POLYMER REACTOR DESIGN, OPTIMIZATION AND CONTROL IN LATEX PRODUCTION TECHNOLOGY

by

ALEXANDER PENLIDIS, DIPL. CHEM. ENG.

A Thesis

Submitted to the School of Graduate Studies

in Partial Fulfilment of the Requirements for the Degree

Doctor of Philosophy.

McMaster University

 September, 1986

LATEX PRODUCTION TECHNOLOGY - REACTOR DESIGN CONSIDERATIONS

"Research can represent the revolt of man against the conditions of life, against creation itself At the same time, it is an aspiration toward clarity - even, paradoxically, toward order and unity of thought - thought that recognizes limits".

An effort by the author to paraphrase Albert Camus

Στους γονείς μου και

στη μνήμη Ευθυμίου

Παπαδοπούλου

DOCTOR OF PHILOSOPHY — McMASTER UNIVERSITY

(Chemical Engineering) — Hamilton, Ontario

TITLE: Polymer Reactor Design, Optimization and Control in Latex Production Technology.

AUTHOR: Alexander Penlidis, Dipl. Chem. Eng. (Aristotle University of Thessaloniki, Greece)

SUPERVISORS: Professor J.F. MacGregor; Professor A.E. Hamielec

NUMBER OF PAGES: xxvi, 438

ABSTRACT

During continuous emulsion polymerization of many monomers (e.g. vinyl acetate, vinyl chloride), sustained oscillations (limit cycles) occur in conversion and all the latex and polymer properties. This creates severe problems with the commercial application of continuous reactors. As shown by Pollock (1984) advanced control theory is inadequate for controlling these reactors. However, it was shown that the limit cycle behaviour could be eliminated through redesign of the reactor train configuration. The redesigned production train was shown via simulation to be free of oscillations and to offer greatly increased flexibility in controlling particle size and monomer conversion.

In this thesis the mathematical model of Kiparissides (1978) and Pollock (1984), based on a particle age distribution analysis and incorporating detailed chemistry and physics of the polymerization phenomena involved, is modified and is used to simulate the dynamic behaviour of these reactors for different modes of process operation (batch, semi-batch and continuous train) and monomer systems (PVAc, PVc).

Experimental studies which demonstrate the improved dynamic performance of the redesigned reactor system are carried out in a pilot plant stainless steel reactor train with on-line monitoring of monomer conversion with a set of on- line densitometers. Control of the final latex particle size and conversion is achieved through manipulation of the initiator feed rate to the first particle nucleating reactor, and the split of the monomer and water flow rates between the first two reactors of the train.

The effect of monomer and water soluble impurities on the emulsion polymerization of Case I monomers is further investigated both theoretically and experimentally. Experimental identification and verification of the main source of stochastic disturbances in these systems was thus obtained.

ACKNOWLEDGEMENTS

I wish to thank Drs. J.F. MacGregor and A.E. Hamielec for their guidance, patience, confidence and encouragement throughout this work. Thanks are also due to Dr. G.A. Irons for his service in the dissertation committee, and to the staff of the Engineering Word Processing Centre for typing this manuscript. My gratitude is extended to Drs. O. Chiantore, H.A. Meyer and N.T. Ali for their lively discussions during the numerous aspects of this research. I particularly wish to thank the McMaster Institute for Polymer Production Technology (MIPPT) for providing facilities for this project. To Pavlos and Vina Kanaroglou I wish to express my appreciation for their help and friendship through many years. To the Department of Chemical Engineering, McMaster University, I wish to express my gratitude for providing financial support. Finally my everlasting love goes to my parents and sister, for their support throughout my many years of study.

TABLE OF CONTENTS

LIST OF FIGURES

LIST OF TABLES

NOMENCLATURE

a	thermal expansion coefficient, lit/°K, in equation (I-106)
$a_p(t,t)$	initial particle surface area at birth, dm^2
$a_{to,t}$	particle area corresponding to $v_{vo,t}$, dm^2
A	constant in the free volume expressions, equation (I-112)
$A_d(t)$	area of monomer droplets, dm^2/l-latex
$A_m(t)$	total surface area of micelles, dm^2/l-latex
A_p, $A_p(t)$	total polymer particle surface area, dm^2/l-latex
B	constant in the free volume expressions, equation (I-113)
$\bar{B}_N(t)$	average number of long-chain branch points per polymer molecule, 1/l-latex
c	constant defined in equation (2.17)
C_{fx}	ratio of k_{fx} to k_p
CI	concentration of initiator in the initiator feed stream, gmole/lit of stream
C_m	ratio of k_{fm} to k_p
C_p	ratio of k_{fp} to k_p
C_w	concentration of radicals in the water phase, gmole/l-latex
d_M	density of pure monomer, gr/lit
d_p	density of pure polymer, gr/lit
$d_p(t,t)$	initial polymer particle diameter, equal to the final diameter of micelles, dm
$d_p(t_f,t_i)$	particle diameter of a particle born at time t_i, now being at time t_f, dm
D_{ave}	some average particle diameter, dm
$\bar{D}_N$	number average polymer particle diameter, dm or Å .

D_p	diffusion coefficient of nomomeric radicals in polymer particles, dm^2/sec
$D_p(t)$	total (cumulative) polymer particle diameter, dm/l-latex
$\bar{D}_p^*(t)$	polymer particle diameter based on a monomer free basis, dm
DP_{max}	maximum degree of polymerization
$\bar{D}_w$	weight average polymer particle diameter, dm or Å
D_w	diffusion coefficient of monomeric radicals in the water phase, dm^2/sec
E(t)	exit age distribution (residence time distribution) function for an ideal CSTR, sec^{-1}
f	efficiency factor for initiator decomposition
f_1	mole fraction of unreacted monomer 1 in the reactor (copolymer case)
f(t)	net particle generation rate, 1/(l-latex)-sec
$F(d_p)$	number frequency of the PSD
F_1	mole fraction of monomer 1 in the copolymer chain (instantaneous copolymer composition)
FI	volumetric flow rate of initiator stream, lit of stream/sec (ml/min in Chapter 7)
FTOT	total volumetric flow rate (ml/min) to reactor 2 (Chapter 7)
I	denotes initiator
I(R1)	initiator volumetric flow rate to R1 (ml/min), Chapter 7
$I_F(t)$, I_F	initiator concentration in the feed, gmole/l-latex
I_{w_o}	initiator concentration in the reactor at time t = 0, gmole/l-latex
$I_w(t)$	initiator concentration in the water phase, gmole/l-latex
k_{ab}	radical capture (absorption) rate constant, dm/sec
k_{cj}	radical capture rate constant (homogeneous nucleation), dm^3/sec
k_d	rate coefficient of initiator decomposition, sec^{-1}

k_{de}	radical desorption coefficient, sec^{-1}
$k_{de}(t,\tau)$	rate coefficient of radical escape (desorption) from polymer particles of the class $n(t,\tau)$, sec^{-1}
k_{fx}	rate consant for radical transfer to CTA, lit/gmole-sec.
k_{fm}, k_{fp}	rate constants for transfer to monomer and polymer, respectively, lit/gmole-sec
k_h	specific homogeneous nucleation rate constant, dm^3/lit-sec, i.e. 1/sec
k_{ho}	rate coefficient of homogeneous nucleation, 1/sec
k_m	rate coefficient of micellar nucleation, i.e. absorption of a radical by a micelle, dm/sec
k_{MI}	rate coefficient for radical reactions with monomer soluble impurities, lit/gmole-sec
k_p^*, k_p	rate constants for terminal double-bond and propagation reactions, respectively, lit/gmole-sec
k_p^1	pseudo-propagation rate constant for the copolymer molecular weight development, 1/sec
k_t, k_{tc}, k_{td}	rate constants for termination by combination and disproportionation, respectively, lit/gmole-sec
k_{tp}, k_{tw}	rate constants for termination in the polymer particle and water phase, respectively, lit/gmole-sec
k_v	ratio of volume of emulsion phase over the volume of aqueous phase, (l-latex)/lit
k_{WI}	rate coefficient for radical reactions with water soluble impurities, lit/gmole-sec
K	extinction coefficient in the light scattering functions, Chapter 3, or ratio of k_p^*/k_p
K_o	mass transfer coefficient for radicals other than initiator ones, sec^{-1}
K_{MSI}	partition coefficient of monomer soluble impurities between polymer particle and emulsion phase
L	critical diffusion length of radicals, dm
m, m_o	partition coefficient of monomeric radicals between water and particle phase

M_F, $M_F(t)$	concentration of monomer in the feed stream, gmole/l-latex
MI, MSI	denotes monomer soluble impurity in general
MI(t), MSI(t)	concentration of monomer soluble impurities in the reactor, gmole/l-latex.
$(MI)_F(t)$	concentration of monomer soluble impurities in the feed stream, gmole/l-latex
$(MI)_p(t)$	concentration of monomer soluble impurities in the polymer particles, gmole/lit
$M_{MON}(t)$	concentration of free monomer in the reactor, gmole/l-latex
$\bar{M}_n$, $\bar{M}_w$	number and weight average molecular weights (of the accumulated MWD), gr/gmole
M_p	monomer concentration in the polymer particles (i.e. in the polymer phase), gmole/lit of particle
M_{TOT_o}	initial concentration of total monomer, units existing as free monomer and as units in polymer chains, gmole/l-latex
$M_{TOT}(t)$	concentration of total monomer in the reactor, gmole/l-latex
M(R1)	volumetric flow rate of monomer to R1 (ml/min).
M_{wc}, M_w	saturation concentration of monomer in the water phase and monomer concentration in the aqueous phase, respectively, gmole/lit
MW	monomer molecular weight, gr/gmole
MWI	initiator molecular weight, gr/gmole
MWS	emulsifier (soap) molecular weight, gr/gmole
n, $\bar{n}$	number of radicals in a particle and average number of radicals per particle, respectively
$n(t,\tau)$	number of polymer particles in the reactor at time t that were born between times τ and $\tau+d\tau$, 1/l-latex
n_p, n_m	refractive indices of polymer particles and dilution medium, respectively
N_A	Avogadro's number, 6.023×10^{23} molecules/gmole
N_{M_o}, N_M	gmoles of monomer in the system initially and at any instant, respectively

N_n	number of polymer particles containing n free radicals, 1/l-latex
$N_p(t,\tau)$	explained in Appendix III
N_p, $N_p(t)$	total number of polymer particles per liter of latex, 1/l-latex
$N_1(t)$	moles of monomer one (unreacted or unbounded) in the reactor (copolymer case)
$p(t,\tau)$	some physical property associated with the class of particles $n(t,\tau)$
$p(t,t)$	property $p(t,\tau)$ at birth, i.e. at $t=\tau$
$P(t)$	total property obtained by summing property $p(t,\tau)$ over all classes of particles in the reactor
$P_r(t,\tau)$	gmoles of dead polymer of chain length r per particle of the class $n(t,\tau)$
$P_r^{\bullet}$	denotes a growing polymeric radical of chain length r
P_s	denotes dead polymer of chain length s
$P_1(t)$	moles of monomer 1 in the copolymer chain (reacted or bounded)
$\bar{q}$, $\bar{q}(t,\tau)$	average number of radicals per particle associated with the class of particles $n(t,\tau)$
$Q_i(t)$	modifid i^{th} moment of the MWD, $Q_i(t) = (Q_n(t)/V_p(t))$, gmole/l-latex
$Q_n(t)$	defined by equation (I-148), associated with the moments of the MWD, gmole/lit
$\bar{Q}_1(t)$	average number of monomer units in polymer molecules per unit volume of particle phase, gmole/lit
r	denotes chain length or radius (dm)
r_c	critical chain length for oligomer precipitation
$\bar{r}_n$, $\bar{r}_w$	number and weight average chain length
r_1, r_2	reactivity ratios for monomer 1 and 2, respectively, (copolymer case)
R	universal gas constant, 1.987 cal/gmole-°K. It also denotes radius of a sphere or a particle, dm. With a dot; it represents a radical in the water phase
$R_r(t,\tau)$	gmoles of radicals of chain length r in a particle of the class $n(t,\tau)$
RATIO	defined in equation (2.27)

R_c	radical capture rate by existing particles, gmole/l-latex-sec
R_{fm}	rate of transfer to monomer reactions, gmole/l-latex-sec
R_I, $R_I(t)$	initiation rate, 1/(l-latex)-sec
R_{p_n}	polymerization rate in a single polymer particle containing n radicals, gmole/particle-sec
R_p, $R_p(t)$, $R_{pTOT}(t)$	total polymerization rate, gmole of monomer/(l-latex)-sec
$R_{pAQ}(t)$	polymerization rate in aqueous phase, gmole/(l-latex)-sec
$R_{p_{POLY}}(t)$	polymerization rate in polymer phase, gmole/(l-latex)-sec
R_t	rate of termination reactions, gmole/(l-latex)-sec
$R_w^{\cdot}$, $R_w^{\cdot}(t)$	concentration of oligomeric radicals in the reactor, 1/l-latex
$R_{w,F}^{\cdot}(t)$	concentration of oligomeric radicals in the feed stream, 1/l-latex
R1, R2	denote reactor 1 (small seeding reactor) and reactor 2 (first large reactor) of the continuous latex train
s_p	flow split
S,[S]	emulsifier concentration, gmole/l-latex
S_{CMC}	critical micelle concentration, gmole/l-latex
$S_p(t)$	area of polymer particles stabilized by polymer end groups rather than soap, dm^2/l-latex
S_{T_0}	total soap concentration in the reactor at time t = 0, gmole/l-latex
$S_F(t)$, $S_T(t)$	soap concentration in the feed and total emulsifier concentration in the reactor, respectively, gmole/l-latex
S(R1)	emulsifier flow rate to reactor 1 (ml/min)
S_a	area occupied by an emulsifier molecule, dm^2/molecule of soap
t, t_f	denotes time and time corresponding to the end of stage 1, respectively, sec
T	temperature, °K
[T]	concentration of chain transfer agent, gmole/lit

$v_t, v_{to,t}$	volume of a single particle (lit) and volume of a particle formed at-time t_o, now at time t, lit
$v(t,\tau)$	polymer volume associated with the class of particles $n(t,\tau)$, lit of polymer/lit of latex
v_{in}	volumetric flow rate into the reactor, lit of latex/sec
v_{out}	volumetric reactor outflow, lit of latex/sec
$v_p(t,\tau)$	particle volume associated with the class of particles $n(t,\tau)$, lit of particle/lit of latex
$v_p(t,t)$	initial polymer particle volume, dm^3
$V, V_{latex}, V_R(t)$	volume of reacting mixture, lit of latex
V_F	free volume fraction, equation (I-106), lit
$V_p, V_p(t)$	total volume of monomer-swollen polymer paticles, lit/l-latex
W	denotes water
WI, WSI	denotes water soluble impurity in general
WI(t), WSI(t)	concentration of water soluble impurities in the reactor, gmole/l-latex
$WI_F(t)$	concentration of water soluble impurities in the feed stream, gmole/l-latex
W(R1)	volumetric water flow rate to reactor 1 (ml/min)
W(r), W(M)	distribution of chain length r and molecular weight distribution
W_p	weight fraction of polymer in polymer particles
x, x(t)	total monomer conversion level at some time t
x_c	conversion at which the separate monomer phase (droplets) disappears. Also, mass fraction of polymer in the polymer phase
[X]	concentration of transfer agent, gmole/lit
$Y_{AVE}(t)$	defined as $Y_{o-or}(t)/V_p(t)$, average number of radicals per particle volume
$Y_{o-or}(t)$	total concentration of radicals in the reactor, gmole/l-latex
$Y_n(t)$	defined in equation (I-149), associated with the moments of the MWD, gmole/lit

Greek Letters

γ	ratio of k_{wl}/k_m or surface tension
δ	lumped monomeric radical diffusion coefficient
$\delta(t-\tau)$	Dirac Delta function
Δt	denotes a (short) time interval, sec
ε	ratio of k_{ab}/k_m
$\varepsilon(t)$	time function, sec^{-1}
θ	mean reactor residence time, sec
λ	denotes wave length of light in general
λ	constant, $dm^2/gmole^{1/2}$-sec
μ	ratio of k_{ho}/k_m, dm^{-1}
$\xi(t)$	time function, $gmole^{1/2}/dm$
π	constant equal to 3.14159
ρ	denotes density in general
$\rho(t)$	radical production (generation) rate into water phase by initiator decomposition and by desorption from polymer particles, 1/(l-latex)-sec
$\rho_{des}(t)$	rate of radical desorption from polymer particles, gmole/(l-latex)-sec
$\rho_i(t)$	rate of radical initiation, gmole/(l-latex)-sec
$\rho_{MI}(t,\tau)$	radical reaction rate with monomer soluble impurities in the class of particles $n(t,\tau)$
ρ'	rate of radical absorption into particles (i.e. entry of radicals), gmole/(l-latex)-sec
σ	denotes variance of a distribution
τ	birth time of the polymer particles in the reactor vessel. It defines the particle phase space
$\phi(t)$	monomer volume fraction in a polymer particle
ϕ_p	volume fraction of polymer in a polymer particle

$\psi(t)$	defined in Appendix XIV

Subscripts

a,ab	denotes absorption (capture, entry) of radicals
AGG	agglomeration
ave, AVE	average
AQ	aqueous phase
c, cr, crit	critical. c may also denote capture events
d	initiator decomposition
de, des	radical desorption
g	glass transition temperature
GEN	generation
f	final time or transfer reaction or flocculation
F	feed stream or free volume
h	homogeneous
IN, in	denotes contribution to a certain total property by inflow
i	initial or initiation or index or interface
l	liquid
n	number of radicals in a polymer particle or n^{th} moment
N	nucleation
out	outflow
p	polymer or polymer particle or polymerization rate or propagation
POLY	polymer phase
R	reacting mixture or reactor
s	solvent
T, TOT	total

ij	in rate constant symbols for the copolymer case: radical of type i reacting with monomer j
∞	infinite (bulk) conditions

Superscripts

•	denotes terminal double-bond reactions
0	self-diffusing conditions
TOT	total
1	denotes pseudo-rate constants for the molecular weight development in the copolymer case

CHAPTER 1

INTRODUCTION AND OBJECTIVES

This introductory chapter will pose the general problem, define the objectives and suggest a general stepwise strategy to satisfy them. It will further briefly describe the contents of each of the nine remaining chapters (in an effort to show from the very beginning that the organization of the thesis is such that consecutive chapters form a logical sequence and continuity, lead to the solution and, in addition, reflect the general stepwise strategy employed).

Research on the modelling, optimization, design and control of emulsion polymerization (latex) reactors and processes has been expanding rapidly as the chemistry and physics of these systems become better understood, and as the demand for new and improved (specialty) latex products increases. The objectives are usually to maximize production rates and/or to control product quality variables such as polymer particle size distribution, particle morphology, copolymer composition, molecular weights, long chain branching, crosslinking frequency and gel content.

Although in recent years considerable advances have been made in all the above mentioned areas, the following very important questions, both academically and industrially, were still unanswered upon initiation of this thesis:

(i) Is the understanding of latex reactors sufficient to satisfy industrial and academic needs? Are the existing model frameworks refined and general? Can existing models successfully predict conversion and other latex and polymer properties? How effectively can models be applied to several modes of reactor operation to suggest open-loop optimization strategies that are feasible and practical? Can one measure latex process variables on-line

effectively? Can existing models be used with other monomer systems with only minor changes?

(ii) Can one eliminate the serious operational and control problem of sustained property oscillations, in continuous latex production? If yes, do the solutions have practical value?

(iii) Why is it that some mathematical models fail to adequately predict real process behaviour? What are the main reasons for this divergence?

All the above questions form an open-ended problem and set specific objectives-targets, that the present investigation attempted to satisfy.

To meet these objectives (and this is true for any attempt in general to develop control schemes for any product quality variable) a general approach-strategy consisting of four basic steps was adopted:

(i) specification of reactor/process model forms: one tries to incorporate detailed process knowledge into a mathematical model

(ii) laboratory and pilot-plant experimentation: data collection and development of measurement methods

(iii) testing of the model's predictive powers: one tries to evaluate model consistency and validity over a wide range of operating conditions, and

(iv) design, optimization and control.

The previously mentioned steps are not independent of each other. In fact, they are highly interrelated and information from each step should be used in an iterative way back and forth, since experience from step (ii) could improve or further shed light to the final model formulation (i.e. step (i)), and similarly, a reliable model from the first three steps could indicate possible bounds concerning the level of sophistication of the proposed control schemes in step (iv).

Following this stepwise strategy, the thesis outline is as follows:

The existing process knowledge with details concerning the several chemical and physical phenomena operative in an emulsion system is translated into mathematics and incorporated into a general dynamic model, based on a population balance approach, in Chapter 2. The model is a modification of the models presented by Kiparissides (1978) and Pollock (1984). Information from the excellent reviews by Blackley (1966), Ugelstad et al. (1967, 1969), Fitch and Tsai (1971), Min and Ray (1974), Ugelstad and Hansen (1976), Nomura et al. (1976), Poehlein and Dougherty (1977), Hansen and Ugelstad (1978), Nomura (1981), Lichti et al. (1983) and Gilbert and Napper (1983), which extensively and comprehensively cover many aspects of emulsion polymerization, is used and incorporated into the mathematical framework. Several model refinements and extensions are suggested.

The link between process modelling and process monitoring or product characterization is made in Chapter 3. Characterization and measurement methods are critically discussed, with the final aim to develop on-line measures of process variables.

Chapters 4 and 5 are concerned with the model testing phase. They represent a theoretical and experimental investigation of batch and semi-batch emulsion polymerization modes for the production of poly(vinyl acetate) latex.

Before proceeding to the final step (i.e. step (iv) of the previously proposed strategy), Chapter 6 critically discusses the state of the art concerning the design, optimization and control of polymerization reactors.

Chapter 7 states once more the operational and control problem related to continuous Case I latex production, explains it theoretically, discusses its serious implications, suggests possible methods of solution and finally, shows an experimental verification of a novel stable reactor train configuration and further illustrates its flexibility and other operational advantages.

Experience with the modelling and experimental stages of the emulsion polymerization of vinyl acetate is extended and applied to another polymer system, that of poly (vinyl chloride), in Chapter 8. A copolymerization model based on population balances for the system vinyl chloride/vinyl acetate is also developed. An emulsion copolymerization model for this comonomer system has to date not been published.

Chapter 9 identifies the source of stochastic disturbances in polymerization reactors and experimentally verifies the effect of impurities in Case I latex systems. It also explains why many theoretical models do not simulate real process data well and it concludes with some general prescriptions for both Case I and II kinetics, as far as impurity effects are concerned.

Finally, Chapter 10 concludes the thesis, discussing on-line control considerations for emulsion reactors, recommending future work, and highlighting the significance of the present work.

In scientific research one builds on the findings of previous researchers. Research, as the word itself signifies, is a perpetual dynamic event. It is believed that the author of this thesis has made a small but very positive contribution towards mining out the rich vein of polymer reactor design and control.

CHAPTER 2

MATHEMATICAL MODELLING OF EMULSION HOMOPOLYMERIZATION REACTORS

2.1 Introduction

Research on the modelling, optimization and control of emulsion polymerization reactors and processes has been expanding rapidly as the chemistry and physics of these systems become better understood, and as the demand for new and improved latex products increases. The objectives are usually to optimize production rates and/or to control product quality variables such as polymer particle size distribution (PSD), particle morphology, copolymer composition, molecular weights and molecular weight distribution (MWD), long chain branching (LCB) and crosslinking frequency, and gel content.

Considerable research in both academic and industrial circles on the optimization of polymer (or latex) quality through the use of batch reactor temperature policies, semi-batch (or semi-continuous) monomer feed policies, etc., has been performed in recent years. However, the succcess of these optimization efforts (or, of any of the subsequent control efforts) depends heavily upon having valid dynamic (or, in some cases, steady-state) models of the physical and chemical phenomena occurring in these complex polymerization systems.

Polymer production technology involves a diversity of products produced from even a single monomer. Polymerizations are carried out in a variety of reactor types: batch, semi-batch and continuous flow stirred tank or tubular reactors. However, very few commercial or fundamental polymer or latex properties can be measured on-line. Therefore, if one aims to develop and apply control strategies to achieve desired polymer (or latex) property trajectories

under such a variety of conditions, it is important to have a valid mechanistic model capable of predicting at least the major effects of the process variables.

In other words, it is very useful to incorporate our knowledge from physics or chemistry (provided, of course, that one has a good understanding of the various phenomena underlying the specific process) into a concise, compact mathematical scheme (the model), which will subsequently be employed to simulate the process and study its special characteristics.

2.2 Models for Emulsion Polymerization

Models for emulsion polymerization reactors vary greatly in their complexity. The level of sophistication needed depends upon the intended use of the model. One could distinguish between two levels of complexity. The first type of model simply involves reactor material and energy balances, and is used to predict the temperature, pressure and monomer concentrations in the reactor. Second level models can not only predict the above quantities but also polymer properties such as particle size, molecular weight distribution and branching frequency. In latex reactor systems, the level one balances are strongly coupled with the particle population balances, thereby making approximate level one models of limited value (Ray (1980)).

In recent years, considerable advances have been made in the modelling of emulsion polymerization reactors. In general, until 1974, models for these systems did not include the particle nucleation phenomena, nor did they consider population balances to account for the PSD's. Now, both homogeneous nucleation (Fitch and Tsai (1971b), Hansen and Ugelstad (1978, 1982)), and micellar nucleation mechanisms (collision or diffusion theory) are usually included in the models. Again, two levels of model are used to account for particle size development. The "monodispersed approximation" model is based on modelling the

development of the number of polymer particles and the total particle volume. Assuming monodispersed particles, the particle size is calculated as proportional to the cube root of the total volume of polymer phase divided by the number of particles. The surface area of polymer particles (needed to calculate the micellar area) is also obtained as proportional to the two-third power of the volume. The second level of emulsion polymerization model employs a population balance approach (or, an age distribution analysis) to obtain the full PSD. By treating the moments of these population balance equations to obtain total or average properties, the set of equations that must be solved is simplified. Since the method of characteristics gives the PSD as a function of (birth/growth) displaced back along the age axis, the moment equations may provide sufficient information to obtain the PSD.

Two of the most comprehensive discussions of these models were presented by Min and Ray (1974), and by Poehlein and Dougherty (1977). Min and Ray (1974) gave a very general model framework which should be capable of modelling most emulsion polymerization systems. Of course, decisions must be made on the relative importance of the various phenomena occurring in a particular system. Other, more recent efforts on the modelling of emulsion reactors include the ones of Table 2-1.

A problem in modelling emulsion systems is that of accounting for the equilibrium partitioning or the dynamic transport of monomers, modifiers, etc., between the several phases involved. The simplest approach employs constant partition coefficients, but more recent work on using thermodynamics (e.g. UNIFAC/UNIQUAC programs, Morton equations) (Hoffman (1984)), has shown promise in accounting for non-ideal solution behaviour (Guyot et al. (1981)).

As in most free radical polymerizations, another phenomenon, the "gel-effect" or "Trommsdorff effect", which results in an autoacceleration of the polymerization rate, may

Table 2-1

Recent Work on the Modelling of Emulsion Polymerization Reactors

Literature Source	Polymer System	Reactor Type: Batch	CSTR: Dyn	CSTR: SS	Level of Model
Thompson and Stevens (1977)	G		X		PB
Cauley et al. (1978)	G		X		PB
Kirillov and Ray (1978)	MMA		X	X	PB
Min and Ray (1978)	MMA	X			PB
Chiang and Thompson (1979)	VAc		X		ADA
Kiparissides et al. (1979)	VAc		X		ADA
Min and Gostin (1979)*	VCM				PB
Sundberg (1979)	G		X		PB
Kiparissides et al. (1980a)	VAc		X		ADA
Schork et al. (1980)	MMA		X		MA
Ballard et al. (1981)**	G		X		
Lichti et al. (1981)	STY	X			PB
Lin et al. (1981)**	STY/AN	X			MA
Hoffman (1981)	SBR	X	X	X	MA
Kiparissides and Ponnuswamy (1981)	STY	X			PB
Lichti et al. (1981)	STY		X		PB
Pollock et al. (1981)	VAc		X		ADA
Gilbert and Napper (1983)	STY	X			PB
Hamielec et al. (1983)	SBR		X	X	PB, MA
Lichti et al. (1983)	STY	X			PB
Broadhead (1984)	SBR	X	X	X	PB, MA
Broadhead et al. (1984)	SBR	X	X	X	PB, MA
Gilbert et al. (1984)	STY	X			PB

* Semi-batch

** Copolymerization

Symbols: G = general polymer system; PB = population balance model; ADA = age distribution analysis; MA = "monodispersed" approximation; Dyn = dynamic; SS = steady-state; CSTR = continuous stirred tank reactor

have to be accounted for. It results from diffusion-controlled termination reactions involving large polymer radicals. At very high conversions, the propagation rates may also become diffusion-controlled if the polymerization temperature is below the glass transition temperature of the polymer being synthesized. These effects have often been accounted for by empirical correlations of the rate constants with conversion. Recently, more fundamental approaches using free volume theory or de Gennes reptation theory have been used quite successfully to model these effects for homopolymers (Marten and Hamielec (1979, 1982), Chiu et al. (1982), Tulig and Tirrell (1981), Hamielec et al. (1982), Tirrell and Tulig (1983), Soh and Sundberg (1982a-1982d)), and for copolymers (Hamielec and MacGregor (1983)). It is this "gel-effect" that is often responsible for multiple steady-states in a CSTR. These multiple steady-states, and the very interesting behaviour that they lead to, have been investigated in several papers (Jaisinghani and Ray (1977), Hamer et al. (1981) and Schmidt et al. (1982, 1984)).

A summary of recent studies of diffusion-controlled termination and propagation reactions in free radical polymerization which are pertinent to emulsion polymerization kinetics is given in Harris et al. (1981) and in Hamielec (1983). Also included are discussions of the effects of diffusion-controlled termination and propagation on molecular weight and branching development, with particular reference to the synthesis of poly(vinyl chloride) (PVC) at high conversions and to the significant reduction of its thermal stability which occurs at these conversion levels.

2.2.1 Uses of Models

Future advances in latex production technology will be achieved largely through the efficient use of these comprehensive emulsion polymerization reactor models. Obvious uses of the models include the simulation and design of batch and/or continuous reactor systems.

Novel operating strategies or recipe modifications which give higher productivity or improved quality can be identified. Control policies can be developed through simulation of various schemes of operation, or by using the model directly to develop advanced multivariable control algorithms for a production system in place. Reactor venting systems can be designed, which will reduce the risk of vessel rupture during a runaway polymerization (Huff (1982)). Operators can be trained using iterative graphics terminals along with the simulation model. Analysis of the consequences of system failures or upsets, which is an important safety consideration, can be greatly simplified. Finally, a less obvious use of the models is to offer guidance in the selection and development of on- or off-line sensors for reaction monitoring or product characterization (Duijfjes (1975), Pollock (1984)).

2.3 Model Development

2.3.1 General

In this section, a mathematical dynamic model will be developed for the emulsion polymerization of vinyl acetate (VAc). The model derivation will be general enough to easily apply to any Case I kinetics monomer (e.g. vinyl acetate, vinyl chloride) and to a variety of different modes of reactor operation (e.g. batch, continuous, etc.).

Subsection 2.3.2 is concerned with the development of the ingredients' mass balances, whereas subsections 2.3.4 and 2.3.5 contain the development of differential equations which describe the evolution of particle size and molecular weight properties, respectively, during the course of the polymerization. This development is based on a population balance approach, a quite general model framework which is discussed in subsection 2.3.3. Finally, subsection 2.3.6 contains the model equations in a compact form.

2.3.2 Material Balances

Material (mass) balances for the ingredients of an emulsion recipe are of the general form: (Accumulation) = (Input) − (Output) + (Production) − (Loss) and are developed in Appendix I. The same form of balance also applies to the oligomeric radical concentration, which is going to be used in subsection 2.3.3, where an expression for the net polymer particle generation rate (nucleation rate), f(t), is developed.

2.3.3 Population Balance Approach

The use of mass and energy balances alone to model polymer reactors is inadequate to describe many cases of interest. Examples are suspension and emulsion polymerizations where drop size or micelle distribution may also be of interest. In such cases, an accounting for the change in number of droplets or micelles of a given size range is often required. This is an example of a population balance.

A population balance is a balance on a defined set of countable or identifiable entities, which accounts for the net accumulation of such entities in a given system as a result of all phenomena which add or remove entities from the set. If the set in question is the number of droplets between diameter D and (D + dD) in a vessel, the set may receive droplets by flow into the vessel, by coalescence or by growth from smaller droplets. The set may also lose droplets by outflow from the vessel, by coalescence or by growth out of the set's size range.

General discussions of the basic ideas have been presented by Hulburt and Katz (1964) and by Randolph (1964). Their application to crystallization systems were reported by Moyers and Randolph (1973) and Chang and Wang (1984), and to polymerization reactors by Stevens and Funderburk (1972), Min and Ray (1974), Thompson and Stevens (1977), Cauley et al. (1978), Kiparissides et al. (1979) and Pollock et al. (1981) (see also Table 2-1).

A further discussion of the population balance approach in modelling particulate systems and the derivation of the general population balance equation are given in Appendix I.

2.3.4 Particle Size Development

The particle size development is based on the expression which gives the rate of change of polymer volume in a particle of a certain class. That expression will lead to an expression for the rate of change of polymer particle volume, $v_p(t,\tau)$, with time. The latter expression will be incorporated in the general total property balance developed in Appendix I to finally yield an ordinary differential equation for $V_p(t)$, the total polymer particle volume in the reactor.

Expressions can also be obtained in a similar way for $D_p(t)$ and $A_p(t)$ and they are also developed with more details in Appendix I.

2.3.5 Molecular Weight Development

The idea of following classes of polymer particles born in the reactor during an infinitesimal time interval $d\tau$ can also be employed for the molecular weight development. The development of expressions for the moments of the molecular weight distribution is outlined in detail in Appendix I of this thesis.

2.3.6 Vinyl Acetate Mathematical Model

The population balance approach in developing the mathematical model equations eventually results in 11 ordinary differential equations. These equations together with the accompanying (auxiliary) algebraic expressions are listed below.

$$\frac{dI_w(t)}{dt} = \frac{I_F(t) - I_w(t)}{\theta} - k_d I_w(t) \qquad (2.1)$$

$$\frac{d\,S_T(t)}{dt} = \frac{S_F(t) - S_T(t)}{\theta} \tag{2.2}$$

$$\frac{d\,x(t)}{dt} = \frac{R_p(t)}{M_{TOT}(t)} - \frac{x(t)\,M_F(t)}{\theta\,M_{TOT}(t)} \tag{2.3}$$

$$M_{TOT}(t) = M_{TOT_0}\,e^{-t/\theta} + M_F(t)\,(1 - e^{-t/\theta}) \tag{2.4}$$

$$x(t) = \frac{M_{TOT}(t) - M_{MON}(t)}{M_{TOT}(t)} \tag{2.5}$$

$$\frac{d\,M_{MON}(t)}{dt} = \frac{M_F(t) - M_{MON}(t)}{\theta} - R_p(t) \tag{2.6}$$

$$R_p(t) = (1 - \phi(t))\,\frac{d_p}{MW}\,\lambda\,\xi(t)\,A_p(t) \tag{2.7}$$

$$\frac{d\,N_p(t)}{dt} = \frac{N_{p_{IN}}(t) - N_p(t)}{\theta} + f(t) \tag{2.8}$$

$$f(t) = \rho(t)\,\frac{A_m(t)k_v + \mu(1 - L\,A_p(t)k_v/4)}{A_m(t)k_v + \mu\,(1 - L\,A_p(t)k_v/4) + \varepsilon\,A_p(t)k_v} \tag{2.9}$$

$$\rho(t) = 2\,f k_d\,I_w(t)\,N_A + \left(\frac{12\pi f k_d N_A D_w \delta k_{fm}}{m k_p}\right)^{1/2}\frac{I_w^{1/2}(t)}{A_p^{1/2}(t)}\,N_p(t) \tag{2.10}$$

$$A_m(t) = (S_T(t) - S_{CMC})\,S_a\,N_A - A_p(t) \tag{2.11}$$

$$\lambda = \left(\frac{k_p d_M}{N_A d_p}\right)\left(\frac{f k_d m k_p N_A}{12\pi D_w \delta k_{fm}}\right)^{1/2} \tag{2.12}$$

$$\xi(t) = \frac{\phi(t)}{(1-\phi(t))} \frac{I_w^{1/2}(t)}{A_p^{1/2}(t)} \tag{2.13}$$

$$\frac{d D_p(t)}{dt} = \frac{D_{p_{IN}}(t) - D_p(t)}{\theta} + f(t) d_p(t, t) + 2\lambda \xi(t) N_p(t) + \frac{\varepsilon(t)}{3} D_p(t) \tag{2.14}$$

$$\phi(t) = \frac{1-x(t)}{1-(x(t)\cdot c)}, \; x(t) = x_c \text{ if } x(t) \le x_c \tag{2.15}$$

$$\varepsilon(t) = \left(\frac{1}{1-\phi(t)}\right) \frac{c-1}{(1-c\,x(t))^2} \frac{d x(t)}{dt}, \; \varepsilon(t) = 0 \text{ if } x(t) \le x_c \tag{2.16}$$

$$c = \left(1 - \frac{d_M}{d_p}\right) \tag{2.17}$$

$$\frac{d A_p(t)}{dt} = \frac{A_{p_{IN}}(t) - A_p(t)}{\theta} + f(t) a_p(t, t) + 4\pi\lambda \xi(t) D_p(t) + \frac{2}{3} \varepsilon(t) A_p(t) \tag{2.18}$$

$$\frac{d V_p(t)}{dt} = \frac{V_{p_{IN}}(t) - V_p(t)}{\theta} + f(t) v_p(t, t) + \lambda \xi(t) A_p(t) + \varepsilon(t) V_p(t) \tag{2.19}$$

$$\frac{d Q_0(t)}{dt} = \frac{Q_{0_{IN}}(t) - Q_0(t)}{\theta} + k_p M_p Y_{AVE}(t) \left(C_m V_p(t) - K \frac{Q_0(t)}{M_p}\right) \tag{2.20}$$

$$M_p = \phi(t) \frac{d_M}{MW} \tag{2.21}$$

$$Y_{AVE}(t) = Y_{0_{TOT}}(t) / V_p(t) \tag{2.22}$$

$$Y_{0_{TOT}}(t) = \lambda\, \xi(t) \left(\frac{d_p}{k_p d_M} \right) \left(\frac{1-\phi(t)}{\phi(t)} \right) A_p(t) \tag{2.23}$$

$$\frac{dQ_1(t)}{dt} = \frac{Q_{1_{IN}}(t) - Q_1(t)}{\theta} + k_p M_p Y_{AVE}(t)(1 + C_m) V_p(t) \tag{2.24}$$

$$\frac{d(Q_0 B_N)(t)}{dt} = \frac{(Q_0 B_N)_{IN}(t) - (Q_0 B_N)(t)}{\theta} + k_p M_p Y_{AVE}(t) \left(C_p \frac{Q_1(t)}{M_p} + K \frac{Q_0(t)}{M_p} \right) \tag{2.25}$$

$$\frac{dQ_2(t)}{dt} = \frac{Q_{2_{IN}}(t) - Q_2(t)}{\theta} + k_p M_p Y_{AVE}(t) \Big((1 + C_m) V_p(t) +$$

$$+ 2(\text{RATIO}) \left((1 + C_m) V_p(t) + C_p \frac{Q_2(t)}{M_p} + K \frac{Q_1(t)}{M_p} \right) \Big) \tag{2.26}$$

$$\text{RATIO} = \frac{1 + K \dfrac{\overline{Q}_1(t)}{M_p}}{C_m + C_p \dfrac{\overline{Q}_1(t)}{M_p}} \tag{2.27}$$

$$\overline{Q}_1(t) = Q_1(t) / V_p(t) \tag{2.28}$$

The underlined equations (2.1), (2.2), (2.3), (2.8), (2.14), (2.18), (2.19), (2.20), (2.24), (2.25) and (2.26) constitute the dynamic model while the other ones accompany them as definitions or expressions for terms (or auxiliary groups of terms) which already appear in the model.

A listing of the assumptions made during the model derivation is given in Appendix I and a detailed documentation of the computer program written to handle the numerical solution of the dynamic model is cited in Appendix II and in Penlidis et al. (1984).

2.4 Model Parameter Estimation

A detailed discussion concerning parameter values and model parameter estimation will be given in Chapter 4. Chapter 4 discusses batch vinyl acetate emulsion polymerization data, on which parameter estimation was mainly based.

2.5 Particle Size Distribution Determination

2.5.1 General

Polymer particles in an emulsion system generally have a distribution of sizes. This distribution is due to two factors. Firstly, particles nucleated over a prolonged period of time will be of different sizes as a result of their different durations of growth. Secondly, particles nucleated at the same time will have a statistical distribution of periods of radical residence and growth. Furthermore, larger particles will have a broader distribution of radical residence periods.

Experimentally determined particle size distributions can serve as "fingerprints", providing clues for the identification of basic mechanisms prevailing in an emulsion system. Theoretical predictions are useful in analyzing experimental PSD's, as illustrated by the work of Lichti et al. (1981, 1983), who postulated a nucleation mechanism based on fitting theoretical PSD's to experimental ones. PSD's also play an important role in controlling latex properties such as bulk viscosity. It is important, therefore, to be able to manipulate PSD's for polymers used as paints, adhesives and spray coatings.

The coalescence of particles, which has not been widely studied, may play an important and, indeed, controlling role in the development of PSD's. In most of the modelling approaches surveyed, it is assumed that enough emulsifier is present to completely stabilize the particles. The accuracy of this assumption is vitally important to the validity of PSD models. This aspect is discussed in more detail in Gilbert et al. (1984), in an effort to model early time PSD's.

There are mainly two common particle size modelling approaches. The simplest approach to modelling the PSD is to assume all particles of the same size (i.e. "monodispersed" approximation). Then, the mass balance equations will give the total polymer volume in the system, and the volume of a single particle is subsequently calculated from the knowledge of the total particle volume and an estimate of the number of particles. In other words,

$$\text{Mass balance equations} \rightarrow V_{polymer,\,total} \tag{2.29}$$

$$V_{particle,\,total} = V_{polymer,\,total} / 1 - \phi(t) \tag{2.30}$$

and

$$V_{particle} = V_{particle,\,total} / N_p(t) \tag{2.31}$$

Particles are generally assumed spherical so that particle diameter and surface area are easily calculated from particle volume. In the "monodispersed" approximation, another common assumption is that the average number of radicals per particle is implicitly considered equal in all particles.

To consider the full PSD, a population balance or age distribution analysis on particles must be employed. Table 2-2 gives a summary of recent work concerning the determination of PSD's in emulsion systems, using both approaches. More details can be found in the literature sources cited in the Table.

2.5.2 Population Balance Approach PSD

The methods suggested in the literature sources of Table 2-2 for the calculation of the full PSD require systems of integro-differential, partial differential or difference differential equations to be solved, which in most of the cases is a tedious task requiring considerable computation time. Furthermore, although the Min and Ray (1974, 1978) model can give the full PSD and it theoretically is the most general mathematical model to date, their moment method needs a separate set of equations for each additional particle generation, thus making it less convenient for the simulation of a CSTR.

The conceptual approach used in this thesis to modelling the full PSD is to discretize the particle population according to age. Each subdivision is then referred to as "a generation". The diameters of all subsequent particle generations are inferred from the diameter of particles of the first generation (i.e. those particles nucleated in the beginning of the reaction) and the nucleation time of the generation of interest with respect to final time at which the PSD is required. In this way, only the diameter of the particles of the first generation is integrated. The appropriate differential equation is

$$\frac{d}{dt} d_p(t_f, t_i) = 2\lambda\, \xi(t) + \frac{\varepsilon(t)}{3} d_p(t_f, t_i) \tag{2.32}$$

where $d_p(t_f, t_i)$ denotes diameter of a particle born at time t_i, now at time t_f.

So, the diameter of a particle of a particular subsequent generation at any time will be equal to the difference between the first generation particle diameter at the time of interest and at the time of nucleation of the generation of interest. If $d_p(f_f, t_i)$ represents the diameter of a particle at time t_f, which was nucleated at time $(t_i + \alpha\, \Delta t)$, then the aforementioned relationship may be expressed by:

$$d_p(t_f, t_i + \alpha\, \Delta t) = d_p(t_f, t_i) - d_p(t_i + \alpha\, \Delta t, t_i) \tag{2.33}$$

where t_i is the time of the first generation. Schematically, one can translate equation (2.33) into the picture of Figure 2-1.

Table 2-2
Recent Work on the Modelling of PSD's in Emulsion Polymerization Reactors

Literature Source	Approach	Comments
Nomura et al. (1971)	MONO	VAc EP
Min and Ray (1974)	PB	GRP
Dickinson (1976)	ADA	STY EP
Poehlein and Dougherty (1977)	MONO	GRP
Cauley et al. (1978)	PB	GPS
Min and Ray (1978)	PB	MMA EP
Kiparissides et al. (1979)	ADA	VAc EP
Poehlein (1979)	MONO	GPS
Sundberg (1979)	PB	GPS
Ray (1980)	PB	GRP
Ballard et al. (1981)	MONO	ECP
Hoffman (1981)	MONO	SBR ECP
Kiparissides and Ponnuswamy (1981)	ADA	STY EP
Lichti et al. (1981)	MONO, PB	STY EP
Nomura and Harada (1981)	MONO	VAc EP
Bataille et al. (1982)	MONO	STY EP
Lichti et al. (1983)	PB	STY EP
Tsai et al. (1983)	MONO	STY EP
Broadhead (1984)	MONO, ADA	SBR ECP
Gilbert et al. (1984)	PB	GPS
Hoffman (1984)	PB	SAN ECP
Pollock (1984)	ADA	VAc EP
Lin (1984)	PB	EP

Symbols:
MONO = "monodispersed approximation"
PB = population balance approach
ADA = age distribution analysis
EP = emulsion polymerization
GRP = general review paper
GPS = general polymer system
ECP = emulsion copolymerization.

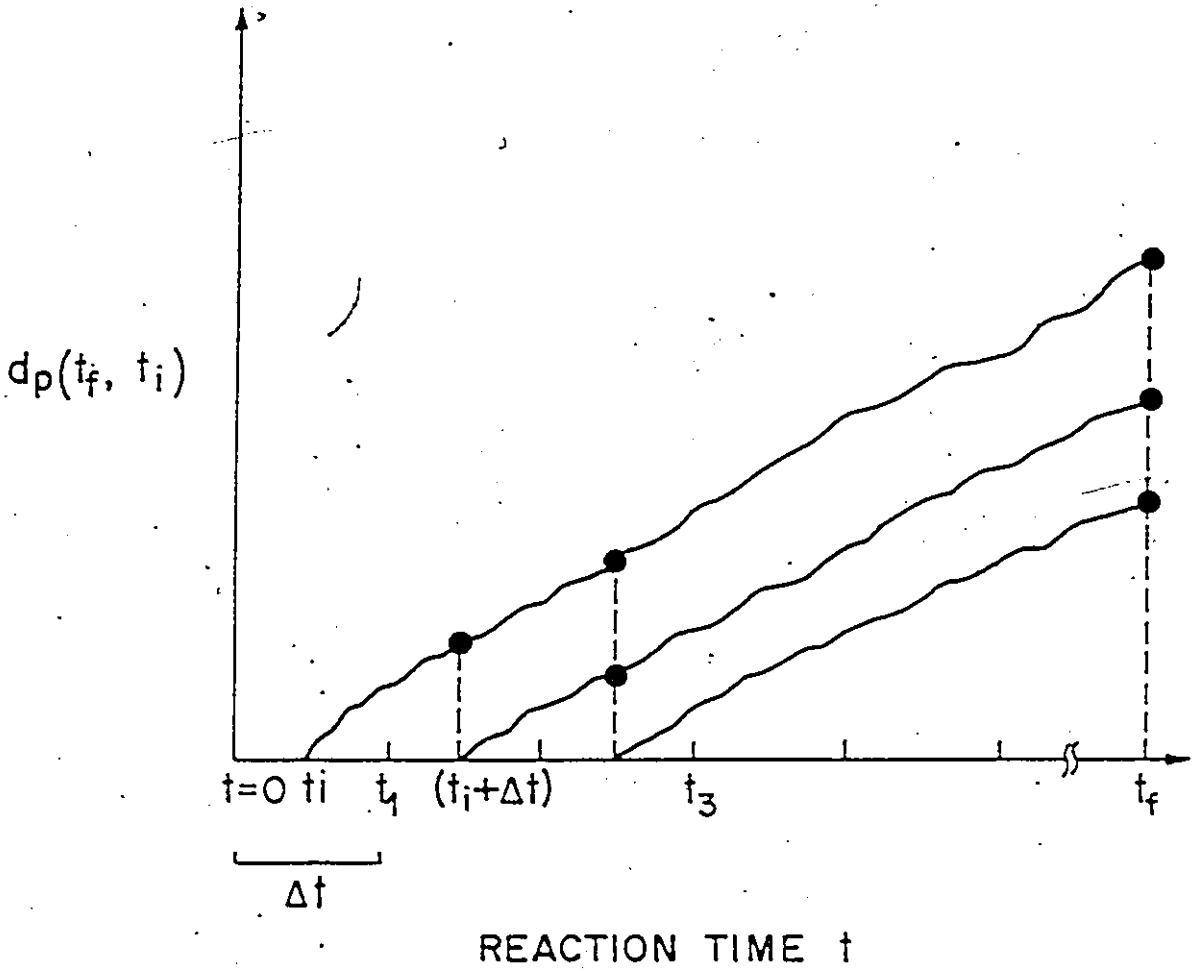

Figure (2-1). Schematic Representation of Relationship (2.33)

Then, the PSD is constructed by storing the number of particles and the diameter of a single particle of each generation. The method is illustrated in detail in Appendix III.

Finally, the PSD is presented as a plot of the normalized number frequency of particles versus particle diameter. The number frequency is calculated as:

$$F(d_p) = \frac{N_p(t, \tau)}{N_p(t)\,\Delta d_p} \tag{2.34}$$

where Δd_p represents the difference in particle diameters between consecutive generations.

The advantage of the PSD calculation method outlined in this subsection and also in Pollock (1984) and Broadhead (1984), is that only one additional differential equation need be integrated, a fact which considerably simplifies matters and saves in computation time. A drawback of the present approach (and also of the other approaches of Table 2-2) is that the statistical variation of the distribution arising from the variation of the number of radicals per particle in a class of a certain size is missing. The PSD's thus calculated indicate the average particle diameter growth of each generation.

Appendix III also illustrates a somewhat different method of calculating PSD's in an emulsion system.

2.6 Conclusions

The objective of this chapter was to present a simple but adequate model for emulsion homopolymerization reactors based on a particle age (residence) distribution analysis. The model contains a minimum number of adjustable parameters which can be readily estimated from experimental data. Important latex and polymer properties related to particle size and molecular weight distributions are accounted for in the present model.

The unquestionable commercial importance of all the above properties for a latex makes such a model useful for the simulation, optimization, design and control of latex

reactors. The ability of the model to provide reactor simulations by simply specifying reactor operating conditions and its importance to every step towards emulsion polymer reactor control will be clearly demonstrated in the subsequent chapters of this thesis.

CHAPTER 3

LATEX AND POLYMER PROPERTY CHARACTERIZATION AND MEASUREMENT METHODS

3.1 Introduction

It is obvious that no attempt can be made towards a more efficient latex reactor design, optimization or control, if one does not have the ability to monitor the process itself during the reaction, i.e., if one can not use information from the process in the form of latex or polymer property measurements. To take one step further, one can not talk about on-line measurements, if of course specific measurement or characterization methods are not first fully developed off-line and later modified so as to be used on-line. And it is needless to add that without feedback of information from a system, there is no direct link between modelling and design or control efforts.

The development of polymer property characterization methods became a very important part of polymer reactor research a long time ago. Measurement techniques represent the probe which can be used by the researcher in order to pose certain questions to nature and receive specific answers. How reliable these answers or indications are, it all is a matter of how well developed and understood the characterization methods are.

It is extremely important to have well developed characterization methods for the following reasons:

(a) Measurements are the link between reactor modelling and reactor design or control. Without measurements, there is no way one can exploit feedback information from a system. Without well developed measurement techniques, reactor optimization efforts are of no practical significance. There are cases (most of the industrial situations in fact) when it is

practically impossible to have measurements on all polymer properties. Even a few measurements are very helpful, though, as it will become evident from Chapter 6.

(b) A few years ago, conversion measurements only were being used by industries to fully characterize their product. The fact that two latex products may have the same conversion but totally different average particle size (or molecular weight) is sufficient to show that conversion measurements alone are not enough. Particle size (or molecular weight) are important properties of a latex sample and they define the end use of the latex product (e.g. if a resin is to be used in a coating, then the resin should not contain particles with a diameter approaching the thickness of the coating, because otherwise a non-uniform film results. Also, if one wants to reduce the viscosity of a latex, one should produce a latex with a bimodal (or possibly multi-modal) PSD).

Despite the evident importance of well developed characterization methods, only in the past two decades have techniques been developed which are reliable, accurate and yield reproducible results. A chapter therefore, which will briefly discuss and summarize our observations and experience with latex and polymer property measurements, is a necessary and logical bridge between reactor modelling and reactor design. The present chapter will not only serve as a guide to several important characterization methods, but it will also tie together the modelling and design chapters of this thesis.

Conversion measurements will be dealt with first. Off-line gravimetry and on-line densitometry are discussed. Then, particle size characterization techniques are critically reviewed (turbidity spectra, hydrodynamic and size exclusion chromatography and electron microscopy). The applicable range of the most common particle size analytical methods is given in Figure 3-1 and a complementary to the present development overview can be found in Collins (1983). Finally, molar mass measurements with specific emphasis on laser light scattering are examined at the end of the chapter.

3.2 Determination of Conversion

Conversion measurements (or equivalently, determination of the concentration of the produced latex or solids content) are one of the most important measurements in polymer characterization, in a sense that conversion is not only a means of sample characterization by itself, but it is also necessary before further analysis (e.g. turbidity spectra) is attempted. One method for conversion determination is widely accepted, the method being the so-called off-line gravimetry. In the present study, off-line gravimetry was employed to determine the latex sample conversion levels, and information from off-line gravimetry was further used and compared to information from an on-line technique, namely on-line densitometry (Abbey (1981), Shork and Ray (1981)). Both methods yield sample conversion levels and are further discussed in what follows.

3.2.1 Off-line Gravimetry

The underlying idea behind off-line gravimetry is to determine the weight of (pure) polymer (produced) contained in a sample and to compare this weight with the weight one would have obtained, had the conversion been 100% (i.e. had the conversion of monomer to polymer been complete). Variations of the above idea are employed in all gravimetric methods, depending upon recipes or reactor mode of operation.

In the case of a batch reactor (or a continuous reactor which starts (full of recipe) with identical feed and initial reactor recipe), conversion is defined as the weight of polymer formed per weight of initial monomer present. A sample is taken from the reactor ($\sim$ 10 ml), a drop of inhibitor (hydroquinone solution in deionized water, 1% by wt.) is added to it and the sample is shaken well. The addition of hydroquinone stops further polymerization. The

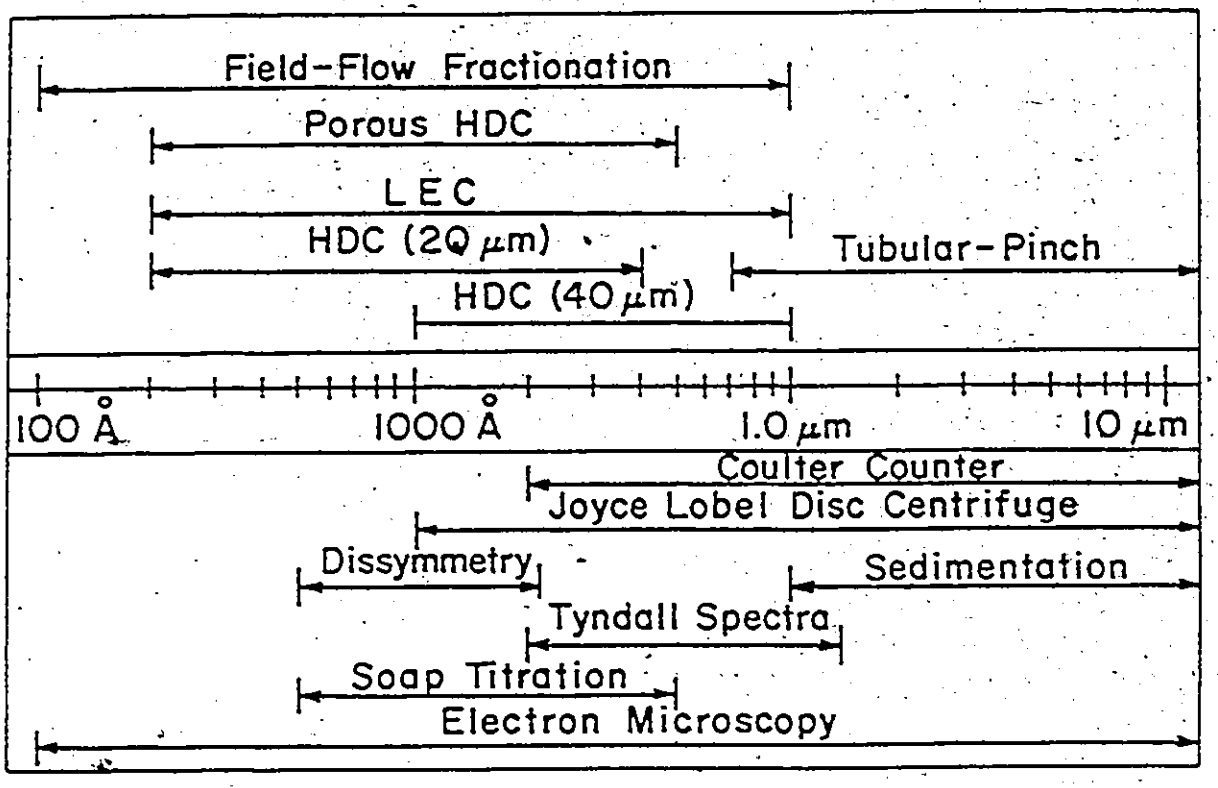

Figure (3-1). Applicable Range of the Most Common Particle Size Analytical Techniques

sample vial is subsequently placed for 10 to 15 minutes into ice (~ 0°C) (an additional measure to quench any further reaction in the vial). Then, two different paths can be followed for conversion determination, both of which should yield the same result, if they are properly done. According to the first one, an 1 or 2 ml aliquot is transferred into a preweighed glass dish (petri dish) and weighed. The exact volume of the aliquot is of no importance for this path. The content of the dish is then dried to a constant weight in a vacuum oven (~ 24 hours at 40 to 45°C) and the dish with the dry residue is weighed again. The fraction solids is then given by:

$$FSOL = \frac{(DISH + DRY) - (DISH)}{(DISH + SAMPLE) - (DISH)} \tag{3.1}$$

For the specific sample and from the experimental recipe employed, one knows the weight fraction of initiator (FI) and emulsifier (FS) and the weight fraction of monomer initially present (FM). Then,

$$x(t) = \frac{FSOL - FI - FS}{FM} \tag{3.2}$$

Totally equivalent is the second path, where one tries to transfer in the preweighed dish an exact volume of latex. Then,

$$x(t) = \frac{(w/A)}{(MW) \cdot M_F} \tag{3.3}$$

where w = weight of dry polymer = (Dish + DRY) – Dish, A = volume of latex transferred in the dish to be dried, MW is the monomer molecular weight and M_F the initial monomer concentration (in gmoles/l-latex). For the case of a batch reactor and always depending on the recipe used, FI and FS in equation (3.2) can be set equal to zero, since they may be negligible.

In the case of a continuous reactor, if the feed and initial reactor concentrations are not identical, then conversion is defined according to equation (I-17). $M_{TOT}(t)$ is given by equation (I-16) and $(M_{TOT}(t) - M_{MON}(t))$ is the weight of (pure) polymer formed, i.e. given by the numerator of (3.2). Obviously in such a case, conversion is defined as the weight of

polymer formed per weight of total monomer present at the time of the sample. FI, FS and FM are all known from the experimental conditions.

3.2.2 On-line Densitometry

An on-line densitometer (a DPR-YWE model, with a PTE-98-EV-72 excitation cell and a DPR-2000 electronic board, by Anton Paar) was employed for the on-line conversion determinations. The instrument can also be used for off-line determinations, if a certain sample volume is injected into its cell. For on-line determinations, the latex is continuously flowing through a vibrating U-tube with a Y-mode oscillator. The U-tube is continuously excited by a current of constant amplitude produced by the PTE-98-EV-72 excitation cell. The period of oscillation T of the tube is proportional to the square root of the mass contained within the tube, and therefore density is obtained as:

$$T = a + b\rho \tag{3.4}$$

where T is the period of oscillation (output from the instrument), ρ is the density of the fluid inside the tube in gr/cm^3, and a and b are calibration constants. An alternative calibration curve can also be given as:

$$\rho = \frac{1}{A}(T^2 - B) \tag{3.5}$$

where A and B are new calibration constants. The calibration constants are obtained at given temperatures by using known density fluids (e.g. water and methanol).

If density is known, then for a batch reactor a simple mass balance relates the measured density $\rho(t)$ with the sample's conversion x(t). The relationship follows:

$$x(t) = \frac{(\rho(t) - \rho^\circ)(1 + w)\, d_M\, d_{pol}}{\rho(t)\, \rho^\circ (d_{pol} - d_M)} \tag{3.6}$$

In equation (3.6), x(t) is the calculated conversion, $\rho(t)$ the measured latex density (all densities are in gr/lit in (3.6)), d_M and d_{pol} are the monomer and pure polymer densities,

respectively, w is the ratio of water to monomer in the emulsion mixture (i.e. grs of water/grs of monomer), and ρ°, the density of the reacting mixture at 0% conversion, is given by:

$$\rho^\circ = \frac{1+w}{\frac{1}{d_M} + \frac{w}{d_w}} \tag{3.7}$$

where d_w is the density of water. All densities are evaluated at the temperature of the U-tube (output from the instrument). A temperature compensation circuit accounts for density fluctuations due to temperature changes. A similar expression to the one in equation (3.6) can also be employed for a continuous reactor.

Schork and Ray (1981) used the following relationship between x(t) and measured density $\rho(t)$:

$$x(t) = \frac{\rho(t) - \rho^\circ}{\rho^{100} - \rho^\circ} \tag{3.8}$$

where ρ^0 and ρ^{100} are the emulsion densities at 0% and 100% conversion levels, respectively. Calculations of x(t) with equation (3.8) gave exactly the same results as with calculations with (3.6).

3.2.3 Comments on Conversion Determination

Conversion determination by off-line gravimetry is, in general, quite accurate and reproducible (the estimated experimental error with gravimetry is in the order of magnitude of 1.5%). However, if a very large number of samples are analyzed, some time delay occurs between sampling and analysis. Settling, agglomeration and some evaporation may all occur. This could cause problems in the final translation of the gravimetric results and discrepancies between off-line gravimetry and on-line densitometry.

3.3 Particle Size Determination: Turbidity Spectra

The experimental simplicity of turbidity spectra analysis (i.e. measurement of the intensity of the scattered light at a fixed angle $\theta = 180°$) is the main reason why the technique has received such attention in the past years (Heller and Pangonis (1957), Meehan and Beattie (1960), Maxim et al. (1969), Varra and Bocko (1979), Kiparissides et al. (1980), Muly and Frock (1980), Zollars (1980), Koch et al. (1981), Rowell and Ford (1981), Zollars (1981 b), Mehta and Shah (1982), Koch et al. (1983) and Melik and Fogler (1983)). For a polydisperse suspension, turbidity τ is given by:

$$\tau = N \int_0^\infty \frac{\pi D^2}{4} K\left(\frac{D}{\lambda_m}, \frac{n_p}{n_m}\right) f(D)\, dD \tag{3.9}$$

f(D) is the suspension's normalized PSD, and

$$\tau = \frac{1}{\ell} \ell n\left(\frac{I_o}{I}\right) \tag{3.10}$$

where I_o and I represent intensity of the incident and the emerging (from the scattering solution) beam, respectively, and ℓ is the length of the optical path. Of course, for a monodisperse suspension with N non-absorbing spherical particles of diameter D (in the absence of multiple scattering), equation (3.9) is considerably simpler. $K(D/\lambda_m, n_p/n_m)$, the extinction coefficient, is in the general case a complicated function of the particle diameter D, the wavelength in the medium λ_m, and the refractive indices n_p and n_m of the particles and the medium, respectively. K can be calculated from the general Mie theory (Heller and Pangonis (1957)). λ_m is the ratio of λ_o to n_m, where λ_o is the wavelength in vacuum.

The concentration C of polymeric solids (polymer particles) in the latex (in gr/cm^3 of latex) is subsequently given by:

$$C = N \rho \int_0^\infty \frac{\pi D^3}{6} f(D)\, dD \tag{3.11}$$

where ρ is the particle density in gr/cm^3 of particle.

Combination of equations (3.9) and (3.11) gives a ratio, the specific turbidity, independent of N, as:

$$\frac{\tau}{C} = \frac{3}{2\rho} \frac{\int_0^\infty D^2 K f(D)\, dD}{\int_0^\infty D^3 f(D)\, dD} \tag{3.12}$$

where the functional dependence of K has been omitted for the sake of brevity. It is evident from equation (3.12) that for a known size distributional form, (τ/C) is a function of the refractive index of the medium, the refractive index and density of the particles, the wavelength of the incident light and the parameters describing the PSD.

Therefore, in principle, the parameters of the PSD can be estimated from (τ/C) measurements at different wavelengths. This is not true, however, in the Rayleigh regime (i.e. small particles for which (D/λ_m) is less than 0.1). In this case, K is proportional to $(D/\lambda_m)^4$ and

$$\frac{\tau}{C} = L \frac{\int_0^\infty D^6 f(D)\, dD}{\int_0^\infty D^3 f(D)\, dD} = L\, \overline{D}_\tau^3 \tag{3.13}$$

where $\overline{D}_\tau$ is a "turbidity" average particle diameter and

$$L = 4\pi^4 \rho^{-1} \lambda_m^{-4} (m^2 - 1/m^2 + 2)^2 \tag{3.14}$$

m is defined as the ratio (n_p/n_m) and lies between 1.1 and 1.2 for PVAc. It is clear from equation (3.13) that use of different wavelengths will not provide additional information; hence, only a "turbidity" average diameter is determined in the Rayleigh regime.

In the Mie scattering regime it should be possible to obtain both particle number and size distribution through measurements of turbidity as a function of wavelength. However, without prior knowledge of the shape of the PSD, it is impossible to find a unique distribution function. Moreover, even if one knows the distributional form of the unknown

PSD it is very difficult, if not impossible, to avoid multivalued solutions for the parameters of the PSD (Kourti et al. (1984)). However, for purposes of on-line determination of some diameter average for particle size control it may not be necessary to know the precise distribution. The establishment of desirable time trajectories for some average particle size should be adequate to ensure that the specifications of the final latex product can be attained. A technique for solving directly for the moments of the unknown PSD can be developed through the method of moments (Kiparissides et al. (1980)), where one approximates K in equation (3.9) with a polynomial, whose coefficients and order are then estimated at given wavelengths from measured turbidity data.

An alternative approach to the interpretation of turbidity spectra and to relating turbidity measurements to reactor states is to use strictly empirical regression models. In other words, rather than building on the theoretical relationship of equation (3.9), one can develop empirical regression models for a particular system which will enable one to predict (or at least gain some information about) particle size at different times from measured turbidity curves.

3.3.1 Experimental

A Bauch and Lomb Spectronic-20 spectrophotometer with a bandwidth of 20 nm and with a cell length of 1.165 cm, operating from 380 to 580 nm (and occasionally, a Hewlett-Packard UV-Vis 8450A, with a cell length of 1 cm and a bandwidth of 2 nm) were employed for turbidity measurements. More details concerning the experimental part can be found in Kourti et al. (1984, 1985).

3.4 Particle Size Determination: Hydrodynamic and Size Exclusion Chromatography of Particle Suspensions

3.4.1 General

The chromatographic separation of particle suspensions using packed beds has attracted considerable attention in recent years. It has the potential to provide accurate measurement of particle size and size distribution for spherical particles in the submicron range. There are two complementary approaches to the use of chromatography to separate particle suspensions according to size. Size exclusion chromatography (SEC) utilizes porous packing and relies mainly on steric exclusion from the pores of the packing. Hydrodynamic chromatography (HDC) utilizes non-porous packing and relies mainly on the velocity profile in the interstitial regions for size separation. In this section, the developments in the understanding of these processes are critically examined and shortcomings of present theory are pointed out. Signal detection and chromatogram interpretation methods are reviewed.

3.4.2 Introduction

For over a decade, chromatographic methods using packed beds have been successfully used for the separation according to size of colloidal dispersions. Though vast strides have been made in the understanding of the separation process, some basic problems still remain pertaining particularly to the holdup of colloid particles in the packed beds and the excessive broadening of colloid peaks (axial dispersion). While earlier research was mainly qualitative, adequate theory now exists to enable quantitative particle size measurement. A number of applications have been reported which demonstrate the considerable ease, rapidity and reliability of chromatographic techniques. These applications include detection of particle agglomeration and swelling effects (Small (1974) and Small et al. (1976)), measurement of particle growth kinetics (Small (1974), Singh and Hamielec (1978)

and Kiparissides et al. (1980)), calculation of particle size distribution (McGowan and Langhorst (1982)), etc.

In this section, we critically review the theoretical and experimental developments concerning colloidal separations in packed columns. New insight is provided and new ideas are suggested for future research which will help to resolve present problems.

3.4.3 Review of Experimental Investigations

Chromatography has until recently been concerned exclusively with the separation of matter at the molecular level. One result of this restriction to the molecular domain was that, from a practical point of view, chromatographic methods invariably dealt with species in solution. Recently, however, chromatographic separations have been reported where the materials resolved were in suspension rather than in solution. Four major areas of particle chromatography have evolved; non-porous packed systems (HDC), porous packed systems (SEC), capillary chromatography (CPG) (Noel et al. (1978)) and field-flow fractionation (FFF) (Giddings and Myers (1978) and Giddings et al. (1978)). Here, we will be dealing with the first two.

Hydrodynamic chromatography (HDC) is a technique for separating small particles by flow through a packed bed of non-porous particles. This technique was invented by Small (1975). Similar developments using porous beds appeared through an independent study by Krebs and Wunderlich (1971). Studies on HDC have since been actively pursued by Stoisits et al. (1976), McHugh et al. (1976), Silebi and McHugh (1978, 1979), Nagy and co-workers (1979, 1981a, 1981b, 1981c) and McGowan and Langhorst (1982), whose major contribution is the development of a theory to explain colloid migration and then the application of this theoretical background to practical cases.

The object of using porous packing in size exclusion chromatography has been to improve resolution over the non-porous HDC system by superimposing a steric exclusion effect on the flow separation. Particles smaller than the pore diameter can diffuse into the pores giving a second and more efficient mechanism of retardation and size separation.

Of course, there are relative advantages and disadvantages and the choice between HDC and SEC always depends on the physical system and the final objectives of the researcher. We will now discuss briefly the experimental developments in HDC and SEC. To keep generality as much as possible, the principal results of these investigations are summarized at the end of the discussion.

(i) Hydrodynamic chromatography:

When colloidal materials are carried in suspension through non-porous packed beds, it has been observed (Small (1974), Small et al. (1976) and Small (1977)) that the rate of transport of the colloidal particles depends on such factors as the size of the colloid, the size of the particulate material that constitutes the packed column and the flow rate and ionic composition of the eluant. The rate of migration (transport) of a colloid may be conveniently expressed by a dimensionless quantity, the R_F number, where:

$$R_F = \frac{\text{rate of transport of colloid through the bed}}{\text{rate of transport of the eluant}} \tag{3.15}$$

R_F gives the rate of migration of a colloid peak relative to a marker species.

In general, particle transport may be governed by one or a combination of the following effects: the hydrodynamic effect, the ionic effect and the Van der Waals effect (Small (1974) and Small et al. (1976)). Figure 3-2 shows data from Small (1974) on the rate of transport of polystyrene latexes through ion exchange beds of different diameter $\overline{D}$ (packing diameter). The fact that R_F clearly increases with increasing particle diameter of the latex, D, provides the basis for a chromatographic size separation. As the packing diameter is

reduced, R_F increases. Furthermore, the slope of the R_F versus D curve increases as the size of the packing is reduced, thereby resulting in improved resolution of different particle sizes. Most significantly, R_F is always greater than unity or in other words, the latex particles move more rapidly through the bed than either the carrier fluid or low molecular weight soluble species.

The dependence of R_F on the ionic strength of the eluant (Small (1974)) is shown in Figure 3-3. Depending on the ionic strength, the colloidal forces can either enhance or hinder the average velocity of the particle. Decreasing the ionic strength, increases the volume of the relatively slow moving fluid in the interstitial regions from which particles are effectively excluded. Obviously, larger particles are excluded to a greater extent. Consequently, the mean velocity of the particle exceeds that of the fluid; the factor increases with the ratio of particle size to packing diameter. At high ionic strength, Van der Waals forces cause the larger particles to spend a greater fraction of their time in the sluggish interstitial regions, so that the R_F dependence on particle size may reverse.

Two approaches have been taken to modelling the role of the colloidal forces in HDC. The capillary model (Small (1974), Stoisits et al. (1976), McHugh et al. (1976), Silebi and McHugh (1978) and Prieve and Hoysan (1978)) considers the interstitial space as a system of interconnecting parallel capillaries of equal size. In the second approach (Buffham (1978)), the speed of the chromatographic transients are calculated from the behaviour of a colloidal suspension in equilibrium in the vicinity of a plane interface. Expressed in this form, the theory is independent of the geometry of the particulate material that constitutes the HDC column. The capillary model approach, however, tends to be more universally accepted.

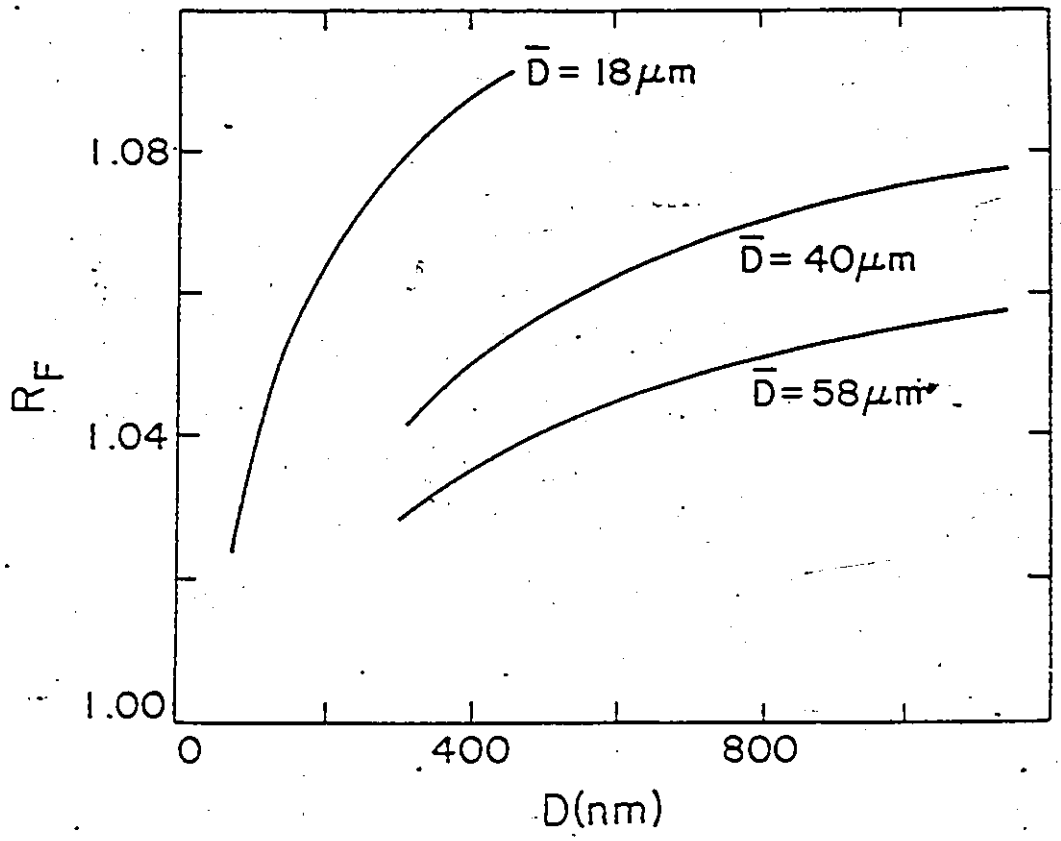

Figure (3-2). Dependence of R_F on Latex Particle (D) and Packing Diameter ($\bar{D}$)

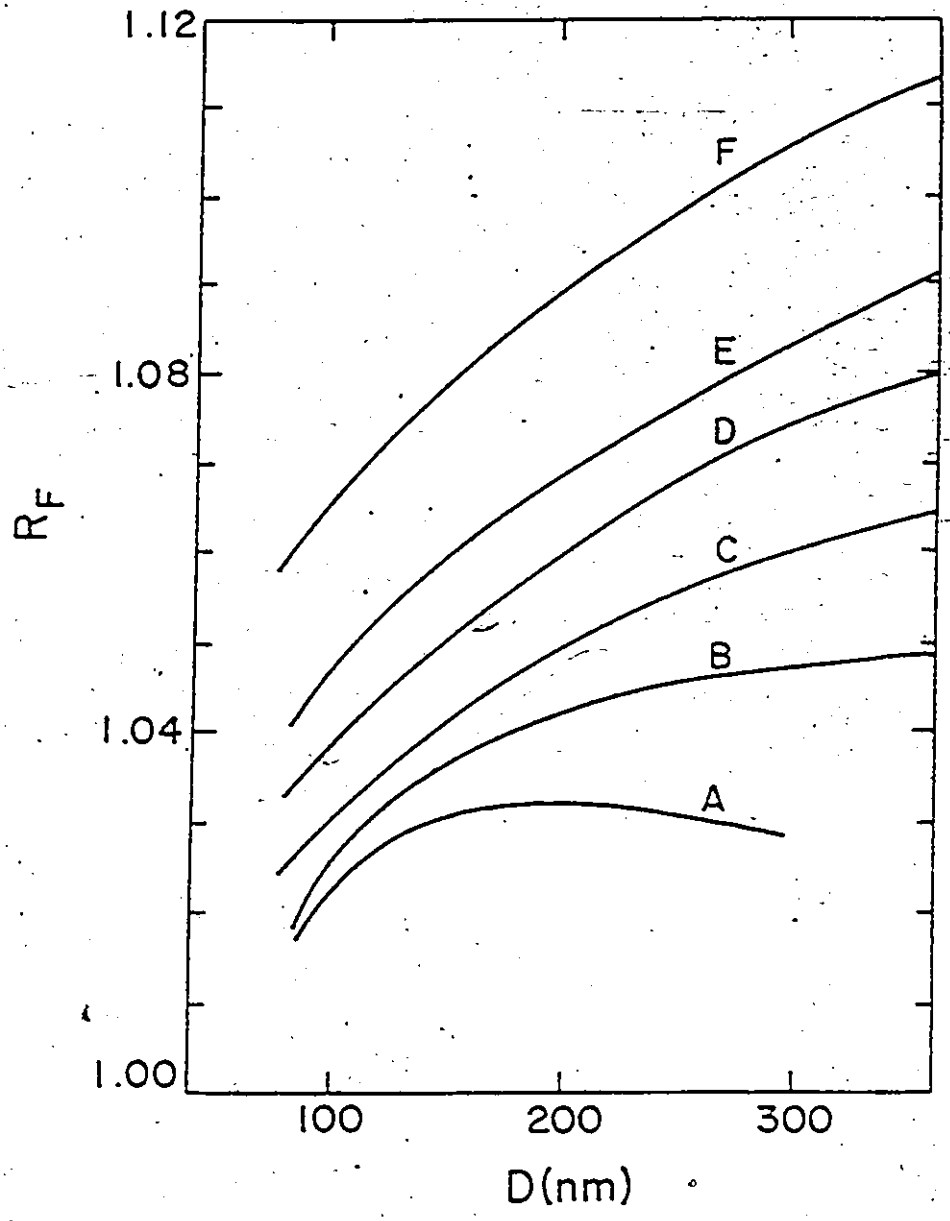

Figure (3-3). Effect of Ionic Strength of the Eluant on the R_F of Polystyrene Latexes (Eluant Concentrations in gmoles of NaCl per liter: A, 1.76×10^{-1}; B, 9×10^{-2}; C, 2.96×10^{-2}; D, 4.6×10^{-3}; E, 1.7×10^{-3}; F, 4.25×10^{-4})

The experimental observations of Small (1974) were subsequently confirmed and further extended by McHugh et al. (1976) and Nagy (1979). Recently, Nagy and co-workers (1981a, 1981b) reported a method for improving signal resolution in latex particle size analysis by HDC. Then, in a companion article (Nagy et al. (1981c)), they presented a comparison of the column resolution characteristics of porous and non-porous packing systems. More recently, Roof et al. (1980) and McGowan and Langhorst (1982) reported on an improved technique for the practice of HDC, which utilizes columns of higher efficiency and resolving power, thereby reducing the analysis time from 1.5 hours to 6 minutes. The integrated, computerized HDC that they described calculates the actual particle size distribution of the sample from its chromatogram from molecular size to greater than 1 μm in an additional 3 to 5 minutes. Several examples and experimental applications of their improved technique were discussed concerning HDC size distribution of a butyl acrylate/butadiene latex and a polybutadiene latex reacted with methyl methacrylate.

(ii) Size exclusion chromatography:

Krebs and Wunderlich (1971) were the first to report a separation of polymethyl methacrylate and polystyrene latexes using silica gel having very large pores (500 to 50,000 Å). This was followed by the work of Gaylor and James (1975) who fractionated polymeric latexes and inorganic colloidal silica, using columns packed with porous glass and water compatible polymeric porous gels. Coll and co-workers (1975, 1980) experimenting with porous glass packing (CPG, 500 to 3,000 Å pore size), found it necessary to add electrolyte as well as surfactant to the aqueous eluant. In the absence of electrolyte, the colloids could not sample the pore volume. Peak broadening was observed to be more extensive than in SEC of polymer molecules. They also observed that in SEC there is no limit as to how small the particle to be separated can be. The upper limit is a result of a greatly reduced diffusion

coefficient for large particles and is probably about 4,000 Å. On the other hand, there appears to be a practical lower limit for HDC (Mori et al. (1974)). Singh and Hamielec (1978), Hamielec and Singh (1978) and Singh (1977) presented the first comprehensive theoretical and experimental investigation of SEC. Using porous glass and silica packing (100 to 30,000 Å pore size), they established at low ionic strength the universality of the particle diameter-retention volume calibration curve. The slope of the calibration curve was essentially independent of the eluant flow rate; however, it became smaller (corresponding to a better resolution) with a reduction in packing size. The effects of the mobile phase flow rate and latex particle size on peak variance are shown in Table 3-1. Analytical expressions were derived to correct measured diameter averages for imperfect resolution. They concluded that SEC is sufficiently rapid for the off-line monitoring of latex particle growth in emulsion polymerization. With some modification it could be used in an on-line mode as a sensor for latex reactor control. However, the present state of SEC does require the development of a proper method for the complete extraction of a PSD from a chromatograph peak profile.

TABLE 3-1

Peak Broadening Data for Polystyrene Latexes Measured by Hamielec and Singh (1978)

Eluant Flow rate (mℓ/min)	Chromatogram Variance (mℓ²) PS 1000 Å	PS 2340 Å	PS 3120 Å
0.94	23.09	20.66	19.39
2.58	29.75	28.69	27.88
7.50	34.47	32.89	29.34

Nagy (1979) and Nagy and co-workers (1980, 1981c) investigated the chromatography of polystyrene latexes using porous glass packing materials (CPG, 500 to 10,000 Å and Fractosil, 25,000 Å pore size). In a distinct departure from previous practice, only (anionic) emulsifier was added to the aqueous eluant, resulting in significantly reduced material loss within the packed bed.

Johnston et al. (1980) reported on the feasibility of chromatographing polystyrene latexes using porous CPG columns (100 and 3,000 Å pore size). A reduction in packing size caused a small increase in R_F, but it significantly increased sample loss. In general, the peak variance increased with particle size, attained a maximum and then started to decrease, analogous to the behaviour of polymer molecules (Table 3–1 gives this decreasing trend). An attempt was made to correlate the statistical properties of the chromatograms of narrow distribution latexes with their mean retention volumes. Such an attempt is valid, provided that the latexes are sufficiently narrow to permit equating their spreading functions with the corresponding measured chromatograms. This condition was not fulfilled, however, for the Dow latexes used by Johnston et al. (1980), as it was easily demonstrated theoretically (Husain, 1980)).

Husain (1980) and Husain et al. (1980) also examined the chromatography of polystyrene latexes using porous CPG columns (1,000, 2,000 and 3,000 Å pore sizes). They advocated the merits of calibrating columns individually to weed out those with inadequate peak resolution and significant particle holdup. Common with previous observations, the extent of skewing in the chromatograms of narrow distribution latexes was observed to increase with particle size.

Finally, Kirkland (1979) investigated the properties of small porous silica microspheres (less than 10 μm compared with approximately 35 μm CPG packing size, pore size less than 75 nm) and superficially porous particles (solid core, porous crust, packing size less than

25 μm) for characterizing inorganic silica sols in the range of 1 to 50 nm. Columns with both types of packing material exhibited high resolution due to the rapid equilibration of slowly diffusing colloids with the pores. The effect of flow rate on peak broadening and the role of ionic strength in colloid separation were observed to be similar to those from earlier studies.

3.4.4 Summary of Main Observations

A brief summary of the main results of the above investigations is now given under three classifications, namely peak separation, peak broadening and material loss:

(i) Peak separation:

1. The particle diameter-retention volume calibration curve, in general, is composed of two linear segments: a segment at low retention volumes beyond the exclusion limit of the porous packing corresponds to HDC size separation, while, a segment at high retention volumes corresponds to SEC size separation.
2. The calibration curve is insensitive to flow rate variations.
3. Increasing the ionic strength of the aqueous eluant causes a shift in the calibration curve to high retention volumes due to increased accessibility of the column voids. At low ionic strength, a universal calibration is obtained.
4. Reducing the packing size improves peak separation.
5. SEC is not limited by a minimum particle size. However, the effectiveness of separation in HDC decreases as the ratio of particle to capillary diameter approaches zero.

(ii) Peak broadening:

1. In general with SEC the peak variance increases with colloid size, reaches a maximum and then starts to decrease as the exclusion limit of the porous column is approached. In HDC, it decreases with increasing particle size.
2. An increase in flow rate causes increased peak broadening in SEC. In HDC, the effect is not known.
3. In SEC, dispersion increases at higher ionic strength due to increased pore permeability. A similar effect may be expected in HDC; however, no experimental data have been reported.
4. The chromatograms of narrow distribution particle standards are generally skewed.
5. A well designed packing can significantly reduce dispersion.

(iii) Material loss:

1. Increasing the electrolyte concentration of the eluant decreases sample recovery. However, if the ionic strength is adjusted by addition of an ionic emulsifier (within limits), material loss is reduced.
2. Sample loss increases with colloid size.
3. Reduction in the size of the packing, enhances material loss.

While factors governing peak separation are fairly well understood, those that affect peak broadening and particularly sample recovery are not. A systematic study to determine the role of colloid composition, packing type, pore size, operating temperature etc. is required in order to offer a better understanding of these phenomena.

3.4.5 Detection of Colloidal Particles

Light transmission has been a standard method for the measurement of size of colloidal spherical particles for many years. The fundamental theory has been developed by Mie. Heller and co-workers (1957), Wallach and Heller (1961) and Stevenson et al. (1961) outlined the theory which gives size distribution curves in heterodisperse systems of non-absorbing colloidal spheres from turbidity spectra. The assumption was made that the unknown PSD followed a log normal distribution, a distributional form commonly encountered in latex systems.

Two of the most commonly used modes of colloidal particle detection, namely turbidimetric and differential refractometry detection, are now briefly examined.

(i) Turbidimetric detection:

The turbidity for very small particles which behave as Rayleigh scatterers is proportional to the sixth power of the particle diameter. For larger particles obeying Mie scattering theory, the corresponding dependence is lower. As a consequence of the above, the small particle signal is comparatively weak, though it can be amplified by using shorter wavelengths. However, to obtain particle size distributions, the relative signal is of greater importance than the absolute signal. Calculations by Silebi and McHugh (1979) indicate that a change of wavelength (or refractive index) has a small influence on the relative signal for non-absorbing particles. However, the relative signal is improved for absorbing particles due to a significant enhancement of the extinction coefficient of the smaller particles. These theoretical observations were confirmed by Nagy (1979) and Nagy et al. (1980) who chromatographed mixtures of polystyrene latexes at 220 and 254 nm (controversy exists as to whether particles absorb at 254 nm; at 220 nm, however, strong absorption occurs). One-of

Nagy's (1979) results, shown in Figure 3–4, demonstrates the dramatic improvement in the 88 nm peak measured at a wavelength of 220 nm compared to that at 254 nm.

As Heller and Tabibian (1957) indicated, appreciable error may result if instruments which are perfectly suitable for ordinary absorption measurements are used for turbidity measurements without proper modifications and precautions. According to them, there are three main sources of error in turbidity measurements: (1) interference of laterally scattered light, (2) the corona effect, and (3) the effect of the solid angle. While such errors were believed to be negligible by earlier workers (Silebi and McHugh (1979)), their existence was unequivocally demonstrated by Husain and co-workers in a series of papers (1979, 1980, 1981). They compared the detector response to a suspension of polystyrene spheres with the response to a solution of sodium dichromate. Furthermore, they showed that impurities (such as residual styrene monomer in polystyrene particles) and additives (such as emulsifier) may cause the measured extinction coefficient to differ from theoretical calculations based on Mie theory. The discrepancy may theoretically be accounted for by employing an effective imaginary refractive index ratio (colloid to medium) (Nagy (1979), Nagy et al. (1980)).

Maron et al. (1963) applied turbidimetric techniques to measure the size distribution of polydisperse polybutadiene-styrene latexes. Gledhill (1961) described a method for constructing a graphical calibration grid for a system of known optical constants and known distributional form, from which the weight mean diameter and standard deviation of the distribution corresponding to observed turbidity measurements could be read directly. However, as Maxim et al. (1969) indicated in their publication, the turbidity spectra analysis, though very attractive because of the simplicity of the experimental technique, should not be used alone for particle size analysis. This was further discussed in Kiparissides et al. (1980). Recently, Nagy et al. (1981b) reported a method for improving signal resolution in latex

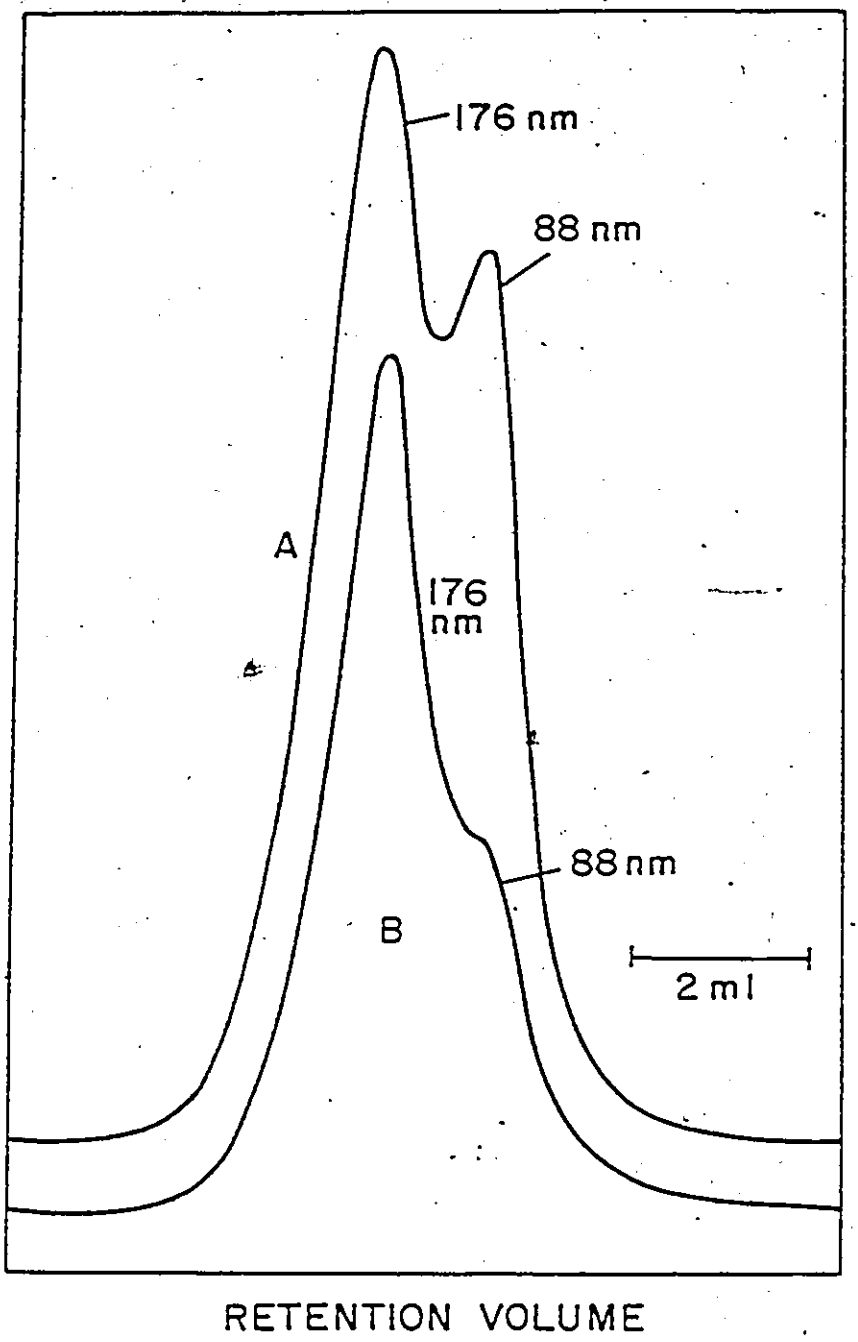

Figure (3-4). HDC Separation of a Bimodal Mixture of 88 nm and 176 nm Polystyrene Latexes. (A, Response at 200 nm; B, Response at 254 nm)

particle size analysis and data for the specific extinction coefficient for polystyrene indicates that improvement can be obtained for the small particle end of broad size distributions by using turbidity detection at wavelengths less than 254 nm.

(ii) Differential refractometry detection:

Zimm and Dandliker (1954) derived a general refractive index expression based on the Mie theory. Their expression for the dispersion refractive index, n_s, is given by:

$$\frac{dn_s}{dc} = \frac{3n_m}{2a^3\rho_p} \mathrm{Re}\left[\sum_{n=1}^{\infty} \frac{2n+1}{2n(n+1)}(a_n - b_n)\right], \qquad (3.16)$$

where c is the weight concentration in gr/cm^3, ρ_p is the particle density, a is a dimensionless size parameter ($a = \pi D/\lambda$, where D and λ are respectively the particle diameter and the wavelength in the medium), n_m and n_s are the refractive indices of the medium and the dispersion, respectively, and a_n and b_n are functions of a and m (m is the refractive index ratio of particle to medium). The above equation (3.16) does not contain the restriction that a be small and allows calculation of the effect of light scattering on the refractive index of a colloidal dispersion. In the limit, as parameter a goes to zero, equation (3.16) reduces to:

$$\frac{dn_s}{dc} = \frac{3n_m}{2\rho_p}\frac{(m^2-1)}{(m^2+2)}, \qquad (3.17)$$

a result derivable from Heller's (1965) equation. In accordance with equations (3.16) and (3.17), dn_s/dc is expected to be independent of c and at small values of a, independent of a as well.

Nakagaki and Heller (1956) confirmed the validity of equation (3.16) for particle diameters as large as 500 nm. Measurements by Silebi and McHugh (1979) showed a surprising agreement of measured data with equation (3.17) for polystyrene latexes as large as 350 nm. Both sets of measurements were made with polystyrene at a wavelength of 546.1 nm. Subsequent data measured by Nagy (1979) in the same laboratory indicated that dn_s/dc

reversed in sign with increasing particle size; the implication, therefore, is that the signal is null for some intermediate particle size. Coll and Fague (1980) observed that dn_s/dc was independent of c for a given latex, though its value increased linearly with particle diameter. Neither Nagy (1979) nor Coll and Fague (1980) were at the time able to explain their results satisfactorily. Interpretation of their data became even more complicated due to the use of a broad wavelength source.

Husain's (1980) opinion is that the above seemingly conflicting data is in fact consistent with the Zimm and Dandliker (1954) equation. Calculations by Zimm and Dandliker (1954) and Nakagaki and Heller (1956) indicate that, depending on the values of m and a, dn_s/dc may either increase with particle size or decrease and eventually change sign.

Differential refractometry shows a less dramatic dependence on particle size (third order) than turbidimetry of non-absorbing particles (sixth order). This advantage of differential refractometry is, however, counterbalanced by the requirement of a higher sample concentration compared to the amount necessary for a photometric detection due to the limited sensitivity of available differential refractometers. Of course, with the advent of more sensitive detectors this drawback will likely be overcome.

3.4.6 Theoretical Analysis of Peak Separation

The passage of an injected sample through the columns and detector generates an output trace on the recorder, the chromatogram. For several reasons, a chromatogram can never fully represent the distribution of colloid sizes in the injected sample. Instrumental spreading (or axial dispersion) causes elution of a single species to occur over a range of retention volumes. The chromatogram of the sample is the superposition of these distributions. When the number of species is small, one might obtain a chromatogram involving many obvious but overlapping peaks. However, with a large number of species, the peaks of

individual species are not evident; one usually obtains a unimodal chromatogram and sometimes a more complex one. Interpretation of a chromatogram must, therefore, account for this superposition and involve an evaluation of instrumental spreading and correction of the detector response to obtain the true concentrations of the component species.

While theory adequately predicts peak separation in HDC, a similar comprehensive treatment is lacking for SEC. Attempts by Nagy (1979) to predict peak separation in SEC have not been very successful. We will now briefly examine the theories proposed to explain peak separation in HDC and SEC.

(i) Hydrodynamic chromatography:

As mentioned earlier, two approaches have been taken to model HDC:

(a) The capillary model: A solute particle does not spend the same fraction of its total residence time at each radial position. If interactions between particles are negligible, the residence time distribution for the solute during a transient will be the same as in the case where the solute is continuously injected. From an analysis of the particle continuity equation in the presence of a radial force field, for the case of continuous injection, it can be shown that the radial concentration distribution is a Boltzmann one, given by:

$$C(r) \propto \exp[-\phi(r)/kT], \tag{3.18}$$

where $\phi(r)$, the particle-wall total interaction energy is given by the superposition of the repulsive potentials arising from the double layer and Born repulsive forces and the Van der Waals attractive potentials, as

$$\phi(r) = \phi_{DL} + \phi_B + \phi_{VW} \tag{3.19}$$

k in equation (3.18) is the Boltzmann constant and T the absolute temperature.

Then, the average particle velocity can be calculated by weighting the local particle velocity $v_{pz}(r)$ at a given radial position with the concentration at that position, to obtain

$$\bar{v}_p = \frac{\int_0^{R-\delta} v_{pz}(r) \exp[-\phi(r)/kT]\, r\,dr}{\int_0^{R-\delta} \exp[-\phi(r)/kT]\, r\,dr} \qquad (3.20)$$

where the upper integration limit accounts for the inability of a particle to approach the capillary wall closer than its radius, δ. $v_{pz}(r)$ is given by a modified Poiseuille equation which takes the wall effect into account.

For an ionic marker, ϕ_B and ϕ_{VW} are negligible and its average velocity, v_M, is obtained by taking the limits of the above integrals in (3.20) as the particle radius δ tends to zero. R_F is then given by definition as:

$$R_F = \bar{v}_p / \bar{v}_M \qquad (3.21)$$

(b) The equilibrium model: The corresponding expression for R_F is given by:

$$R_F = \frac{V}{A} \frac{1}{\int_0^{\infty} \exp[-\phi(h)/kT]\, dh}, \qquad (3.22)$$

where V is the volume of the mobile phase and A is the surface area of the packing. The R_F dependence on packing diameter is manifested by the presence of A.

Both models adequately predict the variation of R_F with particle diameter over a wide range of ionic strength. Unlike the capillary model, equation (3.22) predicts an increase in R_F with hydraulic radius V/A or packing diameter, contrary to the observed dependence. Therefore, the capillary model seems to be more powerful, as mentioned already.

(ii) Size exclusion chromatography:

In addition to the factors governing the separation of colloids in HDC, the use of porous packing introduces the possibility of size separation due to steric exclusion from the pores. Due to the complex flow patterns in porous packed beds, the difficulty in predicting the migration of a colloid peak is obvious. Nagy (1979) and Nagy et al. (1980) attempted to

simplify this problem by using very large pores relative to the size of the colloids being separated (they used a porous column with a mean pore size of 2.5 μm). Their analysis, therefore, assumes that all particles enter the pores and accordingly, describes one extreme of SEC where permeation by all species occurs. No electrolyte was used and the ionic strength was varied by using surfactant alone, at concentrations below and above the critical micelle concentration. The qualitative features of their data were similar to those observed in HDC, and the R_F values obtained were larger due to partial penetration of the pores by the particles.

Nagy (1979) modelled his data using a flow-through-bank model as shown in Figure 3-5. The large tubes in a given bank represent the totality of interstitial regions at the same level in the column, while, the small tubes represent the total of the pores within the packing at the same level. The spaces between the banks have zero volume and serve as a mixing region for altering particle trajectories. The probability of a particle entering a tube at the start of a bank has been assumed equal to the ratio of flow through all such tubes to the total flow rate through all tubes in the bank. The principal result of this analysis predicts that:

$$\frac{1}{R_F} = \frac{(V_{pc}/V)}{R_{F,pc}} + \frac{(V_{ic}/V)}{R_{F,ic}} , \qquad (3.23)$$

where $R_{F,ic}$ and $R_{F,pc}$, the separation factors corresponding to the interstices and pores respectively, are calculated as before. V_{pc}, V_{ic} and V represent the pore volume, interstitial volume and total void volume, respectively.

It can be shown that the result in equation (3.23) may be obtained using a simpler model, which regards the column voids as a system of parallel capillaries of the interstitial and pore type (no mixing region is considered and capillaries are continuous across the length of the column). The peak retention volume of the colloid peak, V_p, is given by:

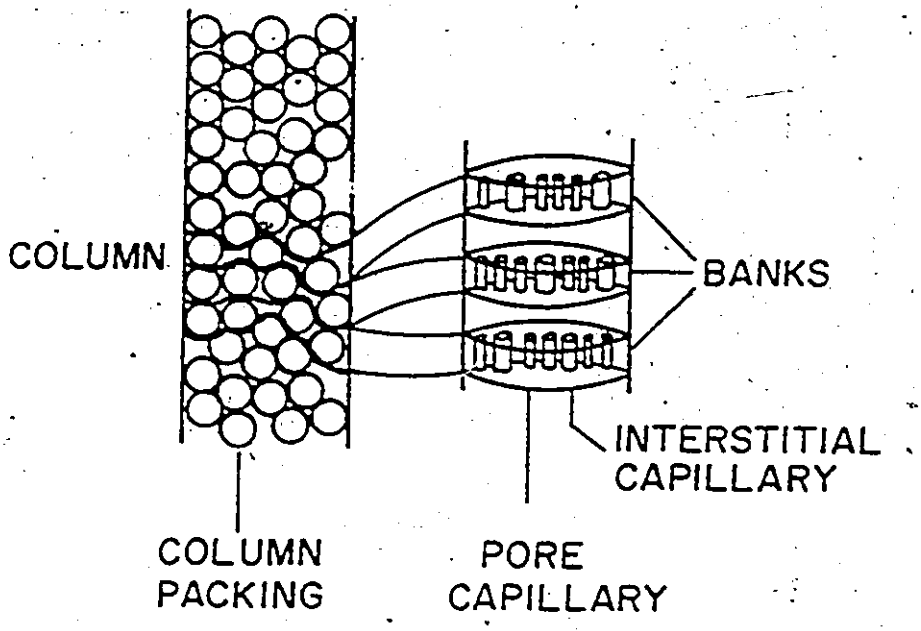

Figure (3-5). Flow-through-bank Model of a SEC Column

$$V_p = n_{pc} Q_{pc} \bar{t}_{pc} + n_{ic} Q_{ic} \bar{t}_{ic} \tag{3.24}$$

where n, Q and $\bar{t}$ denote tube number, flow rate and average residence time, respectively. It follows, therefore, that:

$$1/R_F = (n_{pc} Q_{pc} \bar{t}_{pc} + n_{ic} Q_{ic} \bar{t}_{ic})/V_m \tag{3.25}$$

where V_m, the retention volume of a marker peak, is equal to V. If the length of the column is L and the cross-sectional area of a capillary A, then:

$$\begin{aligned} 1/R_F &= L/V_m [n_{pc} Q_{pc}/(\bar{v}_p)_{pc} + n_{ic} Q_{ic}/(\bar{v}_p)_{ic}] \\ &= L/V_m [n_{pc} A_{pc} (\bar{v}_m/\bar{v}_p)_{pc} + n_{ic} A_{ic} (\bar{v}_m/\bar{v}_p)_{ic}] \\ &= (n_{pc} A_{pc} L/V_m)/R_{F,pc} + (n_{ic} A_{ic} L/V_m)/R_{F,ic} \\ &= (V_{pc}/V)/R_{F,pc} + (V_{ic}/V)/R_{F,ic} \end{aligned} \tag{3.26}$$

The derived result is identical to equation (3.23). The apparent equivalence of the two models is a direct consequence of assigning, in the bank model, the probability that a particle travels through a given tube as equal to the ratio of flow through all such tubes to the total flow rate through all tubes. Therefore, it is not surprising that calculations based on equation (3.23) agree rather poorly with experimental data since, the equivalent model (which allows no fluid intermixing) considered here, is hardly representative of the flow process in a packed column.

Nagy (1979) cites several reasons, chief among which is the slow diffusion coefficient of colloids, to justify the use of a flow model as opposed to a diffusion model. As pointed out by Small (1977), if a bank model is considered, separation by flow would seem unlikely, since very little fluid would flow through the extremely fine pores of the packing when the much less restricted pathway around the particles is available to it. It is beyond the scope of this section to consider alternate models for SEC. It has been, however, suggested (Husain (1980)) that, since the equilibrium theory for HDC is essentially independent of the complex flow goemetry, it may be possible to extend the treatment to predict colloid behaviour in SEC. Further work in this direction would undoubtedly be facilitated by a critical review

by Casassa (1972) who has examined various models proposed to explain peak migration in SEC.

3.4.7 Calculation of Particle Size Distributions

As we have mentioned before, the axial dispersion phenomenon is a serious imperfection in the chromatography of particle suspensions. The input sample W(y) is distorted as a result, so that the diameter frequency distribution calculated based on the measured response F(v) may be significantly in error.

All rigorous methods of correcting detector response for peak broadening (or axial dispersion) use the following integral equation as the basis:

$$F(v) = \int_0^\infty W(y)\, G(v,y)\, dy\,, \tag{3.27}$$

where F(v) is the detector response at retention volume v (i.e. it is related to the true chromatogram W(y) by equation (3.27)) and G(v,y) is the normalized detector response or spreading function for a particle of diameter D(y) or for a species with mean retention volume y at retention volume v. G(v,y) is often called the instrumental spreading function and is frequently considered to be uniform, i.e.

$$G(v,y) = G(v-y)\,, \tag{3.28}$$

which considerably simplifies the mathematical treatment of equation (3.27). W(y)dy is the area under the detector response due to particles of diameter D(y). W(y) is called the detector response corrected for dispersion. Equation (3.27) is a Fredholme integral equation of the first kind and has been used extensively in various science and engineering applications. When detection is turbidimetric, both F(v) and W(y) represent turbidities while, in the case of differential refractometry, they represent refractive index increments.

The response for a general detector is given by:

$$F(v) = \int_0^\infty W(v,y)\,dy\,, \tag{3.29}$$

where:

$$W(v,y) \propto N(v,y)\,D^{\gamma}(y) \tag{3.30}$$

for the Rayleigh scattering regime ($\gamma=3$ for a refractive index and $\gamma=6$ for a turbidity detector) and

$$W(v,y) \propto N(v,y)\,D^2(y)\,K(y) \tag{3.31}$$

for the Mie scattering regime, where K(y) is the extinction coefficient for particles of diameter D(y). In both (3.30) and (3.31), N(v,y) represents number of particles of diameter D(y) at retention volume v.

Comparing equations (3.27) and (3.29), it is clear that:

$$W(v,y) = W(y)\,G(v,y) \tag{3.32}$$

and

$$W(y) = \int_0^\infty W(v,y)\,dv \tag{3.33}$$

Equations (3.32) and (3.33) can be used to derive correction equations for dispersion in the detector cell itself.

Equation (3.27) may be solved both numerically and analytically. Numerically, it is solved either for G(v–y) (Husain et al. (1981a)), when F(v) and W(y) are known, or, as is usually the case, the integral equation is solved for W(y), when F(v) and G(v–y) are known, which may then be converted into a particle size distribution. In contrast, analytical solutions enable the direct calculation of the moments of the size distribution function; the PSD itself is not obtained. Both methods of solution will be discussed later in what follows.

(i) Forms of the spreading function:

(a) Uniform spreading function: In other words, its shape parameters are independent of retention volume, i.e. the shape parameters are the same for particles of

different diameter. This limiting form should be valid for samples with relatively narrow particle size distributions. For this case, equation (3.27) becomes (Hamielec and Ray (1969), Provder and Rosen (1970a)):

$$F(v) = \frac{1}{\sqrt{2\pi\sigma^2}} \int_0^\infty W(y) \exp(-(v-y)^2/2\sigma^2)\, dy \tag{3.34}$$

where σ^2, the variance of the uniform Gaussian spreading function is independent of retention volume.

(b) Non-uniform Gaussian spreading function: The integral equation (3.27) now takes the form:

$$F(v) = \int_0^\infty W(y) \frac{1}{\sqrt{2\pi\sigma^2(y)}} \exp(-(v-y)^2/2\sigma^2(y))\, dy \tag{3.35}$$

(c) General spreading function: Provder and Rosen (1970a,b) have proposed the use of a general statistical shape function to account for deviations of the spreading function from the Gaussian shape. It has the form:

$$G(x) = \phi(x) + \sum_{n=3}^{\infty} (-1)^n A_n \phi^n(x)/n! \tag{3.36}$$

where

$$\phi(x) = \frac{1}{\sqrt{2\pi\sigma^2}} \exp(-x^2/2)$$

$$x = \frac{v - y}{\sigma} \tag{3.37}$$

and $\phi^n(x)$ denotes n^{th}-order derivative. The coefficients A_n are functions of μ_n, the n^{th}-order moments about the mean retention volume, μ, of the normalized detector response for a single species.

(ii) Numerical solution of the integral equation:

Several numerical methods have been reported for the solution of the integral equation. These have been reviewed by Friis and Hamielec (1975c) and evaluated by Silebi and McHugh (1979). The main conclusion is that the method of Ishige et al. (1971) performs better than other available methods. A noteworthy undesirable feature of the method, however, is its tendency to overestimate the number of small particles in a polydispersed sample. Modifications of Ishige's algorithm failed to overcome this defect (Friis and Hamielec (1975c)). Unless a more effective numerical method is developed to solve for the corrected detector response, W(y), it is recommended that analytical methods be used in addition to the numerical method of Ishige et al. (1971) to calculate particle diameter averages. A new promising method that is numerically very "robust" has been recently suggested by Alba and Meira (1985). According to this method, Kalman Filter based techniques are adapted to solve the most general form of Tung's (1966) integral formula, i.e. when a non-uniform, non-symmetric calibration model is employed to correct chromatograms obtained in SEC from instrumental broadening errors. Through this method, the inverse smoothing of a chromatogram contaminated with measurement noise of known statistics is optimally performed by minimizing the estimation error variance.

(iii) Analytical solution of the integral equation:

Three analytical methods for solving the integral equation have been reported (Hamielec and Singh (1978), Husain et al. (1981b) and Husain et al. (1979b)). Their main features are compared in Table 3-2. It is important to realize that the solution derived for a Gaussian spreading function $G_o(v-y)$ is equally applicable to a whole family of functions of the form:

$$G(v,y) = G_o(v-y)\,\psi(y) \qquad (3.38)$$

TABLE 3-2

Comparison of the Analytical Methods for Solving the Integral Equation

		Method*		
		1	2	3
	Attributes	Hamielec and Singh (1978)	Husain et al. (1981b)	Husain et al. (1979b)
1.	Calibration curve	Linear	Nonlinear	Nonlinear
2.	Spreading function	Eqn. (3.38) or Provder and Rosen's shape function	Eqn. (3.38)	Eqn. (3.38) or Provder and Rosen's shape function
3.	Light scattering theory which may be applied	Rayleigh	Mie	Mie
4.	Chemical absorption may be present in turbidimetric detection	No	Yes	Yes
5.	Diameter averages are calculated as a function of retention volume	No	Yes	No

* The refractive index detector (dn_s/dc = constant) can be treated using all the above methods. However, Method 3 is most general.

where $\psi(y)$ is an unspecified function of y. This considerably extends the applicability of the solution for a Gaussian spreading function to an infinite set of non-Gaussian, non-uniform functions (Husain et al. (1979b)).

The first solutions of this kind were based on the use of bilateral Laplace transformations and uniform instrumental spreading functions (Hamielec and Ray (1969) and Provder and Rosen (1970a)) and they were applied to the SEC of polymer molecules. The first application to the chromatography of spherical suspensions was made by Hamielec and Singh (1978) and Husain et al. (1979b). Yau et al. (1976) obtained similar solutions for the case of a uniform spreading function and a linear molecular weight calibration curve (equivalent to a linear particle diameter-retention volume calibration curve in this context). Yau et al. (1976) focused on dispersion in the detector cell as did Hamielec (1980) and Hamielec et al. (1981) in accounting for a non- uniform Gaussian spreading function and a non-linear calibration curve.

The case of a non-uniform spreading function and a non-linear particle diameter-retention volume calibration curve has been treated by Husain and co- workers (1980, 1981). A novel method for identifying and estimating the parameters of the instrumental spreading function for column chromatography has been developed and applied to the SEC of particle suspensions. This has revealed that for SEC, the spreading function of polystyrene latex standards in the size range of 85 to 312 nm is skewed towards longer retention volumes. The Provder and Rosen (1970a,b) general spreading function gives reasonable fit to experimentally measured spreading functions for particles in the size range of 85 to 220 nm. This is clearly demonstrated in Figures 3-6, 3-7 and 3-8. In these three figures (Husain (1980)), F(v) represents the experimental chromatogram and $G(v-v_p)$ the estimated spreading function. Figure 3-9 gives the change of the variance σ^2 with particle diameter, and Figure 3-10 shows a

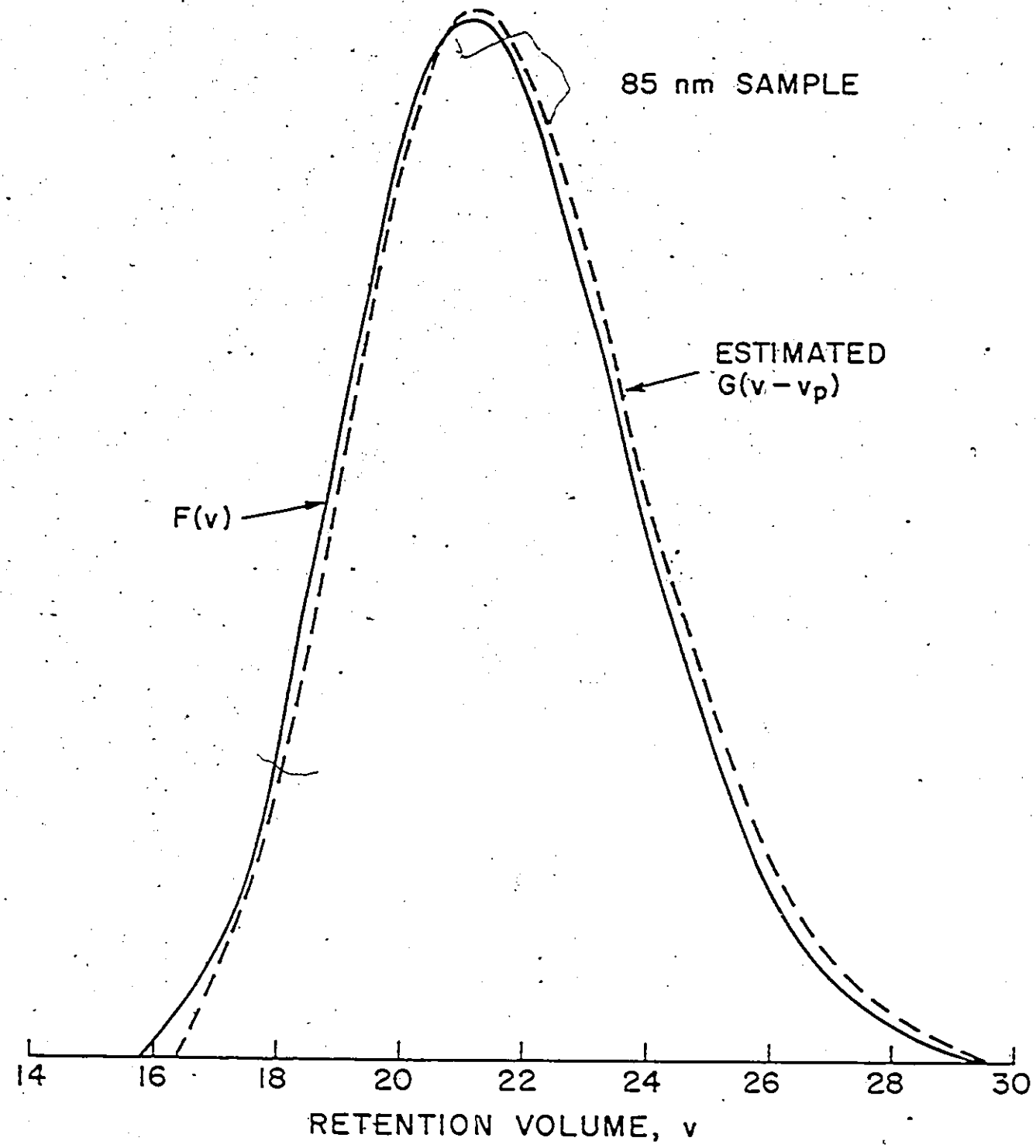

Figure (3-6). Estimation of the Spreading Function from Experimental Chromatogram (85 nm Sample)

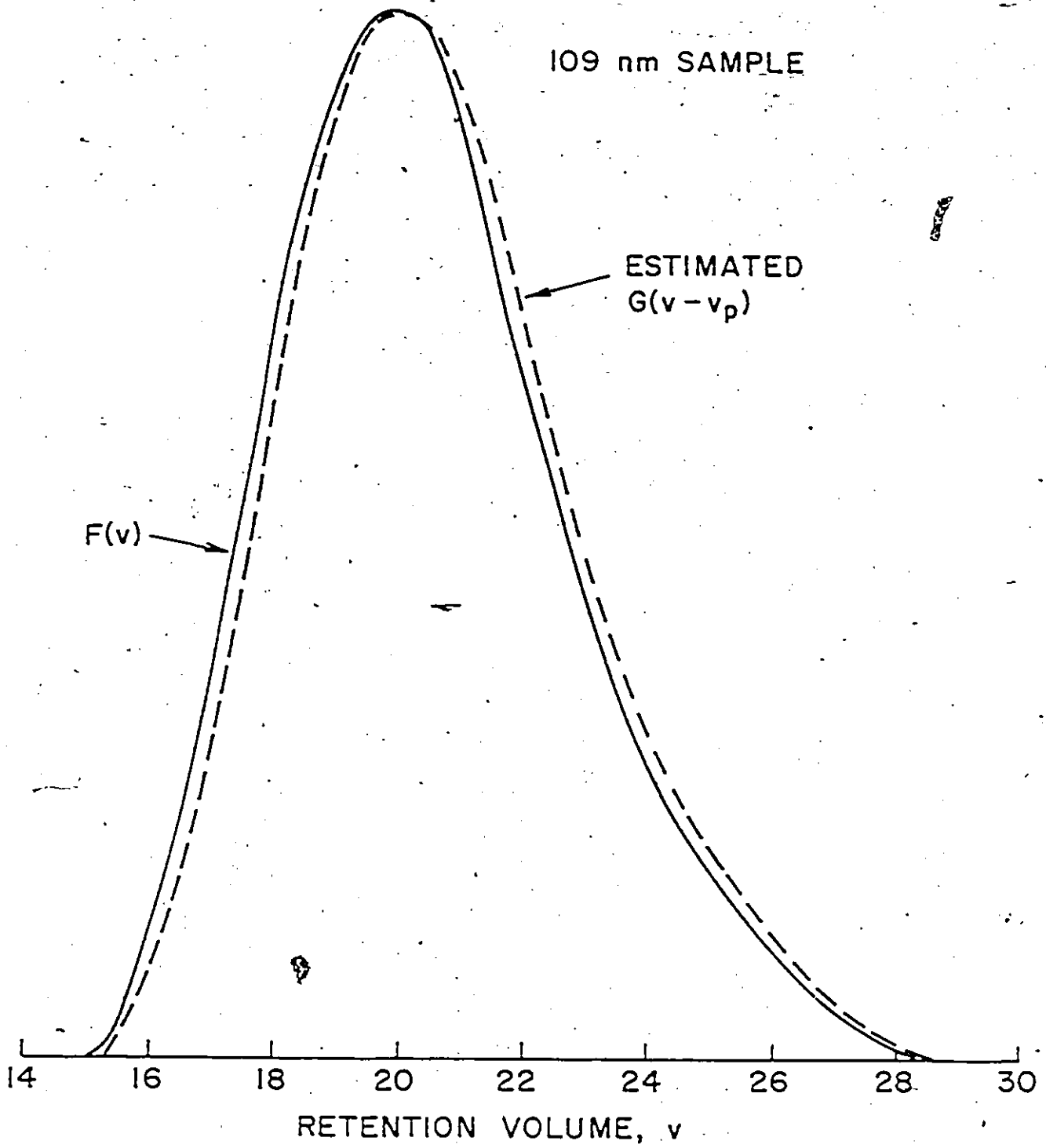

Figure (3-7). Estimation of the Spreading Function from Experimental Chromatogram (109 nm Sample)

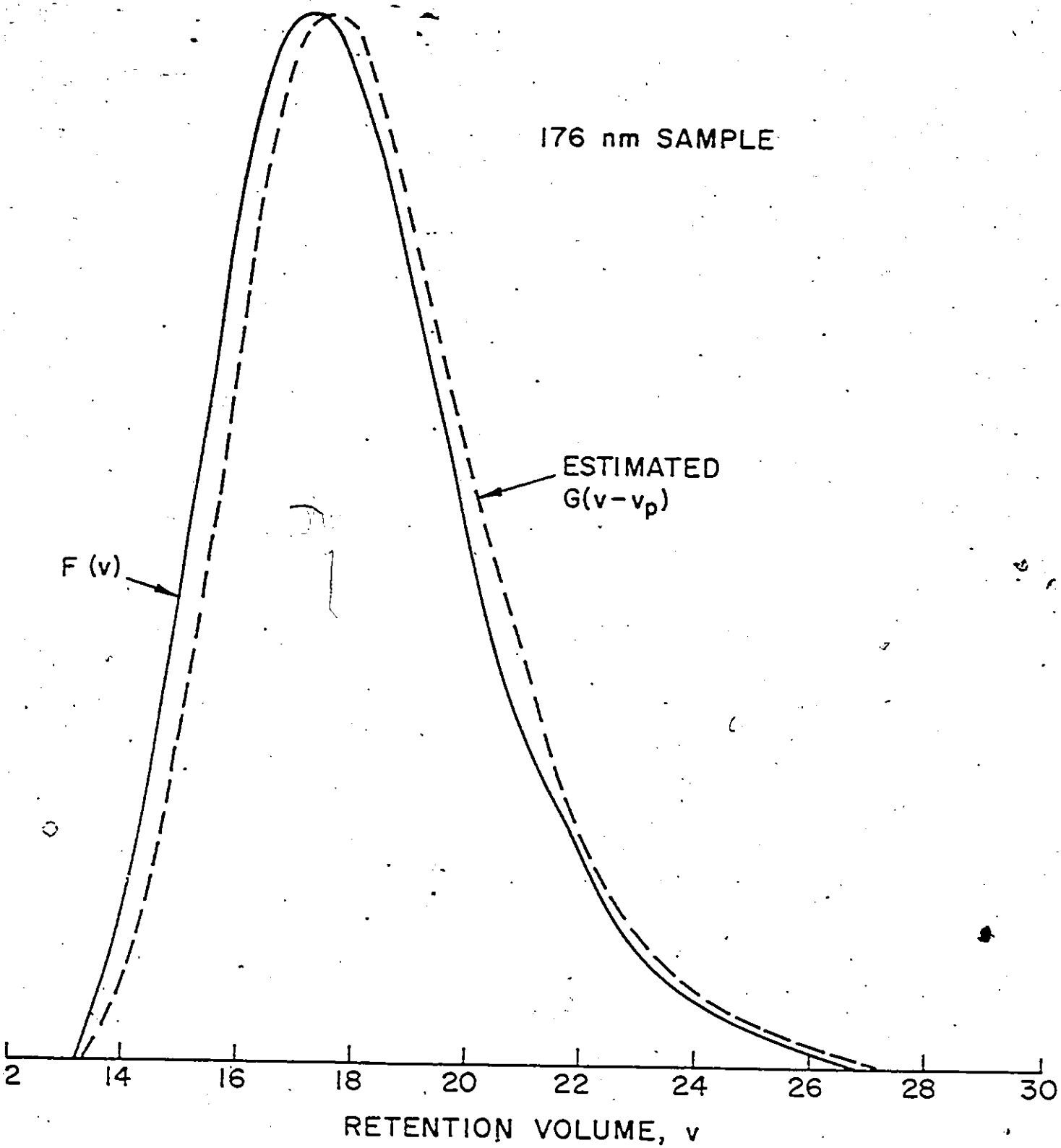

Figure (3-8). Estimation of the Spreading Function from Experimental Chromatogram (176 nm Sample)

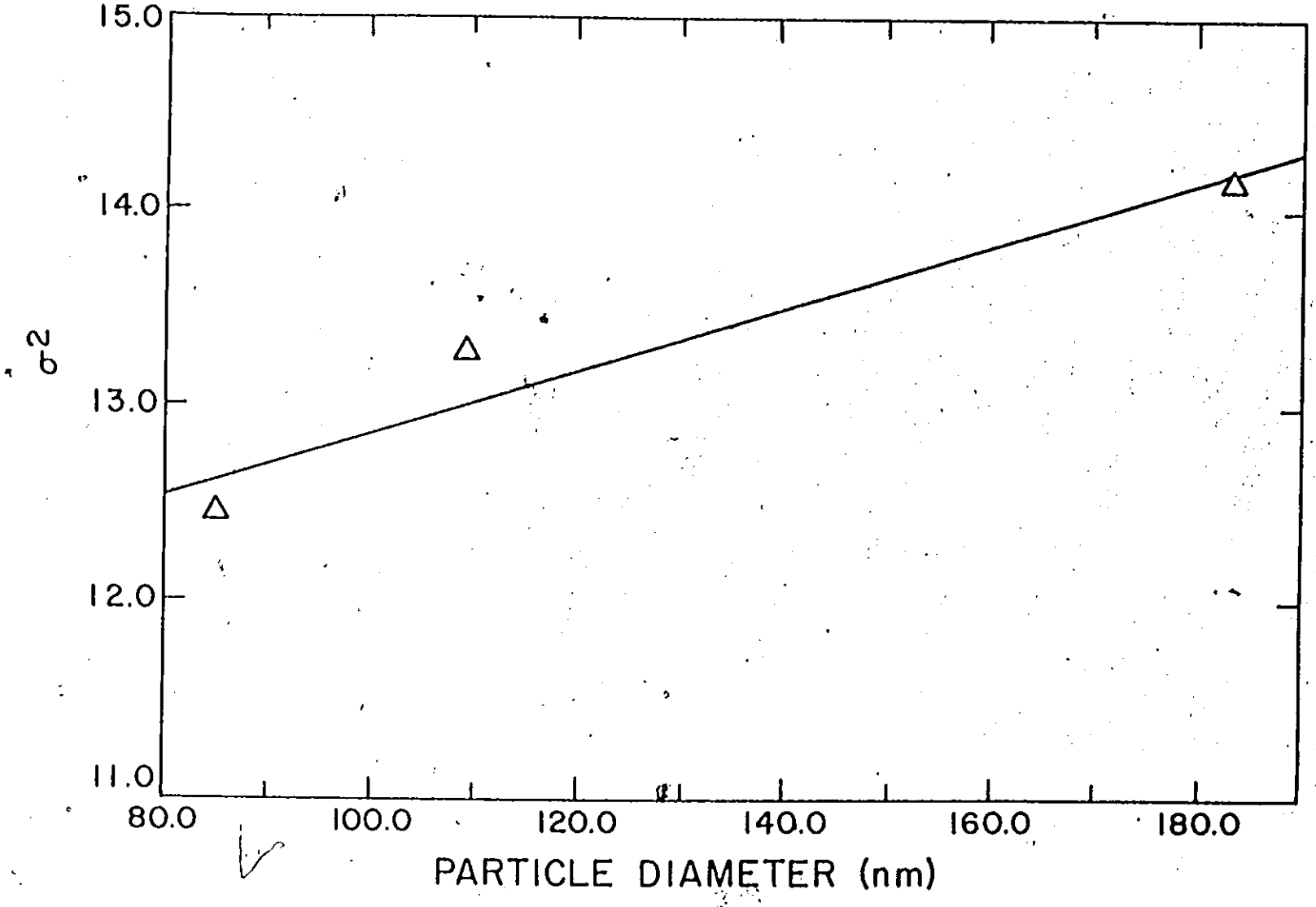

Figure (3-9). Variance σ^2 versus Particle Diameter, Equation (3.36)

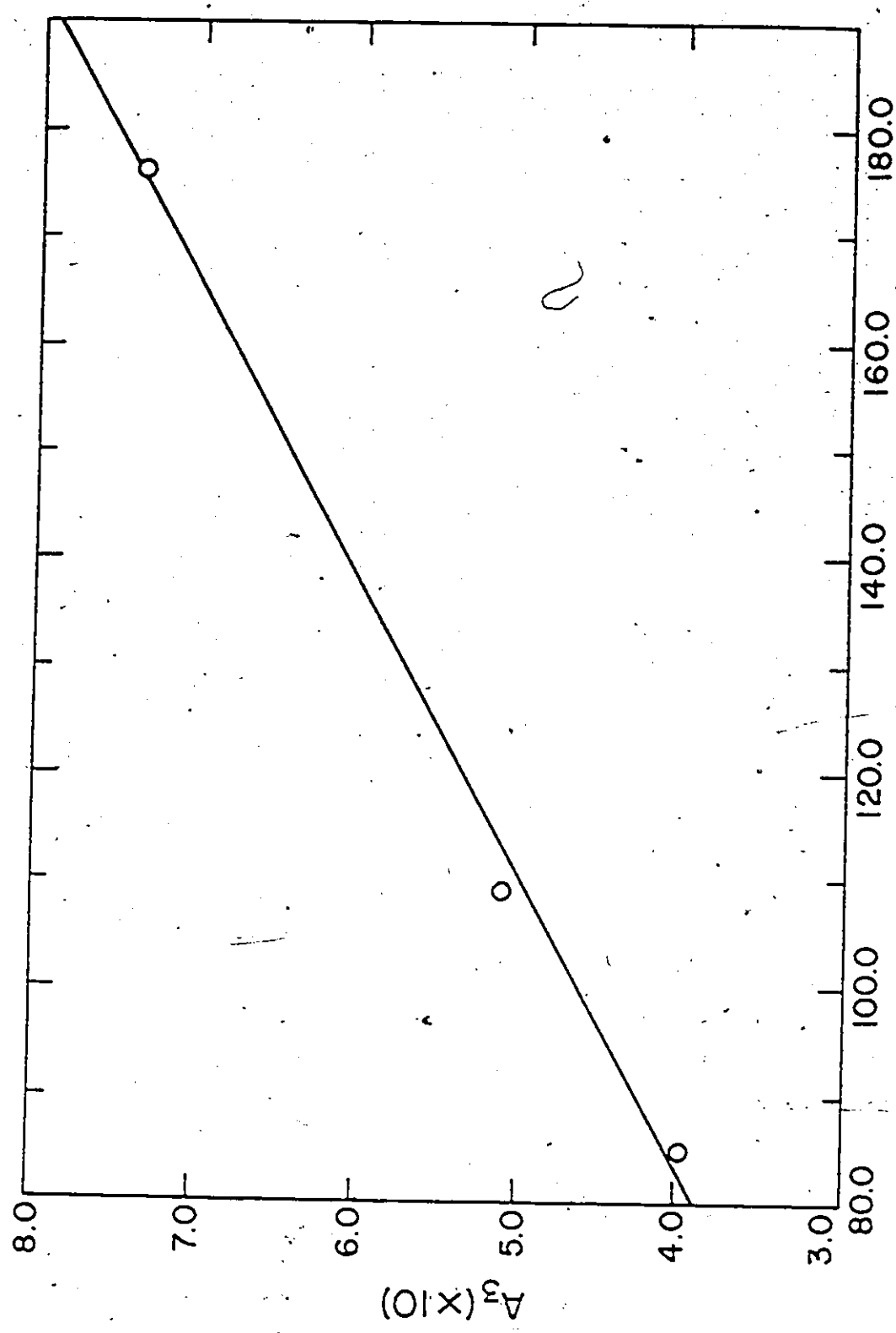

Figure (3-10). Coefficient A_3 versus Particle Diameter, Equation (3.36).

plot of the coefficient A_3 in equation (3.36) versus particle diameter, as they were used in fitting the general spreading function given by equation (3.36) to experimentally measured spreading functions. As it is easily understood from Figures 3-9 and 3-10, the change of σ^2 and A_3 with particle diameter is consistent with experimental data (Husain (1980)), which showed an increase in the skewness of the chromatograms with an increase in particle diameter of the sample. For the 312 nm standard, the fit was poor. It would be of interest to compare experimental G(v,y) with the spreading function predicted by the plug flow dispersion model. It appears that for the HDC or SEC of particles, a skewed instrumental spreading function should be used to properly account for dispersion.

(iv) Instrumental correction for dispersion:

An HDC or SEC operating with normal resolution should provide unimodal and relatively narrow frequency distributions of particle size in the detector cell across the chromatogram of a whole sample. Therefore, a detector system which can provide, say, two moments of the frequency distribution and the particle concentration of the detector cell contents should in principle provide a measure of the frequency distribution of the whole sample and this measure should be largely independent of the resolution of the chromatograph.

To date, the use of a detector system to this end has not been reported. There are, however, at least two detector systems based on turbidity spectra (Husain et al. (1979a) and Hamielec (1978)) and quasi-elastic light scattering or photon correlation spectroscopy (Chu (1970, 1974), Berne and Pecora (1976), Derderian and MacRury (1981) and Zollars (1981b)) which appear promising and seem to have the potential for this task.

(v) Fitting the plug-flow dispersion model:

When we previously discussed the different forms of the spreading function G(v,y), we have seen that a general statistical shape function can account for deviations from the Gaussian shape (Provder and Rosen (1970)). If we consider equation (3.36) again and especially the coefficients denoted by A_n, we can see that the first two coefficients are of direct statistical significance. They also represent the two most useful terms in the infinite series for applications in chromatography:

$$A_3 = \mu_3/\mu_2^{3/2} \tag{3.39}$$

$$A_4 = (\mu_4/\mu_2^2 - 3) \tag{3.40}$$

μ_2 is the variance of the distribution and is equivalent to σ^2. The coefficient A_3 provides an absolute statistical measure of skewness (when $\mu_3 = 0$, the spreading function is symmetrical about the mean retention volume μ_1 or y. When $\mu_3 > 0$, skewing is towards larger retention volumes). The coefficient A_4 provides a statistical measure of flattening or kurtosis (when $A_4 > 0$, the shape function is taller and slimmer than a Gaussian and so forth). Tung and Runyon (1969) used a simpler form to fit skewed detector responses in the SEC of polymer molecules. Silebi (1981) has recently shown that skewed instrumental spreading functions derived from the plug-flow dispersion model (Hess and Kratz (1966)) adequately fitted data for particle separations by HDC. This spreading function has the form:

$$G(v,y) = \frac{1}{2\sqrt{\pi (Pe)^{-1}(v/y)}} \exp(-(v-y)^2/4\,(Pe)^{-1}(v\,y)) \tag{3.41}$$

where (Pe) = (uL/D) is the Peclet number, u is the superficial velocity in the column, L is the length of the packed bed and D is a dispersion coefficient. The plug-flow dispersion model predicts symmetrical broadening in the packed-bed; however, when dispersion is large, the detector gives a response which is skewed towards larger retention volumes. For small dispersion, (Pe) > 100 and G(v,y) reduces to a Gaussian shape.

Efforts by the authors to use equation (3.41) to fit data for particle separations by SEC were proven unsuccessful. It seems that equation (3.41) should be used with HDC data and it is our future intention to check the validity of the plug-flow dispersion model using vinyl acetate latexes from continuous emulsion reactors.

(vi) Particle size determination:

The frequency distribution of the particle sizes is related to the number of particles eluting at volume v by the following equation:

$$f(D)\,dD = \frac{N(v)\,dv}{\int_0^\infty N(v)\,dv} \tag{3.42}$$

or, otherwise written as:

$$f(D) = \frac{N(v)}{\left(\int_0^\infty N(v)\,dv\right)\frac{dD}{dv}} \tag{3.43}$$

For a known calibration curve of the general form

$$\ell n\, D = a + bv + cv^2, \tag{3.44}$$

(dD/dv) is a known function of retention volume v. Then, considering equations (3.30) and (3.31), the frequency distribution is given by:

$$f(D) = \frac{W(v,y)}{\left(\int_0^\infty \frac{W(v,y)}{D^2(y)\,K(y)}\,dv\right) D^2(y)\,K(y)\frac{dD}{dv}} \tag{3.45}$$

or by:

$$f(D) = \frac{W(v,y)}{\left(\int_0^\infty \frac{W(v,y)}{D^Y(y)}\,dv\right) D^Y(y)\frac{dD}{dv}}, \tag{3.46}$$

respectively.

The averages of the distribution are then calculated as:

$$\overline{D}_N = \int_0^\infty D\, f(D)\, dD \tag{3.47}$$

and

$$\overline{D}_w = \frac{\int_0^\infty D^4 f(D)\, dD}{\int_0^\infty D^3 f(D)\, dD} \tag{3.48}$$

3.4.8 Experimental

The apparatus employed for particle chromatography consisted of the following basic parts: (a) pump, (b) sample injector, (c) packed columns, (d) detector and (e) recorder and chromatogram integrator. The calibration latex standards used to obtain a linear calibration curve were Dow (880 and 1260 Å) and Polysciences (570, 980 and 1500 Å) narrow size distribution polystyrene latexes. The samples to be injected were prepared by dispersing a few drops of latex in roughly 10 mℓ of carrier fluid (to eventually yield a sample concentration of 0.5 to 1% by wt.).

The solvent delivery system was a WATERS ASSOCIATES 1 - Model 6000A. A constant carrier fluid flow rate has been used throughout, equal to 2 mℓ/min. A Rheodyne six port syringe loading sample injector was employed to inject a sample volume of 10 μℓ.

A dry packed column with porous material was used for the separations according to size. The packing material employed was CPG 2000 Å, 200 to 400 mesh size. Before use, the column was equilibrated by flushing with five to six column volumes of eluant.

A turbidity detector (Beckman UV - model 1-160 with a cell length of 1 cm operating at a wavelength of 254 nm) and (in some cases) a refractive index (RI) detector (ERMA-RI-model ERC-7510 operating at 40°C) were connected in series with the column (column-turbidity detector - RI detector) to monitor particle sizes eluting from the columns.

The mobile phase (carrier fluid) was deionized water with 0.8 gr/lit Aerosol O.T, 0.8 gr/lit sodium nitrate and 0.4 gr/lit sodium azide (to prevent bacteria formation). The mobile phase was always degassed before use.

Before use, the column, the calibration line and the detectors were rechecked with monodispersed polystyrene standards, which were prepared by soap-free emulsion polymerization at 70°C (from a recipe according to Singh (1977)) and characterized by electron microscopy.

More details about the experimental part can be found in Kourti et al. (1984, 1985).

3.5 Monitoring of Emulsion Polymerization Reactors by Turbidity Spectra and Size Exclusion Chromatography

Particle number and size distribution are key properties in emulsion polymerization processes because not only do they affect polymerization rate and polymer quality, but they also determine application properties of the final latex such as stability, viscosity, film forming, etc. Efforts to manipulate these two important parameters should obviously precede any attempt to control latex reactor performance. But even prior to such efforts, one should be able to determine these two parameters as accurately as possible, thereby the need for techniques which would give an on-line measure of these two factors. Various techniques have been already developed for the determination of particle size of colloidal dispersions but are time consuming and unsuitable for on-line application. Light scattering and chromatographic sizing techniques seem to be the most promising for this purpose.

3.5.1 Latex Particle Size Determination by Turbidity Spectra

Details concerning the polymerization procedure and the experimental set- up are given in Chapter 4. Four runs from Table 4-3, which will be discussed in more detail here, are briefly summarized in Table 3-3.

TABLE 3-3
Classification of Batch Runs

Run #	Emulsifier Level	Expected Particle Diameter
BR7	low	large
BR10-BR11 (replications)	medium	medium
BRS	high	small

Specific turbidity histories are shown in Figure 3-11 for runs BR7, BR10 and BR11 and in Figure 3-12 for runs BR7 and BRS (Kourti et al. (1984)). The obtained results are as expected (see Table 3-3). Note that the degree of dilution was such that a monomer-free particle diameter was measured at such (low) wavelengths which excluded the Rayleigh regime complications.

3.5.2 Discussion of Turbidity Results

Details about the approaches that have been used to translate the specific turbidity measurements into latex particle size can be found in Kourti et al. (1984, 1985) and will not be repeated here again. Kourti et al. (1985) concluded that specific turbidity measurements can provide a weight average diameter and therefore follow the progress of the reaction reasonably well.

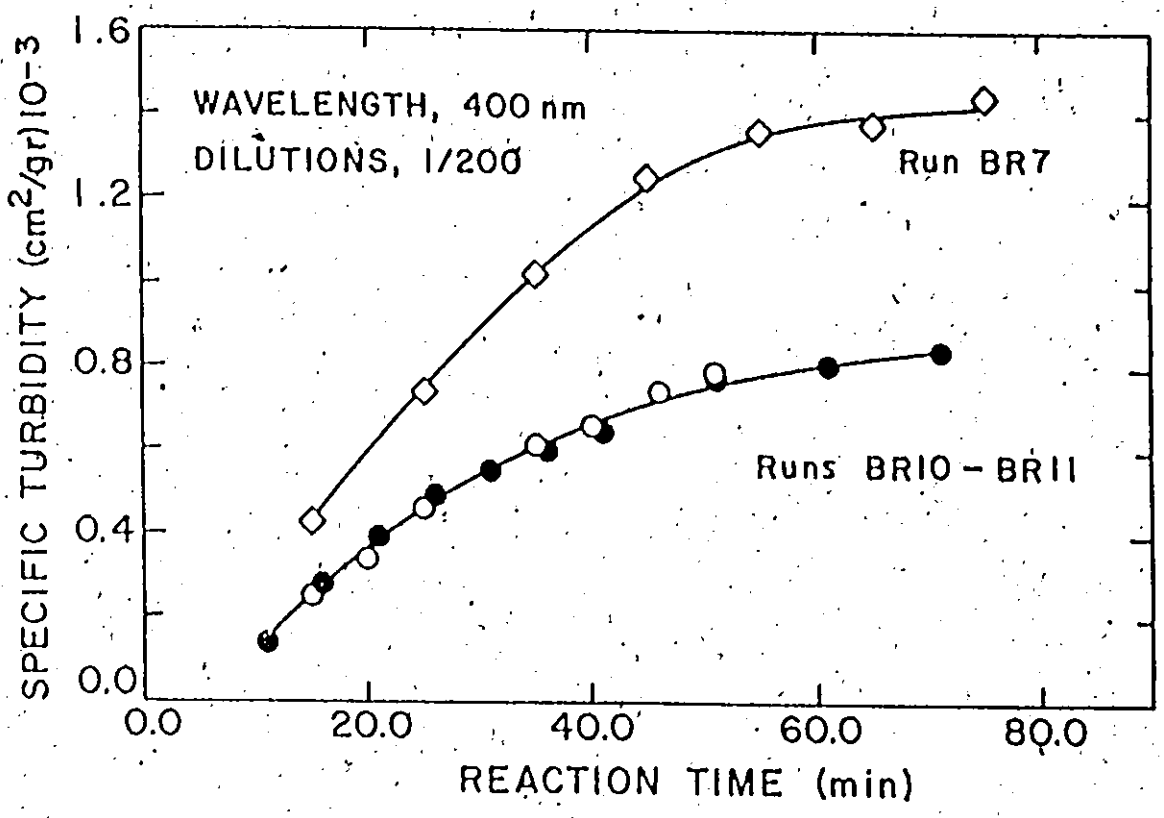

Figure (3-11). Specific Turbidity Behaviour for Runs BR7, BR10 and BR11

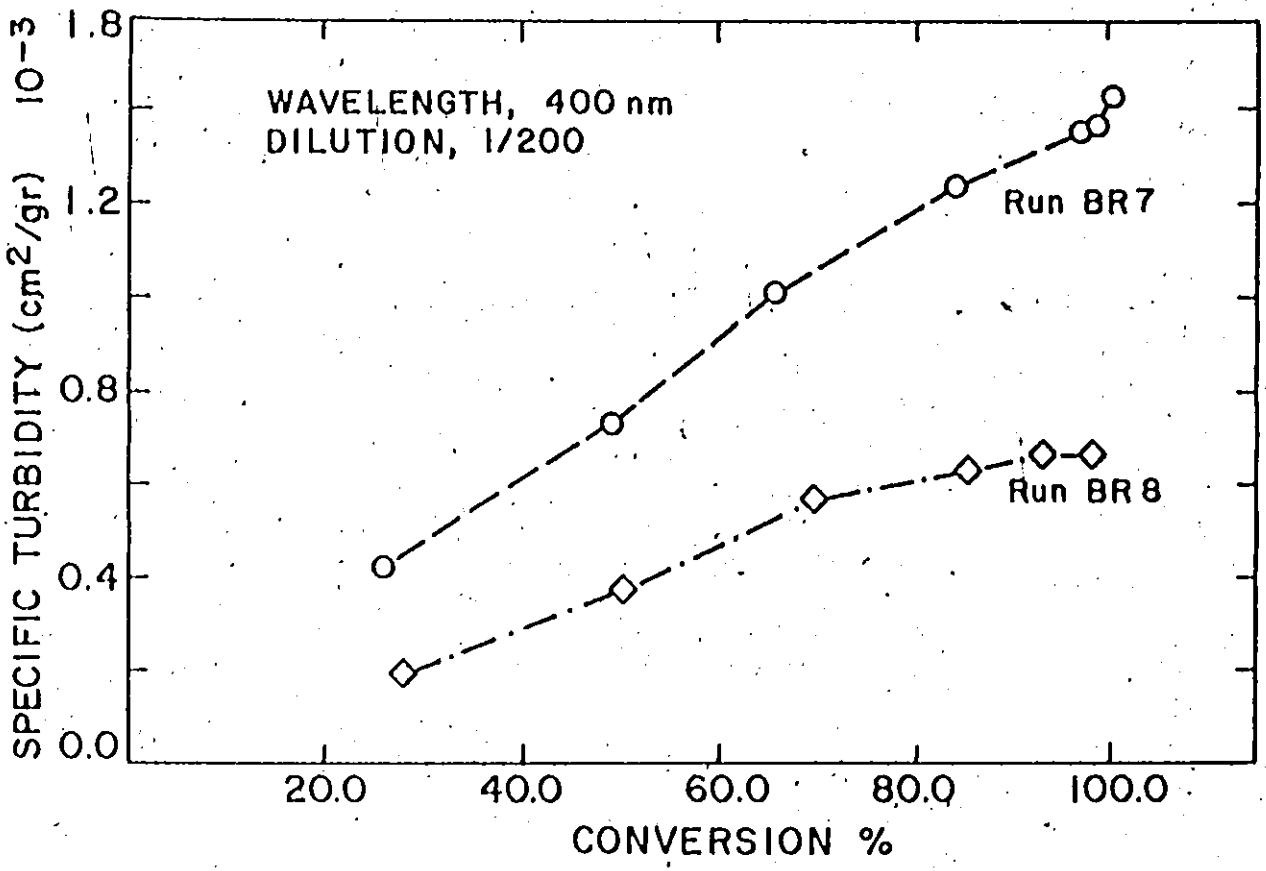

Figure (3-12). Specific Turbidity versus Conversion for Runs BR7 and BR8

3.5.3 Latex Particle Size Determination by SEC

In order to verify and check the turbidity results, the samples which were previously characterized by turbidity spectra, were also characterized by SEC. A particle size-peak retention volume calibration curve was constructed from commercially available polystyrene standards. In the final chromatographic set-up two columns in series were employed, a CPG 75 Å and a 2000 Å one. Typical chromatograms (i.e. SEC responses) can be found in Penlidis et al. (1985).

Figure 3-13 shows "peak" average diameters versus conversion for runs BR10 and BR11. The reproducibility is excellent. Note that in all experiments an increasing diameter was obtained; in other words, the sizes correspond to "almost" monomer-free particles. This was expected since the injected samples were so much diluted in the mobile phase that monomer was extracted from particles into the mobile phase.

3.5.4 Discussion of SEC Results

To correctly interpret a chromatogram one must account for instrumental spreading (peak broadening or axial dispersion), which causes elution of a single species over a range of retention volumes. This of course involves an evaluation of axial dispersion and correction of the detector response to obtain the true picture in an injected sample. Chromatograms of monodispersed samples can be used for the estimation of the instrumental spreading function.

The chromatograms of the several injected poly (VAc) samples were corrected for axial dispersion (Ishige et al. (1971), Husain et al. (1980)) and number and weight average diameters were estimated. The resulted distributions and averages showed that the latex samples were "almost" monodispersed. This was further supported by the fact that estimated

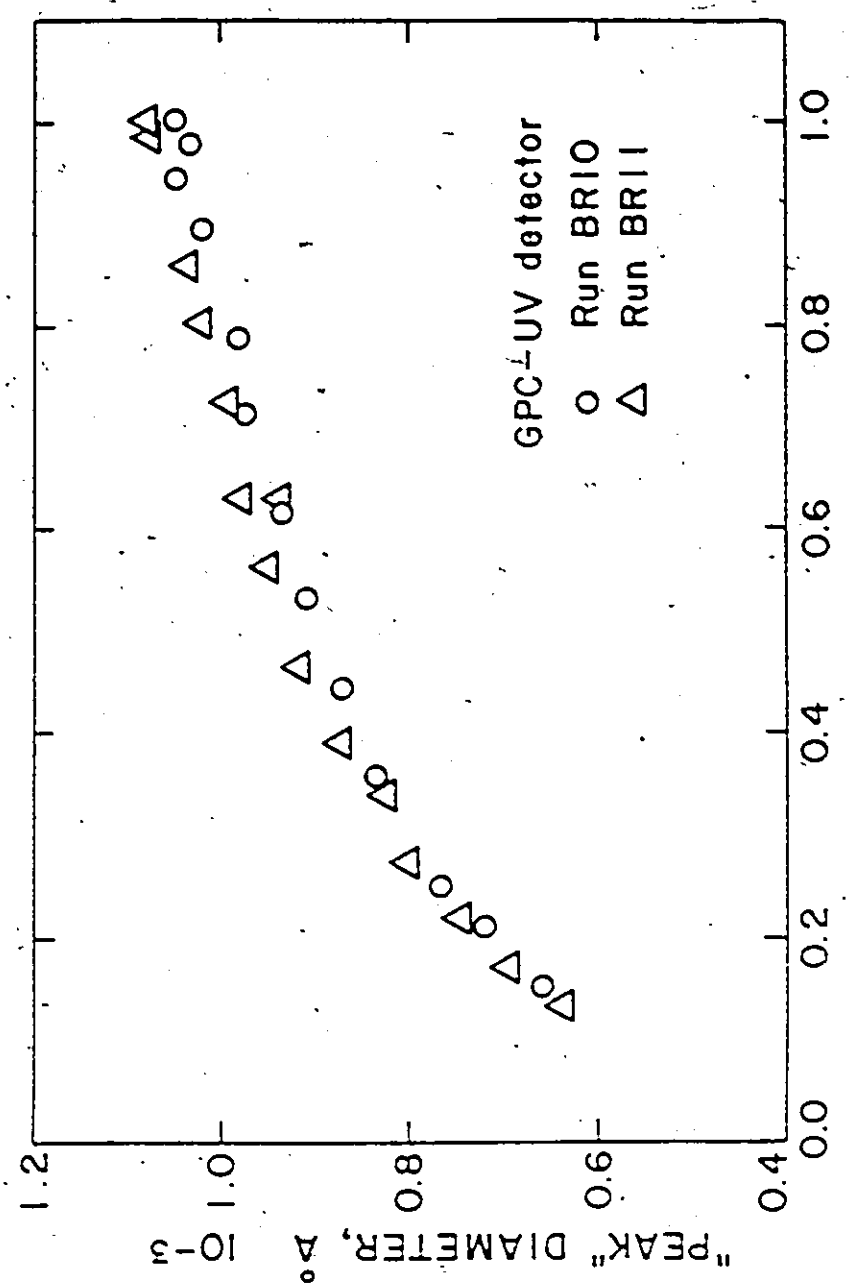

Figure (3-13). Diameters Corresponding to Peak Retention Volumes for Runs BR10 and BR11

average diameters were very close to the "peak" average diameters. These "peak" average diameters were read directly from the calibration curve which had been constructed from the peak retention volumes of monodispersed standards. Again, more details can be found in Kourti et al. (1984, 1985).

3.5.5 Concluding Remarks on Turbidity Spectra and SEC

Turbidity measurements are simple, fast and reproducible. Specific turbidity can successfully follow the particle size evolution during the course of emulsion polymerization and can be translated into weight average diameters. A combination of an on-line spectrophotometer with an on-line densitometer (to yield concentration) would provide the potential to estimate $\overline{D}_w$ on-line, as well. An on-line determination of PSD's, however, would seem quite difficult due to the high correlation of their parameters.

A limitation of turbidity spectra is the so-called "dilution" effect (Kourti et al. 1984)). The degree of dilution must be taken into account to properly correct ρ and n_p, otherwise the obtained results will translate into "false" (non-representative) particle sizes. At low conversions, where high dilutions cannot be employed, SEC can be used as a complementary technique, since it can also successfully follow particle growth and therefore, yield particle sizes.

3.6 Particle Size Determination: Electron Microscopy

The principle of electron microscopy (for more details see Hayat (1978)) is that a narrow beam of electrons is produced in an electron gun at one end of a vacuum column and then focused on as small a spot as possible on the surface of a specimen placed at the far end of the column. Along its path, the electron beam passes through several electromagnetic lenses and deflector coils, with which focusing of the beam is achieved. The beam is directed to the

specimen surface and knocks electrons out of the specimen surface. These secondary electrons are picked up by a collector and conveyed to an amplifier. The secondary electrons that emerge from each point on the specimen surface are characteristic of the surface at that point. In other words, the current received from any point is determined by the characteristics of the surface. Any changes in composition, texture or topography at the point where the electrons strike the surface affect variations in the electron current reaching the collector. The image, therefore, is a display of the received signals in their correct relative positions, and is a picture of the specimen surface. The image in the case of scanning electron microscopy (SEM) is built up point-by-point, and not all at once, as in the case of transmission electron microscopy (TEM). Thus the final picture is a magnified image of the surface of the specimen.

Microscopy represents the only method of obtaining particle size and size distribution by direct measurement of individual particles. However, microscopic methods have always been slow and tedious until the recent advent of television-computer combinations which are capable of automatically analyzing the microscopic image. Systems of this type can however be quite costly.

In a conventional microscopic measurement, a drop of highly dilute suspension is placed on a coated screen or metallic stub and the dried specimen is examined in the microscope and the particles photographed. The size of the photographed particles is then determined, and from the magnification employed, the particle size is computed.

The method is quite straightforward for hard rigid polymer particles such as polystyrene ones (if of course one overcomes the other serious problem of electron microscopy, namely the difficulty in obtaining a representative sample). However, in the case of soft polymers such as polyvinyl acetate and rubber latexes the method cannot be used since the particles flatten and distort. Various techniques have been developed to overcome this difficulty, and from these techniques, two appear to be most attractive: (i) the "particle

hardening" technique (Vanzo et al. (1964), Morganson (1967)) and (ii) the "freeze-drying" or "cold-stage" technique (de la Court and Vogt (1969), Talmon and Miller (1978)). Both these techniques, along with the osmium tetraoxide (O_sO_4) staining technique (Ugelstad et al. (1978), Lee (1981)), have been employed in the present study.

3.6.1 Experimental

In all cases (i.e. for both SEM or TEM and for both the "cold stage" or the "cross-linking" techniques) the latex samples were diluted to a concentration ranging from 2.5×10^{-3} to 4.5×10^{-4} gr/mℓ. The dilution medium was deionized water saturated with sodium lauryl sulphate.

According to the "cold-stage" or "freeze-drying" technique, a small drop from the diluted sample is "quick frozen" in nitrogen slush (liquid nitrogen). The specimen is then sputter coated with gold and transferred under vacuum to the microscope cryo-stage (a typical temperature range of the cold stage is between – 170° to – 150°C). The microscope used for this technique was an ISI-DS- 130 SEM scope 2000.

In the "particle hardening" or "cross-linking" technique, a drop of styrene is added to the dilute sample (roughly 10% of the polymer weight). The sample has to be shaken very well and subsequently irradiated with a total dose of 1–2 megarads of γ-radiation from a Cobalt-60 source. Then the sample can be processed in the microscopy unit.

In our analysis (some typical pictures from which can be found in Penlidis et al. (1985)), we tried to consistently measure ~ 500 particles per latex sample, when possible (~ 4–7 pictures per sample, ~100 particles per picture). The "particle hardening" technique appeared to give better results than the "cold-stage" one. A SEM 501 and a TEM 300 Philips were employed for these measurements.

Microscopic sizing has been recently simplified by the introduction of television-computer systems which automatically analyze the microscope image. An MOP-1.2.3 Carl Zeiss digital image analyzer (Quantimet) has been employed in the present study (Liegeois (1976)). The main problem in the use of this equipment is of course the problem of particle dispersion (i.e. the computer is not able to analyze the form of agglomeration). Thus, unless the particles are well dispersed, the instrument will give erroneous results.

Concluding this brief section on electron microscopy, it is important to emphasize that, although the method is quite precise (estimated experimental error ± 10%), the particle size distributions obtained from electron microscopy may underestimate the presence of very small particles. These particles' sizes are often less than 30 nm and difficult to measure from the micrographs, since they tend to aggregate or deposit on larger particles, thus making themselves invisible.

3.7 Particle Size Determination: Other Measurement Methods

There are several other techniques, which could be employed to characterize a latex sample. A few of the most important or commonly used as complementary techniques to the ones already mentioned for particle size characterization are briefly developed in Appendix IV.

3.8 Molar Mass Measurements

A typical synthetic polymer sample contains a multitude of individual molecular chains many of which may have widely differing molecular weights. When distinguishing between different samples of the same polymer, it is therefore necessary to define an average molecular weight. The breadth of the sample distribution of molecular weights and the average molecular weight of the polymer are determined by the conditions of its polymeri-

zation; these, in turn, control the final thermal, physical, mechanical, and processing properties of the product. Successful market competition of a plastic, therefore, depends on the ability of the engineer to control molecular weight during the polymerization process and on his understanding of how molecular weight influences those properties that are important for the principal application of that plastic.

Two techniques widely used to measure polymer molecular weight are membrane osmometry and light scattering. These are primary methods because average molecular weights are determined absolutely: M_n in the case of osmometry and M_w from light scattering. For routine molecular weight determinations, the techniques of intrinsic viscosity measurement and gel-permeation chromatography (GPC) are very often used. These are called secondary methods because average molecular weight can be determined only indirectly - by calibration with standards of known molecular weights in the case of GPC, and by use of empirical relationships when intrinsic viscosities are measured. More details on the principles of both primary and secondary molecular weight measurement techniques can be found in Yuan (1963) and in the excellent overview by Billingham (1977).

3.8.1 Light Scattering

Light waves are not only refracted and reflected, but also scattered by material particles.

Light scattering may be regarded as an interaction of the electromagnetic field of light with the molecules of the medium. It is the oscillating electric field which is responsible for scattering. Scattering occurs because the local electric field of the light beam induces polarization of the electrons of the molecules. Then, the induced dipoles oscillate in phase with the electric field and emit radiation in all directions.

In calculations of the intensity of scattering the interference of the waves scattered by the dissolved particles (molecules) must be taken into consideration. If the size of particles is small as compared to the wavelength of the incident light, and if the distance between the particles is sufficiently large so that the particles do not interact with one another, the waves scattered by these particles will not interfere, and the intensity of the waves scattered by the medium is the resultant of a simple superposition of the intensities of the waves scattered by the individual particles.

However, when the particles are present in high concentrations, they strongly interact with one another, and the scattered light waves interfere. The intensity of the light scattered by the medium is then calculated by adding up the amplitudes of the waves scattered by individual particles. This interference is called external interference. When the particle size is comparable with the wavelength of the incident light, the waves scattered by different parts of the molecule will be in different phases and will consequently interfere. In such a case one has the so-called internal interference.

In measurements of the intensity of the light scattered by polymer solutions, very dilute solutions are usually employed in order to eliminate external interference. Internal interference will then occur if the molecular weight of the polymer is very high and if the size of its molecules is greater than (λ/20), where λ is the wave length of the incident light. For most of the vinyl monomers, however, the size of molecules is less than (λ/20) for reasonably high molecular weights and internal interference can be minimized.

In the general case in a light scattering experiment, light of wavelength λ_o and intensity I_o is incident on a cell of volume V. Light scattered at an angle θ is detected with intensity I_θ at a certain distance r from the center of the scattering cell. This is shown in Figure 3-14. Note that the intensity envelope is symmetrical about the beam, the scattering

being the same in corresponding forward and backward directions in relation to the direction of the beam incidence.

V, the scattering volume, is defined by the cross-sectional area, A_o, of the illuminating beam and a length, ℓ, of the scattering volume. ℓ is determined by the optics of the detection system and is parallel to the incident beam. In other words, $\ell = V/A_o$.

A useful parameter in light scattering experiments is the so-called Rayleigh ratio or factor, denoted as R_θ. R_θ is defined as the radiant intensity, I_θ, scattered in direction θ, per unit irradiance I_o of the illuminating beam, per unit length of the scattering medium, i.e.

$$R_\theta = \frac{I_\theta r^2}{I_o V} \quad cm^{-1} \tag{3.49}$$

If one regards the polymer solution as an ideal gas of solute molecules (ideal point scatterers) dispersed in the solvent and applies the Einstein-Debye-Rayleigh-Mie theory (see Bilingham (1977)), then one obtains the following expression:

$$\frac{KC}{R_\theta} = \frac{1}{RT}\left(\frac{\partial \pi}{\partial C}\right) \tag{3.50}$$

where K is the so-called extinction coefficient, C the solution concentration, T the absolute temperature and π the osmotic pressure, which is related to the free energy required to create a concentration gradient in the solution. The osmotic pressure is given by:

$$\pi = \frac{RTC}{M} \tag{3.51}$$

therefore,

$$\frac{KC}{R_\theta} = \frac{1}{M} \tag{3.52}$$

where M is some molecular weight average.

For a polydisperse solute in solution,

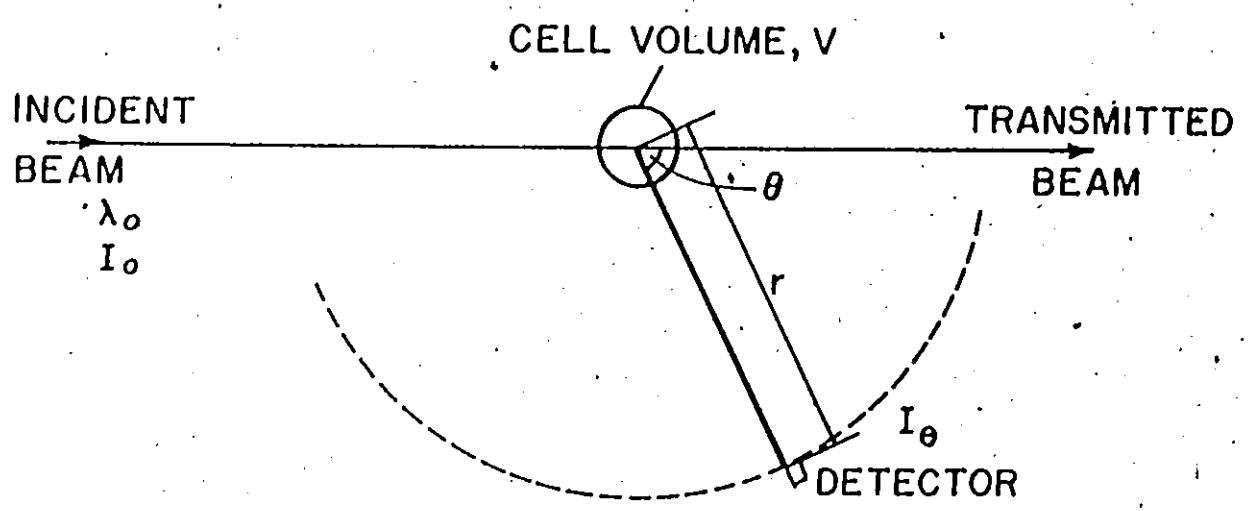

Figure (3-14). A Typical Light Scattering Experiment

$$(R_\theta)_{C\to 0} = \sum_i R_{\theta_i} = \sum_i K C_i M_i$$

$$= K \sum_i \frac{w_i M_i}{V} \tag{3.53}$$

But the concentration of the solution is given by:

$$C = \sum_i \frac{w_i}{V} \tag{3.54}$$

therefore, equation (3.52) becomes:

$$\frac{KC}{R_\theta} = \frac{\sum_i w_i}{\sum_i w_i M_i} = \frac{1}{\overline{M}_w} \tag{3.55}$$

where w_i is the weight fraction of species i with corresponding molecular weight M_i.

In the general case, equation (3.55) becomes:

$$\lim_{\substack{C\to 0 \\ \theta\to 0}} \left(\frac{KC}{R_\theta}\right) = \frac{1}{\overline{M}_w}\left(1 + \frac{16\pi^2}{3\lambda^2} \langle s^2 \rangle \sin^2 \frac{\theta}{2}\right) \tag{3.56}$$

where the limit denotes extrapolation to zero concentration (to avoid external interference) and to zero angle (to avoid internal interference). $\langle s^2 \rangle$ is an important quantity, called the mean square radius of gyration, which in the general case can give information about the dimensions and even the shape of the polymer coils.

3.8.2 Low Angle Laser Light Scattering (LALLSP)

Low angle laser light scattering photometry (LALLSP) is based on measurements of the intensity of light scattered at low forward angles (less than 6°) to determine the R_θ of solvents and polymer solutions, without the use of cumbersome computational techniques such as the Zimm plot. Red vertically polarized light from a HeNe laser (wavelength λ = 633 nm) is focused onto the sample contained between two thick silica windows and a teflon spacer. The measured quantity is the ratio of the scattered to the transmitted radiant power

and is measured with a Chromatix KMX-6 photometer. The method of calibration is based upon geometry, hence the resulting measurements are absolute rather than being referenced to some external standard.

With the KMX-6,

$$R_\theta = \frac{G_\theta}{G_o} (\sigma' \lambda')^{-1} D \tag{3.57}$$

In equation (3.57) G_θ and G_o coincide with I_θ and I_o of equation (3.52) and their ratio is the quantity actually measured with the KMX-6, proportional to radiant power. The group $(\sigma'\lambda')^{-1}$ is a quantity proportional to the solid angle θ over which G_θ is viewed and to ℓ. It is determined by the geometry of the KMX-6 (no reference to external standards is required). Finally, since $G_\theta \sim 10^{-9} G_o$, a series of attenuators is inserted into the beam when measuring G_o. The quantity D in equation (3.57) is a function of these attenuators employed. Note that the largest uncertainty in the measurement of most Rayleigh factors is the transmittance D of the attenuators used.

Typical equipment responses from the KMX-6 are cited in Penlidis et al. (1985) and more details about the experimental measurement of weight average molecular weights are given in Appendix V.

3.8.3 On-line SEC-LALLSP

This method employs size exclusion chromatography (GPC, SEC) (Altgelt (1968), Janca (1981), Giddings (1982), Barnes et al. (1985)) to separate samples of polydisperse polymers into fractions of narrower molecular weight distribution. Then, an on-line LALLSP photometer is used as a molecular weight detector.

Typical equipment responses are again given in Penlidis et al. (1985). For the molecular weight analysis with GPC/LALLSP, a WATERS M45 pump with a WATERS

ASSOCIATES differential refractometer R401 were employed, on line with a Chromatix KMX-6. Two bimodal DUPONT columns were used and the flow rate was kept constant, equal to 1 mℓ/min. The carrier fluid was THF stabilized with 0.025 % BHT and the temperature was kept constant at 25° C. The polymer solutions were 0.1% by weight in THF.

The method is very powerful and can also give information about branching frequency as well. No more details will be mentioned herein, but reference is made to the work by Hamielec et al. (1978), Dietz (1980) and Hamielec (1982), and to the excellent paper by Hamielec and Meyer (1984) for a more in-depth approach.

3.9 Conclusions

Several techniques which can give information about important latex or polymer properties have been critically discussed in this chapter. The great practical significance of all these methods will become more clear during the development of the last chapters of this thesis, at which stage information from these characterization techniques and from the dynamic model application will be combined towards a better and more efficient design and control of the reactor system for the commercial production of emulsion polymers.

CHAPTER 4

BATCH REACTOR STUDIES - PVAc

4:1 Introduction

A general mathematical model has been developed in Chapter 2 for the emulsion homopolymerization of VAc. This model will be tested in the present and subsequent chapters in order to see whether it can accurately simulate reactor behaviour under several modes of operation, the final aim being to assess the model's applicability to existing industrial situations and to further appreciate its use in the design of more sophisticated or complex novel operating schemes.

It is then the logical starting point to initiate this model evaluation from the simpler mode of operation, namely batch polymerization. With the word "simpler" we mean simpler than semi-batch or continuous operation. Investigations reported in the literature concerning batch emulsion polymerization of vinyl acetate are in general disagreement. This is mainly due to the complex physical and chemical phenomena which occur in VAc emulsion polymerization. However, most of the authors agree that the following major conclusions hold for the batch process:

(1) The rate of polymerization is half order with respect to initiator concentration.

(2) Polymerization takes place in the polymer particles.

(3) The number of polymer particles can be considered independent of initiator concentration.

(4) The number of polymer particles becomes constant in 5 – 10 minutes after initiation of particle nucleation.

(5) The order of reaction with respect to particle number is small and lies between 0.05 and 0.2.

(6) The average number of radicals per particle is much less than one half and usually in the order of $0.01 - 0.001$.

(7) Termination reactions are of little importance in molecular weight development, and

(8) The molecular weight of the polymer is independent of particle number and size and initiator concentration.

Several authors in the literature have attempted to provide data or models in order to explain the behaviour of vinyl acetate emulsion polymerization. A very good review of these efforts and a thorough presentation of the interesting peculiarities of emulsion polymerization of VAc can be found in El-Aasser and Vanderhoff (1981). Our objective in this chapter is to present a model for batch emulsion homopolymerization of VAc with a minimum number of adjustable parameters that can be easily estimated from experimental data. To illustrate then the application of this model, we simulate and predict experimental results from the literature (Nomura et al. (1971), Friis and Nyhagen (1973), Keung (1974), Singh and Hamielec (1978)) and from our pilot-plant scale-reactors. Important latex and polymer properties related to particle size and molecular weight distributions are accounted for in the present model. The unquestionable commercial importance of these properties for a latex makes such a model useful for the design, optimization and control of latex reactors.

4.2 Batch Reactor Model

Litt et al. (1970), Friis and Nyhagen (1973), Friis and Hamielec (1975a) and Friis et al. (1974) were the first who examined both theoretically and experimentally the batch emulsion polymerization of VAc with the final aim to model data on conversion, molecular

weights and branching. Later on, Min and Ray (1978) discussed a computational algorithm for the detailed simulation of a batch latex reactor and they successfully applied their model to the polymerization of methyl methacrylate.

Particles in a batch emulsion reactor are mainly formed during the first five or ten minutes of the reaction. At the end of stage 1, particle nucleation ceases since there is no free soap (emulsifier) left to form micelles. Therefore, the total number of polymer particles after nucleation has stopped remains practically constant. This has been shown in numerous experimental studies (Friis and Nyhagen (1973), Keung (1974), Fitch (1971)).

The derivation of the equations for the VAc batch emulsion polymerization model follows exactly the development in section 2.3. The only difference of course is that the inflow and outflow terms in the equations of subsection 2.3.6 should be set equal to zero, since we are dealing here with a batch reactor.

The differential equation that describes the rate of change of conversion in a batch reactor is given by:

$$\frac{d\,x(t)}{dt} = \frac{R_p(t)}{M_F} \qquad (4.1)$$

since $M_{TOT}(t)$ from equation (2.4) is equal to M_F, the monomer concentration in the initial charge (feed), and $M_{TOT_0} = 0$. All the other equations are identical with the equations of subsection 2.3.6 and will not be repeated here again.

4.2.1 Numerical Values of Model Parameters and Rate Coefficient Expressions

There are several parameters and rate constants which are used in the previously developed VAc model. Their values and the sources from which these values (or the kinetic expressions) were obtained are discussed and cited in this subsection.

Table 4-1 contains the expressions for the various kinetic rate constants used in the model (e.g. initiator decomposition rate constant, propagation rate constant, etc.), together with the literature sources from which they were obtained. Similarly, Table 4-2 contains numerical values of the other constants employed. These values and expressions have been extensively tested in the past in simulations of VAc emulsion systems and they are further discussed in Appendix VI.

Also included in Appendix VI is additional information concerning the VAc emulsion system, information that might help one to further clarify the system's peculiarities.

4.2.2 Model Parameters and Parameter Estimation

Inspecting again the model equations of subsection 2.3.6 together with Tables 4-1 and 4-2, one will notice that the only parameters which have not been yet assigned values are the ones denoted by ε and D_w, namely the ratio of the radical capture rate constant (radical absorption) by particles (k_{ab}) to the rate coefficient of micellar nucleation (k_m), and the diffusion coefficient of monomeric radicals in the water phase. It proved very difficult to find reliable and consistent values for ε and D_w from the literature and since it is a very tedious task, if not an impossible one, to directly measure them, we decided to keep ε and D_w as the two adjustable model parameters. These parameters can be easily estimated from experimental data on conversion and particle size.

According to the diffusion theory for radical capture, micelles and small particles should have larger capture rates per unit area than larger particles. In conflict with this theoretical prediction, experimental evidence suggests that micelles are significantly less efficient in capturing radicals.

Table 4-1

Kinetic Rate Constants

	Reference
$k_p = 1.8669 \times 10^7 \exp(-5606/RT)$	Friis et al. (1974)
$k_{fm} = 3.7237 \times 10^6 \exp(-9895/RT)$	Friis et al. (1974)
$k_{fp} = 1.4183 \times 10^6 \exp(-8947/RT)$	Hamielec (1981)
$k_p^* = (kp^*)_o \exp(-(A_1 x(t) + A_2 x^2(t) + (A_3/2.) x^3(t)))$	Friis & Hamielec (1975a)
	Friis et al. (1974)
	Hamielec (1981)
$(kp^*)_o = 9.0963 \times 10^6 \exp(-5510/RT)$	Friis et al. (1974)
$A_1 = -6.8782 + 0.01961 * T$	
$A_2 = 64.733 - 0.185 * T$	
$A_3 = -149.099 + 0.43044 * T$	
$k_d = 0.2540 \times 10^{18} \exp(-33320/RT)$	see Appendix VI

Table 4-2

Numerical Values of Model Constants

Constant	Units	Reference
$a_p(t,t) = \pi \times d_p^2(t,t)$	dm^2	
$d_M = 930.$	gr/lit	Brandrup and Immergut (1975)
$d_p = 1150.$	gr/lit	Brandrup and Immergut (1975)
$d_p(t,t) = 50. \times 10^{-9}$	dm	see Appendix VI
$f = 0.7$		see Appendix VI
$L = 8. \times 10^{-5}$	dm	Fitch and Tsai (1971)
$m = 27.1$		Nomura et al. (1976)
$MW = 86.$	gr/gmole	Brandrup and Immergut (1975)
$MWI = 270.$	gr/gmole	Brandrup and Immergut (1975)
$MWS = 288.$	gr/gmole	Brandrup and Immergut (1975)
$N_A = 6.02283 \times 10^{23}$	molecules/gmole	
$S_{CMC} = 3.2 \times 10^{-3}$	gmole/lit	see Appendix VI
$S_a = 5. \times 10^{-17}$	dm^2/molecule	see Appendix VI
$v_p(t,t) = \pi \times d_p^3(t,t)/6.$	dm^3	
$x_c = 0.2$		see Appendix VI
$\delta = 0.5$		see Appendix VI
$\mu = 0.55$	dm^{-1}	see Appendix VI
$\pi = 3.1415926531$		

Harada et al. (1971) suggest that the rate of entry of a radical into polymer particles is larger by several orders of magnitude than the rate of entry into micelles. They suggest that this observation may be due to: (i) an electrical energy barrier between radicals and micelles or (ii) significant radical desorption from micelles. From their experiments, they suggested that ε, on an area basis, was ~ 1.28×10^5.

Nomura et al. (1972) analyzed the particle formation in styrene emulsion polymerization and found that the value of ε was 1.3×10^5. This value was about 10^2 times greater than that predicted by the diffusion theory which assumes that $k_{ab} = 2\pi D_w \delta d_p M_m$ and $k_m = 2\pi D_w \delta d_m$, where d_p and d_m denote particle and micelle diameter, respectively, and M_m is the aggregation number of a micelle.

On the other hand, in VAc emulsion polymerization, the value of ε was estimated by Nomura et al. (1976) to be ~ 1.2×10^7. This value is also about 10^4 times greater than that predicted by the diffusion theory. According to their arguments, ε is a lumped factor that represents "the radical capture efficiency of a particle relative to a micelle".

Ugelstad et al. (1976) and Ugelstad (1977) made the following observations: (i) only monomeric radicals formed by chain transfer may desorb from the polymer particles (ii) one would expect that the uncharged monomer radicals which have desorbed from the polymer particles may be reabsorbed at a higher rate than the charged oligomer radicals stemming from initiator decomposition, and (iii) a particle containing a radical will tend to absorb a second radical at a much higher rate. They also concluded that the radical capture by particles is greater than radical capture by micelles and reported a range of values for ε from 10^2 to 10^7 depending on the monomer type.

Pramojaney (1982) argued that since an excessively large number of particles is obtained when it is assumed that a desorbed radical may participate in the generation of new particles in the same manner as a newly-produced initiator radical, it is reasonable to suspect

that the desorption and re-absorption scheme may take place only locally. In other words, a radical that desorbs from a particle stays in the vicinity of the particle (he estimated the thickness of the diffusion film barrier surrounding a particle as being in the order of 10^{-7} dm) and there is a high probability that this radical will be re-absorbed (recaptured) by the same particle. He further argued that a high value for ε can also be explained in a sense that in the absence of particle coagulation, the effectiveness of micelles in generating particles should decrease or assume a small value, so as to prevent a boundless increase of the total number of polymer particles with an increase in emulsifier concentration.

We have decided to estimate ε and D_w from experimental conversion-particle size-molecular weight versus time data using a non-linear parameter estimation package (e.g. UWHAUS, ZXSSQ, etc.). Old estimates of ε and D_w, which had been obtained from parameter estimation based on experimental conversion versus time data from Keung (1974), were used as starting values. It was eventually found that $\varepsilon = 0.784 \times 10^{3}$ and $D_w = 0.102 \times 10^{-6}$ dm^2/sec. The value of ε agrees with the postulations and estimates of the previously mentioned authors. For the soap-free VAc case, ε was estimated to be 0.684. This is in agreement with Pramojaney (1982) and Hoffman (1984), who have estimated a $k_m \sim 10^{-4} - 10^{-5}$ dm/sec and a $k_{ab} \sim 0.25 \times 10^{-4}$ dm/sec, respectively, for a case where homogeneous nucleation was important. Therefore, their estimate for ε is roughly 0.25, which is in agreement with our estimate. Furthermore, our D_w estimate is surprisingly close to 0.19×10^{-6} dm^2/sec, used by Nomura and Harada (1981) and based on the theoretical predictions by Wilke and Chang (1955).

The values of ε and D_w which are reported herein have been extensively used in simulations and continuously checked with experimental results from our laboratories and the literature over a period of more than four years (Keung (1974), Singh and Hamielec (1978), Kiparissides et al. (1979), Pollock et al. (1981) and Pollock (1984)). Exactly the same

values were employed throughout the present research when simulating either literature or our experimental results.

4.3 Application of Model Equations

4.3.1 Comparison of Model Predictions with Literature Data

A certain controversy exists in the literature as far as emulsion polymerization of VAc is concerned. This controversy is mainly due to two reasons: (1) the inherent complexity of the physical system itself, and (2) the fact that every experimenter used different reaction conditions, initiator and/or emulsifier levels, purities of reactants, etc. In this chapter, the most consistent batch experimental data from the literature are simulated using the batch model equations. These batch experimental data (Nomura et al. (1971), Friis and Nyhagen (1973), Keung (1974) and Singh and Hamielec (1978)) are mainly concerned with conversion-time histories and final number of particles, and very few of them with other latex or polymer properties (Keung (1974) and Singh and Hamielec (1978)).

Figure 4-1 shows plots of total polymer particle diameter, surface area and volume versus batch time. It is a simulation for a VAc emulsion system at 50°C, with $\bar{I} = 2.22 \times 10^{-3}$ gmoles/liter of water and $\bar{S} = 0.0417$ gmoles/liter of water. The ability of the model to account for particle volume shrinkage in stage 3 is clearly shown. Results of further model predictions and their comparison with reported data are shown in Figures 4-2 to 4-7.

Figures 4-5 to 4-7 show simulations of Keung's experiments (1974). In all these experiments, the recipe consisted of 1000 ml distilled water, 400 ml purified VAc monomer and varying amounts of potassium persulphate (KPS) initiator and sodium lauryl (dodecyl) sulphate (SLS) emulsifier. Emulsion samples were drawn from the reactor in ten- to twenty-minute intervals. The percentage conversion was determined gravimetrically.

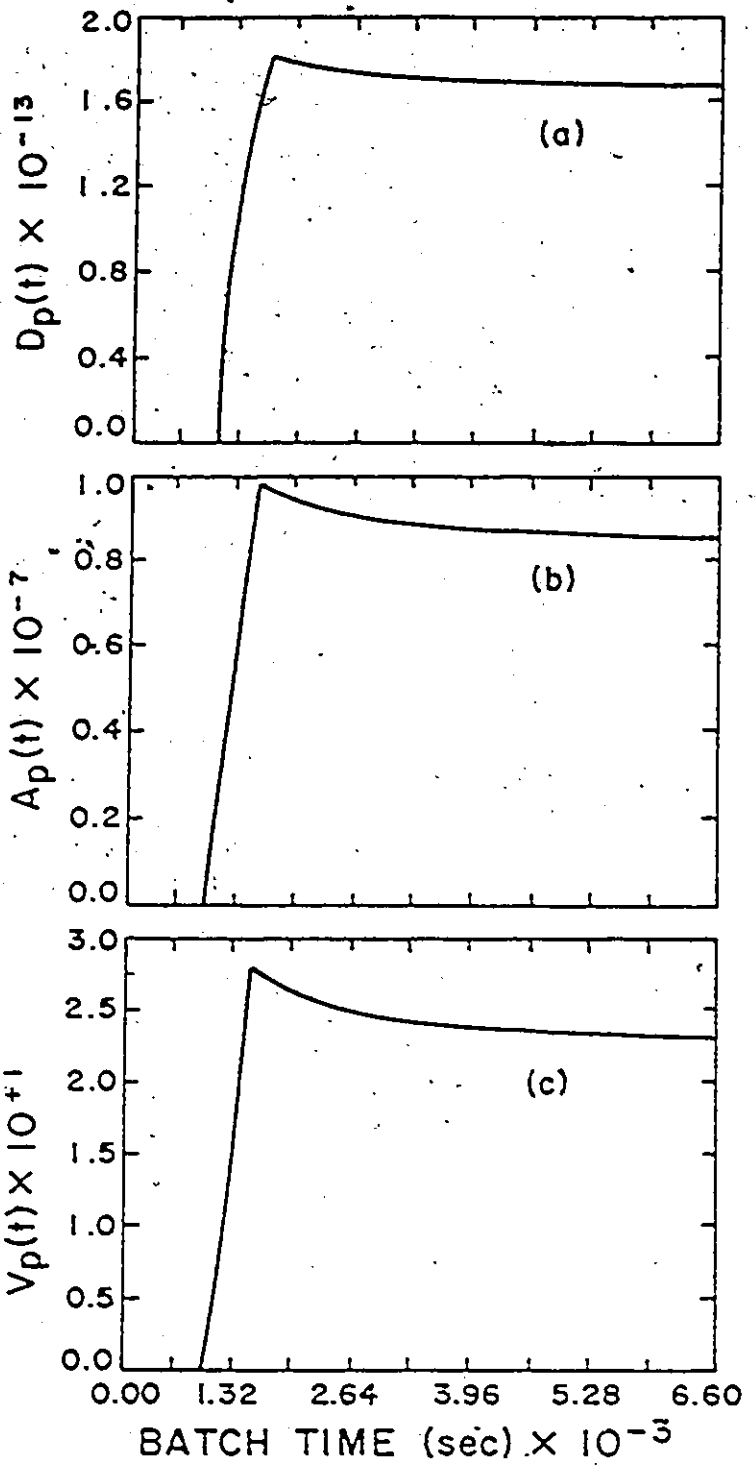

Figure (4-1). Batch VAc Emulsion Polymerization Model Predictions for (a) Particle Diameter, (b) Surface Area, and (c) Particle Volume

The latex samples were subsequently diluted 100 to 200 times with water containing emulsifier and their absorbance was measured with a Beckmann DU spectrophotometer. Their number- and weight-average diameters were obtained from the ratios A/c (absorbance over concentration) and calibration curves established from electron microscopic work.

Molecular weight averages of the polymer samples were determined using a Waters Associates Chromatograph (Model No. ALC-201). Poly (VAc) samples were dissolved in tetrahydrofuran (THF) to form a solution of 0.25% by weight. The chromatograph was operating at room temperature (25°C) and carrier solvent flow rate of 2.5 ml/min.

4.3.2 Comparison of Model Predictions with Experimental Results Measured Herein

Reactor configuration: A schematic representation of the experimental reactor set-up for the batch experiments is shown in Figure 4-8. It is a bench scale 1 gallon (~ 5 liters) stainless steel reactor by Chemineer-Kenics, jacket-heated, with a turbine agitator, a removable top head and teflon gasket and mounted on a hydraulic lift stand. Heating of the reaction mixture is carried out by injecting steam from the main steam line into the jacket inlet line through a diaphragm control valve. The jacket inlet line is connected to the main water line. Through the above mentioned heating and cooling facility and a Gulton WEST 2070 controller, it is very easy to adjust the reaction temperature to a desired value ($\pm$ 1°C).

The top head of the reactor was used for the following: thermocouple, venting, vacuum and nitrogen inlet lines, a pitched blade turbine agitator adjusted to 320 rpm, an inhibitor line (1% by wt. hydroquinone (HDQ) solution) for cases of emergency (e.g. reactor runaways), a rupture disc (145 psig at 500°F) for safety reasons, a manifold connected to the feeding cylinders and a line which comes back from the pump-around sampling loop.

During polymerization, the reaction mixture was continuously circulated through an on-line densitometer (a U-tube DPR-YWE model with a Y-mode oscillator, with a PTE-98-EV-72 excitation cell and a DPR-2000 electronic board, by Anton Paar, Austria). This was accomplished through a sampling loop built around the reactor, from the bottom of the vessel back to its top head. A pump pumped the material from inside the reactor vessel through a sampling valve, a photo-detector and a densitometer back to the top head of the reactor, where the material returned in the reacting mixture through a sparge dip tube. The photo-detector was nothing but a simple light source which produced a voltage signal upon interruption by flowing polymer particles. Its function will become evident later.

Materials and polymerization procedure: The chemicals used in these runs were VAc monomer with its inhibitor (CIL Co., Toronto), deionized water, specially pure SLS and assured grade (ACS) KPS (both from BDH Chemicals). Deionized water was used as the dispersion medium for the reaction and solvent for the initiator and emulsifier solutions. The monomer inhibitor was hydroquinone.

Good care was taken to degas the initiator solution in its feeding cylinder by bubbling UHP (ultra high purity) nitrogen through it. Monomer, emulsifier solution and water were all charged into the reactor vessel, the mixture was stirred at 320 rpm and the reactor was purged with nitrogen for ~ 15 minutes. At the same time, the reaction mixture was heated up to the desired temperature level and the polymerization initiated by injecting the initiator solution. A nitrogen blanket of 2-4 psig was kept over the reacting mixture during polymerization.

More details about the reactor set-up and the polymerization procedure can be found in Appendix VII.

Sampling and off-line analysis: Samples (~ 5 ml each) were drawn off every 10 minutes, starting after initiation of the reaction. Addition of a drop of HDQ solution was to

prevent further polymerization in the samples, which were then placed into ice (0°C) for 10-15 minutes and subsequently stored for further analysis.

Conversion was recorded on-line from the densitometer. It was also determined off-line by gravimetric analysis, thus allowing an independent check of the densitometer readings.

Particle diameter was determined by off-line turbidity spectra and size exclusion chromatography. Occasional electron microscope measurements were taken as well. The number of polymer particles was estimated from conversion and particle size data.

Finally, off-line low angle laser light scattering spectroscopy (LALLSP) and LALLSP on-line with gel-permeation chromatography (GPC) were employed for weight average molecular weight and long-chain branching determinations.

Experimental runs: Table 4-3 gives a summary of the batch VAc runs performed and their operating conditions. As it can be seen from the recipes used, the solids content of all these runs (and all the following continuous runs) was close to 30%, which is representative of a typical recipe. Figures 4-9 to 4-13 show the comparison of our model predictions with measured data from these runs. Appendix VIII contains tables of the data measured.

4.4 Discussion of Experimental Results

Figure 4-2a shows number average particle diameter experimental data versus reaction time. The diameters (in Ångstroms) were measured by Singh and Hamielec (1978) using electron microscopy and liquid exclusion chromatography; therefore, they are particle diameters based on a monomer free basis. In other words, they are based on total monomer-free and not on monomer swollen polymer particle volume. They are estimated as:

$$D_p^*(t) = \left[\frac{6}{\pi} V_p(t) (1 - \phi(t)) \right]^{1/3} \qquad (4.2)$$

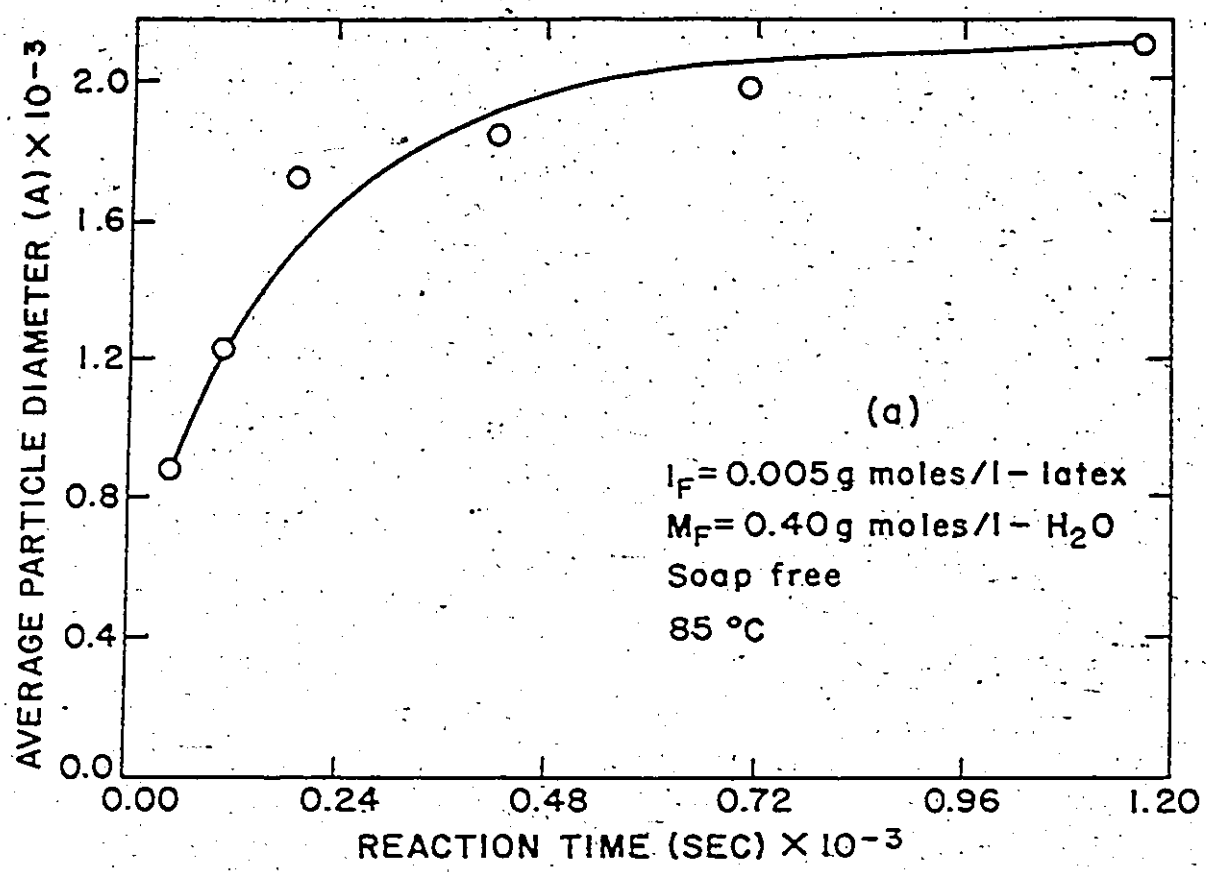

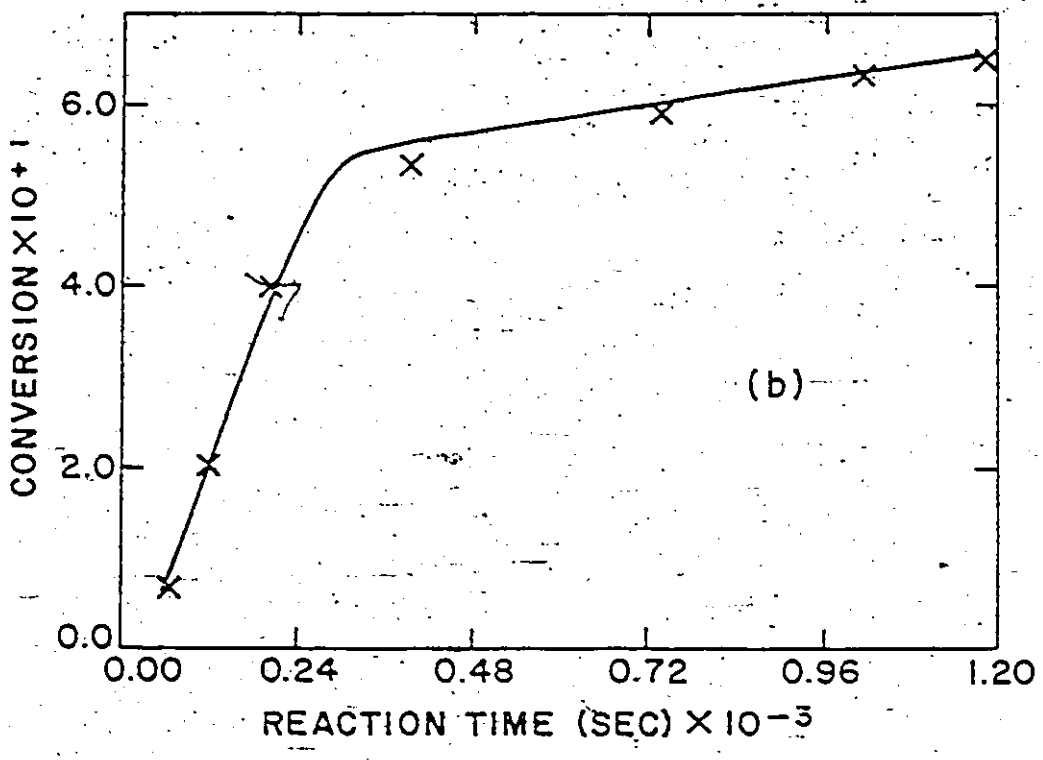

Figure (4-2). (a) Average Particle Diameter and (b) Conversion versus Reaction Time for a Soap-free Case

The polymerization was a soap-free one, i.e. no micellar particle nucleation occurred. Singh and Hamielec (1978) estimated the final number of polymer particles in the latex using measurements of conversion and diameter and they reported a final number of 0.4×10^{16} particles/liter of latex. Our model predicted 0.38×10^{16} particles/liter of latex. The good agreement between our model predictions and their diameter data is evident from Figure 4-2a. Figure 4-2b shows the corresponding to Figure 4-2a conversion versus time history. Conversion shows a tendency to level off after ~50%, which is consistent with the action of the redox system that they employed. By setting the initiator concentration in the computer program effectively equal to zero after ~300.0 seconds of reaction, the model was quite successful in predicting their conversion results as well.

In Figure 4-3, conversion versus time results from Nomura et al. (1971) are simulated. There are two sets of data plotted, which were obtained under exactly the same experimental conditions except for emulsifier concentration. The well known fact that emulsifier concentration does not significantly affect conversion levels is clearly illustrated. Nomura et al. (1971) estimated a final number of 0.7×10^{18} particles/liter of latex and the model's prediction was $2. \times 10^{18}$.

Figure 4-4 shows conversion results from Friis and Nyhagen (1973) taken under the same experimental conditions except for initiator concentration. Again, the agreement between model predictions and conversion measurements is very satisfactory. A higher initiator concentration gives higher polymerization rates and hence, higher conversion levels, as it would be expected.

A conversion-time history for a typical batch run from Keung (1974) is shown in Figure 4-5a. All experimental results that are shown in Figures 4-5 to 4-7 are coming from the same run, namely initiator concentration: 2.22×10^{-3} gmoles/liter of water; emulsifier

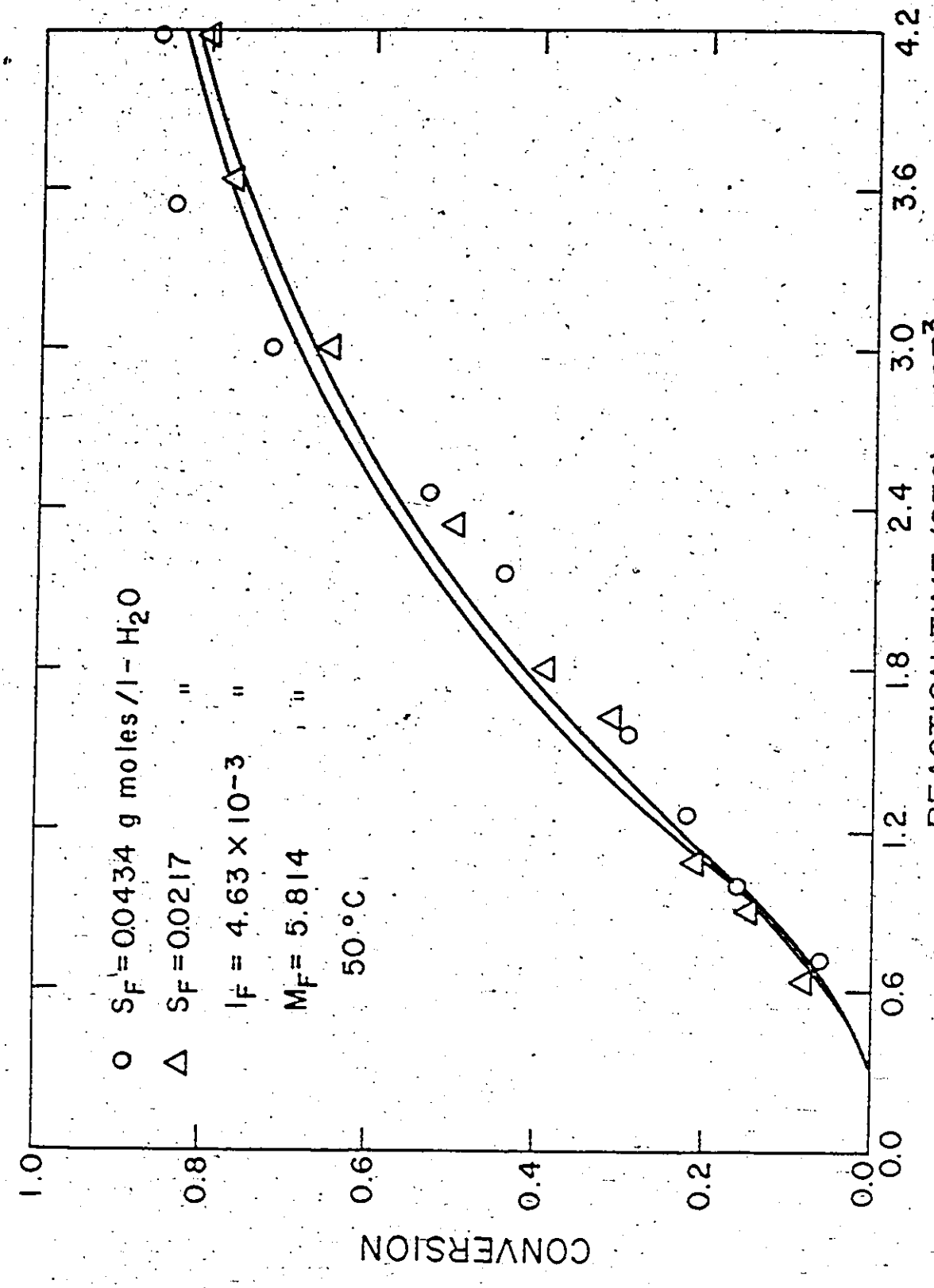

Figure (4-3), Batch Emulsion VAc : Conversion vs. Time for Two Different Emulsifier Concentrations

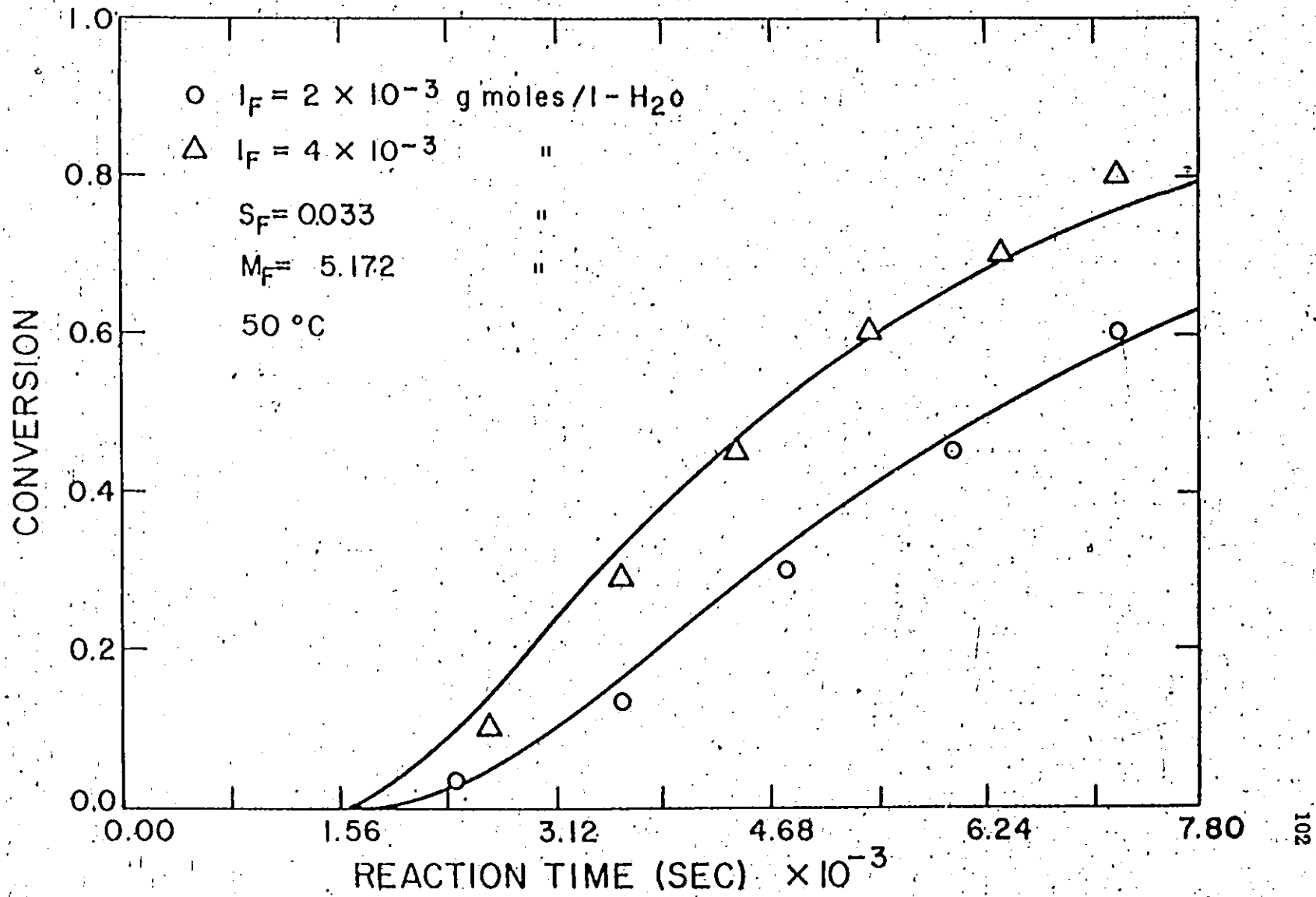

Figure (4-4). Batch Emulsion VAc : Conversion vs. Time for Two Different Initiator Concentrations

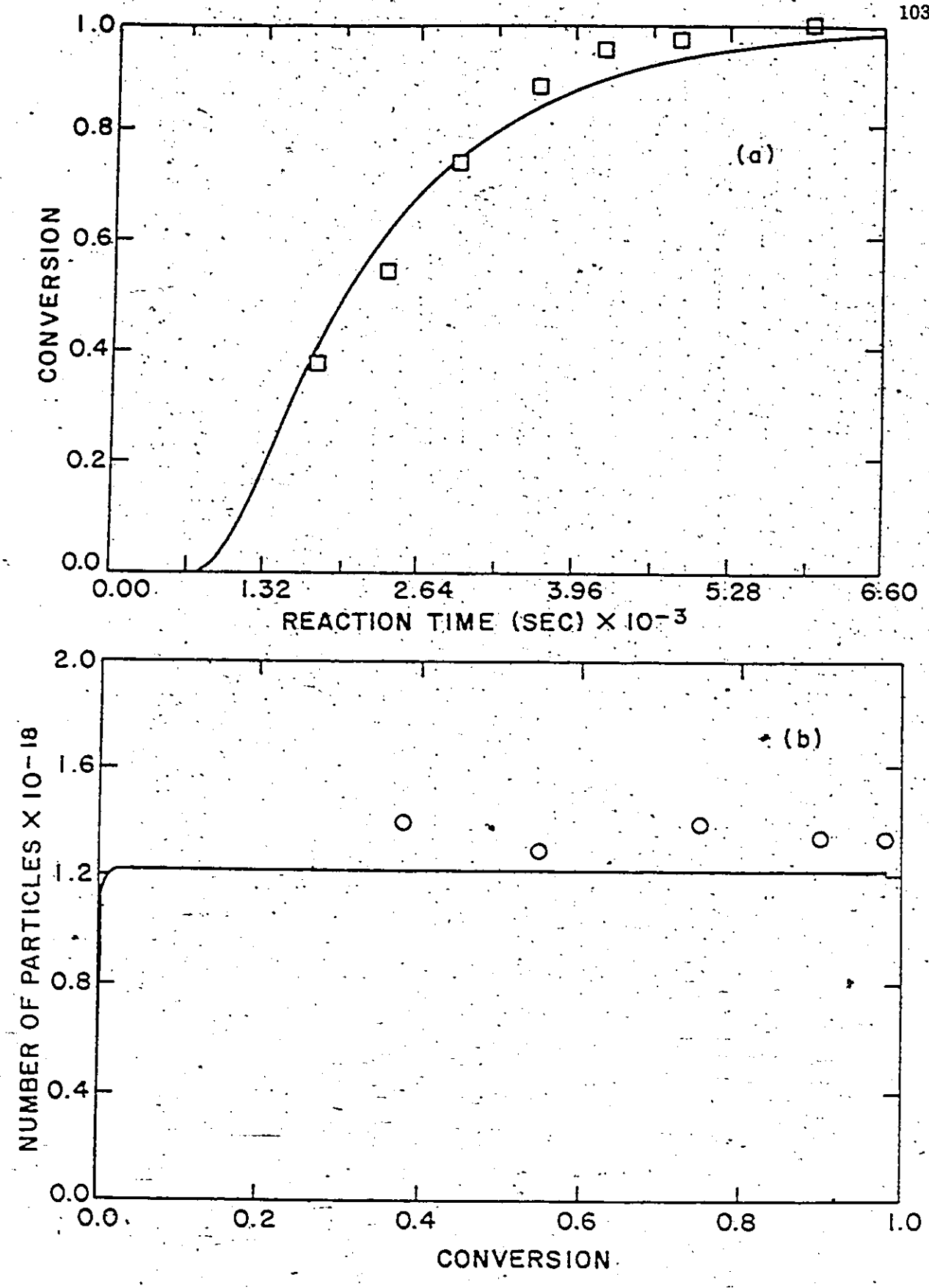

Figure (4-5). Batch Emulsion VAc: (a) Conversion vs. Time, (b) Number of Particles vs. Conversion

concentration: 12 gr/liter of water; monomer concentration: 4.32 gmoles/liter of water; ratio of latex volume to water volume: 1.4; volume of monomer: 400 ml; volume of water: 1000 ml; temperature: 50°C.

In Figure 4-5a, as well as in Figures 4-3 and 4-4, it can be seen that there is an induction (delay) time before polymerization starts. This is due to the presence of traces of dissolved oxygen and other impurities or inhibitors in the reaction mixture. It is virtually impossible to eliminate these from the system. These impurities consume the first radicals that are produced by initiator decomposition, thus causing a delay in the start-up of the reaction.

Inhibitors other than oxygen are assumed to be present in the aqueous phase, where they may react with the aqueous free radicals via a bi-molecular reaction. It has also been shown (Kolthoff and Dale (1945, 1947)) that oxygen acts like a typical inhibitor with persulphate as "catalyst". It does not only act as an inhibitor in the beginning of the polymerization but also, if added to a latex during the course of the reaction, it acts like a "temporary short-stop". Oxygen reacts readily with free radicals to form peroxides.

Although oxygen inhibits the polymerization of VAc, it does not have a critical effect on the course of the reaction. The course of the reaction when little oxygen is present initially appears to be identical after the end of the inhibition period with that observed when oxygen is removed completely by vacuum degassing (Dunn and Taylor (1965)). This is the main difference between inhibitors and retarders. A retarder retards the polymerization throughout the entire reaction period, without giving rise to induction periods. A retarder acts as a typical chain-breaker (Kolthoff and Bovey (1948)). It should reduce the molecular weight of the polymer, although this effect may not be large when effective CTA's are present.

Oxygen as an inhibitor does not affect the course of the reaction. Nevertheless, soluble oligomers are formed during the inhibition period which are surface active and which

are adsorbed on the latex particles once they form. Burnett et al. (1958) found out by a light scattering method that the diameter of a VAc particle was 293 nm when vacuum degassing was used, 260 nm when most of the oxygen was displaced with a stream of nitrogen, and 219 nm when the oxygen concentration was increased by passing in oxygen (Dunn (1981)).

In the experimental runs that we have performed in our laboratories, we have decided to use VAc monomer with its commercial inhibitor (hydroquinone), something that considerably simplifies the preparation procedure (no monomer distillation) and more closely approaches an industrial environment. Furthermore, obtaining a measure of the induction time using an on-line spectrophotometer and knowing the amount of the inhibitor present, one might theoretically be able to model initiator radical consumption by impurities or dissolved oxygen and incorporate it in the model.

Figure 4-5b is a plot of the total number of polymer particles versus conversion (Keung (1974)). The total number of particles that was estimated is about 1.35×10^{18} particles/liter of latex. The model predicted 1.2×10^{18} particles/liter of latex.

As was observed in several experimental studies (Friis and Nyhagen (1973), Keung (1974) and Fitch (1971)), in the batch emulsion polymerization of VAc a massive generation of polymer particles takes place during stage 1, which has typically a duration of 5 to 10 minutes. Friis and Nyhagen (1973) concluded that the number of particles remain constant from 10% to 100% conversion. Therefore, in a very short time, one obtains the final number of polymer particles ($\sim 10^{18}$), which subsequently start to grow during stage 2. Also, since all particles start to grow nearly at the same time, their growth rate in stage 2 will virtually be the same and the final particle size distribution will be almost monodispersed. Thus, all properties of the final product dependent on particle number and size are strictly defined from stage 1.

The duration of stage 1 (i.e., the particle nucleation stage) is approximately 5-10 minutes. This interval is, of course, not sufficient for feedback control action to be taken according to the progress of the reaction, especially if one would like to apply on-line feedback control based on latex property trajectories. Therefore, it might be of interest to find a strategy which might extend the duration of stage 1. An introductory theoretical investigation of the problem will be presented and discussed in Chapter 5 of this thesis, which is concerned with semi-batch latex reactors.

Figure 4-6 shows number-average diameter versus conversion for two different emulsifier concentrations (Keung (1974)). The results indicate that emulsifier concentration has a great influence on particle size development. Again, the agreement of our model predictions with experimental results is very good.

Since the polymerization rate can be determined from the slope of the conversion versus time curve and $N_p(t)$ can be calculated from diameter and conversion data, then $\bar{q}$ can be calculated through:

$$R_p(t) = \frac{k_p M_p N_p(t)}{N_A} \bar{q} \tag{4.3}$$

It was found by this rather imprecise calculation (Keung (1974)), that $\bar{q}$ changed from 0.015 to 0.075 as conversion changed from 0.1 to 0.8. The model predicted a $\bar{q}$ ranging from 0.025 to 0.03 radicals per polymer particle, a result which is in agreement with Case I kinetics.

Finally, to conclude the simulations of literature data, Figure 4-7 shows the change of number and weight average molecular weights, respectively, with conversion (Keung (1974)). As it can be seen, the data agree very well with the model's predictions within the limits of experimental errors.

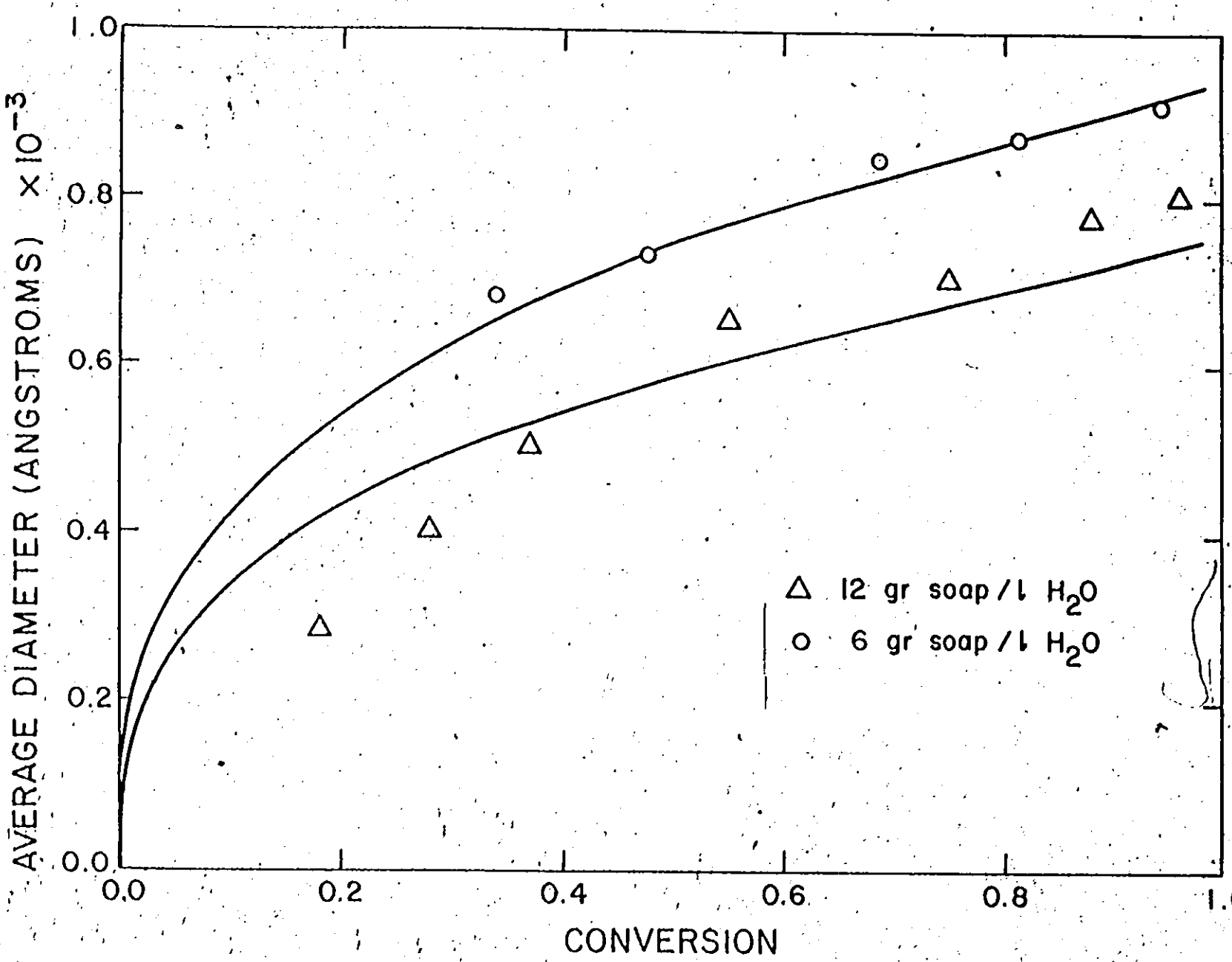

Figure (4-6). Batch Emulsion VAc : Diameter vs. Conversion for Two Different Emulsifier Concentrations.

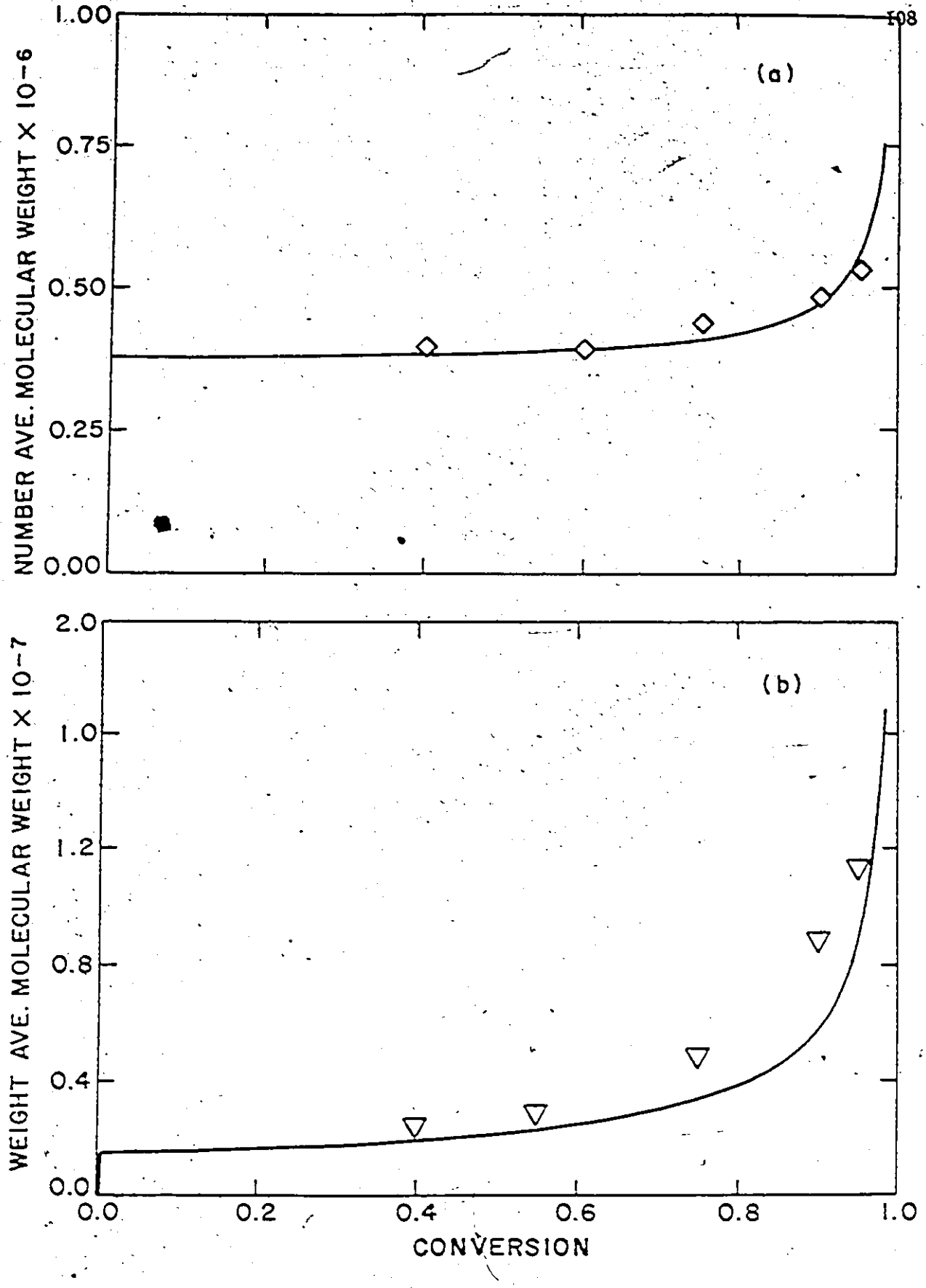

Figure (4-7). Batch Emulsion VAc : Number and Weight Average Molecular Weights vs. Conversion

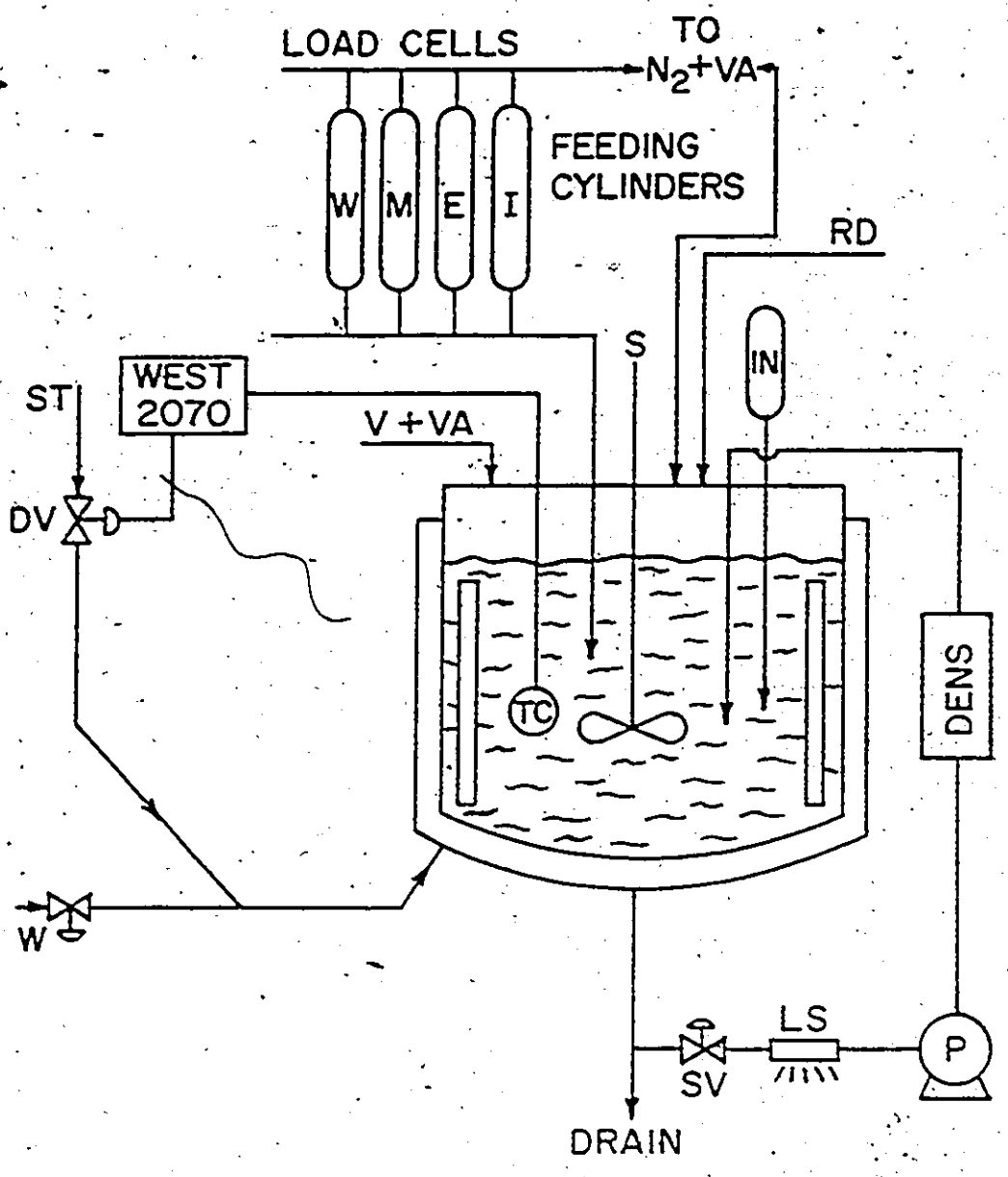

Figure (4-8). Schematic Representation of the Experimental Set-up for the Batch Runs

Figures 4-9 to 4-13 show a comparison of the experimental results obtained in this project from our pilot plant scale reactors with the batch model predictions. Table 4-3 gives a summary of the batch runs performed in terms of operating conditions (temperature and amounts of initiator, emulsifier, monomer and water). These conditions are the only input data that need be supplied to the batch computer model. A detailed discussion of these batch runs and their results will now follow in the remainder of this section.

Figure 4-9 shows conversion vs. reaction time data for runs BR2 (batch run 2) and BR3. Conversion data from both the on-line densitometer and the off-line gravimetric analysis are reported. The agreement between on-line densitometry and off-line gravimetry is very good and so is the agreement between experimental conversion and theoretical model predictions. A diaphragm pump was first used to pump the material around the sampling loop in BR2 (see Figure 4-8). The pump failed at a conversion of ~60%, possibly due to latex coagulation which subsequently caused the pump-around loop lines to clog up. In BR3 a gear pump replaced the diaphragm pump, but it also failed at almost the same conversion level (~65%), possibly for the same reason. All subsequent runs were performed using a screw pump with a gear reducer to pump the reacting material around.

As previously mentioned, all our experimental runs were performed using VAc monomer with its commercial inhibitor (i.e. no monomer distillation took place, which saves preparation time and effort). The observed (and expected) induction time (i.e. time elapsed before polymerization started) was ~ 35 minutes for BR2 and ~ 44 minutes for BR3 (see Figure 4-9). This induction time was estimated from three sources for runs BR2 and BR3: (i) as soon as polymerization starts, due to the highly exothermic reaction, one could see the (steam) control valve start closing, thus denoting the peak of the exotherm (ii) a blue haze was detectable from the sample vials after the first polymer particle generation, due to the

Table 4-3

Summary of Batch Runs

Run	Temperature (°C)	Weight of initiator (grs)	Weight of emulsifier (grs)	Volume of monomer (ml)	Volume of water (ml)
BR2	50	2.5	33.6	1100	3000
BR3	50	1.8	33.6	1100	2800
BR4-BR5	50	2.5	33.6	1100	3000
BR6	50	3.0	28.8	1150	2860
BR7	50	3.0	8.3	1150	2860
BR8	50	3.0	49.4	1150	2860
BR10	50	3.0	28.8	1150	2860
BR11	50	3.0	28.8	1150	2860
BR14	60	3.0	28.8	1150	2860
BR21	40	16.0	28.8	1150	2860
BR22	70	1.5	28.8	1150	2860

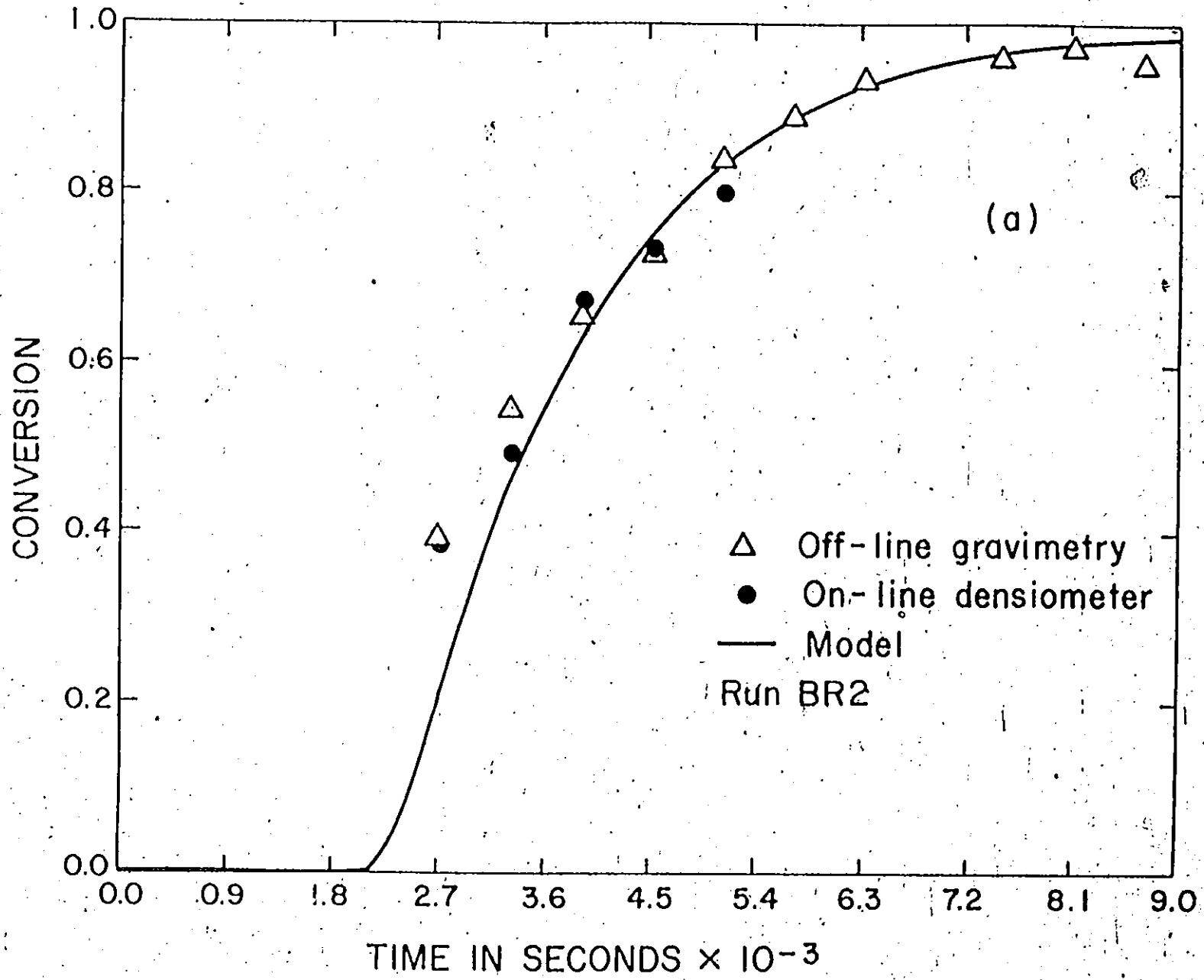

Figure (4-9). Run BR2 : On-line Densitometer Conversion vs. Time

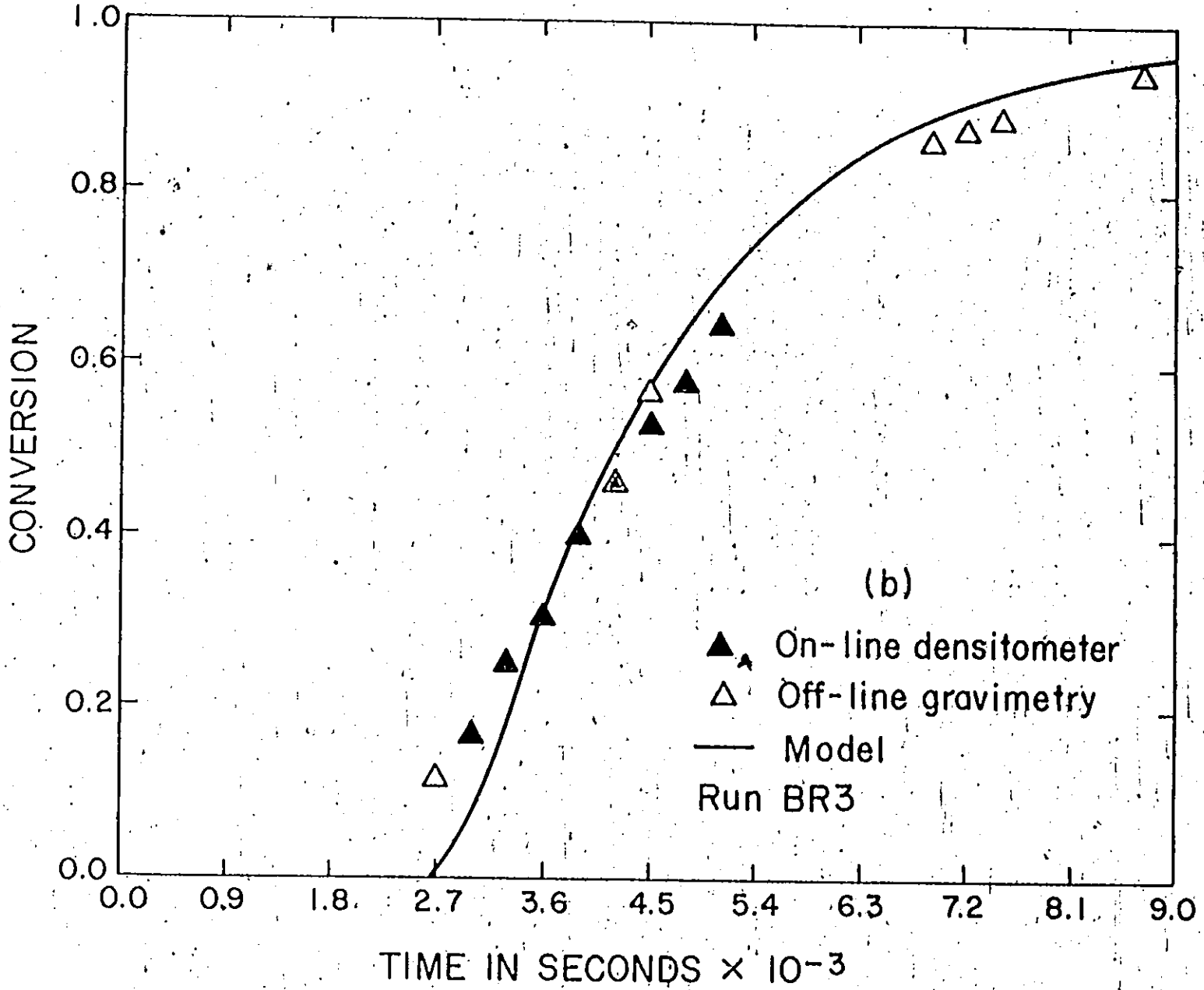

Figure (4-9) cont'd. Run BR3 : On-line Densitometer Conversion vs. Time

Tyndall effect (also, a few drops of methanol added in a latex sample should cause visible coagulation of the latex, if polymer particles are present) (iii) the on-line densitometer easily picked up density differences as soon as the first polymer particles are generated (this is clearly illustrated in Figure 4-10a, where density is plotted versus time for run BR4. The long induction time of run BR4 was caused by intentionally letting oxygen in the system through a feeding valve. As soon as polymerization started, the on- line densitometer at once picked up the density differences due to polymer formation. Figure 4-10b shows another interesting result. It is again a plot of density versus time (from the on-line densitometer) for runs BR2, BR4 and BR5. As can be seen from Table 4-3, the recipe and the conditions for all these three runs were identical. What was not identical was the amount of induction time for each run. What is very interesting, however, is the fact that the slopes of the three curves, once the reaction gets going, are very nearly the same, as they should be, verifying once more the observation that oxygen does not have a critical effect on the course of the reaction, which was previously discussed). In the subsequent runs, an on-line light source (see again Figure 4-8) was used to detect the first particle nucleation (and, therefore, the induction time) and information from this source was also combined with indications from the three aforementioned ones.

Figure 4-11 shows the conversion vs. time histories (measured and predicted) for runs BR6, BR7, BR8, BR10, BR11, BR14, BR21 and BR22. The good reproducibility of our measurements is evident from Figure 4-11a, where data from three identical runs (BR6, BR10 and BR11) are plotted. The three runs were performed in time intervals of 15 days between each other. The data in Figure 4-11c are coming from runs performed at different temperature levels (BR10, BR14, BR21 and BR22). The ability of the model to satisfactorily follow conversion in emulsion polymerization is very well illustrated in Figures 4-11a, b and c.

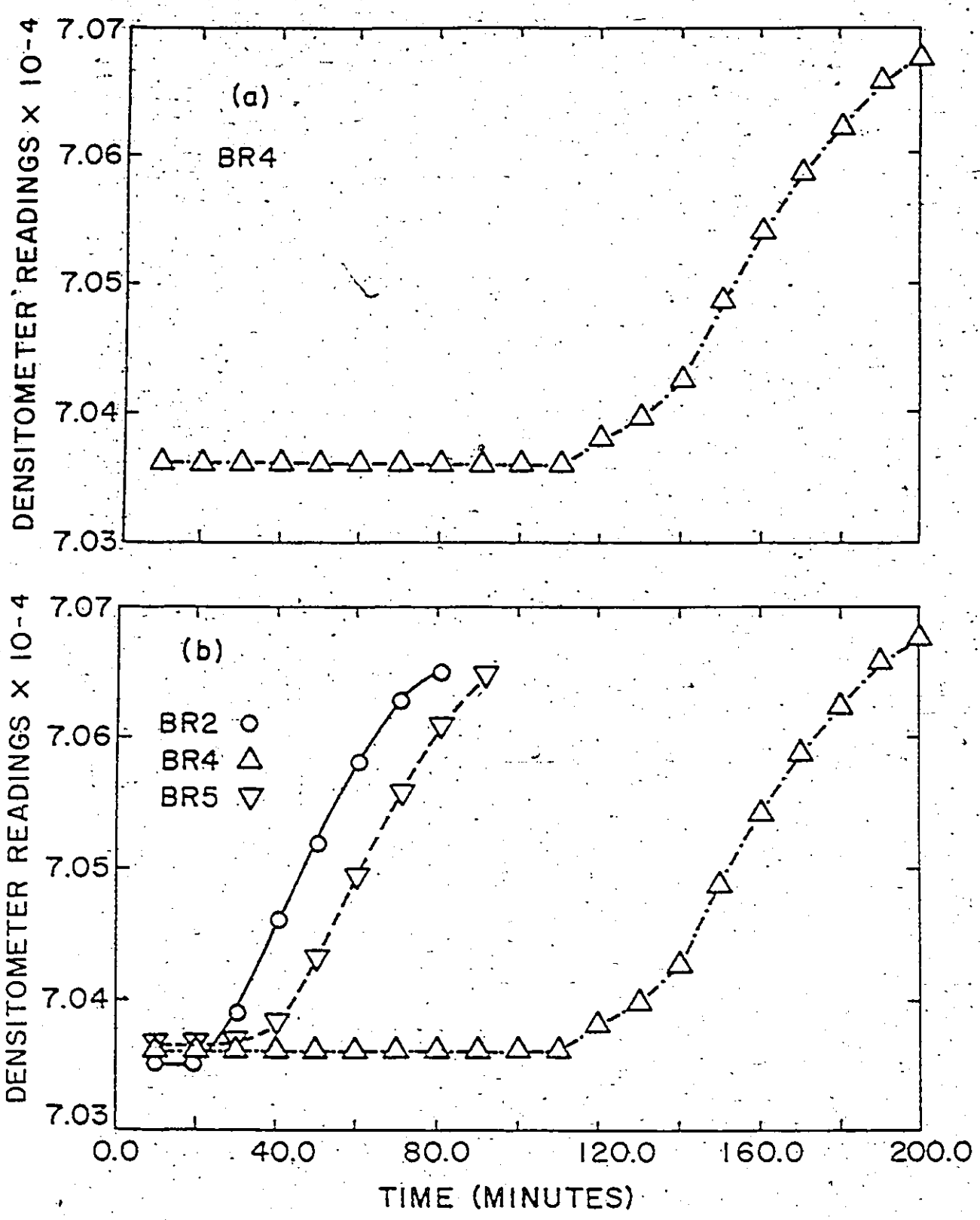

Figure (4-10). On-line Densitometry : (a) Run BR4, (b) Runs BR2, BR4 and BR5. Induction Time Effects

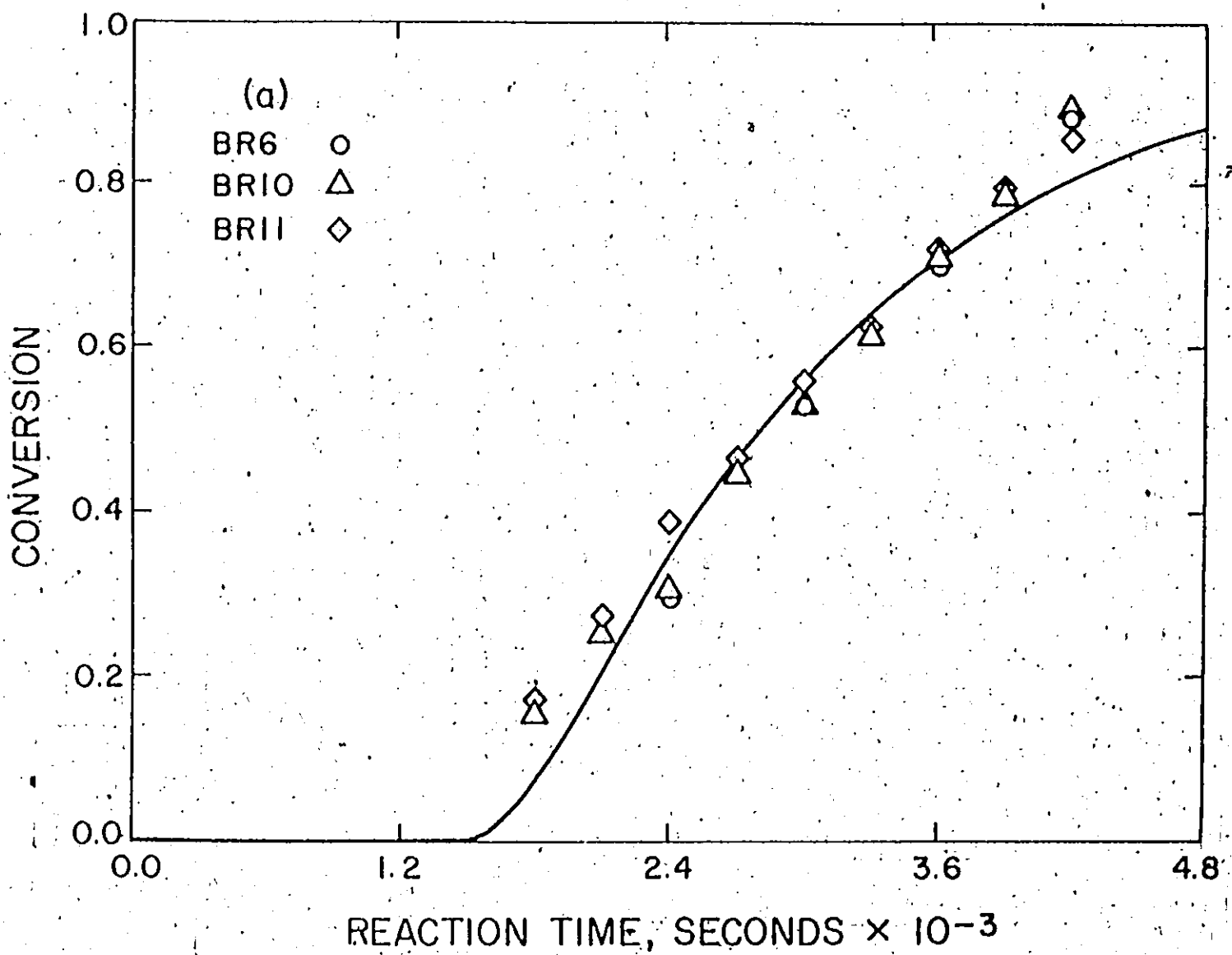

Figure (4-11). Conversion-Time Histories for Runs BR6, BR10 and BR11

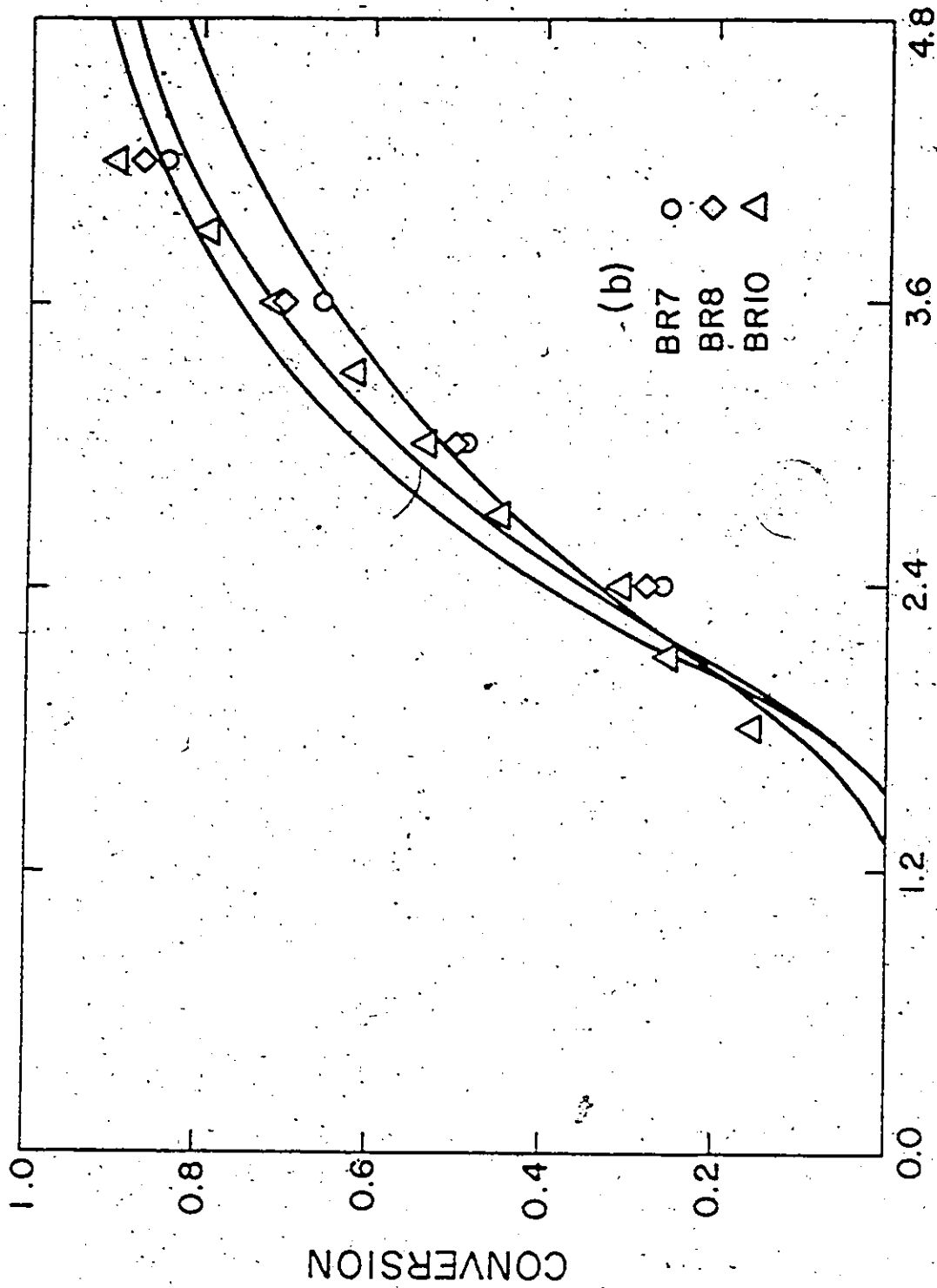

Figure (4-11) cont'd. Conversion-Time Histories for Runs BR7, BR8 and BR10

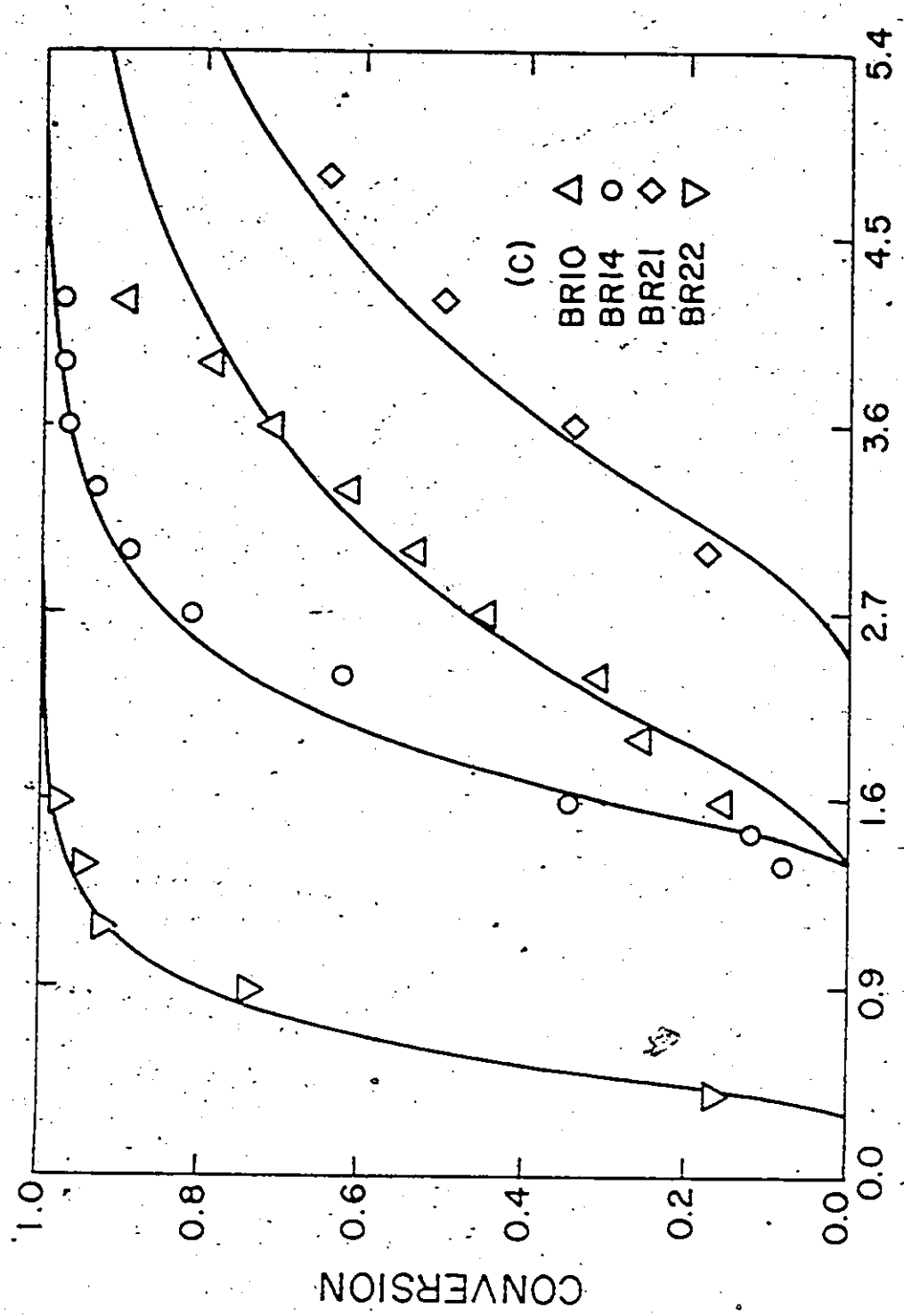

Figure (4-11) cont'd. Conversion-Time Histories for Runs BR10, BR14, BR21 and BR22

Prediction of particle size is probably the weakest point of emulsion polymerization models. The mechanisms which determine particle diameter in an emulsion system are often not only difficult to model but also difficult to even visualize or understand. Another important fact which makes the situation even more complicated is that the measurement of particle size is not a trivial task. Herein, information from several methods (which were discussed in more detail in Chapter 3) was combined in order to obtain a measure of latex particle diameter: electron microscopy (both the "cold stage" and the "particle hardening" techniques), hydrodynamic chromatography, dynamic light scattering and turbidity spectra analysis. Data from the turbidity spectra analysis for runs BR7, BR8 and BR10, BR11 are given in Figure 4-12, along with the model predictions. The agreement is quite satisfactory.

Polydispersities of the samples, calculated as ($\bar{D}_W/\bar{D}_N$) from electron microscopy, ranged from 1.010 to 1.060, an indication that the produced latex was quite monodispersed. This is in disagreement with the observations of Min and Ray (1974), Stannett et al. (1975) and Pramojaney (1982), who claimed that the particle size distributions of poly (VAc) latexes formed in batch reactors were found to be polydisperse, due to reappearance of micelles in "stage 4". Note also that the increase in polydispersity of latex particles claimed by Pramojaney (1982) was shown by simulations to considerably lower the "apparent" value of q for a polydisperse latex, which then reduced the relative growth rates of the smaller particles depending on how radicals were distributed in the polydisperse particle population, thereby producing an unexpectedly broad PSD.

The same indication about the polydispersity of the produced latexes was also obtained from turbidity analysis results, where the "apparent" particle diameter based on the monodisperse hypothesis was found to be very close to the weight average particle diameter, which is plotted in Figure 4-12.

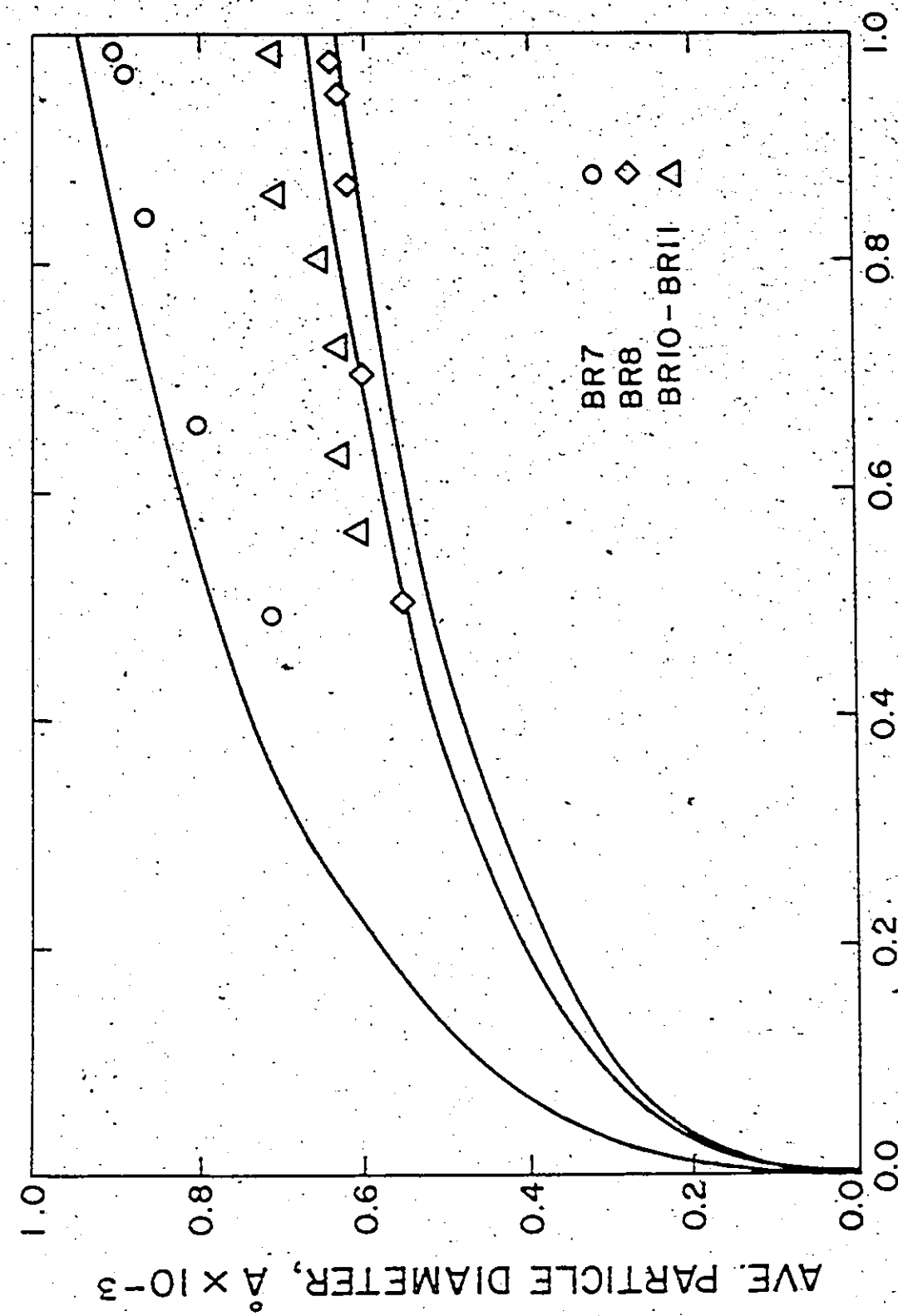

Figure (4-12). Particle Size vs. Conversion Histories for Runs BR7, BR8, BR10 and BR11

Figure 4-13 shows the molecular weight versus conversion experimental data. The experimental points in Figures 4-13a and 4-13c are coming from off-line LALLSP measurements, whereas the ones in 4-13b are coming from LALLSP on-line with GPC. The solid lines in the figure represent our model predictions. It is evident that the model agrees quite well with the experimental measurements and furthermore, both our measurements and the model's response are consistent with the fact that a higher temperature gives lower molecular weights. Looking at Figure 4-13b, one would think after the first impression that there is a quantitative discrepancy between measurements and predictions, although the trend is qualitatively the same. This is not true, however, if one considers that the experimental points are coming from LALLSP on-line with GPC. This being the case, any gel that might have been formed has been filtered out while the solution passes through the GPC column, therefore the LALLSP spectrophotometer does not see its contribution. On the other hand, an off-line LALLSP does take into account the contribution of gel, and since the model had been initially tuned with off-line LALLSP molecular weight measurements, it is expected and it should give predicted values for the weight average molecular weight higher than the measured ones from LALLSP-GPC. More on the estimation of molecular weights and branching frequency have already been given in Chapter 3.

Before concluding the Discussion section, three more points are worth noting: (i) the effect of agitation rate on the batch emulsion polymerization of VAc (ii) a few things concerning the numerical solution of the mathematical model equations, and (iii) possible extensions of the developed model. These three points are briefly discussed in what follows.

(i) The small influence of agitation rate may be seen from the conversion-time curves of Figure 4-14, where the agitation rate was varied from 80 to 200 rpm (Pramojaney (1982)). The small variation in the conversion-time curves and the negligible coagulum

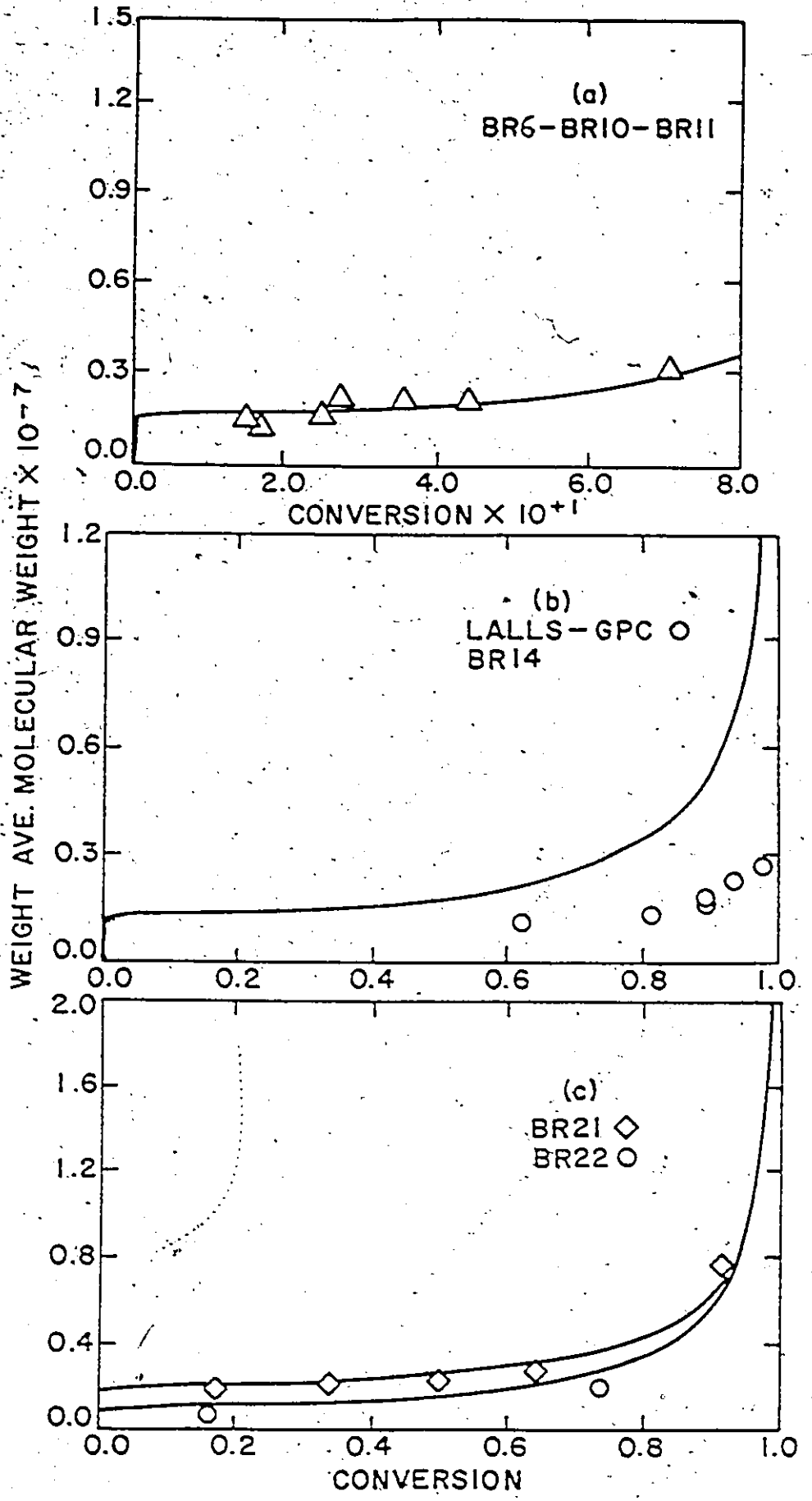

Figure (4-13). Weight Average Molecular Weight vs. Conversion Histories for Runs BR6, BR10, BR11, BR14, BR21 and BR22

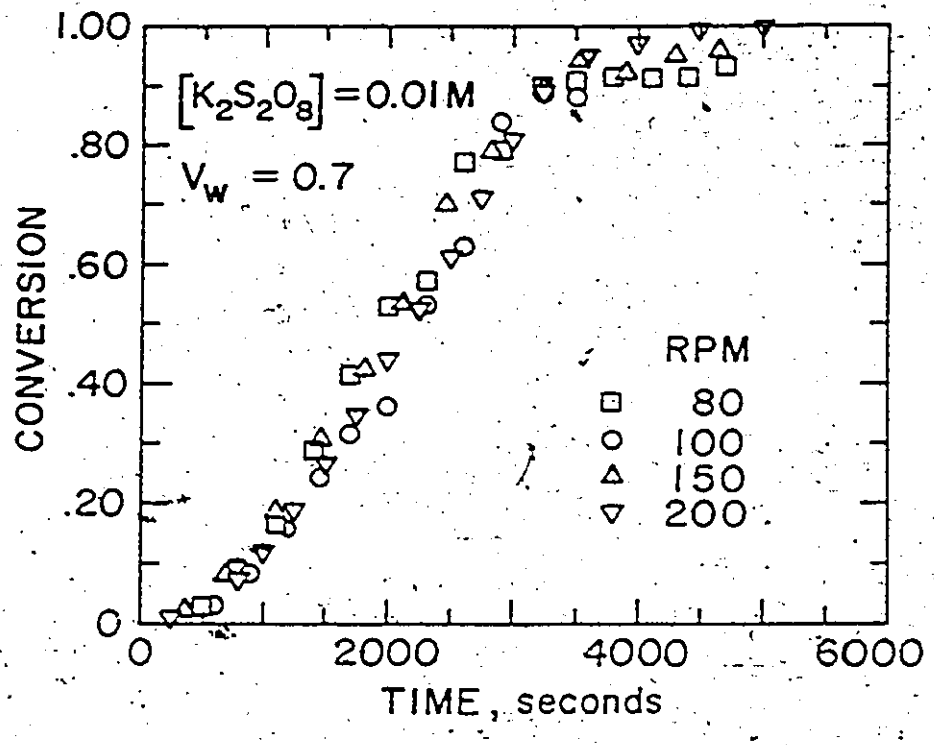

Figure (4-14). Effect of Agitation Rate on Conversion for the Batch Emulsion Polymerization of VAc

obtained experimentally indicate that the latex system is reasonably shear-stable, and the degree of agitation does not affect the reaction rate. This is consistent with our observations during this project.

(ii) Details about the numerical solution of the mathematical model equations can be found in Penlidis et al. (1984). One should remember that to economize computation time, by considering the fact that very small time-step sizes are required during the nucleation stage, but considerably larger time-steps can be safely used during particle growth, an automatic (variable) step size adjusting scheme has to be employed (e.g. the IMSL routine DGEAR).

It is rather difficult to compare the computational efficiency of the various existing models, since the extent of information expected from these models is quite different. However, it is fair to state that, despite the excessive computation time required (~ 12 minutes on a CDC 6400 computer), Min and Ray's (1978) model for a batch reactor can produce the most informative simulation, but only for a narrow range of polymerization recipes. The present model needs ~ 6.5 CPU seconds on a VAX 11/750 compared to ~ 600 CPU seconds of Min and Ray's (1978), or ~ 75 CPU seconds if a parameter estimation routine is also used for a wide variety of recipes.

(iii) The presently developed model is very versatile. It has been designed for great flexibility regarding future modifications, additions or corrections of the existing kinetic or transport mechanisms. This is illustrated in Appendix IX, where a redox initiation mechanism is developed and discussed. Information from this Appendix has been already successfully implemented in different systems (Wong (1984), Kanetakis (1984) and Broadhead (1984)).

4.5 Conclusions

A theoretical and experimental investigation of the batch emulsion polymerization of VAc has been reported. A batch reactor model, based on a polymer particle age distribution analysis, has been shown to adequately follow latex and polymer property trajectories through the treatment of experimental results from the literature and our laboratories. The model is simple, based on a minimum number of adjustable parameters and flexible enough to be further extended and modified. It provided successful latex reactor simulations under a variety of operating conditions. An investigation of particle nucleation with the model revealed that the nucleation rates are extremely rapid and very sensitive to the emulsifier level. It is clear that latex properties are very much dependent on the control of emulsifier level during polymer particle nucleation.

CHAPTER 5

SEMI-BATCH CONTROL POLICIES FOR THE PARTICLE SIZE DISTRIBUTION

5.1 Introduction

The second mode of latex reactor operation that will be studied during the development of this thesis and the progress towards more complicated reactor systems, will be that of semi-batch or semi-continuous reactors. The model which has been developed in Chapter 2 will again be used for this purpose.

Generally, semi-batch polymerization involves the continuous or intermittent addition of monomer or any other ingredient to the batch during the progress of the reaction. In emulsion systems, the monomer-swollen polymer particles can be kept starved for monomer, which leads to higher polymerization rates and also, easier control of the reaction rate. Semi-batch systems are greatly superior to batch systems for handling copolymerization reactions, as it will become evident in Chapter 6. The addition of monomer during polymerization also has the beneficial effect of providing extra cooling of the reaction mixture and thus, permitting better temperature control. Finally, semi-batch polymerization allows the potential for better particle size control of the product, as it will hopefully become obvious from the development of the present chapter.

5.2 An Interesting Control Problem

To develop effective control strategies for polymer particle concentration and subsequently, for polymer particle size, it is of considerable importance to establish the time scale for polymer particle nucleation (i.e. of stage 1). The effectiveness of any control scheme would then depend on the nucleation time. For a typical Case II system (e.g. styrene), the

number of polymer particles, $N_p(t)$ generated up to any time t during stage 1, is generally given by:

$$N_p(t) = R_I N_A t \tag{5.1}$$

Therefore, the finally produced number of particles is:

$$N_p(\text{final}) = R_I N_A t_f \tag{5.2}$$

where t_f is the nucleation time (i.e. time of completion (duration) of stage 1). If one substitutes typical values in equation (5.2), e.g. $K_sS_2O_8$ initiator at 50°C gives an R_I of about 6. x 10^{-9} gmoles/liter of latex-sec, then, to nucleate ~10^{18} polymer particles per liter of latex, the time t_f required is in the order of magnitude of 5 minutes. For Case I kinetics, this time interval can be even less than 5 minutes (see Friis and Nyhagen (1973) or Figure 4-5b of the previous chapter).

From this rough result it is clear that manipulation of initiator and/or emulsifier concentrations or flowrates to control polymer particle nucleation would not at all be an easy task, under the above time scales. In other words, the time that one has got available to interfere in the system during its first stage is very limited. What is more, equation (5.2) does not apply to Case I systems like vinyl acetate, since the total radical entry in these systems is much greater than the initiation rate, a fact that leads to nucleation periods of even shorter duration.

The particle size distribution of a fully converted latex depends on the conditions in stages 1, 2 and 3. It depends on the original PSD at the end of stage 1 and the subsequent particle growth rate of various sized particles in stages 2 and 3. The controlled addition of emulsifier during particle growth stabilizes particles without further particle nucleation. A second aspect in the control of PSD is related to the particle sticky stage which often occurs at intermediate conversion levels. During the sticky stage wall fouling and formation of

coagulum often occur. The use of semi-batch strategies is considered more effective to eliminate the sticky-stage as well as the problems that it leads to.

Min and Gostin (1979) developed a mathematical model for the semi-batch emulsion polymerization system of vinyl chloride. The model was shown to predict the bimodal particle size distribution in seeded emulsion polymerization and the results were in good agreement with pilot plant data. The following characteristics and assumptions were built into their model: (1) All temperature fluctuations of the reactor, including the initial period of heat-up, were taken into account. (2) The polymer particles were considered homogeneous with no internal structure. (3) Polymer particles were considered to be stabilized both by emulsifier and by polymer chain ends on the particle surface. (4) Polymer particle agglomeration was empirically accounted for in the model. (5) The Trommsdorf effect was considered to be present from the very early stages of the reaction. (6) Shrinkage of reacting volume due to polymerization was recognized, and (7) The reactor was considered well mixed and homogeneous with regard to temperature and reaction ingredients. The particle size distribution equations were transformed into a set of moment equations for computational efficiency and the effects of the following variables on the final latex particle size distribution were investigated: seed particle size, quantity of seed, solid content of seed and initial amount of initiator. Some of their observations follow:

(1) A large amount of seed in their runs made micelles appear at a high conversion (~32%), resulting in a bimodal PSD at higher conversions.

(2) The predicted size of small particles was 0.07 μm smaller than that experimentally measured. This was due to a much higher rate of agglomeration between small particles in the experiments than that predicted by the model. Due to the same agglomeration, the concentration of small particles decreased after micelles had disappeared.

(3) Higher solids concentration in the seed led to a greater number of particles growing into large particles. This required more emulsifier coverage and left less emulsifier available to form micelles. Therefore, only few second generation particles were formed.

(4) The model was finally used to theoretically develop techniques of metering surfactant and initiator to control the growth of small particles.

In a similar study, Gordon and Weidner (1981) developed an interesting way to control the particle size distribution of emulsion PVC by varying the rate of emulsifier addition during the polymerization. For reproducibility, the emulsifier solution should be metered according to a reaction dependent variable such as percent conversion. By monitoring the heat liberated by the reaction, the rate of monomer conversion, and therefore, the progress of the reaction could be followed. This liberated heat was accurately quantified with precise conversion measurements. The common, steady-state method of measuring the heat given off was shown to be inadequate and to lead to an appreciable error in the conversion measurements. An unsteady-state heat balance was shown to be better suited for heat transfer calculations. With conversion thus accurately measured, they developed control algorithms which would regulate the addition of emulsifier as a function of conversion and therefore, would eventually affect the PSD of the final product.

5.3 A Possible Approach to Controlling the PSD

In the batch emulsion polymerization of vinyl acetate a massive generation of polymer particles takes place during stage 1, which lasts less than 5 minutes. This is clearly shown in Figure 5-1, which represents the simulation of a typical batch run with 0.0417 gmoles/liter of water emulsifier (SLS) and 0.00222 gmoles/liter of water initiator

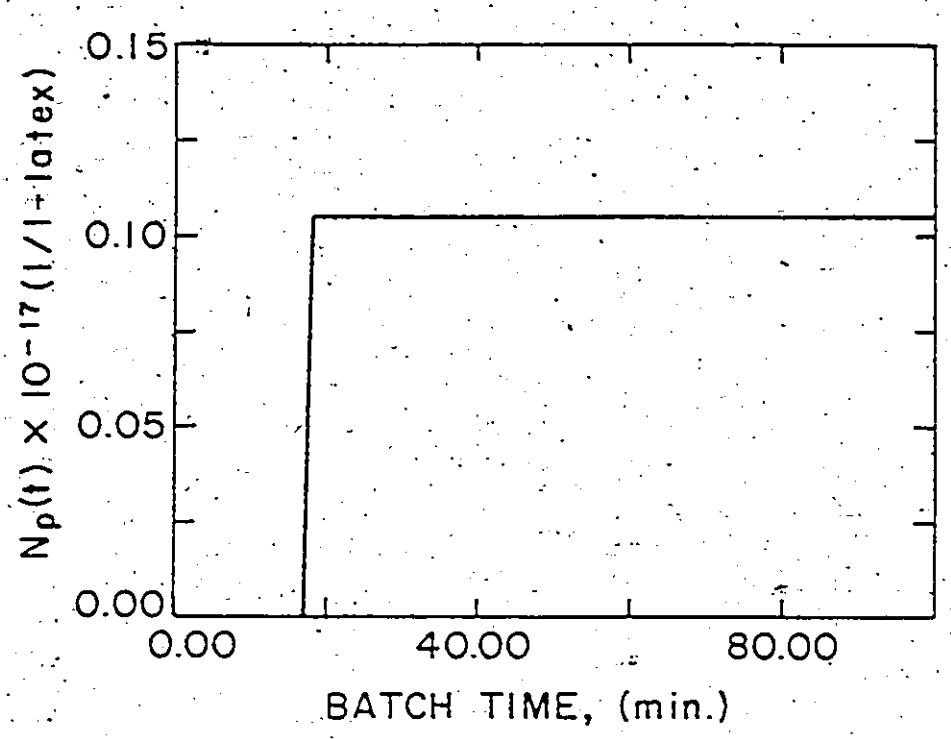

Figure (5-1). Number of Particles vs. Reaction Time for a Typical Batch Emulsion VAc Run

($K_2S_2O_8$). As it can be seen from Figure 5-1, the nucleation time or the duration of stage 1, i.e. the time elapsed from the beginning of the polymerization reaction until the number of polymer particles $N_p(t)$ assumes a constant final value, is about 3 minutes. Therefore, in a very short time one obtains the final number of polymer particles, which subsequently start to grow during stage 2. Since all polymer particles start to grow nearly at the same time, their growth rate in stage 2 will be roughly the same and the final particle size distribution will be quite monodispersed. Thus, all properties of the final product dependent on polymer particle number and size are strictly defined from stages 1 and 2, which are both completed in roughly less than 15 minutes. This time interval of 15-20 minutes was experimentally observed by several workers (Keung (1974), Friis and Nyhagen (1973)) and is also correctly predicted by the batch model. This interval is, of course, not sufficient for feedback control action to be taken according to the progress of the reaction, especially if one would like to apply on-line feedback control based on latex property trajectories. Furthermore, if the initial PSD is narrow, the final PSD will be narrow and one has to be satisfied with the final product without having the capability and flexibility of interfering in the system and thus regulating the final properties according to the various demands. Therefore, it would be of interest if one could find a method, which would be able to extend the particle nucleation time (i.e. the duration of stage 1), and thereby broaden the PSD and control the number of particles generated.

In the vinyl acetate case the situation is complicated by the fact that the critical conversion x_c is ~20%, i.e. droplets disappear at low conversions, as compared to x_c for vinyl chloride which is ~75%. Depending on the recipe, homogeneous nucleation can be important for the early stages of polymerization, since $\sim 10^{12} - 10^{15}$ polymer particles can be generated by homogeneous nucleation in the absence of micelles (a typical homogeneous batch run is shown in Figure 5-2). The amount of emulsifier has to be chosen such that it would guarantee

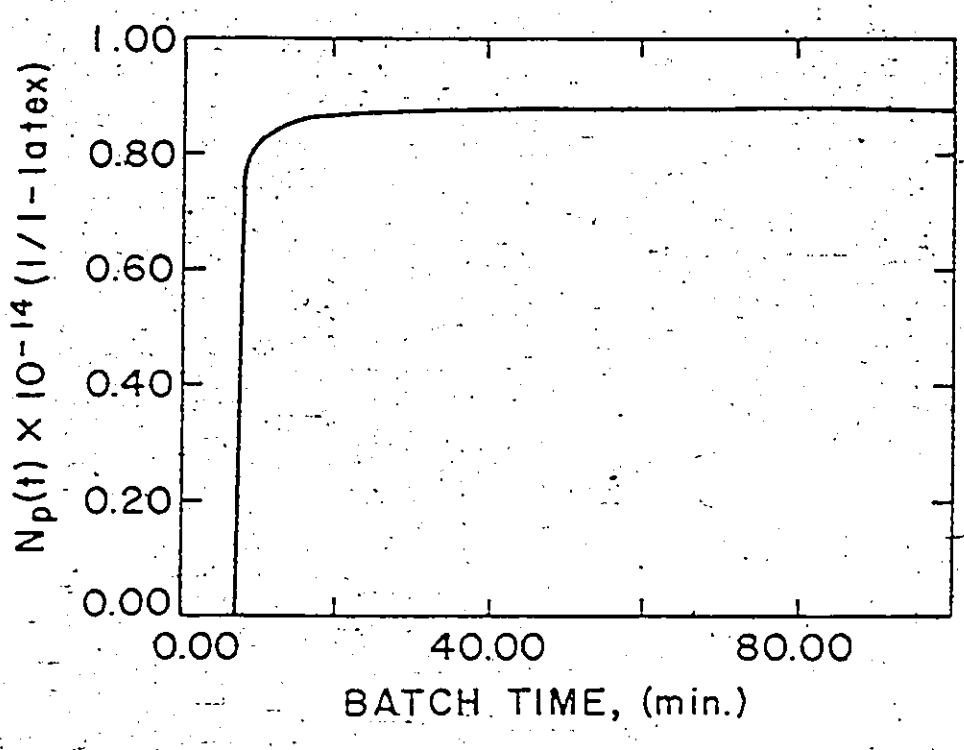

Figure (5-2). Number of Particles vs. Reaction Time for a Typical Batch Homogeneous Emulsion VAc Run (I_F = 0.005 gmoles/lit water)

a particle surface coverage of ~70% during the whole range of conversion, since the system is very sensitive to particle agglomeration. Finally, desorption of radicals from polymer particles into the water phase is very important, causing at any instant the total radical entry into particles to be greater than the radical generation by initiator decomposition.

In the vinyl acetate case, the number of polymer particles generated is almost independent of initiator concentration. On the other hand, the emulsifier concentration has a pronounced effect on the number of particles formed. Therefore, this latter variable might be used in the effort to extend the nucleation time. The idea to be tested would be to feed the emulsifier in pulses or use a very slow constant feed rate and thus cause a series of consecutive particle generations, each one of them lasting until the free emulsifier level in the reaction mixture $A_m(t)$ becomes less than the critical micelle concentration (CMC). The pulses or the slow emulsifier feed rate will stop when $N_p(t)$ reaches a desired constant value. This point would be the end of stage 1. It might also be possible by feeding the emulsifier in pulses or by using a very slow feed rate to generate bimodal or multimodal particle size distributions. (Equally, one could use the alternative approach of seeding with particles at prespecified times without causing any internal particle generations). In other words, the previously mentioned manipulation of emulsifier feed rate in the semi-batch mode would not only provide a time period sufficient to exploit feedback information from the reacting system, but it would also enable one to achieve effective control over the particle size distribution of the produced latex.

5.4 Extension of Stage 1

A series of simulation runs were performed using arbitrarily chosen pulses of emulsifier and manipulating the emulsifier feed rate or the total amount of emulsifier in the reaction mixture. The results proved once more that the system was extremely sensitive to

emulsifier adjustments. Since developing feed policies for emulsifier directly appeared to be very difficult due to the sensitivity of the particle generation period to small changes in it, a more fundamental approach was taken whereby $A_m(t)$, the free emulsifier level in the reactor, was manipulated to give the desired PSD. The emulsifier feed rate policy needed to give this $A_m(t)$ was then solved for. If $A_m(t)$ is less than zero, then no micelles exist in the system and the micellar contribution to particle generation is zero. If $A_m(t)$ is zero, then this means that the amount of total emulsifier present in the system is such that it can bring the micellar concentration up to the CMC and cover the existing polymer particles. Finally, if $A_m(t)$ exceeds the zero level, then the total emulsifier present in the system is used partially to completely cover the surface of the existing polymer particles, to bring the micellar concentration up to the CMC level, and the remainder to exceed the CMC level and thus form micelles. These micelles will contribute in generating new polymer particles, which in their turn will contribute in causing an increase in the total particle surface area, which has to be covered by soap. Thus $A_m(t)$ will fall again and the previously described cyclical process will occur again, if soap is fed at a high enough rate.

If $N_p(t)$ is the desired total number of polymer particles, then theoretically, if $A_m(t)$ is forced to exceed the zero level N times by such an amount which would be capable of generating a number of $(N_p(t)/N)$ polymer particles each time, $N_p(t)$ polymer particles will be finally generated in N consecutive particle generations. And since each generation can be forced, at least in the simulations, to occur between desired points in time, the above method would be able to extend the duration of stage 1 to some desired time scale.

Figure 5-3 shows the adjustment of $A_m(t)$ which would give five successive particle generations. Figure 5-4 gives the number of polymer particles as a function of time. The five consecutive generations can be easily seen and a comparison with Figure 5-1 clearly shows

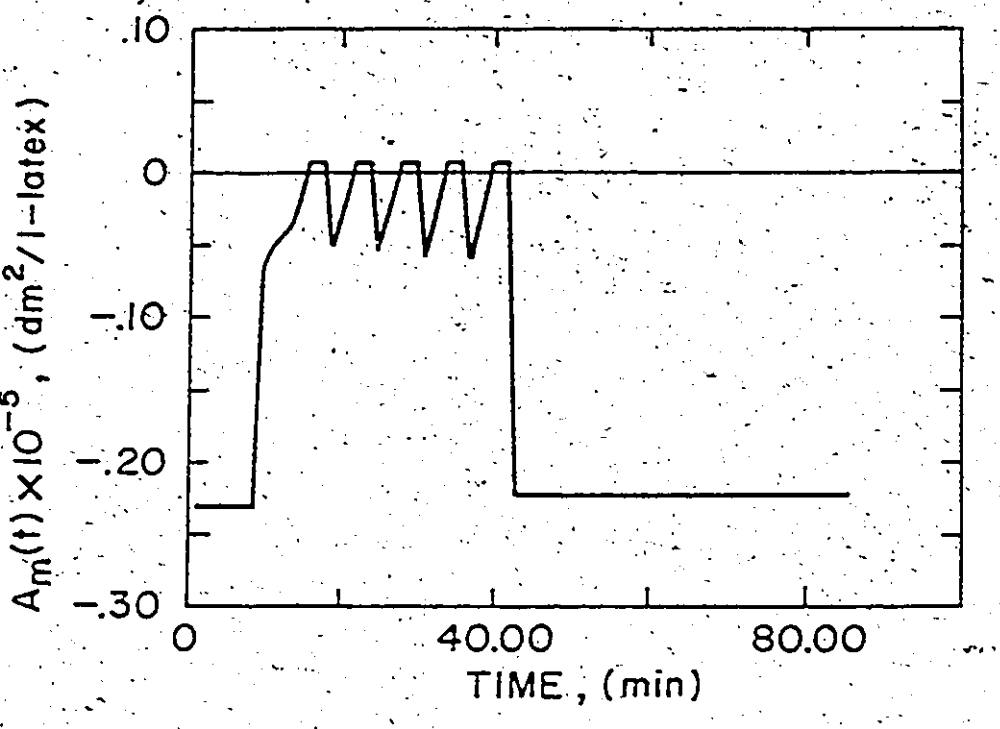

Figure (5-3). Variation of $A_m(t)$ in order to Obtain Successive Particle Generations (I_F = 0.005 gmoles/lit water)

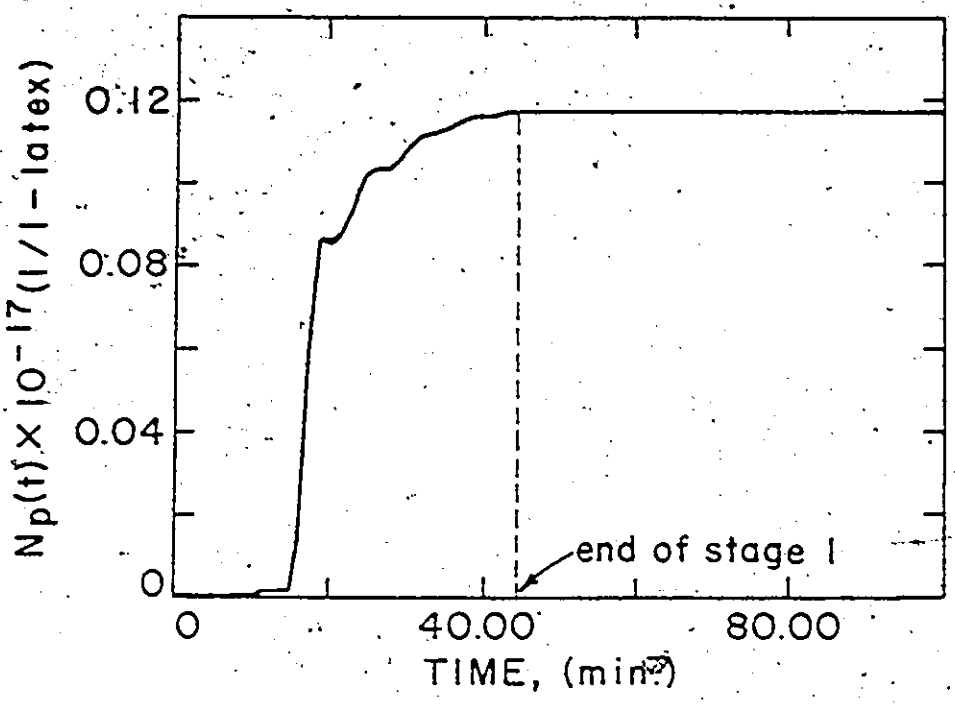

Figure (5-4). Number of Particles vs. Time Corresponding to the $A_m(t)$ Variation of Figure (5-3).

the improvement as far as the duration of stage 1 is concerned. In Figure 5-4 the number of polymer particles assume their final constant value after ~40 minutes, which was the final objective. In Figure 5-5 the previous picture of $N_p(t)$ versus time is compared with the new one, which was obtained by adjusting $A_m(t)$.

5.5 Emulsifier Feed Rate Policy

Although $A_m(t)$ was used in the simulations as the adjusted variable to extend the particle nucleation time, it cannot be used in practice because it is difficult to follow it during the course of the reaction. Additionally, even if it were possible to follow it during the reaction, its level would be regulated from the emulsifier feed rate. Therefore, it is necessary to see what sort of emulsifier feed rate policy the previous $A_m(t)$ versus time history shown in Figure 5-3 would suggest. Before doing that, it should be mentioned here that a series of simulation runs were performed using the identical adjusted $A_m(t)$ policy of Figure 5-3 and different initiator levels, all of which gave the same results and the same final $N_p(t)$ versus time picture, since $N_p(t)$ does not depend on initiator level. The run with an initiator level of 0.005 gmoles/liter of water was chosen to be presented here.

Figure 5-6 shows the total particle surface area as a function of time for the adjusted $A_m(t)$ policy of Figure 5-3, and an initiator level of 0.005 gmoles/liter of water. Figure 5-7 shows the total emulsifier level in the reaction mixture as a function of time, as it was back calculated from the $A_m(t)$ changes. Since

$$\frac{dS_T(t)}{dt} = S_F(t) \tag{5.3}$$

where $S_F(t)$ represents the emulsifier feed rate in gmoles per unit time per unit volume, Figure 5-7 suggests a constant emulsifier feed rate given by the slope of the total emulsifier level in the reactor versus time curve.

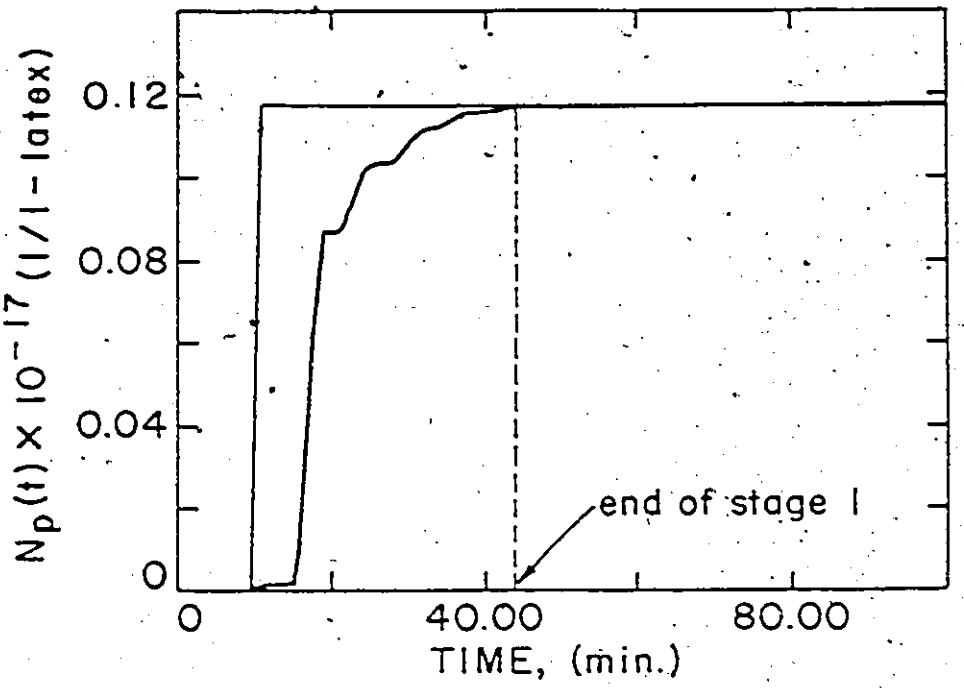

Figure (5-5). Comparison of $N_p(t)$ Between the Usual and the Extended Case (I_F = 0.005 gmoles/lit water; S_F = 0.0437 gmoles/lit water for the Usual Case).

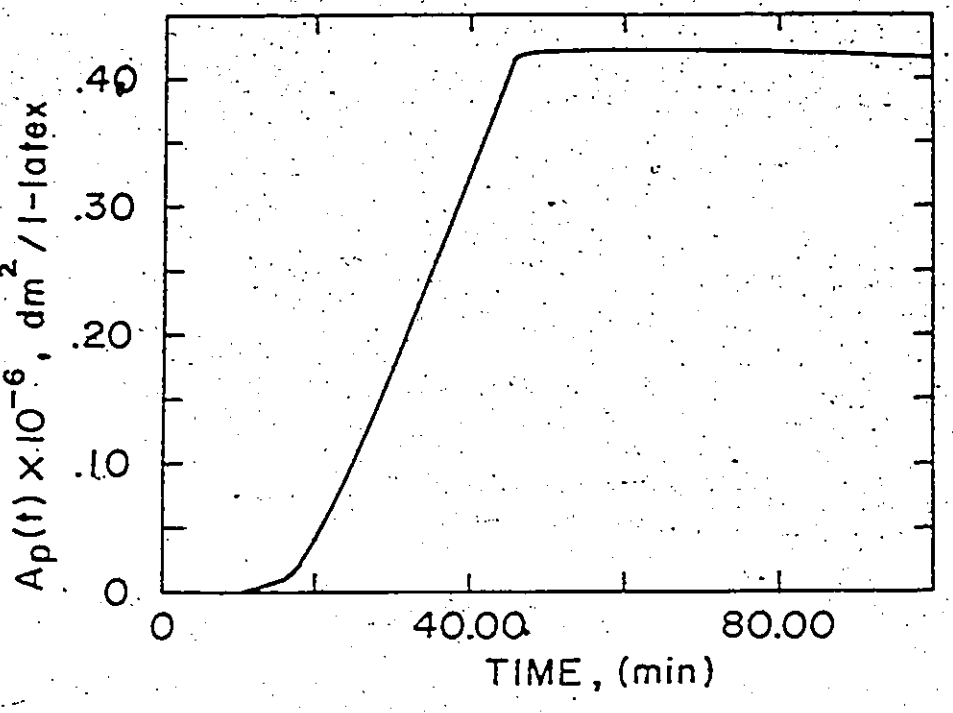

Figure (5-6). Total Polymer Particle Surface Area Corresponding to Figure 5-3 Variations

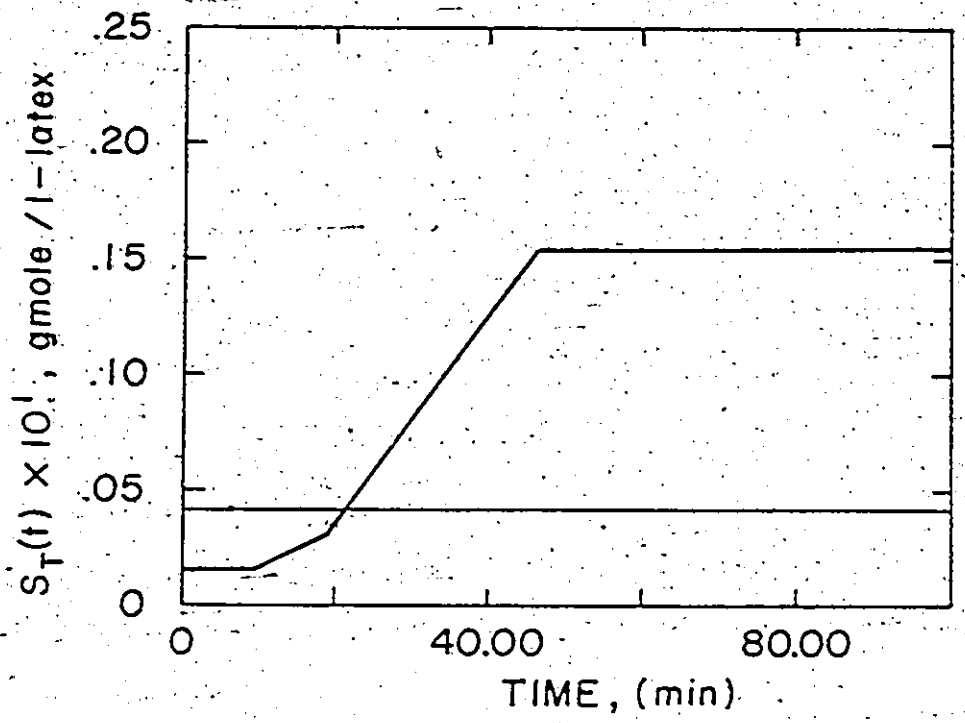

Figure (5-7). Total Emulsifier Level in the Reactor Corresponding to Figure 5-3

5.6 Conclusions

It has been shown how by treating $A_m(t)$ as a manipulated variable, a valid dynamic model can be used to identify and propose a theoretical strategy which would enable one to extend the nucleation stage 1 in the semi-batch emulsion polymerization of VAc. This approach would also allow one to manipulate particle size and create multimodal particle size distributions if so desired. It is recognized of course that, in practice, nobody could guarantee a linear evolution of $A_p(t)$ as the one described in Figure 5-6. The fine control over the emulsifier feed rate necessary to achieve the desired $A_m(t)$ may be possible. Also, the assumption of instantaneous equilibration of the emulsifier among the water, particles and micelles may not be valid. Events in Case I systems happen so fast and particle generation is so massive that, perhaps, the proposed strategy is not very easily applicable. The proposed strategy could be applicable, though, in systems where things happen in a slower fashion, e.g. Case II systems like styrene or butadiene. Anyhow, the major contribution of the chapter is to show that a valid mathematical model can easily be employed to identify and suggest strategies, the feasibility of which can be subsequently tested or not, depending on mere engineering common sense and understanding of the process in question.

CHAPTER 6

CONTROL OF POLYMERIZATION REACTORS

6.1 Introduction

Due to the complexity and non-linearity of the problem of polymer reactor control, little work is available in the literature on this topic, especially concerning practical experimental applications. Many workers in the area of process control readily acknowledge that there is a wide gap between process control theory and its application to the polymerization, or more generally, to the chemical industry. Part of reason for this gap is that most conventional control theory is for continuous processes with measured outputs, and can often be superimposed on top of an existing system. On the other hand, in complex polymerization processes a detailed mechanistic understanding of the process is often necessary to develop a valid control policy. Only recently have adequate theoretical models been developed.

Before attempting an application of the theories developed in the previous chapters in an effort to solve the main control problem with conventional latex reactor trains (Chapter 7), a critical discussion concerning control of polymer reactors in general, will be given in this chapter.

6.2 General Trends

The demand for polymers and polymer latexes having special properties and improved performance has led to a rapid increase in industrial and academic interest in advanced computer modelling and control of polymer reactors. This chapter presents a survey of recent literature on the optimization and control of specific polymer and latex properties,

including: particle size distributions, copolymer composition, molecular weights and branching frequencies. Mathematical models and on-line sensors which are of central importance to these methods are also reviewed.

The automation of batch and semi-batch polymerization reactors has gained rapid acceptance over the past decade. The ability of digital computers and programmable controllers to handle precisely the monitoring and sequencing of the many steps necessary in charging, heating and running batch reactors has resulted in improved quality, safety and operating costs. Excellent reviews of some of the methods used and some reported industrial applications have been given by Amrehn (1977) and Hoogendoorn and Shaw (1980). Those reviews also covered the considerably fewer applications of computer control to continuous processes. Most of the reported installations fall under the heading of what one might call computer automation. Either existing sequencing and control procedures have been taken over by the computer or more complex automation made possible by the computer has been initiated. Polymer quality improvements have largely resulted from the greatly reduced variation in these procedures from one batch to the next.

Improvements in quality that might be possible through the use of optimal policies in feedback control schemes are still limited by the lack of reliable and robust on-line polymer characterization instrumentation. In spite of the difficulties yet to be overcome, enormous improvements in the quality of models for polymerization processes, in polymer characterization techniques, and in on- line instrumentation have been made in recent years. The trend is continuing so rapidly that we expect that the 1980's will see the appearance of higher level optimization and computer control schemes throughout the polymer industry. It is therefore our intention in this chapter to survey recent literature on the modelling, measurement and control of polymer and latex properties. In doing this, we obviously will put

much less emphasis on current industrial practice and more on current research and development work.

The chapter is organized as follows. Models for various polymerization reactors are reviewed in the next section. Some of the on-line monitoring instruments currently being used or else in the development stage are reviewed with respect to their potential utility in controlling polymer reactors. Optimization and control policies for batch and semi-batch reactors are surveyed with respect to the property being controlled (molecular weight, branching, composition, conversion, particle size, etc.). Finally, literature on continuous reactors is discussed with respect to the optimization of operating policies, the design of reactor systems, the estimation of unmeasured states, and the potential for on-line control of polymer or latex properties.

6.3 Polymerization Models

Polymer reactor control is a fascinating area because of the diversity of products obtained from even a single monomer. Polymers may be produced with wide ranges of molecular weights and compositions. They may be produced in a homogeneous reaction medium (bulk or solution polymerization) to produce a plastic, fiber, or rubber product, or in a heterogeneous medium (emulsion polymerization) to give a latex product. The polymerizations are also carried out in a variety of reactor types: batch, semi-batch, and continuous flow stirred tank or tubular reactors. However, very few commercial or fundamental polymer properties can be measured on-line. Therefore, if one is to develop control strategies to achieve desired polymer or latex properties under such a variety of conditions, it is important to have a good mechanistic model capable of predicting at least the major effects of the process variables.

As stated earlier in this thesis, models for polymerization reactors vary tremendously in their complexity. The level of sophistication needed depends upon the intended use of the model. In practice, there are two levels of mechanistic model. The first type of model simply involves the reactor material and energy balances, and is used to predict the temperature, pressure and monomer concentrations in the reactor. Such models are useful for the design of reactor and control systems for homogeneous polymerization. However, they do not predict polymer quality variables such as molecular weights or branching frequencies. Second level models, which predict these as well, can be used to optimize the reactor operation to achieve a desired final polymer quality or to infer these properties throughout the course of the reaction. As illustrated by Ray (1980), the coupling of the model equations often is such that the level one models do not depend strongly on polymer properties, and so the two parts of the second level models can be solved separately. In emulsion polymerization, however, the level one balances are strongly coupled with the polymer particle population balances, thereby making approximate level one models of limited value.

A review of recent work on dynamic models for polymerization reactors was given by Ray (1980). In the following subsections, we shall add to his review and discuss some different aspects of these models.

6.3.1 Homogeneous Polymerization (Bulk and Solution)

Many common polymers are produced in a homogeneous reaction medium; the free radical bulk polymerization of styrene and methylmethacrylate, the condensation polymerization of polyesters and nylons, and the ionic polymerizations of butadiene and styrene, to mention a few. Suspension polymerization, although two phase, can be treated as a homogeneous system as well.

At low conversions and viscosities the material and energy balances for these polymerization systems are reasonably straightforward. General overviews of these models are given in Ray (1972) and Ray and Lawrence (1977).

At high viscosities, fluid dynamic and heat transfer considerations become very important. The model predictions will depend critically upon how these mixing and heat transfer phenomena are handled. Hamer et al. (1981) and Schmidt et al. (1982) have modelled the homopolymerization and copolymerization of MMA and VAc in an ethyl acetate solvent carried out in a CSTR. Multiple steady-states were predicted in various operating regions depending upon heat transfer rates and solvent flow rates. Hamer (1983) modelled the same polymerizations in a tubular reactor. The mixing and heat transfer were shown to be dominant effects in predicting results.

With soluble-coordination catalysts, the major problem is an inadequate understanding of the nature of the catalytic mechanisms. A number of different proposed kinetic mechanisms are able to explain the same observable effects of the catalyst components on the conversion and molecular weight behaviour. Kelly (1985) has recently summarized some of the mechanisms and proposed some dynamic models for the solution polymerization of butadiene.

6.3.2 Heterogeneous Polymerization (Emulsion, Precipitation, Solid Catalyzed Ionic)

Heterogeneous polymerization systems present additional difficulties for the modeller. In these systems there is more than one phase, and hence material balances and, in some cases, heat balances are required for each phase. Furthermore, their behaviour is critically dependent upon the concentration of polymer particles, and on the particle size distribution.

Emulsion polymerization systems have been discussed in Chapter 2 and the reader is referred back to that chapter to review recent efforts on the modelling of emulsion reactors (see Table 2-1) and the accompanying problems.

Precipitation or dispersion polymerization occurs when the polymer is insoluble in its monomer or a solvent and so precipitates out to form polymer-rich particles. It is carried out in solution, bulk, or suspension systems. Examples are the bulk polymerization of vinyl chloride and acrylonitrile, and the suspension polymerization of vinyl chloride. Models which ignore the formation, growth, and coalescence of the individual particles have been shown to give good predictions of conversion and molecular weights (Abdel-Alim and Hamielec (1972)). Population balances have been treated by Liss et al. (1972). Precipitation of polymers in the water phase (e.g., acrylonitrile) can be treated as emulsion polymerization with only homogeneous particle nucleation operative. One of the most difficult problems to account for is particle coalescence.

Modelling the solid catalyzed (Ziegler-Natta) polymerization of olefins (polyethylene and polypropylene) involves treating the additional problem of mass and heat transfer in the growing polymer particles (Böhm (1978), Boor (1979)). Some recent attempts at modelling these systems are reported by Nagel et al. (1980), Michael and Reichert (1982), Lawrence and Chiovetta (1983), Meyer (1983), and Michael and Reichert (1983).

6.4 Measurements

The weakest link in polymer reactor control schemes is undoubtedly the on- line instrumentation. Without some form of on-line polymer characterization, the monitoring and feedback control of polymer quality is not possible. Recently, advances have been made in the development of on-line measurements, but as yet, the use of these instruments has largely

been confined to the monitoring of laboratory reactors. Other measurement problems arise in the monitoring and control of the reactor environment - its temperature, level and flows.

6.4.1 Measurements for Reactor Operation

(i) Temperature: Even temperature measurements can sometimes present problems in polymer reactors due to fouling of the measuring element, which can result in an increased time lag in the sensor dynamics. An interesting solution to severe problems of this sort is to control the reactor head space pressure instead of the temperature, and infer temperature through vapour-liquid equilibrium relationships (Hopkins and Alford (1973)). Some schemes of compensating for the dead time in the control loop have been reviewed in Hoogendoorn and Shaw (1980).

(ii) Flows: One of the most consistently troublesome problems is that of regulating accurately the flows of monomers, initiators, modifiers, etc., to the reactor. Emulsion polymerization is particularly sensitive to small variations in emulsifier and initiator flows (particularly in redox systems). Precision metering pumps, although expensive, allow accurate and reproducible flow. Equipped with variable speed motors or variable stroke activators, they also provide a means of regulating these flows to achieve improved polymer quality. The recent introduction of very accurate mass flow meters based on the Coriolis principle, offers another more accurate means of monitoring and controlling these flows (see Micro Motion Model C, Mass flow meter instruction manual, Micro Motion Co.). Batch feed make-up in tanks on load cells has been used extensively, but is awkward and offers little flexibility for on-line control. The accurate metering of solids continues to be a problem in continuous and semi-batch operation.

(iii) Level: In some instances, there are substantial advantages to running continuous reactors full (no head space), but in other situations, such as in condensation

polymerization where this is not possible, level control can be a problem. Differential pressure measuring systems are subject to plugging. Nuclear instruments are usually more satisfactory, provided the signals are properly conditioned and foaming is controlled.

6.4.2 Polymer and Latex Property Measurements

Most polymer and latex properties are difficult to measure even off-line in the laboratory. Gel permeation chromatography is used extensively with a variety of detectors to obtain molecular weight, composition, and sequence length information. Nuclear magnetic resonance (NMR) instruments can be used to obtain composition, sequence length and other structural information about the polymer produced. Low angle laser light scattering instruments provide precise weight-average molecular weights, and osmometry provides number-average molecular weights. Hydrodynamic or size exclusion chromatography can be used to obtain particle size distributions. Electron microscopy is also a powerful, but tedious way of obtaining particle size information. Although not practical for on- line measurements, these instruments are necessary in polymer reaction engineering research to assess the effects that reactor variables have on polymer properties, and to develop comprehensive mathematical models that can be used for optimization and control. Presently, there are only a limited number of on-line measurements that can be related to more fundamental polymer and latex properties, or to polymerization conditions in the reactor. A few of these will be briefly discussed below. Details concerning density measurements, hydrodynamic chromatography, turbidity spectra and surface tension measurements have already been given in Chapter 3 and will not be repeated here again.

(i) Reactor heat balances: On-line enthalpy balances around the reactor and the reactor cooling jacket can be used to monitor the instantaneous heat release by reaction. This can be used directly in temperature control schemes (Amrehn (1977)), or it can be used to

monitor the instantaneous rate of reaction or the conversion in the reactor (Gordon and Weidner (1981), Harris and Rushing (1982)). The major difficulty lies in accounting for the propagation of all the temperature and flow rate measurement errors into the calculated heat release term. Acceptable results are usually achieved by rapid sampling, and then averaging or filtering all the measurements over short periods of time.

(ii) Viscosity: The progress or status of the degree of polymerization in batch or continuous reactors can be measured using on-line viscometers. Correlated measures of melt viscosity such as stirrer power, pump speed or power, or pressure drop in exit lines from a continuous reactor are often used for this purpose.

(iii) Gas chromatography: Copolymer composition can be inferred by on- line measurements of the residual monomer composition combined with a reactor material balance. Gas chromatography with automated sampling valves can be used to obtain this analysis on-line (Guyot et al. (1981), Campbell (1985)). In some instances, the gas in the reactor head space is analyzed, and the composition and conversion of the monomers in the reacting liquid are inferred through vapour- liquid equilibrium relationships.

(iv) Optimal sensor selection: This is a fairly new area and a very interesting one. The development of on-line sensors is a very costly and time- consuming process. Therefore, if one has available a dynamic model of the process which predicts the various polymer (or latex) properties of interest, then this can be used to guide one in the selection and development of sensors. Pollock (1984) uses ideas from the optimal statistical design of experiments together with models expressed in the form of a Kalman filter to select those combinations of existing or hypothetical sensors which would maximize the information that could be obtained on the states of the polymerization system. Both the type of sensors and the precisions necessary for them are easily investigated in this way. Duijfjes (1975) approached

a similar problem using measurements of observability and controllability to select measurements most suitable for control.

6.5 Batch and Semi-Batch Reactor Control

Most batch or semi-batch polymerization control systems consist of a preprogrammed recipe addition, a start-up and shut-down scheduler, and temperature controls based perhaps on a heat balance. However, few of these systems are aimed at optimizing polymer properties through implementing a selected trajectory, or through changing reactor conditions based on the feedback information from on-line measurements. In this section, we survey work that has been performed in these latter two areas, namely optimization policies, and on- line monitoring and control aimed at achieving desired polymer properties.

Batch reactors are used extensively for homopolymerizations, but in general, they are not ideal for polymerizations involving more than one monomer because of the composition drift that results from the different reactivities of the various monomers. By operating the reactor in a semi-batch mode, one has the flexibility to eliminate this composition drift, and to respond to property variations resulting from batch to batch variations in the polymerization conditions. Several optimizing and control policies aimed at handling such important properties as molecular weights, composition and conversion, branching, and particle size distributions in batch and semi-batch polymer reactors, have been suggested.

6.5.1 Molecular Weight Distribution Control

Several authors looked at the problem of attaining the desired MWD in bulk free radical polymerizations using either temperature variations or semi- continuous operations

involving adding combinations of initiator, monomer, transfer agent or chain stopper (Hoffman et al. (1964), Beste and Hall (1966), Osakada and Fan (1970), Sacks et al. (1973) and Kwon and Evans (1975)). The necessary temperature variations or feed rate trajectories or even the optimal design and selection of the reactor system (Shastry et al. (1973a, 1973b)) were theoretically derived using such methods as Pontryagin's maximum principle, pattern search techniques or nonlinear system synthesis techniques. Only a few papers have reported experimental verification of these methods. Sacks et al. (1973) reported experimental results on temperature policies using methyl methacrylate and styrene initiated by 2,2'-azobisisobutyronitrile (AIBN). Wu et al. (1982) were concerned with the determination of optimal (minimum time) temperature histories for the bulk thermal polymerization of styrene. They gave a good literature review of similar efforts, and compared their theoretical predictions with experimental measurements of conversion and molecular weights. The good agreement suggested that policy improvements are possible in batch polymerizations. A time saving of 18% was realized in an "optimal" polymerization when compared to the isothermal process. Macoveanu et al. (1977) used a model to establish temperature programs for obtaining certain average molecular weights in poly(vinyl chloride) suspension polymerization at constant rate. For an allowed temperature range and polymerization rate, a computer would solve for the required temperature program. Chen and Jeng (1978) studied the minimum end time problem for the bulk polymerization of styrene in a batch reactor by considering the polymerization temperature and the initial initiator concentration as the two control variables. Experimental verification of the results of their numerical calculations seemed promising for conversion but not so for the number average chain length.

6.5.2 Conversion and Composition Control

On-line enthalpy balances around the reactor and cooling jacket are used widely throughout the polymer industry to monitor the heat release by reaction, and thereby the conversion in the reactor. For batch or semi-batch reactors, unsteady-state balances are usually needed to achieve acceptable results (Gordon and Weidner (1981)).

The problem of using temperature variations to maintain a specified copolymer composition distribution in a batch (or a plug-flow) reactor was considered by Ray and Gall (1969), when MWD effects were not critical. The advantages of temperature control, rather than monomer addition, were discussed and the necessary and sufficient conditions for temperature control in the face of monomer depletion were mathematically derived. Tirrell and Gromley (1980) used these ideas to investigate optimal temperature policies for composition control in the styrene/acrylonitrile batch copolymerization. However, such temperature policies are not really practical. They are based on small changes occurring in the monomer reactivity ratios with temperature. These changes are usually so small that the statistical confidence intervals for the changes are much wider than the magnitude of the changes, and, even accepting these changes as known, the temperature variations necessary for composition control could be in the order of 100°C. Obviously, the molecular weights and other properties would suffer greatly even if the reactor heating system could handle the demands upon it.

There are several semi-batch feed policies that can be used to maintain constant copolymer composition throughout the polymerization. One policy would add all of the slowest reacting monomer and part of the faster monomers to the reactor at time zero to provide the monomer ratio which would give the correct instantaneous copoymer composition. The faster monomers are then fed in over time at feed rates which will maintain the monomer molar ratios constant at this initial value. In general, for constant copolymer composition,

these feed rates will differ and vary with time. With this policy, the reaction rate must be controlled by initiator feed rate or temperature, so that the heat removal capabilities of the reactor are not exceeded. This may pose a problem if the polymerization system exhibits a severe gel-effect. A second policy would feed in all the monomers over time in order to maintain constant monomer concentrations in the reactor, thereby maintaining constant polymer composition. A short batch finishing step would be necessary to deplete the monomers at the end, but the composition drift during this stage would usually have little influence on the total batch. Again, some initiator or temperature policy to control the reaction rate would be necessary. A third policy would premix all monomers and feed them to the reactor at a convenient rate. The policy would give some composition drift, but if the standing monomer concentrations in the reactor were kept small, the drift would be small because the composition of the copolymer would essentially be the same as the composition of the monomers in the feed. The choice of feed rate would depend upon the heat removal capabilities of the reactor at any instant.

The above three composition control policies were discussed in Hamielec and MacGregor (1983), and illustrated using a model for a vinyl acetate/vinyl chloride copolymerization which accounted for the gel-effect. Although all of the policies will give constant composition, they will give different production rates (batch times) and they will yield polymer with very different molecular weights and long chain branching frequencies.

Guyot et al. (1981) investigated some of these policies experimentally for the emulsion polymerization of styrene/acrylonitrile in a CSTR. An on-line gas chromatograph was used to measure the monomer composition ratio in the liquid phase, and then a feedback scheme was used to adjust the feed rate of monomers to maintain this ratio constant (first policy). Their subsequent analysis of the copolymers showed that, rather than obtaining a desired constant composition polymer, the polymer composition drifted towards compositions

too rich in styrene. They showed that this was clearly due to not accounting for the partitioning of the monomers between the three phases. A high solubility of acrylonitrile in water coupled with its low solubility in the polymer leads to a much higher styrene/acrylonitrile ratio in the polymer particles than in the total system. This partitioning would have to be accounted for in any control scheme for emulsion systems using monomers with greatly different solubilities.

Johnson et al. (1982) developed a model-reference feed-forward control strategy based on the first policy (maintaining constant monomer molar ratios) for the production of compositionally homogeneous copolymers. Models were used to provide the flow rate profile for the more reactive monomer, which was then used to generate the set-points for an experimental semi-batch reactor. The policy was shown to be fairly successful for the copolymerization of styrene with methyl acrylate in a toluene solution. The same reaction system was studied by Pittman-Bejger (1982), who demonstrated, via simulation, the use of an off-line optimization combined with an on-line self-tuning controller. Ahn et al. (1983) considered the emulsion polymerization of a vinyl chloride/acrylonitrile copolymer of constant composition by controlling the addition rate of the more reactive acrylonitrile monomer.

6.5.3 Long Chain Branching Control

For polymers in which any of the reactions, radical transfer to polymer, terminal double bond, or internal double bond polymerization are important, then branched polymers will be formed. Since the branching frequency (i.e., average number of branch points per molecule) usually has a pronounced effect on the polymer properties and particularly on processability, it is desirable to investigate policies for controlling it. The effect of a number of policies on branching frequencies has been reported by Hamielec and MacGregor (1983) for styrene/butadiene and vinyl acetate/vinyl chloride copolymers. In general, a batch (or plug-

flow) reactor operation will minimize branching frequencies compared to a CSTR or semi-batch operation at the same conversion. In fact, the three semi- batch composition control policies discussed in the preceding section give widely different branching behavior.

6.5.4 Particle Size Distribution Control

In general, particle size distribution in semi-batch emulsion polymerization can be controlled through seeding of the reactors, or through controlling particle nucleation by manipulating the emulsifier and/or initiator feed rates. Some policies using both of these methods have been investigated. Min and Gostin (1979) used initial seeding of the reactor, followed by a controlled emulsifier feed rate to produce a secondary particle generation. The bimodal PSD's obtained in a pilot plant reactor for poly (vinyl chloride) emulsion polymerization were well predicted by their population balance model. The effects of the following variables on the final latex PSD were investigated: seed particle size, quantity of seed, solid contents of the seed, and initial amount of initiator.

Gordon and Weidner (1981) used the ideas of Min and Gostin (1979) to control the PSD in the emulsion polymerization of vinyl chloride by manipulating the emulsifier feed rate as a function of conversion. An on-line measure of conversion was obtained from an unsteady-state heat balance and then used as the feedback variable to control the emulsifier feed rate.

Emulsifier feed rate policies which produce multiple particle generations, or extend the period of particle nucleation have been studied in Chapter 5 for vinyl acetate emulsion polymerization. These policies significantly broaden the resulting PSD over that of a batch reactor operation. In a similar study, Lin et al. (1980) tried to control the particle size in vinyl chloride polymerizations by varying the ratio of monomer to water at the beginning of the reaction.

6.5.5 Temperature Control

Temperature control in batch and semi-batch reactors can be divided into two phases: a heating phase in which the objective is to raise the reactor temperature to its target as fast as possible while avoiding overshoot, and a stabilizing phase in which the objective is to maintain the reactor temperature at a set-point or set-point trajectory throughout the remainder of the polymerization.

Amrehn (1977) and Hoogendoorn and Shaw (1980) give surveys of the literature on temperature control during these two phases. For the heating phase, the control policies are bang-bang in nature, with maximum heating followed by maximum cooling when the temperature approaches to within a certain deviation from target. In some instances, these policies have been arrived at empirically, while in other cases, the Maximum Principle has been used (e.g., Keyes and Kennedy (1974)). In some cases reactor heat balances have been used on-line to calculate set-points for the cooling water temperature at the start of the stabilization phase (Amrehn (1977)).

The problem during stabilizing control is the very uneven heat load on the cooling system during the run because of the acceleration in the reaction rate as a result of the gel-effect. Time-varying heat transfer coefficients also cause problems. More advanced control schemes use either feedforward terms from a reactor heat balance or adaptive controllers. Recent papers by Cluett et al. (1982) and Kiparissides and Shah (1983) have evaluated the performance of various adaptive controllers (including self-tuning regulators) for stabilizing temperature control on a simulated PVC batch polymerization reactor. All their schemes appeared to be robust and superior to fixed parameter proportional integral derivative (PID) controllers.

6.6 Continuous Reactor Control

Where production volume warrants it, continuous reactors can offer many advantages, including lower operating and capital costs, improved heat removal capabilities, and potentially more consistent product quality. Examples of continuous polymerization processes include the emulsion polymerization of styrene/butadiene rubber (SBR), the solution polymerization of butadiene, the bulk polymerization of styrene, polyester and nylon, and the heterogeneous polymerization of ethylene. In this section, we survey some of the recent literature on continuous reactors from the following viewpoints: steady-state optimization, dynamic optimization, reactor design optimization, state estimation and on-line control. As with batch reactors, good process models again play a dominant role.

6.6.1 Steady State Optimization

Steady-state models of continuous polymerization reactors are very useful for simulating the behaviour of these systems for various changes in the recipes and/or operating conditions. Conditions which yield increased productivity or improved quality can be investigated prior to implementing changes in the plant.

The steady-state computer modelling of latex reactor trains used in the manufacture of cold SBR was treated in Hamielec et al. (1983). Their models predict copolymer composition, molecular weight averages, and long chain branching frequencies, as measures of polymer quality, plus the particle size distributions throughout the train. Several modified operating procedures which give higher production rates and/or improved SBR quality were identified. Procedures for modifying the PSD were also investigated. Lin and Chiu (1982) studied the simulation and optimal design of reactors for a seeded continuous emulsion polymerization process. They found that, in general, an increase in the number of stages inside the seeder can reduce the volume of a CSTR for a required production rate. In a

similar work, Lin et al. (1980) studied the performance of an emulsion CSTR for styrene comparing continuous flow operations with and without recycling.

Hoftyzer et al. (1964), Reimschuessel and Nagasubramanian (1972), and Mochizuki and Itoh (1978) were concerned with the optimization of caprolactam polymerization. They were mainly interested in determining an optimum course for temperature and for water content. Balaraman et al. (1983) studied the steady-state multiplicity in the bulk copolymerization of styrene-acrylic esters. They illustrated an innovative way of operating a CSTR in the unique steady-state region to produce copolymers at higher conversion and uniform composition by recycling part of the product.

6.6.2 Dynamic Optimization

Dynamic models for continuous polymerization reactors allow one to investigate their transient behaviour and stability under various conditions, such as start-up, forced oscillations, or upsets due to equipment failures, impurity variations, etc.

Hicks et al. (1969) were concerned with determining the temperature and initiator control policy which brings a CSTR to the desired steady-state while minimizing some objective functional (e.g. start-up time). They applied their mathematical analysis to simulation models of free radical and linear condensation polymerization systems. A theoretical investigation of the optimal start-up problem for styrene emulsion polymerization reactor trains was carried out by Dickinson (1976). He developed numerical algorithms and applied them to the problem of achieving steady-state conversion in the shortest possible time. Simulation results showed that a considerable reduction in start-up time without extended transient oscillatory behaviour or excessively large steady-state conversion overshoots can be attained by application of an optimal soap start-up program. A similar start-up problem for a simulated vinyl acetate emulsion polymerization CSTR was treated by

Kiparissides et al. (1981), using suboptimal control algorithms. Hamielec et al. (1983) used a simulation model to study the stability of an SBR reactor train during start-up and under various upset conditions, and they investigated ways of adding and removing a reactor from the train.

Modifying molecular weight distributions of polymers through operating continuous reactors with forced oscillations in the total flow rate, or the flow rates of monomer, initiator or modifier, or other operating variables, has been treated by a number of authors. Simulations and, in some cases, experimental work, have been performed on free radical, step growth, Ziegler-Natta, and "living" anionic polymerization systems. Meira (1981) presents a thorough survey and discusssion of these works. Molecular weight distributions can be broadened by such forced oscillations in all of these systems. Meira and Johnson (1981) performed both simulations and experimental studies on a tubular reactor to show that with "living" anionic polymerizations, one has particularly great flexibility in producing polymers with prespecified molecular weight distributions.

Problems encountered with the development of continuous reactor systems and some of the ways of dealing with these problems are extensively discussed in Poehlein (1979), Poehlein et al. (1983) and Ray (1983). A stochastic approach was employed by Nassar et al. (1981) to analyze and model, in a uniform fashion, both emulsion polymerization and dispersive mixing in a CSTR. Tsai et al. (1983) presented a model for continuous emulsion polymerization of styrene to predict the particle size and conversion for various operating conditions, accounting for the effects of residence time, initiator and surfactant level. Finally, Lynch and Kiparissides (1981) and Nigam and Nigam (1983) were concerned with the mathematical modelling of a tubular emulsion polymerization reactor and the simulation of its performance under various operating conditions.

6.6.3 Reactor Design Optimization

The use of comprehensive polymerization reactor models provides a deeper understanding of the polymer production process, and permits the design of improved processes which might not otherwise be apparent. Control problems can be anticipated and eliminated at the design stage, giving very stable and more flexible systems.

Two major sources of problems encountered in industrial liquid-phase bulk polymerization processes are the heat released by the highly exothermic reactions and the great increase in viscosity of the reacting medium over the course of polymerization. Shervin et al. (1982) developed a two-stage process to circumvent the aforementioned problems in continuous bulk MMA polymerization. Their process utilizes a CSTR as a first-stage polymerizer and a spray tower as the second-stage finishing reactor. Spraying the partially polymerized mixture into the tower as fine droplets prior to the onset of gel-effect eliminates the problem of transporting, agitating, or mixing a reacting system with rapidly increasing viscosity.

What can be done in the area of emulsion polymerization (particularly with Case I systems such as vinyl acetate and vinyl chloride) as far as reactor design optimization is concerned, is exactly the subject of Chapters 7 and 8 of this thesis.

6.6.4 On-line State Estimation

Realistically, it is very difficult to have on-line measurements of all the major polymer or latex properties of interest, but perhaps one could rely upon one or two of the sensors discussed earlier for the on-line measurement of a few states (e.g., conversion). In order to estimate some of the other states (e.g., molecular weights or particle diameter

averages), Kalman filters or Observers could be used. A number of papers have investigated these state estimation schemes.

Hyun and Bankoff (1976) used a semi-empirical model for the kinetics of the free-radical polymerization of VAc in t-butanol, with a continuous measurement of the reaction mixture viscosity related to conversion and molecular weight, to evaluate the performance of an extended Kalman filter for early detection of process drifts. Their work, carried out on a simulation of the process, indicated that some form of filtering can provide good state estimates, even with significant noise present. Jo and Bankoff (1976) also used the Kalman filter approach to obtain state estimates of conversion and MW average using a refractometer and a viscometer on a CSTR for the polymerization of vinyl acetate in t-butanol. They found that adequate state estimation was achieved on their experimental reactor system, and that the filter could track the system states even with significant disturbances introduced into the system. Schuler (1980) discussed the use of Observers and Kalman-Bucy filters to estimate the unmeasured states in a styrene polymerization reactor. An extended Kalman filter was investigated by Kiparissides et al. (1981) to estimate some of the states in the emulsion polymerization of vinyl acetate from turbidity measurements.

As mentioned earlier, in most polymerization models, the material balance and particle growth parts of the model are independent or only weakly dependent upon the molecular weight development part. Hence, the molecular weight moments and branching frequencies are unobservable from measurements of the former states. Conversely, the molecular weight part of the model is usually coupled with the material and particle population balances. Hence, the latter states are observable from molecular weight related measurements. Pollock (1984) discussed these ideas in studying the optimal selection and development of sensors. By changing the choice of the measurement matrix and the measurement covariance matrix, the choice of sensors or sensor combinations which

optimized the generalized variance of the state estimates of interest (obtained from the Kalman filter) was made.

6.6.5 On-line Control

There are few reported applications of on- line control over the properties of the polymers being produced in continuous reactors. Amrehn (1977) reported on a few applications: conversion control in an SBR reactor train, and quality control in a polyethylene plant. Without providing much technical detail, Ahlberg and Cheyne (1979) gave a summary of their experiences with implementing an adaptive control scheme based on optimal control and extended Kalman filtering. The scheme was designed to control quality and productivity in the face of stochastic disturbances (impurities) and changing heat transfer coefficients. Their application to a full scale continuous solution polymerization process for the production of butyl rubber represents probably the most ambitious utilization to date of advanced control ideas in the polymer production industry. One of the interesting aspects of their paper is the discussion of the numerous practical problems that had to be overcome to obtain a robust system suited to the plant environment.

Harris and Rushing (1982) used a simple kinetic model to show that by controlling conversion one should reduce the variability in the specific viscosity and the end-group formation in the aqueous copolymerization of acrylonitrile in a CSTR. They used on-line unsteady-state heat balances around the reactor and jacket to infer changes in conversion, and then adjusted initiator flow rates in a feedback loop to maintain the conversion at a fixed set-point. Significant reductions in the variability of the specific viscosity and conversion were demonstrated over a ten-day test period on the industrial reactor.

MacGregor and Tidwell (1980) illustrated some of the steps involved in running plant experiments and identifying empirical dynamic models on some continuous

condensation polymerization reactors. Univariate stochastic controllers designed from the identified models were implemented to control the viscosity of the final polymer by manipulating reactor pressures. A number of similar applications based on controlling Mooney viscosity in rubber production (Kelly (1985)), and melt index in polyethylene production have also been investigated in industrial environments.

Arnold et al. (1980) discussed a model reference control strategy for the production of predefined molecular weight distributions for "living" anionic polymers. A GPC set-up was used to measure the molecular weight distribution and forced oscillations in the monomer feed rate to a tubular reactor were used to alter the distribution. Timm et al. (1982) and Hild et al. (1985) used a simulation of the anionic polymerization of styrene is a CSTR to develop a multivariable feedback controller for control of the number average molecular weight and the production rate. The algorithm was based on proportional integral (PI) controllers combined with a steady-state decoupler. Manipulated variables were the flow rate and the input concentrations of monomer and initiator.

Several investigations have been made into using control theory to try to eliminate or dampen the oscillations in the continuous emulsion polymerization of vinyl acetate in a CSTR by manipulating the flow rates of soap and initiator. Leffew and Desphande (1981) applied PI controllers with dead-time compensation to the simulation model of Kiparissides et al. (1979), but their results indicated no success. Of course, from an understanding of the particle nucleation phenomena involved, it is obvious that unless one uses large amounts of soap, it is impossible to eliminate oscillations in this manner. Kiparissides et al. (1981) and Pollock (1984) investigated the possibility of damping down the oscillations by using optimal control and extended Kalman Filtering. Little improvement was obtained (for more details the reader should see Chapter 7). A much more effective way of eliminating these oscillations

was theoretically discussed by Pollock et al. (1981) and will be further developed and experimentally evaluated in Chapter 7 of this thesis.

6.7 Conclusions

It should be apparent from this survey that the control of polymer and latex properties in polymer reactors is not something that can be tackled in the same manner as many of the traditional control problems in the petrochemical industry where the measurement and modelling problems are often more straightforward. Polymer reaction systems are extremely non-linear and complex processes, and the properties that one would like to control are rarely measured on-line. Mathematical models, usually fairly comprehensive in nature, are needed to develop operational and control policies for these reactors. We expect that the 1980's will see rapid developments in the control of these polymerization processes. The control will often be achieved simply through heuristic approaches, or redesigned reactor systems made possible by the improved understanding of the processes gained from the experimental and modelling efforts now under way.

CHAPTER 7

CONTINUOUS REACTORS: DESIGN AND CONTROL CONSIDERATIONS FOR CSTR TRAINS

7.1 Introduction

The majority of industrial polymer latex production take place in batch or semi-batch emulsion polymerization reactors. Where production volume warrants it, however, continuous reactors can offer many advantages, including lower operating and capital costs, improved heat removal capabilities, and potentially more consistent product quality. In spite of these advantages, continuous emulsion polymerization has only been used for the production of a few high volume elastomers such as SBR, ABR, Neoprene, and for some PVC products. A major reason for the extensive use of semi-batch production is the great flexibility that this reactor system provides for making a variety of products in the same reactor. However, even where production volumes might justify it, continuous emulsion polymerization is rarely used. One reason for this is certain dynamic phenomena which characterize the operation in a conventional continuous stirred tank reactor (CSTR) or reactor train.

Gershberg and Langfield (1961), Nomura et al. (1971), Gerrens et al. (1971), Gorber (1973), Greene et al. (1976), Dickinson (1976), Poehlein and Dougherty (1977), Kirillov and Ray (1978), Brooks et al. (1978), Kiparissides et al. (1979), Poehlein (1979), Schork et al. (1980), Nomura and Harada (1981b), Pollock et al. (1981), Lin and Chiu (1982), Poehlein et al. (1983), Badder and Brooks (1984) and Broadhead et al. (1984) are a few literature references which have dealt with dynamic phenomena in emulsion CSTR's, such as conversion overshoots during start-up procedures, different start-up and changeover policies and the existence of multiple steady-states and oscillations.

This chapter is concerned with the pheneomenon of sustained oscillations or limit cycles which are observed to occur in the emulsion polymerization of many monomers (e.g. vinyl acetate, vinyl chloride, neoprene, and methyl methacrylate) in CSTR trains. For a system which exhibits the phenomenon, all the latex and polymer properties (e.g. particle size, monomer conversion, and molecular weight) will oscillate in a limit cycle behavior even though all the feedrates to the reactors are being held constant. These oscillations lead to excessive coagulation and reactor fouling, as well as unacceptable latex and polymer property variations.

Kiparissides et al. (1979, 1980) developed a detailed mathematical model for these systems based on a polymer particle age distribution analysis and were able to fully explain the source of these oscillations as being due to periodic particle generations. Extensive experimental results were used to confirm these model predictions. Kiparissides et al. (1981) and Pollock (1984) further showed that advanced control theory by itself could not be used to eliminate these oscillations through manipulation of the feeds to the reactor(s). However, Pollock et al. (1981) and Pollock (1984) using the dynamic model showed that this limit cycle behaviour could be eliminated through redesign of the continuous reactor train configuration, and that this redesigned system also offered greatly increased flexibility in controlling the conversion and latex particle size. In this chapter, we present an extensive experimental evaluation of this proposed continuous reactor configuration, and confirm the simulation, design and control results of Pollock et al. (1981) and Pollock (1984).

7.2 Oscillations in Conventional CSTR's

7.2.1 An Explanation of the Phenomenon

The oscillating behaviour of some continuous emulsion polymerization processes can be explained as follows (Kiparissides et al., 1979): At the beginning of the reaction, a

rapid generation of a large number of particles occurs, due to micellar and/or homogeneous nucleation mechanisms, leading to the formation of a large and growing particle surface area. This new surface area is rapidly covered with emulsifier molecules, which stabilize the newly formed polymer particles. At some point in time, the particle surface area becomes great enough to deplete the free emulsifier (soap) in the latex with the result that the soap micelles disappear. This leads to a period in which the particle generation (nucleation) rate is very low or even zero. The duration of this period depends on the soap feedrate and the residence time of polymer particles in the reacting vessel. When no new particles are being generated in the reactor, the total number of particles decreases due to the wash-out of the existing particles. Meanwhile, new emulsifier is being fed to the reactor at a steady rate. Eventually, the emulsifier concentration becomes sufficient to stabilize the fewer remaining particles, saturate the water phase, and form another generation of micelles, thereby leading to another particle generation.

This mechanism will lead to periodic formation of discrete particle populations and consequently, to fluctuations in polymerization rate, conversin and particle size. It is clear, therefore, that under many operating conditions in a CSTR, oscillations will prevail, and a steady-state will be impossible to achieve.

The sustained oscillation phenomenon was studied in great detail by Kiparissides (1978). He investigated the effects of initiator and soap concentrations, residence time, stirring rate and oxygen level in the reactor on the conversion and production rate in a single 1.2 liter CSTR. In his study he employed distilled VAc monomer at 50°C for a monomer to water ratio of 4/10.

Figure 7-1 represents simulation results using the presently developed model for one of the experimental conditions of Kiparissides (1978) (I = 0.01 gmole/lit, S = 0.01

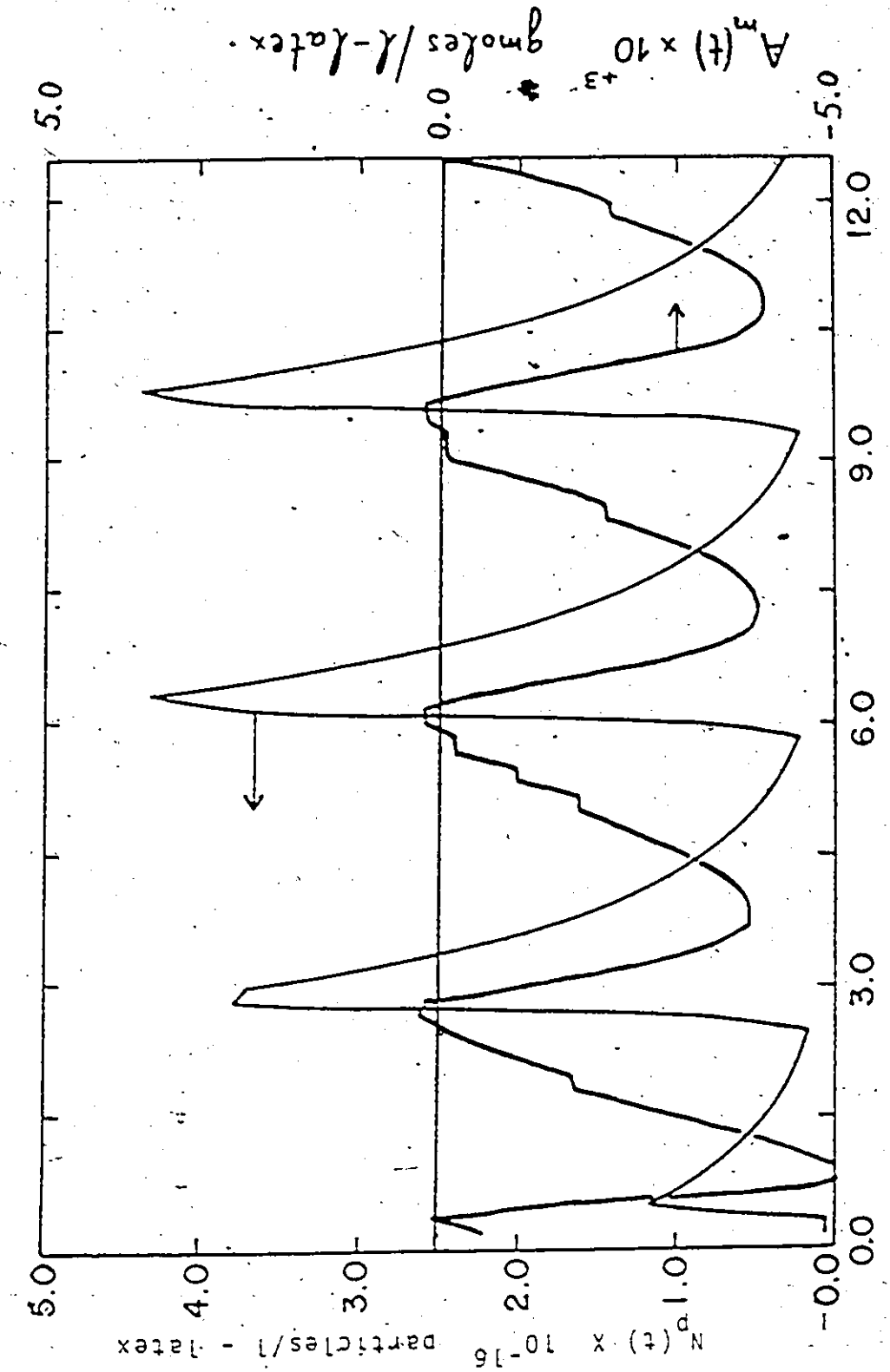

Figure (7-1). Free Micellar Soap and Number of Polymer Particles Variations for a Typical Continuous Emulsion Polymerization Case in a Single CSTR.

gmole/lit, M/W = 4/10, T = 50°C, reactor starting full of water, θ = 30 min.). The figure shows free emulsifier area versus dimensionless time and the corresponding number of polymer particles. The oscillations in $A_m(t)$ are evident. Everytime that $A_m(t)$ exceeds the zero level, indicating the presence of micelles, a new particle generation occurs. The free soap is then rapidly consumed to stabilize the new particle surface area, and the micelles disppear. The periodicity of the phenomenon is also clear.

Although in an industrial environment one would usually have only conversion measurements in which to observe oscillations, note should be made of the fact that limit cycles in the particle number and average diameter are much more extreme. Also, oscillations occur in other polymer properties as well, thereby affecting the final product processability. This oscillating behaviour in conversion, number of particles, average particle diameter and average number of branch points per polymer molecule can be seen in Figures 7-2 and 7-3 for a typical emulsion recipe in a CSTR.

As previously mentioned, oscillations can lead to increased coagulation of latex particles in the reactor, sometimes with catastrophic results (Kiparissides et al., 1980). Since oscillations result from the rapid periodic generation of particles, the particle surface area oscillates wildly while the available amount of soap to stabilize it is fixed. This often results in inadequate stabilization of the particles leading to coagulation. It is sometimes observed that shortly after a new particle generation, the particle surface coverage by soap may fall to a value as low as 35 to 45 percent.

Another undesirable event which is likely to happen is excessive long chain branching during the high conversion portion of the oscillations. Molecular weights will increase accordingly and gel formation may take place, thus leading to a final product with very poor processability. In fact, polymer collected during the oscillation period (Pollock (1984)) never fully dissolved in usually good solvents (due to gel formation).

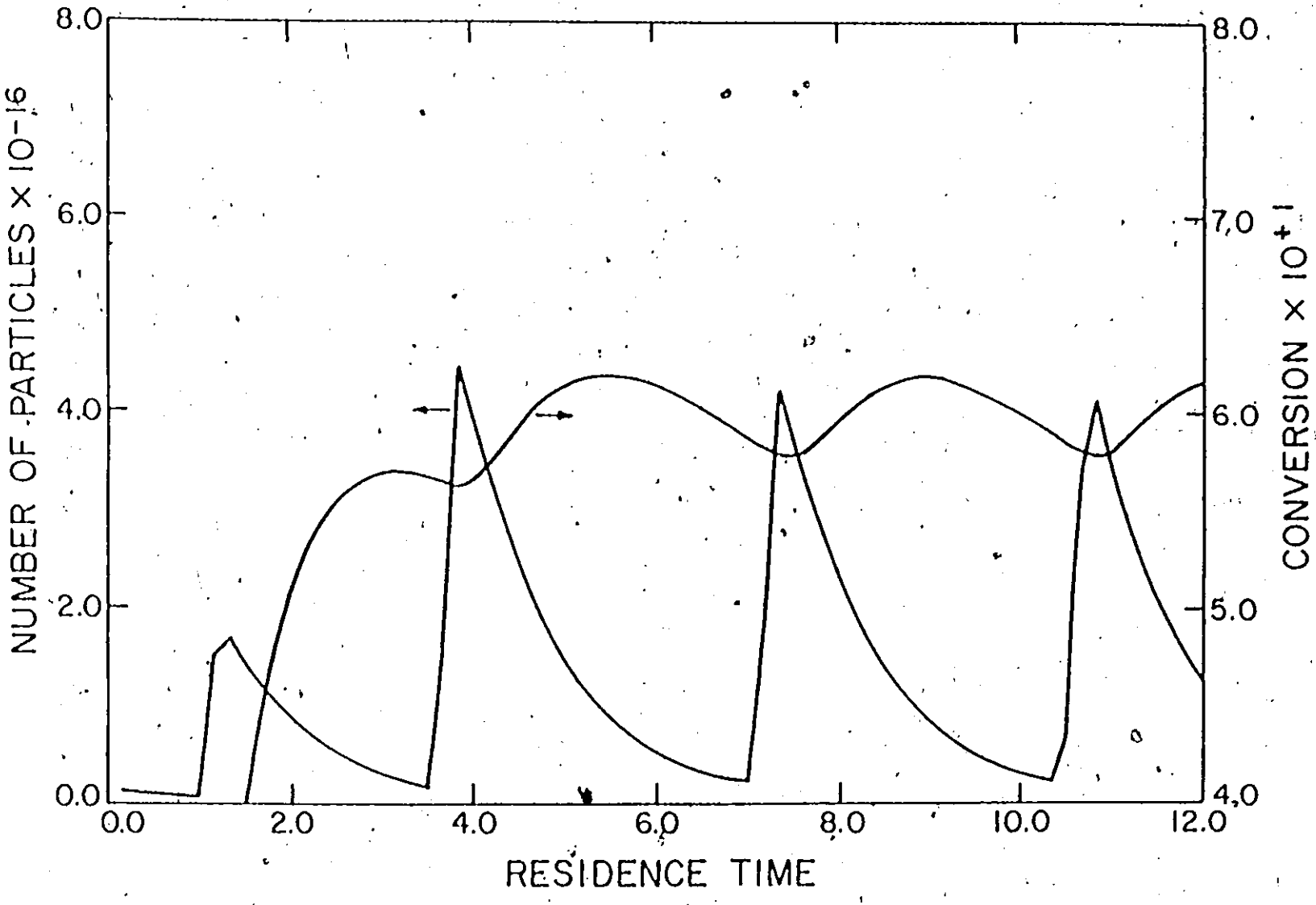

Figure (7-2). Conversion and Number of Particles versus Number of Residence Times for a Single CSTR. Conditions: θ = 1800 sec., I = 0.01 qmole/lit., S = 0.01 qmole/lit.

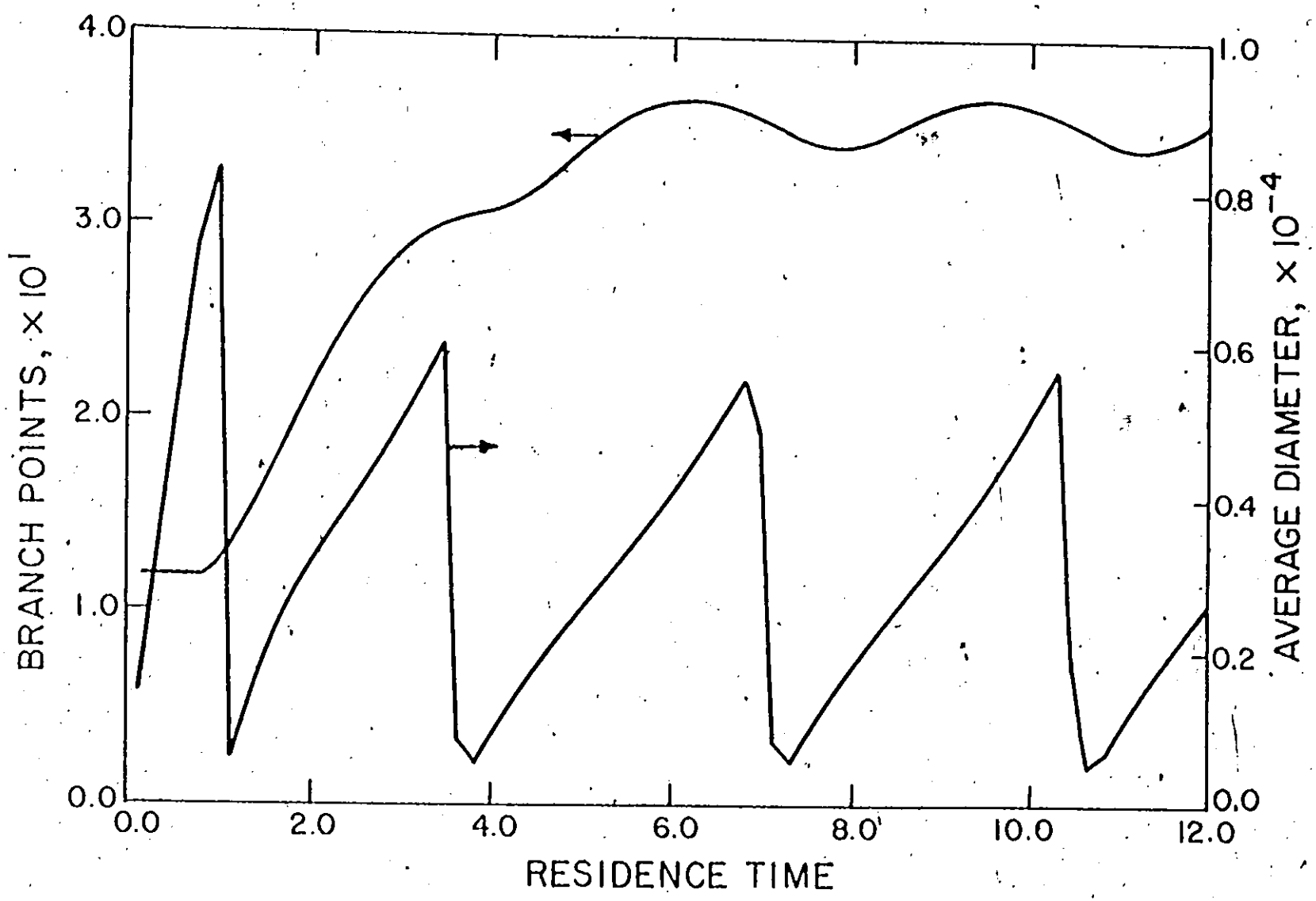

Figure (7-3). Average Number of Branch Points per Polymer Molecule and Average Particle Diameter versus Number of Residence Times for a Single CSTR. Same Conditions as in Figure (7-2).

Another serious implication that is not very obvious with laboratory or bench-scale pilot plant reactors, but is very important for industrial-scale vessels, is the possibility of reactor runaway during the high portion of the conversion swing. Due to the sudden particle nucleation (a massive burst a 10^{16}–10^{19} particles/lit), the polymerization rate becomes very high and one might exceed the cooling capacity of the reactor's jacket.

Sustained oscillations are phenomena which characterize the continuous production of "Case I" monomers (e.g. vinyl acetate, vinyl chloride). In the continuous production of "Case II" monomers (e.g. styrene, styrene-butadiene) and when the average number of radicals per polymer particle does not appreciably deviate from the typical value of 1/2, the newly generated particles tend to grow much faster compared to "Case I" systems, where the average number of radicals per particle is much less than 1/2. The rapidly growing surface area in "Case II" systems is thus "consuming" the excess emulsifier not allowing the formation of new micelles, thereby not causing sizeable upswings in the reaction rate, conversion and size. It is therefore the relative importance of the particle nulceation rate to the particle growth rate that is responsible for the oscillation phenomenon. This ratio apears to be the important parameter in an emulsion system. Whenever this ratio is large, one will observe oscillations, and whenever it is small enough to support a continuous steady-state generation and growth of particles, a steady-state behaviour will result. Hence, "Case I" systems oscillate, since they exhibit a large ratio (large nucleation rate due to a large radical entry rate, and slower growth rate due to a smaller average number of radicals per particle), whereas "Case II" systems exhibit a steady-state behaviour since the aforementioned ratio is small enough (smaller nucleation rate and faster particle growth rate).

7.2.2 Possible Solutions to the Oscillation Problem

It is clear from the previous discussion that the oscillation phenomenon is highly undesirable industrially. It is evident, therefore, that the primary consideration in the operation of continuous reactors is the elimination of these limit cycles.

Kiparissides (1978) in some of his experimental runs used larger quantities of soap. These runs with a higher emulsifier concentration (~0.04–0.06 gmole/lit) showed less pronounced conversion overshoots upon start-up and did not always oscillate. This was attributed to the fact that a high soap concentration prevented on-off nucleation of polymer particles, which upon growth did not deplete the reactor from emulsifier micelles. However, oscillations in conversion of about 5-8% were sometimes observed, even with high soap concentration, depending upon the initiator concentration used.

The use of large quantities of soap in order to eliminate or dampen the oscillations is not a practical solution to the problem. More emulsifier means a more expensive operation as far as cost of raw materials is concerned and perhaps a higher cost in any subsequent stripping and coagulation operation. Additionally, soaps act as contaminants of the final product if present in excess, and they may affect the water repellency of a coating or the subsequent product processability of a rubber. Furthermore, the use of large amounts of soap leads to the generation of large numbers of particles, and hence provides little ability to control particle size, since in such a case, one cannot easily obtain larger particle diameters.

Another possible solution to the problem (Kiparissides (1978) and Pollock (1984)) was the application of advanced control schemes (linear quadratic stochastic optimal control) to a single CSTR. Application of advanced control schemes on a simulation of the process showed in many cases some improvement of the reactor performance upon start-up, but the control scheme was not able to eliminate the oscillations at reasonable soap levels. Pollock (1984) clearly showed that although these policies may possibly dampen the limit cycles in

some cases, they cannot eliminate them, because to eliminate them would involve stopping the particle nucleation altogether.

Following a different idea, Greene et al. (1976) showed results for methyl methacrylate emulsion polymerization where a plug-flow reactor with no feed splitting was used to seed a CSTR train, yielding stable operation and constant conversion. Omi et al. (1969), Ueda et al. (1971), and Nomura and Harada (1981b) used steady-state models in order to maximize the number of particles formed in the emulsion polymerization of styrene, by using optimally sized tubular seeding reactors. The latter authors also discussed a CSTR seeder with the possible splitting of the monomer feed stream. It seems therefore, that seeding of the continuous reactor is another possible solution to the undesirable oscillatory behaviour of CSTR's, with the way of seeding in this case being the primary design consideration.

Batchwise production of seeds for a CSTR is costly and has the additional disadvantage that there may be batch to batch variability in the system. Also, the use of seed particles produced in a batch reactor is not recommendable if a broader particle size distribution is desired to give lower suspension viscosities.

A PFTR used as a seeder for the system in question might create serious operational and cleaning problems due to agglomeration, wall fouling, and plugging. The need to maximize the number of polymer particles nucleated for a given emulsifier level is not relevant as the limiting factor is the surface coverage to give particle stability. The emulsifier level required should be that which gives a stable suspension of polymer particles. It is an easy matter to nucleate sufficient polymer particles at much lower emulsifier levels.

Additionally, a PFTR seeder should be short, since a longer reactor would have all nucleation accomplished in the early stages and thus, the remaining section of the tube would be used in an inefficient manner since no more nucleation would occur. Since the PFTR

seeder would then be a short tube, there would be little difference between the use of a "small" CSTR as a PFTR for the production of seeds for the successive reactors in the train. Thus, the better mixing, operational and cleaning capabilities of a CSTR make the small CSTR seeder prereactor a better choice. The small CSTR could also act as a more efficient preemulsifying stage for the whole train.

An obviously more acceptable solution to the problem through a fundamental redesign of the continuous reactor configuration was suggested by Pollock et al. (1981) and Pollock (1984) and is discussed in the next section.

7.3 A Split-feed Seeding Reactor Design

Pollock et al. (1981) suggested a new design, consisting of a conventional CSTR train but with a very small preliminary split-feed seeding reactor. In order to increase the flexibility of the new reactor system to produce latexes with different properties, a split was suggested for the monomer and water streams. To keep emulsifier and initiator levels high in the small seed reactor all initiator and the majority of emulsifier were fed to the seed reactor. Only enough soap to stabilize the emulsion was then used in the bypass stream to the main (first large) reactor of the train.

With this configuration, the control variables can be the initiator and emulsifier concentrations of the product plus the degree of split of monomer and water. This extra control variable will allow changes to be made in latex properties without changing emulsifier levels, thus preventing downstream problems and increasing flexibility.

In the new reactor train the first large reactor is preceded by a very small initial CSTR. The volume of the pre-reactor is approximately one tenth (or less) of the size of the subsequent reactors in the train. The effect of the size of the small reactor was extensively investigated in simulation studies. Sizes ranging from 1/5 to 1/16 of the large reactor were

checked and it was found that sizes close to 1/5 or larger started being unstable. Sizes ranging from 1/7 to 1/16 of the first large reactor in the train were all found to operate in a stable fashion.

All of the initiator and most or all of the soap stream are fed to the small reactor. Soap can be divided in such a way that the majority is fed to the first reactor while just enough soap to stabilize the dispersion is fed to the second reactor in the train. Only a fraction (10% to 40%) of the monomer/water stream is fed to the small reactor, while the remaining water and monomer are fed to the second reactor (i.e. the first large one). Due to the bypass of some of the monomer and water, the small reactor in the new configuration operates under a high concentration of initiator and emulsifier, thus leading to nucleation of a sufficient number of particles for the downstream reactors.

Simulations revealed that a feed split to the small reactor greater than 0.4 (i.e. 40% of the monomer and water being added to the first reactor) caused the train to oscillate. This is expected because if the split is greater than 40%, then the small reactor has a small residence time and it merely acts as a pre- emulsifying vessel for the train. Nucleation is not complete in the first reactor, thus causing problems to the rest of the train. On the other hand, a split less than 10% is not practical, since the monomer that goes to the small reactor in this case might not be enough to start the polymerization reaction.

The logic behind the new design is that generation of polymer particles can entirely be accomplished in the first small reactor by running under conditions of high soap and initiator concentrations, and the subsequent reactors used only for particle growth and to further finish off the reaction. In this way one achieves either a steady-state generation of particles in the first reactor, or else a very rapid periodic generation which has no destabilizing effect on the much larger downstream reactors. In effect, the small early reactor becomes a continuous seeding reactor.

One can compare the behaviour of a single CSTR of Figures 7-2 and 7-3 to the behaviour of the same reactor with a seeding reactor present, which is shown in Figures 7-4 and 7-5. With the seeder present, all property oscillations are eliminated, while maintaining essentially the same polymer product in terms of conversion and particle size. In addition, the new configuration yields approximately 70% particle coverage by soap at all times while in the single reactor case the coverage dropped to only 40% or less immediately after each particle generation.

Pollock (1984) performed an extensive simulation study on the new configuration, which was also verified from simulations in the present study. From the simulations it was shown that the new system was able to produce a latex with the same average diameter and conversion as the single reactor case but with fewer branches per polymer molecule, and with less initiator and emulsifier requirements. The 10% reduction in the average number of branch points per polymer molecule observed would yield a more processable product in terms of reduced viscosity and die swell, or better adhesive properties.

Thus, the redesigned configuration can achieve superior performance in terms of a more stable operation and lower raw material costs and give a higher productivity or improved product quality when compared to a conventional continuous train. Another less obvious cost saving is that only the small percentage of the monomer/water feed that is going to the important first reactor needs to be purified. Also, recycle monomer streams containing impurities from either the train or the downsteam monomer recovery units will have less adverse effects on the train operation when directed back to the second reactor and thus will not interfere with particle nucleation.

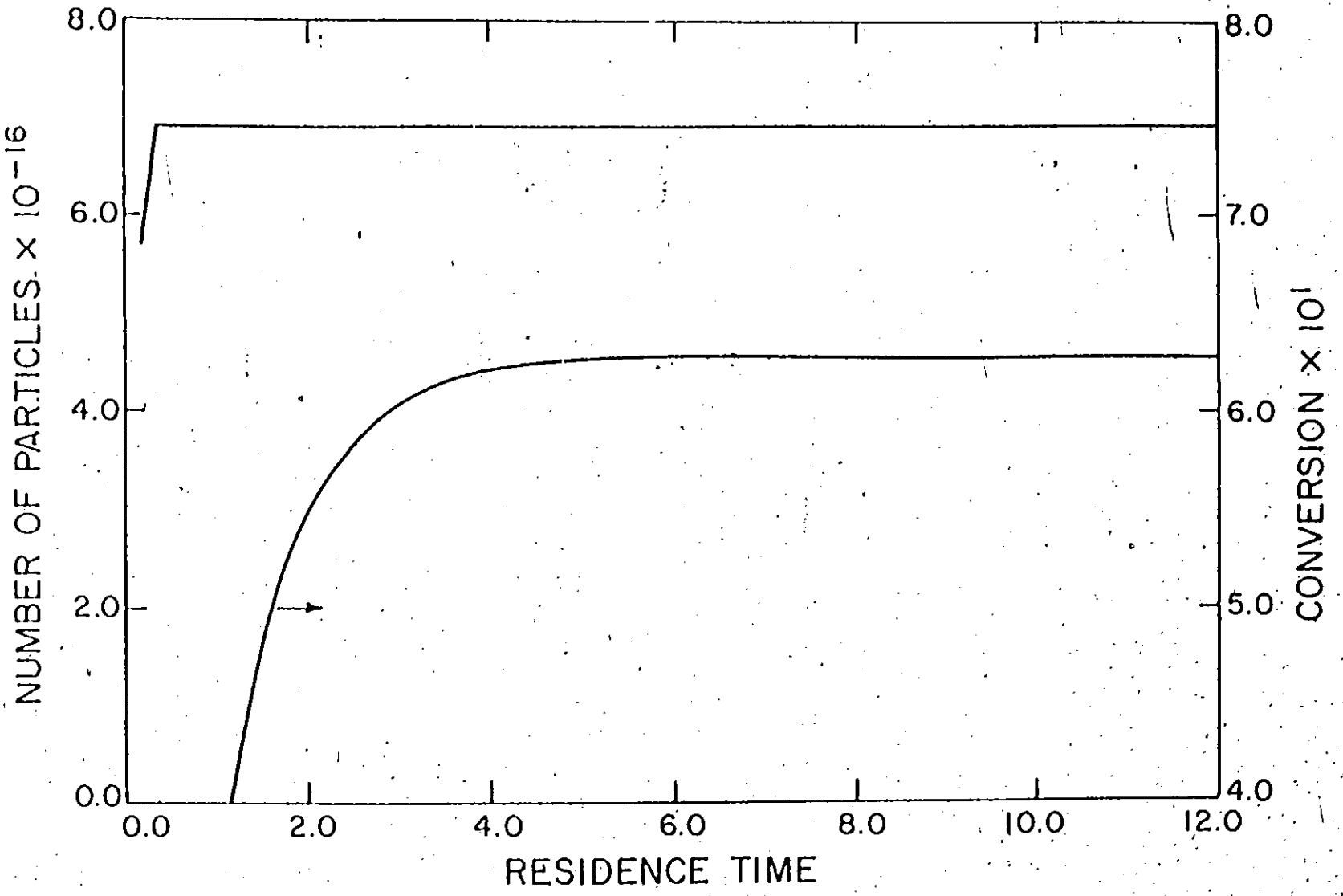

Figure (7-4). Conversion and Number of Particles versus Number of Residence times for the New Configuration. Conditions: θ = 1800 sec., I = 0.01 gmole/lit., S = 0.01 gmole/lit., v_1 = 75 ml., split = 0.4.

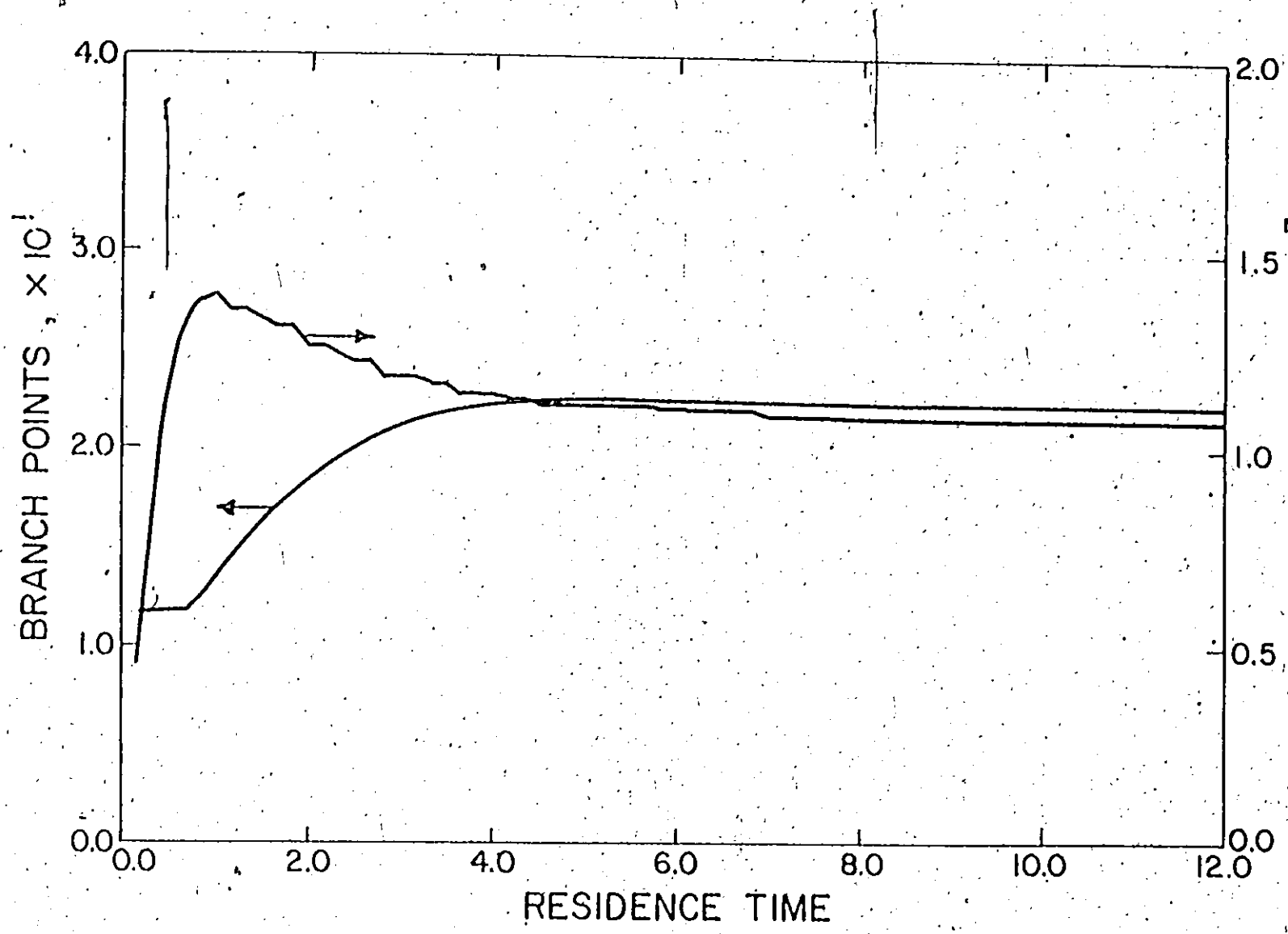

Figure (7-5). Average Number of Branch Points per Polymer Molecule and Average Particle Diameter versus Number of Residence Times for the New Configuration. Same Conditions as in Figure (7-5).

7.3.1 The Effect of Process Control Variables

Under the usual industrial configuration where all feed streams enter the first of several large reactors in series, the main variables which can be used for control over conversion and particle diameter are the initiator and emulsifier feed rates, and the reactor temperatures. Since reactor temperature can be changed only slowly and its effect is similar to that of initiator, it is not considered further in this study. Although initiator and emulsifier feed rates can be easily varied, plant personnel are understandably reluctant to make very large changes, particularly in the emulsifier feed rate. Furthermore, as shown by Pollock (1984), even the use of optimal control theory and extended Kalman filtering cannot dampen the oscillations appreciably in the usual configuration, unless large increases in the emulsifier level are allowed.

However, under the new configuration, the oscillations have been eliminated at the design stage by using a dynamic model to design the seeding reactor and to optimally split the feeds among the reactors. One can therefore concentrate now on the simpler but fundamental control problem of producing a latex with a prespecified conversion, particle size, molecular weight, etc. In the proposed reactor system, one has a much greater flexibility in controlling these properties over a very wide range. This greatly increased flexibility comes from the ability to manipulate a new physical variable, namely the flow split of the monomer/water stream between the first and second reactor. Small changes in this feed split greatly affect the number of particles generated in the seeding reactor, thereby allowing for fine manipulation over particle size. Small changes in initiator flow can then be used to maintain or change the conversion. Soap flow rate could also be used as an additional manipulated variable, but it was decided not to, since once soap concentration has been fixed, it is seldom changed due to its effect on downstream operations. Therefore, the main control variables are

two: initiator flow rate to the small reactor and feed split of monomer/water between the first small and subsequent large reactors of the train.

Some steady-state effects of changing the split and initiator feed rate are shown in Table 7-1. The effect of changing only the feed split is illustrated in the first four rows. By changing the split from 40% of the monomer/water entering the seed reactor to only 10%, the average particle diameter can be reduced from ~ 1200 Å to ~ 600 Å. However, by changing the split alone, the conversion, weight average molecular weight and average number of branch points are seen to increase, the latter two due to the increase in conversion. The next four rows of Table 7-1 illustrate that, by changing the initiator feed rate as well (to obtain the concentrations shown in the second reactor), essentially the same range of particle diameters can be achieved, while maintaining conversion constant. The increases in weight average molecular weight and average number of branch points are not so dramatic now and they would usually be further controlled by addition of a chain transfer agent in most practical applications. The simulated dynamic behaviour of the new reactor system was perfectly stable and non-oscillatory during all of these changes.

Obviously, any further control scheme must be centred around the control of the seeding reactor, and the only control necessary on subsequent reactors in the chain is to ensure that the emulsifier concentration is maintained both below the CMC to ensure that no secondary generation of particles will occur and yet high enough to maintain a stable latex. This can be checked by using an on-line measure of surface tension in the downstream reactors and adding more emulsifier if necessary. However, if proper control is maintained over the number of particles generated in reactor one, there should be no difficulty in satisfying this constraint in the later reactors.

TABLE 7-1

Comparison of Povmer Latex Properties from Reactor 2

When Using Different Bypass Percentages as Control Variable*

Split	I (gmole/lit)	x(t)	D_P (Å)	N_P (x10^{-18})	M_N (x10^{-5})	M_W (x10^{-6})	B_N
0.4	0.01	0.616	1150	0.069	5.06	2.40	0.250
0.3	0.01	0.637	1050	0.075	5.33	3.29	0.920
0.2	0.01	0.666	980	0.17	5.77	6.22	1.20
0.1	0.01	0.702	610	0.62	6.32	8.75	1.67
0.4	0.01	0.616	1150	0.069	5.06	2.04	0.250
0.3	0.0085	0.616	1070	0.078	5.21	2.75	0.833
0.2	0.0069	0.617	1000	0.16	5.49	3.73	0.93
0.1	0.005	0.618	640	0.58	5.79	8.06	1.20

* $\theta_2 = 1800$ sec., $v_1 = 75$ ml, S = 0.01 gmole/lit

7.4 Experimental Set-up

It was shown in the previous sections that one of the advantages of the new train configuration is stable reactor operation. With the seed reactor present no property oscillations in the latex product are observed. Even if the seed reactor is undergoing property oscillations, the combination of dilution of the seed reactor effluent by the bypass stream with the large difference in residence time between the seed and main reactors (in a typical case, less than 10 minutes versus 30 minutes) can dampen out any seed reactor oscillations which may occur.

Another advantage of the redesigned system is that feed purification is only needed for the small reactor. The nucleation step in an emulsion system is highly sensitive to the presence of impurities. Since all nucleation occurs in the small seed reactor and only small feed flows are used due to bypass of feed material, purification of the feed stream may be

feasible leading to enhanced reproducibility if feed stocks are changing and a higher efficiency in nucleating polymer particles. This reproducibility in the long run may be economical for an industrial situation.

In other words, a redesigned configuration has been suggested by a mathematical model and it has been found by applying the model over a variety of operating conditions that the new design offers many advantages over the conventional system, namely stable operation and high operational flexibility. It is therefore the next logical step to try and verify these theoretical results, i.e. experimentally evaluate the new train configuration.

The train configuration is shown schematically in Figure 7-6. In the final experimental set-up, all initiator goes to the first small reactor. A two-way valve on the initiator solution line can be used to divert the initiator stream to the first large reactor of the train, in which case the small reactor acts merely as a pre-emulsifying vessel for the train and the train is expected to show oscillatory behaviour. All the soap is fed to the first seeding reactor (denoted from now on as R1), thus leaving the flow split and the initiator flow rate as the two control variables (degrees of freedom). The arrow denoted as "recycle" in Figure 7-6 indicates that any recycle streams from the downstream reactors or processes should go back to the first large reactor of the train (denoted as R2). Thus, any impurities coming back with the recycle streams would not affect the first sensitive nucleating reactor R1.

Experimental details concerning the employed reactor set-up and the on-line instrumentation, and other useful information about flow rate profiles, solution concentrations, off-line analysis, etc. can be found in Appendix X. Note should be made of the fact that the flow split was now defined in a slightly different way, which is more easily applicable on-line and is discussed in the same Appendix. Appendix XI contains useful information concerning safety considerations with this kind of experiments. Finally, Appendix XII is a record of the experimental data obtained.

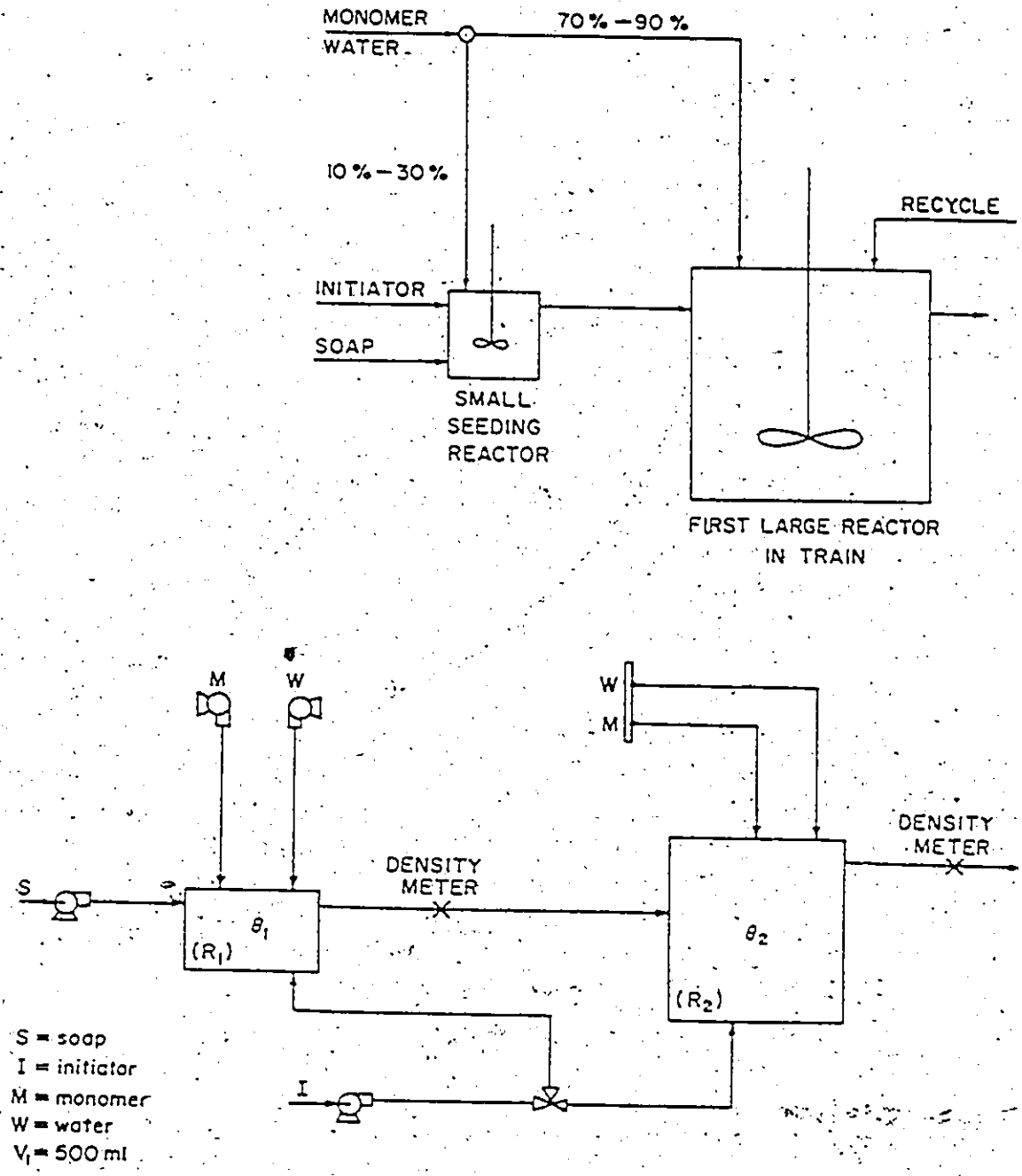

Figure (7-6): New Latex Reactor Train Configuration Experimental Layout.

All continuous experimental runs (CR#) were performed at 50°C. The agitation rate was kept constant between 300 and 320 rpm. The R2 residence time was $\theta_2 = 30$ minutes (1800 sec). To reduce wall fouling during the course of the polymerization care was taken to satisfy the following points: (a) the reactors were operated full (i.e. there was no vapour space in the vessels, since this can cause latex to dry on the wall and present a site for growth); (b) the location of the feed and effluent nozzles was selected in such a way so as to ensure rapid mixing and prevent short-circuiting; (c) care was taken for good reactor cleaning and smooth internal reactor surfaces; (d) the agitation rate guaranteed good mixing (which involves a fine balance between flow and turbulence); and (e) the cooling jacket covered as much of the reactor as possible to prevent nonuniformities in wall temperature (which can cause the reaction to be faster on any deposit near the wall). In all of the experimental runs one start-up procedure was used, that of starting the train vessels full of deionized water.

7.5 Discussion of the Experimental Results

The purpose of the continuous runs were threefold: firstly, to evaluate the new train configuration and to check whether it was free of oscillations; secondly, to investigate the effect of split and initiator flow rate on conversion and average particle size and to verify the simulation results; and thirdly, to gain experience with the new experimental set-up and use this experience later in this thesis while investigating the potential for on-line computer control for polymer reactors.

Figure 7-7 represents a plot of conversion versus dimensionless time (t/θ) for a typical continuous run using the conventional configuration (i.e. only one large reactor, part A of CR1). The oscillating behaviour is self-evident. The main reason for this part of CR1 was to experimentally show the oscillations once more and use it as a basis for comparison with the modified configuration. Kiparissides et al (1979, 1980) and Pollock et al. (1981) observed

that in the poly (VAc) case, the periods of particle generation had a duration of less than or close to 5 minutes, whereas the period of oscillations was around 3 to 4 reactor mean residence times. The results of Figure 7-7 verify once more their observation.

Figure 7-8 shows experimentally measured conversion data from the second reactor in the train versus dimensionless time (t/θ_2). The plot corresponds to parts A and B of run CR1, the oscillatory behaviour of which was also clearly demonstrated in Figure 7-7, where only part A was plotted. The good reproducibility of our gravimetric conversion results and their agreement with conversion from the on-line densitometer are well illustrated in Figure 7-7 (see also Appendix XII). The experimental points on Figure 7-8 are coming from off-line gravimetry for part A (up to $t/\theta_2 = 12.0$) and from on-line densitometry for part B. During part A of CR1, the initiator was all diverted to the second reactor of the train, therefore the small seeding reactor was not in operation and hence the train exhibited an oscillatory behaviour, as expected. The switch to R1 took place exactly after $t/\theta_2 = 12.0$, during the lower portion of an oscillation. As can be clearly seen from Figure 7-8, very shortly after the small seeder became operative, conversion became non-oscillatory and in fact assumed a very steady value. The initial overshoot in R2 conversion during part A is not due to the reactor start-up procedure but due to a temporary increase in the temperature set-point. To avoid a long induction time after the flows to the train had started, the temperature in reactor 1 was increased to 70°C for 5 minutes (instead of the usual set-point of 50°C). This caused the initial conversion overshoot in the very beginning of the reaction. In this way the initial induction time was less than 25 minutes. Conversion measurements from reactor 1 for parts A and B are shown and discussed in Appendix X.

Figure 7-9 shows conversion measurements only for part B of CR1. The points are coming from off-line gravimetry (which was occasionally checked for reproducibility) and on-

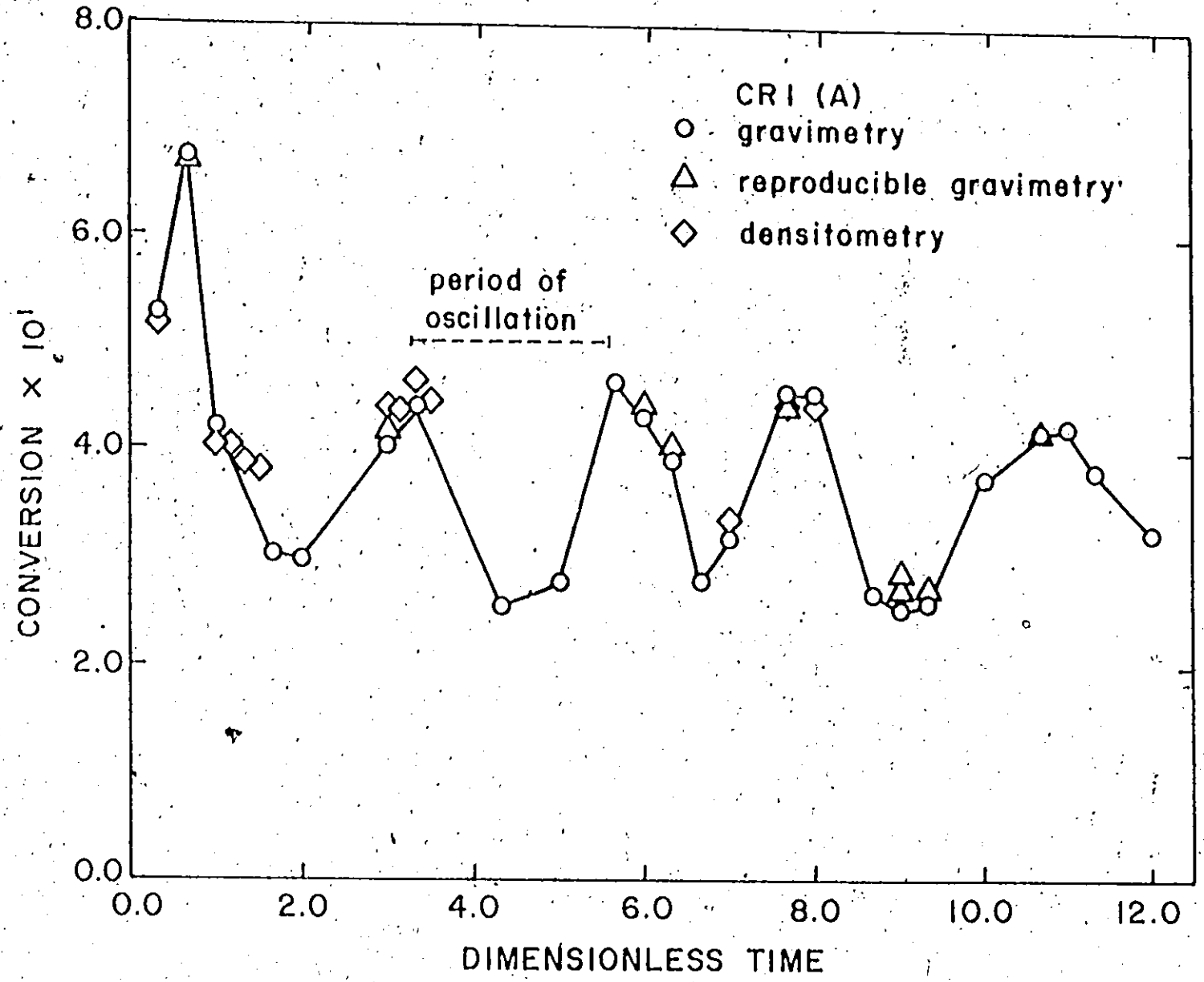

Figure (7-7). Experimental Conversion versus Dimensionless Time for a Typical Continuous Run with the Conventional Train.

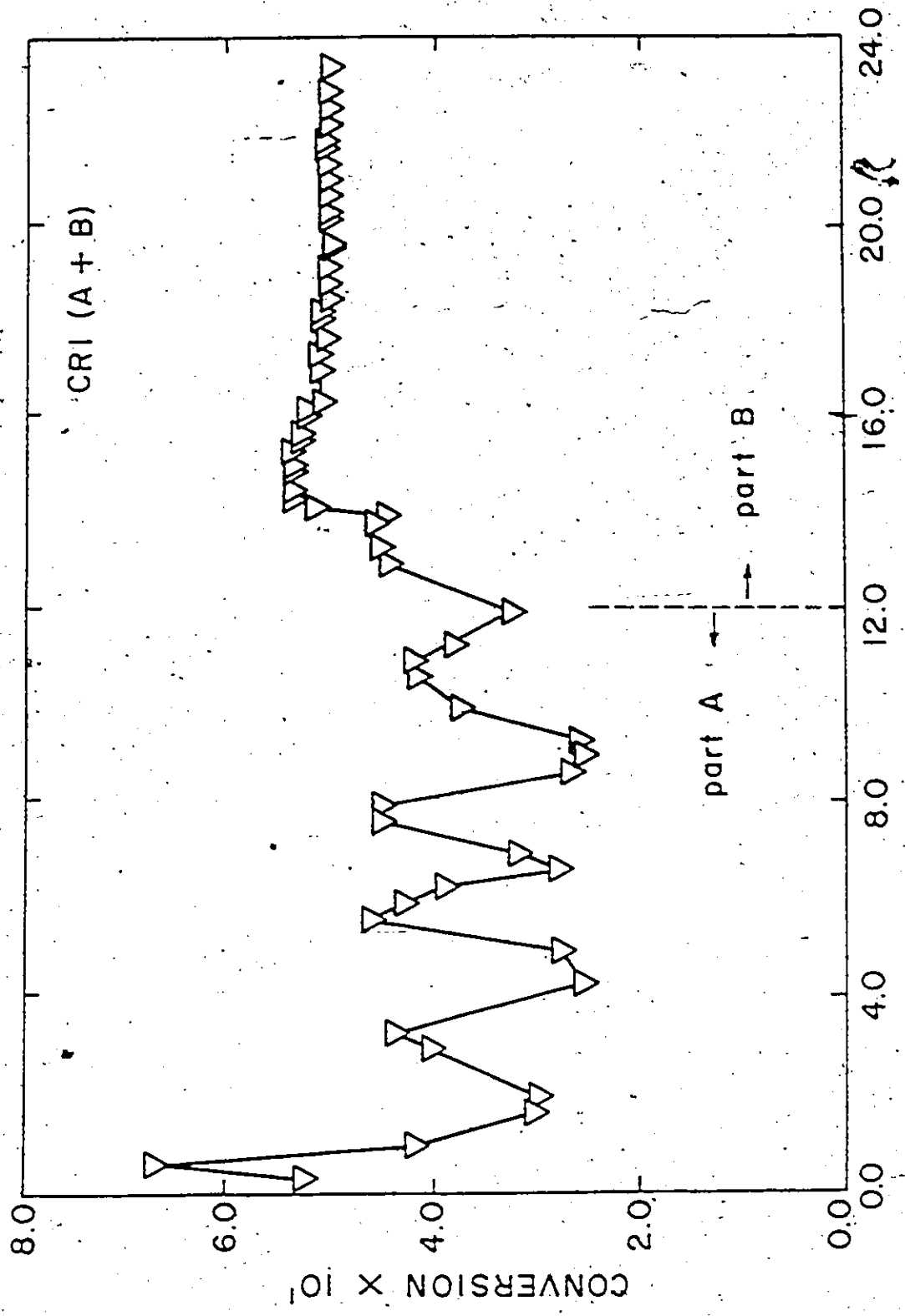

Figure (7-8). Run CR1, Parts A and B: R2 Conversion versus Dimensionless Time.

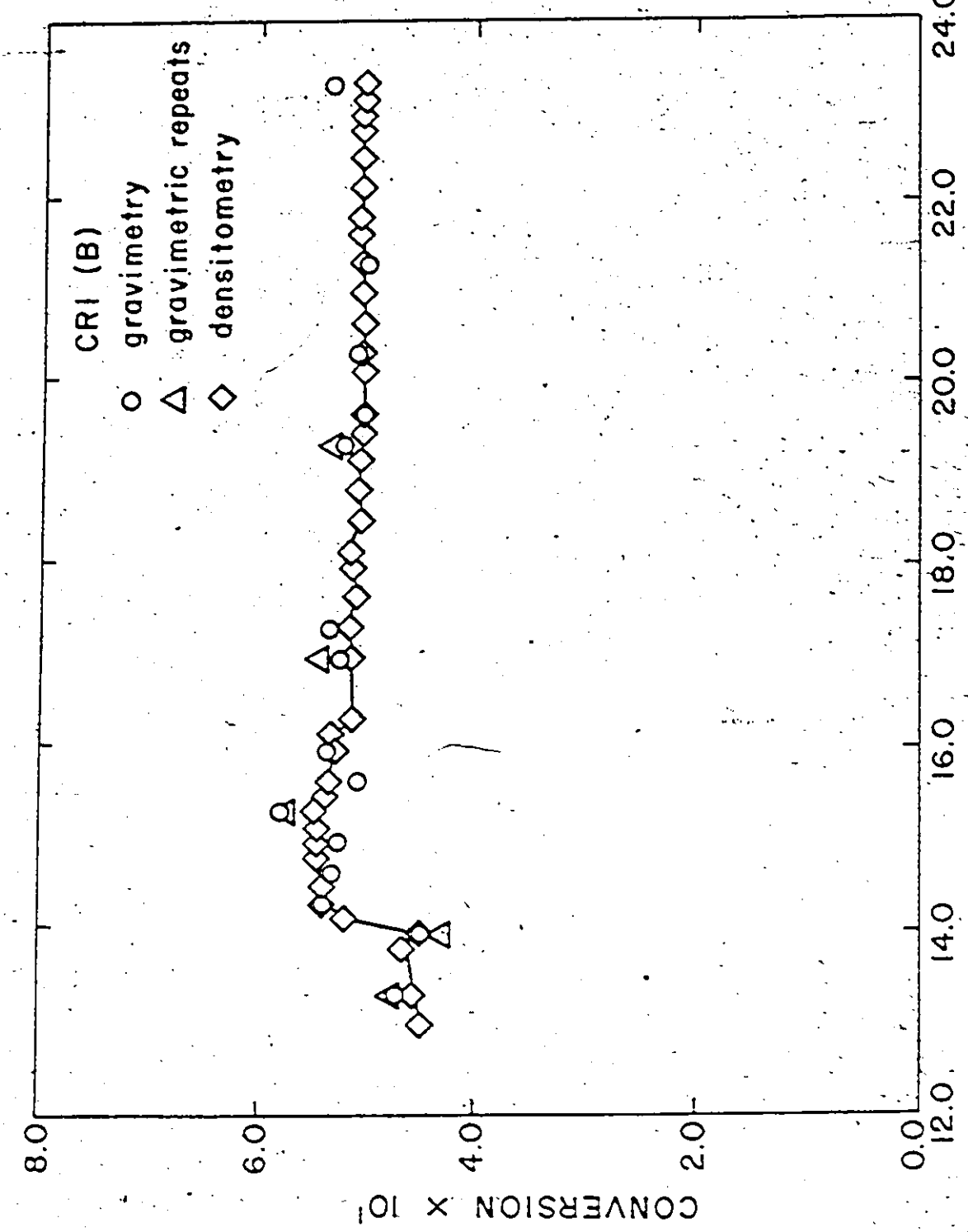

Figure (7-9). Run CR1, Part B: R2 Conversion versus (t/θ_2)

line densitometry. The agreement between the two methods is excellent. Also, the stable behaviour of the train with the seeding reactor present is clearly illustrated. The kick in conversion around $t/\theta_2 = 14.0$ clearly coincides with the overshoot in $x_1(t)$ in Figure X-1. In other words, the overshoot in conversion from reactor 1 forced conversion in reactor 2 to go upwards and stabilize at a new level.

Figure 7-10 gives the experimental picture conversion-wise for parts A, B and C of CR1. The points for part C are from on-line densitometry. Midway through part C of CR1 the AC soap pump-motor got superheated and from that point on the pump was not able to deliver the desirable flow rate to R1 (see flow rate profiles in Appendix X). Almost at the same point the MPI monomer to R1 pump had a major leakage, and therefore we decided to analyze only half of the samples taken from part C. Part D was not further analyzed, because a major coagulation problem was observed in reactor 1, due to the inability of the soap pump to deliver enough soap to stabilize the emulsion. The important thing here is that the reactor train response corresponding to this problematic behaviour can be perfectly explained. The drop in reactor 2 conversion is due to the decrease in monomer to R1 and soap to R1 flow rates. Less monomer means a lower polymerization rate and less soap means a lower number of polymer particles which in turn also gives a lower polymerization rate and hence, lower final conversion. The dashed line represents our model predictions, which are quite close to the observed behaviour. The model parameter values for D_w and ε were kept the same as the ones found in Chapter 4.

From our extensive simulation study, we have noticed that for a conventional train (i.e. the oscillating region of part A in Figure 7-10), a lower value of ε tends to give narrower and more abrupt peaks, closer to the ones experimentally observed in Figure 7-10. However, low values of ε tend to give very low average diameter values, much lower than the ones

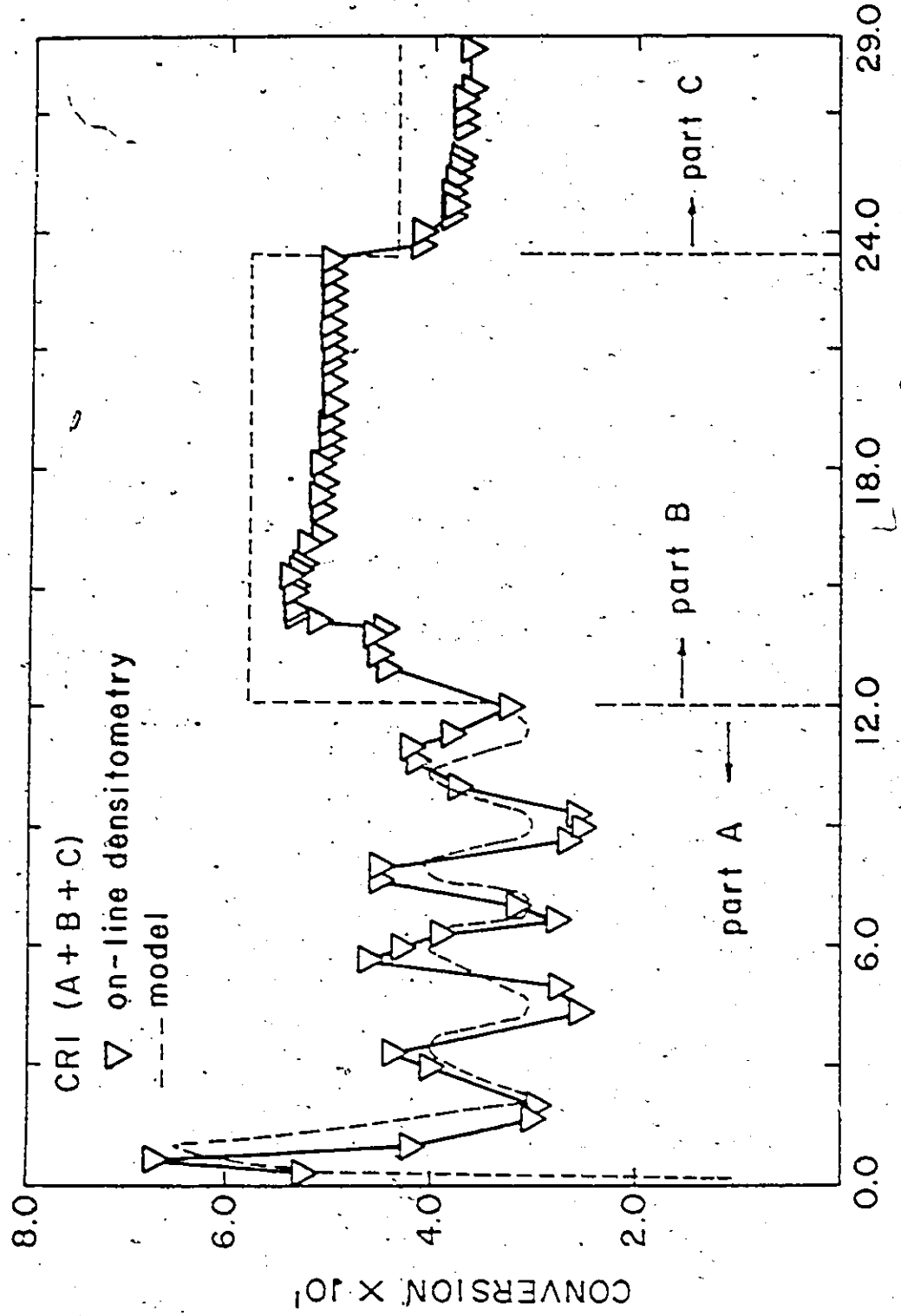

Figure (7-10). Run CR1, Parts A, B and C: R2 Conversion versus (t/θ_2)

experimentally measured for the new train design (Figure 7-12). Therefore, it is evident that, in order to successfully simulate both the oscillating and stable regions and both conversion and average particle size data, a somehow compromising set of values for D_w and ε should be sought for. Hence, we have decided to use the same parameter values throughout the thesis, since they gave very satisfactory results for all different modes of reactor operation. This is an additional indication that our model is finely tuned, but the reader and the future researcher should bear in mind that probably both D_w and ε should change in order to finely tune the model even further. No further model parameter fitting to CSTR data was attempted. Another point worth noting here is that the noticeable tendency of ε to assume higher values in order to account for both conversion and particle size is in agreement with the analysis presented in Chapter 4. One should remember that in all the figures of this chapter, the model is meant to show general predicted behaviour. The model parameters (ε, D_w) were not adjusted to fit the CSTR data but were taken from prior batch experimental data (see Chapter 4). Aside from the fact that the model parameter values were not further adjusted in the present study to fit the CSTR data, the slight discrepancy between the predicted and experimental results can be attributed to reactive impurity effects (see Chapter 9).

An on-line surface tension meter was used during CR1 to record changes in surface tension of the reaction mixture during the polymerization. The surface tension meter was placed after the densitometer from reactor 2. Pollock (1984) had observed from simulation results that conversion showed a time lag behind number of particles in its changes. That is, if the number of particles underwent a massive change due to a new nucleation, it would be around one half of a residence time before conversion would bottom out and start to rise again during an oscillation. However, a massive generation of new particles causes a large increase in surface area, hence a decrease in free soap and an increase in surface tension. Thus, it was felt that peaks in surface tension would lead an increase in conversion by roughly 15 minutes

(if θ_2 = 1/2 hour). In other words, although changes in surface tension may be small, they might be able to forecast conversion changes and thus detect particle generation points in the system.

Figure 7-11 is a plot of the surface tension changes during CR1. Comparing Figures 7-8 and 7-11 one could say that the peaks in surface tension denoted with a, b and c on Figure 7-11 do correspond to new particle generations at t/θ_2 = 2.0, 6.5 and 10.5, respectively, in Figure 7-8. The peak at ~ 57 dyn/cm is not due to a particle generation but rather due to plugging problems with the left surface tension probe. These problems started around t/θ_2 = 8.0, in which cases the probes were being cleaned up and re-immersed in the effluent stream. With clean probes, the surface tension readings assumed their previous levels quickly. During the early stages of the run, when no plugging problems had occurred, the surface tension measurements were between 30 and 38 dyn/cm, consistent with the actual surface tension of poly(vinyl acetate) latex which is close to 35 – 37 dyn/cm. When the switch to R1 took place, surface tension showed the tendency to find a stable point and become constant there, as can be seen from the last points in Figure 7-11. Unfortunately, due to latex deposits inside the probes from part A, probe plugging was still a problem and the surface tensiometer was isolated from the flow path. Although inconclusive, the surface tension results showed a tendency to stabilize at the level of 29 dyn/cm during the seeding reactor operation. This level is the same as observed by Pollock (1984) from off-line surface tension measurements.

Continuing the analysis of CR1, turbidity measurements, hydrodynamic chromatography and occasionally electron microscopy were employed to follow the evolution of average particle diameter during the polymerization. Details on the turbidity measurements for parts A and B and the interpretation of the results can be found in Kourti et al. (1985).

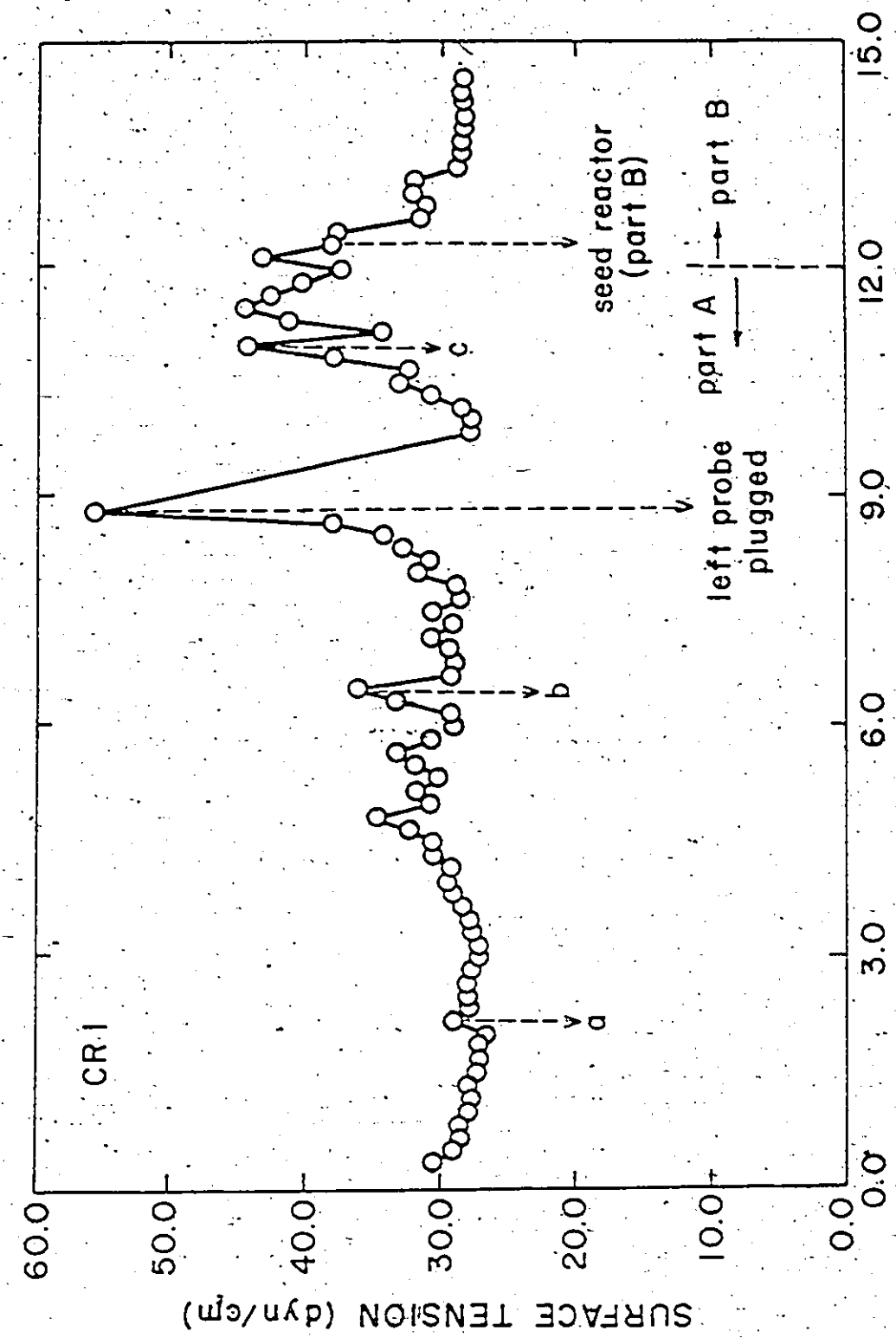

Figure (7-11). Run CR1: On-line Surface Tension versus (t/θ_2)

To investigate the oscillating region of part A electron microscopy was employed (see also Chapter 3). The concentration of the samples that were finally analyzed was close to 0.2×10^{-4} gr/lit. Sample #8 at a conversion level of ~ 40% and at $t/\theta_2 = 1.0$ showed a bimodal PSD, with the population of the large particles having an average diameter between 1000 and 1200 Å and of the small particles between 700 and 850 Å. For the same sample HDC gave a (peak) average diameter of 1250 Å. Sample CR1 #14 at conversion ~ 41% and $t/\theta_2 = 3.0$, which was taken while conversion was going towards a peak (see Figure 7-8), showed a rather broad PSD with sizes between 1900 and 2100 Å. A second population of smaller particles was not observed. The HDC result for #14 was 1500 Å. The behaviour of sample #14 is consistent with the physical picture during the oscillatory mode: a peak in diameter means that the particles residing in the reactor are growing, meanwhile depleting the reactor from free soap, thus not allowing a second generation of particles to appear. The latter was seen in sample #25, taken at ~ 28% conversion and $t/\theta_2 = 6.666$, during the valley of an oscillation. Electron microscopy again revealed two particle populations (consistent with the appearance of a second generation), one being between 2700 and 3300 Å and the other (the new one) between 600 and 1000 Å. HDC for the same sample gave 2200 Å.

One could say that the HDC values for part A were reasonably close to the electron microscopy results. For the stable part B, HDC was again close to electron microscopy and the chromatograms showed quite broad PSD samples, consistent with the operation of a continuous train. Figure 7-12 shows the picture for part B, given as average particle diameter versus t/θ_2. The circles are average diameters from hydrodynamic chromatography, while the triangles represent results from electron microscopy and are merely shown in the plot in order to independently verify the HDC measurements. The behaviour of particle size when the seeding reactor was operative is very stable. Two outliers at $t/\theta_2 = 14.333$ and 15.0 are

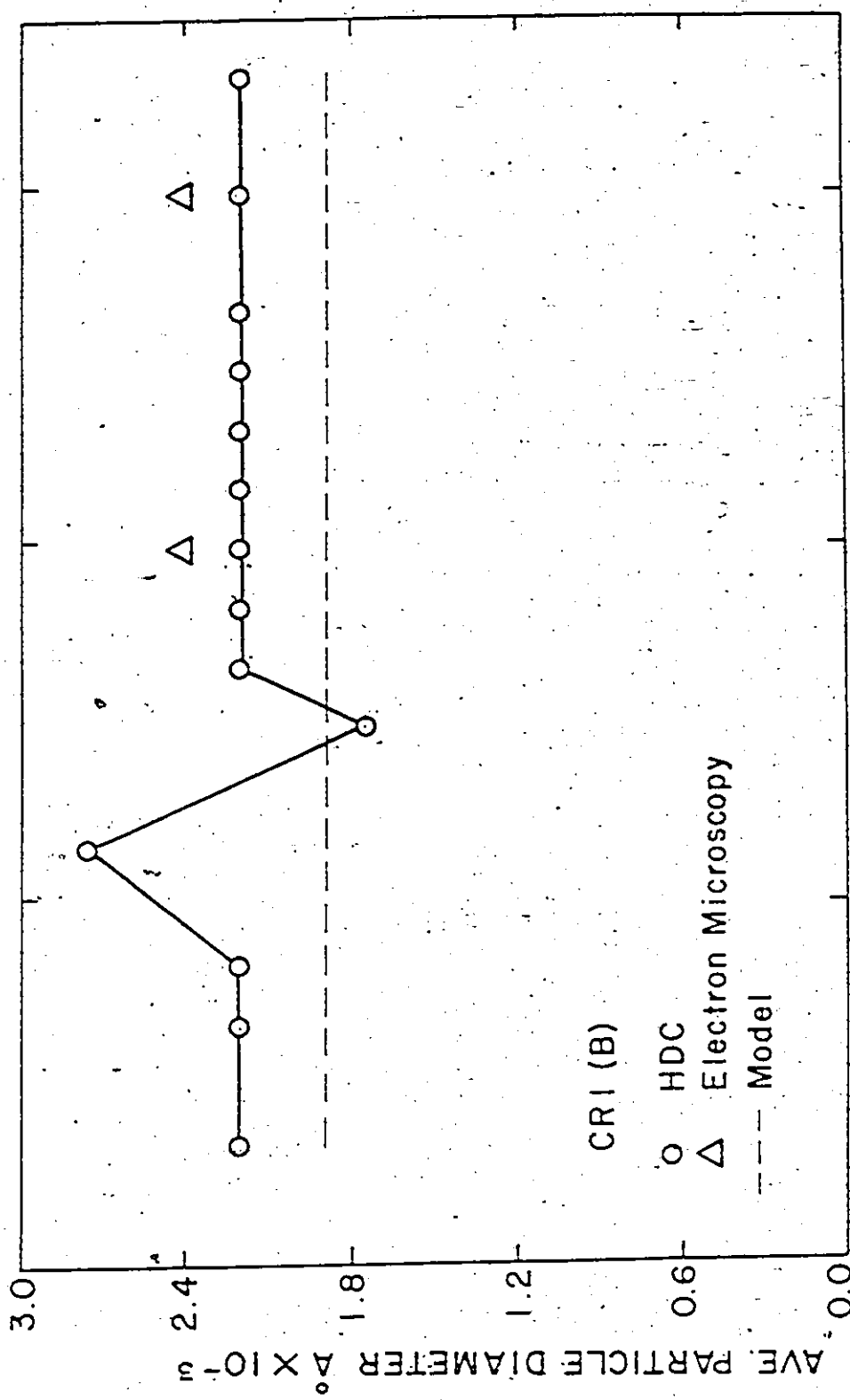

Figure (7-12). Run CR1, Part B: Average Particle Diameter versus (t/θ_2)

positively due to experimental measurement error. The electron microscopy micrographs for part B showed broad distributions (compared with the almost monodispersed samples from a batch reactor in Chapter 4) but they did not reveal an appearance of new particle populations. HDC measurements on some of the part C samples clearly showed evidence of latex coagulation (the agglomerates never came out from the columns) and hence no further analysis was performed for parts C and D of CR1.

The dashed line in Figure 7-12 is the model predictions for the sizes of part B of CR1. Model and experimental data are quite close. It is evident that the model slightly underestimates particle size, but a higher value for ε (see previous discussion on Figure 7-10) would yield results in better agreement. The picture, though, as it stands, is very satisfactory, considering that particle size is one of the most difficult properties to theoretically predict, especially when the prediction is a simultaneous one with conversion and for different modes of process operation.

The good reproducibility of our off-line gravimetric conversion data is very well illustrated in Figure 7-13 for continuous run #2 (CR2), parts A and B. The triangles represent gravimetric data obtained two days after the run and the circles are data that were obtained five days after the run. One can also notice that theoretical predictions and observed behaviour are in good agreement, keeping exactly the same values for the model parameters as in CR1. Figure 7-14 shows again conversion data for parts A and B of CR2. The inverted triangles now represent conversion results from the on-line densitometer, which was placed at the R2 outlet. The off-line gravimetry and on-line densitometry are in excellent agreement. As can be seen from both figures, the induction time which was observed during CR2 was again less than 30 minutes (i.e., roughly 1/2 R2 residence time, which is consistent with CR1 and the observations by Kiparissides (1978)).

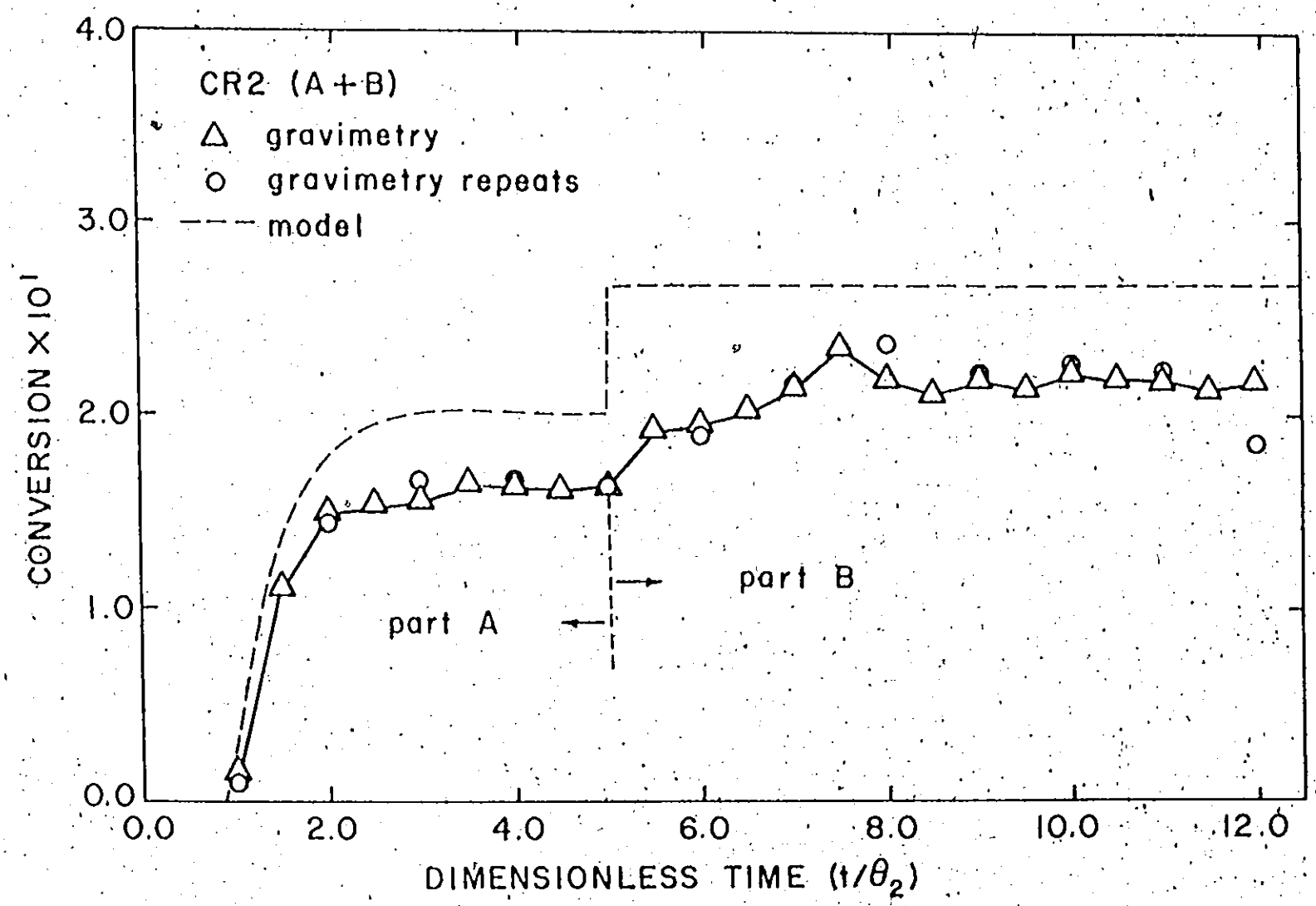

Figure (7-13). Run CR2, Parts A and B: Conversion versus Dimensionless Time

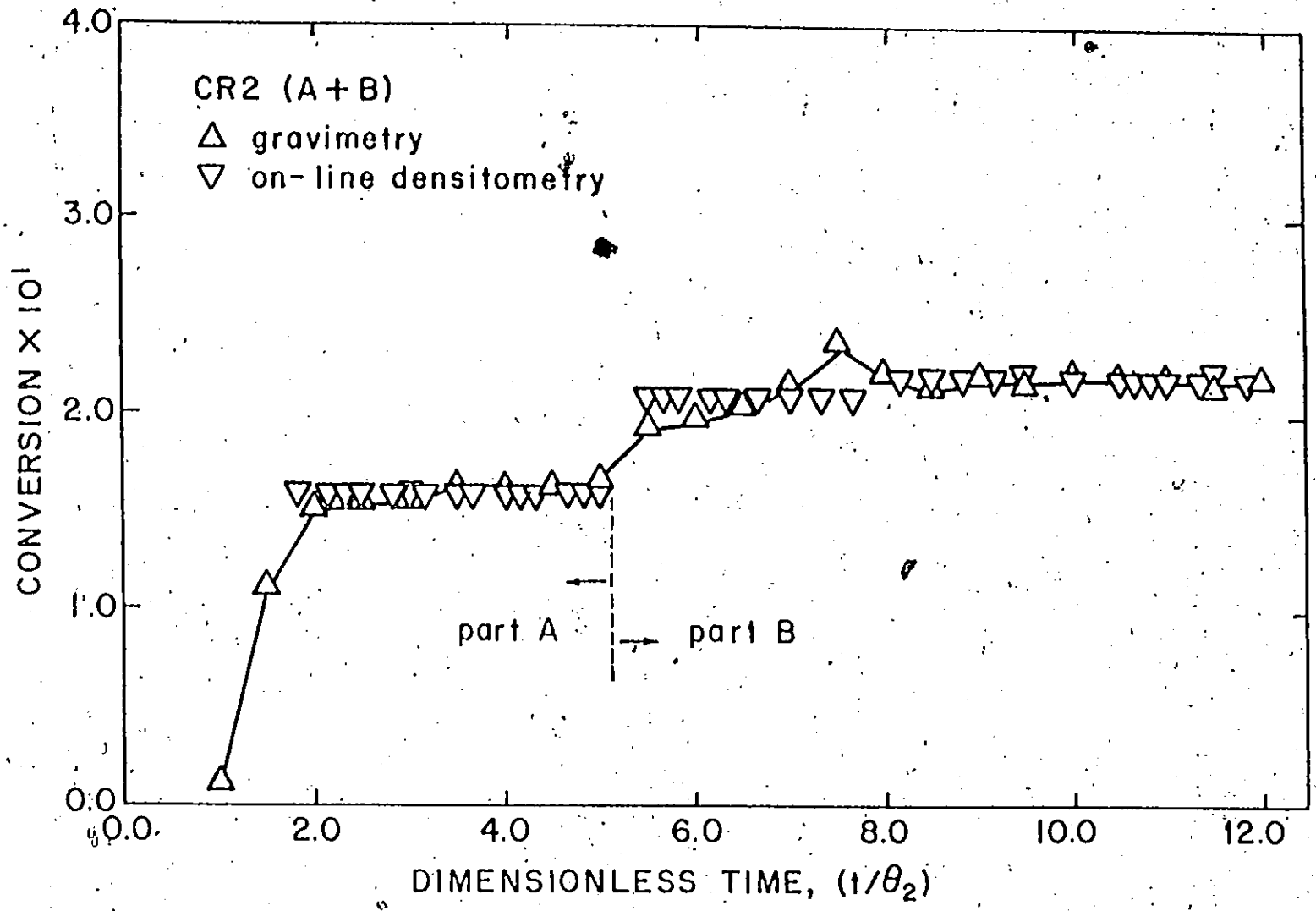

Figure (7-14). Run CR2, Parts A and B: On-line Conversion versus (t/θ_2)

During the switch from part A to part B the flow split was decreased from 0.401 to 0.269. This was accomplished by setting the W_1 flow rate equal to zero, so the water going to R1 during part B was the water with the initiator and emulsifier solutions. This created an environment in the seeding reactor of higher initiator and soap concentrations, which led to the increase in conversion level during part B. Again, the train behaviour during both parts was very stable.

The stable behaviour of the train is also very well illustrated in Figure 7-15, which plots average particle diameter (in Ångstroms) from hydrodynamic chromatography versus dimensionless time. The triangles on the plot represent reproducibility checks of the HDC results. Part A gave a particle diameter close to ~ 1600 Å, while during part B the average size was close to 1500 Å, due to the decrease in split. The HDC results were also independently confirmed with electron microscopy (concentration of the electron microscopy solutions ~ 4.5×10^{-4} gr/lit).

Parts C and E from run CR2 are discussed in Appendix X and more experimental results are presented there.

7.6 Conclusions

The use of comprehensive reactor models which incorporate detailed chemistry and physics of the polymerization phenomena involved gives a deeper understanding of polymer production processes and permits the design of improved systems which otherwise might not be apparent. Control problems can therefore be anticipated and largely eliminated at the reactor design stage, giving control systems which are relatively simple and highly effective.

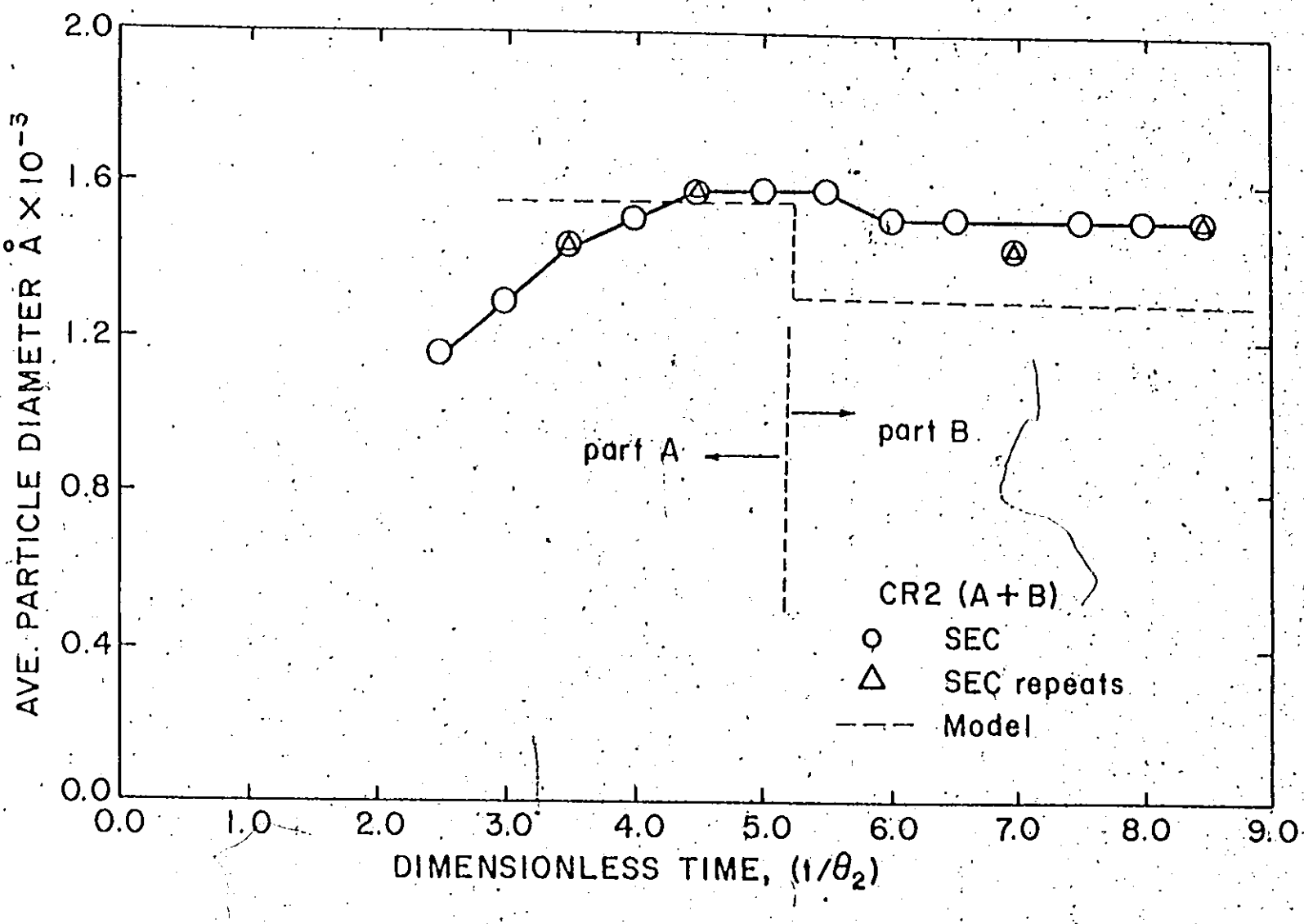

Figure (7-15). Run CR2, Parts A and B: Average Particle Diameter versus Dimensionless Time

Theoretical and experimental studies concerning the continuous production of poly(vinyl acetate) latex have clearly demonstrated the highly improved dynamic performance of a redesigned reactor system over that of the conventional CSTR train. This system used a small prereactor as a continuous seeder for a conventional CSTR train together with a judicious splitting of the monomer and water feeds between the prereactor and the subsequent large reactors. The new configuration is stable (oscillation-free) and very flexible in controlling particle size and conversion. This control is accomplished by manipulating the initiator feedrate to the first (small) reactor, and the flow split of the monomer and water feedrates between the small and the first large reactor of the train.

The split feed reactor design is not only appropriate for the continuous emulsion polymerization of "Case I" oscillatory systems, but it also alows much more flexible control of conversion and particle size for any type of emulsion system. It has many benefits for non-oscillatory "Case II" systems as well, since it offers better control potentials and less sensitivity of the reacting system to impurities (see Chapter 9). By recycling all recovered streams into the second reactor of the train, thus not disturbing the small first nucleating reactor, the split feed configuration gives a system which is much more stable to reactive impurty effects. Consequently, the subsequent fundamental control problem is considerably simplified as well.

CHAPTER 8

EXTENSIONS OF THE MODEL TO THE PRODUCTION OF POLYMER AND COPOLYMER LATEXES OF VINYL CHLORIDE

8.I Introduction

Poly(vinyl chloride) (PVC) is produced today by three major processes: suspension, emulsion, and bulk polymerization. Although there have been a variety of reports in the literature concerning bulk and suspension PVC reactors, very few papers have been published on VCM emulsion polymerization and even fewer on continuous VCM emulsion systems.

A model for the bulk and suspension polymerization of vinyl chloride has been developed and experimentally evaluated by Abdel-Alim and Hamielec (1972, 1974). The model was shown to agree quite well with experimental rate data for several typical commercial initiator systems. The effect of diffusion-controlled reactions on the polymerization rate and the molecular properties of poly(vinyl chloride) was also studied by Hamielec et al. (1982) and Hamielec (1983a, 1983b) for PVC bulk and suspension reactors. Polymer reactor operating procedures which could give higher productivity with minimal loss in the thermal stability of PVC were suggested. Recently, Kelsall and Maitland (1983) developed a mathematical model for the production of PVC by suspension polymerization. A major difference from most previous models was the incorporation of mass transfer for various species between the different phases involved, and the possibility of nonuniform partitioning of initiator concentration and its efficiency. An attempt was also made to model particle morphology.

Keyes and Kennedy (1974) were concerned with the optimal temperature control problem in PVC suspension reactors. First, they developed a non-linear process model and then derived a regulator from the model utilizing variational techniques, in an effort to apply an adaptive temperature control scheme to their reactor. Macoveanu et al. (1977) used the Abdel-Alim and Hamielec (1972, 1974) model to establish temperature programs to obtain specified molecular weight averages for PVC suspension polymerization at constant rate. For an allowed temperature range and polymerization rate, the model gave a suitable temperature program.

Very few studies have been carried out on the modelling of VCM emulsion polymerization. After a brief discussion of these studies, a model for the continuous emulsion polymerization of vinyl chloride, with a minimum number of adjustable parameters that can be easily estimated from experimental data, will be presented. The model will then be extended to cover emulsion copolymerization of vinyl chloride/vinyl acetate and finally used to simulate latex reactor performance under a variety of operating conditions.

8.2 Emulsion Polymerization of Vinyl Chloride

Emulsion PVC resins are produced commercially by batch, semi-batch, and continuous processes. One of the first detailed studies on the kinetics of emulsion polymerization of vinyl chloride was reported by Ugelstad et al. (1969), followed by a similar investigation by Friis and Hamielec (1975a). Ugelstad (1977) gave a very thorough and critical review of existing models for VCM polymerization in solution, bulk and emulsion processes. His model is the most general one for bulk and suspension PVC polymerization. Theory and data from the three previously mentioned sources will be extensively used for the development of a dynamic PVC latex reactor model in the following section.

The only reported experimental investigation of the continuous emulsion polymerization of VCM was by Berens (1974). A simplified mathematical model for the rate of change of conversion in a single continuous stirred-tank reactor was derived. Experimental data on conversion and particle size were in good qualitative accord with the predictions of this empirical model using adjustable parameters estimated from batch polymerization data. Gatta et al. (1969) have published an extensive set of data for semi-continuous seeded VCM emulsion polymerization. Their aim was to find the conditions required to obtain uniform growth of the seeded particles in a single step. Min and Gostin (1979) developed a mathematical model for the semi-batch emulsion polymerization of vinyl chloride. The model was shown to predict a bimodal PSD in seeded emulsion polymerization, which was in good agreement with pilot plant data. The effects of the following variables on the final latex PSD were investigated: seed particle size, quantity of seed, solid content of seed, and initial amount of initiator. Their model could be used to identify practical techniques for metering surfactant and initiator to control the growth of small polymer particles. Gordon and Weidner (1981) used the ideas of Min and Gostin (1979) to control the PSD in the emulsion polymerization of vinyl chloride by manipulating the emulsifier feed rate as a function of conversion. An on-line measure of conversion was obtained from an unsteady-state heat balance and then used as the feedback variable to control emulsifier feedrate. Finally, Lin et al. (1980) tried to control particle size in vinyl chloride emulsion systems by varying the ratio of monomer to water at the beginning of the reaction. They were thus able to produce PVC latexes which had a particle size of about 1 μm in a single step.

8.3 PVC Latex Reactor Model Development - Dynamic CSTR

8.3.1 Homopolymerization Case

Vinyl chloride is a monomer which conforms to Case I emulsion polymerization kinetics. It is generally concluded that monomer consumption occurs predominantly in the polymer particles and that the average number of free radicals per particle is much less than one half as a consequence of rapid radical desorption (see Nomura and Harada (1981a) for a further discussion concerning radical desorption).

A general model for Case I homopolymerizations has been developed in Chapter 2 of this thesis and applied to describe vinyl acetate latex reactor performance. VAc is another monomer (similar to VCM in many ways) which conforms to Case I kinetics. Since both vinyl chloride and vinyl acetate conform to the same reaction kinetics scheme, the same mathematical description should theoretically apply to both systems, when differences in characteristic kinetic or physical constants are appropriately accounted for. The VAc model was thus modified to apply to VCM emulsion polymerization.

Equation (I-33) was now employed to describe the rate of change of the number density function in the phase plane of the system for the general population balance equation. In this way a varying volume reactor case could be easily tackled and several options were investigated, namely starting up the reactor full or half full of water or emulsion recipe and empty. Both seeded and unseeded feed streams were considered. The computer program which was written for the numerical simulation of the system could handle a variety of modes of reactor operation: batch, semi-batch, single CSTR, train of CSTR's and CSTR- tube. An extensive simulation study was initially carried out to check whether the model was able to give reasonable trends. These results and more details can be found in Smith et al. (1985).

8.3.2 Copolymerization (VCM/VAc) Case

The copolymer model development followed the homopolymer model development, properly accounting though for the presence of two monomers, two types of radicals and other implications that a comonomer system can give rise to. Information from Hamielec and MacGregor (1983) was found very helpful.

To our knowledge, this is the first time that a copolymerization model has been developed based on a population balance approach. The resulting differential equations are more involved than those of the homopolymer case, hence it was felt appropriate to include a few useful hints concerning the copolymer model development and some of the difficulties encountered during the development stages in Appendix XIII.

The copolymers of vinyl chloride/vinyl acetate are widely produced all over the world, however, there has yet to be experimental data published in the open literature concerning this system. Direct comparison of the model's predictive power with pilot plant data was not possible due to the lack of literature sources for the specific system. However, the trends in the model's predictions were compared with theoretical postulations or experience from similar systems and were found in good agreement. An extensive simulation study by Murray et al. (1985), results from which are also shown in Appendix XIII, serves as a forerunner for investigating this particular system.

8.4 Model Applications and Discussion

The previously developed PVC latex reactor model is now applied to several modes of emulsion homopolymerization reactor operation. Simulation results concerning the application to emulsion VCM/VAc copolymerization systems are shown in Appendix XIII.

8.4.1 Batch Reactors

As a first application of the reactor model, batch emulsion polymerization was simulated. The model equations are used with the inflow and outflow terms both set equal to zero. Values of the rate constants or other physical constants used in the simulation computer program are given in Table 8-1, along with the literature sources. For more details on other values employed see Chapter 4.

Figure 8-1 shows measured and predicted conversion-time histories for batch VCM emulsion polymerization. The experimental data were measured by Ugelstad et al. (1969). In all these runs, the recipe consisted of 510.0 gr of vinyl chloride, 780.5 gr of water, and varying amounts of potassium persulphate (KPS) initiator and sodium lauryl sulphate (SLS) emulsifier. All polymerization runs were performed at 50°C. To obtain the model predictions shown in Figure 8-1 the diffusion coefficient of monomeric radicals in the water phase (D_w) and the ratio (ε) = (k_{ab}/k_m) of the radical capture rate constant (radical absorption by polymer particles) to the rate coefficient of micellar nucleation were adjusted differently from the VAc case. D_w was set equal to 0.2780×10^{-6} dm^2/sec and ε equal to 0.6980×10^2 for all batch simulation runs. In the case of Figure 8-1e, Ugelstad et al. (1969) reported a number of polymer particles per liter of water corresponding to a conversion level of 18.9% equal to 0.47×10^{19}. The model prediction for the same conversion level was 0.61×10^{19}. Figure 8-2 is a plot of the logarithm of number of particles per liter of water versus the logarithm of emulsifier concentration (gr of emulsifier/lit water). The triangles represent experimental observations from Ugelstad et al. (1969), whereas the solid curve represents our model predictions.

TABLE 8-1

Kinetic Parameters and Other Physical Constants

Used in the PVC Computer Program

C_m	$1.098\times10^{-3}\exp(-2741.82(1/T-1/323))$*	Friis and Hamielec (1975a)
d_M (gr/lit)	$(0.9479-0.00189(T-273))\times1000$	Abdel-Alim and Hamielec (1972)
d_p(gr/lit)	1400.	
f	0.7	Chapter 4
k_d (sec^{-1})	$0.05\times10^{18}\exp(-33320/RT)$	Hamielec (1984)
k_{fp} (lit/gmole-sec)**	$5.\times10^{-1}$	Friis and Hamielec (1975a)
k_p* (lit/gmole-sec)***	$1.\times10^{5}$	Friis and Hamielec (1975a)
k_p (lit/gmole-sec)	$3.694\times10^{4}\times(MW/d_M)^{1/2}\exp(-864.62(1/T-1/323))$	Friis and Hamielec (1975a)
m	35.	Nomura and Harada (1981a)
MW (gr/gmole)	62.5	
S_a (dm^2/molecule)	4.2×10^{-17}	Vijayendran (1971), Liegeois (1976), Maron et al. (1954), Palmgren (1976), Pramojaney (1982)
x_c	$1.409633-(0.002\times T)$	Friis and Hamielec (1975a)
VCM solubility	1.06% by wt (25°C)	Friis and Hamielec (1975a)
δ	0.5	Chapter 4

* T is temperature in degrees Kelvin

** C_p (VAC) ~ $4.\times10^{-4}$, C_p (VCM) ~ $5.\times10^{-5}$

*** PVC: ~ $2.\times10^{-4}$ branch points per repetition unit
VAC: ~ 1.5×10^{-3} branch points per repetition unit

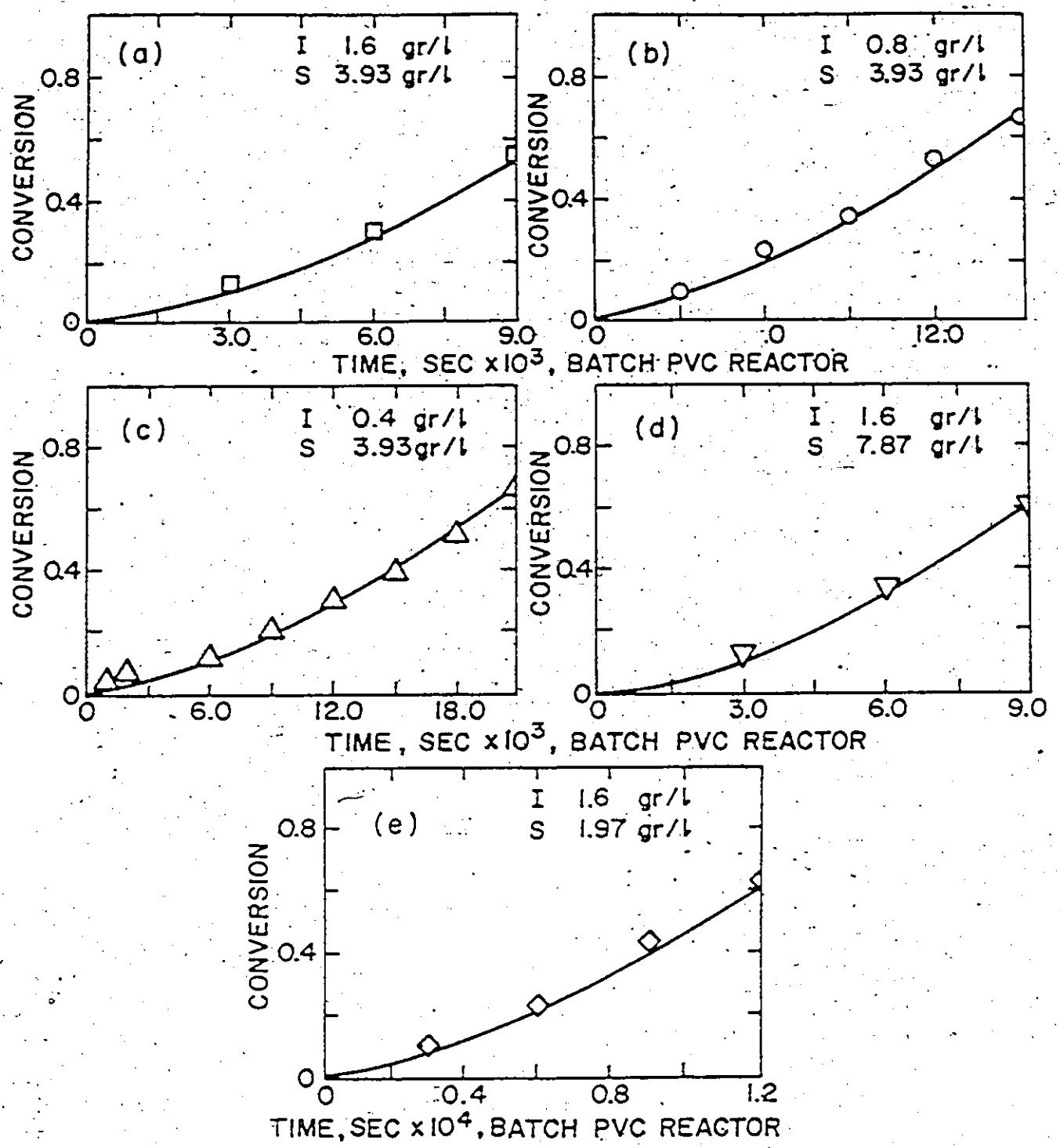

Figure (8-1). Batch PVC Emulsion Polymerization: Conversion-Time Histories

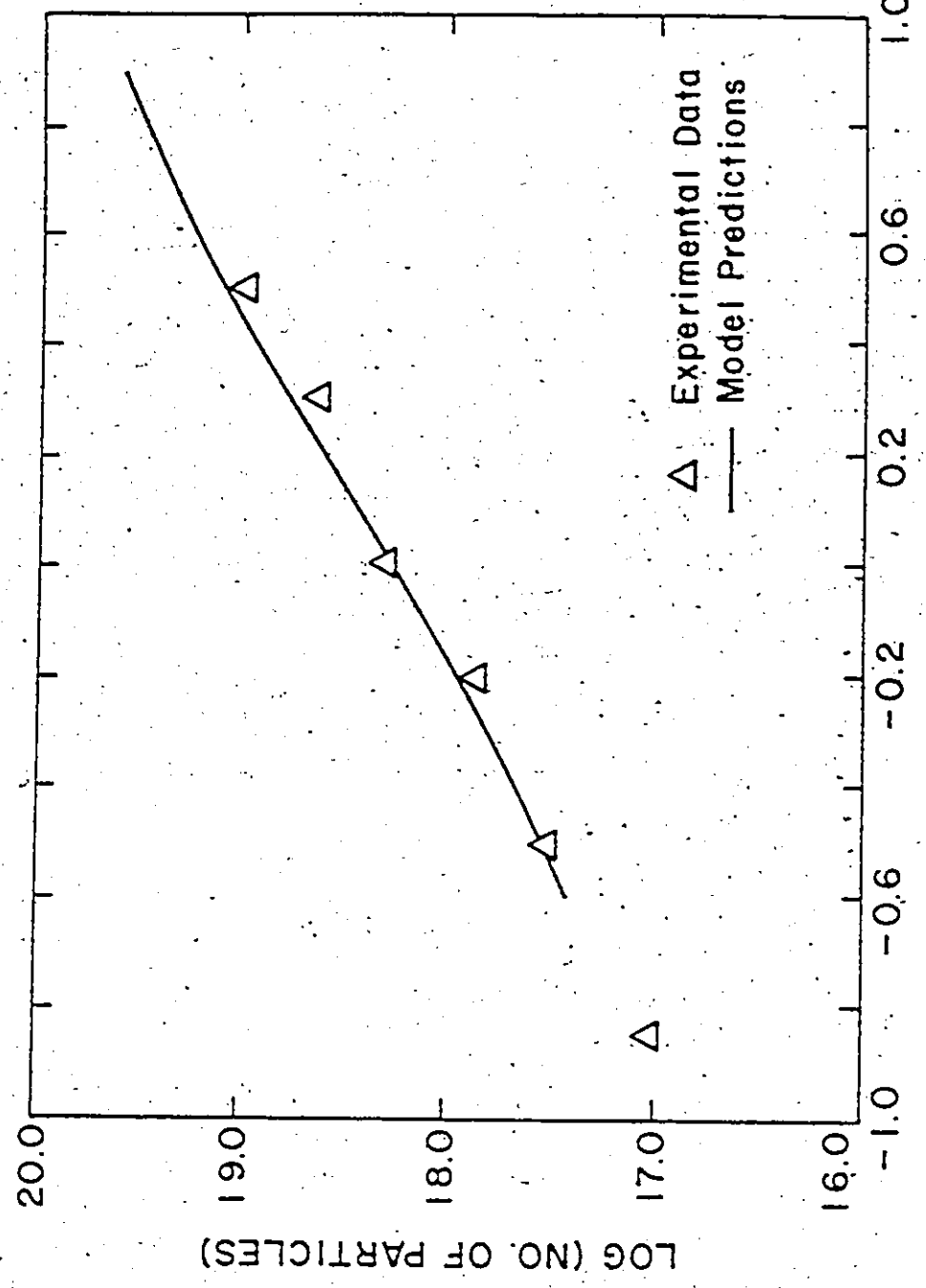

Figure (8-2). Log (Number of Polymer Particles) vs. Log (Emulsifier Concentration) in Batch PVC Emulsion Polymerization

More conversion-time histories from Behrens (1974) for batch emulsion reactors are shown in Figure 8-3, together with the model predictions. The recipe used consisted of 1.0 liter of water, 0.47 liters of VCM and again varying amounts of soap and initiator, as indicated on the figure. For the cases of Figure 8-3b, Berens (1974) measured 0.68×10^{18} particles per liter of latex for the upper curve (I = 1.0 gr, S = 3.0 gr) and 0.34×10^{17} for the lower one corresponding to I = 1.0 gr and S = 1.15 gr. Our model's predictions were 0.2×10^{18} and 0.14×10^{17}, respectively. In Figure 8-3a, the same amount of emulsifier was used for both runs. Berens (1974) estimated $\sim 0.38 \times 10^{17}$ particles per liter of latex for both cases, while our model's prediction was close to $\sim 0.22 \times 10^{17}$.

Liegeois (1976), using 400.0 ml of water, 280.0 gr of VCM, 280.0 mgr of KPS and 2.5 gr of SLS at 50°C, measured by electron microscopy PVC latex particle diameters approximately 190 Å and estimated a number of $\sim 34 \times 10^{15}$ polymer particles per ml of water, for a conversion level of 24%. The model predicted an average particle diameter equal to 200 Å for the same conversion level and for the same experimental conditions.

Ugelstad et al. (1969) reported that the average number of radicals per polymer particle should range between 10^{-1} and $5.\times10^{-4}$ (see also Ugelstad (1977)) in a typical batch emulsion case. Figure 8-4 gives the model prediction for this number ranging from $\sim 0.5 \times 10^{-4}$ to 2.0×10^{-4}, which is in agreement with the physical picture in Case I emulsion kinetics.

A comparison between theoretical and experimental molecular weight distributions in vinyl chloride batch emulsion polymerization was given in Friis and Hamielec (1975a), where they simulated experimental results from Lyngaae- Jorgensen (1971). For a case of batch emulsion PVC polymerized at 50°C, Lyngaae-Jorgensen (1971) measured a weight average molecular weight equal to 0.1078×10^{6}, a number average molecular weight equal to 0.508×10^{5} and a polydispersity ratio equal to 2.12. Our model

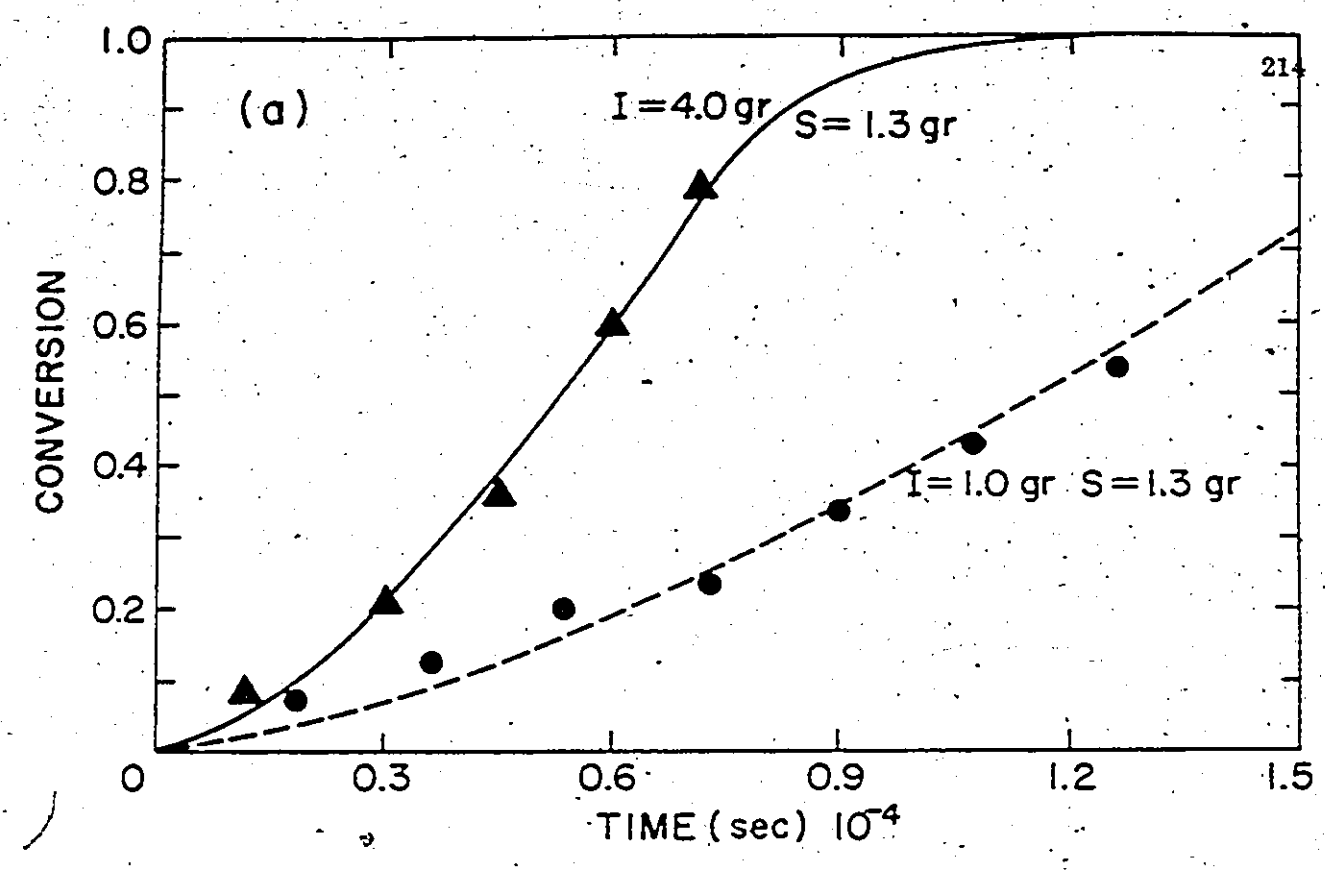

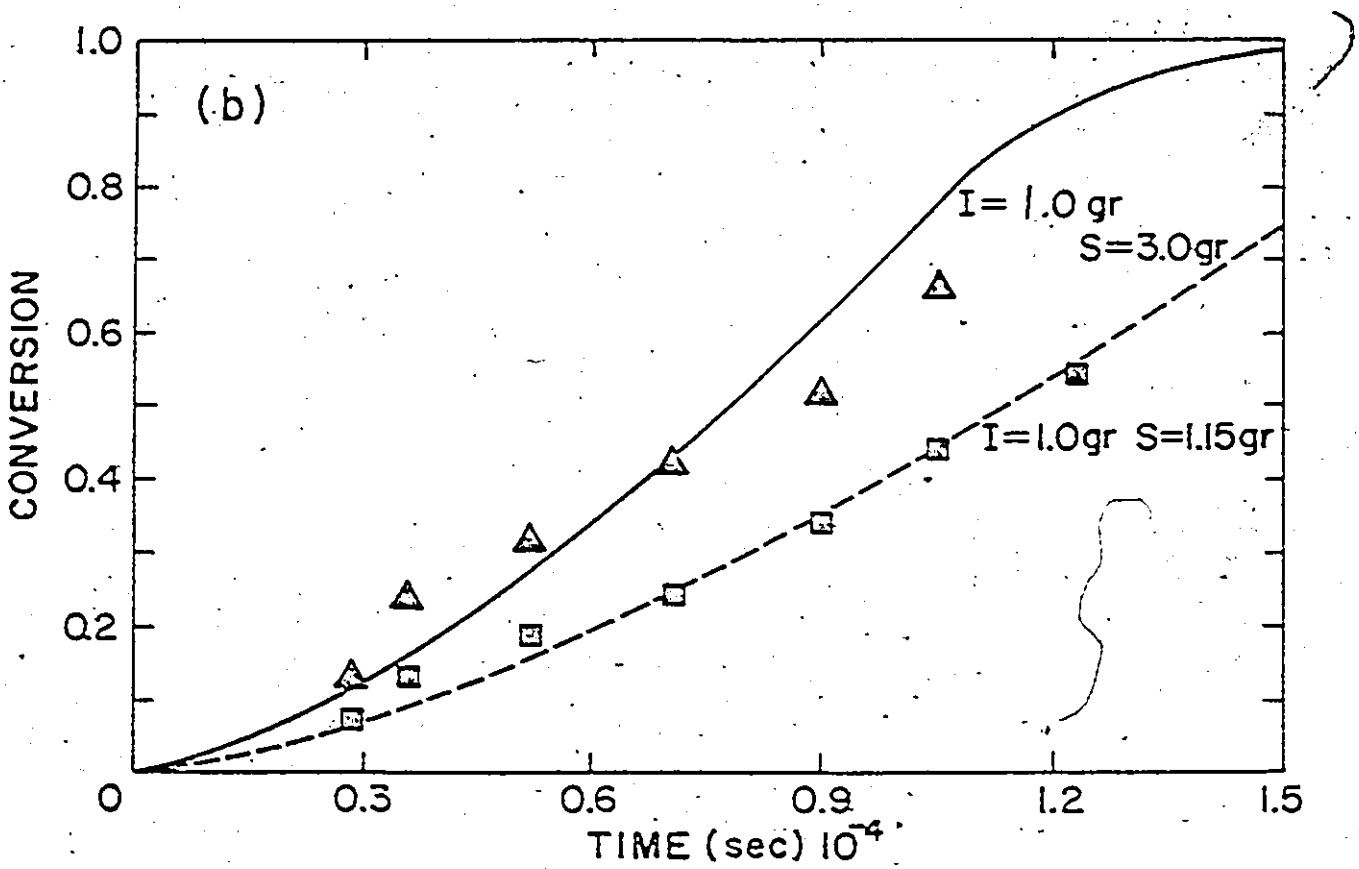

Figure (8-3). Conversion-Time Histories in Batch PVC Emulsion Polymerization for Different Initiator and Emulsifier Concentrations

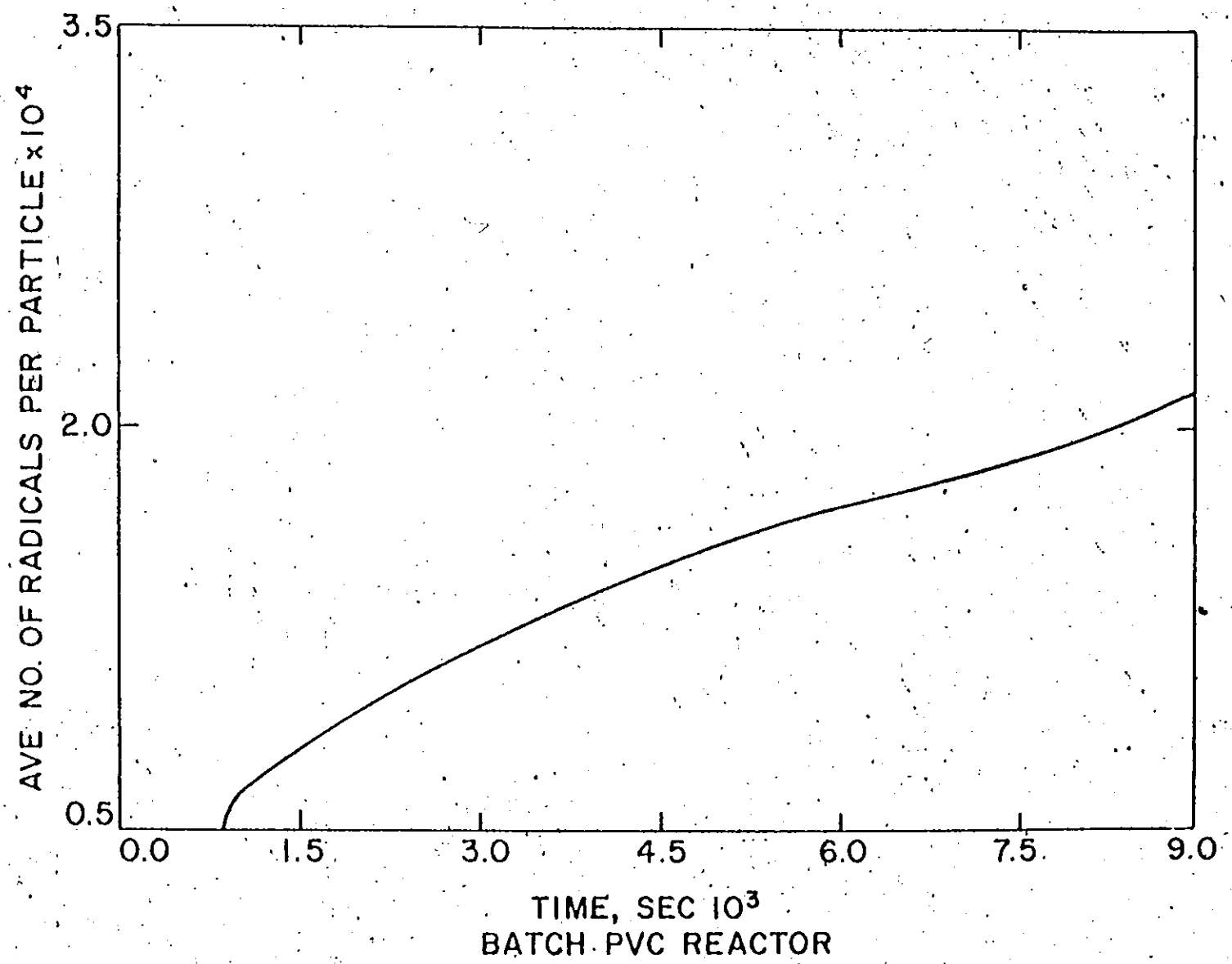

Figure (8-4). Average Number of Radicals per Particle During the Course of a Typical Batch VCM Emulsion Run

predictions were 0.1139×10^6, 0.570×10^5, and 2.0, respectively. The same article reported that the polydispersity ratio changed from 2.02 to 2.09 for conversions between 92.5 and 5.7%, which is in agreement with the model prediction of 2.0 (see also Friis and Hamielec (1975a)).

The excellent agreement of our model predictions with experimental data for batch emulsion PVC production is evident from the previous discussion and Figures 8-1 through 8-4. The model was shown to successfully simulate batch reactor performance and to adequately predict conversion, number of polymer particles, average particle size, average number of radicals per particle, and molecular weights.

8.4.2 Semi-batch Reactors

The application of the model to semi-continuous reactor operation was implemented in the following way: the reactor would start with an initial batch charge (which could be seeded or unseeded). Nucleation of polymer particles was completed during this initial stage. Then, at a prespecified conversion level, the semi-batch part would start (i.e. inflow of ingredients), which could also be seeded or unseeded. The purpose of this part was to grow the polymer particles as fast and as much as possible, according to the final target. A finishing (batch) stage would then be optional, from a prespecified conversion level or reactor volume on. The purpose of this final stage was to completely react the residual VCM.

Illustrative simulation results from the semi-batch portion of the model can be found in Smith et al. (1985). One point worth mentioning here is that the model was able to successfully simulate the behaviour experimentally observed by Lin et al. (1980) in a semi-batch emulsion polymerization of VCM, where the weight ratio of VCM to water was varied at the beginning of the reaction with the final aim to effectively control latex particle size. The result is shown in Figure 8-5 and is in agreement with what Lin et al. (1980) measured.

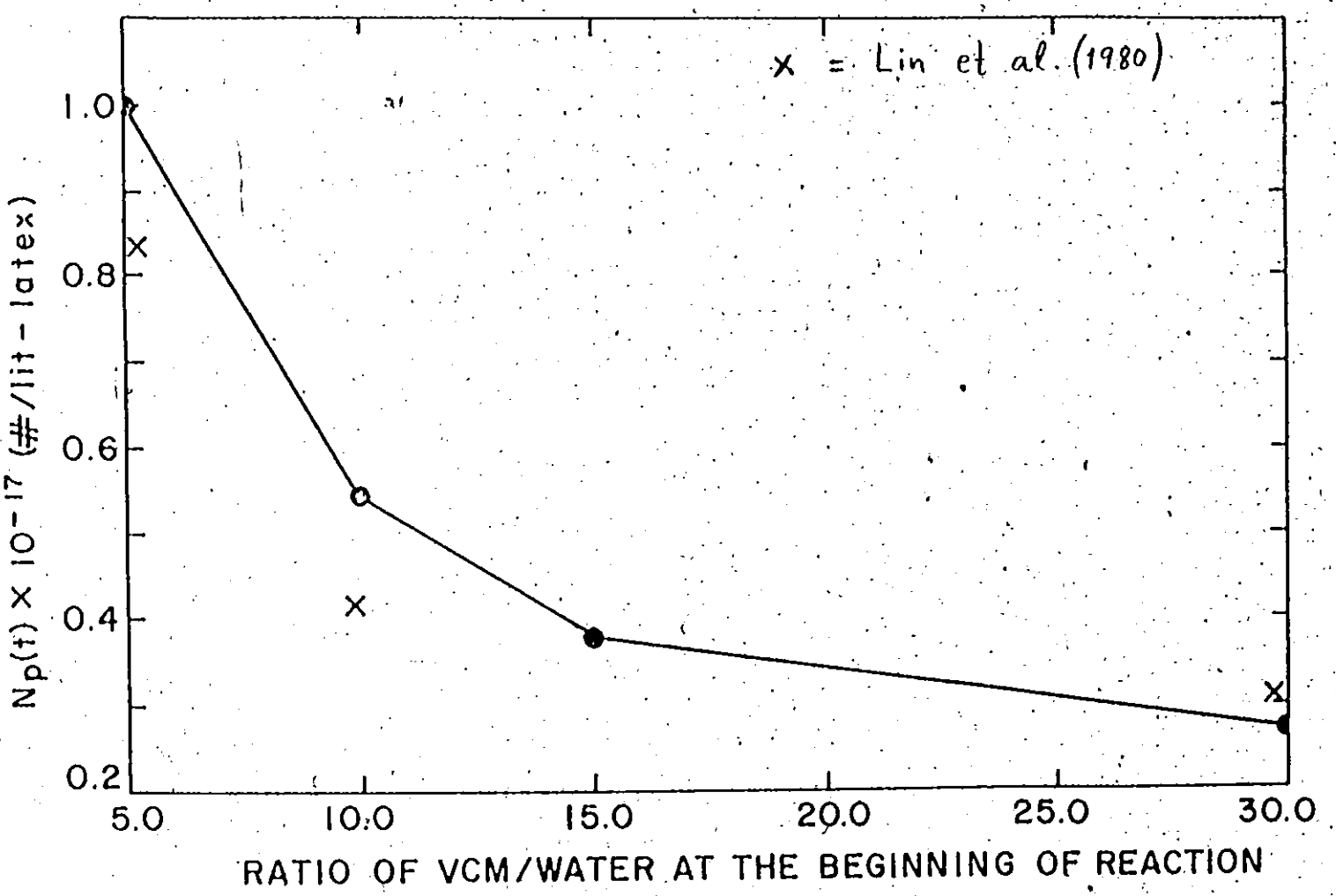

Figure (8-5). Semi-batch VCM Emulsion Polymerization: Number of Particles vs. Ratio of (VCM/water)

8.4.3 Continuous Reactors

With the exception of Berens (1974), very little work has been done on continuous PVC emulsion reactor modelling. In his article, Berens (1974) presented a simple, empirical relation for predicting the behaviour of a continuous PVC system from rate data on batch polymerizations in corresponding recipes. His batch data were in agreement with the data of Ugelstad et al. (1969). As he mentions, "the kinetic relations developed by Ugelstad, particularly the dependence of rate upon particle number and conversion, are sufficiently complex that their rigorous application to a continuous process will be difficult". We think that our model is "sufficiently complex" to incorporate "rate dependence upon particle number and conversion", and yet simple enough to be easily and successfully used in describing continuous reactor performance.

Berens (1974) conducted experiments in a single CSTR at 50°C, using SLS emulsifier and KPS initiator (and trisodium phosphate buffer). The start-up procedure that he used was to charge the reactor with the emulsion recipe (except initiator) and then, at time zero, to inject initiator and start at the same time feeding and withdrawal of the several streams. The feed streams contained ingredients at the same proportions as the recipe in the reactor.

We will now try, in what follows in this subsection, to show that our model predictions give the same trends, lead to the same observations and conclusions, and can successfully follow Berens' (1974) experimental results reported in his interesting article.

(i) Single CSTR:

Figures 8-6a, 8-7a and 8-8a show the simulated behaviour for a single unseeded CSTR. The recipe consists of 400 gr vinyl chloride/liter of water and 0.01 gmoles/liter of latex

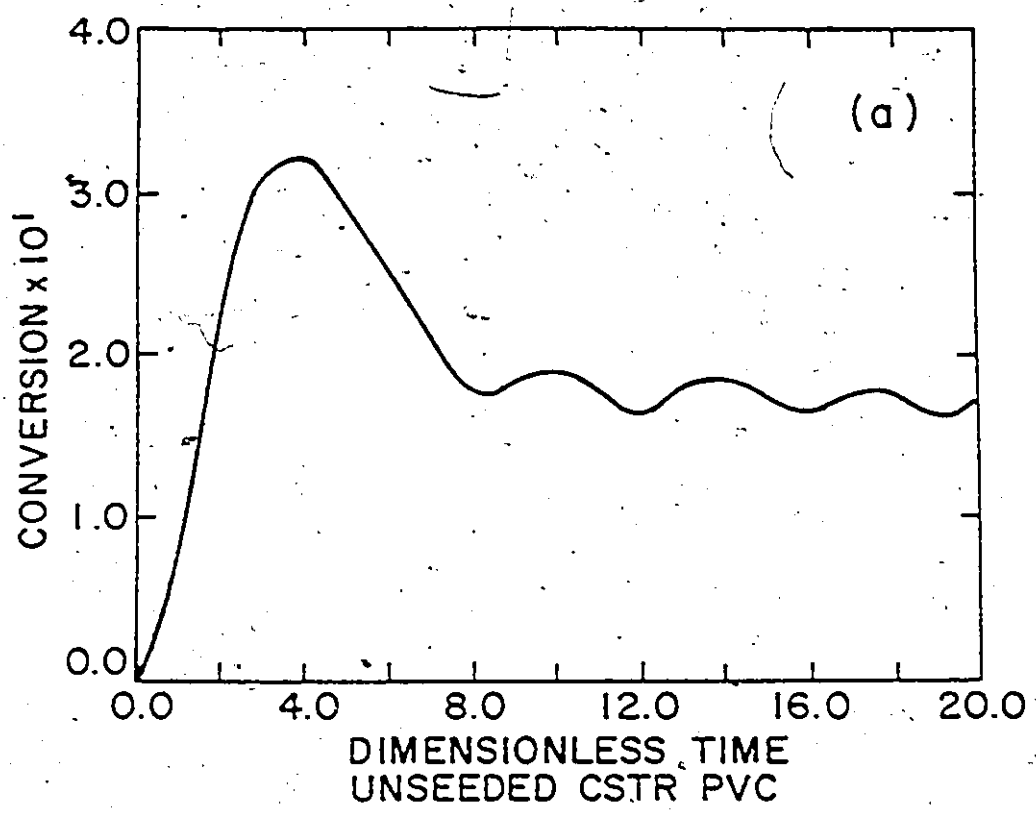

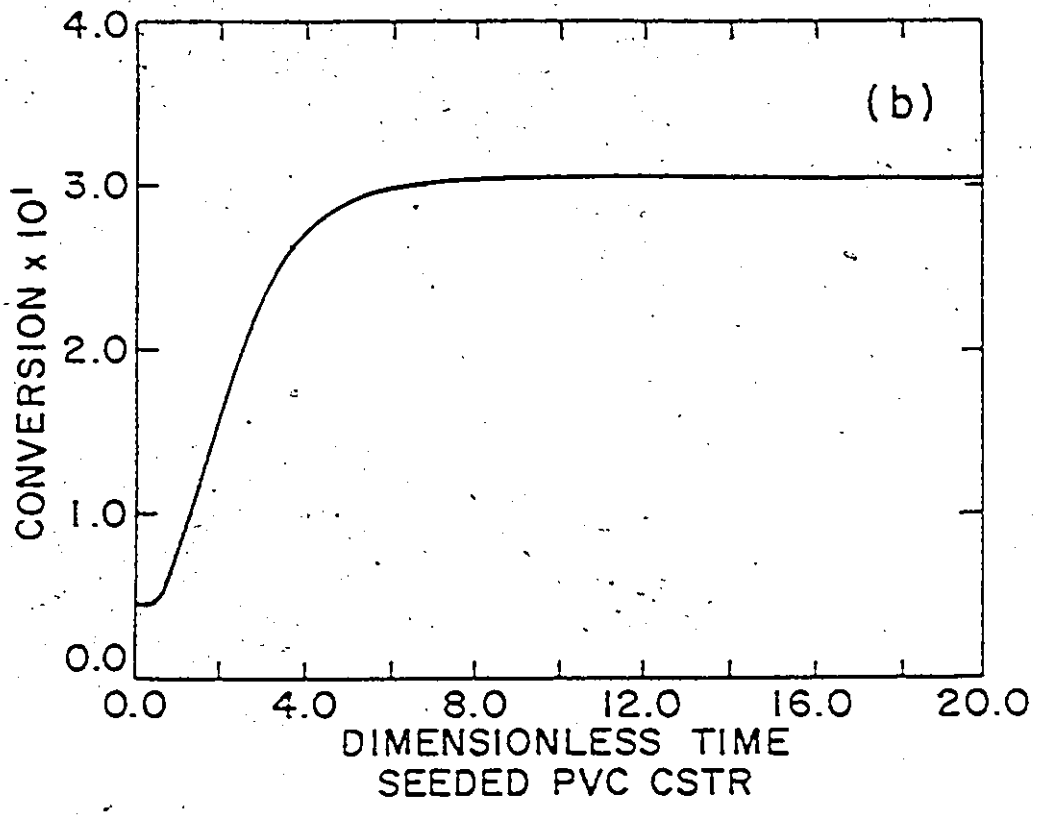

Figure (8-6). Conversion vs. Dimensionless Time: Unseeded vs. Seeded PVC CSTR

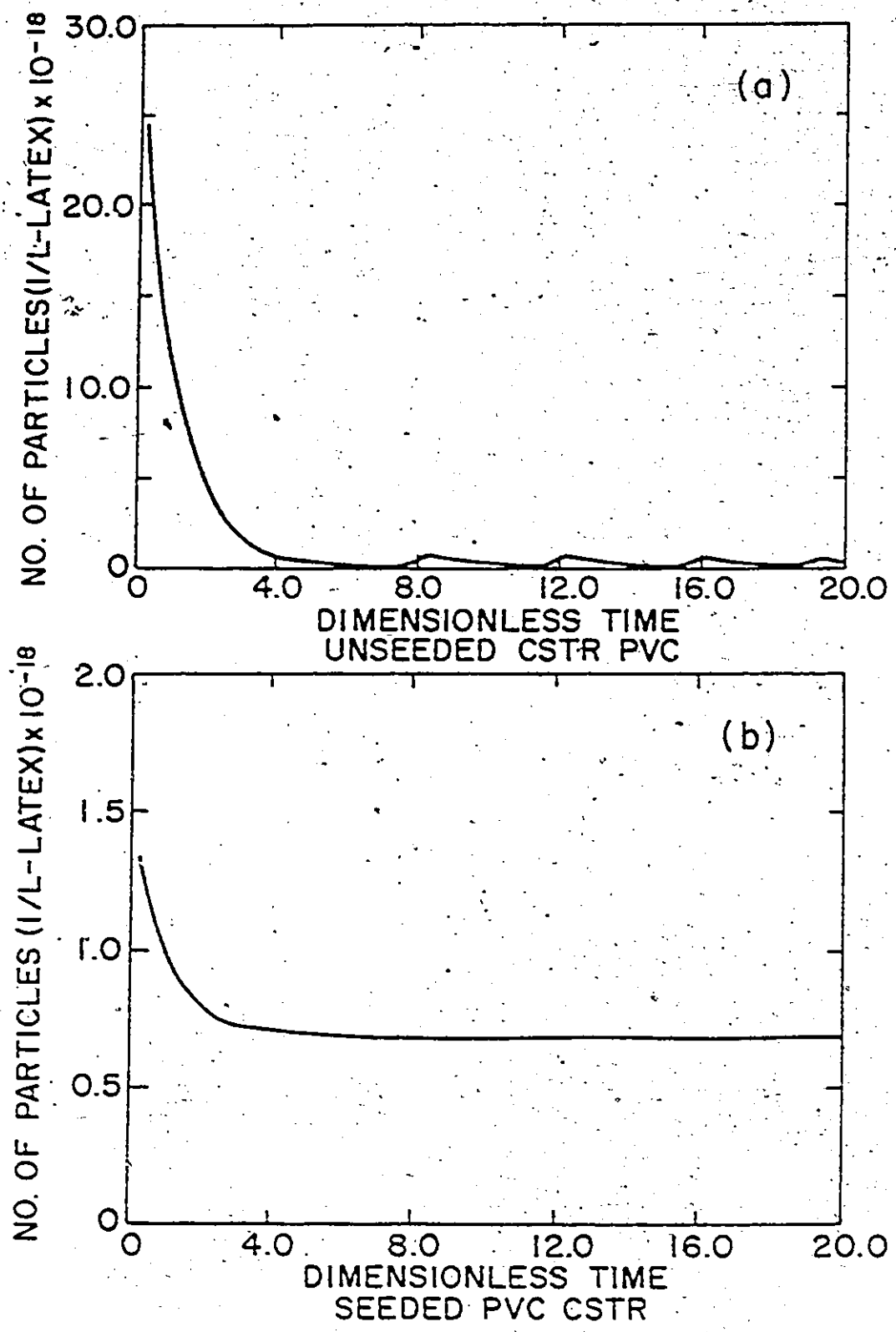

Figure (8-7). Number of Particles vs. Dimensionless Time: Unseeded vs. Seeded PVC CSTR.

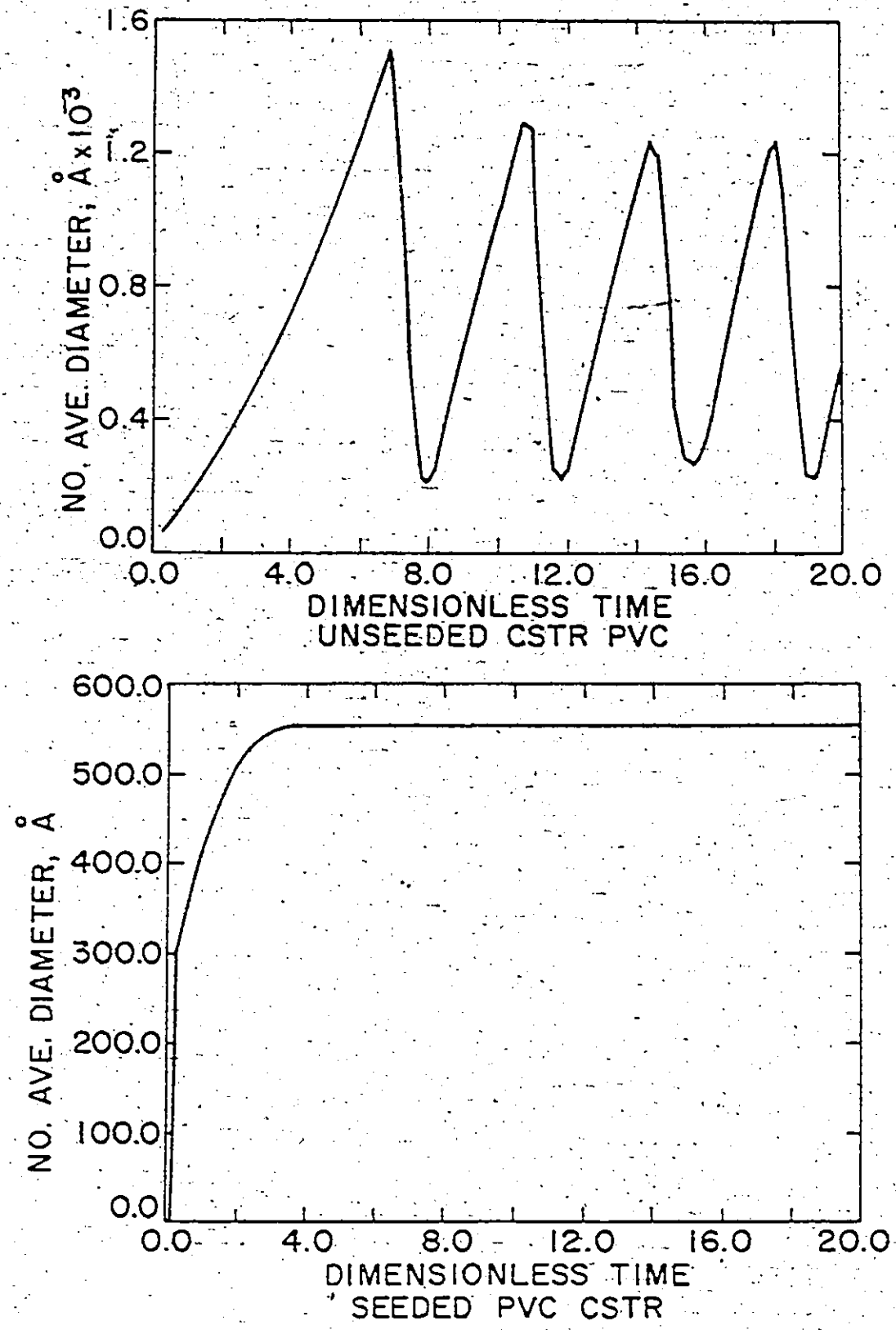

Figure (8-8). Number Average Diameter vs. Dimensionless Time: Unseeded vs. Seeded PVS CSTR.

of emulsifier and initiator, respectively. The mean residence time θ is 30 minutes. Conversion, number of polymer particles and average diameter are all plotted against dimensionless time (t/θ).

The oscillatory behaviour of the single (unseeded) CSTR is evident from these figures. Note again that although in an industrial situation one would usually have only conversion measurements available in which to observe oscillations, the limit cycles in the particle concentration (Figure 8-7a) and average size (Figure 8-8a) are much more extreme. The periods of particle generation last less than 10 minutes, as it can be seen from Figure 8-7a, while the period of oscillation is around 3 mean reactor residence times, which are in agreement with similar observations in VAc emulsion reactors (see Chapter 7). Although in the VAc case (see Figure 7-3) oscillations in the average number of branch points are quite distinct, the PVC model did not show an oscillatory behaviour for $B_N(t)$ (for the experimental conditions employed). This is probably due to the fact that for PVC transfer to polymer and terminal double-bond polymerization reaction rates are very small, whereas for VAc they play a more important role. This, coupled with the facts that conversion does not oscillate as much as in the VAc case and that the conversion levels employed were low, accounted for the lack of limit cycles in the polymer properties. The model prediction for the conversion behaviour is in very good agreement with Berens' (1974) observation that the "PVC concentration remained essentially constant over the period of the polymerization, i.e. the system appeared to be at a steady-state, although the particle size distribution fluctuated widely".

Figure 8-9 shows measured PSD's at various times from Berens' (1974) results. The simulated behaviour of Figure 8-8a is consistent with these experimental observations on PSD. As he states, "in the unseeded continuous run the single narrow peak in the PSD at t=60 minutes indicates that particle formation occurred during a brief interval early in the run and then stopped. By t=120 minutes, this peak has shifted to a larger particle size than

the corresponding batch-charge sample, reflecting a decrease in $N_p(t)$ (due to dilution) and greater growth per particle in the continuous case. At the same time, a new narrow peak at small particle size shows that a second generation of particles has formed over a short time interval. In the 240-minute sample, there are at least three distinct peaks in the distribution, indicating further intermittent formation of new particles".

An extensive simulation study of the single CSTR behaviour and a sensitivity analysis were performed, the results of which are shown in Smith et al. (1985). These results are not shown here, because by now the reader should have developed a very good feel concerning the emulsion process and the effects of the various model parameters and operating conditions on the system response. The point worth mentioning is that this simulation study was done during the final year's design course (ChE 4W4) in the Department of Chemical Engineering (McMaster University), and it clearly shows to what extent the dynamic process model helped the students to understand the fundamentals of emulsion polymerization and latex reactor operation. One can easily see that a good process model may effectively assist in the initial training of new potential polymer engineers.

(ii) Single seeded CSTR:

The case of a single seeded CSTR is treated in Figures 8-6b, 8-7b and 8-8b. The experimental conditions are exactly the same as in Figures 8-6a to 8-8a, with the only difference that a stream of seed particles is now continuously fed to the reactor. The seed consists of 300 Å particles, $1.x10^{18}$ particles/liter of water and corresponds to a conversion level that would give 20 gr PVC/liter of water (~ 5% conversion). Again, the same properties (as in Figures 8-6a to 8-8a) are plotted versus (t/θ) for reasons of comparison.

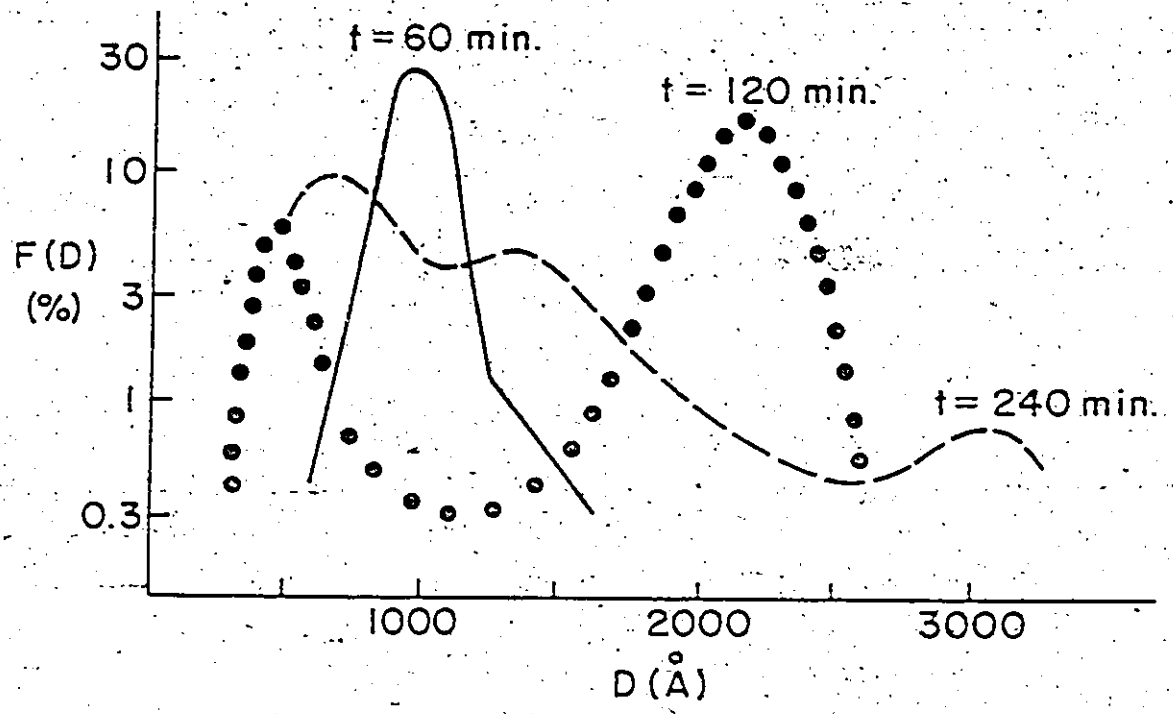

Figure (8-9). Measured PSD's During the Continuous Production of Emulsion PVC.

The observations from the previous paragraph, based on the model predictions for a seeded PVC emulsion CSTR, are again in excellent agreement with Berens' (1974) experimental data. As he observed, "in the seeded continuous run, the PSD shows a single peak throughout. The continuous addition of seed particles prevents new particle formation. The distribution simply broadens, compared to that of the seed, as might be expected due to a distribution of residence times among different particles. The PSD's of the 120- and 240-minute samples were virtually identical; the steady-state here involves constant size distribution and number of particles, as well as conversion".

In an attempt to further test the predictive powers of our model, three experimental recipes from Berens (1974) were simulated. In all these simulation runs, D_w was kept constant to 0.1580×10^{-6} dm^2/sec and ε was set equal to 0.6980×10^2 (equal to the ε used in the batch case). Table 8-2 cites the three recipes from Berens (1974) and Figures 8-10 and 8-11 show the obtained results.

Triangles or inverted triangles in Figures 8-10 and 8-11 represent experimentally measured conversion data. The agreement between model predictions and experimental results is excellent. Inspecting closer Figures 8-10 and 8-11 one can also see the effect of several operating variables, such as soap concentration, residence time and seed characteristics, on the final productivity. An additional simulation study is also reported in Smith et al. (1985). As a final exercise in this examination of a seeded CSTR, the model prediction at $t = 3600$ seconds for average size was compared to Berens' (1974) measured diameter for recipe B. Berens (1974) reported an average diameter close to 1200 Å, whereas the model predicted quite satisfactorily 1070 Å.

TABLE 8-2

Summary of Seeded CSTR Recipes

(Berens (1974))

Recipe	A	B	C
Monomer (gr VCM/lit)*	400	400	400
Soap (gr/lit)**	1.25	2.0	2.0
Initiator (gr/lit)	1.0	1.0	1.0
Temperature (°C)	50	50	50
Residence time (sec)	3600	1800	1800
Seed x(t)	0.05	0.045	0.1
Seed $N_p(t)$ (#/lit)	$1.x10^{18}$	$1.x10^{18}$	$2.2x10^{18}$
Seed diameter (Å)	900	300	630

* In all cases, VCM was in excess, i.e. $M_F(t) = M_p(x(t)=x_c)$.

** In all cases, lit means liter of water.

(iii) Split feed reactor system:

A new reactor configuration for the non-oscillatory production of poly(vinyl acetate) in continuous emulsion trains has already been suggested and discussed in Chapter 7 of this thesis. The PVC dynamic model was now applied to the two reactor case in order to illustrate that this design willeliminate the oscillations. Results from this simulation can be seen in Figure 8-12. These results should be compared with Figures 8-6a to 8-8a (oscillatory behaviour) and 8-6b to 8-8b (seeded single CSTR, batchwise production of seeds). Conditions used for the computer program are as follows: T=50°C, volume of small reactor = 75 ml, concentrations of emulsifier and initiator in the feed stream = 0.01 and 0.02 gmole/lit respectively, mean residence time of second reactor (θ_2) = 1800.0 sec and feed split = 40%. With the seeding reactor present all property oscillations are eliminated.

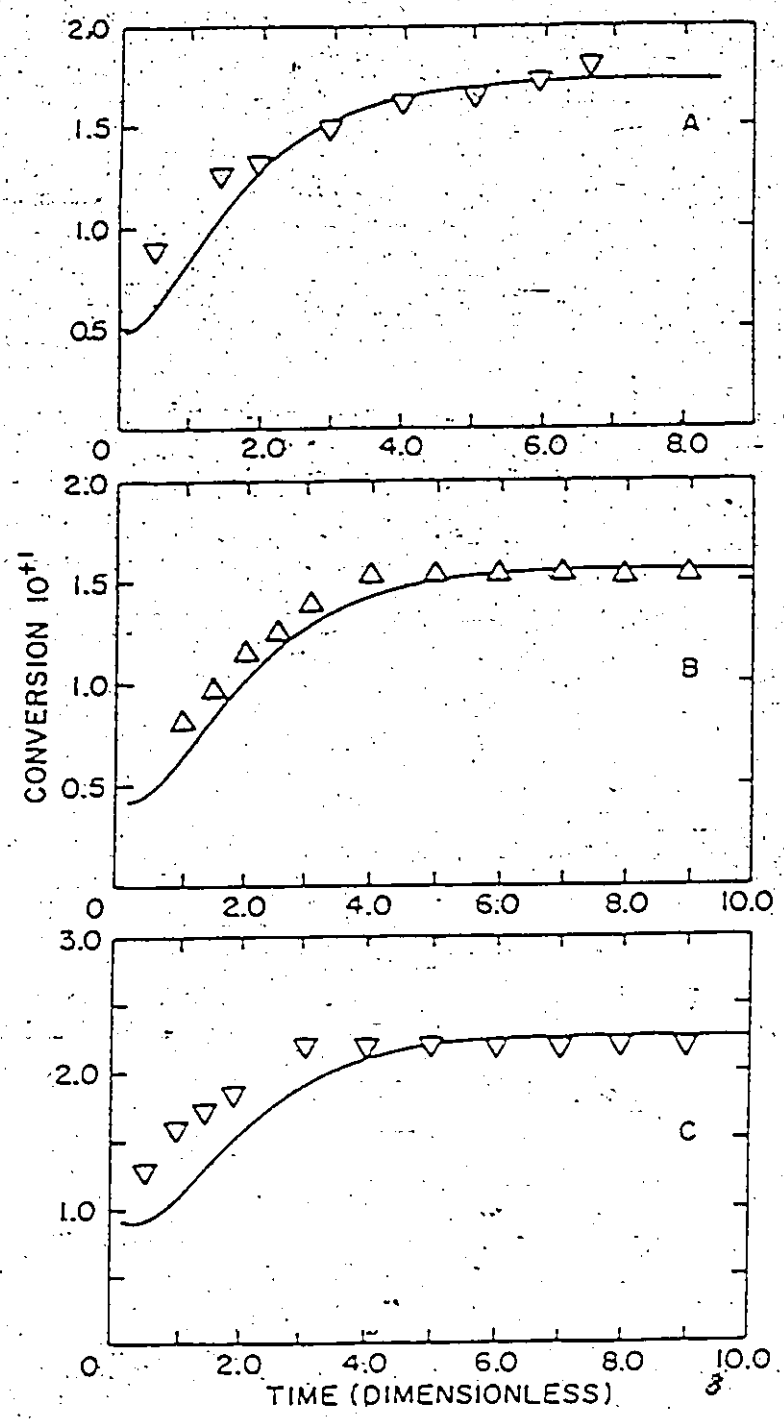

Figure (8-10). Seeded Overflow CSTR Starting Full of Recipe for the Production of Emulsion PVC (See Table 8-2): Conversion vs. Dimensionless Time

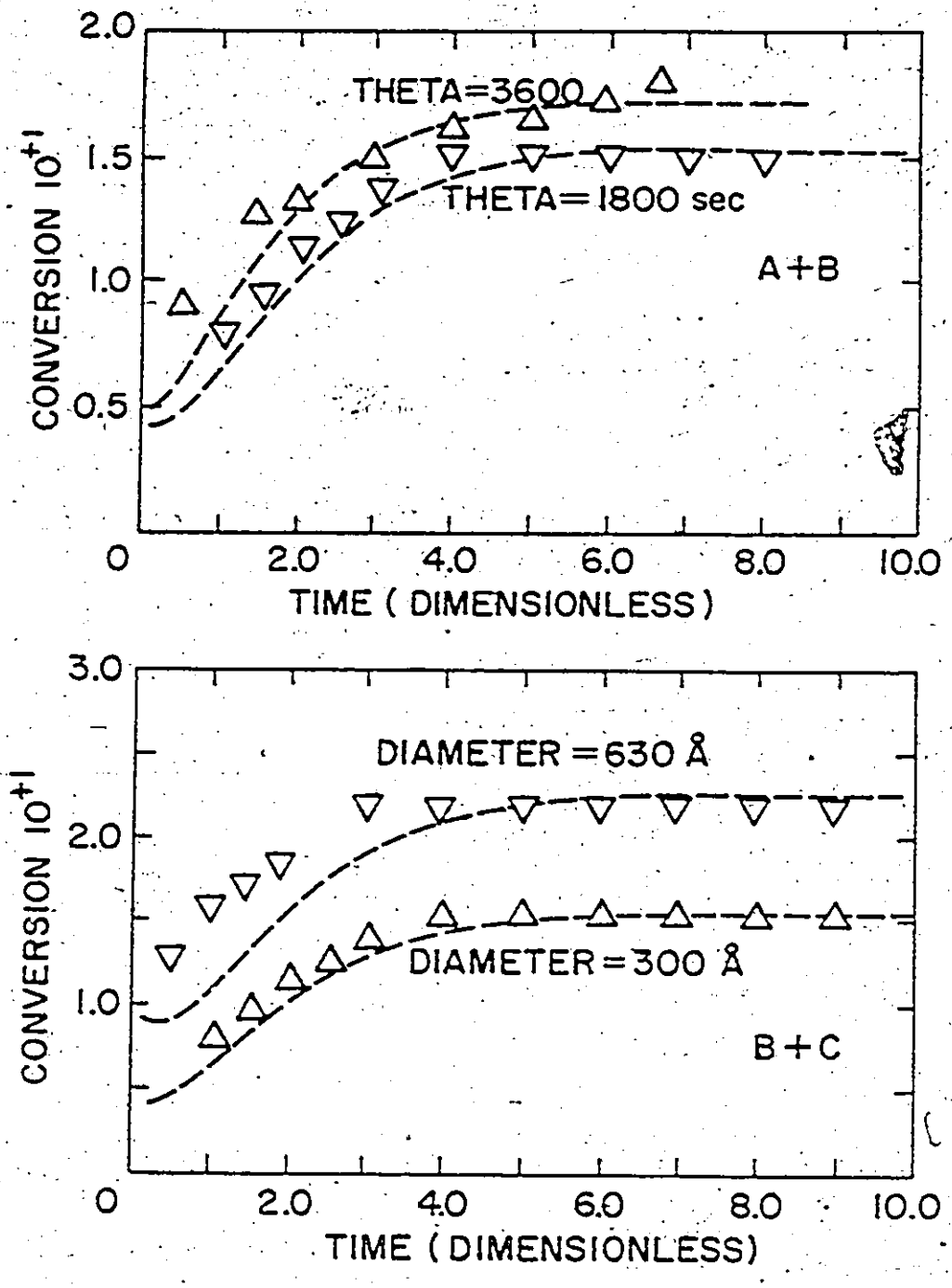

Figure (8-11). Seeded Overflow CSTR, Conversion vs. Dimensionless Time: Effect of Process Variables (See also Table 8-2).

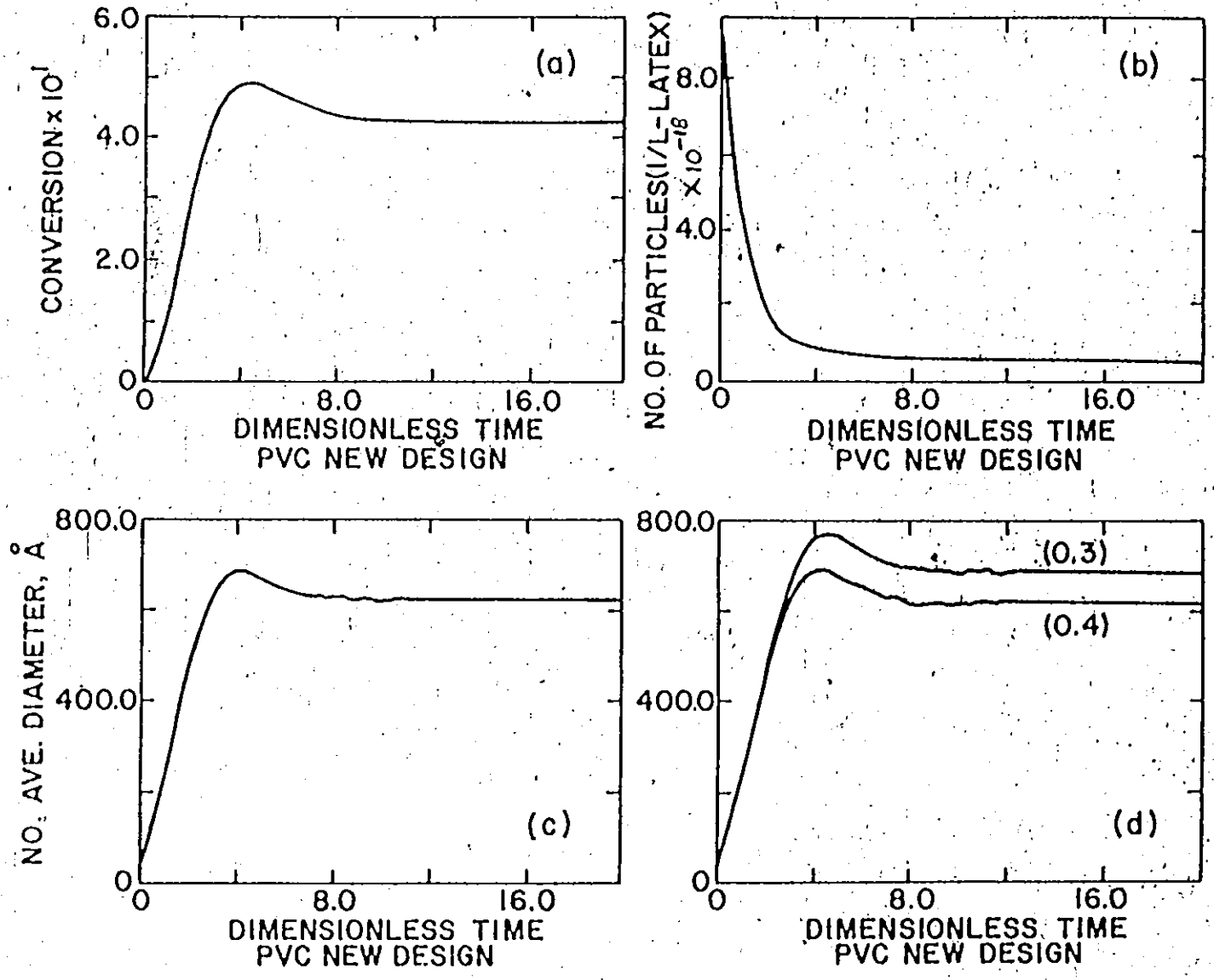

Figure (8-12). Conversion, Number of Particles and Average Diameters vs.(t/θ): Split Feed Reactor System.

An additional step during the study of the split feed reactor system was to again check the predictive powers of our model. The idea which was tested was the following: as shown in Chapter 7, the first reactor in the new train configuration acts as a continuous seeder for the second (i.e., the first large) reactor of the train. If then reactor 1 were operated in such a way so as to produce exactly the seed characteristics of one of Berens' (1974) recipes (say, recipe A), reactor 2 should theoretically give the same results that Berens (1974) measured out of his single seeded CSTR, since reactor 2 simply grows the incoming seed particles. The result is shown in Figure 8-13. The train produced the same latex as a single seeded CSTR and the model was very successful in predicting that. The slight discrepancy at the beginning is most likely due to induction time effects, which was unknown to us from the article. The model response shifted slightly to the right would have been closer to the experimental points.

8.5 Conclusions

Emulsion PVC is widely used for plastisol or coating applications. Lately, PVC from emulsion processes has begun to replace suspension PVC for the production of rigid window frames in Germany. This trend may be due to the fact that emulsion particles are more stable than suspension particles. In light of this appearing trend and since there are only a few reported studies concerning the emulsion PVC process, this initial investigation into the extension of our Case I population balance model to cover emulsion PVC takes on even more importance. The results of the modelling and PVC latex reactor design investigations were very promising and should provide a good starting point for future experimental investigations toward emulsion PVC homo- and copolymerizations.

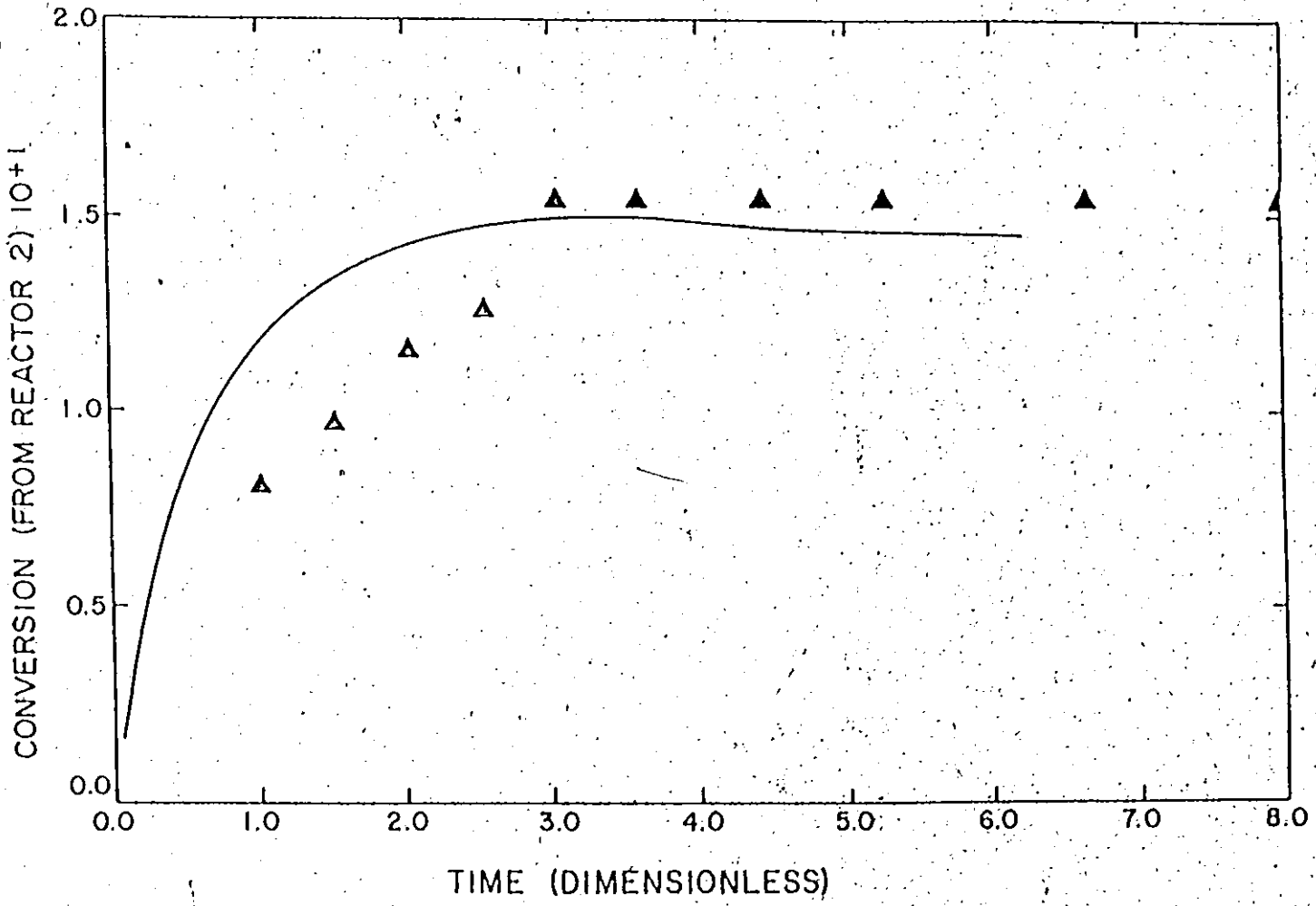

Figure (8-13). Prediction of the New Train Configuration Behaviour: Production of Emulsion PVC

CHAPTER 9

IMPURITY EFFECTS IN CASE I EMULSION POLYMERIZATION

9.1 Introduction

A valid approach to polymer reactor design (and, in general, to the design of any chemical process) should follow the three basic steps: (i) process understanding and subsequent incorporation of this knowledge in a computer process model, (ii) laboratory, pilot-plant and plant experimentation to check the validity of the process model, and (iii) application of the experience gained in the previous steps with optimization, reactor design and control theories to achieve an effective process design and operation.

Things would be more or less straightforward if one could reasonably closely mimic in the laboratory or pilot plant the operating and environmental conditions prevailing in the plant environment. Then, the mathematical models and control theories that are being developed in academia would be directly applicable to industrial systems of the "real world" and there would be no problem - no gap - between theory and practice.

One of the major discrepancies between research and industrial polymerizations is due to the presence of impurities in the latter. Both monomer and water soluble impurities exist in the feeds to industrial reactors and build up in recycle streams.

Experiments done in an academic environment are usually conducted with purified chemical components. Initiators and emulsifiers are of analytical high purity grade, water is distilled or deionized, the bench-scale reactors are kept very clean and monomers are used free of inhibitors and other impurities. This is likely a major cause of disagreement between academic data and those found in an industrial environment.

It is the purpose of this chapter to first review what has been done in the emulsion polymerization literature as far as impurity effects are concerned, secondly model these effects and thirdly, discuss the results of batch PVAc experimental runs specifically designed to investigate the effect that impurities have on Case I emulsion systems. Chapter 10 will extend the ideas of Chapter 9 to cases where the change or drift in impurities over time is not exactly known.

9.2 Impurity Effects in Emulsion Polymerization: Literature Review

Very few papers on the effect of impurities on the kinetics of emulsion polymerization have been published. Most of the experimental investigations include purified monomers, small reactors and carefully degassed systems.

Another point is that most of the investigators recognize the effect of oxygen, which acts as a radical scavenger and inhibitor for almost all emulsion systems, without having a critical effect on the subsequent course of the reaction once the inhibition (induction) period is over. These reports have been discussed in Chapter 4 of this thesis (section 4.4) and will not be repeated here again.

With the exception of Hoffman (1981), who first modelled impurity effects in "Case II" systems (styrene-butadiene), and of Campbell (1985), who used the ideas of Hoffman (1981) to model monomer soluble impurities and further discussed experimental observations in styrene emulsion systems, there is virtually nothing else in the literature. It is evident, therefore, that an investigation on impurity effects in Case I emulsion polymerization systems is well justified.

Since it is acceptable to distinguish emulsion systems as "Case I" and "Case II" systems it is pertinent to first discuss the observations of Campbell (1985) for Case II systems, before proceeding with a different modelling approach for Case I systems.

9.3 Impurity Effects in Case II Systems

The presence of impurities, either water or monomer (oil) soluble, can create serious problems in the modelling of industrial scale reactors. Since most industrial scale processes use either unpurified or partially purified monomers, and what is more, almost all use monomer recycle streams back to the reactors from downstream monomer recovery units containing unknown amounts of contaminants and polymerization by-products, the problem of applying models verified by laboratory experiments to pilot plant or industrial scale reactors is obvious. In fact, it is likely these impurity effects that cause theoretical model predictions and real process data to eventually diverge. The effect of impurities is significant and must be modelled if valid predictions based on laboratory studies are to be made in the plant. Once impurity effects are accounted for then other problems in modelling plant reactors may be identified.

Impurities may in general be divided into two main categories: (i) water soluble (WSI) and (ii) monomer soluble (MSI). Not all impurities consume radicals and slow down the reaction rate. The impurities of interest here are those that react with radicals and slow down the polymerization rate. These two types of impurities are postulated to act in very different ways.

Water-soluble impurities act mainly by consuming reactive free radicals in the water phase. The rate at which this reaction occurs for oxygen is not known. What is known from experimental evidence is that the rate is quite fast (similar to the rate of radical termination), which would cause the rate of initiation to be very low, or essentially zero, until all free oxygen is consumed, resulting in a reaction induction period for a batch reactor. Oxygen is also soluble in the organic phase, but its consumption of radicals in the water phase is so great that radicals formed in the water phase never reach monomer droplets or micelles

to any significant extent. In continuous emulsion polymerization, however, oxygen levels are low in both water and organic phases and there radicals are scavenged in both phases. On the other hand, if the water soluble impurity is something other than oxygen (e.g. hyroquinone (HDQ)), which may react with radicals in a slower way (e.g. in the same order of magnitude as the propagation step), initiation would not be zero but very slow. Campbell (1985) assumed that the main water soluble impurity in his system was oxygen, which was believed to react almost instantaneously with free radicals in the water phase until it was entirely consumed. The phenomenon was very satisfactorily modelled by simply including an induction period (see also Chapter 4 of this thesis).

On the other hand, monomer soluble impurities are proposed to behave in a totally different manner. On pilot plant scale, these impurities are mainly the radical scavengers added to the monomer to prevent autopolymerization (e.g. 4-tert-butyl catechol (TBC) in the case of styrene, or HDQ in the case of vinyl acetate), although in an industrial environment with monomer recycle streams, these impurities can be anything from inhibitors to solvents and other polymerization by-products. Due to their monomer solubility, these impurities reside in the monomer droplets (when present) or in polymer particles with monomer during stages 1 and 2. By scavenging radicals in the polymer particles they decrease $\bar{q}(t)$, thus reducing the reaction rate. Due to this effect, Campbell (1985) argued that the nucleation period for Case II systems is consequently prolonged, since the initiated nuclei grow at a slower rate than if no inhibitor were present, resulting in a larger number of particles being formed, since not as much soap is being used to stabilize growing particles. The net result of this effect is an "apparent pseudo-retardation" early in the reaction and an accelerated rate later in stages 2 and 3 due to the high $N_p(t)$. Of course, the increased number of particles and the reduced $\bar{q}(t)$ have opposite effects on the polymerization rate, where the net effect will depend on the level of impurities. Another not so obvious problem that this effect may cause

during the later stages of the reaction is catastrophic coagulation due to the increased number of polymer particles formed.

Campbell (1985) modelled the effect of oil soluble impurities in Case II systems (styrene) following the approach of Hoffman (1981). Since the impurity reaction affects $\bar{n}$, he rederived the radical and particle balances originally derived by Smith and Ewart (1948). In this way, the general solution derived by O'Toole (1965) was modified with m now being:

$$m = \frac{k_{de}\, v\, N_A}{k_{tp}} + \frac{k_{MI}(MI)_p\, v\, N_A}{k_{tp}} \qquad (9.1)$$

The second term in the RHS of equation (9.1) describes the contribution of monomer soluble impurities in reducing the "net" number of radicals in a polymer particle.

Campbell's (1985) observations from a simulation study where he varied the amount of TBC inhibitor from 10 to 40 ppm, are summarized below:

(i) An increasing amount of inhibitor slows the reaction to some point at which the reaction rate accelerates. The impurities decrease $\bar{n}$, which has the effect of slowing the particle growth rate, thus prolonging interval I of the polymerization, resulting in more particles being formed. Once stage 3 of the polymerization is reached, the inhibitor effect on $\bar{n}$ will be diminished, since its concentration in the polymer particles will decrease. This results in an increase in $\bar{n}$ during stage 3 and this behaviour, coupled with the fact that more particles have been nucleated results in the rate acceleration above that normally expected.

(ii) For increasing impurity levels, the polymer particles at the same conversion are smaller indicating that a larger number of particles have been nucleated. This illustrates the argument presented in (i) that by retarding

the growth rate of particles, stage 1 is prolonged and the number of particles nucleated is increased.

(iii) The value of $\bar{n}$ increases through interval I as particles are being formed, and remains almost constant throughout stage 2, while M_p and $(MI)_p$ remain constant in the particles. Then, as discussed in (i), the value of $\bar{n}$ increases dramatically through stage 3 as $(MI)_p$ decreases. The growth rate of particles can be seen to mirror the $\bar{n}$ behaviour, as would be expected.

(iv) An increase in k_{MI} causes a prolonged nucleation period, resulting in an increased $N_p(t)$, which eventually leads to an accelerated rate of polymerization once the impurity is depleted in interval III. It is interesting to note that this rate increase is so pronounced that the curves with a larger value of k_{MI} actually cross those of lower k_{MI} values. This illustrates how sensitive the system is to the k_{MI} parameter. In practical terms, the more effective the inhibitor, the greater the number of particles that will be formed and the higher will be the rate of polymerization in stage 3.

Campbell (1985) and Huo et al. (1986) verified the above observations by running experiments with inhibited versus uninhibited styrene monomer. They finally concluded that the effect of monomer soluble impurities on the particle nucleation mechanism of Case II systems is significant. In order to successfully model an industrial or pilot plant reactor which uses inhibited monomers, it is obvious that this effect must be accounted for, particularly if inhibitor levels are changing perhaps due to recycle.

9.4 Case I Systems: Modelling Impurities

The model development to include water and monomer soluble impurity effects for Case I systems is described in Appendix XIV. The approach is somewhat different than the

one employed by Hoffman (1981) and Campbell (1985). Also included in Appendix XIV is a different approach to evaluating $\bar{n}$ in Case II systems.

9.4.1 Model Impurity Parameter Values

From the model modification in Appendix XIV, it is evident that new parameters have been inserted (parameters concerning water and monomer soluble impurities). These will be discussed herein before any simulations with the extended model are attempted.

In equation (XIV-3), γ is the ratio of k_{WI} to k_m. The rate coefficient of micellar nucleation k_m, was considered equal to $\sim 10^{-5}$ dm/sec, consistent with the discussion in Chapter 4. Hoffman (1981) in his investigations used $k_{WI} = k_{MI} = 10^5$ lit/gmole-sec, values which denote quite fast reactions of radicals with impurities. Accepting an order of magnitude for k_{WI} (which should be considerably larger than k_p) close to that used by Hoffman (1981), γ becomes $\sim 1. \times 10^{10}$ dm^2/gmole.

In the balance for monomer soluble impurities (XIV-20), $(MI)_p(t)$ denotes concentration of MSI in the polymer particles. The same discussion concerning $(M)_p$ in Chapter 4 holds for $(MI)_p(t)$ as well. $(MI)_p(t)$ can be related to (MI)(t) through a partition coefficient, as follows:

$$K_{MSI} = \frac{(MI)_p(t)}{(MI)(t)} \tag{9.2}$$

Hoffman (1981) chose K_{MSI} to be equal to $\phi(t)$, and the same assumption is employed in the present analysis with no particular justification.

9.5 Case I Systems: Simulations with Impurities

The effect of monomer soluble impurities on the polymerization kinetics of Case I systems should be quite different from their effect on Case II systems because of the different

manner by which they affect both particle growth and particle nucleation. We consider both of these effects in turn.

Effect on particle growth: The rate of polymerization in particles of any class is directly proportional to $q(t, \tau)$ (see equation (I-78)). This term is directly affected by the MSI as shown by equation (XIV-17). The extent of the MSI effect will depend upon the magnitude of the two terms involing $(MI)_p(t)$ on the right hand side of equation (XIV-17) relative to that of the last term which is independent of the MSI. For values of $(k_{MI}(MI)_p(t)) << (8\pi A R_I(t)/A_p(t))$ the MSI will have little effect on $\bar{q}(t, \tau)$ and hence on the particle growth rates, while for larger values of $(k_{MI}(MI)_p(t))$ the effect can become substantial. These situations are illustrated in the simulations of Figures 9-1 and 9-2.

Figure 9-1 gives results for the emulsion polymerization of poly(vinyl acetate) in a train of two continuous stirred tank reactors. Conversion from the second reactor is plotted against dimensionless time (t/θ) with a residence time in the second reactor of $\theta = 30$ minutes. Three cases are plotted in Figure 9-1a: a case with a constant concentration of both water and monomer soluble impurities in the feed stream of 20 ppm, and two other cases where both impurity concentrations were varied by $\pm 50\%$. No discernible effect of the impurities can be observed at this low impurity concentration level. In Figure 9-1b, three cases are again plotted: 0, 20 and 200 ppm of MSI. Again, there is no discernible effect at low impurity levels (0 and 20 ppm). However, at 200 ppm, the MSI have an effect, reducing the conversion by approximately 10% below that for the 0 and 20 ppm cases.

Figure 9-2 shows the model predictions for conversion, average particle diameter and MSI concentration for different MSI levels in the batch emulsion polymerization of vinyl acetate. The conversion versus time plots in Figure 9-2a show little difference for low MSI concentrations, but again much larger effects at higher MSI concentations (100 – 400 ppm).

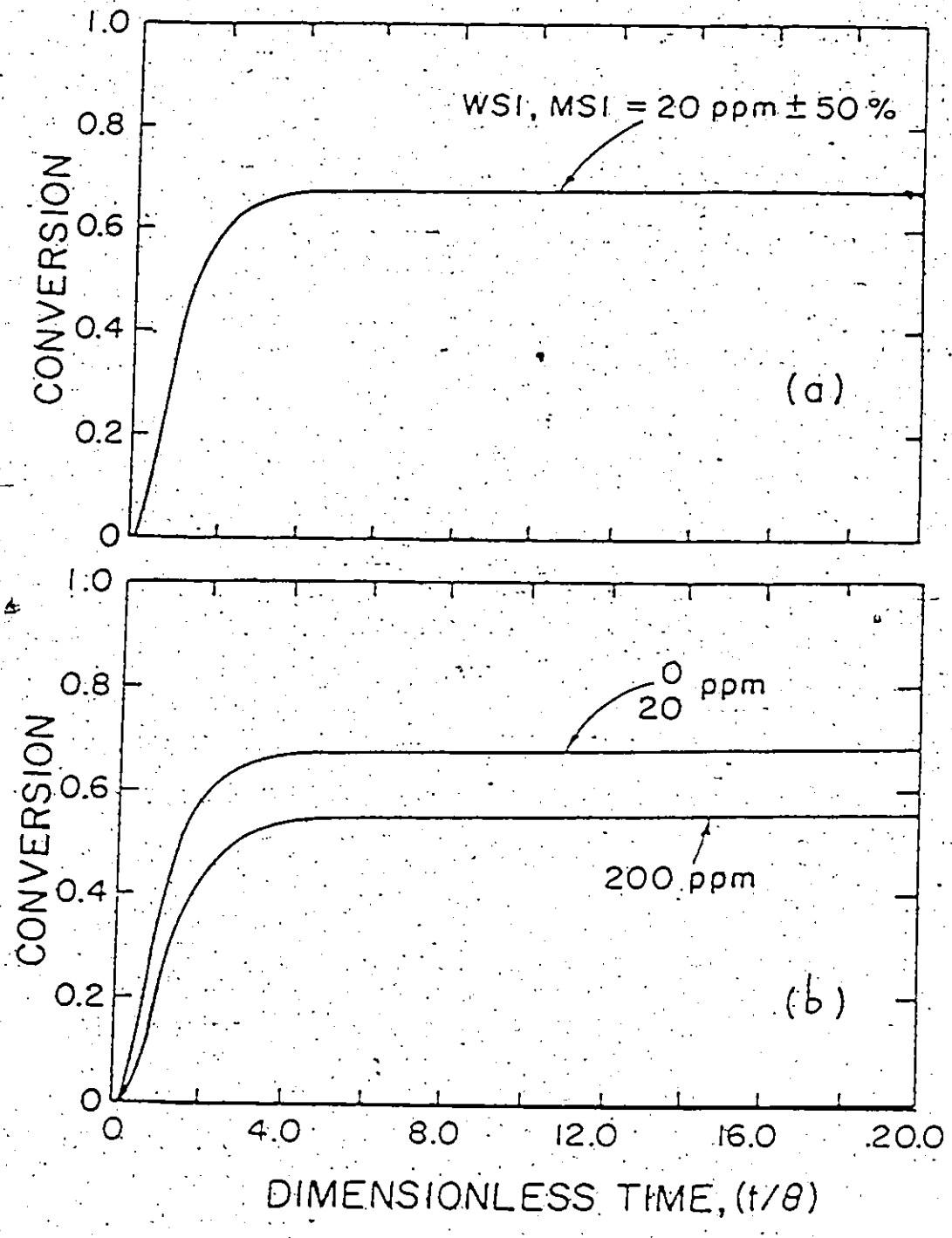

Figure (9-1). Simulation results: Continuous latex train conversion vs. (t/θ) for sevefal impurity levels.

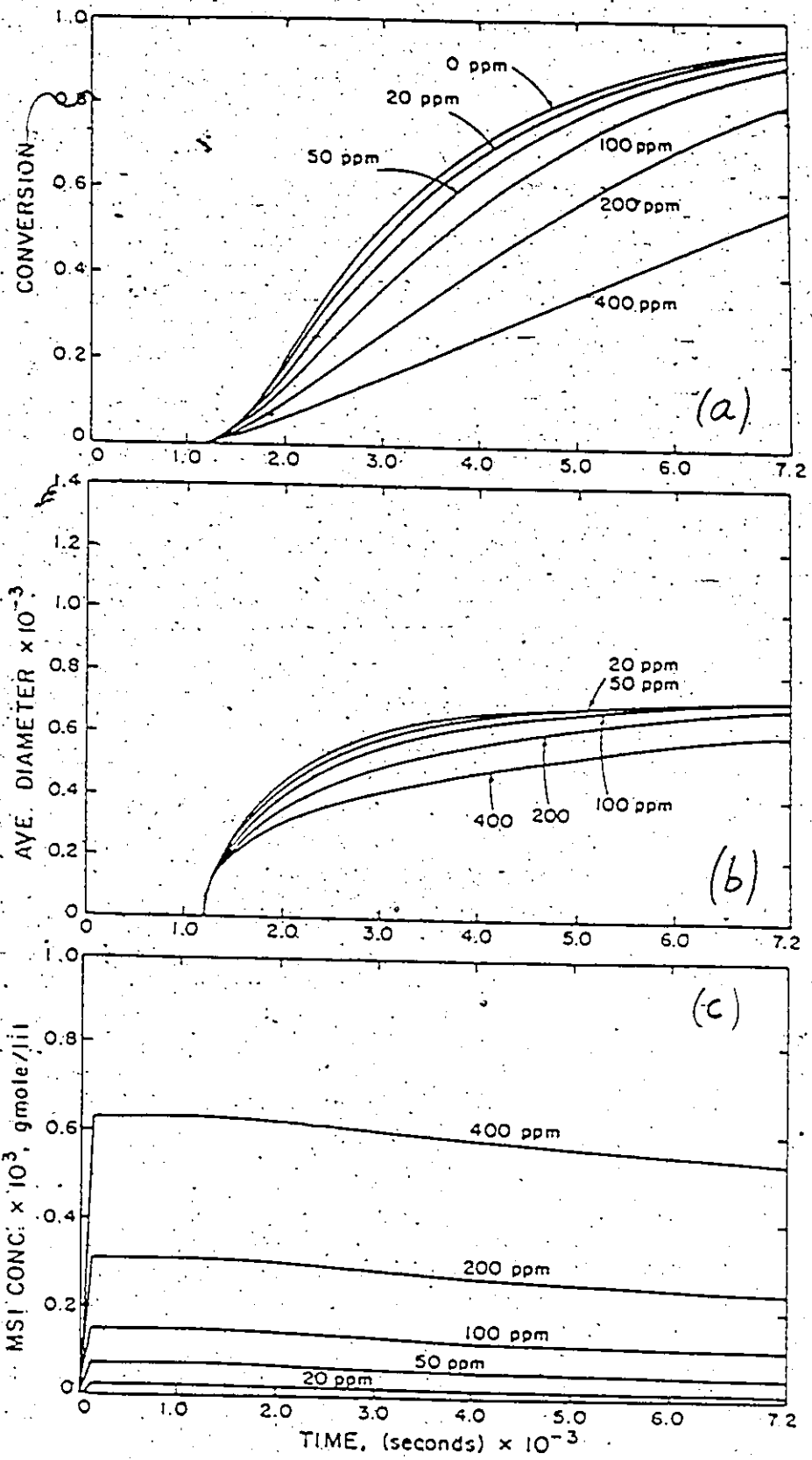

Figure (9-2). Simulation results: Batch reactor operation

In Figures 9-1 and 9-2, the rate constant for reaction between MSI and radicals (k_{MI}) was taken to be equal to the propagation rate constant (k_p). Figure 9-3 shows the effect on the polymerization rate of changing the value of k_{MI}.

Effect on particle nucleation: The MSI have two competing effects influencing the final number of particles generated. Consider the expression for the overall rate of particle nucleation in Case I systems by both homogeneous and micellar mechanisms given by equation (9.3):

$$f(t) = \rho(t) \frac{k_m A_m(t) k_v + k_h}{k_m A_m(t) k_v + k_h + k_{ab} A_p(t) k_v} \qquad (9.3)$$

The rate at which particles are nucleated and the total number of particles nucleated depend upon the time behaviour of the radical entry rate, $\rho(t)$, and the micellar and particle surface ares, $A_m(t)$ and $A_p(t)$, respectively. Typically, for Case I polymerizations, the particle generation rate is very high and lasts only a few minutes. This is a result of the very high value of $\rho(t)$ given by equation (XIV-8) in which the contribution from radical desorption, $\rho_{des}(t, \tau)$ is usually much larger than that from initiator decomposition ($R_i(t) A_n(t, \tau) d\tau / A_p(t)$). From equation (XIV-9), $\rho_{des}(t, \tau)$ is directly proportional to $\bar{q}(t, \tau)$ which is affected by the MSI through equations (XIV-16) and (XIV-17). As $(MI)_p(t)$ increases, $q(t, \tau)$ and hence $\rho(t)$ will decrease. However, from equation (I-78), the rate of growth of particle volume is also directly proportional to $\bar{q}(t, \tau)$. Hence, as $(MI)_p(t)$ increases and $\bar{q}(t, \tau)$ falls, the particle surface area, $A_p(t)$, will grow more slowly, and the micellar area, $A_m(t)$, will decrease more slowly. The particle generation period will therefore be prolonged and the term multiplying $\rho(t)$ in equation (9.3) will decrease less rapidly in the presence of impurities. The above two effects are compensating in that the former reduces the number of particles generated in a given time, while the latter increases the time period for nucleation. The

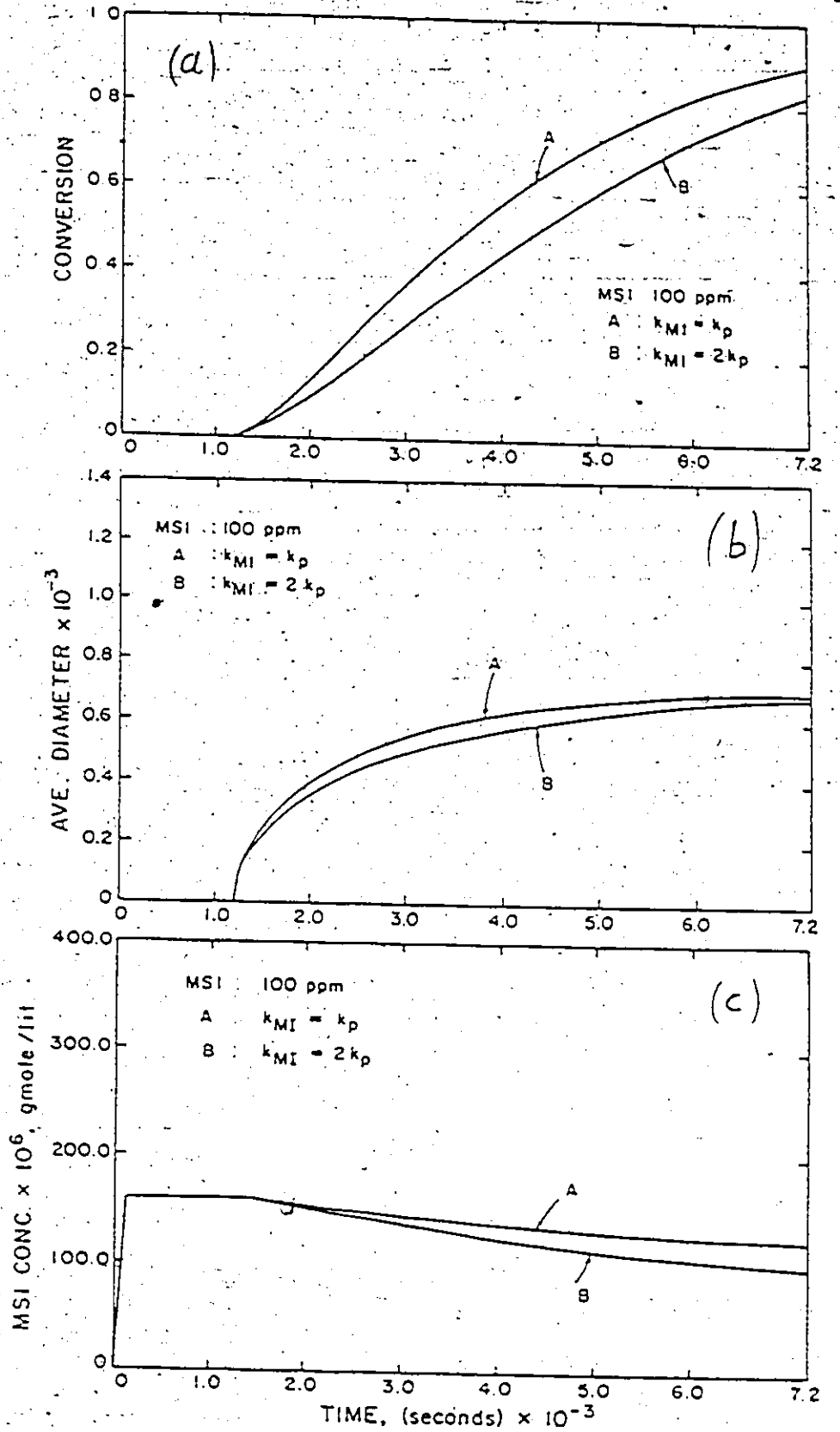

Figure (9-3) Simulation results: Batch reactor operation, MSI level of 100 ppm. Effect of k_{MI}

resulting effect is that there may be little change in the total number of particles generated, and hence on the final particle diameters.

The total affect of increasing the MSI level on the rate of particle generation and the number of particles generated is illustrated via simulation in Table 9-I (and Figure 9-2c) for the batch polymerization of vinyl acetate. The total number of particles generated is very little changed for MSI level ranging from 0 to 400 ppm.

Campbell (1985), in order to fit his experimental data, statistically estimated the initial amount of impurity and the impurity rate constant from conversion and diameter observations, since no information was available on either one, which resulted in significant correlation. Due to the great industrial importance of impurity effects, and since it seems that the two major cases in emulsion polymerization behave in a different way, it would be well justifed to further investigate and clarify the effect of inhibitors in Case I emulsion reactions. So, it was decided in the present study to run a series of experiments by cleaning the monomer, adding a known amount of inhibitor and studying the polymerization kinetics. In this way the initial concentration of inhibitor would be known and could be statistically separated from the impurity reaction rate constant, resulting in a more useful and industrially applicable model.

9.6 Discussion of the Experimental Plan

Reactor configuration: The reactor which was used for these runs was identical to the one described in Chapter 4.

Materials and polymerization procedure: The vinyl acetate used was 99+% pure (Aldrich, catalog number V150-3), inhibited with only 3-5 ppm HDQ. This remaining inhibitor was removed prior to polymerization by passing the monomer 3 times through a bed

Table 9-1

MSI Effect on Number of Particles

(MSI) (ppm)	$N_p(t)$ (x10^{-19})
0	0.110
20	~0.110
50	0.115
100	0.120
200	0.128
400	0.133

of Rohm and Haas Amberlyst A-27 ion exchange resin, strongly basic (Aldrich, catalog number 21643-7), using a low flowrate (~5 ml/min), as described in Schork (1981).

Water, initiator and emulsifier were as described in Chapter 4 and the rest of the chemicals employed (sodium bicarbonate ($NaHCO_3$) buffer, 4-tert-butyl catechol (TBC) and HDQ) were BDH ACS (analytical) reagents.

This time, monomer, water, initiator and emulsifier solutions and any other chemicals were all charged into the reactor vessel, the mixture was stirred at 320 rpm and 20-25°C while being degassed for ~10 minutes, and then the reaction started by raising the temperature to 50°C. Time zero (t=0) for sampling was considered to be the point when temperature was equal to 35°C. In this way, one had the opportunity to investigate a different starting procedure than the one described in Chapter 4, which at the same time closely resembled common industrial practice.

Sampling and off-line analysis: Samples were drawn off every 5 minutes. Conversion was measured gravimetrically and particle size by SEC. A Corning pH meter 140 was occasionally used to verify pH measurements done on the samples by common pH paper indicator.

Experimental runs: Table 9-2 gives a summary of the batch VAc runs performed and their operating conditions. Appendix XV contains tables of the data measured.

9.7 Discussion of Experimental Results

As can be seen from Table 9-2, the employed base case recipe for the impurity (IM) runs was somewhat different than the recipes used in Chapter 4. The reason for this change was that in this way one had an additional base case recipe coming from different operating conditions with which one could further test the validity of our model.

Table 9-2

Summary of Batch VAc Impurity Runs

Run*	IM1 (base case)	IM2	IM3	IM4	IM5	IM6
$NaHCO_3$ (gmole/l-H_2O)	–	0.01	–	–	–	–
TBC (ppm)	–	–	20	200	100	50

*For all IM runs: VAc = 1150 ml, water = 2860 ml,

I = 2.0 grs, S = 15.0 grs, Temp. = 50°C and HDQ present < 1 ppm

Campbell (1985) observed that in some of his emulsion polystyrene runs the latexes produced were very viscous. This observation was attributed to the low ionic strength of the solution, which significantly affects the surface chemistry of the system. The low concentration of ions present in the water due to the efficient deionization process can result in the electrical double layer about the particle expanding.

This effect is extenuated when the concentration of soap and initiator is low, since both of them are species which contribute counterions to the solution. Therefore, due to the extended ionic double layer, the repulsive ionic influence of the particle extends further than if the solution ionic strength were higher, thus increasing the effective particle diameter. If the solution ionic strength is low enough, the double layer will extend to the point where the movement of the particles is hindered, which results in the highly viscous latex that was observed by Campbell (1985). He further argued that the effect that this phenomenon might have on the particle nucleation mechanism is not clear, although some effect would be expected due to the significant change in the surface chemistry of the system. For this reason, and in agreement with Schork (1981), he employed in all his subsequent runs recipes that included an ionic buffer ($NaHCO_3$) in order to raise the solution ionic strength. In the buffered runs the latex viscosity was greatly reduced.

In his runs, Schork (1981) also employed NaCl and NaOH (on top of $NaHCO_3$) in order to adjust the solution ionic strength (and pH). As pointed out by Dunn (1981), the ionic strength of the aqueous phase affects the stability of the latex particles and the rate of reaction. The effect of increasing ionic strength is to reduce the electrostatic repulsive energy barrier so that ultimately the latex coagulates. When enough emulsifier is present this factor is less obvious and it has been generally neglected, although it has been taken into account by Klein et al. (1973) and by Goodwin et al. (1973). What these two groups of researchers observed, though, was a dramatic decrease in polymerization rate corresponding to a concen-

tration of KCl close and above ~0.06 gmoles/lit, which is quite high. A reasonable level of NaCl or KCl typically employed for ionic strength adjustment is between 0.01 and 0.02 gmole/l-H_2O).

In the experimental runs done in the present thesis, we have never observed ionic strength effects similar to the ones described by Campbell (1985), as far as latex sample viscosity is concerned. This was probably due to the fact that the anionic emulsifier levels employed in our recipes were never extremely low, but were rather in a medium range, one that would be industrially preferable, and thus the observations appeared to be in agreement with those of Dunn (1981).

However, we decided to compare results from two recipes during the IM runs, one with and one without $NaHCO_3$ buffer. We felt that the sodium ions resulting from the dissociation of $NaHCO_3$ would be enough to adjust the emulsion ionic strength with use of NaCl redundant. Also, we decided not to employ NaOH at all (to affect the solution pH), because a different pH might have caused different partitioning of inhibitors (impurities) between the monomer and water phases, and this would only complicate things further. Nevertheless, pH control in an emulsion reactor is an important industrial problem.

In the remainder of this section results from the impurity PVAc batch runs will be discussed. First, we discuss the results in terms of conversion, and then in terms of average particle size.

9.7.1 Impurity Runs: Conversion

Figure 9-4 shows results from the impurity-free run IM1 (which will serve as a base case). The monomer was purified and no $NaHCO_3$ buffer was present. The pH was close to 6 at the beginning of the run and closer to 5 in the final stages. The induction time (due to

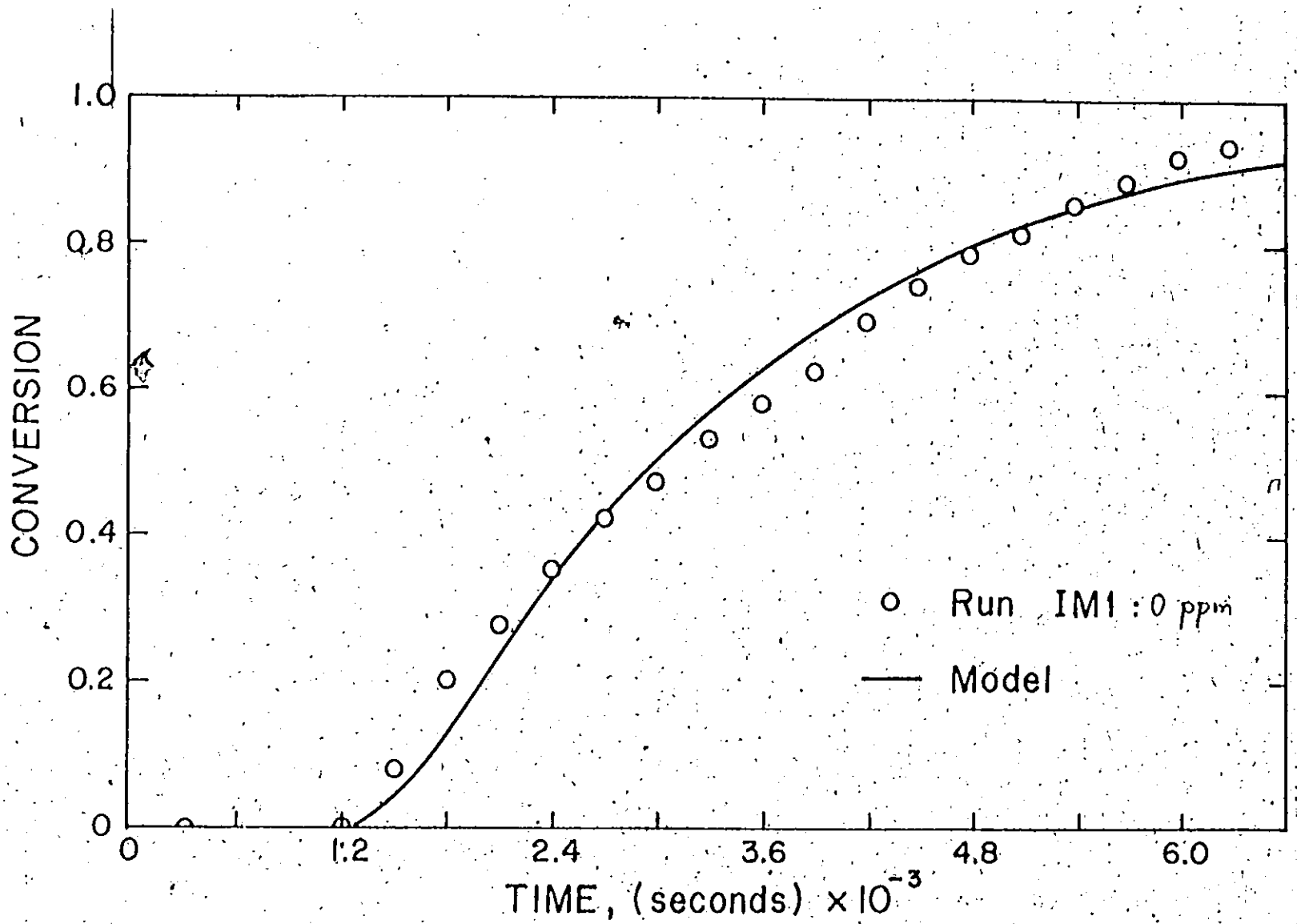

Figure (9-4) Run IM1 : Conversion vs. Time Data and Model Predictions

traces of O_2) was ~1200 sec, a very typical value according to the discussion in Chapter 4. The solid line in the figure represents our model predictions, and as one can clearly see, the agreement between model and experimental conversion is quite good. In general, the conversion levels of the IM runs are lower than the levels of the BR runs (described in Chapter 4), as they should be, since the initiator level employed during the IM runs is lower.

Figure 9-5 compares runs IM1 and IM2. Run IM2 is identical to run IM1 recipe-wise, and it also contains $NaHCO_3$ buffer. The conversion-time history from both runs is almost identical, an indication that the employed level of $NaHCO_3$ did not affect the rate of the polymerization. The pH during IM2 was more constant, closer to ~5.5. The final pH was ~5.1. Two observations that we have made during IM2 are worth mentioning here: (i) The late latex samples from IM2 ($x(t) > 40\%$) were "thinner" than the corresponding samples of IM1, an indication that the latex viscosity was a bit lower at higher conversions. This was expected due to the ionic strength effect. (ii) The reactor wall was quite clean, when the reactor contents were emptied. The reactor hardly needed any further cleaning procedure but just a warm water rinse. There were no spots with coagulated latex on the walls (i.e. no wall fouling). This was again attributed to the somewhat lower final latex viscosity.

Run IM3, the conversion-time history of which is shown in Figure 9-6, was identical to IM1, with the extra addition of 20 ppm monomer soluble TBC. This level of inhibitor is typical for a pilot plant or laboratory environment. IM3 exhibited about the same induction period as run IM1, a further indication that monomer soluble impurities act in a different way than water soluble ones, since they are residing in the polymer particles. In addition, the fact that IM1 and IM3 exhibited the same induction time was a verification of the good reproducibility of our experimental procedures. The pH during IM3 was again between 6 and 5. No visible difference in latex appearance was observed. The experimental results of Figure 9-6

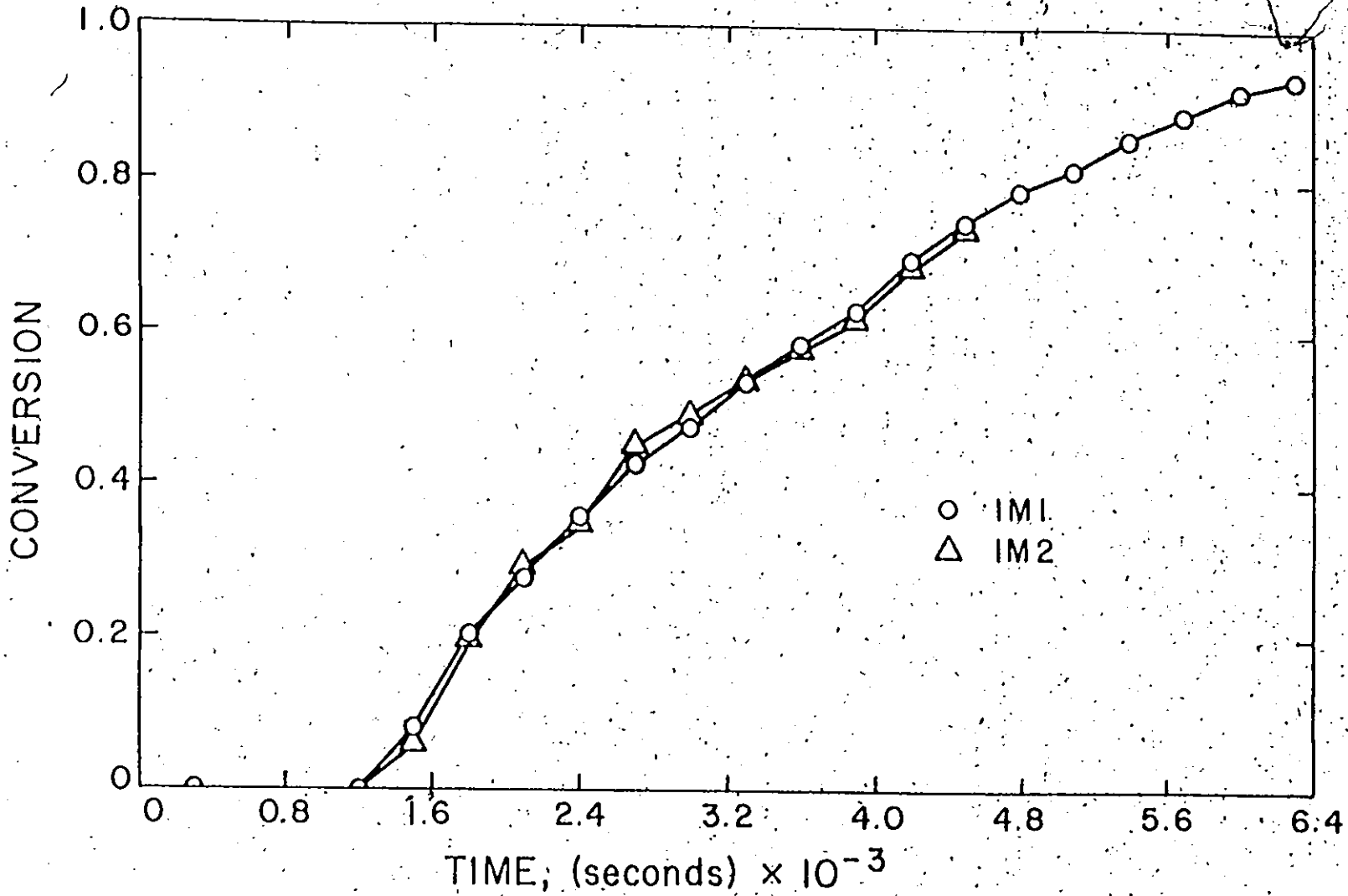

Figure (9-5). Conversion vs. Time Data from Runs IM1 and IM2

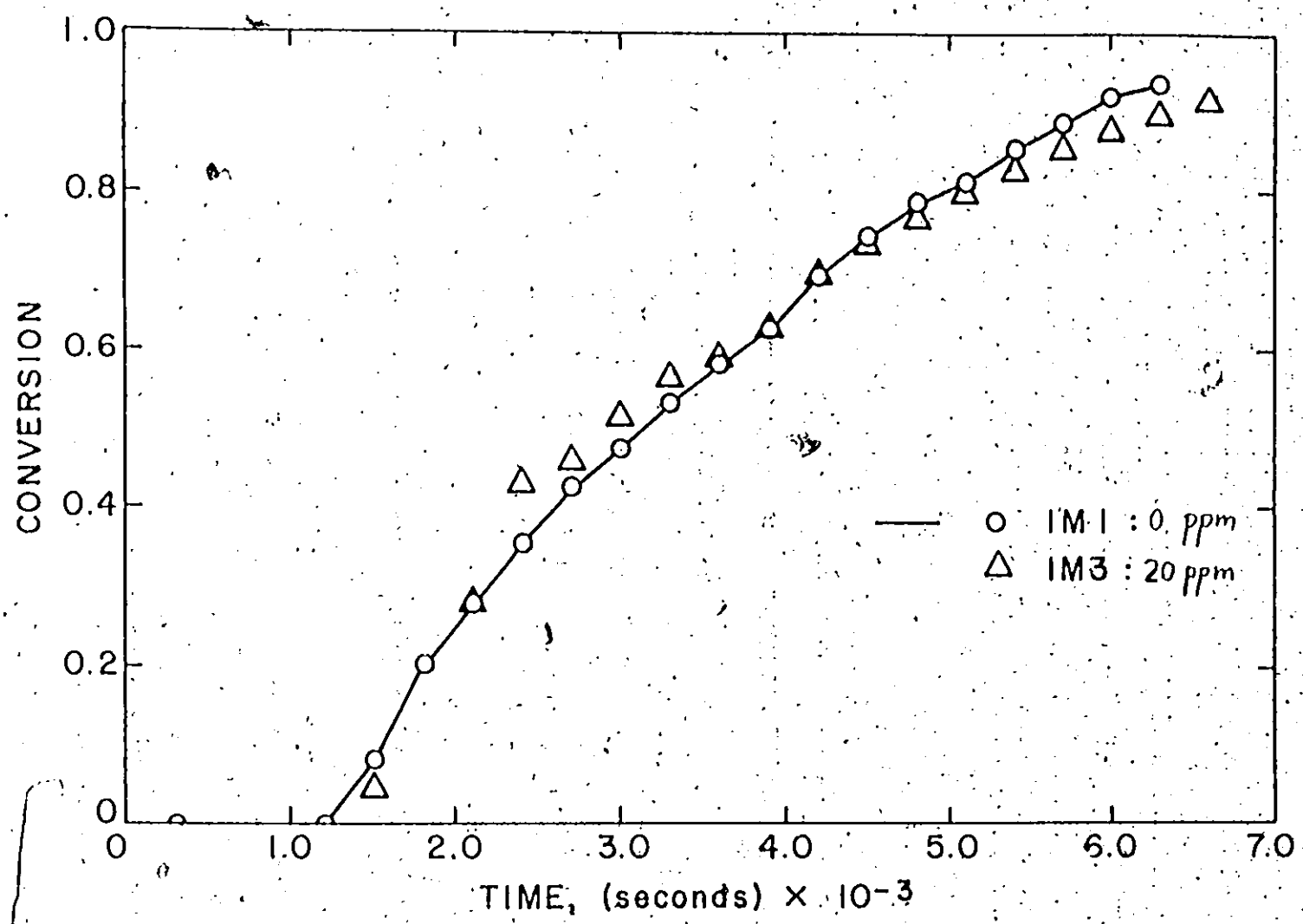

Figure (9-6). Conversion vs. Time Data from runs IM1 and IM3

clearly suggest that a MSI level of 20 ppm does not affect the polymerization rate appreciably, an observation consistent with our previous postulations with the mathematical model.

A comparison between the conversion histories in runs IM3, IM4, IM5 and IM6 is given in Figure 9-7. A level of 200 ppm TBC (Run IM4) is considered high and can result in practice from monomer recycle streams back to the main reactor from downstream monomer recovery units. All four runs gave nearly the same pH levels and induction times as previously. Of course, a more precise interpretation of the results of Figure 9-7 depends strongly upon having precise estimates of the induction periods. However, one can clearly see the small effect on conversion in the 0–50 ppm cases and the larger effect in the 100–200 ppm range, which is in agreement with the simulations of Figure 9-2.

We have decided at this stage not to further investigate the effect of WSI other than O_2 on the VAc emulsion system, mainly for three reasons: (i) We expect WSI to act exactly as oxygen, a behaviour that was described in Chapter 4 of this thesis, (ii) We thought that it would be a good idea to study the MSI effect uncoupled from the WSI effect, and (iii) The problem of studying the effect of hydroquinone on the VAc emsulsion system is quite complicated. HDQ is being used as an inhibitor for VAc monomer, but its behaviour during polymerization is not very well understood. Depending on the emulsion pH, it can preferentially partition between the two phases (monomer and water). Therefore, we did not want to add another factor of uncertainty in an already complicated system. The effect of pH on HDQ partitioning between monomer and water and its effect on the reaction rate is being currently studied by Huo et al. (1986).

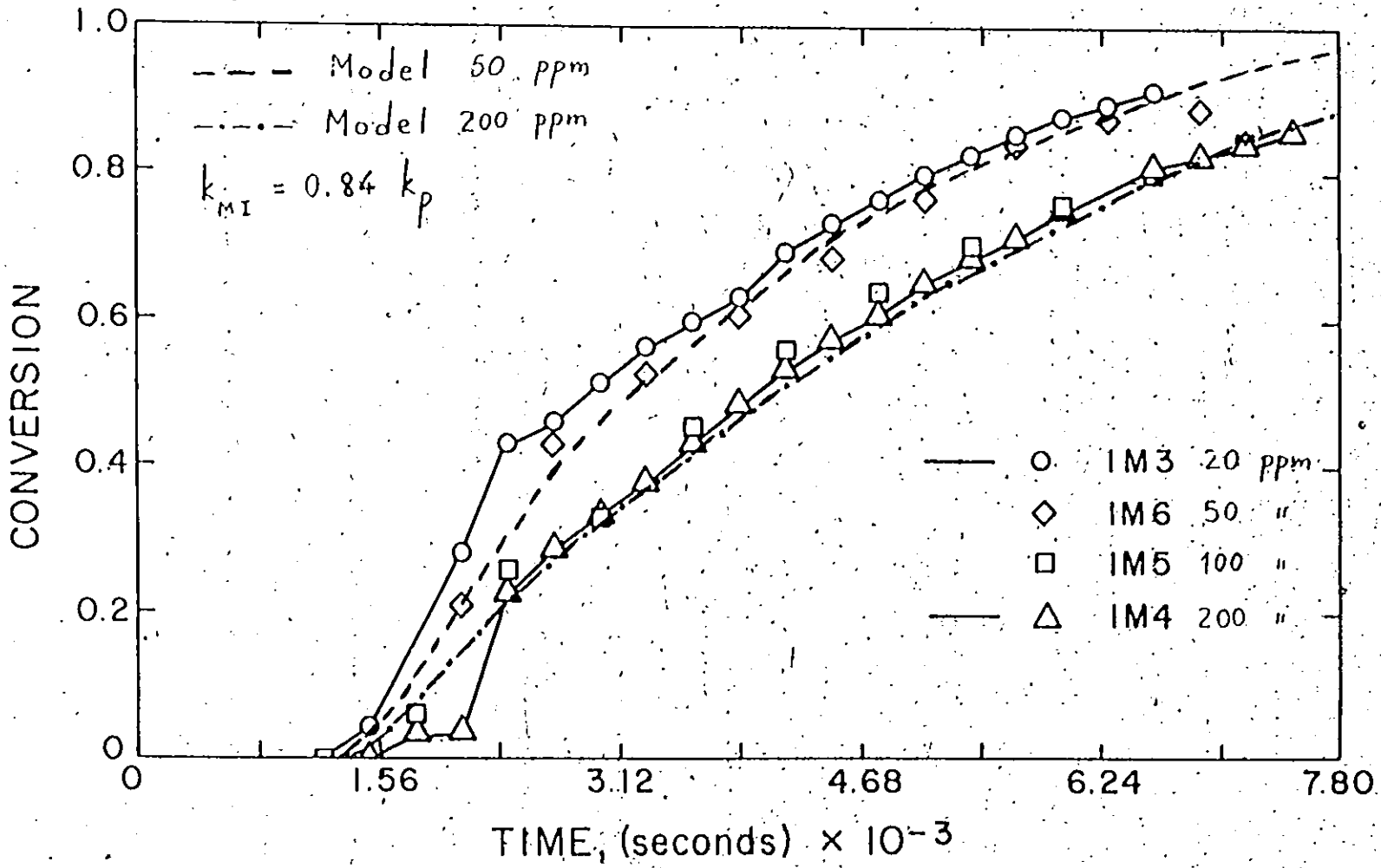

Figure (9-7). Conversion-time histories for runs IM3, IM4, IM5 and IM6.

9.7.2 Impurity Runs: Particle Size

Figure 9-8 is a plot of the HDC average particle size versus time for the base case (run IM1). The solid curve represents model predictions, and the agreement is again very good. Particle size measurement data is plotted in Figure 9-9 for runs IM1 and IM2. One can clearly see that the effect of $NaHCO_3$ at the level employed was not significant on particle diameter.

Figure 9-10 shows average diameter data versus batch reaction time for runs IM1 (base case, no impurity), IM3 (20 ppm TBC) and IM6 (50 ppm TBC). As the monomer soluble impurity level increases, particle diameter decreases, but note that for the same final conversion level (~85%), the difference between runs IM3 and IM6 is ~25Å (see Appendix XV).

Figure 9-11 summarizes the particle size histories for runs IM6 (50 ppm TBC), IM5 (100 ppm) and IM4 (200 ppm). The obtained sizes are lower than the sizes of IM1 and lie together roughly in the same range for all three runs (IM6, IM5 and IM4).

In order to check for reproducibility of the HDC measurements, a few repeats were run randomly one month apart from each other. The results which were obtained follow: for sample IM4#8, 578, 585 and 580 Å, respectively; for sample IM4#20, 746 and 740 Å; and sample IM5#8 gave 685 and 689 Å, respectively.

The obtained experimental results in Figures 9-4 through 9-11 were satisfactorily predicted by the mathematical model. The model showed that for reasonably low MSI levels, there should be no or very little difference in conversion. For high impurity levels (greater than 100 ppm), it correctly predicted that there should be a modest difference. At low MSI levels, desorption is still dominant and the difference negligible (see equation (XIV-11)). At high MSI levels, however, q(t) decreases (see equation (XIV-16)), resulting in a subsequent

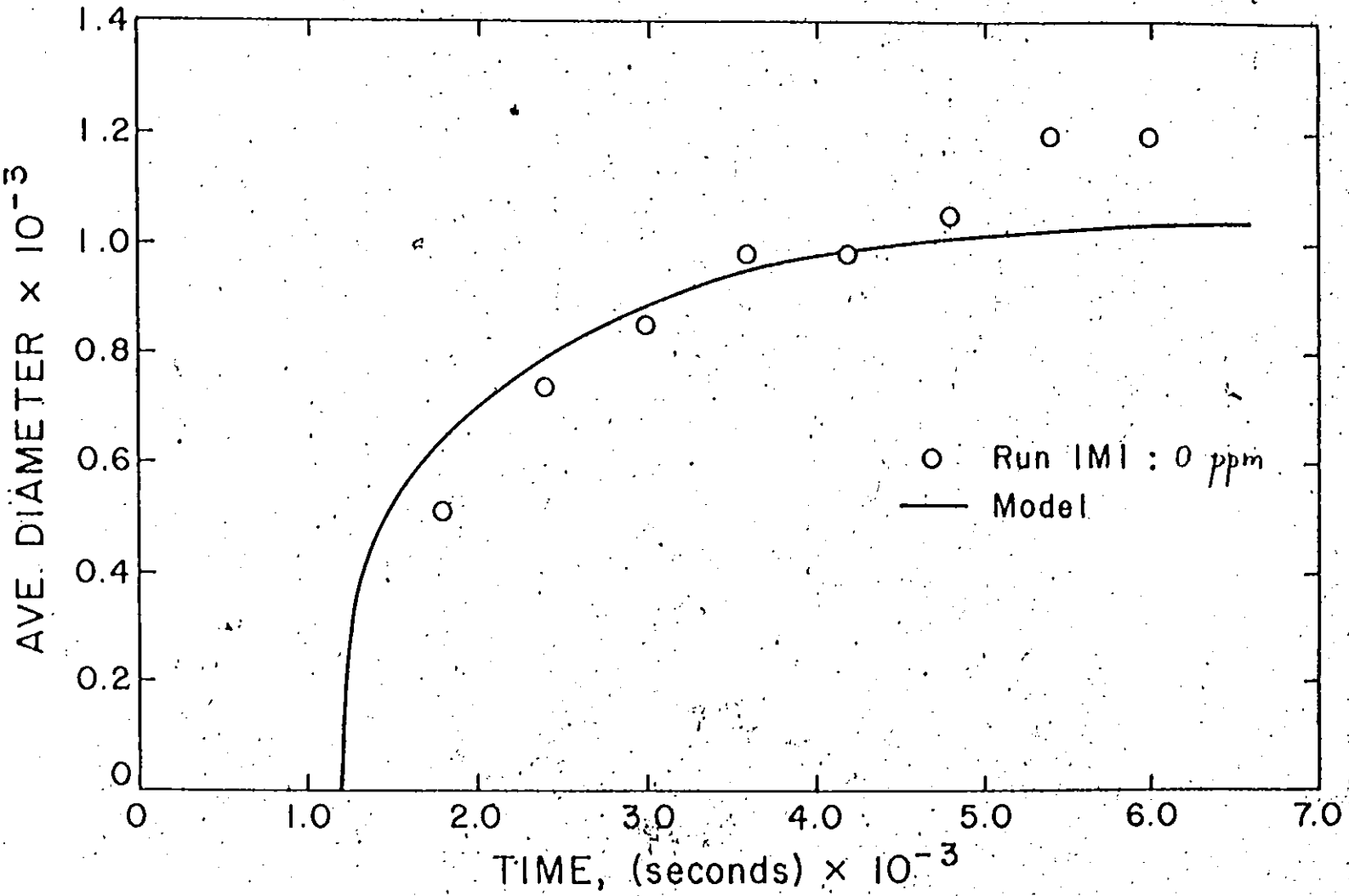

Figure (9-8). Average Particle Diameter vs. Time: Data and Model Predictions

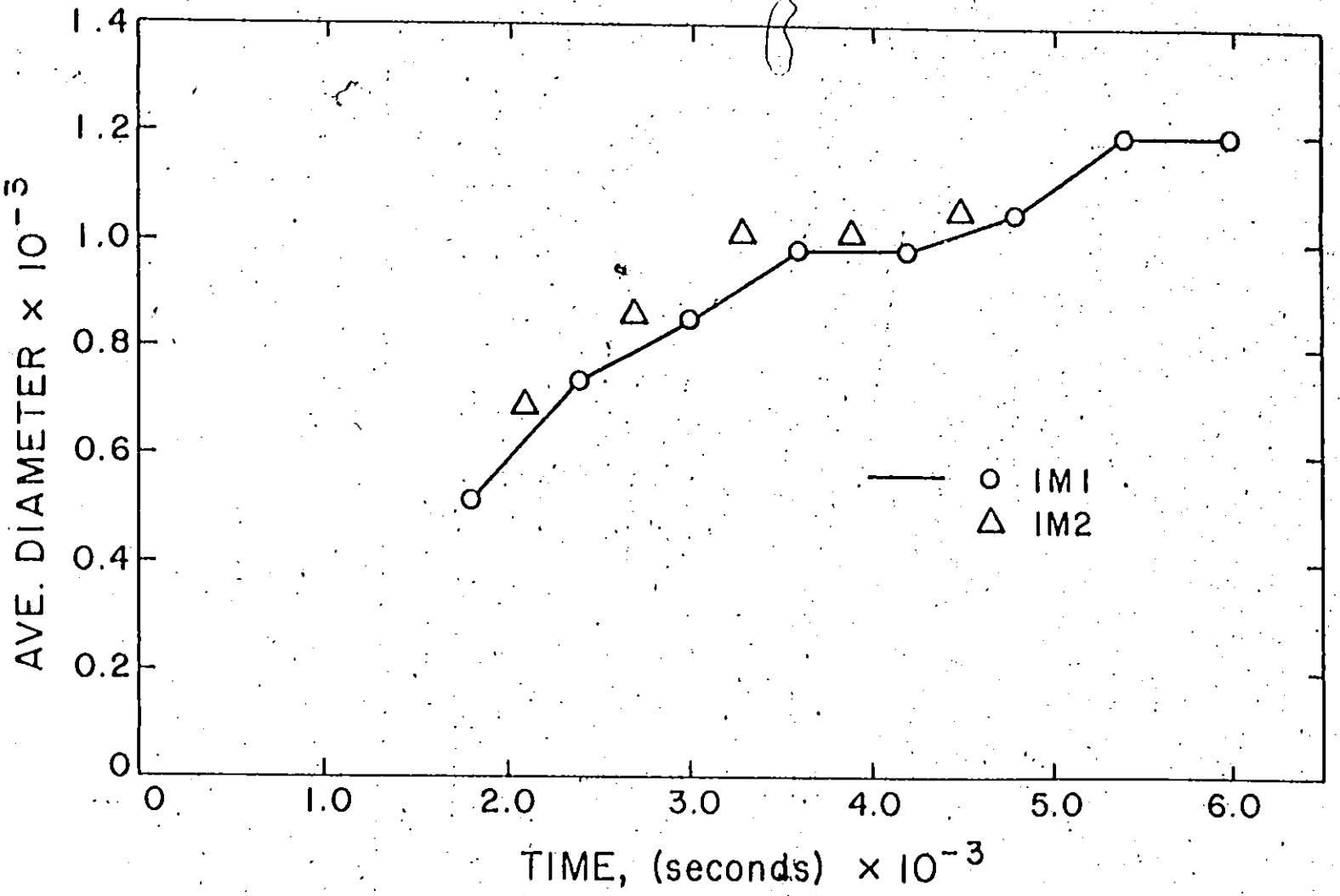

Figure (9-9). Evolution of Particle Size with Time for Runs 1M1 and 1M2

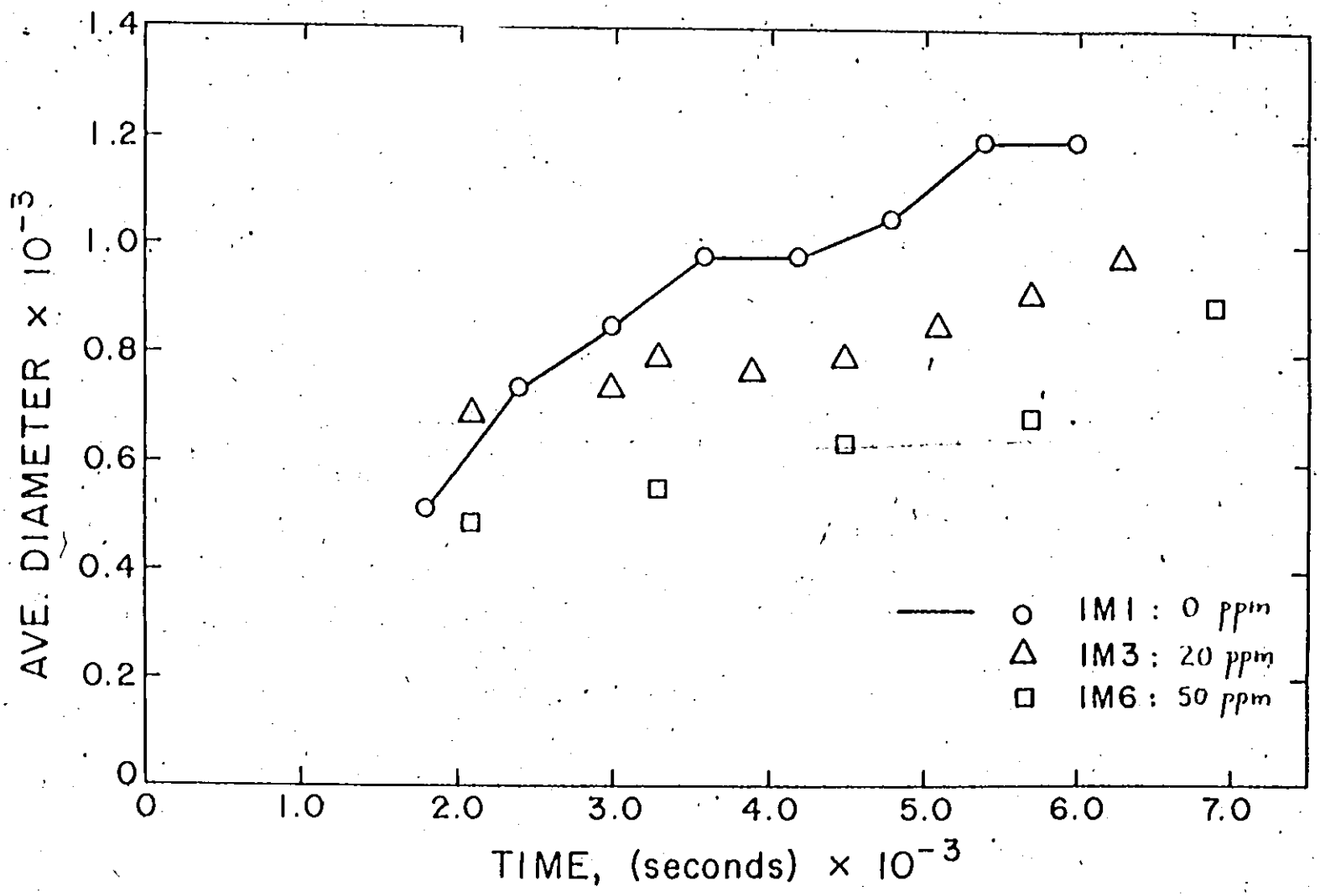

Figure (9-10). Runs IM1, IM3 and IM6: Diameter vs. Time.

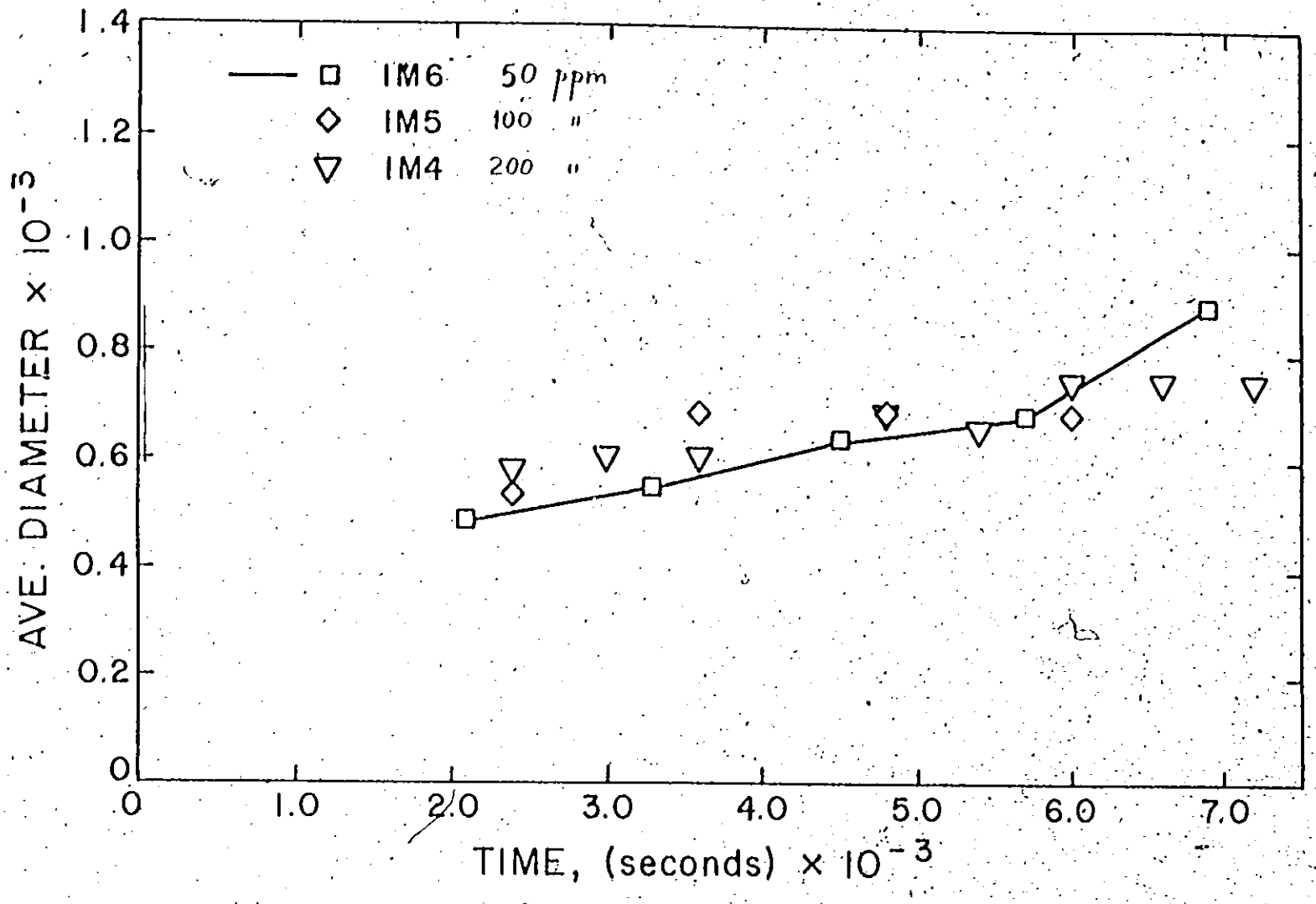

Figure (9-11). Average Particle Size vs. Batch Time for Runs 1M6-1M5-1M4

drop in $R_p(t)$ and conversion. As for polymer particle size, the presence of MSI may cause a slight reduction in $\bar{q}(t)$. This, combined with the competing effect on $A_p(t)$, as discussed previously, will finally yield particle diameters somewhat lower compared to the ones of the impurity-free case.

9.8 General Prescriptions for Case I and II Systems: Impurity Effects

This section contains a summary of our experience and observations concerning impurity effects in emulsion polymerization systems of Case I and II kinetics:

(i) Both Case I and II systems, effect of oxygen: Oxygen acts as an inhibitor which gives an induction period but causes no after-effects in the subsequent course of the polymerization reaction. If introduced in the system as a slug, it may reduce the polymerization rate for some period of time, but the rate will assume its previous value when all of the O_2 is consumed. If introduced in the system in larger quantities, it may completely stop the polymerization reaction.

(ii) Both Case I and II systems, effect of water soluble impurities other than oxygen (e.g. hydroquinone): WSI affect the radical production initially, thus manifesting themselves as induction periods. The induction period is usually proportional to the amount of WSI present in the emulsion. No appreciable effects on the course of the reaction once the induction time is over.

(iii) Case II systems, effect of monomer soluble impurities: MSI prolong stage 1, increase $N_p(t)$, reduce $\bar{q}(t)$ during stages 1 and 2 and cause a dramatic increase in $R_p(t)$ during stage 3. Higher levels of MSI yield lower conversion and particle size, higher number of particles, higher viscosity

and lower molecular weights. A deliberate addition of MSI in the emulsion recipe can therefore be possibly used in order to extend the nucleation time of stage 1, to produce finely monodispersed small particle populations, and to reduce batch times, if of course the reactor's cooling system can take the load during stage 3.

(iv) Case I systems, effect of monomer soluble impurities: For levels less than 50 ppm there is almost no effect on conversion. Higher levels reduce the polymerization rate and conversion, but not as appreciably as for Case II systems. The final particle diameter is defined by a competing effect of the MSI on $\bar{q}(t)$ and $A_m(t)$, and is usually lower compared to an impurity-free case. The new continuous train configuration, which was discussed in Chapter 7, presents additional advantages now that the MSI effects have been quantified. One can direct all the recycle streams back to R2. If the streams contain low levels of impurities, there will be no observable effect on conversion. If the levels are high (i.e. greater than 100-200 ppm), then one can easily compensate for the effect of MSI on conversion or diameter by ensuring tight control on R1 and postfeeding initiator. This is a much easier task to accomplish.

9.9 Conclusions

The effects of monomer soluble impurities on conversion and particle size of emulsion polymerization systems of Case I kinetics have been identified and studied both theoretically and experimentally. These effects, which represent the most important unknown stochastic disturbances in an emulsion system, can play a dominant role in the

meaningful design and safe operation of emulsion polymerization reactors and can explain many not well understood phenomena in these processes.

CHAPTER 10

FINAL CONSIDERATIONS CONCERNING THE ON-LINE CONTROL OF EMULSION POLYMERIZATION REACTORS, GENERAL RECOMMENDATIONS AND CONCLUDING REMARKS

10.1 Introduction

Polymer reactors present a variety of unique problems not present in most control situations. Many of the important process responses are not readily measured and, those that are, are often taken only at discrete intervals of time, usually with relatively long sampling intervals and with large analytical errors. Classical continuous control theory is most often inadequate in its extension to these situations, while some of the modern powerful discrete stochastic control concepts are limited by a lack of reasonable measurement loops.

Stated in a different way by Ray (1985), "the principal difficulties in achieving good control of polymerization reactors are related to inadequate on-line measurements, a lack of understanding of the dynamics of the process, the highly sensitive and nonlinear behaviour of these reactors, and the lack of well-developed techniques for the control of nonlinear processes".

What this thesis has done so far is that it has taken a polymer process from its modelling stage, and through a three-step strategy (see Chapter 1), it has brought the process to such a point where one can actually talk about implementation of on-line control schemes to the process. In other words, the previous chapters of this thesis have added enough to our understanding of process dynamics and behaviour, and of on- or off-line measurements, that one is now ready to tackle the control problem.

The present chapter has been divided into three parts. Part 1 deals with considerations concerning the on-line feedback control of PVAc emulsion polymerization reactors. It is not an exhaustive study but it may provide the basis for a future project on on-line control. Then, part 2 contains some more general recommendations for future work, and finally, part 3 concludes the present thesis by citing its major contributions.

10.2 Part 1: On-line Control of Emulsion Processes

10.2.1 General

An overview of the situation has already been given in Chapter 6. More specifically, Kiparissides et al. (1981) concluded that an extended Kalman filter in conjunction with a suboptimal linear quadratic stochastic control algorithm appeared to have some good features for handling the complexity of the polymer reactor control problem. This combination would provide good state estimates, would take into account any disturbances and large measurement errors and, in addition, the uncertainty in the model parameters could be included in the filter algorithm to account for these model inadequacies (Astrom (1970)).

Obviously, before such an advanced control strategy can be developed, a valid mathematical process model is required which can accurately predict the response of the system to various control actions and can be solved in real time by a process control computer. With the availability of modern process control computers, the practical implementation of such schemes is certainly a reasonble possibility.

To implement such near optimal control algorithms would possibly require considerable space and time on a process minicomputer because of the severe non-linearities of the process, and therefore it would be probably impractical in many situations. However, off-line simulations of these control policies can show some upper-limits as to what could

possibly be accomplished and the nature and magnitudes of the input variable(s) manipulations that are necessary. This could then lead to the development of simple heuristic-type control algorithms which capture the important aspects of optimal control but are more easily implemented on-line.

In a real situation, perfect models do not and will never exist. Uncertainties arise because of imprecise knowledge of physico-chemical parameters, experimental measurement errors and the existence of process disturbances that are difficult to account for in a model, i.e. disturbances that are stochastic in nature (e.g. impurities, see Chapter 9). A dynamic system such as a polymer reactor which also contains elements of a random or statistical nature is termed a stochastic one.

The main stochastic disturbances in a polymer reactor that cannot be accounted for in a deterministic mathematical model of the process and how they can be accounted for is the subject of the next subsection.

10.2.2 Kalman Filters for Emulsion Polymerization Systems

In the preceding chapters of this thesis, we have developed a valid deterministic mathematical process model (Chapter 2), and a reliable on-line measurement, conversion via densitometry (Chapter 3). In addition, all material and particle balance states, i.e. $N_p(t)$, $D_p(t)$, $A_p(t)$, $V_p(t)$ and $x(t)$, are observable from the on-line measurement of $x(t)$. Therefore, one could use a Kalman Filter to track particle size development.

Consider a non-linear stochastic process, modelled by:

$$\dot{\underline{x}} = \underline{f}(\underline{x}, \underline{u}, \underline{k}, t) + \underline{w} \qquad (10.1)$$

where $\underline{x}$ is the (nx1) state variable vector, $\underline{f}$ the non-linear process model, $\underline{u}$ the (rx1) control variable vector, $\underline{k}$ the system parameter vector, t denotes time and $\underline{w}$ is the (nx1) model process noise vector.

Assuming that:

$$\underline{v} = \underline{h}(\underline{x}, t) + \underline{v} \tag{10.2}$$

represents an observation from the system, with $\underline{v}$ being the (mx1) measurable output vector, $\underline{h}$ the non-linear measurement model and $\underline{v}$ the (mx1) measurement noise vector, then the state model equations (10.1) can in general be linearized and discretized.

If one has a very complex model or, if one cannot easily define a nominal steady-state arodnd which to linearize equations (10.1) (e.g. oscillations in a polymer reactor), then the normal variational approach does not work. Instead, one can resort to the so-called "instantaneous apparent linearization", first introduced by Pearson (1962) and Weber and Lapidus (1971), and later employed by Kiparissides (1978) and Pollock (1984).

Although not guaranteeing a unique selection of matrices A and B, the "apparent linearization" of equations (10.1) would yield:

$$\dot{\underline{x}} = A\,\underline{x} + B\,\underline{u} + \underline{w} \tag{10.3}$$

where matrices $A(\underline{x}, \underline{u}, t)$ and $B(\underline{x}, \underline{u}, t)$ ((nxn) and (nxr) respectively) are linearized at a certain time.

Then, discretization of equations (10.3) would eventually give:

$$\underline{x}_{k+1} = \Phi\,\underline{x}_k + \Delta\,\underline{u}_k + \underline{w}_k \tag{10.4}$$

where:

$$\Phi = \exp(AT) \tag{10.5}$$

and

$$\Delta = \int_0^T e^{A(T-s)} B\,ds \tag{10.6}$$

with T being the discrete time interval.

Equations (10.2) would also take the form:

$$\underline{v}_k = H\,\underline{x}_k + \underline{v}_k \tag{10.7}$$

where H is the linearized form of $\underline{h}(\underline{x},t)$. Φ, Δ and H are evaluated by assuming $\underline{x}$ and $\underline{u}$ constant over the time interval T.

For a linearized model, the Kalman Filter provides an optimal estimate of the state vector $\underline{x}_k$ (in a Bayesian or a minimum mean squared error sense) based on information available at the current time t through the measurement vector $\underline{y}_k$. Even if some states are not directly measured, provided that they are observable, the Kalman Filter can provide the optimal estimates of these states as well. The estimate of the state at any instant is a weighted sum of the prediction based on past data and the information from the new observation.

$\underline{w}_k$ and $\underline{v}_k$ in equations (10.4) and (10.7) are assumed to be independent white Gaussian noise vectors with zero mean and covariances given by:

$$E(\underline{w}\,\underline{w}^T) = R_w \tag{10.8}$$

$$E(\underline{w}_t\,\underline{v}^T_{t+j}) = 0 \qquad \text{for all } j \tag{10.9}$$

$$E(\underline{v}\,\underline{v}^T) = R_v \tag{10.10}$$

where E denotes expectation and superscript T denotes transpose of a matrix (vector).

Then, the Kalman Filter equations are given by:

$$\hat{\underline{x}}_{k+1/k} = \hat{\underline{x}}_{k/k} + \int_{t_k}^{t_{k+1}} \underline{f}(\underline{x}, \underline{u}, t)\,dt \tag{10.11}$$

where $\hat{\underline{x}}_{k+1/k} = \hat{\underline{x}}_{t+1/t}$ is the one-step ahead forecast of the state vector, and

$$P_{k+1/k} = \Phi_k P_{k/k} \Phi_k^T + R_w \tag{10.12}$$

Once a set of measurements become available, then:

$$\hat{\underline{x}}_{k+1/k+1} = \hat{\underline{x}}_{k+1/k} - K_{k+1/k}(\underline{y}_{k+1} - H\,\hat{\underline{x}}_{k+1/k}) \tag{10.13}$$

and

$$P_{k+1/k+1} = P_{k+1/k} - K_{k+1/k} H\, P_{k+1/k} \tag{10.14}$$

where $P_{k+1/k+1}$ and $P_{k+1/k}$ denote the variance-covariance matrices of the state estimates, i.e. the matrices that show how precise the state estimates are.

Finally, the Kalman gain matrix K is given by:

$$K_{k/k-1} = P_{k/k-1} H^T (H P_{k/k-1} H^T + R_v)^{-1} \qquad (10.15)$$

Equations (10.11) to (10.15) give the so-called "extended Kalman Filter" (Jazwinski, 1970). The extended Kalman Filter is such that predictions of the state one-step ahead estimate $\hat{\underline{x}}_{k+1/k}$ are calculated using the non-linear model, while the covariance matrices depend on the linearized model form.

The necessary steps to implement the extended Kalman Filter are the following:

(a) At a given time period k, use equations (10.11) and (10.12) to get $\hat{\underline{x}}_{k+1/k}$ and $P_{k+1/k}$.

(b) Use equation (10.15) to obtain $K_{k/k-1}$.

(c) As an observation becomes available, update state estimates and covariance matrix using equations (10.13) and (10.14).

(d) Increase k by 1 and repeat steps (a) through (c).

Some useful hints are worth mentioning at this point:

(i) If the process model is perfect, $R_w = 0$.

(ii) If R_v has diagonal only and large elements (~ 10), then the measurement vector contribution is effectively ignored.

(iii) A state is said to be observable using a given property measurement, if by taking the measurement it is possible to make an inference about the state level using the developed model. The structure of the present model in a state-space form is:

$$\begin{pmatrix} \underline{x}_{PSD} \\ \hline \underline{x}_{MWD} \end{pmatrix}_{k+1} = \left(\begin{array}{c|c} A_1 & 0 \\ \hline A_3 & A_4 \end{array}\right) \begin{pmatrix} \underline{x}_{PSD} \\ \hline \underline{x}_{MWD} \end{pmatrix}_k + \underline{w}_k \qquad (10.16)$$

with a possible on-line measurement equation:

$$\underline{y}_k = \left(H_{11} \; 0 \right) \left(\begin{array}{c} \underline{x}_{PSD} \\ \hline \underline{x}_{MWD} \end{array} \right)_k \qquad (10.17)$$

From equations (10.16) and (10.17) one can clearly see that the MWD states depend on the PSD states ($A_3 \neq 0$), because of the dependence on x(t) and $V_p(t)$. PSD states, on the other hand, do not depend on the MWD states ($A_2 = 0$). Hence, the MWD states are not observable from measurements on the PSD states.

(iv) The term $(\underline{y}_{k+1} - H\,\hat{\underline{x}}_{k+1/k})$ in equation (10.13) represents the prediction error. Equation (10.13) gives the filtered state estimate $\hat{\underline{x}}_{k+1/k+1}$.

(v) The first step in the implementation of the Kalman Filter (step (a)) starts with a choice of initial conditions for the state vector $\hat{\underline{x}}_{0/0}$ and the covariance matrix $P_{0/0}$.

(vi) The Kalman Filter is a conventional low pass filter. Substituting equation (10.13) into (10.4), the structure becomes:

$$\hat{\underline{x}}_{k+1/k} = \phi\,\hat{\underline{x}}_{k/k-1} + \Delta\,\underline{u}_k + \phi\,K_{k/k-1}(\underline{y}_k - H\,\hat{\underline{x}}_{k/k-1}) \qquad (10.18)$$

New state estimate — Model contribution — Data contribution

One can now see the effect of R_w or R_v on the state estimates. If, for example, the precision of the measurements is poor, R_v increases, causing the Kalman gain $K_{k/k-1}$ to decrease, and therefore, the data contribution to be weighted less heavily.

From the above discussion, one can see that the Kalman Filter resembles an ordinary low pass noise filter in that it filters out the effects of the measurement noise $\underline{v}_k$ in order to give a better estimate of the true state of the system. However, rather than using an arbitrary filter structure (e.g. the usual first order low pass filter) it uses the model of the system.

The Kalman Filter is the only way of coupling a process dynamic model with a small set of measurements in order to allow one to track all the states of the model (assuming of course that observability conditions are satisfied). In other words, it is the only way to bring process data into the process model.

Assuming that one has a good mathematical process model and a good measurement to satisfy observability, the main problem in implementing a Kalman Filter is the stochastic states. The key to a good filter is how one introduces the stochastics.

10.2.3 Application of Kalman Filters to the Two Reactor System

The sources of the major stochastic disturbances in all industrial free radical and ionic polymerizations are the reactive impurities (see Chapter 9). In general, all stochastic disturbances in the system like variations in the quality of raw materials, effect of oxygen, etc., can be attributed to and summarized as "impurity effects".

The process model noise vector $\underline{w}_k$ (see equation (10.4)) contains in general model inadequacies, which are basically due to uncertainties in the nucleation term, f(t), feed rate variabilities and statistical fluctuations of the distribution of radicals in the polymer particles, i.e., stochastic fluctuations of the polymerization rate, $R_p(t)$. One usually has a good handle on these inadequacies, coming from a good process understanding.

Applying the Kalman Filter to the two reactor system, the process state vector $\underline{x}_k$, containing the particle size states $N_p(t)$, $D_p(t)$, $A_p(t)$ and $V_p(t)$, conversion x(t), the initiator and emulsifier concentrations $I_w(t)$ and $S_T(t)$, and the water and monomer soluble impurity concentrations in the reactor WSI(t) and MSI(t); was further augmented by two more states; these two additional states described the impurity concentrations in the feed (incoming) streams, which are unknown and purely stochastic. By using impurity concentrations in the

feed streams as the two new stochastic states, one can effectively and easily account for O_2 slugs in the system, which would not be accounted for as easily with flow rate states.

The equation for the two new states is the following:

$$(CIM_F)_{t+1} = (CIM_F)_t + a_t \tag{10.19}$$

where CIM_F denotes concentration of impurities in the feed streams and a_t is white noise. For the first approach, the measurement equation (10.7) contained information on the conversion level from reactor 2 only.

If the impurities come from two different sources (e.g. feed tanks plus recycle streams), then one can run the Kalman Filter for each reactor separately, provided that there exist conversion measurements from both reactors. In such a case, both state vectors should be augmented with the two additional equations for CIM_F. In the present case, since all impurities come from the same source, i.e. feed streams, and since the same impurities affect both R1 and R2, then the augmentation is as follows:

$$\underline{z}_k = \begin{pmatrix} \underline{x}_{1k} \\ \underline{x}_{2k} \\ (CIM_F)_k \end{pmatrix} \tag{10.20}$$

The same approach, which closely parallels the physical picture, can also be used in an extension to biological or fermentation reactors and processes (Parulekar et al. (1985), Yoo et al. (1985)).

Eventually, one ends up with a (20x1) state vector $\underline{z}_k$. To give more details about the case study, it could be as lengthy as the previous part of the thesis. Since section 10.2 is the basis for immediate future work, the reader is referred for more details to Penlidis et al. (1986). One thing that should be mentioned herein, however, is that for the Kalman Filter implementation on the continuous latex train of Chapter 7, the impurity levels in the feed were considered to be in the typical pilot-plant range of 20 ppm, and to vary by $\pm$ 20 ppm as well.

The results from the Kalman Filter application, i.e. the effort to see whether the filter was able to track conversion variations due to stochastic impurity level variations in the feed, are shown in Figure 10-1, for conversion and average particle diameter, respectively. It is clear from the figure that the model prediction $\hat{\underline{x}}_{t+1/t}$ and the filtered estimate $\hat{\underline{x}}_{t+1/t+1}$ almost coincide. The slight discrepancy which is observed is only due to the numerical integration scheme.

When the model prediction coincides with the filtered estimate, i.e. when $\hat{\underline{x}}_{t+1/t} = \hat{\underline{x}}_{t+1/t+1}$, then this means that there is virtually no information on the state estimates coming from the new measurement, and hence the Kalman gain is set equal to zero, which was the case in this exercise. The reason for that is explained in what follows.

Let's consider first the effects of the "apparent linearization" method. Kiparissides (1978) and Pollock (1984) linearized the system by diagonalizing matrix A in equation (10.3). This was a very "ad hoc" scheme, since it did not necessarily represent the true physical picture of the system. In our "apparent linearization", matrix A was not diagonal, but dominantly dependent on $A_p(t)$ and $S_T(t)$, since f(t), the nucleation term, is a function of particle surface area and total emulsifier concentration. What we observed, however, was that during the Kalman Filter implementation steps matrix A (or ϕ) was just being updated, without permitting information to propagate to other positions of the matrix. In other words, one was just updating matrix A without passing in the uncertainty due to impurity effects.

Let's discuss now the main reason why the Kalman Filter analysis gave the results of Figure 10-1. Chapter 9 clearly showed that Case I systems conversion is insensitive to typical pilot-plant impurity variations (which had been actually employed in the simulation exercise). Hence, the Kalman Filter could not obtain any additional information from the measurements. Therefore, the Kalman gain $K_{t+1/t}$ was set equal to a small value or zero, and

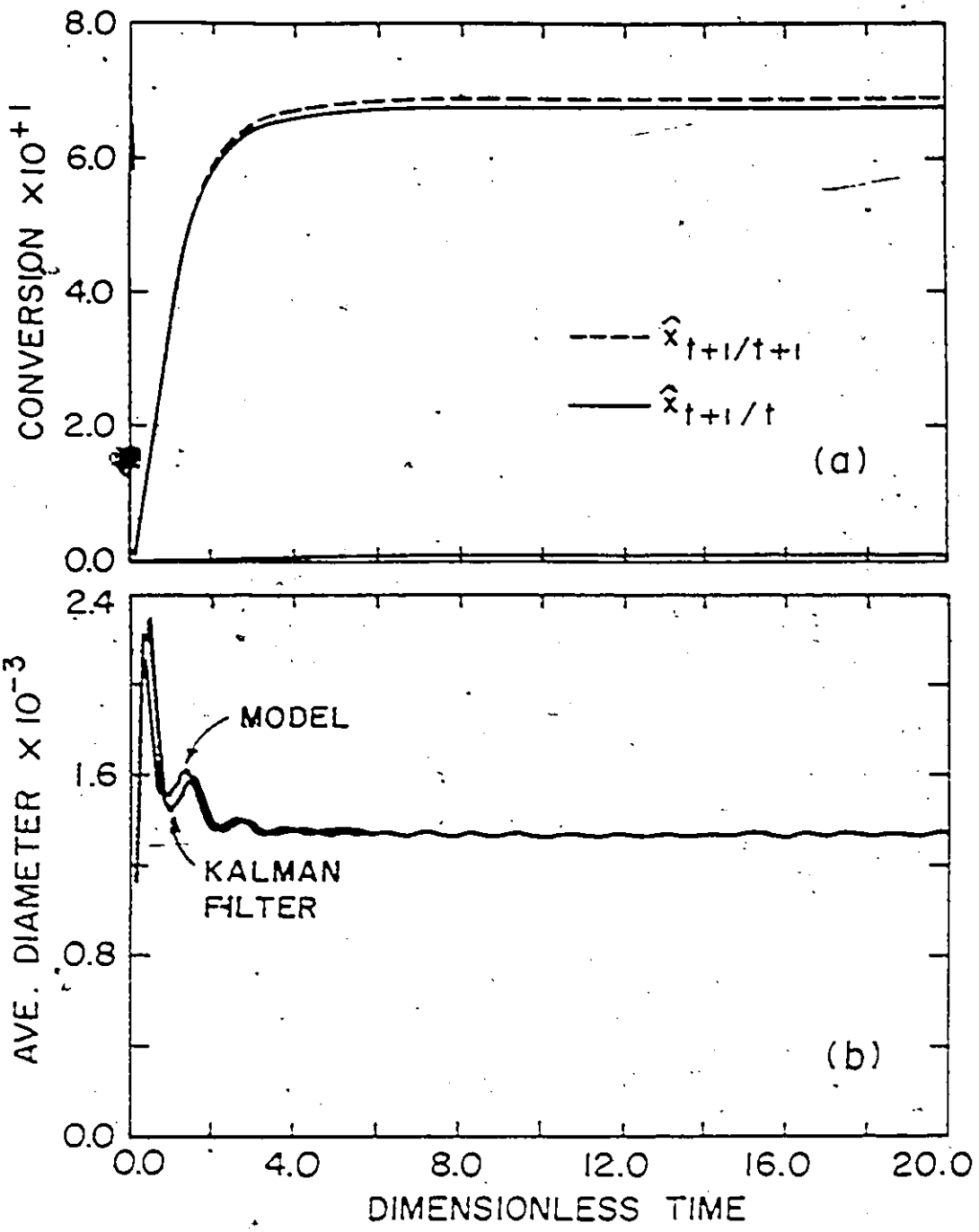

Figure (10-1). Model Prediction and Filtered Estimate for Conversion and Average Size from the Kalman Filter Analysis

since no new additional information was propagating through the states, the Kalman Filter simply agreed with the model prediction, as it should have done, and hence $\hat{\underline{x}}_{t+1/t} = \hat{\underline{x}}_{t+1/t+1}$.

Another thing that this Kalman Filter analysis revealed is that there may be no point including the effect of monomer soluble impurities, because they have virtually no effect on the system response at typical pilot-plant levels. The Kalman Filter analysis could be repeated by including only the water soluble impurity effects, provided that a more efficient linearization technique for the system would permit information from WSI(t) to propagate to the other states through the f(t) term. Therefore, what is needed is a Taylor series type of linearization for f(t), i.e. an expansion for $[\partial f(t)/\partial WSI(t)]$. Such an expansion gave the following result:

$$\frac{\partial f(t)}{\partial WSI(t)} = -(R_w^{\bullet})\left(1 + \frac{L k_v}{4}\right) + \frac{\partial A_p(t)/\partial t}{\partial WSI(t)/\partial t} \qquad (10.21)$$

Equation (10.21) looks more promising in that the last derivative ratio can be evaluated at any time t from the computer program.

Departing from the traditional approach of "local linearization" followed by linear designs for the thus "linearized" systems, the papers by Soliman (1981) and Ogunnaike (1985) could also be helpful in near future applications.

To conclude the Kalman Filter section, one could say that the Kalman Filer analysis in combination with the results of Chapter 9 clearly suggested that a simpler Filter can be used for Case I systems to account for stochastic impurity variations and their effects.

10.2.4 The Potential for On-line Particle Size Measurement

The difficulties associated with even off-line particle size determination have been highlighted in detail in Chapter 3. Chapter 3 also made clear that particle size measurement is maybe the most important of the latex characterization techniques. It would be redundant to try and justify here how important the on-line particle size determination would be for

industrial emulsion processes. It should be mentioned, however, that on-line latex particle diameter measurement on an industrial scale could be a project by itself..

Kiparissides et al. (1980) were probably the first to report on a lab-scale experimental effort to monitor polymer particle size during the continuous emulsion polymerization of VAc on-line. The method employed was turbidity spectra and a Beckman DU spectrophotometer was used for turbidity measurements. Absorbance values at 350 nm wavelength plotted against reaction time were able to follow the behaviour of conversion for both cases of sustained oscillations and steady-state reactor operation. They concluded that by monitoring continuously the absorbance (turbidity) at even a single wavelength (the discussion in Chapter 3 further illustrates and extends this point), one can determine whether the reactor operates at a stable or limit cycle mode, and additionally one can detect induction times or rate and extent of particle flocculation.

Zollars (1980) also employed turbidity measurements for the determination of particle size and described equipment for the on-line application of the technique during a latex polymerization. Pointing out that the dilution system is probably the most crucial part of the on-line set-up, he used two wavelengths to continuously monitor the evolution of particle size in batch VAc emulsion polymerization. The dilutions employed were in the range of 0.3-0.4 mg/cm^3. Erratic readings were reported at higher conversions due to latex precipitation in the flow-through cells.

Pollock (1984) tried to use the same ideas but his initial runs indicated problems with the experimental apparatus. First, the dilution cell of the UV spectrophotometer was subject to settling out of the polymer, which resulted in misleading readings. In addition, other severe problems were encountered in attempts to dilute the samples accurately.

From the analysis of Chapter 3 and from the experience accumulated during the several stages of this thesis, we think that two wavelengths (in the range between 350 and

600 nm) combined with the precise flow rates of a peristaltic pump would enable one to rather inexpensively set up a dilution loop for the on- line determination of latex particle size. Inexpensively because there are obviously some fully automated set-ups available commercially for this purpose, but, besides the fact that they are in the range of $10,000 or more, nobody can guarantee their success with latex systems. Using a dilution loop with two wavelengths, one could also employ the two spectrophotometers as calibrated instruments, i.e., construct calibration curves of sample absorbance or turbidity over concentration versus diameter determined from another off-line characterization technique (e.g. HDC), a way which could simplify the analysis appreciably. Another solution would be the use of the two spectrophotometers off-line, in which case one would simply have to increase the sampling interval during which diameter information would become available.

Finally, one could resort for additional information or ideas to more sophisticated techniques, such as laser nephelometry, high speed multiangle scattered light measurements, pulse shape analysis, differential light photometry or recording of the rms value of turbidity fluctuations, and dynamic light scattering. All these techniques are recent, probably more expensive, they have only been tested with perfectly monodispersed suspensions as usually and they are all based on light scattering principles. Ideas from these more sophisticated techniques (see, for instance, Bartholdi et al. (1980), Salzman et al. (1980), Lee and Groves (1981) and Gregory (1985)), could be eventually exploited in order to suggest a set-up well suited for an industrial environment.

10.2.5 Final Step: Emulsion Reactor Control

Chapter 7 of this thesis gave a solution to the main operational and control problem in Case I emulsion polymerization reactors, that of the sustained oscillations phenomenon. With the new oscillation-free and operationally very stable and flexible reactor configuration,

one can now safely concentrate on the simpler but fundamental control problem of producing a latex in a range of specifications.

Of course, there is a wide spectrum of different control algorithm sophistication that can be used in these reactor control studies. One could start from simple single loop feedback control, based on measurements of density and turbidity which can show one how to change initiator flow rate and split in order to achieve effective control over conversion and particle size. The design of multivariable decouplers could be another possibility in the intermediate range with optimal control combined with extended Kalman filtering being a possibility at a higher level of sophistication.

We would like to conclude this subsection with a proposal of possible control schemes, which can eventually be attempted on our new reactor design in the immediate future. The control algorithms that can be developed can cover set-point changes and disturbance rejection. In the case of set-point changes the controller can bring the process either from one conversion level to another with particle size being unaltered or from one particle diameter to another keeping conversion the same or from one operating point to another with new conversion and average size. In the case of disturbance rejection, the controller can compensate for the following: (i) system contamination by oxygen and (ii) effect of water (or monomer) soluble impurities.

Two approaches can be taken for the final controller design. In the first approach, the process can be modelled as:

$$\underline{y}(s) = \underline{G}(s) \cdot \underline{u}(s) \qquad (10.22)$$

where $\underline{y}(s)$ is the process output and $\underline{u}(s)$ the process input vector (see the possible schematic representation of Figure 10.2). $\underline{G}(s)$ is the process transfer function matrix, identified from step testing on a simulation model of the reactor configuration around a nominal operating

point (this study has already been initiated). In the second approach, the dynamic model can be used in its state-space form:

$$\dot{\underline{x}}(t) = A\,\underline{x}(t) + B\,\underline{u}(t) \tag{10.23}$$

$$\underline{y}(t) = C\,\underline{x}(t) \tag{10.24}$$

to finally yield an open-loop transfer function of the form:

$$\underline{G}(s) = C(sI-A)^{-1}\,B \tag{10.25}$$

The following control algorithms can be examined: (i) single loop feedback on conversion and average particle size from the second reactor, with proportional-integral (PI) control plus dead-time compensation. The objective of this part of the control study (although the study may result in mutually fighting controllers) is to investigate how effectively one can achieve set-point changes (ii) single loop feedback of average particle diameter to split and a combination of feedforward plus feedback of conversion to initiator flow rate. Variations of this scheme depending upon whether one uses information after the second reactor only and/or information on conversion after the first reactor as well. This appears to be a very practical scheme and it will essentially reduce to the design of a decoupler (iii) fully multivariable feedback based on transfer function models (e.g. IMC, Huang and Stephanopoulos (1985)) or full optimal control combined with extended Kalman Filters.

10.3 Part 2: Other General Future Recommendations

This part contains some more suggestions and ideas, other than control ones, for future work and thought. These suggestions came up during the course of the present thesis. They will be cited in reference to the chapter where they first originated from, so that it might be easier for the reader to put them in a broader perspective. The following investigations might be considered:

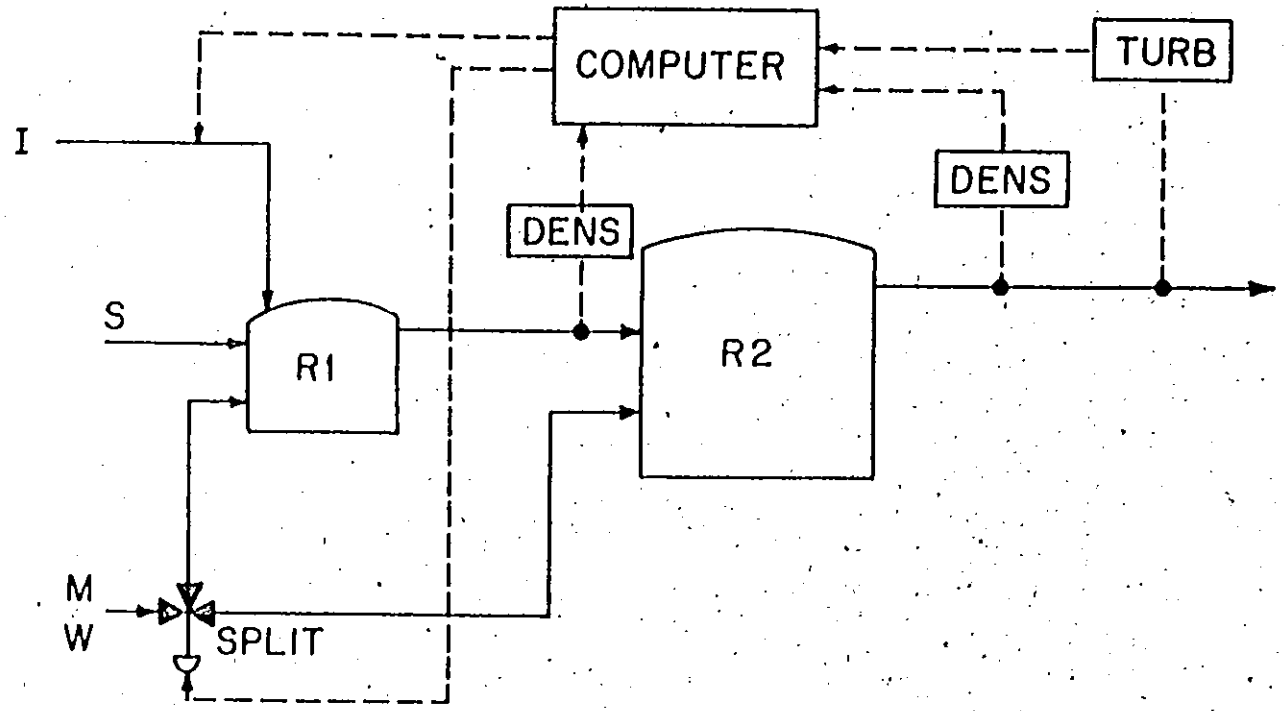

Figure (10-2). Computer Control of Continuous Latex Reactors

(a) Chapter 2: A more-in-depth study of particle coalescence and agglomeration kinetics; experimental differentiation between collision and diffusion theories and study on the use of seeded latexes in batch, semi-batch or continuous reactors which would again help in discriminating between the two theories; influence of ionic strength or degree of agitation on particle generation; applications and refinements of the DLVO theory; a closer study on homogeneous nucleation; influence of pH on polymerization kinetics; statistical variations in PSD calculations; extension of modelling framework in order to cover as many monomers (Cases I and II) as possible.

(b) Chapter 3: An extensive evaluation of various packing materials with differing pore geometry is required. The optimum packing particle, to minimize dispersion or particle loss in the columns, is probably one with a solid core and superficial surface pores. Factors affecting particle loss such as ionic strength of eluant, use of ionic surfactant alone as opposed to a mixture of surfactant and electrolyte, effect of glass transition temperature of particles, effect of packing type and effect of column temperature need to be better understood. A multiple wavelength UV/Visible light turbidity detector has been theoreticaly evaluated and found to have reasonable potential as an analytical tool for particle size measurement (Husain et al. (1979a)). Likewise, IR detection has been shown to have some useful features (Nagy (1979)). An experimental investigation of both these detectors is desirable. Also, more sensitive refractometers with a monochromatic light source should be evaluated. The theory of HDC should be extended to investigate the possibility of predicting the chromatogram shape. The corresponding development of a theory for SEC to adequately predict peak separation as well as peak shape may be facilitated by the use of model porous spheres. The numerical treatment of chromatographic data is rather inadequate. It is desirable to develop new improved methods for the recovery of W(y), i.e. of the true

chromatogram. A more detailed study concerning the mathematics, the interpretation and the application of dynamic light scattering on latex size characterization is required.

(c) Chapter 4: A combination of an on-line spectrophotometer with addition of a known amount of water soluble inhibitor in the emulsion recipe would offer great help in the attempt to investigate and model rates of radical scavenging by contaminants.

(d) Chapter 5: Experimental verification of the semi-batch strategies for Case I kinetics and extension to Case II kinetics; derivation of open-loop semi- batch strategies using optimization techniques (e.g. Pontryagin's maximum principle); effort to obtain bimodal or multi-modal PSD's, if so desired, with semi-batch seeding.

(e) Chapter 7: Different start-up policies with the new reactor configuration; appropriate start-up of the seeding reactor is believed to be able to bring the second reactor (or the rest of the train) very rapidly to a desirable prespecified set-point. Experimental verification of start-up policies; extensions to Case II systems.

(f) Chapter 8: Experimentation with emulsion VCM or VCM/VAc and further testing of the predictive powers of the VCM homo- and copolymerization models.

(g) Chapter 9: Effect of pH on hydroquinone partitioning between the monomer and water phase; regulation (control) of pH in an emulsion reactor; experimentation with known (monomer or water soluble) and unknown (slugs of oxygen) amounts of impurities in the new continuous train configuration.

10.4 Part 3: Concluding Remarks

The etymology of the ancient greek word for "human being" is "someone who always looks higher". Attempting a somehow free metaphorical translation of its meaning, one could say that a human being always tends to set high objectives. Human beings are

involved in scientific research, hence the tendency of scientific research in general to set high targets as well.

It is of course the reader's part to judge whether this thesis fulfilled successfully (or not) its objectives. And at this concluding point, it is the author's attempt to summarize the major contributions that this thesis offers in chemical engineering research in general, and more specifically, in the vast field of polymer reactor design:

(a) Modelling and process understanding stage: A very general model framework was further refined and extended to a different system (VCM). The population balance approach was applied for the first time to an emulsion copolymerization system (VCM/VAc).

(b) Experimental stage: a novel continuous latex reactor configuration and its flexible oscillation-free operation were evaluated and experimentally verified. This contributed to further our process understanding and simplify the main control problem, and led to the development of new suggestions for on-line process monitoring and feedback control.

(c) Process design and control stage: The industrially very important and largely unstudied effect of monomer or water soluble impurities on emulsion polymerization reactors (Case I systems) was investigated both theoretically and experimentally. The analysis added to our process understanding, identified the source of the main process disturbances and finally, set the basis for a more meaningful Kalman Filter application on these systems and a more refined way of including the stochastics for the future solution of the on-line feedback control problem.

REFERENCES

Abbey, K.J., in "Emulsion Polymers and Emulsion Polymerization", editors D.R. Bassett and A.E. Hamielec, ACS Symposium Series 165, Washington, D.C. (1981).

Abdel-Alim, A.H. and A.E. Hamielec, J. Appl. Poly. Sci., 16, 783 (1972).

————, J. Appl. Poly. Sci., 18, 1603 (1974).

Adamson, A.W., "Physical Chemistry of Surfaces", 2nd ed., Interscience, N.Y. (1967).

Ahlberg, D.T. and I. Cheyne, AIChE Symposium Series in Chemical Process Control, No. 159, Vol. 72 (1979).

Ahn, Y.O., K.Y. Park and T.K. Park, PACHIEC, Vol. II (1983).

Alba, D. and G.R. Meira, to appear in J. Liq. Chromat. (1985).

Altgelt, K.H., in "Advances in Chromatography", editors J.C. Giddings and R.A. Keller, Vol. 7, N.Y. (1968).

Amrehn, H., Automatica, 13, 533 (1977).

Andersen, H.M. and S.I. Proctor, Jr., J. Poly. Sci., A-3, 2343 (1965).

Arnold, K., A.F. Johnson and J. Ramsay, IFAC PRP-4, Ghent, Belgium (1980).

Astrom, K.J., "Introduction to Stochastic Control Theory", Acad. Press, N.Y. (1970).

Bakon, R.G.R., Trans. Faraday Soc., 42, 140 (1946).

Badder, E.E. and B.W. Brooks, Chem. Eng. Sci., 39, 1499 (1984).

Balaraman, K.S., B.D. Kulkarni and R.A. Mashelkar, Poly. Eng. Sci., 23, 719 (1983).

Ballard, M.J., D.H. Napper and R.G. Gilbert, J. Poly. Sci., 19, 939 (1981).

Bamford, C.H., W.G. Barb, A.D. Jenkins and P.F. Onyon, "The Kinetics of Vinyl Polymerization by Radical Mechanisms", Butterworths Scientific (1958).

Barnes, J.D., B. Dickens and F.L. McCrackin, ACS National Conference, Miami, April 1985.

Bartholdi, M., G.C. Salzman, R.D. Hiebert and M. Kerker, Appl. Optics, 19, 1573 (1980).

Bataille, P., B.T. Van and Q.B. Pham, J. Poly. Sci., Poly. Chem. Ed., 20, 795 (1982).

Battacharya, D., Ph. D. Thesis, Dept. of Chemical Engineering, McMaster University, Hamilton, Ontario (1985).

Berens, A.R., J. Appl. Poly. Sci., 18, 2379 (1974).

Berne, B.J. and R. Pecora, "Dynamic Light Scattering", John Wiley and Sons, Inc., N.Y. (1976).

Beste, L.F. and H.K. Hall, Jr., J. Macro. Chem., 1, 121 (1966).

Bevington, J.C., "Radical Polymerization", Acad. Press, N.Y. (1961).

Billingham, N.C., "Molar Mass Measurements in Polymer Science", Kogan Page Ltd. (1977).

Blackley, D.C., "High Polymer Latices", MacLaren and Sons Ltd., London (1966).

————, "Emulsion Polymerization", Appl. Sci. Publishers, London (1975).

Böhm, L.L., Polymer, 19, 545 (1978).

Boor, J., "Ziegler-Natta Catalysts and Polymerizations", Acad. Press, N.Y. (1979).

Brandrup, J. and E.H. Immergut, editors, "Polymer Handbook", Wiley Interscience, N.Y. (1975).

Broadhead, T.O., M. Eng. Thesis, Dept. of Chemical Engineering, McMaster University, Hamilton, Ontario (1984).

Broadhead, T.O., A.E. Hamielec and J.F. MacGregor, to appear in Makromolec. Chem. (1984).

Brooks, B.W., H.W. Kropholler and S.N. Purt, Polymer, 19, 193 (1978).

Bueche, F., J. Poly. Sci., 43, 527 (1960).

————, "Physical Properties of Polymers", Wiley Intersci., N.Y. (1962).

Buffham, B.A., J. Coll, Inter. Sci., 67, 154 (1978).

Burnett, G.M., M.H. George and H.W. Melville, J. Poly. Sci., 16, 31 (1955).

Burnett, G.M., R.S. Lehrle, D.W. Ovenall and F.W. Peaker, J. Poly. Sci., 29, 417 (1958).

Campbell, J.D., M. Eng. Thesis, Dept. of Chemical Engineering, McMaster University, Hamilton, Ontario (1985).

Casassa, E.F., J. Phys. Chem., 75, 3929 (1972).

Cauley, D.A., A.J. Giglio and R.W. Thompson, Chem. Eng. Sci., 33, 979 (1978).

Chang, K.H.S., M.H. Litt and M. Momura, in "Emulsion Polymerization of Vinyl Acetate", editors M.S. El-Aasser and J.W. Vanderhoff, Applied Science (1981).

Chang, R.Y. and M.L. Wang, Ind. Eng. Chem. Proc. Des. Dev., 23, 463 (1984).

Chen, S.A. and W.F. Jeng, Chem. Eng. Sci., 33, 735 (1978).

Chiang, A.S.T. and R.W. Thompson, AIChE J., 25, 552 (1979).

Chiu, W.Y., G.M. Carratt and D.S. Soong, AIChE National Meeting, Los Angeles (1982).

Chu, B., Ann. Rev. Phys. Chem., 21, 145 (1970).

———, "Laser Light Scattering", Acad. Press, N.Y. (1974).

Cluett, W.R., S.L. Shah, J.M. Martin-Sanchez and D.G. Fisher, CSChE Conference, Vancouver (1982).

Coll, H., G.R. Fague and K.A. Robillard, paper from Eastman Kodak Co., Rochester, N.Y. (1975).

Coll, H. and G.R. Fague, J. Coll. Inter. Sci., 76, 116 (1980).

Collins, E.A., lecture #11 in "Advances in Emulsion Polymerization and Latex Technology", Lehigh University, Bethlehem, PA (1983).

Corrin, M.L. and W.D. Harkins, J. Amer. Chem. Soc., 69, 683 (1947).

de la Court, F.H. and H. Vogt, J. Oil Coll. Chem. Assoc., 52, 587 (1969).

Crowe, C.M., chapter in "An Intensive Short Course on Polymer Production Technology", McMaster University, Hamilton, Ontario (1984).

Derderian, E.J. and T.B. MacRury, J. Disper. Sci. and Techn., 2, 345 (1981).

Dickinson, R.F., Ph. D. Thesis, Dept. of Chemical Engineering, University of Waterloo, Ontario (1976).

Dickinson, R.F. and C.E. Gall, 59th CIC Conference, London, Ontario, June 1976.

Dietz, R., J. Appl. Poly. Sci., 25, 951 (1980).

Duckworth, I.H., Rubber Chem. and Techn., 38, 233 (1965).

Duijfjes, G., Journal A, 16, 93 (1975).

Dunn, A.S. and P.A. Taylor, Macromol. Chem., 83, 207 (1965).

Dunn, A.S., in "Emulsion Polymerization of Vinyl Acetate", editors M.S. El-Aasser and J.W. Vanderhoff, Applied Science (1981).

Edelhauser, H., in "Polymer Colloids", NATO Adv. Study Inst., Trondheim, Norway (1975).

El-Aasser, M.S. and J.W. Vanderhoff, editors, "Emulsion Polymerization of Vinyl Acetate", Applied Science (1981).

Fitch, R.M., J. Paint Technol. Eng., 37, 32 (1965).

————, editor, "Polymer Colloids", Pergammon Press (1971).

Fitch, R.M. and C.H. Tsai, in "Polymer Colloids", editor R.M. Fitch, Plenum Press, N.Y. (1971a), p. 73-102.

————, in "Polymer Colloids", editor R.M. Fitch, Plenum Press, N.Y. (1971b), p. 103-115.

Foss, A.S., AIChE J., 19, 209 (1973).

Friis, N. and L. Nyhagen, J. Appl. Poly. Sci., 17, 2311 (1973).

Friis, N., D. Goosney, J.D. Wright and A.E. Hamielec, J. Appl. Poly. Sci., 18, 1247 (1974).

Friis, N. and A. E. Hamielec, J. Appl. Poly. Sci., 19, 97 (1975a).

————, Polymer Preprints, 16, 192 (1975b).

————, Adv. Chromat., 13, 41 (1975c).

————, in "Emulsion Polymerization", editors I. Piirma and J. L. Gardon, ACS Symposium Series 24, Washington, D.C. (1976).

————, chapter in "An Intensive Short Course on Polymer Production Technology", McMaster University, Hamilton, Ontario (1977).

Gardon, J.L., Br. Poly. J., 2, 1 (1970).

Gatta, G., G. Benetta, G.P. Talamini and G. Vianello, in "Addition and Condensation Polymerization Processes", editor R.F. Gould, Advances in Chemistry Series 91, ACS Publications (1969).

Gaylor, V.F. and H.L. James, Conference on Analytical Chemistry, Cleveland, March 1975.

Gerrens, H., Fortschridde Hochpolymer Forschung, 1, 234 (1959).

Gerrens, H., K. Kuchner and G. Ley, Chem. Ing. Techn., 43, 693 (1971).

Gershberg, D.B. and J.E. Longfield, 45th AIChE Meeting, New York (1961).

Giddings, J.C., in "Advances in Chromatography", editors J.C. Giddings, E. Grushka, J. Cazes and P.R. Brown, Marcel Dekker Inc., N.Y. (1982).

Giddings, J.C. and M.N. Myers, Sep. Sci. Techn., 13, 637 (1978).

Giddings, J. C., M. N. Myers and J. F. Moellmer, J. Chromat., 14, 501 (1978).

Gilbert, R.G. and D.H. Napper, JMS-Rev. Macromol. Chem. Phys., C23, 127 (1983).

Gilbert, R.G., P.J. Feeney and D.H. Napper, 67th CAN-AM Chemical Congress, Montreal, June 1984.

Gledhill, R.J., J. Phys. Chem., 66, 458 (1961).

Goodwin, J.W., J. Hearn, C.C. Ho and R.H. Ottewill, Br. Poly. J., 5, 347 (1973).

Gorber, D.M., Ph.D. Thesis, Dept. of Chemical Engineering, University of Waterloo, Waterloo, Ontario (1973).

Gordon, D.L. and K.R. Weidner, in "Emulsion Polymers and Emulsion Polymerization", editors D.R. Bassett and A.E. Hamielec, ACS Symposium Series 165, Washington, D.C. (1981).

Graessley, W.W. and H.M. Mittelhauser, J. Poly. Sci., A2, 5, 431 (1967).

Graessley, W.W. and J.S. Prentice, J. Poly. Sci., A2, 6, 1887 (1968).

Graessley, W.W., R.D. Hartung and W.C. Uy, J. Poly. Sci., A2, 7, 1919 (1969).

Graessley, W.W. and E.S. Shinbach, J. Poly. Sci. Poly. Phys. Ed., 12, 2047 (1974).

Greene, R.K., R.A. Gonsalez and G.W. Poehlein, in "Emulsion Polymerization", editors I. Piirma and J.L. Gardon, ACS Symposium Series 24, Washington, D.C. (1976).

Gregory, J., J. Coll. Interf. Sci., 105, 357 (1985).

Guyot, A., J. Guillot, C. Pichot and L.R. Guerrero, in "Emulsion Polymers and Emulsion Polymerization", ACS Symposium Series 165, Washington, D.C. (1981).

Hamer, J.W., Ph. D. Thesis, Dept. of Chemical Engineering, University of Wisconsin (1983).

Hamer, J.W., T.A. Akramov and W.H. Ray, Chem. Eng. Sci., 36, 1897 (1981).

Hamielec, A.E. and W.H. Ray, J. Appl. Poly. Sci., 13, 1319 (1969).

Hamielec, A.E., in "An Intensive Short Course on Polymer Production Technology", McMaster University, Hamilton, Ontario (1976).

———, J. Liq. Chromat., 1, 555 (1978).

Hamielec, A.E., A.C. Ouano and L.L. Nebenzahl, J. Liq. Chromat., 1, 527 (1978).

Hamielec, A.E. and S. Singh, J. Liq. Chromat., 1, 187 (1978).

Hamielec, A.E., J. Liq. Chromat., 3, 381 (1980).

———, in "An Intensive Short Course on Polymer Production Technology", McMaster University, Hamilton, Ontario (1981).

----------, in "Emulsion Polymerization of Vinyl Acetate", editors M.S. El-Aasser and J.W. Vanderhoff, Applied Science (1981).

Hamielec, A.E., H.J. Ederer and K.H. Ebert, J. Liq. Chromat., 4, 1697 (1981).

Hamielec, A.E., Pure and Appl. Chem., 54, 293 (1982).

Hamielec, A.E., R. Gomez-Vaillard and F.L. Marten, J. Macromol. Sci.-Chem., A17, 1005 (1982).

Hamielec, A.E. and J.F. MacGregor, in "Emulsion Polymerization", editor I. Piirma, Acad. Press, N.Y. (1982).

Hamielec, A.E., in "Science and Technology of Polymer Colloids", editors G.W. Poehlein, R.H. Ottewill and J.W. Goodwin, NATO ASI Series I (1983a).

----------, Chem. Eng. Commun., 24, 1 (1983b).

Hamielec, A.E. and J.F. MacGregor, in "Workshop on Polymer Reaction Engineering", Berlin, W. Germany, October 1983.

Hamielec, A.E., J.F. MacGregor, T.O. Broadhead, J. Kanetakis and F.Y.C. Wong, 123rd Meeting, ACS Rubber Division, Toronto, May 1983.

Hamielec, A.E., in "An Intensive Short Course on Polymer Production Technology", McMaster University, Hamilton, Ontario (1984).

Hamielec, A.E. and H.A. Meyer, in "Developments in Polymer Characterization - 5", Applied Science, London, England (1984).

Hansen, F.K. and J. Ugelstad, J. Poly. Sci., Poly. Chem. Ed., 16, 1953 (1978).

----------, in "Emulsion Polymerization", editor I. Piirma, Acad. Press, N.Y. (1982).

Harada, M., M. Nomura, W. Eguchi and S. Nagata, J. Chem. Eng. of Japan, 4, 54 (1971).

Harkins, W.D., J. Amer. Chem. Soc., 69, 1428 (1947).

Harris, B., A.E. Hamielec and L. Marten, in "Emulsion Polymers and Emulsion Polymerization", editors D.R. Bassett and A.E. Hamielec, ACS Symposium Series 165, Washington, D.C. (1981).

Harris, T.J. and E.V. Rushing, AIChE National Conference, Orlando, FL (1982).

Hayat, M.A., "Introduction to Biological Scanning Electron Microscopy", University Park Press, Baltimore (1978).

Heller, W., J. Phys. Chem., 69, 1123 (1965).

Heller, W. and W.J. Pangonis, J. Chem. Phys., 26, 498 (1957).

Heller, W. and R.M. Tabibian, J. Coll. Sci., 12, 25 (1957).

Hess, M. and R.J. Kratz, J. Poly. Sci., A-2, 4, 731 (1966).

Hicks, J., A. Mohan and W.H. Ray, CJChE, 47, 590 (1969).

Hild, D.J., R.E. Gilbert and D.C. Timm, ACS Meeting, Division of PMSE, Miami, April 1985.

Hildebrand, F.B., "Advanced Calculus for Applications", Prentice Hall Inc. (1976).

Hoffman, E.J., M. Eng. Thesis, Dept. of Chemical Engineering, McMaster University, Hamilton, Ontario (1984).

Hoffman, R.F., S. Schreiber and G. Rosen, Ind. Eng. Chem., 56, 51 (1964).

Hoffman, T.W., in "An Intensive Short Course on Polymer Production Technology", McMaster University, Hamilton, Ontario (1981).

Hoftyzer, P.J., J. Hoogschagen and D.W. van Krevelen, 3rd Symposium on Chem. React. Eng., Amsterdam (1964).

Hoogendoorn, K. and R. Shaw, IFAC PRP -4, Ghent, Belgium (1980).

Hopkins, B. and G.H. Alford, Instrum. Techn., 20, 39 (1973).

Horn, D., 67th CAN-AM Chemical Congress, Montreal, June 1984.

Huang, H.P. and G. Stephanopoulos, ACC Vol. 3, Boston, June 1985.

Huff, J.E., Plant/Operations Progress, 1, 211 (1982).

Hulburt, H.M. and S. Katz, Chem. Eng. Sci., 19, 555 (1964).

Huo, B.P., J.F. MacGregor, A.E. Hamielec, J.D. Campbell and A. Penlidis, to appear in J. Appl. Poly. Sci. (1986).

Husain, A., Ph.D. Thesis, Dept. of Chemical Engineering, McMaster University, Hamilton, Ontario (1980).

Husain, A., J. Vlachopoulos and A.E. Hamielec, J. Liq. Chromat., 2, 517 (1979a).

----------, J. Liq. Chromat., 2, 193 (1979b).

Husain, A., A.E. Hamielec and J. Vlachopoulos, ACS Symposium Series 138, 47 (1980).

----------, J. Liq. Chromat., 4, 459 (1981a).

----------, J. Liq. Chromat., 4, 425 (1981b).

Hyun, J.C. and S.G. Bankoff, Chem. Eng., Sci., 31, 953 (1976).

Ishige, T., S.I. Lee and A.E. Hamielec, J. Appl. Poly. Sci., 15, 1607 (1971).

Jackson, R.A., R.A. Small and K.S. Whiteley, J. Poly. Sci. Poly. Chem., 11, 1781 (1973).

Jaisinghani, R. and W.H. Ray, Chem. Eng. Sci., 32, 811 (1977).

Janca, J., in "Advances in Chromatography", editors J.C. Giddings, E. Grushka, J. Cazes and P.R. Brown, Marcel Dekker Inc., N.Y. (1981).

Jazwinski, A.H., "Stochastic Processes and Filtering Theory", Acad. Press, N.Y. (1970).

Jo, J.H. and S.G. Bankoff, AIChE J., 22, 361 (1976).

Johnson, A.F., B. Khaligh and R. Ramsay, in "Computer Applications in Applied Polymer Science", ACS Symposium Series 197, Washington, D.C. (1982).

Johnston, J.E., C.L. Cowherd and T.B. MacRury, ACS Symposium Series 138, 27 (1980).

Kanetakis, J., M. Eng. Thesis, Dept. of Chemical Engineering, McMaster University, Hamilton, Ontario (1984).

Kelly, S., M. Eng. Thesis, Dept. of Chemical Engineering, McMaster University, Hamilton, Ontario (1985).

Kelsall, D.G. and G.C. Maitland, in "Workshop on Polymer Reaction Engineering", Berlin, W. Germany, October 1983.

Keung, C.K.J., M. Eng. Thesis, Dept. of Chemical Engineering, McMaster University, Hamilton, Ontario (1974).

Keyes, M.A. and J.P. Kennedy, 2nd Purdue Conference on Process Control, Adaptive Control (1974).

Kim, C.J., Ph.D. Thesis, Dept. of Chemical Engineering, McMaster University, Hamilton, Ontario (1983).

Kiparissides, C., Ph.D. Thesis, Dept. of Chemical Engineering, McMaster University, Hamilton, Ontario (1978).

Kiparissides, C., J.F. MacGregor and A.E. Hamielec, J. Appl. Poly. Sci., 23, 401 (1979).

----------, CJChE, 58, 48 (1980).

Kiparissides, C., J.F. MacGregor, S. Singh and A.E. Hamielec, CJChE, 58, 65 (1980).

Kiparissides, C., J.F. MacGregor and A.E. Hamielec, AIChE J., 27, 13 (1981).

Kiparissides, C. and S.R. Ponnuswamy, Chem. Eng. Commun., 10, 283 (1981).

Kiparissides, C. and S.L. Shah, Automatica, 19, 225 (1983).

Kirillov, V.A. and W.H. Ray, Chem. Eng. Sci., 33, 1499 (1978).

Kirkland, J.J., J. Chromat., 185, 273 (1979).

Klein, A., C.H. Kuist and V.T. Stannett, J. Poly. Sci., 11, 2111 (1973).

Koch, H., H. Dautzenberg and M. Hartmann, Acta Polym., 32 (series 7), 398 (1981).

----------, Acta Polym., 34, (Series 7), 404 (1983).

Kolthoff, I.M. and W.J. Dale, J. Amer. Chem. Soc., 67, 1672 (1945).

----------, J. Amer. Chem. Soc., 69, 441 (1947).

Kolthoff, I.M. and F.A. Bovey, J. Amer. Chem. Soc., 70, 791 (1948).

Kolthoff, I.M. and I.K. Miller, J. Amer. Chem. Soc., 73, 3055 (1951).

Kolthoff, I.M., E.J. Meehan and C.I. Carr, J. Amer. Chem. Soc., 75, 1439 (1953).

Kolthoff, I.M., P.R. O'Connor and J.L. Hansen, J. Poly. Sci., XV, 459 (1955).

Kourti, T., A. Penlidis, J.F. MacGregor and A.E. Hamielec, Symposium on Quantitative Characterization of Plastics and Rubber, McMaster University, Hamilton, Ontario (1984).

Kourti, T., A. Penlidis, A.E. Hamielec and J.F. MacGregor, 190th National ACS Meeting, Chicago, September 1985.

Krebs, V.K.F. and W. Wunderlich, Die Ang. Makrom. Chem., 20, 203 (1971).

Kwon, Y.D. and L.B. Evans, AIChE J., 21, 1158 (1975).

Lawrence, R.L. and M.G. Chiovetta, in "Workshop on Polymer Reaction Engineering", Berlin, W. Germany, October 1983.

Lee, C.K. and T.H. Forsyth, in "Emulsion Polymers and Emulsion Polymerization", editors D.R. Bassett and A.E. Hamielec, ACS Symposium Series 165, Washington, D.C. (1981).

Lee, D.I., in "Emulsion Polymers and Emulsion Polymerization", editors D.R. Bassett and A.E. Hamielec, ACS Symposium Series 165, Washington, D.C. (1981).

Lee, G.W. and M.J. Groves, Powder Techn., 28, 49 (1981).

Leffew, K.W. and P.B. Deshpande, in "Emulsion Polymers and Emulsion Polymerization", editors D.R. Bassett and A.E. Hamielec, ACS Symposium Series 165, Washington, D.C. (1981).

Ley, G.J.M., C. Schneider and D.O. Hummel, J. Poly. Sci., C27, 119 (1969).

Lichti, G., B.S. Hawkett, R.G. Gilbert, D.H. Napper and D.F. Sangster, J. Poly. Sci., 19, 925 (1981).

Lichti, G., R.G. Gilbert and D.H. Napper, J. Poly. Sci., 21, 269 (1983).

Liegeois, J.M., Die Ange. Makromol. Chem., 56, 115 (1976).

Lin, C.C., W.Y. Chiu and L.C. Huang, J. Appl. Poly. Sci., 25, 565 (1980).

Lin, C.C., H.C. Ku and W.Y. Chiu, J. Appl. Poly. Sci., 26, 1327 (1981).

Lin, C.C. and W.Y. Chiu, J. Appl. Poly. Sci., 27, 1977 (1982).

Lin, C.C., AIChE Annual Meeting, San Francisco, November 1984.

Lin, W.S., S.N. Tong, H.K. Hung, M.C. Chang, W.W. Hsu and P.L.C. Hao, J. Vinyl Techn., 2, 74 (1980).

Liss, B., R. Shinnar and S. Katz, 163rd ACS Annual Meeting, Boston, MA (1972).

Litt, M.H., R. Patsiga and V.T. Stannett, J. Poly. Sci., A1, 8, 3607 (1970).

Litt, M.H. and K.H.S. Chang, Symposium on Emulsion Polymerization of Vinyl Acetate, Emulsion Polymers Institute, Lehigh University, Bethlehem, PA (1980).

————, in "Emulsion Polymerization of Vinyl Acetate", editors M.S. El-Aasser and J.W. Vanderhoff, Applied Science (1981a), p. 137.

————, in "Emulsion Polymerization of Vinyl Acetate", editors M.S. El- Aasser and J.W. Vanderhoff, Applied Science (1981b), p. 159.

Lord, G.M., M. Eng. Thesis, Dept. of Chemical Engineering, McMaster University, Hamilton, Ontario (1984).

Lynch, D. and C. Kiparissides, J. Appl. Poly. Sci., 26, 1283 (1981).

Lyngaae-Jorgensen, J., J. Poly. Sci., C33, 39 (1971).

MacGregor, J.F. and P.W. Tidwell, in "Computer Applications to Chemical Engineering", editors R.G. Squires and G.V. Reclaitis, ACS Symposium Series 124, Washington, D.C. (1980).

Macoveanu, M., V. Nagacevschi and D. Feldman, Die Ange. Makromol. Chem., 64, 19 (1977).

Maron, S.H., M.E. Elder and J.N. Ulevitch, J. Coll. Sci, 9, 89 (1954).

Maron, S.H., P.E. Pierce and J.N. Ulevitch, J. Coll. Sci., 18, 470 (1963).

Marten, F.L. and A.E. Hamielec, in "Polymerization Reactors and Processes", editors J.N. Henderson and T.C. Bouton, ACS Symposium Series 104, Washington, D.C. (1979).

———————, J. Appl. Poly. Sci., 27, 489 (1982).

Maxim, L.D., A. Klein, M.E. Meyer and C.H. Kuist, J. Poly. Sci., C27, 195 (1969).

McGowan, G.R. and M.A. Langhorst, J. Coll. Interf. Sci., 89, 94 (1982).

McHugh, A.J., C. Silebi, G.W. Poehlein and J.W. Vanderhoff, J. Coll. Interf. Sci., 4, 549 (1976).

Meehan, E.J. and W.H. Beattie, J. Phys. Chem., 64, 1006 (1960).

Mehta, J. and L.H. Garcia-Rubio, ACS National Meeting, Division of PMSE, Miami, April 1985.

Mehta, K.T. and H.S. Shah, J. Sci. and Ind. Res., 41, 292 (1982).

Meira, G.R., J. Macromol. Sci., Rev. Macromol. Chem., C20, 207 (1981).

Meira, G.R. and A.F. Johnson, Poly. Eng. Sci., 2, 415 (1981).

Melik, D.H. and H.S. Fogler, J. Coll. Interf. Sci., 92, 161 (1983).

Meyer, H.A., Ph.D: Thesis, Technischen Universitat, Berlin, W. Germany (1983).

Michael, R. and K.H. Reichert, CJChE, 59, 602 (1982).

———————, Chem. Ing. Techn., 55, 564 (1983).

Min, K.W., Ph.D. Thesis, Dept. of Chemical Engineering, SUNY at Buffalo (1976).

Min, K.W. and H.I. Gostin, Ind. Eng. Chem. Prod. Des. Dev., 18, 272 (1979).

Min, K.W. and W.H. Ray, J. Macro. Sci.-Revs. Macro. Chem., C11, 177 (1974).

----------, J. Appl. Poly. Sci., 22, 89 (1978).

Mochizuki, S. and N. Itoh, Chem. Eng. Sci., 33, 1401 (1978).

Morbidelli, M., G. Storti and S. Carra, J. Appl. Poly. Sci., 28, 901 (1983).

Morganson, N.E., J. Coll. Interf. Sci., 23, 605 (1967).

Mori, S., R.S. Porter and J.F. Johnson, Analyt. Chem., 46, 1599 (1974).

Morris, C.E.M. and A.G. Parts, Die Makromol. Chem., 119, 212 (1968).

Morton, M., S. Kaizerman and M.W. Altier, J. Coll. Sci., 9, 300 (1954).

Morton, M., P.P. Salatiello and H. Landfield, J. Poly. Sci., 8, 111 (1952a).

———————, J. Poly. Sci., 8, 215 (1952b).

———, J. Poly. Sci., 8, 279 (1952c).

Moyers, C.G. and A.D. Randolph, AIChE J., 19, 1089 (1973).

Muly, E.C. and H.N. Frock, Optical Eng., 19, 861 (1980).

Murray, K.O., G.W. Illmann and K.E. Pascoe, ChE 4W4 Reports, Dept. of Chemical Engineering, McMaster University, Hamilton, Ontario (1985).

Nagasubramanian, K., D. Saito and W.W. Graessley, J. Poly. Sci., A2, 7, 1955 (1969).

Nagasubramanian, K. and W.W. Graessley, Chem. Eng. Sci., 25, 1549 (1970).

Nagel, E.J., V.A. Kirillov and W.H. Ray, Ind. and Eng. Chem. Prod. Dev., 19, 372 (1980).

Nagy, D.J., Ph.D. Thesis, Lehigh University, Bethlehem, PA (1979).

Nagy, D.J., C.A. Silebi and A.J. McHugh, in "Polymer Colloids", editor R.M. Fitch, Plenum Press (1980).

———, J. Coll., Interf. Sci., 79, 264 (1981a).

———, J. Appl. Poly. Sci., 26, 1955 (1981b).

———, J. Appl. Poly. Sci., 26, 1567 (1981c).

Nakagaki, M. and W. Heller, J. Appl. Phys., 27, 9 (1956).

Napper, D.H. and A.E. Alexander, J. Polymer. Sci., 61, 127 (1962).

Napper, D.H. and A.G. Parts, J. Polymer. Sci., 113 (1962).

Napper, D.H. and A. Netschey, J. Poly. Sci., A-1, 9, 81 (1971).

Nassar, R., J.R. Too and L.T. Fan, J. Appl. Poly. Sci., 26, 3745 (1981).

Netschey, A. D.H. Napper and A.E. Alexander, J. Poly. Sci., Poly. Letters, 7, 829 (1969).

Nigam, K.M. and K.D.P. Nigan, J. Appl. Poly. Sci., 28, 887 (1983).

Noel, R.J., K.M. Gooding, F.E. Regnier, D.M. Ball, C. Orr and M.E. Mullins, J. Chromat. 16, 373 (1978).

Nomura, M., M. Harada, K. Nakagawara, W. Eguchi and S. Nagata, J. Chem. Eng. of Japan, 4, 160 (1971).

Nomura, M., M. Harada, W. Eguchi and S. Nagata, J. Appl. Poly. Sci., 16, 811 (1972).

———, in "Emulsion Polymerization", editors I. Piirma and J.L. Gardon, ACS Symposium Series 24, Washington, D.C. (1976).

Nomura, M. and M. Harada, J. Appl. Poly. Sci., 26, 17 (1981a).

————, in "Emulsion Polymers and Emulsion Polymerization", editors D. R. Bassett and A. E. Hamielec, ACS Symposium Series 165, Washington, D.C. (1981b).

Nomura, M., Yamamoto, Horie, Fujita and M. Harada, J. Appl. Poly. Sci., 27, 2483 (1982).

Ogunnaike, B.A., ACC 1, Boston, June 1985.

Omi, S., T. Ueda and H. Kubota, J. Chem. Eng. of Japan, 2, 193 (1969).

Osakada, K. and L.T. Fan, J. Appl. Poly. Sci., 14, 3065 (1970).

O'Toole, J.T., J. Appl. Poly. Sci., 9, 1291 (1965).

Palmgren, O., in "Emulsion Polymerization", editors I. Piirma and J.L. Gardon, ACS Symposium Series 24, Washington, D.C. (1976).

Park, W.S. and W.W. Graessley, J. Poly. Sci.-Poly. Phys. Ed., 15, 85 (1977).

Parulekar, S.J., J.M. Modak and H.C. Lim, ACC 2, Boston, June 1985.

Patsiga, R., Ph.D. Thesis, College of Forestry, New York State University, Syracuse, N.Y. (1962).

Patsiga, R.A., W. Lerdthusnee and I. Marawi, Ind. Eng. Chem. Prod. Res. Dev., 23, 238 (1984).

Paxton, T.R., J. Coll. Interf. Sci., 31, 19 (1969).

Pearson, J.D., J. Electron. Control, 13, 453 (1962).

Penlidis, A., J.F. MacGregor and A.E. Hamielec, Technical Report MIPPT-B-002, Dept. of Chemical Engineering, McMaster University, Hamilton, Ontario (1984).

————————, MIPPT Internal Report, Dept. of Chemical Engineering, McMaster University, Hamilton, Ontario (1985).

Penlidis, A., J.F. MacGregor, A.E. Hamielec and P. Gossen, MIPPT Internal Report, Dept. of Chemical Engineering, McMaster University, Hamilton, Ontario (1986).

Pittman-Bejger, T.P.A., Ph.D. Thesis, University of Minnesota (1982).

Poehlein, G.W., in "Polymerization Reactors and Processes", editors I.N. Henderson and T.C. Bouton, ACS Symposium Series 104, Washington, D.C. (1979).

Poehlein, G.W. and D.J. Dougherty, Rubber Chem. Techn., 50, 601 (1977).

Poehlein, G.W., H.C. Lee and N. Stubicar, in "Workshop on Polymer Reaction Engineering", Berlin, W. Germany, October 1983.

Pollock, M.J., J.F. MacGregor and A.E. Hamielec, in "Computer Applications in Applied Polymer Science", ACS Symposium Series 197, Washington, D.C. (1981).

Pollock, M.J., Ph.D. Thesis, Dept. of Chemical Engineering, McMaster University, Hamilton, Ontario (1984).

Pramojaney, N., Ph.D. Thesis, Lehigh University, Bethlehem, PA (1982).

Priest, W.J., J. Phys. Chem., 56, 1077 (1952).

Prieve, D.C. and P.M. Hoysan, J. Coll. Interf. Sci., 64, 201 (1978).

Provder, T. and E.M. Rosen, Sep. Sci., 5, 437 (1970a).

————————, Sep. Sci., 5, 485 (1970b).

Randolph, A., CJChE, 42, 280 (1964).

Ray, W.H. and C.E. Gall, Macromol., 2, 425 (1969).

Ray, W.H., J. Macro. Sci.-Revs. Macro. Chem., C8, 1 (1972).

Ray, W.H. and R.L. Lawrence, in "Chemical Reactor Theory", editors L. Lapidus and N.R. Amundson, Prentice-Hall, NJ (1977).

Ray, W.H., IFAC PRP-4, Ghent, Belgium (1980).

---------, in "Chemical Reaction Engineering-Plenary Lectures", editors J. Wei and C. Georgakis, ACS Symposium Series 226, Washington, D.C. (1983).

-------, ACC 2, Boston, June 1985.

Reimschuessel, H.K. and K. Nagasubramanian, Chem. Eng. Sci., 27, 1119 (1972).

Roe, C.P., Ind. Eng. Chem., 60, 20 (1968).

Romatowski, J. and C.V. Schulz, Makromol. Chem., 85, 187 (1965).

Roof, L.B., G.T. Porter, E.N. Fuller and R.A. Mowery, Jr., IFAC PRP-4, Ghent, Belgium (1980).

Rowell, R.L. and J.R. Ford, in "Emulsion Polymers and Emulsion Polymerization", editors D.R. Bassett and A.E. Hamielec, ACS Symposium Series 165, Washington, D.C. (1981).

Ruckenstein, E. and R. Nagarajan, J. Phys. Chem., 79, 2622 (1975).

Sacks, M.E., S.I. Lee and J.A. Biesenberger, Chem. Eng. Sci., 28, 241 (1973).

Saito, O., K. Nagasubramanian and W.W. Graessley, J. Poly. Sci., A2, 7, 1937 (1969).

Saltzman, G.C., R.D. Hiebert, J.H. Jett and M. Bartholdi, SPIE Optics in Metrology and Quality Assurance, 220, 23 (1980).

Schmidt, A.D., A.B. Clinch and W.H. Ray, AIChE Meeting, Los Angeles, CA (1982).

————————, Chem. Eng. Sci., 39, 419 (1984).

Schmidt, E. and R.H. Kelsey, Ind. Eng. Chem., 43, 406 (1951).

Schmidt, E. and P.H. Biddison, Rubber Age, 88, 484 (1960).

Schork, F.J., G. Chu and W.H. Ray, AIChE Meeting, Chicago IL (1980).

Schork, F.J., Ph.D. Thesis, University of Wisconsin (1981).

Schork, F.J. and W.H. Ray, in "Emulsion Polymers and Emulsion Polymerization", editors D.R. Bassett and A.E. Hamielec, ACS Syposium Series 165, Washington, D.C. (1981).

Schuler, H., IFAC PRP-4, Ghent, Belgium (1980).

Shastry, J.S., L.T. Fan and L.E. Erickson, J. Appl. Poly. Sci., 17, 3101 (1973a).

————————, J. Appl. Poly. Sci., 17, 3127 (1973b).

Shawki, S., Ph.D. Thesis, Dept. of Chemical Engineering, McMaster University, Hamilton, Ontario (1978).

Shervin, C., G. Carratt and D. S. Soong, AIChE Meeting, Los Angeles, CA (1982).

Shinoda, K., T. Nakagawa, B. Tamamushi and T. Isemura, "Colloidal Surfactants", Acad. Press, N.Y. (1963).

Shinoda, K. and P. Becher, "Principles of Solution and Solubility", Marcel Dekker, N.Y. (1978).

Silebi, C.A., FACSS Symposium, Philadelphia, PA (1981).

Silebi, C.A. and A.J. McHugh, AIChE J., 24, 204 (1978).

————————————, J. Appl. Poly. Sci., 23, 1699 (1979).

Singh, P.N. and Ramkrishna, D., Computers Chem. Eng., 1, 23 (1977).

Singh, S., M. Eng. Thesis, Dept. of Chemical Engineering, McMaster University, Hamilton, Ontario (1977).

Singh, S. and A.E. Hamielec, J. Appl. Poly. Sci., 22, 577 (1978).

Small, H., J. Coll. Interf. Sci., 48, 147 (1974).

————————, U.S. Patent 3, 865, 717 (1975).

Small, H., F.L. Saunders and J. Solc, Adv. Coll. Interf. Sci., 6, 237 (1976).

Small, H., Adv. Chromat., 15, 113 (1977).

Smith, W.V. and R.H. Ewart, J. Chem. Phys., 16, 592 (1948).

Smith, W.V., J. Amer. Chem. Soc., 71, 4077 (1949).

Smith-Powers, S., W.E. Vallesi and P.C. Kwan, ChE 4W4 Reports, Dept. of Chemical Engineering, McMaster University, Hamilton, Ontario (1985).

Soh, S.K. and D.C. Sundberg, J. Poly. Sci., 20, 1299 (1982a).

----------, J. Poly. Sci., 20, 1315 (1982b).

----------, J. Poly. Sci., 20, 1331 (1982c).

----------, J. Poly. Sci., 20, 1345 (1982d).

Soliman, M.A., Computers Chem. Eng., 5, 111 (1981).

Stannett, V., A. Klein and M. Litt, Br. Poly. J., 7, 139 (1975).

Stevens, J.D. and J.O. Funderburk, Ind. Eng. Chem. Proc. Des. Dev., 11, 360 (1972).

Stevenson, A.F., W. Heller and M.L. Wallach, J. Chem. Phys., 34, 1789 (1961).

Stock, R.S. and W.H. Ray, AIChE Meeting, San Francisco, November 1984.

Stockmayer, W.H., J. Poly. Sci., 24, 314 (1957).

Stoisits, F.R., G.W. Poehlein and J.W. Vanderhoff, J. Coll. Interf. Sci., 57, 2 (1976).

Sundberg, D.C., J. Appl. Poly. Sci., 23, 2197 (1979).

Talmon, Y. and W.G. Miller, J. Coll. Interf. Sci., 65, 284 (1978).

Tanford, C., "The Hydrophobic Effect", Wiley, N.Y. (1973).

Tanford, C., J. Phys. Chem., 78, 2469 (1974).

Thompson, R.W. and J.D. Stevens, Chem. Eng. Sci., 32, 311 (1977).

Timm, D.C., R.E. Gilbert, T.T. Ko and M.R. Simmons, in "Computer Applications in Applied Polymer Science", ACS Symposium Series 197, Washington, D.C. (1982).

Tirrell, M. and K. Gromely, 73rd AIChE Meeting, San Francisco, CA (1980).

Tirrell, M. and T.J. Tulig, in "Workshop on Polymer Reaction Engineering", Berlin, W. Germany, October 1983.

Tsai, M.C., W.Y. Chiu and C.C. Lin, PACHIEC II, 76 (1983).

Tulig, T.J. and M. Tirrell, Macromolecules, 14, 1501 (1981).

Tung, L.H., J. Appl. Poly. Sci., 10, 375 (1966).

Tung, L.H. and F.R. Runyon, J. Appl. Poly. Sci., 13, 2397 (1969).

Ueda, T., S. Omi and H. Kubota, J. Chem. Eng. of Japan, 4, 50 (1971).

Ugelstad, J., P.C. Mork and J.O. Aasen, J. Poly. Sci., A-1, 5, 2281 (1967).

Ugelstad, J., P.C. Mork, P. Dahl and P. Ragnes, J. Poly. Sci., C27, 49 (1969).

Ugelstad, J. and F.K. Hansen, Rubber Chem. Techn., 49, 536 (1976).

Ugelstad, J., J. Macromol. Sci.-Chem. A11, 1281 (1977).

Ugelstad, J., T. Ellingsen and K.H. Kaggerud, 4th Inter. Conf. in Organic Coatings Sci. and Techn., Vol. 2, editors G.D. Parfitt and A.V. Patsis (1978).

Vanzo, E., R.H. Marchessault and V. Stannett, J. Coll. Sci., 19, 578 (1964).

Vavra, J. and J. Bocko, Coll. Poly. Sci., 257, 1212 (1979).

Vijayendran, B.R., in "Polymer Colloids", editor R.M. Fitch, Plenum Press, N.Y. (1971).

———————, J. Coll. Interf. Sci., 60, 418 (1977).

———————, J. Appl. Poly. Sci., 23, 733 (1979).

Vrentas, J.S. and J.L. Duda, AIChE J., 25, 1 (1979).

Vrentas, J.S., J.L. Duda and H.C. Ling, J. Poly. Sci Poly. Phys. Ed., 23, 275 (1985a).

Vrentas, J.S., J.L. Duda, H.C. Ling and A.C. Hou, J. Poly. Sci. Poly. Phys. Ed., 23, 289 (1985b).

Wallach, M.L. and W. Heller, J. Chem. Phys., 34, 1796 (1961).

Warson, H., in "Emulsion Polymerization", editors I. Piirma and J.L. Gardon, ACS Symposium Series 24, Washington, D.C. (1976).

Weber, A.P.J. and L. Lapidus, AIChE J., 17, 641 (1971).

Wilke, C.R. and P. Chang, AIChE J., 1, 264 (1955).

Wong, F.Y.C., M. Eng. Thesis, Dept. of Chemical Engineering, McMaster University, Hamilton, Ontario (1984).

Wu, G.Z.A., L.A. Denton and R.L. Lawrence, Poly. Eng. Sci., 22, 1 (1982).

Yasuda, H., C.E. Lamaz and A. Peterlin, J. Poly. Sci., A2, 1117 (1971).

Yau, W.W., J.J. Kirkland, D.D. Bly and H.J. Stoklosa, J. Chromat., 125, 219 (1976).

Yeliseyeva, V.I. and A.V. Zuikov, in "Emulsion Polymerization", editors I. Piirma and J. L. Gardon, ACS Symposium Series 24, Washington, D.C. (1976).

Yoo, Y.J., J. Hong and R.T. Hatch, ACC 2, Boston, June 1985.

Yuan, C.J.; "Determination of Molecular Weights of High Polymers", Israel Program for Scientific Translations, Jerusalem (1963).

Zimm, H.B. and W.B. Dandliker, J. Phys. Chem., 58, 644 (1954).

Zollars, R.L., J. Coll. Interf. Sci., 74, 163 (1980).

----------, in "Emulsion Polymerization of Vinyl Acetate", editors M.S. El-Aasser and J.W. Vanderhoff, Applied Science (1981a).

----------, J. Dispers. Sci. Techn., 2, 331 (1981b).

APPENDIX I

Model Derivation

Initiator balance

A balance can be written for the number of gmoles of initiator, as follows:

$$\frac{d}{dt}\left(I_w(t)\,V_R(t)\right) = (CI * FI) - I_w(t)\,v_{out} - k_d\,I_w(t)\,V_R(t) \qquad (I\text{-}1)$$

or

$$\frac{dI_w(t)}{dt} = \frac{CI * FI}{V_R(t)} - I_w(t)\,\frac{v_{out}}{V_R(t)} - k_d\,I_w(t) - \frac{I_w(t)}{V_R(t)}\,\frac{dV_R(t)}{dt} \qquad (I\text{-}2)$$

Subsequently,

$$\frac{dV_R(t)}{dt} = v_{in} - v_{out} - \text{shrinkage} \qquad (I\text{-}3)$$

or

$$\frac{dV_R(t)}{dt} = v_{in} - v_{out} - R_p(t)\,(MW)\left(\frac{1}{d_M} - \frac{1}{d_p}\right)V_R(t)\,k_c \qquad (I\text{-}4)$$

Equation (I-2) is very general and can be used for several modes of reactor operation (e.g. batch, semi-batch, continuous, start-up, etc.). If the assumption is made that the reactor is a vessel continuously operating full, i.e. overflow ideal continuous stirred tank reactor (CSTR), then the rate of change of V_R is zero (Hoffman (1981)) and equation (I-2) is considerably simplified to yield:

$$\frac{dI_w(t)}{dt} = \frac{I_F(t)}{\theta} - \frac{I_w(t)}{\theta} - k_d\,I_w(t) \qquad (I\text{-}5)$$

The solution of equation (I-5) is the following:

$$I_w(t) = I_{w_o}\exp\left(-((1-k_d\theta)/\theta)\,t\right) + I_F(t)\left(-\frac{1}{1-k_d\theta}\exp\left(-\left(\frac{1-k_d\theta}{\theta}\right)t\right) - \frac{1}{1-k_d\theta}\right) \qquad (I\text{-}6)$$

I_{w_o} denotes concentration of initiator in the reactor at time $t=0$. If one considers that $(1 - k_d\,\theta) \simeq 1$, which is a reasonable assumption for reactor residence times in the order of

magnitude of half an hour and/or longer, then (I-6) collapses to the simpler form:

$$I_w(t) = I_F(t)\,(1 - \exp(-t/\theta)) \tag{I-7}$$

provided that I_{w_o} is zero, as well.

Emulsifier balance

Under the assumption of an overflow ideal CSTR, the rate of change of total soap (emulsifier) concentration in the reactor is given by:

$$\frac{d\,S_T(t)}{dt} = \frac{S_F(t)}{\theta} - \frac{S_T(t)}{\theta} \tag{I-8}$$

In equation (I-8), $S_T(t)$ denotes total soap in the reactor, i.e. free micellar soap plus free dissolved soap plus soap adsorbed on polymer particles and/or monomer droplets. The solution of (I-8) is similar to the solution of (I-5) and given by:

$$S_T(t) = S_{T_o} \exp(-t/\theta) + S_F(t)\,(1 - \exp(-t/\theta)) \tag{I-9}$$

Oligomeric radical concentration balance

If $R_w \cdot(t)$ denotes concentration of oligomeric radicals in the reactor, then use of the collision theory to describe radical capture mechanisms would yield the following equation for the rate of change of $R_w \cdot(t)$:

$$\begin{aligned}\frac{d\,R_w \cdot(t)}{dt} = {} & \frac{R_{w,F} \cdot(t)}{\theta} - \frac{R_w \cdot(t)}{\theta} + \rho_i(t)\,N_A + \rho_{des}(t)\,N_A \\ & - k_m\,A_m(t)\,R_w \cdot(t)\,k_v - k_h R_w \cdot(t) - k_{ab}\,A_p(t) R_w \cdot(t)\,k_v \\ & - k_{tw}\,R_w^2 \cdot(t)\,(k_v/N_A)\end{aligned} \tag{I-10}$$

If one now applies the radical stationary-state hypothesis, neglects radical termination in the water phase and accepts negligible inflow and outflow of radicals, equation (I-10) yields:

$$R_w \cdot = \frac{(\rho_i(t) + \rho_{des}(t))\,N_A}{k_m\,A_m(t)\,k_v + k_h + k_{ab}\,A_p(t)\,k_v} \tag{I-11}$$

or

$$R_w = \frac{\rho(t)}{k_m A_m(t) k_v + k_h + k_{ab} A_p(t) k_v} \tag{I-12}$$

if $\rho(t) = (\rho_i(t) + \rho_{des}(t)) N_A$ represents the total radical formation rate in the water phase.

Free monomer balance

The rate of change of free unpolymerized monomer in the reactor is given by:

$$\frac{d M_{MON}(t)}{dt} = \frac{M_F(t)}{\theta} - \frac{M_{MON}(t)}{\theta} - R_{p_{TOT}}(t) \tag{I-13}$$

where

$$R_{p_{TOT}}(t) = R_{p_{POLY}}(t) + R_{p_{AQ}}(t) = R_p(t) \tag{I-14}$$

The assumption that the total rate of polymerization equals the rate of polymerization in the polymer particle phase holds very well for micellar systems and for monomers which are moderately soluble in the water phase.

Total monomer balance

If $M_{TOT}(t)$ denotes the total concentration of monomer units existing both as free unpolymerized monomer and as bound monomer (i.e. monomer units bound in polymer chains), then:

$$\frac{d M_{TOT}(t)}{dt} = \frac{M_F(t)}{\theta} - \frac{M_{TOT}(t)}{\theta} \tag{I-15}$$

or

$$M_{TOT}(t) = M_{TOT_0} \exp(-t/\theta) + M_F(t)(1 - \exp(-t/\theta)) \tag{I-16}$$

Rate of change of conversion

The instantaneous conversion x(t) in the reactor can be defined as follows:

$$x(t) = \frac{M_{TOT}(t) - M_{MON}(t)}{M_{TOT}(t)} \qquad \text{(I-17)}$$

or

$$x(t) = 1 - \frac{M_{MON}(t)}{M_{TOT}(t)} \qquad \text{(I-18)}$$

Differentiating (I-18) with respect to time and using equations (I-13) through (I-18), one obtains:

$$\frac{dx(t)}{dt} = \frac{R_p(t)}{M_{TOT}(t)} - \frac{x(t)\,M_F(t)}{\theta\,M_{TOT}(t)} \qquad \text{(I-19)}$$

If the tank contents at time t=0 (i.e. just before the initiator stream is started) are the same as the feed streams, i.e. if $M_F(t) = M_{TOT_o}$, then (I-16) yields $M_{TOT}(t) = M_F(t)$ and, therefore:

$$\frac{dx(t)}{dt} = \frac{R_p(t)}{M_F(t)} - \frac{x(t)}{\theta} \qquad \text{(I-20)}$$

If on the other hand the reactor starts full of pure water, then $M_{TOT_o} = 0$, and (I-19) becomes:

$$\frac{dx(t)}{dt} = \frac{1}{(1 - \exp(-t/\theta))}\left(\frac{R_p(t)}{M_F(t)} - \frac{x(t)}{\theta}\right) \qquad \text{(I-21)}$$

Basic ideas on population balances

In transport theory, one develops differential material, energy and momentum balances in the space of geometrical coordinates within the system being analyzed. These balances, together with postulated transport mechanisms, give differential equations in concentrations, temperature, velocity and pressure, as functions of the spatial coordinates.

A phase space is established for a typical particle, whose coordinates specify the location of the particle as well as its quality. Then, ordinary differential equations describe

how these phase coordinates evolve in time. In other words, the state of a particle in a processing system is specified by the values of a number of phase coordinates $z_1, z_2, \ldots$,

$$\underline{z} = [z_1, z_2, \ldots] \tag{I-22}$$

The only requirement on $\underline{z}$ is that they describe the state of the particle fully enough to permit one to write a set of first-order ordinary differential equations of the form:

$$\frac{dz_i}{dt} = u_i(\underline{z}, t); \; i = 1, 2, \ldots \tag{I-23}$$

which show how the z's evolve in time while the particle is in the processing system. u_i is the so-called phase velocity. The set of equations (I-23) is nothing but the equations of motion for the phase coordinates z_i.

The phase coordinates may be external (e.g. position in the system) or internal (e.g. size of a particle, number of free radicals in a particle or molecular weight of a polymer). They may also be continuous or discrete (e.g. clearly the number of free radicals in a particle and the molecular weight of a polymer are integer variables). One may be able, however, to represent such discrete distributions as continuous ones either because the number of entities involved is large, or because one might not think of the actual number of entities but instead, of the expected value of that number.

Putting it in another way, a population balance accounts for all the important mechanisms according to which the value of each phase coordinate changes with time. In this context, equation (I-23) describes evolution, or the process by which a phase coordinate changes with time in the system (e.g. growth of a particle, movement of a particle through space, etc.). u is identical with velocity if z is a positional coordinate.

Finally, a partial differential equation is developed for the number density of particles in the phase space (analogous to the classical Liouville equation that expresses the conservation of probability in the phase space of a mechanical system). In other words, if the particle states (i.e. points in the particle phase space) are regarded at any moment as a

continuum filling a suitable portion of the phase space, flowing with a velocity field specified by the function u_i, then one may ask for the density of this fluid streaming through the phase space, i.e. the number density $n(\underline{z},t)$ of particles in the phase space defined as:

$$n(\underline{z},t) \cdot |d\underline{z}| = \text{number of particles in the system at time } t \text{ with phase coordinates in the range } z_1 \pm dz_1/2, z_2 \pm dz_2/2, \ldots \quad \text{(I-24)}$$

where

$$|d\underline{z}| = dz_1 \cdot dz_2 \ldots \quad \text{(I-25)}$$

is the differential volume element in the phase space.

Further, let

$$f(\underline{z},t) \cdot |d\underline{z}| \quad \text{(I-26)}$$

be the net number of particles introduced into the system per unit time at time t with phase coordinates in the range $z_1 \pm dz_1/2, z_2 \pm dz_2/2, \ldots$ (i.e. (I-26) gives the net effect on the number of particles of (birth-death) events. Examples are coalescence of two droplets or condensation of two polymer molecules. In each case, two particles of given size or molecular weight disappear (die) and one of a different size or molecular weight appears (is born)).

Then, since in any system accumulation is the net result of both evolution and birth/death processes, one can write:

$$\text{Accumulation} = \text{Net evolution} + \text{Net birth} \quad \text{(I-27)}$$

and obtain the classical Liouville equation for particles (Hulburt and Katz (1964)):

$$\frac{\partial n(z,t)}{\partial t} = -\sum_i \frac{\partial}{\partial z_i} (u_i(z,t)\, n(z,t)) + f(z,t) \quad \text{(I-28)}$$

With external (position) $\underline{x}$ and internal coordinates $\underline{r}$, i.e.

$$\underline{z} = [\underline{x} \quad \underline{r}] \quad \text{(I-29)}$$

the general equation (I-28) takes the form:

$$\frac{\partial n(\underline{z},t)}{\partial t} + \sum_{i=1}^{3} \frac{\partial}{\partial x_i}(v_i\, n(\underline{z},t) + \sum_{j} \frac{\partial}{\partial r_j}(G_j\, n(\underline{z},t) = f(\underline{x},\underline{r},t) \qquad \text{(I-30)}$$

Equations (I-28) and (I-30) apply to values of $\underline{z}$ in the interior of the range. At limiting values, such as a minimum value of z_i, a boundary condition would be required since no evolution into the smallest interval of z_i can occur from a smaller interval. Typically, the distribution $n(\underline{z},t)$ will have limiting values of zero for $z_i \to 0$ and/or $z_i \to \infty$.

Methods of solution of the population balance

Since the above complete system characterization is often mathematically intractable, an approximate system description may then be furnished by the leading moments of a distribution (the distribution of internal coordinates of the phase space, e.g. particle size, or other aspects of particle quality), all considered as functions of the external coordinates of the phase space (i.e. coordinates that specify the location or position of the particles in the processing unit).

The moment function can be defined as:

$$\mu_n(t) = \int_{k_o}^{\infty} k^n\, n(\underline{z},t)\, dk\,; \quad n = 0, 1, 2, \ldots \qquad \text{(I-31)}$$

Then, $\mu_o(t)$ gives the total number of particles per unit volume at time t.

Eventually, one obtains a set of differential equations in the moments, which furnish the approximate working description for the system being studied. Of course, if one has to consider more than one internal coordinates, then various complications arise, since there are many more moments (two first ones, three second ones, etc.). In such a case, convergence may also be very slow.

A considerable simplification occurs if one takes all particles to be nucleated at the same size r_o. Then, $f(\underline{x},\underline{r},t)$ can be written as:

$$f(\underline{x},\underline{r},t) = b(c,\theta)\cdot\psi(r) \qquad \text{(I-32)}$$

where $\psi(r)$ is now a Dirac Delta function $\delta(r - r_o)$ (Kiparissides et al. (1979)).

If the moment differential equations form a set that cannot be closed, the difficulty may be overcome by an application of the orthogonal expansion of the particle size distribution. Thus, one may use a knowledge of the moments to reconstruct the distribution. These expansions are simply series of special functions, the coefficients in the series being given in terms of the moments of the underlying distribution, each coefficient in turn involving just one moment of next higher order than the preceding coefficients. A way to do this is to use Laguerre polynomials and develop corresponding orthogonal expansions based on the Γ distribution (Hulburt and Katz (1964)). Another way to overcome the problem is to use the method of weighted residuals (Singh and Ramkrishna (1977)). More literature references concerning the solution of the resulting equations from population balances can be found in Crowe (1984).

The case of a CSTR

In a well-stirred vessel, the particle environment is uniform and one may accordingly dispense with external coordinates altogether, and reduce the whole set of phase coordinates $\underline{z}$ to a single dimension (e.g. that specifying the particle size). Therefore, one ends up with an one-dimensional phase space.

Equation (I-30) can thus become:

$$\frac{\partial n(\underline{r},t)}{\partial t} = \frac{v_o n_o(\underline{r},t) - v\, n(\underline{r},t)}{V} - \sum_j \frac{\partial}{\partial r_i}(G_j\, n(\underline{r},t)) + f(\underline{r},t) \qquad \text{(I-33)}$$

where v_o is the inlet volumetric flow rate in the general case, V is the tank volume, $n_o(\underline{r},t)$ is the inlet distribution function, v is the outlet volumetric flow rate and $n(\underline{r},t)$ is now only a function of the internal phase coordinates $\underline{r}$ and time t. If the tank is an overflow CSTR, then $v_o = v$ and (I-33) becomes simpler.

In the general CSTR case, the source function $f(\underline{z},t)$ must be taken to include particle feed and take off conditions as well as nucleation, since, in the absence of external phase coordinates, one no longer has differential equations in position to which feed and outflow can be appended as boundary conditions.

In this case, $\mu_o(t)$ is the total number of particles in the vessel at time t, $\mu_1(t)$ the cumulated total of their sizes r, etc.

A CSTR case can be furthermore simplified if the population balance approach collapses to a residence time distribution approach. In the latter case, use is made of a single (internal) coordinate, τ, the time a particle has spent in the vessel (Dickinson (1976), Kiparissides et al. (1979), Pollock et al. (1981)).

Population balance equation for a polymer reactor

Any latex particle can be characterized by a set of physical quantities which will specify a given particle or class of particles. The previously developed population balance equation (Liouville equation) (I-28) could also be written as:

$$\frac{\partial n(\underline{z},t)}{\partial t} + \nabla (\dot{\underline{z}}\, n(\underline{z},t)) = f(\underline{z},t) \qquad (I\text{-}34)$$

where $\nabla = (\partial/\partial z_1 + \partial/\partial z_2 + \ldots)$. The first term on the left hand side of (I-34) represents accumulation of the number density function $n(\underline{z},t)$, whereas the second term represents rate of change of $n(\underline{z},t)$ with respect to external and internal coordinates (i.e. rate of movement of particles through a class, e.g. growth into or out of volume range v, v + dv). The right hand side function $f(\underline{z},t)$ represents, in the general case, birth and death in a class (i.e. net nucleation) and inflow and outflow from the reactor.

There is a variety of ways in choosing the phase coordinates $\underline{z}$. Min and Ray (1974) chose $\underline{z}$ to be equal to v (particle volume), in which case $n(\underline{z},t)$ becomes the particle size distribution n(v,t). Gorber (1973), Dickinson (1976), Dickinson and Gall (1976), Kiparissides

et al. (1979) and Pollock et al. (1981) used $\underline{z} = \tau$, in which case the analysis becomes an age or a residence time distribution analysis. Finally, $\underline{z}$ can be set equal to (v,q), in which case the analysis based on n(v,q,t) can become more complex.

In the present analysis, $\underline{z}$ will be set equal to τ, i.e. the birth time of the polymer particles in the reactor vessel. Then $n(\underline{z},t)$ becomes $n(t,\tau)$ and $(n(t,\tau)d\tau)$ represents number of particles in the reactor at some time t which were born between times τ and $\tau + d\tau$. Integration of $(n(t,\tau)d\tau)$ over the time period t would give the total number of particles in the reactor at time t.

Then, since $\dot{\underline{z}}$ in the population balance equation (I-34) is unity (i.e. the particle phase space is the τ-axis), equation (I-34) can be simplified to yield:

$$\frac{\partial n(t,\tau)}{\partial t} + \frac{\partial n(t,\tau)}{\partial \tau} = f(t,\tau) \tag{I-35}$$

with

$$f(t,\tau) = \frac{1}{\theta}\left[n(t,\tau)_F - n(t,\tau)\right] + f_N(t,\tau) + f_{AGG}(t,\tau) \tag{I-36}$$

The first term on the right hand side of equation (I-36) represents net change by flow, the term $f_N(t,\tau)$ represents contribution by nucleation (i.e. new particle generation) and $f_{AGG}(t,\tau)$ is the coalescence (agglomeration) term.

If one neglects the otherwise very complicated agglomeration term, equation (I-36) becomes:

$$f(t,\tau) = \frac{1}{\theta}\left[n(t,\tau)_F - n(t,\tau)\right] + f(t) \tag{I-37}$$

where $f_N(t,\tau)$, the net nucleation term, was set equal to f(t) for the sake of brevity.

An expression for the nucleation term f(t)

The generation (nucleation) of new polymer particles in an emulsion system is basically due to two mechanisms: micellar and homogeneous particle nucleation. Then, the

rate of particle nucleation, f(t), can be expressed as:

$$f(t) = k_m A_m(t) R_w k_v + k_h R_w \tag{I-38}$$

But R_w is given by equation (I-12), therefore substitution of equation (I-12) to (I-38) yields:

$$f(t) = \rho(t) \frac{k_m A_m(t) k_v + k_h}{k_m A_m(t) k_v + k_h + k_{ab} A_p(t) k_v} \tag{I-39}$$

In general,

$$A_m(t) = (S_T(t) - S_{CMC}) S_a N_A - A_p(t) + S_p(t) - A_d(t) \tag{I-40}$$

$S_p(t)$, the area of polymer particles stabilized by polymer end groups rather than soap, might in the general case be important but it is very difficult to obtain an expression for it. $A_d(t)$, the area of monomer droplets, is usually neglected as being quite a few orders of magnitude less than $A_p(t)$. Therefore, the final expression for $A_m(t)$ is the following:

$$A_m(t) = (S_T(t) - S_{CMC}) S_a N_A - A_p(t) \tag{I-41}$$

The specific homogeneous nucleation rate constant, k_h, should be allowed to tend towards zero as the area of polymer particles $A_p(t)$ increases, since the radical capture rate by polymer particles would then be greater than the rate of initiation of new radicals. In other words, there is a higher probability for an oligomer to be captured by a pre-existing particle and thus, not to form a new (primary) particle by homogeneous precipitation. Therefore, according to Fitch and Tsai (1971b):

$$k_h = k_{h_o} (1 - L A_p(t) k_v / 4) \tag{I-42}$$

L in the above expression represents the critical radical diffusion length and is given by Einstein's diffusion law:

$$L = \left(2 D_w \cdot \frac{D P_{max}}{k_p M_{wc}} \right)^{1/2} \tag{I-43}$$

L in (I-43) is given in dm. k_p is the propagation rate constant, D_w is the diffusion coefficient of monomeric radicals in the water phase in dm^2/sec, DP_{max} is the maximum degree of polymerization (Fitch and Tsai (1971b)), and M_{wc} is the saturation concentration of monomer in the water phase in gmole/lit. Since VAc is ~2.1% by weight soluble in the water phase, M_{wc}

is close to 0.25 gmole/lit. DP_{max} is close to 53,(Priest (1952)), therefore an order of magnitude for L would be 10^{-4} dm (see also Fitch and Tsai (1971b)) for 50°C.

If finally one defines the ratios

$$\mu = k_{h_o} / k_m \quad \text{and} \quad \varepsilon = k_{ab} / k_m \tag{I-44}$$

then, equation (I-39) can become:

$$f(t) = \rho(t) \frac{A_m(t)k_v + \mu(1 - LA_p(t)k_v/4)}{A_m(t)k_v + \mu(1 - LA_p(t)k_v/4) + \varepsilon A_p(t)k_v} \tag{I-45}$$

It is also possible to use the Hansen and Ugelstad (1978) approach which is more rigorous for homogeneous nucleation. In this case,

$$f(t) = \rho(t)\left(\frac{1}{1 + \dfrac{k_m A_m(t) + k_{ab} A_p(t)}{k_p M_w / k_v}}\right)^{r_c - 1} \tag{I-46}$$

r_c is the critical chain length for oligomer radical precipitation (r_c is approximately 15 or 16 for VA_c) and M_w is the concentration of monomer in the water phase (i.e. M_w coincides with M_{w_c} in the expression for L).

Total property balance equation

Associated with the class of polymer particles $n(t,\tau)d\tau$ in the polymer reactor is a physical property $p(t,\tau)$ (e.g. $p(t,\tau)$ can be diameter or area of particles of that class, etc.). Then, a total property P(t) (e.g. total particle diameter in the reactor at time t) can be obtained by summing (integrating) the property $p(t,\tau)$ over all classes of particles in the reactor vessel.

The property $p(t,\tau)$ consists of two parts: the contribution from newly generated (nucleated) particles $n_{GEN}(t,\tau)$ which assumed that property and the contribution from newly introduced particles $n_{IN}(t,\tau)$ which either entered the reactor having that property or grew to that property. Therefore:

$$P(t) = \int_0^t p(t,\tau)\, n_{TOT}(t,\tau)\, d\tau$$

$$n_{TOT}(t,\tau) = n_{GEN}(t,\tau) + n_{IN}(t,\tau) \qquad \text{(I-47)}$$

or

$$P(t) = \int_0^t p_{GEN}(t,\tau)\, n_{GEN}(t,\tau)\, d\tau + \int_0^t p_{IN}(t,\tau)\, n_{IN}(t,\tau)\, d\tau \qquad \text{(I-48)}$$

$p_{GEN}(t,\tau)$ and $p_{IN}(t,\tau)$ in the above expression represent the same property $p(t,\tau)$, the distinction being made just to emphasize once more the two different particle types that constitute $n_{TOT}(t,\tau)$ in equation (I-47).

One can differentiate equation (I-48) with respect to time to obtain the evolution of the total property P(t) with time. Using Leibnitz's rule (Hildebrand (1976)),

$$\frac{d}{dx}\int_A^B f(x,t)dt = \int_A^B \frac{\partial f(x,t)}{\partial x}\, dt + f(x,B)\frac{dB}{dx} - f(x,A)\frac{dA}{dx} \qquad \text{(I-49)}$$

which is valid for all values of x in the interval (a,b) when f and $\partial f/\partial x$ are continuous for $a \leq x \leq b$ and $A \leq t \leq B$, and also dA/dx and dB/dx are continuous in (a,b). Therefore:

$$\frac{dP(t)}{dt} = p_{GEN}(t,t)\, n_{GEN}(t,t) + p_{IN}(t,t)\, n_{IN}(t,t) + \int_0^t \frac{dp_{GEN}(t,\tau)}{dt}\, n_{GEN}(t,\tau)\, d\tau + \int_0^t \frac{dp_{IN}(t,\tau)}{dt}\, n_{IN}(t,\tau)\, d\tau + \int_0^t p_{GEN}(t,\tau)\frac{dn_{GEN}(t,\tau)}{dt}\, d\tau + \int_0^t p_{IN}(t,\tau)\frac{dn_{IN}(t,\tau)}{dt}\, d\tau \qquad \text{(I-50)}$$

Equation (I-50) will lead to the final total property balance equation, which is the following:

$$\frac{dP(t)}{dt} = \frac{P_{IN}(t)}{\theta} - \frac{P(t)}{\theta} + p(t,t)\,f(t) + \int_0^t \frac{dp_{GEN}(t,\tau)}{dt}\, n_{GEN}(t,\tau)\,d\tau + \int_0^t \frac{dp_{IN}(t,\tau)}{dt}\, n_{IN}(t,\tau)\,d\tau \qquad \text{(I-51)}$$

Equation (I-51) simply says that the rate of change of the total property P(t) equals the total property inflow minus the total property outflow plus the nucleation term plus the growth terms. The last two integral terms on the right hand side of equation (I-51) can be substituted by one integral term of the form

$$\int_0^t \frac{dp(t,\tau)}{dt}\, n(t,\tau)\,d\tau \qquad \text{(I-52)}$$

without forgetting that, in the general case, there are two types of particles contributing to $p(t,\tau)$; particles nucleated in the vessel which grew to the property $p(t,\tau)$ and particles nucleated somewhere else, which entered the reactor with the inlet streams and grew to $p(t,\tau)$.

Final total property balance equation

A general population balance equation was previously developed (equation (I-34)), which was then applied to a polymer reactor with the τ-axis as the polymer particle phase space (equation (I-35)). With the introduction of the idea of a total property in the reactor (equation (I-47)), equations (I-35) and (I-50) led to equation (I-51), the final total property balance equation. The necessary steps that led from equation (I-50) to (I-51) are summarized below.

Step 1

Consider equation (I-35) at steady-state:

$$\frac{\partial n(t,\tau)}{\partial \tau} = f(t,\tau) \qquad \text{(I-53)}$$

Apply then equation (I-53) to the first type of polymer particles (i.e. the newly nucleated ones):

$$\frac{\partial n_{GEN}(t,\tau)}{\partial \tau} = -\frac{n_{GEN}(t,\tau)}{\theta} + f(t)\,\delta(t-\tau) \tag{I-54}$$

To obtain equation (I-54), the inflow term of equation (I-37) was set equal to zero, since, obviously, there is no inflow of newly nucleated particles. Also, the Dirac Delta function of the second term on the right hand side indicates the time of appearance of a particular class of particles.

Step 2

Take the Laplace transform of equation (I-54):

$$L\left\{\frac{\partial}{\partial \tau} n_{GEN}(t,\tau)\right\} = \int_0^\infty e^{-st}\,\frac{\partial}{\partial \tau} n_{GEN}(t,\tau)\,dt =$$

$$\int_0^\infty e^{-st}\,\frac{\partial}{\partial t}\,\frac{\partial t}{\partial \tau} n_{GEN}(t,\tau)\,dt = \int_0^\infty e^{-st}\,\frac{\partial}{\partial t} n_{GEN}(t,\tau)\,dt =$$

$$L\left\{\frac{\partial}{\partial t} n_{GEN}(t,\tau)\right\} = s\,n_{GEN}(s,\tau) - n_{GEN}(0,\tau) = \tag{I-55}$$

$$s\,n_{GEN}(s,\tau)$$

by virtue of the fact that $(\partial t/\partial \tau) = 1$ and that $n_{GEN}(0,\tau) = 0$.

Also,

$$L\{f(t)\,\delta(t-\tau)\} = \int_0^\infty e^{-st} f(t)\,\delta(t-\tau)dt = \int_0^\infty g(t)\,\delta(t-\tau)\,dt$$

$$= g(\tau) = e^{-s\tau} f(\tau) \tag{I-56}$$

Therefore, the Laplace transform of (I-54) gives:

$$s\,n_{GEN}(s,\tau) = -\frac{1}{\theta}\,n_{GEN}(s,\tau) - e^{-s\tau} f(\tau) \tag{I-57}$$

or

$$n_{GEN}(s,\tau) = f(\tau)\,e^{-s\tau}\,\frac{1}{\left(s+\frac{1}{\theta}\right)} \tag{I-58}$$

Taking the inverse Laplace transform of equation (I-58) one obtains:

$$n_{GEN}(t, \tau) = f(\tau)\, e^{-(t-\tau)/\theta} \qquad \text{(I-59)}$$

Step 3

For the same type of particles, the net rate of change of their number with respect now only to time t is given by:

$$\frac{dn_{GEN}(t, \tau)}{dt} = -\frac{n_{GEN}(t, \tau)}{\theta} + f(t)\,\delta(t-\tau) \qquad \text{(I-60)}$$

(I-60) was obtained again from equations (I-35) and (I-37), by setting now the terms $(\partial/\partial\tau)$ and $n(t,\tau)_r$ equal to zero. Equation (I-60) gives the net evolution of $n_{GEN}(t,\tau)$ with respect to time t (not with respect to the particle class time τ).

Step 4

Repeat steps 1 through 3 for the second type of polymer particles (those which grew to the specific property $p(t,\tau)$ but were not nucleated in the vessel). For these particles $n_{IN}(t,\tau)$ which entered the vessel, one obtains:

$$\frac{\partial n_{IN}(t, \tau)}{\partial \tau} = \frac{1}{\theta}\, n_{IN}(t)\,\delta(t-\tau) - \frac{1}{\theta}\, n_{IN}(t, \tau) \qquad \text{(I-61)}$$

Note that there is no nucleation term for incoming particles and that the Dirac Delta function in the above equation denotes the time of entrance of particles which have the same age in the vessel as all the other particles that outflow with property $p(t,\tau)$.

A similar analysis to the one described in steps 1 through 3 will give:

$$n_{IN}(t, \tau) = \frac{n_{IN}(\tau)}{\theta}\, e^{-(t-\tau)/\theta} \qquad \text{(I-62)}$$

and

$$\frac{d\, n_{IN}(t, \tau)}{dt} = \frac{n_{IN}(t)}{\theta}\,\delta(t-\tau) - \frac{n_{IN}(t, \tau)}{\theta} \qquad \text{(I-63)}$$

Step 5

Functions (I-59) and (I-62) at birth, i.e. at $t=\tau$, are given by:

$$n_{GEN}(t,t) = f(t) \tag{I-64}$$

and

$$n_{IN}(t,t) = \frac{n_{IN}(t)}{\theta} \tag{I-65}$$

Remember that $(t-\tau)$ gives the life (age) of a certain class of particles in the vessel. This is the lifetime of particles which were born at time τ, now at time t.

Step 6

Now, equation (I-50) becomes:

$$\frac{dP(t)}{dt} = p(t,t)\,f(t) + \frac{P_{IN}(t)}{\theta} + \int_0^t \frac{dp_{GEN}(t,\tau)}{dt} n_{GEN}(t,\tau)\,d\tau + \int_0^t \frac{dp_{IN}(t,\tau)}{dt} n_{IN}(t,\tau)\,d\tau + \int_0^t -p_{GEN}(t,\tau)\frac{n_{GEN}(t,\tau)}{\theta}\,d\tau + \int_0^t p_{GEN}(t,\tau)\,f(t)\,\delta(t-\tau)\,d\tau + \int_0^t -p_{IN}(t,\tau)\frac{n_{IN}(t,\tau)}{\theta}\,d\tau + \int_0^t p_{IN}(t,\tau)\frac{n_{IN}(t)}{\theta}\,\delta(t-\tau)\,d\tau \tag{I-66}$$

where $p(t,t)$ is $p_{GEN}(t,t)$ (i.e. a property at birth time) and

$$p_{IN}(t,t)\,n_{IN}(t) = P_{IN}(t) \tag{I-67}$$

Also, it is easy to see that the last integral term of equation (I-66) is zero, since it is equal to

$$\frac{n_{IN}(t)}{\theta}\,p_{IN}(\tau,\tau) \tag{I-68}$$

which is zero, since $p_{IN}(\tau,\tau) = 0$ (i.e. there is no contribution to the property $p(t,\tau)$ exactly at the time of entrance).

Step 7

Examine the fourth integral term on the right hand side of equation (I-66):

$$\int_0^t p_{GEN}(t,\tau) f(t)\,\delta(t-\tau)\,d\tau = f(t)\int_0^t p_{GEN}(t,\tau)\,\delta(t-\tau)\,d\tau$$

$$= f(t)\,p_{GEN}(\tau,\tau) = 0 \qquad \text{(I-69)}$$

since $p_{GEN}(\tau,\tau) = 0$ (i.e. the property $p(t,\tau)$ has zero value at birth time).

Step 8

Now, equation (I-66) can be rewritten as:

$$\frac{dP(t)}{dt} = p(t,t)\,f(t) + \frac{P_{IN}(t)}{\theta} + \int_0^t \frac{dp_{GEN}(t,\tau)}{dt} n_{GEN}(t,\tau)\,d\tau + \int_0^t \frac{dp_{IN}(t,\tau)}{dt} n_{IN}(t,\tau)\,d\tau - \left(\frac{P_{GEN}(t)}{\theta} + \frac{P_{IN}(t)}{\theta}\right) \qquad \text{(I-70)}$$

The last term of equation (I-70) can be set equal to:

$$-\frac{1}{\theta}\left(P_{GEN}(t) + P_{IN}(t)\right) = -\frac{1}{\theta}P(t) \qquad \text{(I-71)}$$

since the growth of newly generated and newly entered particles to the property $p(t,\tau)$ contributes to the total property $P(t)$ in the vessel. Note the difference between equation (I-67) and

$$-\int_0^t p_{IN}(t,\tau)\frac{n_{IN}(t,\tau)}{\theta}\,d\tau \qquad \text{(I-72)}$$

Equation (I-67) gives the total property at time t at inflow conditions, i.e. it gives $P_{IN}(t)$, whereas the integral (I-72) above gives the contribution to the total property $P(t)$ in the vessel from the second type of particles.

Finally, equation (I-70) becomes:

$$\frac{d\,P(t)}{dt} = \frac{P_{IN}(t)}{\theta} - \frac{P(t)}{\theta} + p(t,t)\,f(t) + \int_0^t \frac{dp_{GEN}(t,\tau)}{dt}\, n_{GEN}(t,\tau)\,d\tau + \int_0^t \frac{dp_{IN}(t,\tau)}{dt}\, n_{IN}(t,\tau)\,d\tau \qquad \text{(I-73)}$$

which is identical to equation (I-51), the final general total property balance in the reactor.

Particle size development: rate of change of polymer volume

The rate of change of polymer volume in a particle of a certain class born at time τ, now being at time t, is given by the following expression:

$$\frac{d\,v(t,\tau)}{dt} = R_p(t,\tau)\,\frac{MW}{d_p} \qquad \text{(I-74)}$$

Considering that one particle from a certain class is representative of the whole class, an expression for the rate $R_p(t,\tau)$ can be written for one particle, as follows:

$$R_p(t,\tau) = \frac{k_p M_p}{N_A}\,\bar{q}\,(t,\tau) \qquad \text{(I-75)}$$

Also, assuming that M_p is the same for the whole class, due to a very fast diffusion of monomer from monomer droplets to polymer particles, an expression for M_p can be written as:

$$M_p = \phi(t)\,\frac{d_M}{MW} \qquad \text{(I-76)}$$

with

$$\phi(t) = \frac{1 - x(t)}{1 - x(t)\left(1 - \dfrac{d_M}{d_p}\right)}, \quad x(t) = x_c \text{ if } x(t) \le x_c \qquad \text{(I-77)}$$

Hence,

$$\frac{d\,v(t,\tau)}{dt} = \left(\frac{k_p d_M}{N_A d_p}\right)\phi(t)\,\bar{q}\,(t,\tau) \qquad \text{(I-78)}$$

Average number of radicals per particle

If one applies a steady-state hypothesis on radicals for a particle of a certain class, then this hypothesis would state that the number of radicals which desorb from the class should be equal to the number of radicals that enter the class. Therefore,

$$\rho(t,\tau) = \bar{q}\,(t,\tau)\, k_{de}\,(t,\tau)\, n(t,\tau)\, d\tau \tag{I-79}$$

In the same manner, if one applies a steady-state analysis on radicals for the whole class, the hypothesis would state that radicals which enter the particles of a certain class and subsequently terminate should equal the radicals which initiated that particular class. In other words,

$$R_i(t)\,\frac{A_n(t,\tau)\,d\tau}{A_p(t)} = 2\rho(t,\tau)\,\bar{q}\,(t,\tau) \tag{I-80}$$

Elimination of $\rho(t,\tau)$ from equations (I-79) and (I-80) and the fact that (Chiang and Thompson (1979))

$$A_n(t,\tau)\,d\tau = a_p(t,\tau)\,n(t,\tau)\,d\tau \tag{I-81}$$

give:

$$\bar{q}\,(t,\tau) = \left(\frac{R_i(t)}{2\,k_{de}(t,\tau)}\right)^{1/2}\frac{a_p(t,\tau)^{1/2}}{A_p(t)^{1/2}} \tag{I-82}$$

Desorption rate constant

Harada et al. (1971) and Nomura et al. (1971) have theoretically derived an expression for the rate coefficient for radical desorption using a stochastic approach and have successfully applied it to vinyl acetate (or vinyl chloride) emulsion polymerization. Their result is the following:

$$k_{de}(t,\tau) = \left(\bar{q}\,(t,\tau) + \frac{k_p M_p m d_p^2(t,\tau)}{12\,D_w\,\delta}\right)^{-1}\left(\frac{k_{fm}}{k_p} + \frac{k_{ft}[T]}{k_p M_p} + \frac{R_i(1-\bar{q}\,(t,\tau))}{N_p(t)\,k_p M_p\,\bar{q}\,(t,\tau)}\right)k_p M_p \tag{I-83}$$

The last term in the second expression in brackets of equation (I-83) represents escape (desorption) of initiator radicals. This term can be safely neglected since an initiator radical would be sufficiently reactive to polymerize monomer molecules before escaping. Therefore, the majority of radicals escaping from polymer particles are small, mobile monomeric radicals of lower molecular weight which are produced by some transfer mechanism to small molecules (Romatowski and Schulz (1965)). Also, if the assumption is made that there is no transfer agent present in the reaction mixture, equation (I-83) can be finally written as:

$$k_{de}(t,\tau) = \left(\bar{q}\,(t,\tau) + \frac{k_p M_p m d_p^2(t,\tau)}{12 D_w \delta} \right)^{-1} k_{fm} M_p \qquad \text{(I-84)}$$

Nomura and Harada (1981) derived exactly the same expression as the one in (I-84) following also a deterministic approach. Their expression follows:

$$k_{de}(t,\tau) = \left(\frac{12 D_w \delta}{m d_p^2(t,\tau)} \right) z \left(\frac{k_{fm}}{k_p} \right) \qquad \text{(I-85)}$$

with

$$z = \sum_{j=1}^{s} \left(\frac{k_p M_p}{K_o \bar{q}\,(t,\tau) + k_p M_p} \right)^j \qquad \text{(I-86)}$$

and $0 < z < s$. No radical longer than s units will be found in the water phase due to radical desorption and since it is very unlikely that radicals other than monomeric can desorb, the value of s is unity (this is also in agreement with Friis and Nyhagen (1973)). K_o is a mass transfer coefficient for radicals other than initiator radicals and is given by:

$$K_o = \frac{12 D_w \delta}{m d_p^2(t,\tau)} \qquad \text{(I-87)}$$

If one considers the fact that the product $(K_o\, \bar{q}(t,\tau))$ is usually one order of magnitude less than the product $(k_p M_p)$, then the value of z becomes unity and the expression for $k_{de}(t,\tau)$ reduces to the simplified one:

$$k_{de}(t,\tau) = \left(\frac{12\, D_w\, \delta}{m\, d_p^2(t,\tau)} \right) \frac{k_{fm}}{k_p} \qquad \text{(I-88)}$$

which is exactly how it was employed by Kiparissides et al. (1980a) and Pollock (1984) in their model development. Equation (I-88) can also be obtained from equation (I-84) if one accepts that the average number of radicals per particle $\bar{q}(t,\tau)$ is much less than 0.1 during the whole range of conversions (which is true in most of the cases for vinyl acetate or vinyl chloride).

Parameter m in the previous expressions is the so-called partition coefficient for radicals between polymer particles (polymer phase) and water phase and is defined as (Nomura and Harada (1981)):

$$(R\cdot)_{p_i} = m\,(R\cdot)_{w_i} \qquad \text{(I-89)}$$

where (R·) denotes radical concentration, subscripts p and w denote particle and water phase, respectively, and i represents the interface between polymer particles and water phase.

Alternatively, the partition coefficient (which can be viewed as the ratio of the activity coefficients in each phase) can be obtained as (Harada et al. (1971), Nomura et al. (1971)):

$$m = M_p/M_w \qquad \text{(I-90)}$$

where M_p is the monomer concentration in the polymer particle and M_w in the water phase.

Another parameter which appears in the expressions for $k_{de}(t,\tau)$ and is worth discussing is parameter δ, a lumped diffusion coefficient or, alternatively, the ratio of film mass transfer resistance to overall mass transfer resistance (Nomura and Harada (1981)). δ is given by the following expression:

$$\delta = \left(1 + \frac{6\, D_w}{m\, D_p} \right)^{-1} \qquad \text{(I-91)}$$

according to Nomura and Harada (1981). D_w is the diffusion coefficient of radicals in the water phase and D_p in the polymer particle. In the beginning of the polymerization when monomer droplets exist in the water phase and hence the polymer particles are saturated

with monomer, the value of δ is close to unity because D_w and D_p are of the same order of magnitude. However, in a higher conversion range, the value of D_p will decrease markedly with the progress of the polymerization due to an increase in the viscosity inside the polymer particles. When the condition $(6D_w/mD_p) >> 1$ is satisfied, namely, the diffusion resistance inside the polymer particle becomes dominant,

$$\delta \doteq \left(\frac{6\,D_w}{m\,D_p}\right)^{-1} \tag{I-92}$$

and

$$k_{de}(t,\tau) = \left(\frac{2\,D_p}{d_p^2(t,\tau)}\right) \cdot z \cdot \left(\frac{k_{fm}}{k_p}\right) \tag{I-93}$$

In such a high monomer conversion range, the value of $k_{de}(t,\tau)$ decreases with the progress of polymerization, corresponding to the decrease in the value of D_p.

Previous efforts in the literature to simulate data on the emulsion polymerization of vinyl acetate (Harada et al. (1971), Nomura et al. (1971), Ugelstad et al. (1969), Friis and Nyhagen (1973), Nomura et al. (1976), Kiparissides et al. (1980a) and Pollock et al. (1981)) made use of the simplified expression for $k_{de}(t,\tau)$ given by equation (I-88) and assumed an average constant value for δ throughout the reaction (i.e. no reduction due to particle viscosity increase). If these two assumptions are relaxed, then a more general expression for $k_{de}(t,\tau)$ can be obtained as follows:

$$k_{de}(t,\tau) = \frac{n\,\psi_1\,k_{fm}\,M_p}{n\,\psi_1\,q\,(t,\tau) + k_p M_p\,\psi_2\,a_p(t,\tau)} \tag{I-94}$$

with

$$\psi_1 = 12\,D_w\,D_p \tag{I-95}$$

and

$$\psi_2 = mD_p + 6D_w \tag{I-96}$$

The rate coefficient for radical desorption can also be estimated from the "apparent half-life of propagating radicals" measurement used by Ley et al. (1969).

A more general expression for $\bar{q}(t,\tau)$

An equation was previously derived (equation (I-82)) which gave an expression for the average number of radicals per polymer particle, similar to the expressions derived by Ugelstad et al. (1967), Ugelstad et al. (1969) and Harada et al. (1971).

If the simplified expression (I-89) for $k_{de}(t,\tau)$ is substituted in equation (I-82), together with

$$a_p(t,\tau) = \pi d_p^2(t,\tau) \tag{I-97}$$

and

$$R_i(t) = 2 f k_d I_w(t) N_A \tag{I-98}$$

then the following expression is obtained for the average number of radicals per particle:

$$\bar{q}(t,\tau) = \left(\frac{f k_d m k_p N_A}{12 \pi D_w \delta k_{fm}} \right)^{1/2} \frac{I_w^{1/2}(t)}{A_p^{1/2}(t)} a_p(t,\tau) \tag{I-99}$$

If the more general expression for $k_{de}(t,\tau)$ is used (i.e. equation (I-94)), then equation (I-82) yields:

$$\bar{q}(t,\tau) = \frac{\Psi_3 I_w(t) + (\Psi_3^2 I_w^2(t) + 4 \Psi_4 I_w(t) M_p^2 A_p(t))^{1/2}}{2 M_p A_p(t)} a_p(t,\tau) \tag{I-100}$$

with

$$\Psi_3 = \frac{f k_d N_A}{k_{fm}} \tag{I-101}$$

and

$$\Psi_4 = \frac{\Psi_3 k_p \Psi_2}{\pi \Psi_1} \tag{I-102}$$

Accounting for the gel-effect

Free radical polymerization in a latex particle occurs at polymer concentrations where chain entanglements and low free volume can significantly reduce the translational and segmental mobility of macroradicals. The termination reaction becomes diffusion-controlled and a reduction in the termination rate constant by several orders of magnitude can cause a large increase in the average number of radicals per particle and an acceleration in the rate of polymerization particularly for Case II systems. At higher conversions a glassy-state transition may occur with the propagation reaction rate falling rapidly and approaching rates which are typical of solid state polymerizations (if the polymerization temperature is below the glass transition temperature of the polymer being synthesized). As a result, in the normal time scale limiting conversions of less than 100% are reached.

When molecular weight development is controlled mainly by termination reactions, a dramatic increase in the weight average molecular weight is observed at high conversions. In emulsion polymerizations chain transfer reactions are generally more important and thus molecular weight increases with conversion are not large. However, at very high conversions ($x(t) > 80\%$), abnormal molecular structures have been observed and predicted in the suspension polymerization of vinyl chloride, for example (Hamielec et al. (1982)). These include a large increase in the number of terminal double bonds associated with a sharp decrease in the number average molecular weight and an increase in the number of long branches associated with an increase in the weight average molecular weight. All these abnormal changes are predicted (Hamielec et al. (1982)) due to diffusion-controlled termination and propagation.

The previously mentioned effects have often been accounted for by empirical correlations of the rate constants with conversion. Recently, more fundamental approaches using free volume theory or de Gennes reptation theory have been used quite successfully to

model these effects for homopolymers (Friis and Hamielec (1976), Marten and Hamielec (1979), Harris et al. (1981), Hamielec et al. (1982), Marten and Hamielec (1982), Tulig and Tirrell (1981), Tirrell and Tulig (1983), Soh and Sundberg (1982a-1982d), Chiu et al. (1982) and Hamielec (1983)), and for copolymers (Hamielec and MacGregor (1983) and Lord (1984)).

Kiparissides et al. (1980a) and Pollock et al. (1981) did not account for the gel-effect in their vinyl acetate emulsion polymerization model development. This was reasonable, since vinyl acetate (and vinyl chloride) emulsion polymerizations are examples of systems where radical desorption is important. The decrease in the termination rate constant for VAc is about the same as that for styrene (Friis and Hamielec (1976)), however, the effect of radical desorption in the VAc case counteracts the gel-effect. While this is generally true for both VCM and VAc emulsion polymerizations (Friis and Hamielec (1976)), there might be special situations, such as very high initiation rates with large polymer particles, where the rate of radical desorption could no longer counteract the gel-effect. Therefore, in such cases models for Case I systems should account for diffusion-controlled termination.

In order to estimate the dependence of the termination rate constant on conversion, molecular weight and temperature, the following is assumed: k_t, the termination rate constant, becomes diffusion-controlled when the diffusion coefficient for a polymer radical D_p becomes less than or equal to a critical diffusion coefficient Dp_{cr}. It is further assumed that the termination rate constant beyond this critical conversion can be expressed by:

$$k_t = k_1 \cdot D_p \qquad \text{(I-103)}$$

and at the critical point by:

$$k_{t_{cr}} = k_1 \cdot D_{p_{cr}} \qquad \text{(I-104)}$$

where k_1 is a temperature dependent proportionality constant.

If no chain entanglements are present, the diffusion coefficient of a polymer molecule is given according to Bueche (1960, 1962), as:

$$D_p = \left(\frac{\phi_o \delta^2}{k_2 M}\right) \exp\left(-A/V_F\right) \tag{I-105}$$

where M is the molecular weight of the polymer (monodisperse), ϕ_o is a jump frequency, δ a jump distance, k_2 and A are constants and V_F represents the free volume fraction.

V_F in the general case is equal to:

$$V_F = (0.025 + a_p(T - T_{g_p}))\frac{V_p}{V_T} + (0.025 + a_M(T - T_{g_m}))\frac{V_M}{V_T} + (0.025 + a_s(T - T_{g_s}))\frac{V_s}{V_T} \tag{I-106}$$

where subscripts M, p and s denote monomer, polymer and solvent (if solution polymerization), respectively, T is the polymerization temperature, T_g the glass transition point, V denotes volume and V_T total volume, and

$$a_i = (a_\ell - a_g)_i \tag{I-107}$$

where i = M, p or s, a_ℓ is the expansion coefficient for the liquid state and a_g is the expansion coefficient for the glassy state.

It is further noted that:

$$T_{g_p} = T_{g_\infty} - (Q/\overline{M}_N) \tag{I-108}$$

where Tg_∞ is the glass temperature of the infinite molecular weight polymer, Q is a constant independent of temperature and $\overline{M}_N$ is the cumulative number average molecular weight.

It is also reasonable to expect that D_p would correlate well with the weight average molecular weight, since the diffusion coefficients of entangled polymeric chains in solution will most certainly depend on the viscosity of the medium and vice versa (Marten and Hamielec (1979)). In fact, it was shown by the previously mentioned authors that the best correlation with experimental data was achieved when the cumulative weight average molecular weight to the 1/2 power was used instead of M in equation (I-105).

Therefore,

$$k_t = k_1\left(\frac{\phi_o \delta^2}{k_2 \bar{M}_w^{1/2}}\right)\exp(-A/V_F) \tag{I-109}$$

for unentangled polymer solutions, and

$$k_t = k_1\left(\frac{\phi_o \delta^2}{k_2 \bar{M}_w^{1.75}}\right)\exp(-A/V_F) \tag{I-110}$$

for entangled polymer solutions.

At the onset of gel-effect,

$$K_3 = \frac{k_1 \phi_o \delta^2}{k_{t_o} k_2} = \bar{M}_w^{1/2}\exp(+A/V_F) \tag{I-111}$$

where $k_{t_o} = k_{t_{cr}}$, and hence:

$$\frac{k_t}{k_{t_o}} = \left(\frac{\bar{M}_{w_{cr1}}}{\bar{M}_w}\right)^{1.75}\exp\left(-A\left(\frac{1}{V_F} - \frac{1}{V_{F_{cr1}}}\right)\right) \tag{I-112}$$

where $\bar{M}_{w_{cr1}}$ and $V_{F_{cr1}}$ satisfy equation (I-111).

Similarly, one has for the propagation rate constant:

$$k_p = k_{p_o}\exp\left(-B\left(\frac{1}{V_F} - \frac{1}{V_{F_{cr2}}}\right)\right) \tag{I-113}$$

where k_{p_o} represents the propagation rate constant below the critical conversion where k_p becomes diffusion-controlled and B is unity, according to Bueche (1960).

As was mentioned before, for polymerizations which occur near the glass transition point of the monomer-polymer mixture reactions involving small molecules can also become diffusion-controlled. When the propagation reactions become diffusion controlled, the rate of polymerization rapidly falls to a value close to zero. This was clearly shown (Marten and Hamielec (1979)) for the emulsion polymerization of styrene and methyl methacrylate. However, with VAc where the glass transition point of pure poly (vinyl acetate) (~28°C) is

below the polymerization temperature, a limiting conversion approaching 100% can be reached and one can neglect diffusion-controlled propagation.

Diffusion coefficient of radicals in the polymer particle

While there exist several equations to theoretically estimate the concentration, temperature and molecular weight dependence of diffusion coefficients in amorphous polymer-solvent systems (Vrentas and Duda (1979), Vrentas et al. (1985a, 1985b)), the simple empirical expressions obtained from experiments proved to be the preferred means of describing the conversion dependency inside the latex particles. Since the value of the diffusion coefficient for monomeric radicals inside the particles, D_p, was found to decrease with conversion, Friis and Nyhagen (1973) proposed the following experimentally determined expression (also proposed by Friis and Hamielec (1976) and by Yasuda et al. (1971):

$$D_p = D_p^{\circ} \exp(-\beta x_v (1-\alpha)/(1+\alpha x_v)) \qquad \text{(I-114)}$$

where D_p° is the self-diffusing coefficient of the diffusing compound (monomer radicals) in its own medium (pure monomer), β is the ratio of a critical free volume fraction necessary for diffusion to take place to the free volume fraction of monomer, α is the ratio of the free volume fraction of polymer to the free volume fraction of monomer, and

$$x_v = \frac{1-H}{H} \qquad \text{(I-115)}$$

where H is the volume fraction of the low molecular weight compound (monomer) in monomer-swollen particles, therefore

$$x_v = \frac{x(t)\, d_M}{(1-x(t))\, d_p} \qquad \text{(I-116)}$$

i.e. x_v gives the ratio between volume fraction of monomer and polymer in monomer-swollen polymer particles.

Substituting equation (I-116) into equation (I-114), one finally obtains:

$$D_p = D_p^{\circ} \exp\left(\frac{-\beta\, x(t)\, d_M\, (1-\alpha)}{(\alpha\, x(t)\, d_M + (1-x(t))\, d_p)} \right) \tag{I-117}$$

with $D_p^{\circ} = 1. \times 10^{-8}$ or 10^{-10} dm^2/sec, $\alpha = 0.3$ and $\beta = 3.2$ (Friis and Nyhagen (1973)) or $\alpha = 0.42$ and $\beta = 3.69$ (Zollars (1981)).

Litt and Chang (1980) suggested an alternative expression for D_p which has the following form:

$$D_p = D_p^{\circ} \phi(t)^m \tag{I-118}$$

In equation (I-118) the exponent m assumes the value of 2.

Another expression suggested by Friis and Hamielec (1977) for the emulsion polymerization of VAc, also yields a similar result. This expression follows:

$$D_p = D_p^{\circ} \left(\left(\frac{1-x(t)}{1-0.19\, x(t)} \right)^2 + 0.0017\, x(t) \right) \tag{I-119}$$

Rate expression for particle volume

Combination of equations (I-78) and (I-99) yields the following expression for the rate of change of polymer volume in a particle:

$$\frac{d\, v(t,\tau)}{dt} = \left(\frac{k_p\, d_M}{N_A\, d_p} \right) \left(\frac{f\, k_d\, m\, k_p\, N_A}{12\, \pi\, D_w\, \delta\, k_{fm}} \right)^{1/2} \phi(t)\, \frac{I_w(t)^{1/2}}{A_p(t)^{1/2}}\, a_p(t,\tau) \tag{I-120}$$

or

$$\frac{d\, v(t,\tau)}{dt} = \lambda \cdot \phi(t) \frac{I_w(t)^{1/2}}{A_p(t)^{1/2}}\, a_p(t,\tau) \tag{I-121}$$

where:

$$\lambda = \left(\frac{k_p\, d_M}{N_A\, d_p} \right) \left(\frac{f\, k_d\, m\, k_p\, N_A}{12\, \pi\, D_w\, \delta\, k_{fm}} \right)^{1/2} \tag{I-122}$$

Setting

$$\xi'(t) = \phi(t)\, \frac{I_w(t)^{1/2}}{A_p(t)^{1/2}} \tag{I-123}$$

one obtains:

$$\frac{d\,v\,(t,\tau)}{dt} = \lambda \xi'(t)\, a_p(t,\tau) \tag{I-124}$$

If the more general expression (I-100) for $\bar{q}(t,\tau)$ is used, then one obtains:

$$\frac{d\,v\,(t,\tau)}{dt} = \left(\frac{k_p d_m}{N_A d_p}\right)\left(\frac{\phi(t)}{2\,M_p A_p(t)}\right)(\psi_3 I_w(t) + (\psi_3^2 I_w^2(t) + 4\psi_4 I_w(t)\, M_p^2 A_p(t))^{1/2})a_p(t,\tau) \tag{I-125}$$

Now, recalling that $\phi(t)$ is monomer volume over particle volume and that $(1-\phi(t))$ is polymer volume over particle volume, one obtains the following expression for particle volume:

$$v_p(t,\tau) = \frac{v(t,\tau)}{1-\phi(t)} \tag{I-126}$$

Therefore, the rate of change of particle volume is obtained by differentiating equation (I-126) with respect to time, as follows:

$$\frac{d\,v_p(t,\tau)}{dt} = \frac{1}{1-\phi(t)}\,\frac{d\,v\,(t,\tau)}{dt} + \frac{v\,(t,\tau)}{(1-\phi(t))^2}\,\frac{d\phi(t)}{dt} \tag{I-127}$$

Accounting for particle volume shrinkage during stage 3

During stages 1 and 2, i.e. when $x(t)$ is less than or equal to x_c,

$$\phi(t) = \frac{1-x_c}{1-x_c\left(1-\frac{d_M}{d_p}\right)} = \text{constant} \tag{I-128}$$

Hence, $d\phi(t)/dt = 0$ and equation (I-127) becomes:

$$\frac{d\,v_p(t,\tau)}{dt} = \frac{1}{1-\phi(t)}\,\frac{d\,v\,(t,\tau)}{dt} \tag{I-129}$$

or

$$\frac{d\,v_p(t,\tau)}{dt} = \lambda\,\xi(t)\,a_p(t,\tau), \quad x(t) \le x_c \tag{I-130}$$

if one substitutes:

$$\xi(t) = \frac{\xi'(t)}{1-\phi(t)} \tag{I-131}$$

During stage 3, i.e. when $x(t) > x_c$, $\phi(t)$ ceases to be a constant, and

$$\frac{d\,\phi(t)}{dt} = \frac{c-1}{(1-c\,x(t))^2}\,\frac{d\,x(t)}{dt} \tag{I-132}$$

where:

$$c = \left(1 - \frac{d_M}{d_p}\right). \tag{I-133}$$

Hence, equation (I-127) becomes:

$$\frac{d\,v_p(t,\tau)}{dt} = \lambda\,\xi(t)\,a_p(t,\tau) + \frac{v(t,\tau)}{1-\phi(t)}\,\frac{1}{1-\phi(t)}\,\frac{d\,\phi(t)}{dt} \tag{I-134}$$

or

$$\frac{d\,v_p(t,\tau)}{dt} = \lambda\,\xi(t)\,a_p(t,\tau) + v_p(t,\tau)\,\varepsilon(t), \quad x(t) > x_c \tag{I-135}$$

where

$$\varepsilon(t) = \frac{1}{1-\phi(t)}\,\frac{c-1}{(1-c\,x(t))^2}\,\frac{d\,x(t)}{dt} \tag{I-136}$$

The time function $\varepsilon(t)$ accounts for particle volume shrinkage due to monomer and polymer density differences during stage 3 of the reaction in a batch reactor, where $dx(t)/dt$ is considerable. However, $dx(t)/dt$ is small in the case of a CSTR operating under stable conditions (or, even under oscillatory conditions, when a change in $x(t)$ may be cancelled by the opposite change in $x(t)$ during the conversion swing). Therefore, $\varepsilon(t)$ can be neglected in the case of a CSTR. Obviously, $\varepsilon(t)$ would not be negligible under start-up conditions.

Property balance for total particle volume

Equation (I-135) is nothing but the rate of change of property $p(t,\tau)$ in the reactor vessel with respect to time. In other words, equation (I-135) represents the term $(dp(t,\tau)/dt)$ in the general property balance (I-73) or (I-51). Therefore, the general property balance for total particle volume in the reactor becomes:

$$\frac{d\,V_p(t)}{dt} = \frac{V_{p_{IN}}(t) - V_p(t)}{\theta} + v_p(t,t)\,f(t) + \lambda\,\xi(t)\,A_p(t) + \varepsilon(t)\,V_p(t) \tag{I-137}$$

Expression for total particle diameter

Recalling that

$$v_p(t,\tau) = \frac{1}{6}\,\pi\,d_p^3(t,\tau) \tag{I-138}$$

and differentiating (I-138) with respect to time, one obtains:

$$\frac{d}{dt}\,(d_p(t,\tau)) = 2\,\lambda\,\xi(t) + \frac{1}{3}\,\varepsilon(t)\,d_p(t,\tau) \tag{I-139}$$

Substituting (I-139) in (I-51), the property balance for total particle diameter follows:

$$\frac{d\,D_p(t)}{dt} = \frac{D_{p_{IN}}(t) - D_p(t)}{\theta} + d_p(t,t)\,f(t) + 2\lambda\,\xi(t)\,N_p(t) + \frac{1}{3}\,\varepsilon(t)\,D_p(t) \tag{I-140}$$

Expression for total particle surface area

Since

$$a_p(t,\tau) = \pi\,d_p^2(t,\tau), \tag{I-141}$$

by differentiating equation (I-141) one obtains:

$$\frac{d\,a_p(t,\tau)}{dt} = 4\,\pi\,\lambda\,\xi(t)\,d_p(t,\tau) + \frac{2}{3}\,\varepsilon(t)\,a_p(t,\tau) \tag{I-142}$$

Then, substituting equation (I-142) in the total property balance equation (I-51), the equation for the rate of change of total particle surface area, $A_p(t)$, is obtained as follows:

$$\frac{d\,A_p(t)}{dt} = \frac{A_{p_{IN}}(t) - A_p(t)}{\theta} + a_p(t,t)\,f(t) + 4\pi\,\lambda\,\xi(t)\,D_p(t) + \frac{2}{3}\,\varepsilon(t)\,A_p(t) \tag{I-143}$$

Expression for total number of polymer particles

The equation for the rate of change of total number of polymer particles in the reactor is straightforward and given by:

$$\frac{d N_p(t)}{dt} = \frac{N_{p_{IN}}(t) - N_p(t)}{\theta} + f(t) \qquad \text{(I-144)}$$

Equations (I-137), (I-140), (I-143) and (I-144) describe the evolution of the particle size distribution in the reactor vessel, as it will be also shown later.

Expression for the desorption rate

The desorption rate, $\rho_{des}(t)$, in the reactor is given by:

$$\rho_{des}(t) = \int_0^t k_{de}(t,\tau)\, n(t,\tau)\, \bar{q}(t,\tau)\, d\tau \qquad \text{(I-145)}$$

Equations (I-88), (I-97) and (I-99) or equations (I-94) and (I-100) can be employed in a straightforward manner to obtain a final expression for $\rho_{des}(t)$.

Definition of the moments of the MWD

If

$R_r(t,\tau)$ = gmoles of radicals of chain length r in a particle of the class $n(t,\tau)d\tau$ (I-146)

and

$P_r(t,\tau)$ = gmoles of dead polymer of chain length r per particle of the class $n(t,\tau)d\tau$ (I-147)

then, the n^{th} moment for dead polymer is defined as:

$$Q_n(t,\tau) = \sum_{r=1}^{\infty} r^n P_r(t,\tau) \qquad \text{(I-148)}$$

and the n^{th} moment for a live polymer chain as:

$$Y_n(t,\tau) = \sum_{r=1}^{\infty} r^n R_r(t,\tau) \qquad \text{(I-149)}$$

Live polymer equations

For r = 1,

$$\frac{dR_1^{\cdot}}{dt} = -k_p M R_1^{\cdot} + k_{fm} M Y_0 - k_{fp} R_1^{\cdot} Q_1 - k_p^{*} R_1^{\cdot} Q_0 + k_{fp} P_1 Y_0 \qquad \text{(I-150)}$$

where the summation in the second term of the right hand side of equation (I-150) starts from r = 2, because a transfer to monomer reaction of the form

$$R_1^{\cdot} + M \rightarrow P_1 + R_1^{\cdot} \qquad \text{(I-151)}$$

gives zero net production of $(R_1^{\cdot})$. M in equations (I-150), (I-151) and in all the subsequent expressions in this appendix will denote monomer concentration at some time t in the polymer particle (i.e. $M \equiv M_p$).

Similarly, for $r \geq 2$,

$$\frac{dR_r^{\cdot}}{dt} = k_p M_p R_{r-1}^{\cdot} - (k_{fm} M_p + k_{fp} Q_1 + k_p^{*} Q_0 + k_p M_p) R_r^{\cdot} + k_p^{*} \sum_{s=1}^{r-1} R_s^{\cdot} P_{r-s} + k_{fp} r P_r Y_0 \qquad \text{(I-152)}$$

where the brackets on $R^{\cdot}(t,\tau)$, $P(t,\tau)$, $Y(t,\tau)$ or $Q(t,\tau)$ are not shown to simplify typing.

Summation over $R_r^{\cdot}$ from r = 1, (based on equations (I-150) and (I-151)) gives:

$$\frac{dR_1^{\cdot}}{dt} + \frac{d\left(\sum_{r=2}^{\infty} R_r^{\cdot}\right)}{dt} = \frac{dY_0}{dt} = -k_p M_p Y_0 + k_p M_p \left(\sum_{r=2}^{\infty} R_{r-1}^{\cdot}\right) - k_p^{*} Q_0 Y_0 + k_p^{*} \left(\sum_{r=2}^{\infty} \sum_{s=1}^{r-1} R_s^{\cdot} P_{r-s}\right) \qquad \text{(I-153)}$$

In equation (I-153),

$$\sum_{r=2}^{\infty} R_{r-1}^{\cdot} = \sum_{s=1}^{\infty} R_s^{\cdot} = Y_0 \qquad \text{(I-154)}$$

if s = r−1, and

$$\sum_{r=2}^{\infty} \sum_{s=1}^{r-1} R_s \cdot P_{r-s} = Y_0 Q_0, \tag{I-155}$$

hence, going back to equation (I-153),

$$\frac{d Y_0}{dt} = 0. \tag{I-156}$$

Multiplying equation (I-152) with r and adding equation (I-150) to their product, one obtains:

$$\frac{d Y_1}{dt} = k_p M_p Y_0 + k_{fm} M_p (Y_0 - Y_1) + k_{fp} (Y_0 Q_2 - Q_1 Y_1) + k_p^{\bullet} Q_1 Y_0 \tag{I-157}$$

recalling that:

$$\sum_{s=1}^{\infty} (s+1) R_s = Y_1 + Y_0, \tag{I-158}$$

$$\sum_{r=2}^{\infty} r \sum_{s=1}^{r-1} R_s \cdot P_{r-s} = Q_1 Y_0 + Q_0 Y_1 \tag{I-159}$$

and that $P_0 = 0$.

Introducing now the modified moment

$$Q_i'(t, \tau) = Q_i(t, \tau)\, v_p(t, \tau) \tag{I-160}$$

where $Q_i(t,\tau) = Q_n(t,\tau)$ from equation (I-148), one obtains for $Y_1(t,\tau)$:

$$\frac{d Y_1}{dt} = k_p M_p Y_0 + k_{fm} M_p (Y_0 - Y_1) + k_{fp} \left(Y_0 \frac{Q_2'}{v_p(t, \tau)} - Y_1 \frac{Q_1'}{v_p(t, \tau)} \right)$$

$$+ k_p^{\bullet} Y_0 \frac{Q_1'}{v_p(t, \tau)} \tag{I-161}$$

If a chain transfer agent is present, then instead of the term $(k_{fm} M_p)$ one should have the term $(k_{fm} M_p + k_{ft} T)$, where T is the concentration of chain transfer agent in the reactor at time t and k_{ft} denotes the velocity constant for transfer reactions with the transfer agent.

Similarly, multiplying equation (I-152) with r^2, summing up from $r=2$ and adding equation (I-150), one obtains for Y_2:

$$\frac{dY_2}{dt} = k_p M_p (Y_0 + 2Y_1) + k_{fm} M_p (Y_0 - Y_2) + k_{fp}\left(Y_0 \frac{Q_3}{v_p(t,\tau)} - Y_2 \frac{Q_1}{v_p(t,\tau)} \right) + k_p^*\left(Y_0 \frac{Q_2}{v_p(t,\tau)} + 2Y_1 \frac{Q_1}{v_p(t,\tau)} \right) + \tag{I-162}$$

where:

$$\sum_{r=2}^{\infty} r^2 R_{r-1} = Y_2 + 2Y_1 + Y_0 , \tag{I-163}$$

$$\sum_{r=2}^{\infty} r^2 R_r = Y_2 - R_1 , \tag{I-164}$$

$$\sum_{r=2}^{\infty} r^2 \sum_{s=1}^{r-1} R_s P_{r-s} = Q_2 Y_0 + 2Q_1 Y_1 + Q_0 Y_2 \tag{I-165}$$

and

$$\sum_{r=2}^{\infty} r^3 P_r = Q_3 \tag{I-166}$$

were used during the intermediate steps to obtain (I-162).

Application of the stationary state hypothesis for (dY_1/dt) and $dY_2/dt)$ yields:

$$\frac{Y_1(t,\tau)}{Y_0(t,\tau)} = \frac{k_p M_p + k_{fm} M_p + k_{fp} \dfrac{Q_2(t,\tau)}{v_p(t,\tau)} + k_p^* \dfrac{Q_1(t,\tau)}{v_p(t,\tau)}}{k_{fm} M_p + k_{fp} \dfrac{Q_1(t,\tau)}{v_p(t,\tau)}} \tag{I-167}$$

and

$$\frac{Y_2(t,\tau)}{Y_0(t,\tau)} = \frac{k_p M_p + k_{fm} M_p + k_{fp} \dfrac{Q_3(t,\tau)}{v_p(t,\tau)} + k_p^* \dfrac{Q_2(t,\tau)}{v_p(t,\tau)} + 2\left(k_p M_p + k_p^* \dfrac{Q_1(t,\tau)}{v_p(t,\tau)} \right)\left(\dfrac{Y_1(t,\tau)}{Y_0(t,\tau)} \right)}{k_{fm} M_p + k_{fp} \dfrac{Q_1(t,\tau)}{v_p(t,\tau)}} \tag{I-168}$$

Equations (I-167) and (I-168) describe the (live) active polymer chains in the reactor vessel.

Dead polymer equations

A similar development to the one employed to derive the live polymer equations, would give:

$$\frac{d\,Q_0(t,\tau)}{dt} = k_{fm} M_p Y_0(t,\tau) - k_p^* Y_0(t,\tau)\left(\frac{Q_0(t,\tau)}{v_p(t,\tau)}\right) \tag{I-169}$$

$$\frac{d\,Q_1(t,\tau)}{dt} = k_{fm} M_p Y_1(t,\tau) + k_{fp} Y_1(t,\tau)\left(\frac{Q_1(t,\tau)}{v_p(t,\tau)}\right) - k_{fp} Y_0(t,\tau)\frac{Q_2(t,\tau)}{v_p(t,\tau)} - k_p^* Y_0(t,\tau)\frac{Q_1(t,\tau)}{v_p(t,\tau)} \tag{I-170}$$

and

$$\frac{d\,Q_2(t,\tau)}{dt} = k_{fm} M_p Y_2(t,\tau) + k_{fp} Y_2(t,\tau)\left(\frac{Q_1(t,\tau)}{v_p(t,\tau)}\right) - k_{fp} Y_0(t,\tau)\frac{Q_3(t,\tau)}{v_p(t,\tau)} - k_p^* Y_0(t,\tau)\frac{Q_2(t,\tau)}{v_p(t,\tau)} \tag{I-171}$$

Then, using equations (I-167) and (I-168) one finally obtains:

$$\frac{d\,Q_0(t,\tau)}{dt} = k_{fm} M_p Y_0(t,\tau) - k_p^* Y_0(t,\tau)\left(\frac{Q_0(t,\tau)}{v_p(t,\tau)}\right) \tag{I-169}$$

$$\frac{d\,Q_1(t,\tau)}{dt} = k_p M_p Y_0(t,\tau) + k_{fm} M_p Y_0(t,\tau) \tag{I-172}$$

and

$$\frac{d\,Q_2(t,\tau)}{dt} = (k_p M_p + k_{fm} M_p)\, Y_0(t,\tau)$$

$$+\left(2Y_0(t,\tau)\left(\frac{k_p M_p + k_p^* \dfrac{Q_1(t,\tau)}{v_p(t,\tau)}}{k_{fm} M_p + k_{fp} \dfrac{Q_1(t,\tau)}{v_p(t,\tau)}}\right)\right.$$

$$\left.\left(k_p M_p + k_{fm} M_p + k_{fp} \frac{Q_2(t,\tau)}{v_p(t,\tau)} + k_p^* \frac{Q_1(t,\tau)}{v_p(t,\tau)}\right)\right) \qquad \text{(I-173)}$$

Expression for branch points per polymer particle

If B_N denotes branch points per polymer molecule, then $(Q_0 B_N)(t,\tau)$ denotes branch points per polymer particle of the class $n(t,\tau)d\tau$, and:

$$\frac{d\left(\sum_{r=1}^{\infty} B_N(t,\tau)\right)}{dt} = k_{fp} Y_0 Q_1 + k_p^* Y_0 Q_0 \qquad \text{(I-174)}$$

and that:

$$\frac{d\,((Q_0 B_N)(t,\tau))}{dt} = \left(k_{fp} \frac{Q_1(t,\tau)}{v_p(t,\tau)} + k_p^* \frac{Q_0(t,\tau)}{v_p(t,\tau)}\right) Y_0(t,\tau) \qquad \text{(I-175)}$$

Generalizing the expressions for Q_0, Q_1 and $Q_2(t,\tau)$

Defining the ratios

$$C_m = k_{fm}/k_p, \qquad \text{(I-176)}$$

$$C_p = k_{fp}/k_p, \qquad \text{(I-177)}$$

$$K = k_p^*/k_p \qquad \text{(I-178)}$$

and making use of the assumptions that:

$Y_{AVE}(t)$ = average number of radicals in any given volume for all classes

$$= \frac{Y_{0_{TOT}}(t)}{V_p(t)} = \frac{Y_0(t,\tau)}{v_p(t,\tau)} \qquad \text{(I-179)}$$

and that:

$$\bar{Q}_1(t) = \frac{Q_1(t)}{V_p(t)} = \frac{Q_1(t,\tau)}{v_p(t,\tau)}$$

$$= \text{average number of polymeric radicals} \tag{I-180}$$

are constant and independent of τ (i.e. $Y_{AVE}(t)$ and $\bar{Q}_1(t)$ are not functions of τ), one obtains:

$$\frac{dQ_0(t,\tau)}{dt} = k_p M_p Y_{AVE}(t)\left(C_m v_p(t,\tau) - K\frac{Q_0(t,\tau)}{M_p}\right) \tag{I-181}$$

$$\frac{dQ_1(t,\tau)}{dt} = k_p M_p Y_{AVE}(t)(1+C_m) v_p(t,\tau) \tag{I-182}$$

$$\frac{dQ_2(t,\tau)}{dt} = k_p M_p Y_{AVE}(t)\left((1+C_m)v_p(t,\tau) + 2\left(\frac{1+\dfrac{K\bar{Q}_1(t)}{M_p}}{C_m+\dfrac{C_p\bar{Q}_1(t)}{M_p}}\right)\right.$$

$$\left.\cdot\left((1+C_m)v_p(t,\tau) + \frac{C_pQ_2(t)}{M_p} + \frac{KQ_1(t,\tau)}{M_p}\right)\right) \tag{I-183}$$

and

$$\frac{d((Q_0 B_N)(t,\tau))}{dt} = k_p M_p Y_{AVE}(t)\left(C_p\frac{Q_1(t,\tau)}{M_p} + K\frac{Q_0(t,\tau)}{M_p}\right) \tag{I-184}$$

Expressions for the total moments of the MWD

Substituting equations (I-181) through (I-184) into the general property balance equation (I-51), one obtains the following expressions for the total moments of the molecular weight distribution:

$$\frac{dQ_0(t)}{dt} = \frac{Q_{0_{IN}}(t) - Q_0(t)}{\theta} + k_p M_p Y_{AVE}(t)\left(C_m V_p(t) - K\frac{Q_0(t)}{M_p}\right) \tag{I-185}$$

$$\frac{dQ_1(t)}{dt} = \frac{Q_{1_{IN}}(t) - Q_1(t)}{\theta} + k_p M_p Y_{AVE}(t)(1 + C_m) V_p(t) \tag{I-186}$$

$$\frac{dQ_2(t)}{dt} = \frac{Q_{2_{IN}}(t) - Q_2(t)}{\theta} + k_p M_p Y_{AVE}(t)\left((1 + C_m) V_p(t) + 2\,(RATIO)\left((1 + C_m) V_p(t) + \frac{C_p Q_2(t)}{M_p} + \frac{K Q_1(t)}{M_p}\right)\right) \tag{I-187}$$

where

$$RATIO = \frac{1 + K\dfrac{\overline{Q}_1(t)}{M_p}}{C_m + C_p\dfrac{\overline{Q}_1(t)}{M_p}} \tag{I-188}$$

and

$$\frac{d((Q_0 B_N)(t,\tau))}{dt} = \frac{(Q_0 B_N)_{IN}(t) - (Q_0 B_N)(t)}{\theta} + k_p M_p Y_{AVE}(t)\left(C_p\frac{Q_1(t)}{M_p} + K\frac{Q_0(t)}{M_p}\right) \tag{I-189}$$

In the above expressions, the term $(1 + C_m)$ could easily be approximated by unity, since $C_m << 1$.

Calculation of the molecular weight averages

After having derived equations describing the moments of the molecular weight distribution, one can calculate the number average and weight average molecular weights and the average number of branch points per polymer molecule, as follows:

$$\overline{M}_n(t) = \frac{Q_1(t)}{Q_0(t)}\,MW \tag{I-190}$$

$$\overline{M}_w(t) = \frac{Q_2(t)}{Q_1(t)}\,MW \tag{I-191}$$

and

$$\bar{B}_N(t) = \frac{(Q_0 B_N)(t)}{Q_0(t)} \tag{I-192}$$

Expression for the total number of radicals per liter of latex

The total number of radicals per liter of latex in the reactor is given by:

$$Y_{0_{TOT}}(t) = \int_0^t \bar{q}(t,\tau)\, n(t,\tau)\, d\tau \tag{I-193}$$

in (radicals/liter of latex).

Expression for the total rate of polymerization

Similarly, the total rate of polymerization in the vessl, $R_p(t)$, is given by:

$$R_p(t) = \int_0^t R_p(t,\tau)\, n(t,\tau)\, d\tau \tag{I-194}$$

Comments concerning the molecular weight development

(1) The predictions of the weight average molecular weight, $M_w(t)$, tend to go to infinity for some conversions, for reasonable degrees of branching (as conversion x(t) increases, then transfer to polymer begins to dominate the molecular weight development with respect to branching). Jackson et al. (1973) felt that this was due to outflow of large polymer radicals being neglected in the theoretical analysis. However, for polydispersities of 100 or less, their results indicated that the neglect of the outflow term should not introduce a large error in the numerical solution. The exponential increase in $\bar{M}_w(t)$ at high conversions is likely due to the formation of a few huge polymer molecules (formation of gel).

(2) Transfer reactions generally have activation energies larger then those for propagation reactions; their effect in reducing the average molecular weight of the

polymer will therefore become more pronounced as the temperature is raised. If allowance is made for transfer, the MW passes through a maximum as the temperature is raised. Below the temperature corresponding to this maximum, the MW falls because the kinetic chain length decreases as the temperature is reduced; above this temperature, the MW falls with increasing temperature because the increasing frequency of transfer reactions outweighs the effect due to the increase in the kinetic chain length. Burnett et al. (1955) demonstrated this effect in the case of VAc, the maximum MW being found for a polymer prepared at about 10°C.

Dynamic model assumptions

The assumptions made in the model development in Chapter 2 are summarized herein:

(1) Particle agglomeration (coalescence) is negligible.

(2) $S_p(t)$ and $A_d(t)$ are set equal to zero in the expression for $A_m(t)$.

(3) One polymer particle from a certain class $n(t,\tau)d\tau$ is representative of the whole class. M_p is the same in all classes, due to a very rapid diffusion of monomer from monomer droplets to polymer particles and to and from polymer particles of different age.

(4) The number of radicals that desorb from a certain class is equal to the number of radicals which enter the class. Also, the radicals that terminate in a class are the radicals which initiated the class. Furthermore, for the derivation of an expression for $q(t,\tau)$, it is assumed that instantaneous termination takes place when another radical enters a particle which already contains one radical. In other words, polymer particles contain either zero or one radical.

(5) During the derivation of an expression for $R_w(t)$, use is made of the collision theory or diffusion theory with a large surface resistance (equivalent to the collision theory)

and no distinction between oligomers of different chain lengths is made. No destruction of oligomers takes place with impurities (an accounting for impurity effects is implicitly taken with the induction time, since the velocity constant for reaction of oligomers with impurities is difficult to estimate). The stationary-state hypothesis for oligomeric radicals is applicable, no radical termination in the water phase is assumed and, finally, a negligible inflow and outflow of radicals from the reactor is considered. The reactivity of a macro-radical depends only on the identity of its terminal monomer unit. Effectively, all of the monomer is consumed by propagation reactions (long chain hypothesis).

(6) The amount of polymer produced in the water phase ($R_{p_{AQ}} \sim 0$) is negligible (vinyl acetate's moderate solubility is taken into account while calculating L, the critical diffusion length).

(7). Finally, the following assumptions are made for the molecular weight development:

(a) Termination reactions are insignificant in the production of polymer.

(b) The rate of transfer to monomer is much higher than the rate of radical initiation, therefore, effectively all radicals produced will have a terminal double-bond.

(c) No transfer to solvent occurs.

(d) $Y_{AVE}(t)$ and $\overline{Q}_1(t)$ are independent of τ and constant for all classes in any given volume, and

(e) All rate constants involved in the molecular weight development are independent of τ, i.e. independent of particle size.

APPENDIX II

General Computer Flowchart

A general computer program (DYNAVAC) has been written to handle the dynamics of emulsion polymerization reactors for the production of Case I monomers. The computer program is well documented. The documentation manual is rather long, therefore it was decided not to be included herein, but it is available from the McMaster Institute for Polymer Production Technology, Department of Chemical Engineering, McMaster University, Hamilton, Ontario, L8S 4L7, Technical Report #MIPPT-B-002.

APPENDIX III

Population Balance Numerical Calculation of Particle Size Distributions

In terms of total properties, the rate of change of the total number of particles in the emulsion mixture with time, is given by:

$$\frac{d N_p(t)}{dt} = \frac{N_{p_{IN}}(t) - N_p(t)}{\theta} + f(t) \qquad \text{(III-1)}$$

or

$$\frac{d N_p(t)}{dt} - \frac{N_{p_{IN}}(t) - N_p(t)}{\theta} = f(t) \qquad \text{(III-2)}$$

If one considers a single CSTR with no particle inflow, then equation (III-2) becomes:

$$\frac{d N_p(t)}{dt} + \frac{N_p(t)}{\theta} = f(t) \qquad \text{(III-3)}$$

Rewriting equation (III-3) for a "very small" time interval, Δt, one obtains the following difference equation:

$$\frac{\Delta N_p(t)}{\Delta t} + \frac{N_p(t)}{\theta} = \eta_o(t) \qquad \text{(III-4)}$$

where $n_o(t)$ denotes number of particles "born" during the time interval Δt. Δt is finite but considered "sufficiently small" and t_i, the midpoint of interval Δt, is the point when generation of a class of particles occurs.

Since

$$\frac{\Delta N_p(t)}{\Delta t} = \frac{N_p(t_i + \frac{\Delta t}{2}) - N_p(t_i - \frac{\Delta t}{2})}{\Delta t} \qquad \text{(III-5)}$$

equation (III-4) can be rewritten as:

$$\frac{N_p(t_i + \frac{\Delta t}{2}) - N_p(t_i - \frac{\Delta t}{2})}{\Delta t} + \frac{N_p(t_i)}{\theta} = \eta_o(t_i) \qquad \text{(III-6)}$$

Therefore,

$$\eta_o(t_i)\,\Delta t = N_p(t_i + \frac{\Delta t}{2}) - N_p(t_i - \frac{\Delta t}{2}) + \frac{N_p(t_i)\,\Delta t}{\theta} \qquad \text{(III-7)}$$

where $n_o(t_i)\,\Delta t$ denotes particles of a certain class born at time t_i.

Also,

$$n(t_f, t_i)\,\Delta t = \eta_o(t_i)\Delta t \exp\left(-(t_f - t_i)/\theta\right) \qquad \text{(III-8)}$$

where $n(t_f,t_i)\Delta t$ denotes number of particles at time t_f, which were born at time t_i. (III-8) is obtained by considering the decay rate in a CSTR.

Finally, the (number) frequency of the PSD is given by:

$$f(t, \tau) = \frac{n(t, \tau)\,d\tau}{\int_0^t n(t, \tau)\,d\tau} \qquad \text{(III-9)}$$

where $f(t,\tau)$ in the above expression denotes frequency of the PSD corresponding to the class $n(t,\tau)d\tau$. The denominator in equation (III-9) gives the total number of particles at time t in the reactor vessel.

When particle generation occurs only during certain periods of time and these periods of particle generation are sufficiently short, as in the case of an emulsion Case I system, one can make the assumption that only one class of particles is generated for each discrete period of particle nucleation. Therefore, equation (III-9) can be rewritten as:

$$f_i = \frac{n(t_f, t_i)\,\Delta t}{N_p(t_f)} \qquad \text{(III-10)}$$

f_i corresponds to the class of particles born at time t_i. The numerator in the above expression denotes number of particles of that certain class born at t_i, now at time t_f, and the denominator total number of particles at time t_f.

If one defines the normalized frequency distribution as:

$$F_i = F(d_{p_i}) = \frac{f_i}{\Delta(d_{p_i})}, \tag{III-11}$$

then

$$\sum_{t_i, i=1}^{t_f} F_i = 1. \tag{III-12}$$

An alternative approach for PSD calculations

Herein an alternative method for PSD determination will be developed. More details can be found in Hamielec (1976) and Poehlein (1979).

If E(t) denotes the exit age distribution (or residence time distribution) function for an ideal CSTR, then

$$E(t) = \frac{1}{\theta} \exp(-t/\theta) \tag{III-13}$$

If F(D) now is the normalized size distribution, where D is some diameter, then one obtains the identity:

$$F(D)\,dD = E(t)\,dt \tag{III-14}$$

or

$$F(D) = \frac{E(t)}{\left|\frac{dD}{dt}\right|} \tag{III-15}$$

where the denominator represents the absolute value of the rate of change of particle diameter with time.

But, from equation (2.32),

$$\left|\frac{dD}{dt}\right| = 2\lambda\xi(t) + \frac{\varepsilon(t)}{3} D \tag{III-16}$$

Therefore:

$$F(D) = \frac{(1/\theta)\exp(-t/\theta)}{2\lambda\,\xi(t) + \frac{\varepsilon(t)}{3} D} \tag{III-17}$$

Hamielec (1976) obtained the following expression by a similar approach:

$$F(D) = \frac{D}{K_1\theta} \exp\left(-\frac{D^2}{2K_1\theta}\right) \qquad \text{(III-18)}$$

with

$$K_1 = \left(\frac{2\,k_p M_p (MW)}{\pi N_A d_p}\right)\left(\frac{f k_d I_w(t) N_A}{N_p(t)\, k_{de}}\right)^{1/2}\left(\frac{\pi}{6}\right)^{1/3} \qquad \text{(III-19)}$$

K_1 is given in (dm^2/sec) and k_{de}' (in dm^2/sec) is a specific desorption rate constant which is only a function of temperature.

APPENDIX IV

Other PSD Measurement Methods

Some other techniques which could be used for latex particle size characterization are briefly discussed in this appendix.

Dynamic light scattering

Dynamic light scattering (DLS) is concerned not with the time-averaged intensity, as classical light scattering methods, but rather with the time behaviour of the fluctuations in the scattered intensity. The technique is also referred to as quasi- elastic light scattering or photon correlation spectroscopy.

When a colloidal dispersion is illuminated by a light source, the intensity of scattered light continuously fluctuates around its mean value due to the particle Brownian motion. The technique of DLS makes use of the fact that the time dependence of these intensity fluctuations can be related to the translational diffusion coefficient of the scatterers in the illuminated medium (Derderian and MacRury (1981), Horn (1984)).

The method should give reasonable results for narrow size distributions. For broad distributions, the technique is still at the evaluation stage (Stock and Ray (1984)).

For the DLS measurements, a NICOMP laser particle nanosizer - Model 200 was used (CIL Ltd., Toronto, Canada). The light source was a 632.8 nm laser and no shape of the size distribution was preassumed. The procedure, which is simple, involves the preparation of a dilute latex dispersion (roughly, a drop from the latex sample in 5 ml of a 0.1 molar solution of Aerosol OT in water), which is then illuminated by the laser beam. A precise concentration of the dilute dispersion is not required.

The particle size distribution for sample BR6-#5 (conversion ~ 53%) obtained by DLS can be found in Kourti et al. (1985). The obtained weight average diameter was 68 nm, as compared to 65 nm obtained from the specific turbidity method for the same sample. Note that the dilution problem which may affect turbidity measurements is also present in DLS methods.

Surface tension

Measurements of surface tension provide a way of establishing whether soap micelles are present or not. If the free soap concentration is above the CMC, then the surface tension will remain constant at its lowest value. If the soap concentration is below the CMC, the surface tension will be higher and depend on emulsifier level. In this way, surface tension measurements should in principle provide means to detect oscillations in the particle surface area in an emulsion system, and possibly provide an indication of the degree of soap coverage of the polymer particles.

Several methods of measuring surface tension exist. These are time consuming, are best applicable to "clean" systems, and are not easily adapted for use on-line. In the present study, a Digitec surface tension meter 500, an experimental apparatus developed by Madison Kipp Corporation, was used to record surface tension off- and on-line. It consisted of two glass tubes of different orifice sizes submerged to the same level in the sample to be tested, through which nitrogen bubbles were emitted with a constant frequency (maximum bubble pressure principle). A differential pressure measurement between the two bubbles formed, after being smoothed out by a filter, was translated into surface tension. The method was quick (approximately 30 seconds per sample for off-line measurements) and independent of the depth in which the two tubes were immersed in the sample.

The tensiometer was easily calibrated by tuning two potensiometers to give true readings for two (or more) substances of known surface tension (deionized water has a surface tension of 72.1 dyn/cm, 99.8% pure methanol 22.6 dyn/cm and a mixture of 25% methyl alcohol and 75% water 45 dyn/cm). 99+% pure heptane may also be used (19.7 dyn/cm) but it is very volatile and was therefore not used.

Soap titration

Particle size measurement of a latex or dispersion by soal titration is based on the hypothesis that the quantity of soap adsorbed at a selected end point is proportional to the interfacial area of a unit volume of particles. The end point is considered to be the CMC as determined by means of conductivity or surface tension measurements. The soap titration method yields a surface average diameter.

The method is rapid and can cover a range of diameters from 500 to 5000 Å. However, the amount of soap charged or in solution and the solids content must be accurately known, and the method is not applicable when more than one soap are present in the dispersion.

APPENDIX V

Procedure for Molecular Weight Determination by LALLSP

The determination of weight average molecular weight for a latex sample ($\bar{M}_w$) was done using LALLSP (Low Angle Laser Light Scattering Photometry) with a Chromatix KMX-6. The procedure consists of 4 basic steps: (a) preparation of solvent, (b) preparation of 4 to 5 solutions from each sample, (c) use of the KMX-6 to determine R_θ and (d) determination of $\bar{M}_w$. These four steps will be described in what follows:

(a) Preparation of solvent: Ethyl Acetate (EAc, ACS Reagent Grade, Fisher or Caledon Labs Ltd.) was used to dissolve the dry polymer (PVAc). Tetrahydrofuran (THF) was not used because it appeared very noisy in the LALLSP. The choice of solvent should be based on the fact that solvent and polymer should have a large difference in refractive indices.

(b) Preparation of solutions from each sample: Coagulate the polymer (from 1 or 2 ml of latex) using methanol. Put the polymer into a small dish and wash it with deionized water. Leave it in deonized water for ~ ½ hour and then, place the dish with the washed polymer into a vacuum oven for ~ 24 hours (~ 35 to 40° C). Weigh the dry, clean polymer and dissolve it in EAc. Prepare a solution of ~ 0.5% by wt. PVAc in EAc (i.e. dissolve ~ 0.5 gr of dry clean polymer in 100 ml EAc). To make sure that the polymer is completely dissolved in EAc, leave the dry polymer in EAc for 24 hours. Call this solution S1.

S1: $(.5)(10^{-2})$ gr of dry polymer/cm^3 of solution

Prepare now S2:

20 ml S1 + 5 ml solvent = 25 ml S2

$$\frac{(0.5)(10^{-2}) \times 20}{25} = (0.4)(10^{-2})\ gr/cm^3$$

S3: 20 ml S1 + 15 ml solvent = 35 ml S3

$$\frac{(0.5)(10^{-2}) \times 20}{35} = (0.2857)(10^{-2})\ gr/cm^3$$

S4: 15(S1) + 20(EAc) = 35 ml S4

$$\frac{(0.5)(10^{-2}) \times 15}{35} = (0.2143)(10^{-2})\ gr/cm^3$$

and

S5: 10(S1) + 40(EAc) = 50 ml S5

$$\frac{(0.5)(10^{-2}) \times 10}{50} = (0.1)(10^{-2})\ gr/cm^3$$

Store these solutions in 50 ml (KIMAX) flasks..

Notes: (i) The reason that EAc was chosen for LALLSP was that, besides being a solvent for PVAc, its refractive index increment dn/dc was relatively large and known for the helium-neon laser wavelength. If this were not true, then the laser refractometer KMX-16 would be used to measure dn/dc. dn/dc of a polymer solution is largely independent of molecular weight and remains constant in the working range of concentrations. The literature value for EAc/PVAc dn/dc is 0.077 (Brandrup and Immergut (1975)) and the experimental value for THF/PVAc dn/dc, which was obtained from the KMX-16 is 0.0556.

(ii) Toluene should be occasionally used to check the performance of the KMX-6. The R_θ for toluene is close to 14×10^{-6}. If an R_θ larger than 15.5×10^{-6} is found, this is an indication that the instrument's cell is dirty and requires cleaning.

(iii) For molecular weights higher than 10^6, S1 should be a 0.15% by wt. solution. An "optimum" range of concentrations for the solutions was found to be between 15×10^{-4} gr/cm^3 and 1 or 3×10^{-4} gr/cm^3.

(c) Use of the KMX-6 to determine R_θ: The objective now is to measure the intensity of both the scattered and incident light for each solution with the KMX-6 (a schematic diagram of which is given in Figure V-1). The idea behind it follows: Having these two measurements for each solution and the corresponding values for the solvent, one can subtract the contribution of the solvent in estimating R_θ. The dependence of $\bar{M}_w$ on R_θ is shown in Figure V-2.

The procedure is as follows:

(1) Open laser compartment. Use switch no. 8 (see Figure V-1). In the laser compartment there is the laser cell. Change filter and put one 0.2 μm pore size FG type filter. Change filter every 2 to 3 solutions (or, when considerable backpressure is developed in the syringe, i.e. if the syringe can not pump the solution through). Rinse the injection syringe with solvent and make sure that there are no air bubbles in it. Then, place the syringe on the syringe pump and start injecting solvent through the cell. Switch a in Figure V-1 (green light indicator) indicates that power is on, if β (i.e. mode indicator) is on INFUSE then fluid flows through the laser cell, γ adjusts the flow rate and δ and ε have to do with the syringe size. Try to make sure that there are no air bubbles in the laser cell, set β on INFUSE, see if there is any fluid coming out in the waste flask, adjust γ to 0.3 ml/min and inspect the cell. Put the laser beam on. If the cell is not coloured, then there are no air bubbles. The field stop (no. 12) should indicate 1.5 during this introductory step. Let the solvent flow through the cell for a couple of minutes and close the laser compartment.

(2) Try to focus the beam. Use no. 4 (move clockwise) and nos. 5 and 7. The objective is to get an external circle, as thinner and brighter as possible, and place the laser beam in the center of the external circle. Use no. 13 (down) and no. 14 to inspect the beam.

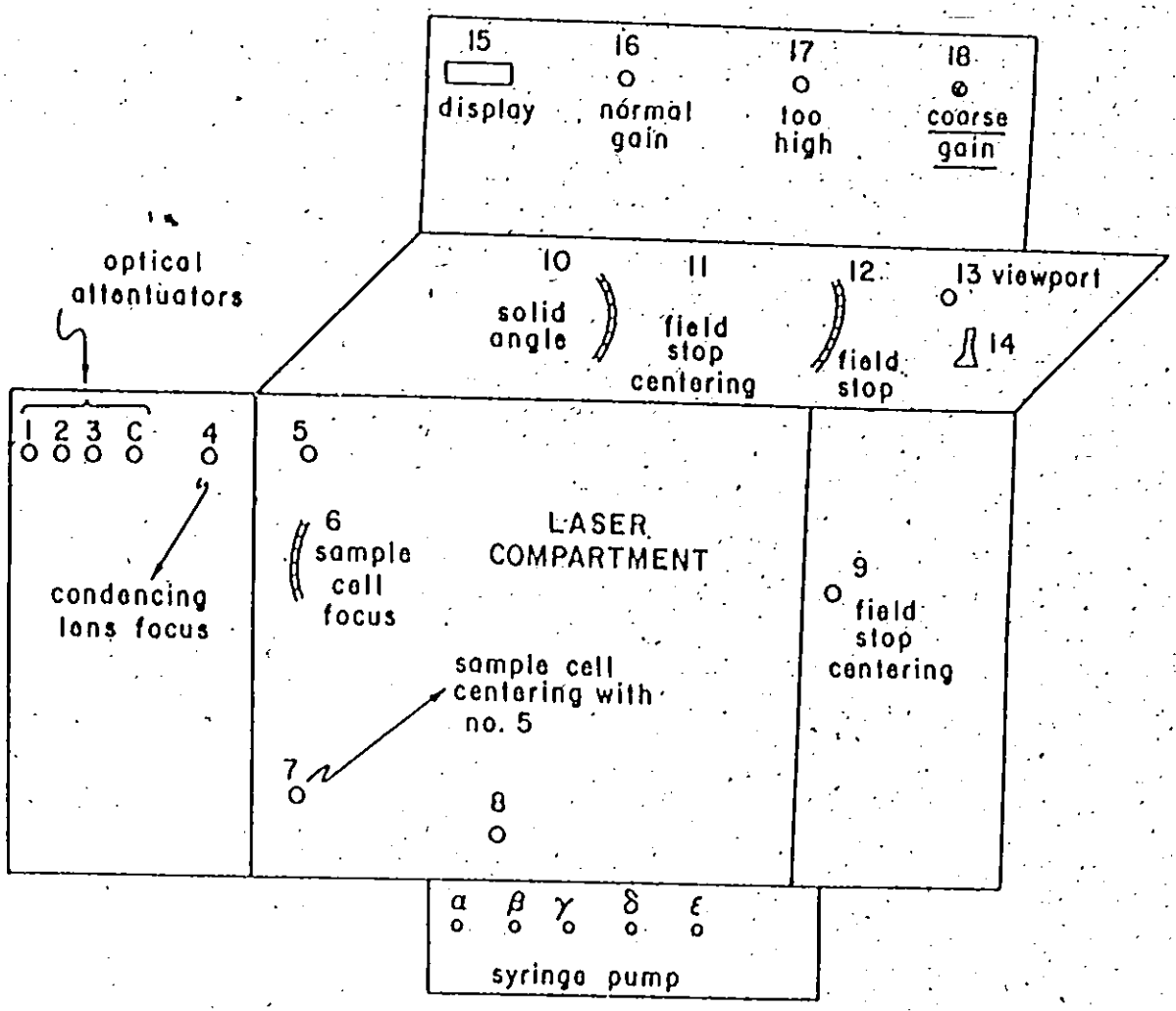

Figure (V-1). Schematic Diagram of the KMX-6 LALLSP

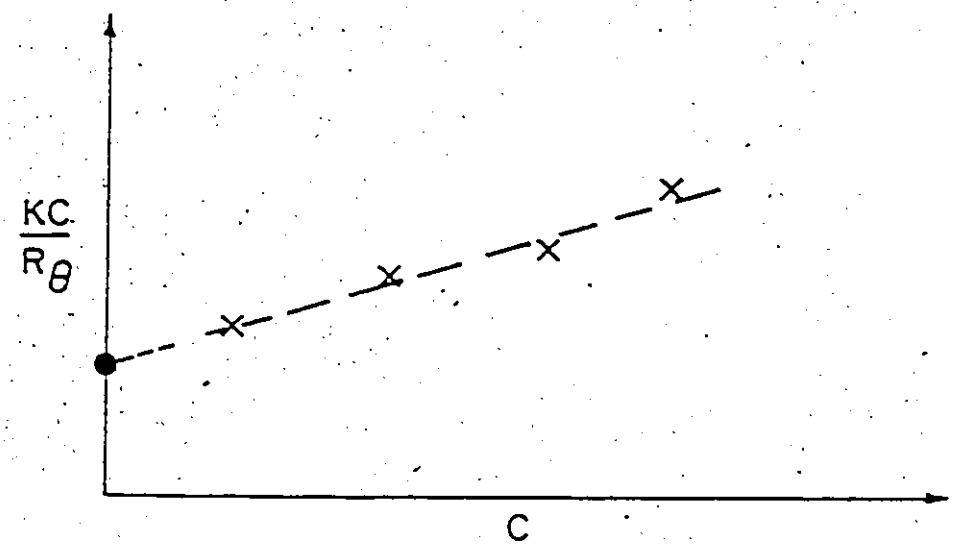

$$\frac{KC}{R_\theta} = \frac{1}{\overline{M}_w} + 2A_2C$$

C in gr/cm^3

Figure (V-2) $\bar{M}_w$-R_θ Relationship

Use also nos. 6, 9 and 11 for the above purpose.

(3) Set no. 12 to 0.2 and no. 10 to 6–7. Now, one is ready for a measurement. Set no. 13 to the upward position and close no. 14 (i.e. optical path is now closed).

In a few words: Use 1.5 and 3–7, attenuators out, and nos. 4, 5, 6 and 7 to inspect the cell. A field stop of 1.5 tells one how clean the cell is. Then, use 0.2 and 6–7 (or 0.2 and P_o) with nos. 9 and 11 to centre the beam.

(4) Measure G_θ: All attenuators (nos. 1,2,3) out and increase the coarse gain (no. 18) to get a number on the display (no. 15) between 900–1000, if possible. The chart recorder should respond accordingly.

Measure G_o: Attenuators 1, 2 and 3 in. No. 10 should indicate P_o and no. 12 should be in 1.5. Adjust the attenuators to get a reading higher than 250. Note which attenuators were used. Remember that attenuator 4 is always in and that if C is in, then no light passes through the cell. Attenuator C should always be out during a measurement. G_o should be very stable on the recorder chart..

(d) Determination of $\bar{M}_w$: While measuring G_θ, leave the recorder pen on for almost 2 to 3 inches on the graph paper. To get a numerical value for G_θ use the lower envelope of the signal obtained. The recorder's paper is already calibrated between 0 and 1000 (numbers corresponding to the KMX–6 display, no. 15).

The calculation procedure is as follows:

$$R_{\theta_{polymer}} = R_{\theta_{solution}} - R_{\theta_{solvent}} \qquad (V\text{-}1)$$

$$R_\theta = \frac{G_\theta}{G_o} \cdot (\sigma'\lambda')^{-1} \cdot D \qquad (V\text{-}2)$$

$(\sigma'\lambda')^{-1}$ is a function of the solid angle (no. 10), field stop (no. 12) and the refractive index.

D is a function of the attenuating filters.

Measure G_θ and G_o for each solution and write down the attenuators that were used in. Start with S5 and go to S1, i.e. for every sample record:

EAc	G_θ	G_o	attenuators in
S5	>>	>>	>>
.	.	.	.
.	.	.	.
.	.	.	.
S1	>>	>>	>>

Check for reproducibility by repeating the measurements for the solvent between samples.

Determination of D:

$$D = \prod_{i=1}^{4} (att)_i \qquad (V\text{-}3)$$

where: $(att)_1 = 0.248$

$(att)_2 = (6.448) \times 10^{-2}$

$(att)_3 = (4.077) \times 10^{-3}$

$(att)_4 = (1.6367) \times 10^{-5}$

If an attenuator is not used in, then $(att)_i = 1$. Remember that attenuator 4 is always considered in.

If, for instance, during a measurement, attenuators 2 and 3 were used in, then:

$$D = 1 \times (att)_2 \times (att)_3 \times (att)_4$$

$$= (4.3026) \times 10^{-9}$$

Determination of $(\sigma'\lambda')^{-1}$:

From tables of the KMX-6 operator's manual one obtains for a solid angle 6-7 and a field stop 0.2, for a

refractive index	$(\sigma'\lambda')^{-1}$
1.37	$(6.518) \times 10^2$
1.38	$(6.566) \times 10^2$

The refractive index for PVAc is $\eta_D = 1.3724$. Therefore, by linear interpolation:

$$(\sigma'\lambda')^{-1} = (6.52952)(10^2)$$

for

$$\eta_D = 1.3724$$

Going now back to Figure V-2 and using C expressed in gr of polymer per cm^3 of solution (gr/cm^3), one obtains:

$$\frac{KC}{R_\theta} = \frac{1}{M_w} + 2A_2C \qquad (V\text{-}4)$$

In equation (V-4), C and R_θ are known. One still needs to calculate the extinction coefficient, K.

Determination of K:

The extinction coeffient K is generally given by:

$$K = 2\pi^2 \eta_D^2 \left(\frac{d\eta}{dc}\right)^2 (1 + \cos^2\theta')/\lambda^4 N_A \qquad (V\text{-}5)$$

For a 6-7° annulus, $\cos^2\theta' = 0.99$, i.e. close to unity, therefore, the expression for K becomes:

$$K = (408.0) \times 10^{-8} \times \eta_D^2 \times \left(\frac{d\eta}{dc}\right)^2 \qquad (V\text{-}6)$$

$\eta_D = 1.3724$ and

$$\left(\frac{d\eta}{dc}\right) = 0.077$$

Therefore, $K = (4.5562) \times 10^{-8}$

At this stage, one knows everything needed to calculate the molecular weight of the sample.

Note:

(i) The base line on the chart recorder of the KMX-6 (paper #EC-144) is sometimes drifting between 10 and 30. To get the base line for each measurement use zero coarse gain, 6–7 and 0.2 and the viewpoint to the "up" position. Then, correct for this base line drift as follows:

$$R_\theta = \left(\frac{G_o - b\ell}{G_o - b\ell}\right) \cdot (\sigma' \lambda')^{-1} \cdot D, \qquad (V\text{-}7)$$

where $b\ell$ denotes the reading for the base line.

(ii) The R_θ that has been measured for EAc during this experimental study was 4.5935951×10^{-6} (i.e. $\sim 4.594 \times 10^{-6}$). Battacharya (1985) in a parallel study with bulk PVAc measured an R_θ for EAc equal to $\sim 4.597 \times 10^{-6}$, which independently confirmed and verified our measurements.

(iii) The specific refractive index increment dn/dc, if not known from the literature, it can be measured with the laser differential refractometer (LDR) KMX-16 at the same wavelength λ, at which the KMX-6 operates.

APPENDIX VI

Model Parameter Values

Numerical values of model constants and kinetic rate expressions which are cited in Tables 4-1 and 4-2 are further discussed in this appendix. These numerical values and expressions were employed in the computer program which handled the simulations of emulsion VAc systems. The parameters are discussed in alphabetical order.

Initial particle surface area, $a_p(t,t)$

The initial polymer particle area (i.e. area upon formation at time zero), $a_p(t,t)$, is given by the formula that represents the surface area of a sphere of diameter $d_p(t,t)$. In other words, all particles are initially assumed to be of a spherical shape and $a_p(t,t) = \pi \times d_p^2(t,t)$.

Monomer density, d_M

The VAc monomer density was taken equal to 930.0 gr/lit, an average of the two values which are reported in Brandrup and Immergut (1975) for the temperature range 25-50°C.

Polymer density, d_p

Brandrup and Immergut (1975) report the following values for the pure poly (vinyl acetate) density: 1191.0 gr/lit at 20°C, 1190.0 at 25°C, 1170.0 at 50°C and 1110.0 gr/lit at 120°C. An average density of 1150.0 gr/lit was used in the model.

Initial particle diameter, $d_p(t,t)$

The initial polymer particle diameter, $d_p(t,t)$, used in the nucleation term of equation (2.14), is assumed to be equal to the diameter of a micelle. A typical diameter for micelles ranges between 50 and 100 Ångstroms. $d_p(t,t)$ was chosen equal to 50 Å, or $50. \times 10^{-9}$ dm.

Efficiency factor for initiator decomposition, f, and initiator decomposition rate constant, k_d

In aqueous solutions, potassium persulphate initiator (KPS) is believed to thermally decompose by the following steps:

$$S_2O_8^{-2} \rightarrow 2\,SO_4^{-\cdot} \qquad \text{(VI-1)}$$

$$2\,SO_4^{-\cdot} + 2H_2O \rightarrow 2\,HSO_4^{-} + 2\,HO\cdot \qquad \text{(VI-2)}$$

$$2\,HO\cdot \rightarrow H_2O + \tfrac{1}{2}\,O_2 \qquad \text{(VI-3)}$$

Step (VI-1) is a symmetrical scission of the O-O bond to form two sulphate ion radicals and is the rate determining step of the decomposition (Kolthoff and Miller (1951)). The activation energy for reaction (VI-1) was found by Kolthoff and Miller (1951) to be ~ 33.5 kcal/gmole.

Kolthoff and Miller (1951) found that the first order rate constant of decomposition for KPS is $\sim 3.0 \times 10^{-4}$ min^{-1} at 60°C in a neutral aqueous medium. Decomposition is more rapid at low pH and is believed to be the result of induced decomposition by hydrogen ions. Also, decomposition is accelerated by many water soluble or partially soluble organic compounds such as methanol and ethanol (Kolthoff et al. (1953)), which cause a large increase in rate.

Patsiga (1962) followed the decomposition of KPS in an aqueous 0.67% sodium lauryl sulphate (SLS) solution at 60°C. He found that the first order rate constant was $\sim 5.07 \times 10^{-4}$ min^{-1}, which is slightly higher than the value obtained by Kolthoff and Miller (1951).

This is reasonable since in Patsiga's work (1962) soap was present in the solution while Kolthoff and Miller (1951) were looking at the neutral aqueous medium.

Patsiga (1962) also found that the KPS decomposition rate was ten times more rapid in the presence of VAc than with soap alone or in styrene emulsion polymerization (see also Kolthoff et al. (1955)). It seems that the KPS decomposition is a function of conversion and other standard variables in an emulsion system, such as organic volume, initiator concentration and particle number.

Litt and Chang (1981a) undertook a study to investigate the effect of the above mentioned variables on the decomposition of KPS. They measured the initiator concentration as polymerization proceeded and they found that the rate of induced decomposition of KPS was dependent on the number of particles to the 0.11 power and the volume of the organic phase per unit volume of aqueous phase to the -0.64 power. These dependencies agreed very well with those predicted by their theory.

The rate constant for induced decomposition of initiator by monomeric radicals calculated by Litt and Chang (1981a) was found to be $\sim 2.1 \times 10^7$ lit/gmole-sec. The high rate constant shows diffusion control of the reaction and implies that the reaction of persulphate with monomeric radicals in the aqueous phase (in other words, a monomeric radical that is in the aqueous phase after desorption from a polymer particle may attack persulphate to generate sulphate and an ion radical $SO_4^{-\cdot}$) proceeds through an electron transfer mechanism.

In a similar study, Morris and Parts (1968) were concerned with the influence of various soaps and monomers on the rate of thermal decomposition of KPS. They found that the presence of sodium lauryl sulphate combined with the presence of VAc caused a marked increase in the rate of KPS disappearance, compared with the values found by Kolthoff and Miller (1951). Their conclusions were that as long as there was soap present in the solution

the rate of disappearance of KPS was increased, being though independent of the concentration of the soap. The dependence of the KPS decomposition on the monomer concentration was obscure.

From the above discussion, it is obvious that in numerical calculations on decomposition rates, the assumption that the rate of production of radicals in the system is given by the rate of thermal decomposition of KPS in water may be seriously in error. We have chosen to follow the results found by Morris and Parts (1968) for the decomposition rate constant of potassium persulphate, which were also successfully used by Nomua et al. (1971) and Nomura and Harada (1981). The expression for k_d is given in Table 5-1 and is the same as the one also employed by Shawki (1978) and Kim (1983). Kim (1983) also suggested an expression for the initiator efficiency factor, as:

$$f = 5.87 \times 10^{-3} (M)^{-0.5} \exp\left(\frac{3530}{RT}\right), \qquad \text{(VI-4)}$$

where M denotes monomer concentration. The above expression for f gives reasonable values for the initiator efficiency for typical values of monomer concentration. Factor f in the model was set equal to a typical value of 0.7.

More details concerning the modelling of the initiation reactions in a polymerization system and more specifically, of the factor fk_d, could be found in a very recent illustrative paper by Mehta and Garcia-Rubio (1985).

Rate constants k_p, k_{fm}, k_{fp} and k_p^*

All the expressions for the above rate constants were obtained from the sources cited in Table 4-1 by fitting conversion and molecular weight versus time data. They are in agreement with expressions or values independently estimated and suggested by Bamford et al. (1958), Bevington (1961) and Chang et al. (1981).

Friis et al. (1974) and Hamielec and MacGregor (1982) have also used an expression for k_p^* which corrects for diffusion-controlled polymerization with terminal double bonds:

$$k_p^* = (k_p^*)_o - (169.6\, W_p + 479.9\, W_p^2 + 1014.0\, W_p^3) \qquad \text{(VI-5)}$$

where W_p is the weight fraction of polymer in polymer particles.

Critical oligomeric radical diffusion length, L

Under conditions where the monomer has an appreciable (or moderate) solubility in the liquid medium and where the stabilizer is either absent or present in amounts far below its critical micelle concentration, the system is initially homogeneous. In such cases initiation and the first stages of chain propagation take place in solution (Fitch (1965)). Chain growth continues in solution until a high degree of "supersaturation" has been reached at which point "homogeneous self-nucleation" is believed to occur (Fitch and Tsai (1971a)). The average degree of polymerization which a growing chain may reach before precipitating out is thus an important factor in determining the rate at which particles are nucleated and consequently the ultimate particle concentration. This also determines the average distance an oligomeric chain radical in solution diffuses before it precipitates out. If, of course, the oligomer is captured by a pre-existing particle prior to its precipitating out, no new particle is formed. Obviously then, the greater the distance travelled in solution, the greater the probability of capture by particles, and therefore the slower the rate of particle formation, and, as it turns out, the smaller the final number of particles will be (Fitch and Tsai (1971a)).

If the maximum degree of polymerization of a growing radical chain is known, then from the time required to polymerize to this chain length and from the Fickian diffusion coefficient, it is possible to calculate the distance, L, a growing oligomer will diffuse before it

precipitates out to form a primary particle (Fitch and Tsai (1971b)). This is required in order to calculate the particle formation rate and final number of particles (see Chapter 2).

According to Fitch and Tsai (1971b), Einstein's diffusion law relates the average distance travelled in Brownian motion, L, to time by means of the Fickian diffusion coefficient, D_w (in this case an average value, since the oligomeric radical is continuously growing). This relationship becomes:

$$L = \left(2\, D_w \cdot \frac{DP_{max}}{k_p M_{wc}} \right)^{1/2} \qquad \text{(VI-6)}$$

Fitch and Tsai (1971b) experimentally estimated values of L for the methyl methacrylate case. The oligomers were prepared by telomerizations and characterized by viscometry, infrared spectroscopy and gel permeation chromatography. The estimated value of L for the MMA case was $\sim 2.8 \times 10^{-4}$ dm. The value of L will of course depend on the monomer concentration M_{wc}.

For other monomers, different values of L can be expected because of different solubilities of the oligomeric radicals, which affect DP_{max}, and different values for propagation rate constants, k_p. For instance, styrene should have a lower value for DP_{max} and roughly the same value for k_p, compared to MMA. Therefore, it will have a smaller value of L. Vinyl acetate, on the other hand, would have a greater solubility than MMA and therefore a larger DP_{max} (the DP_{max} of a growing MMA chain with a sulphate or sulphonate end-group in aqueous solution was estimated (Fitch and Tsai (1971b)) to be in the order of 65 to 75 units). However, VAc has a k_p which is roughly five times as large as that for MMA, which, according to equation (VI-6), would reduce L.

Water soluble chain transfer agents would be expected to have some effect on the DP_{max} of the oligomeric radicals. Their presence would effectively change the nature of end-groups on the radical, markedly reducing solubility and thus DP_{max}.

The value of D_w that has been usually employed is a time averaged value. The oligomeric radicals involved grow from monomeric species to much larger ones, with a concomitant decrease in the Fickian diffusion coefficient with time. However, since L should be a constant average value in the model equations, its time dependence is not involved.

Using equation (VI-6), one could substitute values for the VAc case and calculate an average L for 50°C. k_p can be taken from Table 4-1 for 50°C and D_w can be set equal to 0.1017×10^{-6} dm²/sec. Considering the solubility of VAc in water to be ~ 2.1% by weight (Friis and Hamielec (1976)), M_{wc} is estimated to be ~ 0.25 gmole/lit. Then, using a DP_{max} of ~ 25 units, L becomes equal to ~ 8.0×10^{-5} dm. This value is the same as that which Fitch and Tsai (1971a, 1971b), Litt et al. (1970) and Promojaney (1982) have used. The latter used a DP_{max} of 200, but considered a ~ 4.0% by wt solubility and used a D_w equal to 10^{-8} dm²/sec.

Partition coefficient of monomeric radicals, m

The partition coefficient of monomeric radicals between the polymer particle and water phase, m, was defined in Appendix I in equations (I-89) and (I-90), according to Nomura et al. (1971), Harada et al. (1971) and Nomura and Harada (1981). The value that was employed by them, as well as by Pramojaney (1982), was ~ 28.0.

Dunn (1980) suggested that monomer (VAc) is partitioned between the two phases (monomer and water) according to the following relationship:

$$(M_p) = 13.7\,(M_w)^2 \qquad \text{(VI-7)}$$

where (M_p) and (M_w) are the monomer concentrations by weight in the polymer and water phases respectively. The form of this relation has been confirmed independently (Dunn and Taylor (1965), Napper and Parts (1962)). It arises because the miscibility of VAc with water is limited whereas VAc and poly (VAc) are miscible in all proportions, and consequently the

activity of the monomer increases much more rapidly than its concentration in the aqueous phase.

Considering a constant m during the reaction, given by:

$$m = \frac{M_p \text{ at } x(t) = x_c}{M_w \text{ at } x(t) = x_c} \qquad \text{(VI-8)}$$

and estimating M_p from equation (I-76), the value of m that we obtained for $M_w = 0.33$ gmole/lit (i.e. solubility of VAc at 50°C ~2.8% by weight, see Nomura et al. (1971)) was ~27.1.

Molecular weights of monomer, initiator and soap, MW, MWI, MWS

These were taken from Brandrup and Immergut (1975), i.e. the Polymer Handbook, as: MW = 86.09, MWI = 270.0 and MWS = 288.38 gr/gmole, respectively.

Critical micelle concentration, S_{CMC}

Micellization has been treated either as a stepwise association phenomenon or as a phase transition process (Shinoda et al. (1963)). In the first approach the micellar aggregates and the single molecules of surfactant are assumed to be in association-dissociation equilibrium and the law of mass action is applied. The critical micelle concentration (S_{CMC}) is defined as the concentration above which any added surfactant molecules appear with high probability as micellar aggregates. In the latter approach, micellization is regarded as a phase separation starting at CMC which now represents the saturation concentration of the phase containing single molecules of surfactant. Although both approaches can explain some features of the micelle formation, the available experimental evidence seems to be in agreement with the first of these. In the region close to the CMC, the physico-chemical properties do indeed change rapidly, but continuously, and the concentration of the single surfactant molecules increases slowly. The addition of surfactant above the CMC not only leads to an

increase in the number of aggregates but also gives rise to larger average sizes of the aggregates. It is therefore reasonable (Ruckenstein and Nagarajan (1975)) to assume that for all concentrations of surfactant there are micellar aggregates of various sizes. At low concentrations, however, the number and size of these aggregates is small. As the concentration increases, both the number and the average size of the aggregates increase. The particular kind of behaviour occurring at CMC is caused by an essential change in the shape of the size distribution of the aggregates; above the CMC the participation of the larger sizes is more important.

Ruckenstein and Nagarajan (1975), using a thermodynamic formulation and expressions for the chemical potential suggested by Tanford (1973, 1974), showed that at low concentrations of surfactant the size distribution of the aggregates is a monotonically decreasing function of their size. As the concentration increases, the size distribution of the aggregates changes from a monotonically decreasing function to one which has two extrema, a minimum and a maximum. They derived the following expression for the critical concentration:

$$C_{crit} = \xi_{crit} \exp\left(\frac{\mu_B - \mu_A}{kT} \right) + \int_2^\infty g\, \xi_{crit}^g \exp\left(- \frac{\mu_g}{kT} \right) dg \qquad \text{(VI-9)}$$

where μ_A denotes the standard chemical potential of a single molecule of amphiphile in the aqueous medium, μ_B the size-independent part of the standard chemical potential for a single amphiphile, μ_g the size-dependent part of the standard chemical potential for an aggregate of size g, k is the Boltzmann constant, T the absolute temperature and ξ is defined as:

$$\xi = \left(\frac{N_A}{F} \right) \exp\left(\frac{\mu_A - \mu_B}{kT} \right) \qquad \text{(VI-10)}$$

N_A in equation (VI-10) represents the number of molecules of the amphiphile and

$$F = N_S - N_A - \sum_{g=2}^{\infty} N_g \qquad \text{(VI-11)}$$

with N_S denoting the number of molecules of the solvent and N_g the number of aggregates containing g molecules each.

However, no matter how rigorous all the thermodynamic considerations are, there is still some uncertainty about the S_{CMC} of the emulsifiers typically employed in an emulsion system. The published values of S_{CMC} for sodium lauryl (dodecyl) sulphate (SLS) are found to vary between 0.001 and 0.009 molar depending not only on the method of determination, e.g. surface tension or conductance measurements, but also on the purity and source of the samples (Vijayendran (1977)). Furthermore, S_{CMC} for an ionic surfactant is known to decrease with the number of methylene groups in the hydrophobic portion of the surfactant molecule, and the ionic strength of the solution (Shinoda and Becker (1978)). Nevertheless, it is still not clear exactly how S_{CMC} would change during emulsion polymerization where particles and micelles are present. While most investigators assumed a fixed value for S_{CMC} in the range 0.003 - 0.005 molar, the following expression can be used to account for the ionic strength effect (Blackley (1975), Corrin and Harkins (1947)):

$$\log_{10} S_{CMC} = -0.45774 \log_{10}\left(\sum_{i=1}^{N} Z_i C_i \right) - 3.2485 \qquad \text{(VI-12)}$$

where Z_i and C_i are the ionic charge and molal concentration of the i-th ionic species in the aqueous phase.

For reference reasons, we report here the tabulated values for the S_{CMC} of SLS from Brandrup and Immergut (1975):

Temperature	S_{CMC}	
25 - 60°C	9.0×10^{-3}	gmoles/lit
20°C	6.3×10^{-3}	
40°C	6.7×10^{-3}	
60°C	7.9×10^{-3}	
75°C	9.5×10^{-3}	

The value of S_{CMC} that we used in all our simulations was actually determined experimentally using a Digitec surface tension meter 500, based on the maximum bubble pressure technique, and specially pure SLS from BDH Chemicals. This value was determined using solutions of SLS in water-VAc mixtures and found to be $\sim 3.2 \times 10^{-3}$ gmole/lit, surprisingly close to the value of 3.1×10^{-3} that was employed by Morbidelli et al. (1983).

Area coverage by an emulsifier molecule, S_a

In an aqueous solution, the driving force for the adsorption of a surfactant molecule such as SLS at the monomer/water or polymer/water interface is the favourable free energy change associated with the transfer of the hydrocarbon portion of the surfactant molecule from the aqueous phase to the interface. The free energy change for such a process will depend on the nature of the surfactant and the organic phase (monomer or polymer). If one is concerned with the adsorption characteristics of a given surfactant at various interfaces, then one can make the reasonable assumption that the observed differences in the adsorption characteristics of the chosen surfactant at various interfaces are due to the differences in the energy of interaction of the surfactant molecule with the surface in question. Surfactant adsorption at various interfaces is adequately described by Langmuir type adsorption isotherms (Paxton (1969), Adamson (1967)).

Vijayendran (1971), in an interesting study on the adsorption of SLS at latex/water interfaces, observed the following:

(i) The area occupied by a surfactant molecule on a polymer surface decreases logarithmically with increasing interfacial tension of the polymer/water interface. Further, the logarithm of the area per molecule of surfactant at saturation adsorption increases with the polarity of the polymer surface (since, water solubility of organic liquids, which is a rough measure of polarity, is inversely related to the respective interfacial tension).

(ii) The area per molecule of SLS at various interfaces increases with the mole fraction of monomer in water and depends strongly on the nature of the polymer surface. The molecular areas of a homologous series of soaps, in which the hydrocarbon chain varied from C_{12} to C_{17}, decreased regularly from 0.41 nm^2 to 0.23 nm^2 as the length of the hydrocarbon chain increased. This result can readily be explained by the increase in the energy of adsorption of the soap molecules due to increased hydrophobic interactions as the chain length of hydrocarbon increases.

(iii) The increase in the area per molecule of surfactant on the more polar polymers results in diminished stability against flocculation of primary particles due to decreased surfactant adsorption under saturation conditions. It is therefore reasonable to expect that the stabilizing action of a surfactant will diminish with increase in the polarity of the interface. However, the increased polarity of the monomer may favour self-stabilization due to orientation of the polar groups of the polymer at the water interface.

In another interesting study on the role of micellar equilibria, Morbidelli et al. (1983) argued that the common assumption in previously proposed models that the area occupied by an emulsifier molecule present in a micelle and the area occupied by an emulsifier molecule on the polymer surface are equal and independent of the emulsifier concentration, is a rather poor approximation. In fact, a reliable value of the area coverage in a

micelle can be only obtained through an analysis of the micelles formation equilibria, by taking into account also the effect of the solution ionic strength.

Morbidelli et al. (1983) concluded that two contributions have to be taken into account during micellar formation equilibria: the interaction energy between the micellar hydrophobic core and water, which tends to decrease the aggregate size; and the interaction energy between the head groups of the emulsifier molecules present in the aggregate, which tends to increase its size. The conflict between these two effects determines the equilibrium volume of the micellar aggregates.

The nucleation stage of a Case I system is dominated by a very high concentration of radicals in the water phase caused by the high rate of desorption of radicals from the particles. This results in short nucleation periods and a dramatic increase in the rate of polymerization. From the two parameters in the nucleation part of the model (S_a and ϵ), ϵ has the largest effect on the model predictions. Rewriting the expression for $A_m(t)$ according to Morbidelli et al. (1983), one would obtain:

$$A_m(t) = \left((S_T(t) - S_{CMC})\, a_{sp} - A_p(t) \right) \frac{a_{sm}}{a_{sp}} \qquad \text{(VI-13)}$$

where a_{sp} is identical to S_a and a_{sm} is the area occupied by an emulsifier molecule present in a micelle.

Then, using the conditions of run BR10 and $\epsilon = 0.7839 \times 10^3$, $D_w = 0.1017 \times 10^{-6}$ dm^2/sec and $(a_{sm}/a_{sp}) = 1$ as the base case, we obtained the results shown in Figure VI-1, by varying the ratio (a_{sm}/a_{sp}). One can see from the results of Figure VI-1 that the model predictions for both conversion and number of particles are sensitive to ϵ, but not to (a_{sm}/a_{sp}). In other words, the assumption $a_{sm} = a_{sp}$ seems valid for a Case I system. It is postulated that a large proportion of radicals are in close proximity to the particles due to the large amount of

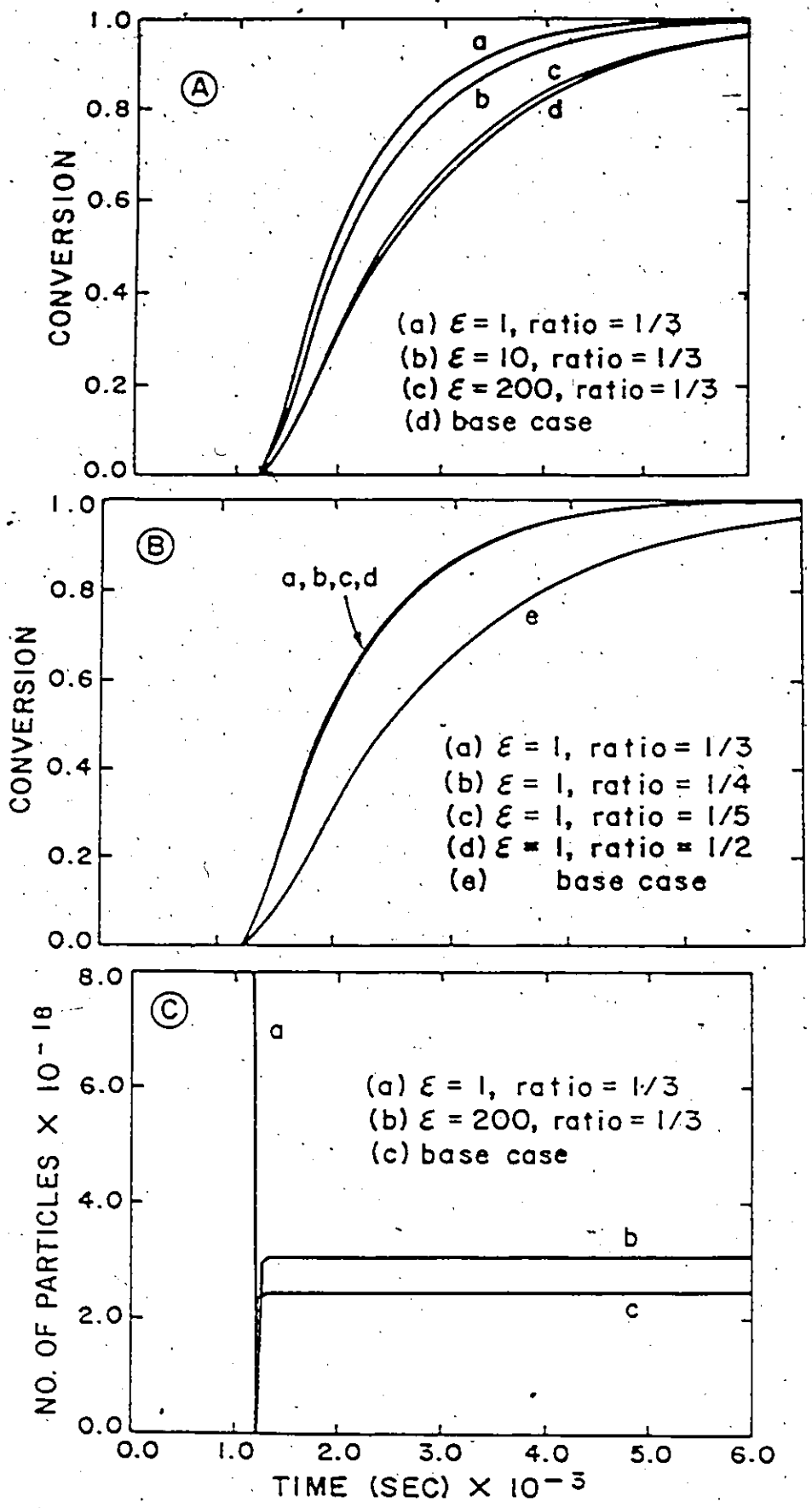

Figure(VI-1). Effect of the Ratio(a_{sm}/a_{sp}) on Conversion and Number of Particles

desorption, thereby making the efficiency of radical capture by particles even larger than it was proposed by Nomura et al. (1972) for a Case II system. For this reason, although both ε and S_a affect particle nucleation, the effect of ε is dominant.

Pramojaney (1982) found that a value of 40-50 x 10^{-16} cm^2/molecule for S_a on the poly (VAc) latex particles tended to give consistently more reasonable results than a value of 110 x 10^{-16} estimated in the literature (Vijayendran (1971, 1979) and Yeliseyeva and Zuikov (1976)). Brandrup and Immergut (1975) report three values for S_a: 49, 52 and 53.4 x 10^{-16} cm^2/molecule, respectively. Broadhead (1984) used ~ 6.0 x 10^{-17} dm^2/molecule for his emulsion SBR simulations and Hoffman (1984) ~ 8.0 x 10^{-17} dm^2/molecule for styrene/-acrylonitrile (SAN) copolymerization reactors. Morbidelli et al. (1983) reported ~ 5.0 x 10^{-17} dm^2/molecule coverage on a latex particle of polystyrene, a value which drops down to ~ 1.0 x 10^{-17} for area occupied in a micelle. The value that we employed in our simulations is 5.0 x 10^{-17} dm^2/molecule, which is consistent with the average value in Brandrup and Immergut (1975), Pramojaney (1982) and Morbidelli et al. (1983).

Initial polymer particle volume, $v_p(t,t)$

$v_p(t,t)$ is the volume of a sphere with diameter $d_p(t,t)$. Therefore, $v_p(t,t) = \pi \times d_p^3(t,t)/6$.

Critical conversion, x_c

Details can be found in Morton et al. (1954) and Friis and Hamielec (1975a).

Lumped monomeric radical diffusion coefficient, δ

δ has also been previously discussed in some detail (Appendix I). Figure VI-2 is a

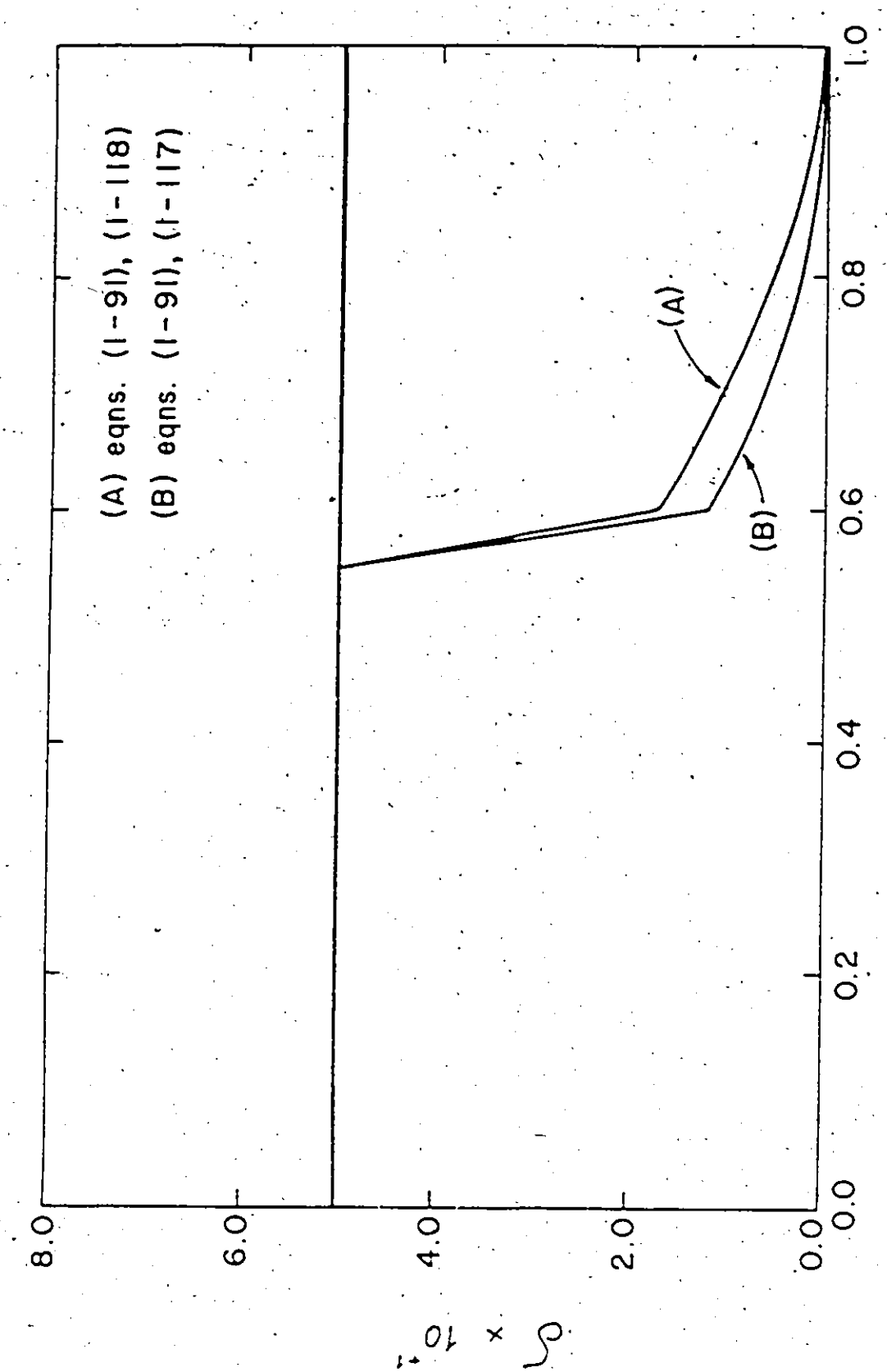

Figure (VI-2). δ versus Conversion.

plot of the general expression for δ, which was discussed in Appendix I. One can compare the more consistent with the real situation changing δ with the constant value of 0.5, which was employed by most of the authors in the literature. δ in this plot is calculated using equations (I-91) and (I-117) for a batch reactor and with parameter values from Friis and Nyhagen (1973).

Ratio μ

μ is the ratio of the rate coefficient of homogeneous nucleation, kh_o, to the rate coefficient of micellar nucleation (i.e. absorption of a radical by a micelle), k_m, and it was defined in equation (I-44). In all our simulations we have used μ = 0.55 according to Fitch and Tsai (1971a, 1971b) and Pollock (1984). Pramojaney (1982) reported that a possible order of magnitude for k_m could be $10^{-4} - 10^{-5}$ dm/sec.

Additional information

(i) Hydrolysis and reacetylation of low conversion poly (VAc) showed no molecular weight change, indicating that there is no back-biting on polymer acetate groups. The degree of polymerization for VAc equals (k_p/kf_m). Only 6% of the chain transfer is on the acetate methyl hydrogens and 94% on the vinyl hydrogens of VAc.

(ii) A puzzling feature of the polymerization of aqueous solutions of VAc is that the percentage contraction corresponding to 100% polymerization is 15.7% at 60°C where the value calculated from the densities of monomer and polymer is 23.6%, which is the value found in bulk polymerization. This is a result of the effect of the solute on the structure of water which even at 60°C retains a large proportion of the tetrahedral hydrogen-bonded structure of ice. Hydration of vinyl acetate increases the mean density of water. Poly (VAc) latex has no effect on the density of water: presumably it is not hydrated to a significant

extent. Consequently, when a solution of VAc polymerizes the water expands, partially compensating the contraction due to polymerization. When a separate monomer phase is present, intermediate values of the percentage contraction are applicable, which makes it difficult to apply the dilatometric method of determining polymerization rates to emulsions of VAc (Dunn (1981)).

(iii) Chemical degradation studies on polyvinyl alcohol obtained by hydrolysis of poly (VAc) confirm that the propagation reaction proceeds by a head-to-tail addition (Bamford et al. (1958)). Bevington (1961) reports that the heat of reaction is $(-\Delta H) = 21.3$ kcal/gmole. Transfer of vinyl acetate to toluene has a rate constant $k_{fs} = 7.73$ lit/gmole-sec, much faster than k_{fm} at 50°C (Bamford et al. (1958)). Pramojaney (1982) assumed that the rate constants for transfer to either water or polymer soluble impurities k_I are equal to k_p (50°C). Hoffman (1981) used $k_{IW} = k_{IM} = 10^5$ lit/gmole-sec.

(iv) The order of dependence of polymerization rate on several experimental variables is the following: initiator concentration 0.5 - 0.6; number of particles 0.12 - 0.2; volume of organic phase remaining in the particles 0.4; ionic strength 0.0 (Chang et al. (1981); soap concentration (SLS) 0.0 - 0.1; and type of soap 0.0. The order of number of particles with respect to initiator concentration is 0.0 and with respect to emulsifier concentration 0.5 - 0.9. All the above dependencies are for the temperature range 45 - 60°C. Dunn (1981) observed that the ionic strength of the aqueous phase affects the stability of the latex particles and the rate of reaction, especially when no ionic emulsifier is used. The effect of increasing ionic strength was to reduce the electrostatic repulsive energy barrier so that the latex ultimately coagulated. When emulsifier was present this factor was less obvious and it has generally been neglected. In the absence of ionic emulsifiers, Dunn (1981) observed a maximum in the polymerization rate with increasing ionic strength.

(v) The degree of solubilization of poly (VAc) could be estimated from the specific viscosity of the solution. The higher the specific viscosity of the solution, the higher the degree of solubilization. SLS gives a specific viscosity of ~ 4.70 dl/gr, which is quite high (Chang et al. (1981)).

(vi) A primary radical is a product of thermal decomposition of the initiator molecule. For simplicity, most of the authors assume for equation (I-10) that a desorbed (nomoneric) radical is kinetically identical to a primary radical (Pramojaney (1982)).

In general, the concentration of radicals in the aqueous phase is extremely small, ranging roughly from 10^{-14} to 10^{-10} gmoles of radicals/lit of latex in a typical reaction system. Also, due to the excessive number of particles generated, the desorbed radicals have to be excluded from participating in the generation of new particles in a typical batch system.

(vii) The effect of non-ionic emulsifiers in emulsion polymerization has been the subject of several investigations. Using cationic (alkyl ammonium bromide), anionic (alkyl sulphate), and non-ionic (Triton X-100) emulsifiers, Napper and Alexander (1962) found that the non-ionic emulsifier did not affect the rate of polymerization. However, anionic emulsifier increased, and cationic emulsifier decreased the initial rate. The slope of the conversion-time curves in most cases approached the same value above 20% conversion. Particle sizes produced by anionic emulsifiers were reportedly much smaller than those obtained without emulsifier, yielding the same particle size as with the non-ionic emulsifier. A much larger particle size was produced by cationic emulsifiers.

Studying the rate of seeded polymerization of VAc, Netschey et al. (1969) and Napper and Netschey (1971) observed a significant reduction in the rate when using steric stabilizers, e.g. poly (ethylene oxide-b-vinyl acetate), poly (vinyl alcohol-g-vinyl acetate), etc. The rate was about one half of that observed with electrostatic stabilizer and twice that observed for mixtures of both types of emulsifiers. The reduction in the polymerization rate

was attributed in general to the decrease in the rate of radical absorption into particles which was caused by the high microscopic viscosity of the thick adsorbed surfactant layer and possible chain transfer reaction to the surfactant molecules. Coulombic repulsion between the radicals and the adsorbed layer, both having negative charges, was believed to be the reason for the low reaction rate in the mixed emulsifier systems.

(viii) Pramojaney (1982) observed a significant increase in the rate of polymerization of batch emulsion VAc when $NaHCO_3$ was excluded from the recipe, while increasing the $NaHCO_3$ level from 0.01 to 0.03 molar had a minimal effect on the conversion-time curves. The primary function of $NaHCO_3$ in emulsion polymerization is to neutralize the excess acidity produced by the decomposition of KPS, and thus to keep the pH of the latex within a permissible range (pH of 4 to 5). Although the high pH in the absence of $NaHCO_3$ may cause a considerable increase in the rate of initiator decomposition via an acid-catalyzed reaction, the data of Kolthoff and Miller (1951) did not yield sufficiently large k_d values to explain the observed increase in the rate of reaction. Alternatively, the decreased reaction rate with $NaHCO_3$ may have arisen from the destabilization and coalescence of primary particles and consequent reduction in particle number, probably due to an increase in ionic strength.

(ix) Monomer concentration inside a particle: The rapid rate of monomer diffusion through the aqueous phase to the particle leads to the assumption that the concentration of monomer in the particles is very close to that at equilibrium. Expressing this thermodynamic equilibrium, Morton et al. (1954) proposed the following equation:

$$\frac{2 v_m \gamma}{r RT} + (1-\phi(t))\left(1-\frac{1}{DP}\right) + \ell n\, \phi(t) + \chi (1-\phi(t))^2 = 0 \qquad \text{(VI-14)}$$

where v_m is the partial molar volume of monomer, in gmole/lit, γ the particle-water interfacial tension, in dyn/dm, r the radius of the monomer-swollen particle at equilibrium, in dm,

DP the degree of polymerization of the polymer molecule, and χ the monomer-polymer interaction parameter (χ is in the range 0.28 - 0.38 for VAc (Gardon (1968c), Klein et al. (1973)).

Since the monomer activity in the aqueous phase decreases during the monomer-starved period, a more applicable version of Morton's equation suggested by Min (1976) can be written, neglecting the 1/DP term:

$$RT\,\ell n\,(M_w/M_{ws}) = 2\,\frac{v_m\,Y}{r} + RT\,[1-\phi(t) + \ell n\,\phi(t) + \chi\,(1-\phi(t))^2] \qquad \text{(VI-15)}$$

where M_w and M_{ws} are the equilibrium monomer concentration in the aqueous phase, and that at saturation, respectively, in gmole/lit of water.

APPENDIX VII

Operating Procedure for MIPPT Reactors

This appendix is a detailed guide for the various steps which had been followed during the latex reactor runs.

Reactor configuration

Bench scale stainless steel reactors by Chemineer-Kenics were used for the experimental runs. A typical reactor consisted of a vessel (almost 6 in. in internal diameter with a volume of 1 gallon or 5 liters), jacket heated (volume of jacket ~ 0.75 gallons), with a removable top head and teflon gasket and mounted on a hydraulic lift stand. The top head was held stationary while the vessel was lowered or raised with the hydraulic lift stand to open or close the reactor. A manual swing-out feature was also provided to facilitate cleaning.

Standard features included a variable speed drive, pitched blade turbine agitator with a mechanical shaft seal assembly, four removable baffles, a sparge dip tube and a thermowell. The internal surface of the vessel and everything else in it were made of stainless steel.

More details on the reactor configuration can be found in the accompanying manuals by Chemineer-Kenics.

Top head description

Stirrer: The reactor was stirred with a pitched blade turbine agitator. The stirrer's motor speed was adjusted to 320 rpm using a stroboscope.

Thermocouple: A type-T thermocouple (Chromel-Alumel, material resistant to VAc) was inserted in the reacting mixture through the reactor thermowell. The signal from

the thermocouple (thermocouple voltage) was fed to the computer front end or to a local electronic controller (in volts) for temperature control of the reactor contents.

Nitrogen line: This line was connected to a nitrogen cylinder and was used to purge (or pressurize) the reactor for ~ 10-15 minutes after charging monomer, water and emulsifier solution and before injecting the initiator into the reactor to start polymerization. The nitrogen cylinder contained prepurified (PREP) or ultra high purity (UHP) nitrogen (oxygen content < 10 ppm or < 2 ppm, respectively). The nitrogen blanket in the reactor was set to less than 5 psi (possibly ~ 2 psi) before initiating the reaction.

Rupture disc: It ruptured at 145 psig at 500°F.

Feed line: It was controlled by a manifold through which monomer, water, emulsifier and initiator solutions were charged into the reactor.

Pump-around loop line: The flow path in this loop was from the bottom of the reactor to the sparge dip tube. A densitometer and a light source were connected in the loop and provision was made for samples to be drawn off through a sampling valve for off-line analysis.

Note: (i) All lines used in the reactor set-up were stainless steel (1/8 in. outside diameter and 0.080 in. inside diameter (~ 2 mm)) tubes.

(ii) Three more lines were used through the top head of the reactor: a vacuum line (to facilitate charging), a vent line (to depressurize the reactor or facilitate purging) and an inhibitor line (to inject a concentrated solution of inhibitor (~ 2.0% by wt.) in cases of emergency).

Reactor's jacket

Two thermocouples, one at the jacket inlet line and one at the outlet line, could be used for cascaded temperature control if desired. The jacket outlet line was connected to the drain. The jacket volume was ~ 0.75 gallons.

The jacket inlet line was connected to the main water line (water at 5-8°C). Steam from the main steam line (100 psi) was injected into the jacket inlet line through a diaphragm control valve. The control valve (trim E ½ in., Linear, Air-to- Open) regulated the flow rate of steam needed for temperature control (if the cooling water flow rate were regulated, then an Air-to-Close valve would have been used). A needle valve regulated the cooling water flow rate, which was adjusted to ~ 0.85 gallons/min. (or 3.75 lit/min.).

Temperature control

To maintain a constant temperature in the reactor (± 1°C) a simple feedback control loop was designed. This was accomplished by inserting a thermocouple in the reactor. The signal from the thermocouple (in volts) was fed to the VAX front end or to a local (Honeywell) electronic controller or to a WEST 2070 controller. The computer's (controller's) output, a signal in amps, after proper conversion into 1-9 volts signal was fed to a pressure-voltage transducer (type 546 electro-pneumatic transducer with a supply pressure of 20 psig and a type 67 FR filter regulator). The pneumatic output of the transducer (3-15 psig) could actuate the diaphragm control valve to regulate the flow rate of the hot stream (steam).

Temperature controller

A proportional-integral (PI) controller with a first order filter were used for temperature control (using the VAX 11/750 front end). Several up and down step changes (of 5-10°C) and several load changes were performed to check the controller's performance. Load

changes were easily performed by adding boiling water (~ 1 lit) in the reactor over a time interval of ~ 1 minute. A load disturbance of 800 cal/sec (1.2 lit of water at 90°C added over an interval of 1 minute) was roughly estimated to be almost 10 times the heat release by reaction (~ 60 cal/sec).

Densitometer

The densitometer was a DPR-YWE (U-tube with a Y-mode oscillator) model, with a PTE-98-EV-72 excitation cell and a DPR-2000 electronic board, by Anton Paar (density measuring systems for process control). More details about the whole unit can be found in the Operator's Manual. It was calibrated using deionized water at ambient temperature and 99% pure methanol. The densitometer readings were checked before every run for reproducibility and consistency (with air, water and methanol).

Polymerization procedure

VAc monomer was not distilled and was used with its commercial inhibitor (this saves time and the effort needed to purify the monomer). The initiator and emulsifier were predissolved in deionized water. Before polymerization was initiated, the mixture of VAc monomer, water and emulsifier were stirred at 320 rpm and purged with nitrogen for ~ 10 minutes.

Sampling

The polymerization reaction usually lasts about two hours after initiation, a time period long enough to reach conversion levels of > 95%. Samples (~ 5 mℓ each) were drawn off every 5 to 10 minutes, starting after initiation of the reaction (~ 20 samples/run). After sampling, addition of a drop of hydroquinone solution (1% by wt.) would stop further

polymerization in the samples, which would then be frozen at 0°C (ice) and kept for further off-line analysis. The hydroquinone solution was prepared by dissolving 1 gr of HDQ in 100 ml of deionized water.

Reactor shut down

Steam was shut off and the cooling water flowrate was maximized. When the mixture reached ~ 30-35°C, the reactor contents were drained into labelled waste drums. Hydroquinone solution (and ice) were added to quench any further polymerization. The drums were subsequently disposed of. This same procedure was used in cases of emergency, as well.

All lines were cleaned with warm water and a solution of methanol in water. Cleaning the lines after every experiment was very important, because it helped to avoid line blockage from polymer and cross contamination from one experiment to another.

Reactor clean-up

After draining the reactor contents into waste-drums, charge the reactor with a solution of methanol in deionized water (700 ml methanol in 3800 ml water) going up to 50°C. Drain the reactor contents and repeat the same procedure with deionized water (and, possibly, soap) going up to 60°C (for almost an hour). When finished, force some air through the densitometer lines (or any other lines in the sampling circuit) and let dry. The next day repeat the procedure with deionized water (60°C, for an hour) and let dry. If there is considerable polymer buildup on the reactor walls or agitator, then use chloroform and pure ethyl alcohol (~ 15-20 ml) and heat the mixture up to 40-42°C. Use the same procedure whenever the reactor is extremely dirty.

APPENDIX VIII

Batch PVAc Results

Measured experimental data from the several batch VAc emulsion runs performed (see Chapter 4) are reported here. The operating conditions for each run can be found in Table 4-3.

BR2

Time (sec)	Conversion	
	Gravimetry	Densitometry
2700.	0.3897	0.3841
3300.	0.5424	0.4915
3900.	0.6531	0.6695
4500.	0.7231	0.7315
5100.	0.8373	0.8000
5700.	0.8887	–
6300.	0.9321	–
6900.	0.8928	–
7500.	0.9099	0.8799
8100.	0.9698	–
8700.	0.9504	–

BR3

Time (sec)	Conversion	
	Gravimetry	Densitometry
2700.	0.1140	–
3000.	–	0.165
3300.	–	0.250
3600.	–	0.304
3900.	–	0.399
4200.	–	0.459
4500.	0.5669	0.530
4800.	–	0.578
5100.	–	0.643
6900.	0.8607	–
7200.	0.8745	–

7500.	0.8874	–
8100.	0.8176	–
8700.	0.8937	–

BR6

Time (sec)	x(t)	$\bar{M}_w \times 10^{-7}$
2400.	0.2974	
3000.	0.5317	
3600.	0.7070	0.328
4200.	0.8849	

BR7

Time (sec)	x(t)	$\bar{D}_W$(Å)
2400.	0.2606	
3000.	0.4892	712.
3600.	0.6566	803.
4200.	0.8390	866.
–	0.9660	892.
–	0.9840	904.

BR8

Time (sec)	x(t)	$\bar{D}_W$(Å)
2400.	0.2765	
3000.	0.5006	550.
3600.	0.7013	600.
4200.	0.8668	618.
–	0.947	629.
–	0.975	637.

BR10

Time (sec)	x(t)	$\bar{M}_w \times 10^{-7}$
1800.	0.1509	0.134
2100.	0.2497	0.148
2400.	0.3037	
–	0.3578	0.206

2700.	0.4437	0.206
3000.	0.5308	
3300.	0.6154	
3600.	0.7103	
3900.	0.7864	
4200.	0.8940	

BR11

Time (sec)	x(t)	$\bar{D}_W$(Å)	$\bar{M}_w \times 10^{-17}$
1800.	0.1709	–	0.109
2100.	0.2735	–	0.209
2400.	0.3899	–	
2700.	0.4649	–	
3000.	0.5622	603.	
3300.	0.6288	625.	
3600.	0.7238	627.	
3900.	0.8012	650.	
4200.	0.8582	704.	
–	0.9830	709.	

BR14

Time (sec)	x(t)	$\bar{M}_w \times 10^{-7}$	
1500.	0.0782	–	
1650.	0.1191	–	
1800.	0.3427	–	
2400.	0.6225	0.113	
2700.	0.8117	0.138	
3000.	0.8898	0.163	(0.187)
3300.	0.9323	0.235	
3600.	0.9684	–	
3900.	0.9746	0.279	
4200.	0.9756	–	

BR21

Time (sec)	x(t)	$\bar{M}_w \times 10^{-6}$
3000.	0.1718	1.733
3600.	0.3385	2.002
4200.	0.4998	2.202
4800.	0.6438	2.652

—	0.9134	7.655

BR22

Time (sec)	x(t)	$\bar{M}_w \times 10^{-6}$
400.	0.1625	0.603
900.	0.7360	1.981
1200.	0.9189	
1500.	0.9460	
1800.	0.9768	

APPENDIX IX

Redox Initiation System

Introduction

A large number of polymerizations, especially those at low temperatures, are initiated by two component systems. These so-called "redox" systems quite generally follow the reaction:

$$A^{n+} + ROOR \rightarrow A^{(n+1)+} + RO\cdot + RO^{-} \qquad \text{(IX-1)}$$

where A is an activator (e.g. metal ion) and ROOR a peroxide. Reaction (IX-1) is an one-electron transfer reaction with concomitant cleavage of the $-O-O-$ bond. The integer n has small values such as two for Fe or zero for N,N dimethylaniline. The peroxide may be inorganic such as the persulphate anion or organic such as benzoyl peroxide. At high monomer concentrations most of the free radicals RO· will initiate polymerization and second-order kinetics are followed. Redox initiations are usually employed in the temperature range 0-50°C. The activator (e.g. iron) and the reducing agent are not destroyed in the redox system.

The most efficient manner of adding the components of a redox system is to add them in stages, by gradual addition or by adding the peroxide at the start and then the reducing agent gradually. A typical redox system for cold SBR production employs sodium formaldehyde sulphoxylate (reducing agent), a hydroperoxide (oxidant) and ferrous (Fe^{2+}) sulphate as an activator plus a chelating agent or a chelating iron salt. The function of the chelator is to complex the ferrous ion and thus limit the concentration of free iron.

Redox systems appear very versatile, permitting polymerization at ambient temperatures and the possibility of control of the rate of radical initiation versus polymeriza-

tion time. This in turn permits control of heat generation and the minimization of reaction time.

Because of the low water solubility of most vinyl monomers redox catalysis has mainly been used in emulsion polymerization. In these aqueous systems it appears that accurate control of pH is required to a value or range specific to the monomer undergoing polymerization. With the persulphate-sulphite system, for example, it was found that acrylonitrile requires acid conditions, and VCM reacts most satisfactorily at pH 8, whereas the rate of polymerization of styrene is independent of pH except at low hydrogen ion concentrations (Bamford et al. (1958)).

Bacon (1946) reported that, in aqueous acrylonitrile polymerizations, the redox systems led to higher MW's and to polymerizations which could be performed at higher rates and at lower temperatures. Edelhauser (1975) and Warson (1976) used the redox system ammonium persulphate together with sodium bicarbonate in water, which proved to be an effective redox initiation system for VAc emulsion polymerization. The reaction was started at 25°C and run nonisothermally to 70°C. The time to almost complete conversion was about 30 minutes. Hoffman (1981) described a redox system comprised of potassium peroxydisulphate (KPS), iron (Fe^{2+}) and sodium formaldehyde sulphoxylate (SFS) in his modelling of emulsion SBR reactors. Finally, Patsiga et al. (1984) studied the titanium (III) - hydroxylamine system and applied it to emulsion polymerizations of styrene, MMA, VAc, isoprene and acrylonitrile at 30°C. Reaction conditions such as emulsifier type, initiator concentration and manner of introduction of initiator were optimized for styrene. VAc showed behaviour similar to styrene and could be polymerized to high (> 80%) yield.

The KPS-Fe-SFS redox system

The KPS-Fe-SFS redox system, on which no detailed kinetic modelling seems to have been published, was studied by Andersen and Proctor (1965) who used inhibition kinetics. With this system the primary cycle comprises the reaction of KPS with ferrous ion (Fe^{2+}) to yield sulphate radicalion SO_4^{-}, followed by reduction of the ferric ion (Fe^{3+}) to ferrous by SFS, thus allowing the iron to cycle. Actually, radicals from reactions other than the KPS-ferrous reaction are also involved.

In using inhibition kinetics to study the rate of radical generation, an inhibitor capable of successfully competing with monomer for the radicals has to be present in the system, so that polymerization is prevented until the inhibitor is consumed. Thus, the inhibition period, from the start of the reaction to the onset of polymerization, is an inverse function of the rate of radical generation. A common inhibitor is oxygen.

The KPS-Fe-SFS redox system is a continuous system where a small amount of persulphate is pumped into the aqueous charge containing Fe^{3+} and the reaction is activated and controlled by sulphoxylate addition. (Equally, one could use persulphate in excess and control the rate by the addition of a ferrous salt). Additional persulphate is added at a rate of ~2.0 gmoles of persulphate per gmole of sulphoxylate.

The kinetics of the KPS-Fe-SFS redox system can be described by the following reactions (Andersen and Proctor (1965)):

$$S_2O_8^{2-} + Fe^{2+} \xrightarrow{k_1} SO_4^{-} + Fe^{3+} + SO_4^{2-} \qquad \text{(IX-2)}$$

$$Fe^{3+} + SFS \xrightarrow{k_2} Fe^{2+} + X \qquad \text{(IX-3)}$$

$$SO_4^{\cdot -} + M \xrightarrow{k_3} R\cdot \qquad \text{(IX-4)}$$

$$R\cdot + M \xrightarrow{k_4} \text{polymer} \qquad \text{(IX-5)}$$

$$S_2O_8^{2-} + SFS + 3O\,H^- \xrightarrow{k_5} 2\,SO_4^{2-} + SO_3^{2-}(HCHO) + 2\,H_2O \qquad \text{(IX-6)}$$

$$Fe^{2+} + SO_4^{\cdot -} \xrightarrow{k_6} Fe^{3+} + SO_4^{2-} \qquad \text{(IX-7)}$$

$$X + S_2O_8^{2-} \xrightarrow{k_8} Y \qquad \text{(IX-8)}$$

where M denotes monomer, R· is a free active monomeric radical, $SO_4^{\cdot -}$ is the sulphate radical, X is a decomposition product of the SFS in the SFS-Fe reduction and is of the form $(HCHO)SO_2^{\cdot -}$, and Y is a non-reactive radical product. The activation energy of reaction (IX-2) is ~ 12 kcal/gmole (Bevington (1961)). The reader should have in mind that the above is not a rigorous development of the reaction mechanism, but a development sufficient for modelling purposes.

If one accepts that $k_6 \sim 0.0$ lit/gmole-sec (Andersen and Proctor (1965)), then the kinetic equations for the unsteady-state may be written as follows:

$$\frac{d(S_2O_8^{2-})}{dt} = B - k_1(S_2O_8^{2-})(Fe^{2+}) - k_5(S_2O_8^{2-})SFS - k_8(S_2O_8^{2-})X \qquad \text{(IX-9)}$$

$$\frac{d(SFS)}{dt} = A - k_2(Fe^{3+})\,SFS - k_5(S_2O_8^{2-})SFS \qquad \text{(IX-10)}$$

$$\frac{d(X)}{dt} = k_2(Fe^{3+})\,SFS - k_8(S_2O_8^{2-})X \qquad \text{(IX-11)}$$

$$\frac{d(Fe^{2+})}{dt} = -k_1(S_2O_8^{2-})(Fe^{2+}) + k_2(Fe^{3+})SFS \qquad \text{(IX-12)}$$

$$\frac{d(Fe^{3+})}{dt} = k_1(S_2O_8^{2-})(Fe^{2+}) - k_2(Fe^{3+})SFS \qquad \text{(IX-13)}$$

and

$$\frac{d(SO_4^{\cdot-})}{dt} = k_1(S_2O_8^{2-})(Fe^{2+}) - k_3(SO_4^{\cdot-})M \qquad \text{(IX-14)}$$

where $M = M_w$, i.e. the concentration of monomer in the water phase and B and A represent gmoles/sec of $S_2O_8^{2-}$ and SFS added, respectively.

Continuous SFS and KPS addition at steady-state

According to this method, a small amount of KPS is pumped into the reactor before the SFS addition is started. SFS and KPS are then added in a given ratio (A/B) to keep the KPS concentration in excess (the opposite, i.e. to keep SFS in excess is not recommended).

Equations (IX-12) and (IX-11) at steady-state yield:

$$k_1(S_2O_8^{2-})(Fe^{2+}) = k_2(Fe^{3+})SFS \qquad \text{(IX-15)}$$

$$k_2(Fe^{3+})SFS = k_8(S_2O_8^{2-})X \qquad \text{(IX-16)}$$

Considering that the SFS concentration will be kept at a small constant value, equation (IX-10) becomes at steady-state:

$$k_5(S_2O_8^{2-})SFS = A - k_2(Fe^{3+})SFS \qquad \text{(IX-17)}$$

or

$$(SFS) = \frac{A}{k_5(S_2O_8^{2-}) + k_2(Fe^{3+})} \qquad \text{(IX-18)}$$

Substituting now equations (IX-15), (IX-16) and (IX-18) in equation (IX-9) one finally obtains:

$$\frac{d(S_2O_8^{2-})}{dt} = \frac{(k_5(S_2O_8^{2-}) + k_2(Fe^{3+}))B - A(k_5(S_2O_8^{2-}) + 2k_2(Fe^{3+}))}{k_5(S_2O_8^{2-}) + k_2(Fe^{3+})} \qquad \text{(IX-19)}$$

Inspection of equation (IX-19) shows that to keep $d(S_2O_8^{2-})/dt$ positive or close to zero, B has to be about twice A. Much below B/A = 2., the KPS concentration in the reactor will decrease and the reaction will slow and eventually die. If, on the other hand, B/A is too high, then the KPS concentration will build up and eventually thermal decomposition of persulphate will be of significance.

Simulation results with the redox initiation model

Several simulations were performed using the redox initiation model, as was described in equations (IX-9) to (IX-14) (see Penlidis et al. (1985)). Since the system described is an SFS controlled one, an initial amount of Fe^{3+} is needed to be reduced to Fe^{2+}, and thus start the iron cycle. The ratio B/A was kept equal to 2., as it was suggested from the previous section. The simulations were performed for a semi-batch system, where $k_3 = k_p$. Also, it was assumed that radicals from reaction (IX-6) do not initiate the polymerization. In such a case, the rate of initiation is given by:

$$R_i = k_3 M_w (SO_4^{\cdot -}) = k_1 (Fe^{2+})(S_2O_8^{2-}) \qquad \text{(IX-20)}$$

Many contradictions were noticed in the literature for the values of k_1, k_2 and k_8. The values that were finally chosen, after a considerable number of simulation runs, are the following:

$k_1 = 0.047$ lit/gmole-sec

$k_2 = 1.078$ lit/gmole-sec

$k_5 = 0.31$ lit/gmole-sec

$k_8 = 0.15$ lit/gmole-sec

Also, concentrations and feed rates used in the simulations are the following:

$(S_2O_8^{2-})_o = 0.027$ gmole/lit

$(SFS)_o = 0.$ gmole/lit

$(Fe^{3+})_o = 0.0012$ gmole/lit

$B = 2A = 0.20 \times 10^{-5}$ gmole/sec

Andersen and Proctor (1965) observed that in about 30 minutes the system had reached steady-state. It was obvious from the simulation results that the redox initiation model agreed quite well with experimental observations from literature.

APPENDIX X

Continuous Runs Experimental Information

Experimental details concerning the continuous runs performed are cited herein. Information concerning the reactor set-up, instrument calibration, and on- or off-line analytical methods, which has already been given previously (see Chapters 3 and 4) will not be repeated again.

Ingredients: Water used for the reaction recipe or as dilution medium for the preparation of solutions was deionized (18 megohm-cm). The monomer was vinyl acetate from CIL Co. (Toronto), ~ 99% pure, the rest being inhibitors, solvents, chain transfer agents and other impurities. The initiator was potassium persulphate, ACS analytical grade, and the soap (emulsifier) sodium dodecyl (lauryl) sulphate, specially pure, both from BDH Chemicals.

Reaction conditions: Temperature = 50°C (± 1), θ_2 = 30 minutes, V_2 = 5000 ml, V_1 = 500 ml, FT = total volumetric flow rate to R2 = 167 ml/min, k_v = 1.4 and the volumetric ratio of monomer to water = 0.4. During the course of the polymerizations, the total volumetric flow rate was being checked every 1/2 hour so as to detect any fluctuations due to pump or check-valve problems, possible coagulation in the vessels or the lines, etc.

Pump flow rate selection: Pump flow rates should satisfy the constraints from θ_2, k_v and minimum/maximum flow rate. The flow rate of monomer to R1 (denoted from now on as M_1 or M(R1)) was fixed to a value of 10 ml/min, because one always needs to have some monomer going to R1 to get the reaction going.

Start-up procedure: R1 and R2 were filled up with deionized water. All the lines were also filled up with water (by running water from all feed tanks for 1/2 hour). In this way it was ensured that there was no air in the lines, and especially in the initiator line, when the switch to R1 occurred. After the feed tanks had been filled with the solutions or other raw materials, they were all carefully deaerated. Nitrogen was bubbled through (using a slow bubble rate) and vacuum was pulled on and off. Nitrogen was not bubbled through the soap solution to prevent excessive foaming.

On-line densitometers: On-line densitometers were used in all continuous runs to follow conversion. The following hints might be useful for their efficient implementation in the future: (a) Densitometer electronic board settings: $\mu_s = 160$, $2^N = 11$, $T_o = 69950$, span = 600–900, $t_o = 50^{+25}$, K = from –0.94 to -2.3×10^{-4} Kelvin^{-1}. A value of -1.08×10^{-4} was frequently used. The sensitivity factor of the oscillator cell E should be always calculated with water/air. (b) The densitometer flow cell can easily handle flow rates up to 400 ml/min. (c) If the densitometer cell tempreature t_o follows the reactor temperature, then this is an indication that the circuit for temperature compensation in the excitation cell is open (probably due to liquid penetration). (d) In some cases, the on-line densitometer readings (period of oscillation T of the vibrating U-tube) were observed to fluctuate ± 300 units about some average (actual) level. To obtain a true reading in these cases the output was recorded and averaged over 2 and 5 minute intervals. These fluctuations were due to latex which coagulated and subsequently was deposited inside the U-tube. Due to the deposit, the vibrating U-tube became heavier and so it did not oscillate as without the deposit. As a result, the reading dropped down. As new free flowing latex was continuously coming in, the coagulated latex pieces were washed out at some point. Consequently, the U-tube assumed its previous weight and under the constant amplitude excitation current the output reading

overshot its previous actual value, before coming back down to it. This observation can explain possible discrepancies between off-line gravimetric conversion and on-line densitometry.

Problems with latex coagulation: In cases of soap pump failure, there was not enough soap to stabilize the polymer particles and consequently the latex coagulated in the reactors and in the flow path lines. This could be easily detected by a reduction in the total volumetric flow rate or a very unreasonable reading from the on-line densitometers. The first thing one should do in cases like this is to isolate the densitometers from the flow path in order to prevent latex coagulation inside the densitometer lines. To dissolve the coagulated poly(vinyl acetate) a 25% by wt. KOH (potassium hydroxide) solution in water heated up to 50°C or chloroform at 45°C were found useful.

Sampling: 5 to 10 ml samples were drawn off for further off-line analysis in time intervals of 5 to 15 minutes. More than 30% of the samples from each run were checked for reproducibility. The final solids content in the continuous runs was ~ 30 - 35%, which is a typical range for this kind of experiments.

Split definition: The definition of the flow split was slightly modified throughout the present work, compared to the one that Pollock et al. (1981) had used. Split was defined as follows:

$$s_p = \frac{M_1 + W_1^{TOT}}{FT} \qquad (X\text{-}1)$$

with M_1 being the flow rate of monomer to reactor 1 (R1), FT the total volumetric flow rate to R2, and

$$W_1^{TOT} = W_1 + I(R1) + S(R1) \qquad (X\text{-}2)$$

An alternative way to define split could be the following:

$$s_p = \frac{M_1 + W_1}{M_1 + W_1 + M_2 + W_2} \qquad \text{(X-3)}$$

However, the definition in equation (X-1) was considered more practical for experimental implementations and was followed throughout this work.

From the pump flow rate constraints, the range of splits that could be obtained were the following: s_p (min) = 0.138 and s_p (max) = 0.647. During the experimental evaluation of the new train configuration, it was decided to keep M_1 and M_2 unaltered during a run, which is very practical for industrial applications. For the same reason and for the additional reason of latex stability, it was also decided not to change S(R1). Then, it is evident from equations (X-1) and (X-2) and from the definition of FT,

$$FT = M_1 + W_1 + I(R1) + S(R1) + M_2 + W_2 \qquad \text{(X-4)}$$

that the only variables that affected split were W_1, I(R1) and W_2.

Continuous runs description: The continuous runs which were performed to evaluate the new train configuration behaviour consisted of several parts. During these parts initiator flow rate and split were being changed in order to assess their effect on conversion and particle size. The flow rate profiles and other characteristics of these runs are cited below:

Continuous Run 1

CR1

part*	A**	B	C	D	end
M_1(ml/min)	10	10	10***	10***	
M_2	38	38	70	70	
W_1	16	16	0	0	
W_2	63	63	63	63	
I	10	10	10	15	
S	30	30	14***	9***	
split		0.395	0.204	0.204	

* For all parts: CI = 0.167 gmoles/lit

CS = 0.139 gmoles/lit.

** In part A all initiator was fed to R2.

*** "Estimated" flow rates, due to pump leakage.

Continuous Run 2

CR2

part*	A	B	C	E**	end
M_1(ml/min)	10	10	10	10	
M_2	38	38	38	38	
W_1	22	0	12	0	
W_2	62	84	62	79	
I	10	10	20	15	
S	25	25	25***	25***	
split	0.401	0.269	0.401	-	

* For all parts: CI = 0.083 gmoles/lit

CS = 0.169 gmoles/lit.

Parts A, B: same FI - different split.

Parts A, C: same split - different FI.

** In part E all initiator was fed to R2.

*** The actual flow rates were somwhat lower due to pump leakage.

R1 conversion for CR1: The conversion behaviour inR1 for parts A and B is shown in Figure X-1. The circles represent conversion in reactor 1 and the inverted triangles conversion in reactor 2 for reasons of comparison. During part A, i.e. up to $t/\theta_2 = 12.0$, the first reactor was just being used as an emulsifying vessel, hence the zero conversion. When the initiator stream was switched to R1 during part B, polymerization started almost immediately in reactor 1 and very soon an overshoot in conversion was observed. This initial overshoot in the

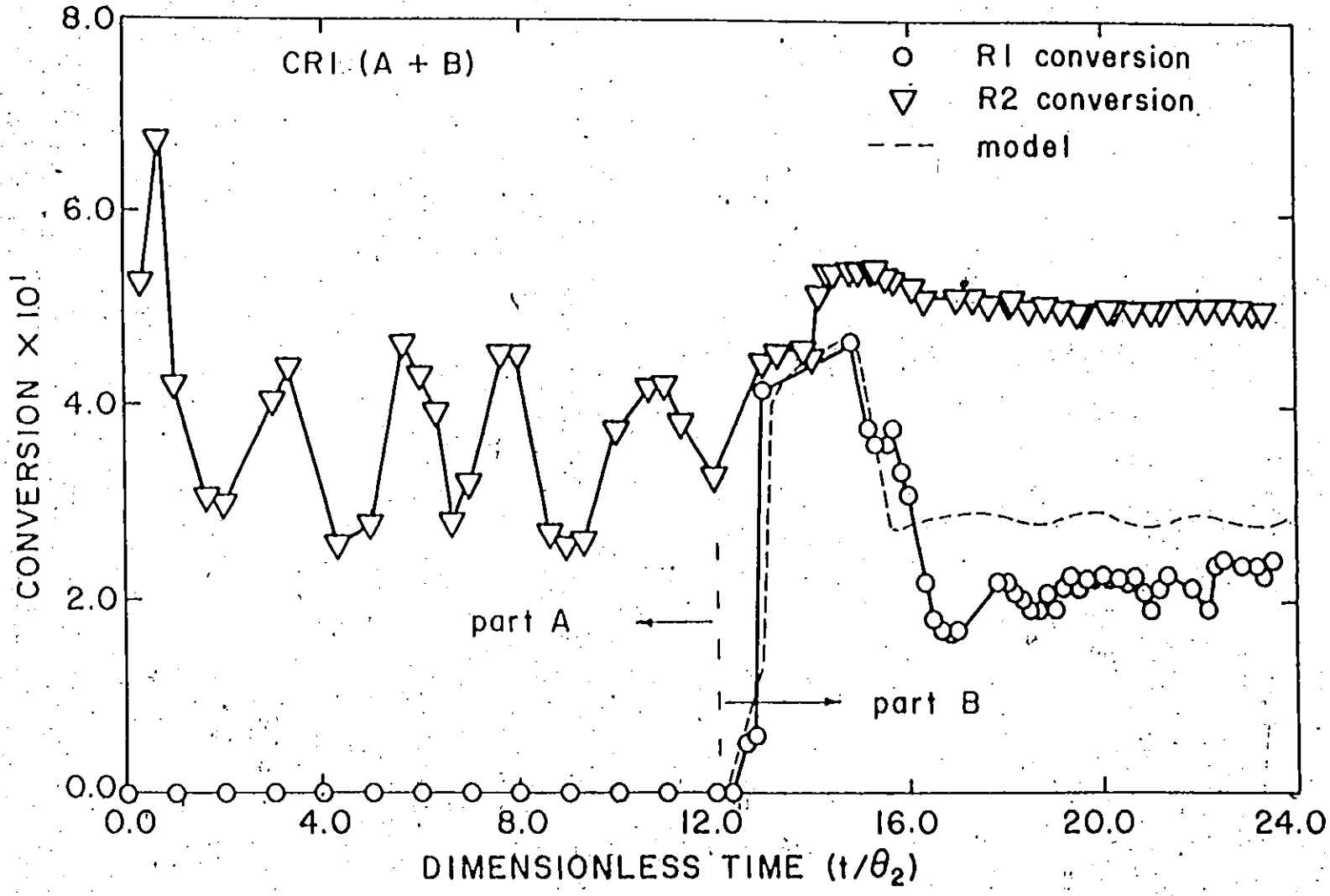

Figure (X-1). Run CR1, Parts A and B: R2 and R1 Conversion versus (t/θ_2)

conversion of R1 (which was followed by densitometry) is due to the R1 start-up procedure. R1 started for part B full of the emulsion recipe and it did give a conversion overshoot which is consistent with this kind of start-up (Kiparissides et al., 1980; Pollock, 1984). This excursion in conversion soon died out and the conversion in R1 assumed a lower level, slightly oscillating around ~ 20.5 - 21%. One can easily realize from Figure X-1 that the oscillatory behaviour of R1 did not have any destabilizing effect on R2. The dashed line in Figure X-1 represents the model predictions for R1 conversion. The experimental results showed that R1 oscillated by ~1%, which is in agreement with the model.

Experimental results from CR2: The complete experimental picture from CR2 is shown in Figures X-2and X-3. Close to $t/\theta_2 = 11.0$ the emulsifier pump started leaking due to a mechanical failure. From $t/\theta_2 = 15.0$ onwards the leakage was quite serious. Since less emulsifier was going to R1 from $t/\theta_2 = 11.0$, a smaller number of particles were being generated and therefore, particle diameter showed an increase, as it is obvious from the last stages of part B in Figure X-3. In an attempt to compensate for the pump leakage, the soap flow rate was increased by ~ 10 ml/min at $t/\theta_2 = 12.0$. More soap was going now to R1, which tended to stabilize particle size during part C. As can be seen from Figure X-2, conversion during part C showed the expected increase, since the initiator flow rate had been increased, but it never assumed a constant level due to an additional kick at $t/\theta_2 = 16.0$ when the soap flow rate was again increased by ~ 5 ml/min. Due to the soap leakage during part C, things in the first reactor were uncertain and therefore, the results of part C are not used to draw any conclusions but to merely show the train's response.

During part E of CR2, all feeds were diverted to the second reactor of the train, in an effort to see whether the large reactor would oscillate or not. Although inconclusive, the

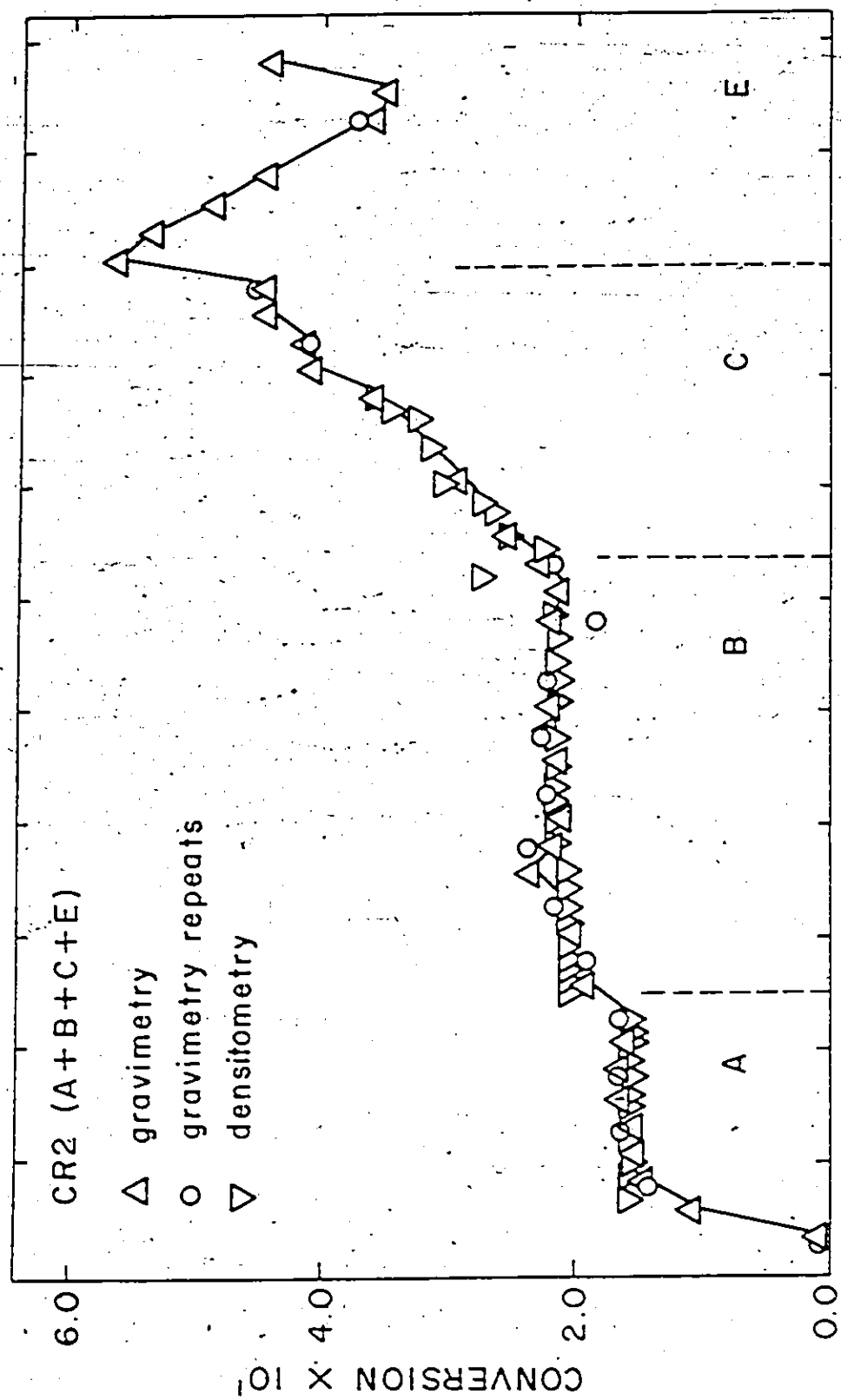

Figure (X-2). Run CR2, Complete Experimental Picture: Conversion

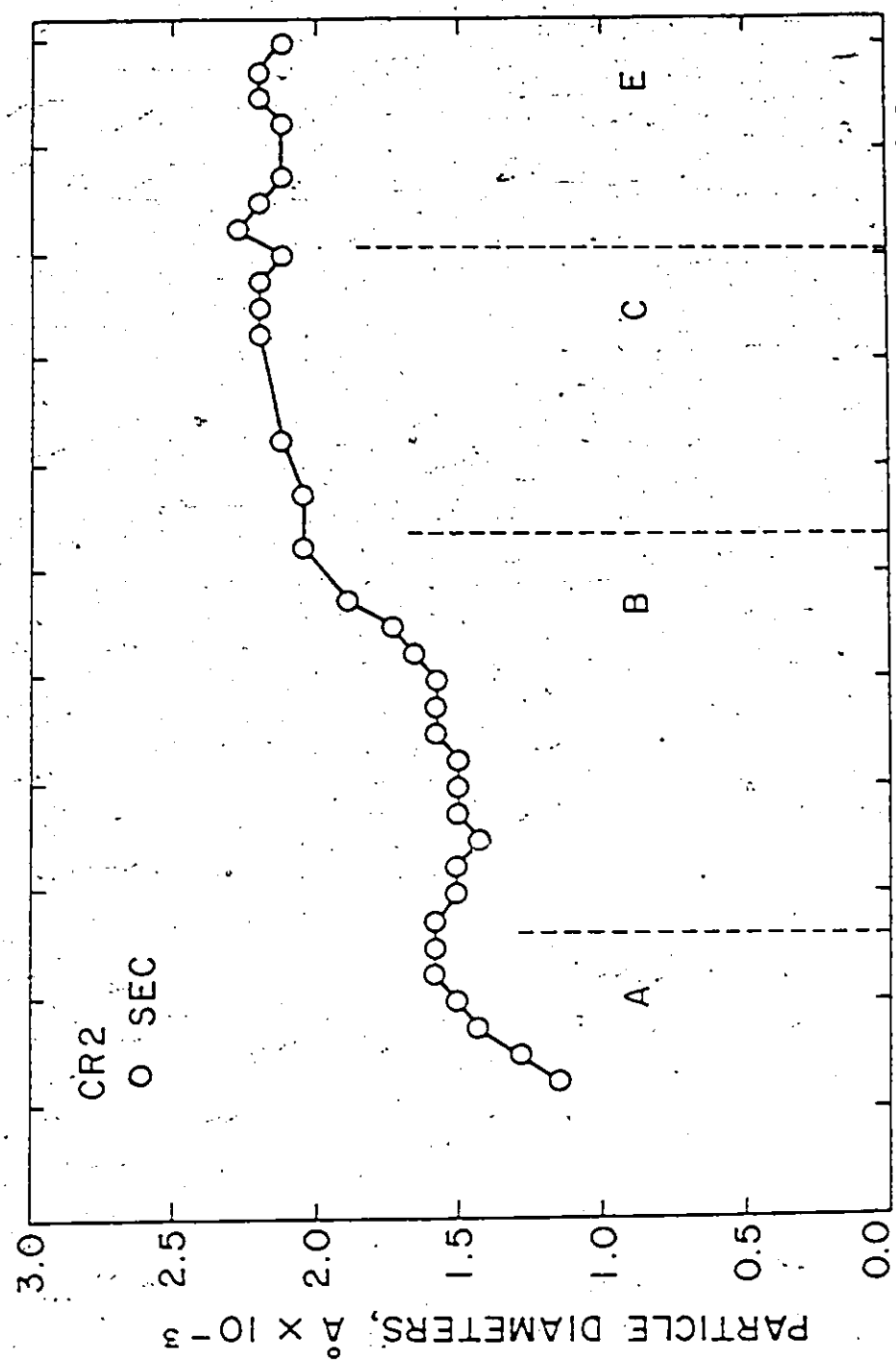

Figure (X-3). Run CR2, Complete Experimental Picture: Particle Diameter

results from Figures X-2 and X-3 do reveal a tendency of the train to oscillate in both conversion and particle size. In fact, the conversion behaviour for part E is very similar to the oscillatory behaviour of Figure 7-4.

Finally, Figure X-4 shows conversion versus (t/θ_2) for reactor 1 from the on-line densitometer. The start-up procedure this time was to start R1 full of deionized water. The results were obtained up to $t/\theta_2 = 12.0$, at which point the densitometer was isolated from the flow path in order to avoid possible latex coagulation in its lines, due to the insufficient amount of soap going to R1 through the leaking soap pump.

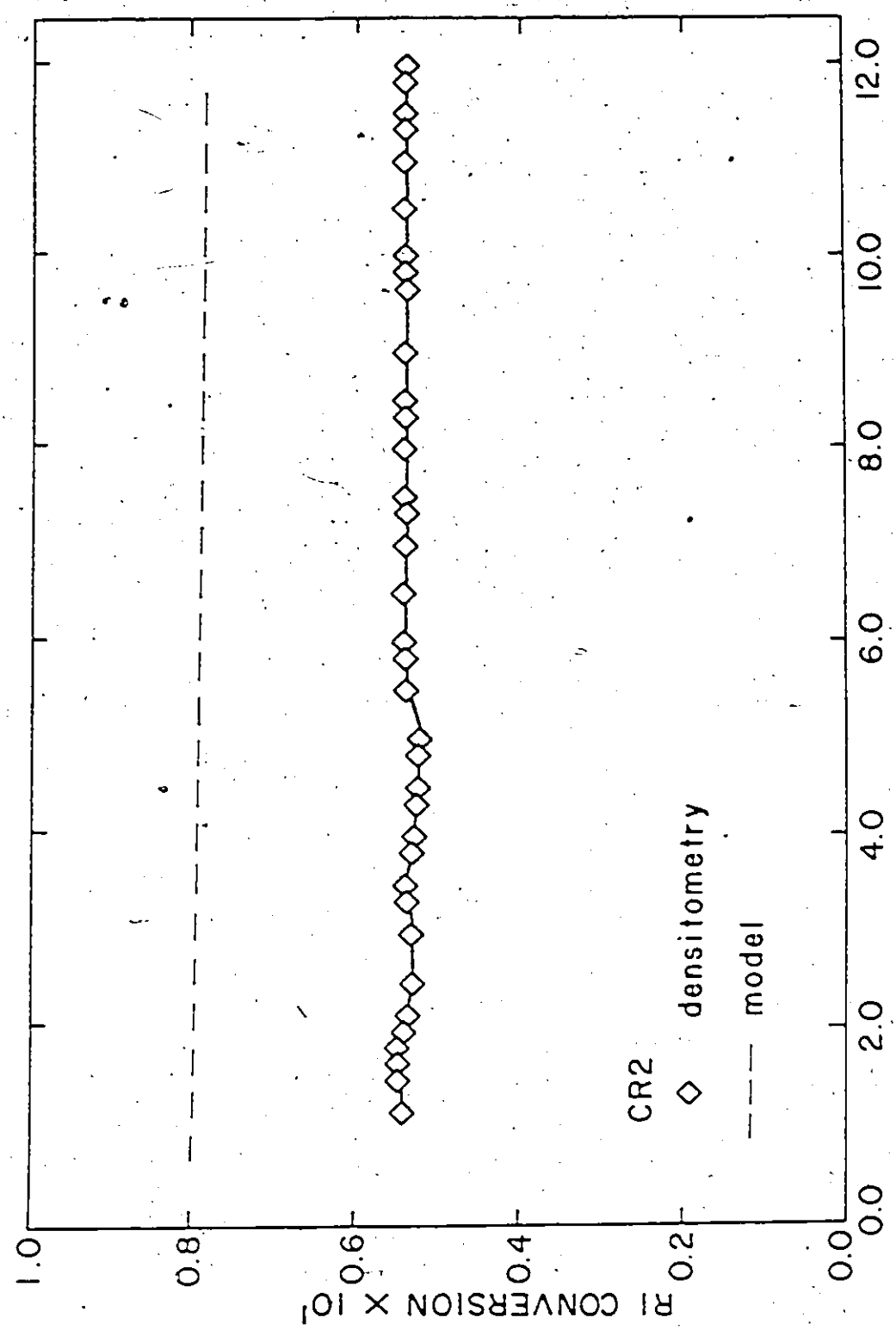

Figure (X-4). Run CR2, Parts A and B: RI Conversion versus (t/θ_2)

APPENDIX XI

Safety Considerations

A brief overview concerning safety and health hazards considerations were deemed necessary at this point and helpful for the future experimenters with this type of materials.

Hazard identification and protection

The hazards associated with the experiments performed could be divided into two categories: (1) hazards related to the nature of the chemicals used, and (2) hazards associated with the equipment. Table XI-1 lists the physical properties and some of the hazards of the major chemicals used, while Table XI-2 provides mortality data based on laboratory animals for the same chemicals.

Chemicals

For each of the major chemicals used hygiene, actual precautions and procedures for handling and storage will be outlined below.

Sodium lauryl sulphate (SLS): It is a white powder used as the emulsifying agent in the reactor. It is water soluble and has a molecular weight of 288.4 gr/gmole. SLS is a skin irritant and allergen, though perhaps not a severe one, as indicated in the literature sources 3 and 5 (for literature source numbers, see end of appendix). It causes readily reversible changes which disappear after the end of exposure. No TLV (threshold limit value) values are available for SLS. It can be dangerous when heated to decomposition because it emits highly toxic fumes. Eye contact could be a problem. SLS should be handled with gloves (single use vinyl examination Tru-Touch gloves) and protective glasses (chemical splash goggles, ENCON 160) and care must be taken so that powder inhalation might be avoided.

TABLE XI-1

Physical Property and Hazard Data for Major Experimental Chemicals Used

Chemical	Formula	MW	Condition at STP	M.P. (°C)	B.P. (°C)
Sodium lauryl sulphate	$C_{12}H_{25}SO_4Na$	288.4	solid (crystals)	–	–
Potassium persulphate	$K_2S_2O_8$	270.3	solid (crystals)	6	–
Hydroquinone	$C_6H_4(OH)_2$	110.1	solid	172	285
Vinyl acetate	$CH_3COOCHCH_2$	86.05	liquid	–100.2	73

TABLE XI-1
(continued)

Chemical	Vapour pressure	Flash point	Ignition point	Health	Fire	Reactivity
Sodium lauryl sulphate	–	–	–	–	–	–
Potassium persulphate	–	–	–	1	0	1
Hydroquinone	4 mm Hg at 150°C 1 mm Hg at 132°C	165°C	516°C	–	–	–
Vinyl acetate	100 mm Hg at 2.5°C	–8°C*	427°C	2	3	2

* explosive limits at STP are 2.6% to 13.4%

Health: 4 - short exposure major injury (even if treated)
3 - short exposure serious temporary injury (even if treated)
2 - intense exposure possible residual injury without treatment
1 - irritation minor even without treatment
0 - no hazard under combustion

TABLE XI-1
(continued)

Chemical	Eye Contact	Inhalation	Skin Penetration	Skin Irritation	Ingestion
Sodium lauryl sulphate	4	-	2	3	2
Potassium persulphate	3	-	-	2	2
Hydroquinone	4	3	3	2	2
Vinyl acetate	1	3	3	1	2

Fire: 4 - vapour at STP which burns readily
3 - liquid and solid which can be limited at most conditions.
2 - moderately heated before ignition
1 - preheat required
0 - no burning possible

Reactivity: 4 - deterioration possible
3 - strong candidate for deterioration
2 - violent chemical changes
1 - unstable at high tempratures
0 - normally stable

TABLE XI-2

Mortality Data for Major Chemicals Used

Chemical	LD_{50} for ingestion in lab rat	LD_{50} for skin penetration in lab rabbit	Other
Sodium lauryl sulphate	1–10 gm/kg	2–20 ml/kg	
Potassium persulphate	1–10 gm/kg	> 20 ml/kg	
Hydroquinone	1–10 gm/kg	2–20 ml/kg	
Vinyl acetate	3 gm/kg	3 ml/kg	LD_{50} for rat inhalation = 4000 pm for 4 hours.

Potassium persulphate (KPS): KPS (white, odourless crystals) is the initiator for the polymerization, an eye and skin irritant according to #3 and #4. It may involve both reversible and irreversible changes, but it is not severe enough to cause death or permanent injury. It decomposes at a temperature lower than 100°C. It liberates oxygen above 100°C when dry or at about ~ 50°C when in solution. When heated to decomposition it emits highly toxic fumes of oxides of sulfur. It can react with reducing materials. It is water soluble. Gloves and eye protection are considered necessary when PKS is used. It must be kept dry and cool.

Hydroquinone: Hydroquinone (colourless, hexagonal prisms) is used to inhibit the reaction and eventually stop the polymerization. It is a strong eye and skin irritant and allergen. Its TLV is 2 mgr/m^3 of air and its presence is indicated by a sweet taste (see #3). Ingestion or inhalation may induce nausea, dizziness, a sensation of suffocation, an increased rate of respiration, vomiting, muscular twitchings, headache, dyspnea, cyanosis, delirium and collapse. It can react with oxidizing materials. If this material accidentally comes into contact with the skin, it should be removed at once and the affected area should be washed with plenty of soap and warm water. Gloves, eye protection and mask are considered necessary.

Methanol: It is a very flammable liquid and it can form explosive mixtures with air. It causes skin irritation and its ingestion can cause blindness and permanent injury. In short exposure it causes dizziness, headache or narcosis. Eye protection, gloves and protective clothing are considered necessary. To fight fire caused by methanol dry chemical, foam or carbon dioxide could be used.

Vinyl acetate (VAc): It is a colourless, mobile liquid which can polymerize even on exposure to light. It is not a strong eye or skin irritant (see sources #4,5) but can be narcotic in high concentrations. It is a very strong fire hazard due to its low flash point (18°F). When

burning highly toxic acid fumes are emitted. Of course, spontaneous heating is out of the question with VAc and in case of fire foam, carbon dioxide, dry chemical or carbon tetrachloride could be used. It should be kept grounded in a solvent room away from oxidizing agents. Gloves and protective glasses should be used with it.

Tetrahydrofuran (THF): It is a colourless, mobile liquid with an ether-like odour. It is very flammable and its vapour can form explosive mixtures with air. It may form organic peroxides when exposed to air or light and hence explode. It is a strong eye, skin and respiratory irritant with narcotic effects. It is reported as causing injury to liver and/or kidney (#3). Its TLV is 590 mgr/m^3 of air or 200 ppm in air. In case of fire, dry chemical or carbon dioxide may be ineffective. Water can be used to disperse its vapours. Eye protection, gloves and protective clothing are recommended. Continued exposure can lead to the development of a sensitivity to it.

Equipment

Distillation equipment: Distillation under vacuum is used to remove the impurities from the monomer. Possible hazards follow: (a) Breakage of the equipment with subsequent spills and high vapour concentrations (increased danger of fire and explosion). (b) Emission of toxic fumes. (c) Formation of explosive flammable mixtures with air. (d) Exposure to high vapour concentrations when opening the equipment, and (e) polymerization in the collecting vessel or inside the distillation column.

Procedures to reduce risks

Monomer distillation: It should be carried out in a fume hood with two traps on the line to prevent releasing of large amounts of VAc to the atmosphere. A heating mantle should be used to remove ignition sources and the collecting vessel should be opaque to prevent

polymerization by light. No smoking or Bunsen burners should be allowed near the still and a self-contained respirator should be available in the event of a spill or large leak. The distilled VAc should be kept in the refrigerator to reduce further risks.

Procedures in event of accident

. Procedures in case of fire, spills and leakage, and first aids in general are described in detail in the reference sources #1 and 2. More specifically, KPS spills should be neutralized with weak reducing agents such as bisulfite and water followed by neutralization with soda ash. In case of fire caused by VAc, the fire should be fought with foam, CO_2 on dry chemical type extinguishing agents, but not water.

General literature references on safety

#1. "Fire protection Guide on Hazardous Materials", 6th Edition, National Fire Protection Association, 1975.

#2. "Toxic and Hazardous Industrial Chemical Safety Manual for Handling and Disposal with Toxicity and Hazard Data", International Technical Information Institute.

#3. "Dangerous Properties of Industrial Materials", 3rd Edition, N.I. Sax (Ed.), Van-Nostrand Reinhold Co., New York, 1968.

#4. "CRC Handbook of Laboratory Safety", 2nd Edition, CRC Press, N.V. Steere (Ed.), Cleveland, Ohio, 1976.

#5. "Industrial Hygiene and Toxicology", Vol. II, 2nd Edition, F.A. Patty, D.W. Fasset and D.D. Irish (Eds.), John Wiley and Sons, New York, 1963.

APPENDIX XII

Continuous PVAc Runs Data Record

CR1, θ_2 = 30 minutes

	t/θ_2	Gravimetry $x_2(t)$	Reproducible checks on $x_2(t)$	Densitometry $x_2(t)$	Average particle size, Å
A	0.333	0.5247		0.5131	
	0.666	0.6710	0.6628		1000
	1.000	0.4190	0.4217	0.3994	1250
	1.166			0.3973	
	1.333			0.3829	1000
	1.500			0.3772	
	1.666	0.3016			
	2.000	0.2967			
	2.333				1200
	3.000	0.4022	0.4142	0.4344	1500
	3.166			0.4314	
	3.333				1500
	3.500			0.4399	
	3.666				1500
	4.333	0.2548			
	5.000	0.2754			
	5.666	0.4615			
	6.000	0.4297	0.4390		
	6.333	0.3900	0.40412		2200
	6.666	0.2782			2200
	7.000	0.3176		0.3314	2200
	7.666	0.4521	0.4384	0.4393	
	8.000	0.4520		0.4394	
	8.666	0.2674			
	9.000	0.2542	0.2840		
	9.000		0.2677		
	9.333	0.2594	0.2704		
	10.000	0.3748			
	10.666	0.4172	0.4135		
	11.000	0.4214			
	11.333	0.3816			
	12.000	0.3251			
B	12.666				2200
	13.000			0.4457	
	13.333	0.4663	0.4714	0.4541	2200
	13.666				2200
	13.833			0.4598	
	14.000	0.4451	0.4279	0.4472	
	14.166			0.5151	
	14.333	0.5335		0.5381	2750
	14.500			0.5372	

	14.666	0.5279			
	14.833			0.5360	
	15.000	0.5221		0.5389	1750
	15.166			0.5398	
	15.333	0.5735	0.5674	0.5422	2200
	15.500			0.5333	
	15.666	0.5034		0.5303	2200
	16.000	0.5318		0.5256	2200
	16.166			0.5247	
	16.333			0.5113	2200
	16.666				2200
	17.000	0.5217	0.5399	0.5131	2200
	17.333	0.5303		0.5145	2200
	17.666			0.5074	
	18.000			0.5111	2200
	18.166			0.5131	
	18.500			0.6035	
	18.666				2200
	18.833			0.5062	
	19.166			0.5050	
	19.333	0.5197	0.5283		
	19.500			0.5008	
	19.666	0.5000		0.5017	
	20.166			0.5026	
	20.333	0.5073	0.5105	0.5038	
	20.666			0.5014	
	21.000			0.5038	
	21.333	0.4977		0.5050	
	21.666			0.5077	
	21.833			0.5053	
	22.166			0.5035	
	22.500			0.5041	
	22.833			0.5047	
	23.000			0.5053	
	23.166			0.5038	
	23.333	0.5316		0.5017	
C	23.666			0.4154	
	24.000			0.4138	
	24.333			0.3872	
	24.666			0.3836	
	25.000			0.3872	
	25.333			0.3836	
	25.666			0.3792	
	26.000			0.3783	
	26.666			0.3776	
	27.000			0.3765	
	27.333			0.3747	
	27.500			0.3765	
	27.666			0.3679	
	28.666			0.3679	

	t/θ_2	CR1 Densitometry $x_1(t)$	
up to	12.333	0.0000	A
	12.666	0.0532	B
	12.833	0.0589	
	13.000	0.4149	
	14.833	0.4648	
	15.166	0.3760	
	15.333	0.3592	
	15.500	0.3592	
	15.666	0.3760	
	15.833	0.3313	
	16.000	0.3090	
	16.333	0.2193	
	16.500	0.1799	
	16.666	0.1687	
	16.833	0.1630	
	17.000	0.1687	
	17.833	0.2193	
	18.000	0.2193	
	18.166	0.2081	
	18.333	0.2025	
	18.500	0.1912	
	18.666	0.1912	
	18.833	0.2081	
	19.000	0.1912	
	19.166	0.2137	
	19.333	0.2249	
	19.500	0.2137	
	19.666	0.2193	
	19.833	0.2193	
	20.000	0.2249	
	20.166	0.2193	
	20.333	0.2193	
	20.500	0.2137	
	20.666	0.2249	
	20.833	0.2081	
	21.000	0.1912	
	21.166	0.2137	
	21.333	0.2249	
	21.833	0.2137	
	22.166	0.1912	
	22.333	0.2362	
	22.500	0.2418	
	22.666	0.2362	
	22.833	0.2362	
	23.000	0.2362	
	23.166	0.2362	
	23.333	0.2249	
	23.500	0.2418	

CR2, θ_2 = 30 minutes

	t/θ_2	Gravimetry $x_2(t)$	Reproducible checks for $x_2(t)$	Densitometry $x_2(t)$	Average particle size, Å
A	1.000	0.01126	0.00920		
	1.500	0.10909			
	1.833			0.15818	
	2.000	0.14855	0.14257		
	2.166			0.15730	
	2.333			0.15739	
	2.500	0.15230		0.15737	1148
	2.833			0.15333	
	3.000	0.15435	0.16408	0.15730	1286
	3.166			0.15728	
	3.500	0.16299		0.15726	1430
	3.666			0.15730	
	4.000	0.16158	0.16523	0.15748	1505
	4.166			0.15756	
	4.333			0.15756	
	4.500	0.16009			1580
	4.666			0.15762	
	4.833			0.15762	
	5.000	0.16409	0.16326	0.15754	1580
B	5.500	0.19158		0.20747	1580
	5.666			0.20756	
	5.833			0.20750	
	6.000	0.19606	0.19027		1505
	6.166			0.20743	
	6.333			0.20748	
	6.500	0.20224			1505
	6.666			0.20747	
	7.000	0.21383	0.21664	0.20758	1430
	7.333			0.20767	
	7.500	0.23516			1505
	7.666			0.20762	
	8.000	0.21832	0.23778		1505
	8.166			0.21767	
	8.500	0.21114		0.21762	1505
	8.833			0.21758	
	9.000	0.21825	0.22237		1580
	9.166			0.21765	
	9.500	0.21376		0.21773	1580
	10.000	0.22199	0.22704	0.21771	1580
	10.500	0.21854		0.21773	1657
	10.666			0.21771	
	10.833			0.21767	
	11.000	0.21805	0.22291	0.21773	1735
	11.333			0.21769	
	11.500	0.21319		0.21771	1891
	11.833			0.21762	
	12.000	0.21814	0.18522		

C	12.166			0.21752	
	12.500	0.21159			2049
	12.833			0.27777	
	13.000	0.22637	0.21888		
	13.333			0.22786	
	13.500	0.25517		0.25799	2049
	14.000			0.26809	
	14.166			0.27834	
	14.500	0.29408		0.30841	2127
	15.166			0.31843	
	15.666			0.32839	
	15.833			0.34843	
	16.000	0.35992		0.35862	
	16.500	0.40911			2205
	17.000	0.41660	0.41416		2205
E	17.500	0.44540			2205
	18.000	0.44671	0.45699		2127
	18.500	0.56567			2281
	19.000	0.53752			2205
	19.500	0.48692			2127
	20.000	0.44503			
	20.500				2127
	21.000	0.35992	0.37694		2205
	21.500	0.35113			2205
	22.000	0.44297			2127

CR2

t/θ_2	Densitometry $x_1(t)$	
1.166	0.05399	A
1.500	0.05436	
1.666	0.05442	
1.833	0.05455	
2.000	0.05380	
2.166	0.05324	
2.500	0.05279	
3.000	0.05299	
3.333	0.05357	
3.500	0.05363	
3.833	0.05283	
4.000	0.05267	
4.333	0.05250	
4.500	0.05225	
4.833	0.05227	
5.000	0.05211	
5.500	0.05382	B
5.833	0.05389	
6.000	0.05416	
6.500	0.05409	
7.000	0.05389	
7.333	0.05370	
7.500	0.05396	
8.000	0.05412	
8.333	0.05396	
8.500	0.05409	
9.000	0.05407	
9.666	0.05388	
9.833	0.05405	
10.000	0.05415	
10.500	0.05409	
11.000	0.05412	
11.333	0.05416	
11.500	0.05409	
11.833	0.05410	
12.000	0.05396	

APPENDIX XIII

VCM/VAc Emulsion Copolymerization

The emulsion copolymerization model development followed the development in Chapter 2. A full development will not be repeated again but enough hints will be given so that the derivation of the new equations and expressions will be evident. The model will then be applied to copolymer latex reactor simulations concerning the specific system VCM/VAc. Lack of experimental literature data made it impossible to directly check the model's predictive powers, however, successful simulation of extreme cases and reasonable trends obtained in the model's predictions are convincing enough about the validity of the mathematical model.

Copolymer model development

Following the development in Chapter 2 of this thesis,

$$\frac{dv(t,\tau)}{dt} = \frac{MW_1 R_{p1}(t,\tau) + MW_2 R_{p2}(t,\tau)}{d_p} \qquad \text{(XIII-1)}$$

$$R_{p1}(t,\tau) = k_{p11}\, k_{p22}\, \frac{r_1 (M_1)_p^2 + (M_1)_p (M_2)_p}{k_{p11} r_2 (M_2)_p + k_{p22} r_1 (M_1)_p}\, \frac{\bar{q}(t,\tau)}{N_A} \qquad \text{(XIII-2)}$$

$$\bar{q}(t,\tau) = \bar{q}_1(t,\tau) + \bar{q}_2(t,\tau) \qquad \text{(XIII-3)}$$

$$M_p = (M_1)_p + (M_2)_p \qquad \text{(XIII-4)}$$

$$r_1 = k_{p11}/k_{p12} = 1.68 \qquad \text{(XIII-5)}$$

$$f_1(t,\tau) = (M_1)_p / M_p \tag{XIII-6}$$

$$\frac{\bar{q}_1(t,\tau)}{\bar{q}(t,\tau)} = \omega_1 \tag{XIII-7}$$

$$\omega_1 = \frac{k_{p21} f_1(t,\tau)}{k_{p12} f_2(t,\tau) + k_{p21} f_1(t,\tau)} \tag{XIII-8}$$

In all the above expressions and in what follows, subscript 1 refers to monomer 1 (VCM), subscript 2 to monomer 2 (VAc), and only the expressions for monomer 1 are shown. Expressions for monomer 2 are totally analogous to the ones for monomer 1. The same nomenclature is kept as for the homopolymer case.

Following Nomura et al. (1982) for the desorption rate constant expressions, one finally obtains:

$$\bar{q}(t,\tau) = \frac{R_i^{1/2}(t)}{\left(2\sigma_{23}\right)^{1/2}} \frac{a_\rho(t,\tau)}{A_\rho^{1/2}(t)} \tag{XIII-9}$$

$$\sigma_{23} = \omega_1 \sigma_6 \left(\frac{12 \pi D_{w1} \delta_1}{m_1} \right) + \omega_2 \sigma_6 \left(\frac{12 \pi D_{w2} \delta_2}{m_2} \right) \tag{XIII-10}$$

$$\sigma_6 = \frac{r_1 C_{m_{11}} (M_1)_p + C_{m_{21}} (M_2)_p}{r_1 (M_1)_p + (M_2)_p} \tag{XIII-11}$$

$$C_{m_{11}} = k_{fm_{11}} / k_{p_{11}} \tag{XIII-12}$$

$$(M_1)_p = \phi_1(t)\, d_{M_1} / MW_1 \tag{XIII-13}$$

$$\phi_1(t) = \frac{\alpha\,(1\ x_1(t))}{\left(\alpha + \beta\,\frac{d_{M_1}}{d_{M_2}}\right) - \alpha\, x_1(t)\left(1 - \frac{d_{M_1}}{d_p}\right) + \beta x_2(t)\, d_{M_1}\left(\frac{1}{d_p} - \frac{1}{d_{M_2}}\right)} \qquad \text{(XIII-14)}$$

In equation (XIII-14), $x_1(t) = x_{c_1}$ if $x_1(t) \leq x_{c_1}$ and $x_2(t) = x_{c_2}$ if $x_2(t) \leq x_{c_2}$. Also,

$$\alpha \equiv \frac{\text{grs of monomer 1}}{\text{grs of monomers 1 and 2.}} \qquad \text{(XIII-15)}$$

and β is defined similarly as the mass percentage of monomer 2.

There is a rough approximation in the above definition of $\phi_1(t)$, i.e. equation (XIII-14). In the specific system VCM/VAc, x_{c_1} and x_{c_2} differ considerably, due to the very different solubilities of the two monomers to their own polymers. A modelling approach using one x_c for the whole system, even empirically or experimentally defined (see Nomura et al. (1982)), would be closer to reality. Another alternative would be the use of partition coefficients for the definition of $(M_1)_p$ (see Hamielec and MacGregor (1983)). An even more sophisticated approach (but maybe less practical because it would insert additional parameters in the model and therefore additional uncertainty) would be to start from thermodynamic considerations (see Ugelstad et al. (1978) or Hoffman (1981)). This part of the model, although sufficient for a start, definitely needs a further refinement for future studies.

Following Hamielec and MacGregor (1983),

$$x_1(t) = \frac{P_1(t)}{N_1(t) + N_2(t) + P_1(t) + P_2(t)} \qquad \text{(XIII-16)}$$

From the previous development,

$$R_{P_1}(t) = \sigma_3\left(\frac{fk_d N_A}{\sigma_{10}}\right) I_w^{1/2}(t)\, A_p^{1/2}(t) \qquad \text{(XIII-17)}$$

$$\sigma_3 = \frac{k_{p_{11}} k_{p_{22}}}{N_A} \frac{r_1\left(M_1\right)_p^2 + \left(M_1\right)_p\left(M_2\right)_p}{k_{p_{11}} r_2\left(M_2\right)_p + k_{p_{22}} r_1\left(M_1\right)_p} \tag{XIII-18}$$

$$\sigma_{10} = \sigma_8 + \sigma_9 \tag{XIII-19}$$

$$\sigma_8 = \omega_1 \frac{12\, D_{w_1} \delta_1}{m_1} \sigma_6 \tag{XIII-20}$$

and

$$\frac{dv_p(t,\tau)}{dt} = \lambda\, \xi(t)\, a_p(t,\tau) + v_p(t,\tau)\left(\varepsilon_1(t) + \varepsilon_2(t)\right) \tag{XIII-21}$$

$$\lambda\xi(t) = \frac{\lambda\xi'(t)}{1 - \phi_1(t) - \phi_2(t)} \tag{XIII-22}$$

$$\lambda\xi'(t) = \sigma_5\left(\frac{f k_d N_A}{\sigma_{10}}\right)^{1/2} \frac{I_w^{1/2}(t)}{A_p^{1/2}(t)} \tag{XIII-23}$$

$$\sigma_5 = \sigma_1\sigma_3 + \sigma_2\sigma_4 \tag{XIII-24}$$

$$\sigma_1 = \frac{MW_1}{d_p} \tag{XIII-25}$$

$$\varepsilon_1(t) = \frac{1}{1 - \phi_1(t) - \phi_2(t)} \frac{d\phi_1(t)}{dt} \tag{XIII-26}$$

$$\frac{d\phi_1(t)}{dt} = \sigma_{19} \frac{dx_1(t)}{dt} - \sigma_{20} \frac{dx_2(t)}{dt} \tag{XIII-27}$$

$$\sigma_{19} = \frac{a}{\sigma_{17}}\left(\frac{(1-x_1(t))\sigma_{12}}{\sigma_{17}} - 1\right) \qquad \text{(XIII-28)}$$

$$\sigma_{20} = \frac{a\sigma_{13}(1-x_1(t))}{\sigma_{17}^2} \qquad \text{(XIII-29)}$$

$$\sigma_{12} = a\left(1 - \frac{d_{M_1}}{d_p}\right) \qquad \text{(XIII-30)}$$

$$\sigma_{13} = \beta d_{M_1}\left(\frac{1}{d_p} - \frac{1}{d_{M_2}}\right) \qquad \text{(XIII-31)}$$

$$\sigma_{17} = \sigma_{11} - \sigma_{12}x_1(t) + \sigma_{13}x_2(t) \qquad \text{(XIII-32)}$$

and

$$\sigma_{11} = a + \beta\frac{d_{M_1}}{d_{M_2}} \qquad \text{(XIII-33)}$$

Now, it is equation (XIII-21) which can be incorporated in the general property balance equation (see Chapter 2) and eventually give a differential equation for $V_p(t)$, the total polymer particle volume in the system. The rest of the PSD differential equations are derived in a completely analogous way as the homopolymer ones and the material balances describing the system can be written following Hamielec and MacGregor (1983).

For the molecular weight part of the model, one can follow Chapter 2 and the development in Hamielec and MacGregor (1983), with

$$k_p^1 = \omega_1\left(k_{p_{11}}(M_1)_p + k_{p_{12}}(M_2)_p\right) + \omega_2\left(k_{p_{31}}(M_1)_p + k_{p_{22}}(M_2)_p\right) \qquad \text{(XIII-34)}$$

$$k_{fm}^1 = \omega_i\left(k_{fm_{11}}(M_1)_p + k_{fm_{12}}(M_2)_p\right) + \omega_2\left(k_{fm_{21}}(M_1)_p + k_{fm_{22}}(M_2)_p\right) \qquad \text{(XIII-35)}$$

$$\omega_2 = 1 - \omega_1 \tag{XIII-36}$$

$$k_p^{*1} = \left(\omega_1 k_{p_1}^* + \omega_2 k_{p_2}^*\right) M_p \left(1 - \text{cum } F_1\right) \tag{XIII-37}$$

$$k_{f_p}^1 = \left[\omega_1\left(k_{fp_{11}} \text{ cum } F_1 + k_{fp_{12}} \text{ cum } F_2\right) + \omega_2\left(k_{fp_{21}} \text{ cum } F_1 + k_{fp_{22}} \text{ cum } F_2\right)\right] M_p \tag{XIII-38}$$

$$\text{cum } F_2 = 1 - \text{cum } F_1 \tag{XIII-39}$$

and

$$Y_{\sigma_{TOT}}(t) = \left(\frac{fk_d N_A}{\sigma_{10}}\right)^{1/2} I_w^{1/2}(t)\, A_p^{1/2}(t)\, V_R(t) \tag{XIII-40}$$

In the above expressions, (cum F_1) represents the accumulated mole fraction of monomer 1 in all dead polymer chains, with F_1 defined as:

$$F_1 = \frac{r_1 f_1^2 + f_1 f_2}{r_1 f_1^2 + 2 f_1 f_2 + r_2 f_2^2} \tag{XIII-41}$$

Copolymer latex reactor studies

The objective of this exercise was to test whether the copolymer latex model was able to give reasonable trends in simulating the specific system VCM/VAc. It was impossible to find reported experimental results in the literature, so the study was limited in the simulation stage (see Murray et al. (1985)). The model could handle batch, semi-batch, single continuous, continuous train and CSTR-tube (Lee and Forsyth (1981)) reactor configurations.

Since there was no experimental data available for the copolymer case, the copolymer model was run as a homopolymer one by setting one of the monomer inputs equal

to zero. In this way one could test two extreme cases and see if there were any flaws in the model's logic. The results for a batch latex reactor are shown in Figure XIII-1a.

A problem that one encounters when producing a copolymer in a batch reactor is that of copolymer compositional drift. This drift occurs due to different reactivities of the two monomers. For the VCM/VAc system, r_1(VCM) = 1.68 and r_2(VAc) = 0.23, therefore VCM is the faster reacting monomer. The theoretical curve for the instantaneous copolymer composition, i.e. F_1 versus f_1, would lie above the 45 degree line for a system of this type, with the drift being in the direction that tends to decrease the mole fraction of the fast monomer. Our model was tested to see whether it could predict the right drift. For the recipes employed, the model prediction is shown in Figure XIII-1b. The portion of the curve generated by the model parallels the theory in that the curve is above the 45 degree line and the drift is in the right direction, as indicated by the arrow.

For a single continuous reactor, the model predicted the expected oscillatory behaviour. The oscillations disappeared when a seeded feed stream was used. Figure XIII-1c shows a single CSTR behaviour when different start-up conditions are applied. The solid line corresponds to the reactor starting up full of water. The expected overshoot, when the reactor starts full of the emulsion recipe, is correctly predicted by the model and furthermore, the model numerical predictions (conversion ~ 25%, diameter ~ 1500 Å) are in a reasonable range. The train configuration was also simulated and shown to eliminate oscillations, as expected (see Chapter 7).

In conclusion, one could say that despite the lack of experimental data with which the copolymer model predictive powers could be tested, its trends when applied to the VCM/VAc system were very reasonable and in agreement with our general experience from systems of this type. There are certain aspects of the model that should be refined in the near future, but at least the basic structure has been successfully set up.

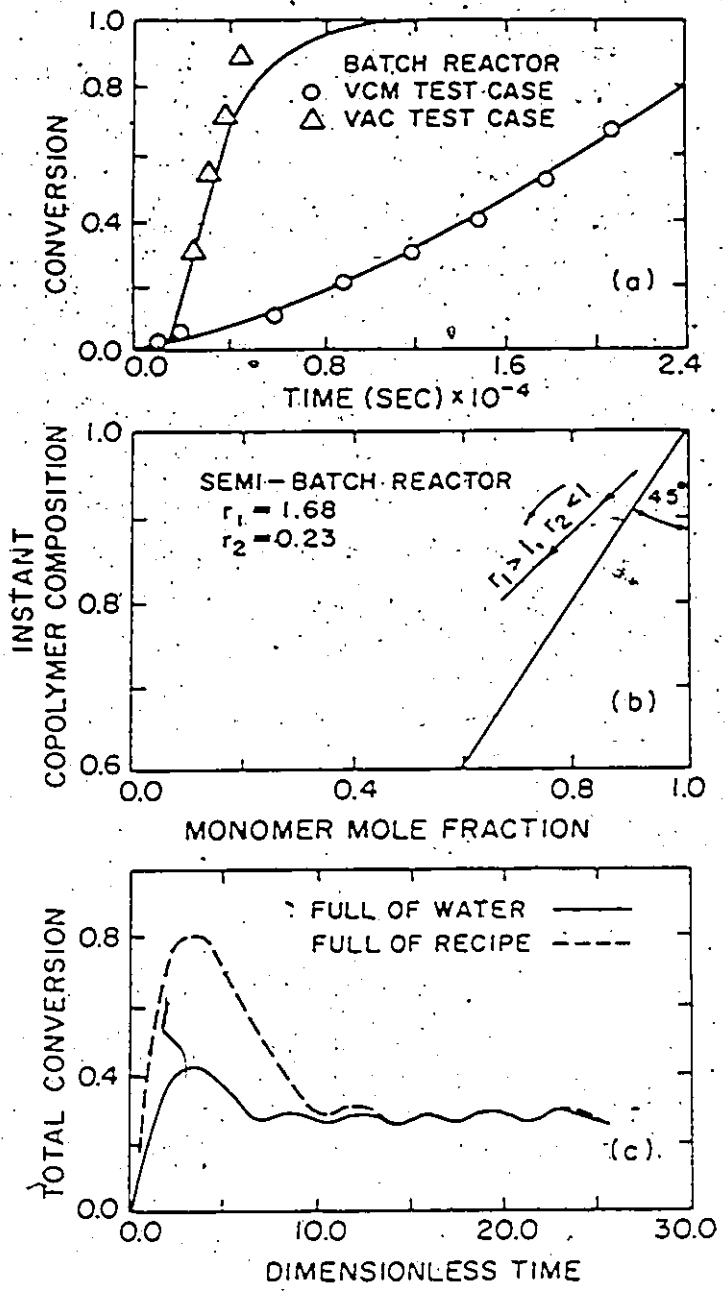

Figure (XIII-1). VCM/VAc Emulsion Copolymerization: (a) Conversion vs. Time in a Batch Reactor for Extreme Cases, (b) Instantaneous Copolymer Composition, (c) Start-up Procedures in an Unseeded CSTR

APPENDIX XIV

Model Modification to Include Impurities

Water Soluble Impurities (WSI, WI)

Water soluble impurities (oxygen or hydroquinone) react with radicals in the water (or emulsion) phase according to the following scheme:

$$R\cdot + WSI \xrightarrow{k_{WI}} R(WSI) \qquad \text{(XIV-1)}$$

Considering reaction (XIV-1), equation (I-12) becomes

$$R_w = \frac{\rho(t)}{k_m A_m(t) k_v + k_n + k_{ab} A_p(t) k_v + k_{WI}(WI)(t) k_v} \qquad \text{(XIV-2)}$$

with (WI)(t) representing concentration of water soluble impurities at time t in gmole/l-latex and k_{WI} being the rate constant of the radical reaction with impurities in gmole/lit-sec.

Then, equation (I-45) becomes:

$$f(t) = \rho(t) \frac{A_m(t) k_v + \mu(1 - L A_p(t) k_v/4)}{A_m(t) k_v + \mu(1 - L A_p(t) k_v/4) + \varepsilon A_p(t) k_v + \gamma(WI)(t) \cdot k_v} \qquad \text{(XIV-3)}$$

with

$$\gamma = (k_{WI}/k_m) \qquad \text{(XIV-4)}$$

The mass balance for water soluble impurities is quite straightforward and can be written as:

$$\frac{d(WI)(t)}{dt} = \frac{(WI)_F(t)}{\theta} - \frac{(WI)(t)}{\theta} - k_{WI}(R_w) k_v \frac{(WI)(t)}{N_A} \qquad \text{(XIV-5)}$$

Monomer soluble impurities (MSI, MI)

Monomer soluble impurities act inside the polymer particles where they are being transferred with monomer during the diffusion of monomer from its droplets. Their reaction with radicals can be represented as follows:

$$\bar{q}(t,\tau) + MSI \xrightarrow{k_{MI}} \bar{q}(MSI) \qquad \text{(XIV-6)}$$

With reaction (XIV-6) in mind, the radical balance for a class (t,τ) viewed in the water phase, equation (I-79), becomes:

$$\begin{pmatrix}\text{Entry to}\\ \text{a class}\end{pmatrix} = (\text{Desorption}) + (\text{Initiation}) - \begin{pmatrix}\text{Water phase}\\ \text{termination}\end{pmatrix} \qquad \text{(XIV-7)}$$

Neglecting water phase termination, equation (XIV-7) can be written as:

$$\rho(t,\tau) = \rho_{des}(t,\tau) + R_I(t)\,\frac{A_n(t,\tau)\,d\tau}{A_p(t)} \qquad \text{(XIV-8)}$$

with

$$\rho_{des}(t,\tau) = \bar{q}(t,\tau)\,k_{de}(t,\tau)\,n(t,\tau)\,d\tau \qquad \text{(XIV-9)}$$

Also, the radical balance for the whole class, equation (I-80), becomes:

$$\begin{pmatrix}\text{Initiation}\\ \text{of a class}\end{pmatrix} = \begin{pmatrix}\text{Mutual termination of}\\ \text{radicals in particles}\end{pmatrix} + \begin{pmatrix}\text{Destruction of}\\ \text{radicals by MSI}\end{pmatrix} \qquad \text{(XIV-10)}$$

The first term in the RHS of equation (XIV-10) is a second order type of termination, whereas the second term describes a first order termination of radicals.

If termination took place only by mutual termination of two radicals inside a polymer particle, then the first term in the RHS of equation (XIV-10) would be identical to the RHS term of equation (I-80). Now, there is also a first order termination of radicals by impurities. Therefore, only the radicals that enter the particles and are not destroyed by MSI can mutally terminate. Hence, equation (XIV-10) becomes:

$$R_I(t)\,\frac{A_n(t,\tau)\,d\tau}{A_p(t)} = 2[\rho(t,\tau) - \rho_{MI}(t,\tau)]\,\bar{q}(t,\tau) + \rho_{MI}(t,\tau) \qquad \text{(XIV-11)}$$

with

$$\rho_{MI}(t,\tau) = k_{MI}(MI)_p(t)\cdot\bar{q}(t,\tau)\,n(t,\tau)\,d\tau \qquad \text{(XIV-12)}$$

Combination of (XIV-8) and (XIV-11) will yield a new expression for $q(t,\tau)$, which accounts for the destruction of radicals by MSI. This expression is the following:

$$\bar{q}(t,\tau) = \frac{-2R_I(t)\dfrac{a_p(t,\tau)}{A_p(t)} - k_{MI}(MI)_p(t) + \Delta^{1/2}}{4\,IMP(t,\tau)} \qquad \text{(XIV-13)}$$

with

$$IMP(t,\tau) = k_{de}(t,\tau) - k_{MI}(MI)_p(t) \qquad \text{(XIV-14)}$$

and

$$\Delta = 4R_I^2(t)\frac{a_p^2(t,\tau)}{A_p^2(t)} + k_{MI}^2(MI)_p^2(t) + 4R_I(t)\frac{a_p(t,\tau)}{A_p(t)}[2k_{de}(t,\tau) - k_{MI}(MI)_p(t)] \qquad \text{(XIV-15)}$$

The expression for $\bar{q}(t,\tau)$ as given by (XIV-13) is quite complicated. Using the previously employed assumption (see Appendix I), which is valid for Case I systems, that desorption of radicals is dominant over the term $(R_I(t)\,A_n(t,\tau)\,d\tau/\,A_p(t))$, equation (XIV-13) becomes:

$$\bar{q}(t,\tau) = \psi(t,\tau)\,a_p(t,\tau) \qquad \text{(XIV-16)}$$

with

$$\psi(t,\tau) = \frac{-k_{MI}(MI)_p(t)}{4\pi A} + \frac{1}{4\pi A}\left\{k_{MI}^2(MI)_p^2(t) + 8\frac{\pi A R_I(t)}{A_p(t)}\right\}^{1/2} \qquad \text{(XIV-17)}$$

$$A = \frac{12\,D_w\,\delta\,k_{fm}}{m\,k_p} \qquad \text{(XIV-18)}$$

and

$$\pi A >> k_{MI}(MI)_p(t)\,a_p(t,\tau) \qquad \text{(XIV-19)}$$

Equation (XIV-19) is true for Case I systems, for a range of sizes from 100 to 4000 Å.

Finally, the material balance for MSI is quite straightforward and can be written as:

$$\frac{d(MI)(t)}{dt} = \frac{(MI)_F(t)}{\theta} - \frac{(MI)(t)}{\theta} - \frac{k_{MI}(MI)_p(t)\cdot N_p(t)\,\bar{q}(t)}{N_A} \qquad \text{(XIV-20)}$$

where (MI)(t) represents the total concentration of monomer soluble impurities, $(MI)_p(t)$ the concentration of MSI in the polymer particles, k_{MI} the reaction rate constant with MSI, and

$$\bar{q}(t) = \left\{ \int_0^t \bar{q}(t,\tau)\, n(t,\tau)\, d\tau \right\} / N_p(t) \qquad \text{(XIV-21)}$$

An alternative approach

An expression for $\bar{q}(t,\tau)$ could also have been obtained for Case I systems, if the original derivations by Smith and Ewart (1948), O'Toole (1965), Ugelstad and Hansen (1976) and Hoffman (1981) were to be followed. In this way, one simply has to substitute $n_{n-1}(t,\tau)$ for N_{n-1}. The result would be the following:

$$\bar{q}(t,\tau) = \frac{\alpha}{4} \frac{I_m(\alpha)}{I_{m-1}(\alpha)} \qquad \text{(XIV-22)}$$

with m defined as in equation (9.1). I_m represents modified Bessel functions of the first kind, which can finally give (Hildebrand (1976)):

$$\bar{q}(t,\tau) \sim \frac{\alpha^2}{8} \cdot \frac{\Gamma(m)}{\Gamma(m+1)} \qquad \text{(XIV-23)}$$

where Γ represents the Gamma function.

From a simulation study using typical values for Case I systems, the two approaches gave almost the same results for a range of particle diameters between 100 and 3000 Å. Some slight discrepancy after a particle diameter of 2000 Å was due to the approximation of equation (XIV-23).

APPENDIX XV

Data of Batch VAc Impurity Runs

	Time (sec)	Conversion	Average Size (Å)
IM1			
	1500	0.0794	
	1800	0.2017	508
	2100	0.2775	
	2400	0.3531	734
	2700	0.4230	
	3000	0.4729	848
	3300	0.5315	
	3600	0.5815	978
	3900	0.6259	
	4200	0.6945	978
	4500	0.7432	
	4800	0.7861	1049
	5100	0.8132	
	5400	0.8532	1193
	5700	0.8852	
	6000	0.9192	1193
	6300	0.9354	
IM2			
	1500	0.0569	
	1800	0.1920	
	2100	0.2918	683
	2400	0.3426	
	2700	0.4489	855
	3000	0.4895	
	3300	0.5351	1006
	3600	0.5750	
	3900	0.6146	1006
	4200	0.6807	
	4500	0.7318	1050

	Time (sec)	Conversion	Average Size (Å)
IM3			
	1500	0.0415	
	2100	0.2780	683
	2400	0.4273	
	2700	0.4567	
	3000	0.5114	734
	3300	0.5614	789
	3600	0.5963	
	3900	0.6293	762
	4200	0.6923	
	4500	0.7299	789
	4800	0.7625	
	5100	0.7967	848
	5400	0.8239	
	5700	0.8524	907
	6000	0.8754	
	6300	0.8934	974
	6600	0.9123	
IM4			
	1800	0.0302	
	2100	0.0349	
	2400	0.2226	578
	2700	0.2824	
	3000	0.3315	603
	3300	0.3751	
	3600	0.4267	603
	3900	0.4837	
	4200	0.5297	
	4500	0.5734	
	4800	0.6077	685
	5100	0.6513	
	5400	0.6831	657
	5700	0.7124	
	6000	0.7458	746
	6600	0.8076	746
	6900	0.8229	
	7200	0.8374	746
	7500	0.8570	

	Time (sec)	Conversion	Average Size (Å)
IM5			
	1800	0.0585	
	2400	0.2538	531
	3000	0.3259	
	3600	0.4517	685
	4200	0.5577	
	4800	0.6377	685
	5400	0.7031	
	6000	0.7558	685
	6600	0.8026	
	7200	0.8424	
IM6			
	2100	0.2055	483
	2700	0.4254	
	3300	0.5242	547
	3900	0.6034	
	4500	0.6830	634
	5100	0.7642	
	5700	0.8340	683
	6300	0.8706	
	6900	0.8847	885